Plant Energetics

Octavian S. Ksenzhek

Alexander G. Volkov

Academic Press

PLANT ENERGETICS

This Page Intentionally Left Blank

PLANT ENERGETICS

Octavian S. Ksenzhek
Ukrainian State University
Dniepropetrovsk, Ukraine

Alexander G. Volkov
University of California
at Los Angeles
Los Angeles, California

Octavian S. Ksenzhek
Ukrainian State University
Dniepropetrovsk, Ukraine

Alexander G. Volkov
University of California
at Los Angeles
Los Angeles, California

ACADEMIC PRESS

San Diego   New York   Boston   London   Sydney   Tokyo   Toronto

Contents

Chapter 3
Arrangement of Energy Relations in Plants

Chapter 4
Problems of Integration and Hierarchy of Structures

Chapter 5
Thermodynamics of Energy Conversion by Plants

Chapter 6

Electrochemistry and the Processes of Energy Conversion in Plants

Chapter 7

Photochemistry of Photosynthesis and Mechanisms of Oxygen Evolution

Chapter 8

Energetics of Dark Respiration and Mechanism of Cytochrome Oxidase Functioning

Chapter 9

Plants and the Atmosphere: Heat and Moisture Exchange

Chapter 10

Energetics of Permeation of Molecules and Ions across Membranes

Chapter 11
Transpiration Stream

Chapter 12
Entropy Balance of the Plant

Chapter 13
Electrical Signals and Long-Distance Communication in Plants

Chapter 14

Artificial Photosynthesis in Organized Assemblies of Photosynthetic Pigments

Chapter 15

Humans and Plants

Preface

Green plants capture solar energy and transform it into the chemical energy of organic matter. The scale of this activity is vast and the results are vital. For thousands of years, the progress of human civilization has been tightly linked with the cultivation of plants. Therefore, it is not surprising that processes of energy conversion by plants are of fundamental significance to the life sciences. This book presents the basic concepts and principal applications of thermodynamics, energetics, electrophysiology, and photobiophysics of green plants. In an effort to make the book as compact as possible, we have included only what is essential to the most important phenomena and concepts of plant energetics.

The first two chapters begin with considerations of the peculiarities of solar light as a form of energy, as well as laws governing light propagation in the atmosphere and its capture by plants. The two next chapters discuss the sequence of energy processes in plants and the corresponding hierarchy of structures. Chapter 5 presents a brief introduction to the thermodynamics of energy conversion by plants. In Chapter 6, we introduce the principles of electrochemistry and discuss the main concepts of plant bioelectrochemistry. Chapter 7 addresses the mechanism of water photooxidation and oxygen evolution in photosynthesis. In Chapter 8, the reader will learn about the thermodynamics of respiration. Chapters 9 through 11 are devoted to water transport in plants, transpiration stream, and heat and moisture exchange. In Chapter 12, an attempt is made, possibly for the first time, to examine the entropy balance of a plant. In Chapter 13, we discuss plant electrophysiology, electrical signals in plants, long-distance communication, and insect-induced electrochemical signals in plants. Chapter 14 is devoted to artificial photosynthesis, and the last chapter considers some general aspects of the interrelations between humans and plants.

The authors intend this book to be used as an introduction to energetics, thermodynamics, biophysics, and the electrophysiology of green plants for scientists and engineers, as a textbook for students, and as a reference resource for researchers in plant energetics.

This Page Intentionally Left Blank

Introduction

Our terrestrial existence is tightly and inseparably linked with the life activity of green plants. Approximately 3.5 billion years ago, the first photosynthetic organisms, which were primitive algae and photosynthetic bacteria, appeared on Earth and gradually changed the initial oxygen-free atmosphere of Earth into one rich in oxygen. Thus, the prerequisites for the origin of animal life were created. Some 400–450 million yeas ago vascular plants appeared and occupied dry land. The first amphibians followed the plants, leaving the water for life on land. These events could not happen until the ozone screen shielded Earth's surface from the hard ultraviolet radiation of the Sun. However, this screen could not be formed before appreciable amounts of oxygen had accumulated in the atmosphere from the activity of photosynthetic organisms.

Two hundred million years later, lush forests of tree ferns and gigantic lycopods covered the land surface of Earth. In the span of 50 million years they extracted almost all of the carbon dioxide from the atmosphere. The carbon was then buried in geological strata, and the atmospheric oxygen content increased to about 20%. Eventually, the remnants of these primeval plant communities became the energy source for our technological civilization.

Life on Earth has been supported by the flux of solar energy that poured onto the planet continually for billions of years. The power of this flux is extremely high: 4.14×10^{15} kW·h per day or 1.5×10^{18} kW·h per year. These values are too vast to be imagined easily unless we express the power of the solar energy flux in other units. According to Einstein's equation $E = mc^2$, the energy equivalent of 1 kg of mass is about 2.5×10^{10} kW·h. The net daily energy flux incident upon Earth can thus be expressed as 165 tons, and the net annual flux is 60,000 tons. By comparison, the annual production of electric energy in the United States corresponds to an equivalent mass of about 100 kg, and the total use of all kinds of energy corresponds to about 800 kg.

The flow of radiant energy coming from the Sun sets into motion practically all active processes on Earth. The only exceptions are volcanic phenomena, earth-

quakes, and tides, but their role in the total energy balance of Earth is negligible. The largest consumers of solar energy are meteorological processes: winds and rains, ocean currents, and hurricanes. An ordinary tropical hurricane consumes 500–1000 or even as much as 2000 kg of energy within the several days of its vigorous existence. This amount is approximately equal to the annual consumption of energy by humans.

The huge "machine" of the biosphere is second to meteorological processes on the scale of consumption of solar energy. The parts of this machine are the innumerable living beings that populate Earth. Total mass of this machine is about 5×10^{12} tons. Its power consumption is about 5×10^{13} kW. The function of this machine is life itself in all its diverse forms and manifestations, and the results of its functioning are the rotating "wheels" of the biogeochemical cycles. Over several years, the biospheric machine renews itself by substitution of its "worn parts" with new ones. The biospheric machine needs 300 years to recycle all of the carbon dioxide contained in the atmosphere and dissolved in oceans. A single cycle of oxygen lasts about 4000 years, and approximately the same time is needed for plants to pass all the water of the seas and oceans through their roots, stems, and leaves. Eight million years is enough for plants to decompose the 1.5 billion km³ of water that exists on our blue planet. During the past billion years of geological history, the water resources of Earth have been decomposed by plants several hundred times.

To provide uninterrupted functioning of the biosphere, 20–30 tons of energy per day or 8000–12,000 tons per year is necessary. This energy comes from the Sun and enters the biosphere through plant leaves and the cells of algae. A small fraction of the energy received, approximately 40 tons per year, is fixed by plants in the form of chemical energy contained in the 200 billion tons of biomass produced annually. These 40 tons comprise the whole energy resource for all heterotrophic organisms. Humankind's share of this energy is only about 250 kg. Although this amount may be rather small by comparison, it is the product of 4 billion acres of cultivated lands over all continents except Antarctica.

If the flow of solar rays is the motive force that actuates the biospheric machine, then plants are its engines or power stations. They capture solar energy, convert it into forms accessible to biological systems, and synthesize all of the material from which organic substances of the biosphere are built. Plants provide the channel through which energy enters living matter. Strictly speaking, there are other paths by which energy enters the biosphere, but their total share of its energy balance is negligibly small. These paths are the relics of ancient forms of life such as sulfur bacteria, ferrobacteria, and some other autotrophs.

About 95% of living matter existing on Earth is the biomass of plants. The plants underpin all food webs, producing oxygen, exerting a strong influence on climate, and creating soil and preventing its erosion. The specific and unique role of plants as the largest scale consumer and transformer of energy naturally attracts

great interest to the problem of plant energetics. The field splits into several levels according to the hierarchical arrangement of biological systems. It comprises the investigation of photosynthetic processes on the molecular level and on the level of chloroplasts, the study of energetics of photosynthesis on the cellular level, the investigation of energy relations of the plant as an entire organism, and the study of the energetics of plant communities. All of these levels are specific and demand appropriate methodology so distinct from each other that the domains of investigation exist almost independently.

The most advanced investigations currently are studies of the mechanisms and energetics of photosynthesis on the molecular level. The results achieved in this field during the past decade are most impressive. However, there are many other questions concerning the energetics of plants that need much further study.

Photosynthesis is the fundamental process in the life of plants. However, its identification as their main goal would hardly be correct. The plant is an organism, the vital aims of which are its individual survival and reproduction. The plant uses photosynthesis to supply itself with materials and energy that are needed to perform all of its vital functions. To obtain an adequate picture of plant energetics, we must examine all of the processes accompanying the production, consumption, and transformation of energy in the plant.

It is relevant to view the plant as an integrated technological system. For such a system to operate, a series of opposing conditions must be met. All of the components of the photosynthetic reaction, i.e., the carbon dioxide, water, and energy needed for performing the reaction, must be delivered into a certain compartment containing appropriate complexes of pigments and enzymes. The products of the reaction need to be continually removed from the reaction compartment and distributed over the macroscopic body of the plant. All of these processes are linked with certain expenditures of energy.

Among the most intriguing questions of plant energetics is the one concerning the explanation of the large gap between the theoretically attainable limit of efficiency of energy conversion by the photosynthetic process and the actual efficiency. Estimates based on thermodynamics give a limiting value for the efficiency of photosynthesis at about 15%, whereas it rarely exceeds 1% in green plants. The discrepancy between these figures arises because the plant consumes a substantial fraction of absorbed energy to provide for its inherent vital needs.

Studies of plant energetics on the level of the whole organism have very practical applications. Plant crops accumulate excess absorbed energy, which remains after the plant has fulfilled its inherent physiological requirements. Various methods intended to stimulate the productivity of the plant must facilitate its physiological functions and provide a redistribution of the plant's energy balance in favor of the productive process. Elaboration of such methods demands a comprehensive knowledge of the energetics of productive mechanisms.

Plant energetics may have a direct relation to problems of the industrial utili-

zation of solar energy. Some problems are caused by the properties of the incident flux of solar radiation. This flux is characterized as having a low density of about 1 kW/m², as well as extreme variability. It varies over a wide range and depends on the season, time of day, geographic position, and weather. Effective use of such dilute and variable energy flux is a very complicated problem. In this respect, plants may be recognized as an example of a successful and reliable solution to this problem. Examination of the principles of organization and functioning of this natural prototype as perfected by evolution may aid in the design of techno-logical systems for solar energy conversion.

One of the problems concerns the productivity and stability of the biospheric machine. Humans as a biological species exist on Earth entirely at the expense of the resources of the biosphere. We consume the fruits of its functioning with high selectivity. Thus, people are interested in the reliable and effective functioning of the energy-transforming biospheric machine. Meanwhile, humanity, with its eco-nomic activity, reduces the power of the biospheric machine continually. Due to the destruction of tropical forests (Myers, 1984), which proceeds at the rate of more than 1 acre per second, the input capacity of the biosphere diminishes daily by a value comparable to that of a large hydroelectric power station. At first glance such a loss may not appear very large when compared with the total capacity of the biosphere. It comes to about 0.1% of the total capacity of the biosphere over the course of a year. Nevertheless, the accumulated loss may become appreciable or even hazardous in a few decades.

The economic activity of humans not only reduces the total capacity of the biospheric machine but also modifies its structure. Natural ecological systems are being replaced by artificial ones. The artificial systems, such as cultivated lands, usually are more productive than the wild ones but, in contrast to the latter, are more homogeneous and consequently less stable. To maintain their stability, an additional energy contribution is required. A field, if not weeded, will soon be choked with weeds or "overgrown." It will spontaneously turn from a cultivated state into a wild one, the former being more stable than the latter but quite useless in economic respects. The problem of an ecological system's stability is connected with the arrangement of energy relations among its components. The stability of any energy-transforming system is determined by the pattern of energy processes that occur. Ecological systems are not exceptions in this respect, although obvious interconnections between the energetics and the stability may be disguised be-cause of the complexity and specificity of biological processes.

Plant energetics may have a particular significance in relation to biotechno-logical systems such as greenhouses. Here reasonable knowledge of plant energy functions is relevant in the realm of both design and operations.

The problems considered in this book have a direct bearing on the question of a crop's energy cost. This value is characterized by the energy coefficient, defined as the ratio of expenditure of technological energy consumed in cultivation to

energy stored in crops. This ratio is usually low in extensive agricultural systems. It is also comparatively low in forestry and sugarcane planting. In the cases when a low energy coefficient is accompanied by a sufficiently high level of productivity, the cultivation of plants may be considered a potentially renewable source of energy. Certain efforts in this direction are being undertaken. For example, large-scale production of ethanol from sugarcane is being realized in Brazil, where this product is used in significant amounts as fuel for cars. Industrial forestry projects for the production of energy are being explored in Sweden.

Intensive agriculture is accompanied by the wide employment of machinery and application of large amounts of fertilizers. Therefore, the energy coefficients in such cases may be rather high. They may attain values of about 0.08 for the industrial production of wheat and even 0.2 for corn. The energy coefficient rises as the yield increases and, as a rule, more rapidly than the latter. Thus, we obtain a crop produced by plants with increasing energy cost. Such a trend evidently is natural and inevitable, but causes concern in the long term because it denotes a progressive increase in energy expenditures for agriculture. Eventually, these expenditures may become excessive. Thus, the problem of optimization of energy invested in agriculture will become more acute, and one may assume that a detailed knowledge of plant energetics, as the main energy-transforming element of agriculture, will become essential to solving this problem.

The authors have taken the risk of writing this book with the intention to focus more attention upon the problem of plant energetics. In our opinion, this problem is not only interesting, intriguing, and worthy of thorough study but also vital to our continued existence.

This Page Intentionally Left Blank

Chapter 1

Light

THE SOURCE

In the beginning we should say a few words about the Sun. The Sun is, essentially, an inexhaustible source of power that has been pouring enormous quantities of energy out into space continually for billions of years. Only one-half of a billionth part of this flow (5×10^{-10}) falls onto Earth, but even this infinitesimal part is huge by human standards, equaling 165 tons of energy per day.

The Sun is an ordinary star like approximately 20 billion others in our galaxy. In a sense we are lucky that our Sun is such as it is. Were it 30% less or 40% more massive, life in its present form on Earth could not have evolved. In the former case, Earth's diurnal rotation would be stopped due to the gravity of a small but too close body, as happened with the Moon under the influence of Earth (a phenomenon known as tidal locking). In the latter case, the life span of a massive Sun would be too short, about 2–3 billion years, to allow evolution to create highly organized forms of life (Dole, 1970). The Sun's age is estimated to be about 5 billion years. Our Sun is now in the middle of its life span and will continue to shine approximately as it does now for another 4–5 billion years.

One may deem, however, that not we but the Sun should be considered "lucky." Our Sun is probably only one in a million or even 10 million stars that is circled by such a beautiful blue planet like Earth populated with higher life forms. At the risk of becoming too poetic, we will not continue with these thoughts.

Energy is generated deep within the Sun (Noyes, 1982; Zirin, 1988). Solar matter is heated there to temperatures of about 15 million K (27 million °F) and compressed to a pressure of about 1 billion atm. The density of the inner core is about 100 g/cm^3, which is almost 10 times that of lead. Under such conditions the

electron shells of atoms are destroyed and free electrons and nuclei, chiefly those of hydrogen and helium with minor amounts of heavier elements, form a state of matter resembling metal. It is very plastic and features high electrical and heat conductivities. In the internal parts of the Sun, profound stillness reigns—no macroscopic movements, no vigorous processes—all is uniformly heated and all is unchanging for millions of years.

However, on the microscopic level the particles of matter in the Sun, nuclei and electrons, take part in extremely fast movements that are small in amplitude but tremendous in energy. The particles collide with each other continually. Occasionally a collision is so energetic that two nuclei of hydrogen (protons) coalesce and form a nucleus of heavy hydrogen (deuteron). Subsequent collisions of deuterons with protons lead to the formation of nuclei of helium. Ultimately four protons fuse to form one nucleus of helium. The mass of four protons exceeds the mass of one nucleus of helium by approximately 0.7%. This excess mass is converted into energy in the form of γ-quanta and neutrinos. Every second 564 million tons of hydrogen is being transformed into 560 million tons of helium, and the difference, 4 million tons, is being converted into energy.

The inconceivably great scale of the generation of nuclear energy in the Sun gives the impression that it occurs very intensively and vigorously. In fact this is not so. The thermonuclear reactions in the entrails of the Sun proceed calmly and extremely slowly. During 1 billion years only a few percent of the available nuclear fuel reacts. The intensity of generation of energy in the Sun per unit of mass is 10,000 times lower than that in the human body.

Most of the energy liberated from the thermonuclear synthesis of helium is carried away as hard γ-radiation. However, the very dense ionized solar matter is opaque for any kind of electromagnetic radiation. The γ-quanta are absorbed immediately after their creation, reradiate, are reabsorbed, and so on. Finally after innumerable acts of absorption and reemission, the energy diffuses from the depth of the Sun to its surface. About 50 million years is needed for the radiation energy to reach the outer strata of the Sun. During this long travel the parameters of the energy change very significantly. The average energy per quantum decreases by several thousand times, while their number increases correspondingly.

Conditions in the outer layers of the Sun are quite different from those in its depths. The rate of transfer of energy here is accelerated greatly due to vigorous convective movements of hot highly ionized matter.

Ultimately the energy raised from the depths of the Sun reaches its atmosphere, where the temperature is about 6000 K. At this temperature hot gases of the solar atmosphere (the photosphere) radiate energy into space. Eight minutes are needed for light to travel the 150 million km that separates the Sun from Earth. Thus, the energy that comes to Earth today was born in the entrails of the Sun as far back as the Eocene epoch when the dinosaurs were yet in existence.

A fraction of the energy that reaches the Earth (approximately 30%) is reflected

back into space, whereas the rest drives all meteorological processes. A small portion of the solar energy is absorbed by green plants, and it is just this part that will be the object of examination in this book.

RADIATION

Because it is an ephemeral substance that set into motion all the processes of life, including plant life, we review here its basic attributes.

Radiation is the process of emission of electromagnetic waves and their propagation through space. One of the fundamental characteristics of the flow of radiation is its intensity (Chandrasekhar, 1960). The intensity of radiation[1] (I) has been adopted as the quantity of radiant energy, dE, incident onto a unit area, $d\sigma$, normal to the direction of flux in the unit solid angle, $d\omega$, in the unit of time dt:

$$I = \frac{dE}{dt \cdot d\sigma \cdot d\omega} \; \text{J/m}^2\text{·s·sr.} \qquad (1.1)$$

The intensity of radiation is a feature of a light beam, and it is determined by the radiative power of the source from which it originated. Intensity does not change when radiation propagates through nonabsorbing and nonscattering media. Thus, the intensity of radiation near the surface of the Sun and near Earth beyond its atmosphere is the same. Furthermore, the intensity remains constant when light passes through optical lenses or is reflected by mirrors. By concentrating solar rays with an optical system a very high energy density may be present at the focus, but the intensity of radiation remains constant.

As shown in Fig. 1.1A, the radiant flow through a given area in plane 2 is less than that through an equal area in plane 1. The intensity of radiation in both cases is the same, however, because the angle of divergence of the light cone is correspondingly less in the second case. Our perception of the brightness of a light source possesses the same nature. The quantity of light that comes from the source and hits the eye of observer 2 in Fig. 1.1B is less than that of observer 1, but the latter sees the source at a correspondingly greater angle. Thus, the brightness of the source is perceived as equal by both observers.

The power that hits a unit area of a surface with the incident flux of radiation is termed irradiance. The irradiance may be found by integration of the intensity of radiation over all directions from which the light falls onto the surface, taking

---

[1] It should be noted that there is some ambiguity in the usage of terminology referred to the flow of radiant energy (Bell and Rose, 1981). The terms used for the specification of radiant flow in astrophysics, photometry, and photochemistry do not always coincide. For example, such terms as luminance, radiance, and brightness are sometimes used to mean something quite close to that of the term intensity of radiation. This term is used only in astrophysics. Thus, one must take pains to avoid confusion when reading books related to different fields.
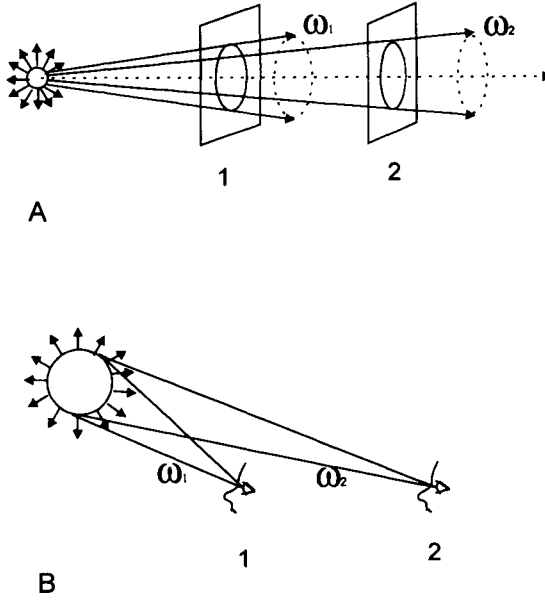
Figure 1.1 Intensity of radiation does not change when light propagates through an optically transparent medium. (A) A lesser radiant flow passes through a unit area on screen 2 than through an equal area on screen 1, but the solid angle changes by the same proportion so that the intensity is invariable. (B) The brightness of a light source is perceived as equal independent of the distance of an observer from the source because the amount of light received and the solid angle at which it arrives change simultaneously by the same proportion. In this respect the notion of brightness is similar to that of intensity.

into account the angle of incidence, α, and the azimuth angle of the rays, ϕ (see Fig. 1.2):

$$E = \int_0^{2\pi} d\phi \int_0^{\pi/2} I(\phi, \alpha) \cos\alpha \, \sin\alpha \, d\alpha. \qquad (1.2)$$

In the case of small-angle sources, such as the Sun, the irradiance simply equals the intensity of radiation multiplied by the value of the solid angle of the source and multiplied by the sine of the incidence angle:

$$E = I\omega \, \sin\alpha. \qquad (1.3)$$

When a surface is illuminated by a source uniformly over the whole hemisphere, as in the case of an overcast sky, the dependence of the irradiance upon the intensity of radiation is quite simple:

$$E = I\pi. \qquad (1.4)$$
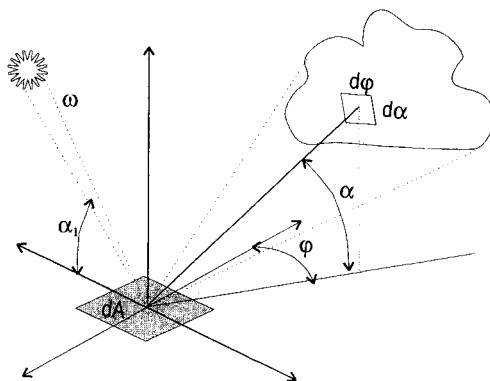
Figure 1.2 Element of area, *dA*, illuminated from a small-angle source and from an extended source, such as a cloud. α and α_1 are inclination angles against the plane of *dA;* ϕ is the azimuth angle against a chosen direction. The irradiation of *dA* from both sources is determined by Eqs. (1.4) and (1.3), respectively.

One should note that radiation of high intensity may originate a very low irradiance if the source emits only at a small angle, while the light flux of comparatively low intensity taken over a large solid angle will give rise to a rather high level of irradiance. So the intensity of radiation incident on Earth from Sirius, the brightest star in the sky, is about 8 times higher than that from the Sun because this star is hotter than our Sun and its surface is correspondingly brighter. Nevertheless, the irradiance from Sirius is less (by approximately 10 billion times) because the solid angle at which Sirius is viewed from Earth is 80 billion times smaller than that of the Sun.

Another much more common example is the case of illumination of the ground through a layer of clouds in overcast weather. In this case the inherent intensity of solar radiation is diminished significantly because of the change of the solid angle at which light falls (see Fig. 1.3). The light flux incident on the upper boundary of the cloudy layer comes in a very narrow cone (the solid angle of the Sun is 6.8×10^{-5} sr). It is scattered by the cloudy layer, spreads over the whole firmament, and falls to ground from a hemisphere at the solid angle of 2π sr. Thus, due to the change of the solid angle of the light cone, the intensity of radiation diminishes by the factor of $2\pi/6.8 \times 10^{-5} = 9.24 \times 10^4$. Beyond that, a significant fraction of the solar energy incident on the upper boundary of the cloudy layer is scattered upwards. By estimating this fraction, say, as about 50% and neglecting absorption, we obtain the rounded value of 2×10^5 for the factor of radiation intensity diminution (the dilution factor) in overcast weather compared with a clear day. At the same time the irradiance of the ground will diminish by only a factor of about 2 because the intensity of radiation decreases as the solid angle of the radiation
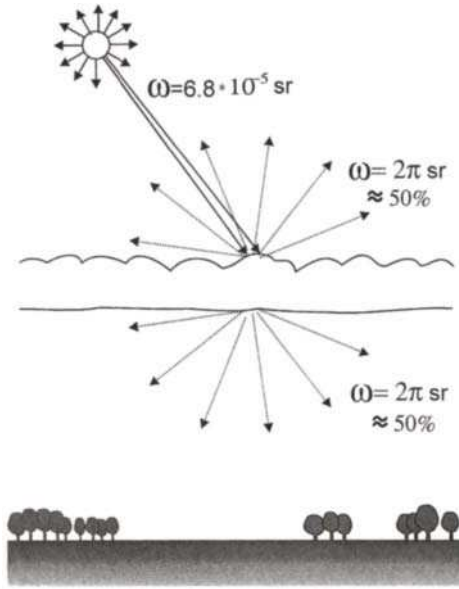
Figure 1.3   The intensity of radiation may diminish by hundreds of thousands of times in scattering due to an increase in the angle of divergence of the light cone.

increases, by the same proportion. Therefore, the decrease in irradiation is due to the upward reflection of light from the clouds.

In addition to the integral intensity of radiation, I, the corresponding differential characteristics such as the intensity of radiation at definite frequency I_ν and that at definite wavelength I_λ are used. These functions define the spectral distribution of energy by frequency or by wavelength, respectively:

$$I_\nu = (dI/d\nu) \quad \text{and} \quad I_\lambda = (dI/d\lambda). \tag{1.5}$$

Because frequency and wavelength are related simply through $\lambda\nu = c$, the intensity functions are related as follows:

$$I_\lambda = (\nu^2/c)I_\nu \quad \text{or} \quad I_\nu = (\lambda^2/c)I_\lambda. \tag{1.5a}$$

Intensity of radiation over a definite range of frequencies or wavelengths (I_{1-2}) may be obtained by integrating the function I_ν or I_λ within the corresponding limits:

$$I_{1-2} = \int_{\nu_1}^{\nu_2} I_\nu \, d\nu = \int_{\lambda_1}^{\lambda_2} I_\lambda \, d\lambda. \tag{1.6}$$

The region of a solar spectrum that is of most interest for plant science is that between the wavelengths 400 and 700 nm or the frequencies 430–750 THz

(1 terahertz $= 10^{12}$ Hz $= 10^{-12}$s^{-1}). It is this region in which the radiant energy can be absorbed by plants and used for photosynthesis. The energy that falls within this region is specified as photosynthetically active radiation (PAR). By integrating I_ν or I_λ within denoted limits of ν or λ, one may find the total intensity of PAR. Its portion of the whole solar spectrum is about 40%.

Radiation of electromagnetic waves is an inherent feature of all physical bodies. Emission of radiation is caused by the thermal motion of charged particles within the matter. Let us imagine a closed cavity within a solid body heated to a certain temperature T_s. This empty cavity containing no matter will be filled, however, with radiation, that is, with the photons emitted continuously and absorbed by the walls of the cavity. The radiation that fills the cavity exists in thermal equilibrium with its heated walls. Thus, it is the equilibrium radiation. One may estimate the density of the equilibrium radiation. As established by Planck (1923), the number of photons within a narrow frequency band between ν and $\nu + d\nu$ contained in a unit volume (the photon density D_ν) at a temperature T equals

$$D_\nu = \frac{8\pi}{N_A c^3}\left(\frac{kT}{h}\right)^2 f_2(\beta) \times 10^{12} \quad \text{E/m}^3\text{·THz.} \tag{1.7}$$

Here $h = 6.626 \times 10^{-34}$ J·s is Planck's constant, $k = 1.38 \times 10^{-23}$ J/K is Boltzmann's constant, $c = 2.998 \times 10^8$ m/s is the velocity of light, and $N_A = 6.02 \times 10^{23}$ is Avogadro's number. The number of photons D_ν is expressed here in moles. One mole corresponds to 6.02×10^{23} photons. The name einstein is used sometimes for this unit with the abbreviation E. The frequencies are expressed here and throughout in terahertz. The function $f_2(\beta)$ describes the adjusted distribution of photons in the adjusted dimensionless "frequencies" β:

$$f_2(\beta) = \frac{\beta^2}{\exp(\beta) - 1}. \tag{1.8}$$

The argument of this function, β, is the ratio of the energy of a photon of certain frequency to the mean energy of heat of motion of a molecule at a given temperature: $\beta = h\nu/kT$. The function $f_2(\beta)$ is invariant with respect to temperature. The plot of the function $f_2(\beta)$ is shown in Fig. 1.5.

Integration of Eq. (1.7) within the whole range of frequencies from zero to infinity gives

$$D = 2.404\frac{8\pi}{N_A c^3}\left(\frac{kT}{h}\right)^3 \quad \text{E/m}^3. \tag{1.9}$$

So the number of photons in a 1 m^3 cavity at room temperature is about 4.8×10^{14} or 0.8×10^{-9} mol. At a surface temperature of the Sun of about 5785 K the corresponding values are 3.9×10^{18} and 6.5×10^{-6} E, respectively.

Now let us imagine that there is an orifice in the wall of the cavity. The photons will escape from the cavity through this orifice and propagate at the velocity of
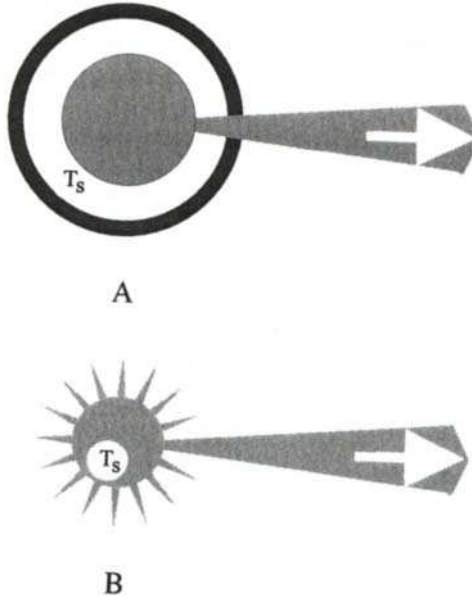
Figure 1.4   (A) Model of a black body: a cavity in heated matter. The equilibrium radiation escapes from the cavity through an orifice in the wall. (B) A heated body emits radiation in all directions at the solid angle 4π sr. A single beam is shown arbitrarily.

light within a certain cone (see Fig. 1.4A). The power of the photon flux will be proportional to the area of the orifice, σ, the volume density of the photons of certain frequency, D_ν, in the cavity, and the velocity of light, c. The value of the flux related to unit area and to a unit solid angle is the intensity of the photon flux. The expression for the intensity of photon flux at a certain frequency is thus as follows:

$$N_\nu = \frac{2}{N_A}\left(\frac{kT}{ch}\right)^2 f_2(\beta) \times 10^{12} \text{ E/m}^2\text{·s·sr·THz.} \qquad (1.10)$$

Accordingly, by integrating Eq. (1.10) over the whole range of frequencies, for the total intensity of photon flux one obtains

$$N = \frac{4.808}{N_A c^2}\left(\frac{kT}{h}\right)^3 (8.02 \times 10^{-10})T^3 \quad \text{E/m}^2\text{·s·sr.} \qquad (1.11)$$

From Eqs. (1.7) and (1.9) one can easily obtain the corresponding expressions for the density of radiant energy in the cavity and the intensity of radiation that leaves the cavity through the orifice. One need only multiply the number of photons by their energy, $h\nu$. As a result, for the density of radiation one obtains

$$U_\nu = \frac{8\pi}{c^3} \cdot \frac{(kT)^3}{h^2} f_3(\beta) \times 10^{12} \quad \text{J/m}^3\text{·THz,} \qquad (1.12)$$
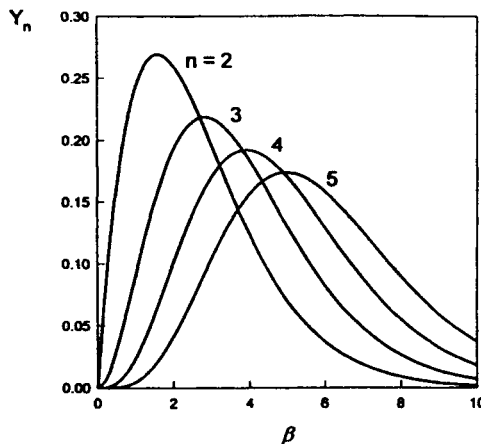
Figure 1.5 The graphs of functions $f_n(\beta)$ that determine the spectral distribution of the number of photons and that of energy in black-body radiation (BB radiation). The functions are shown in normalized form in such a way that the area under each of the curve is taken as unity. To obtain the true values of the function $f_n(\beta)$, the values of Y_n for $n = 2$–5 should be multiplied by the factors 2.404, 6.494, 24.884, and 122.08, respectively.

where $f_3(\beta) = \beta f_2(\beta)$. By multiplying Eq. (1.12) by the value of the velocity of light and dividing by 4π, we obtain the differential intensity of radiation:

$$I_\nu = \frac{2(kT)^3}{(ch)^2} f_3(\beta) \times 10^{12} \quad \text{W/m}^2\cdot\text{sr}\cdot\text{THz}. \tag{1.13}$$

The integral intensity of radiation accordingly equals:

$$I = \frac{2\pi^4 k^4}{15 c^2 h^3} T^4 = (1.805 \times 10^{-8}) T^4 \quad \text{W/m}^2\cdot\text{sr}. \tag{1.14}$$

The model of a cavity surrounded by heated walls is convenient for the theoretical analysis of processes of radiation and is used in precision measurements as a source of standardized equilibrium radiation. One may imagine, however, the orifice opened to its maximum value: the heated matter now constitutes a spherical body, as shown in Fig. 1.4B. Such a body will emit radiation into the surrounding space within a solid angle of 4π sr. The intensity of emitted radiation in this case will depend upon the ability of the body to absorb radiation. This feature is characterized by the absorption factor. The processes of absorption and emission of light are symmetrical in a certain sense: if a body effectively absorbs radiation in a definite range of frequencies, it also effectively emits in the same part of the spectrum. A perfect radiator should also be a perfect absorber. The bodies that completely absorb all incident radiation are termed absolute black bodies. The absorption factor for such bodies equals unity for all frequencies. The intensity of radiation emitted by a black body is the same as the intensity of the equilibrium

radiation escaping from a heated cavity unless the temperatures are equal in both cases. That is why the terms "equilibrium radiation" and "black-body radiation" are sometimes used synonymously. It should be noted that the propagating black-body radiation retains all features of the equilibrium radiation in a closed cavity except its volume density, which decreases with increasing distance from the source.

The emissive properties of Sun are rather close to those of a black body at the temperature of about 5785 K. At the temperature of the Sun, the total intensity of black-body radiation is 2.02×10^7 W/m^2·sr. By multiplying this value by that of the solid angle of the Sun (6.8×10^{-5} sr), we obtain 1374 W/m^2 as the irradiance that should be created by direct solar rays at the surface of Earth in the absence of an atmosphere.

The regularities of radiative processes are often analyzed in alternative units, in terms of the wavelengths and not the frequencies. It is not difficult to pass from one mode of description to the other by taking into account the relation between the frequency and the wavelength. In such notation, the dimensionless factor $\beta = hc/kT\lambda$. From Eq. (1.7) one obtains the expression for the number of photons of a certain wavelength in unit volume:

$$D_\lambda = \frac{8\pi}{N_A}\left(\frac{kT}{ch}\right)^4 f_4(\beta) \times 10^{-9} \quad \text{E/m}^3\text{·nm.} \tag{1.15}$$

Correspondingly, the expression for photon flux is

$$N_\lambda = \frac{2}{N_A}\left(\frac{kT}{ch}\right)^4 cf_4(\beta) \times 10^{-9} \quad \text{E/m}^2\text{·s·sr·nm.} \tag{1.16}$$

For the differential intensity of the black-body radiation one obtains

$$I_\lambda = 2\frac{(kT)^5}{c^3h^4}f_5(\beta) \times 10^{-9} \quad \text{W/m}^2\text{·sr·nm.} \tag{1.17}$$

In these formulae, $f_4(\beta) = \beta f_3(\beta)$ and $f_5(\beta) = \beta f_4(\beta)$.

THE SPECTRAL DISTRIBUTION OF PHOTONS AND ENERGY IN BLACK-BODY RADIATION

As one may see, the expressions describing the spectral distribution of photon flux intensity and that of the energy flux in frequency (Eqs. 1.10 and 1.13) or in wavelength (Eqs. 1.15 and 1.16) consist of two distinct parts. One is dependent on temperature while the other is invariant with temperature and is a function of the dimensionless factor β. This part can be represented by the functions $f_2(\beta)$–$f_5(\beta)$:

$$f_n(\beta) = \frac{\beta^n}{\exp(\beta) - 1}. \tag{1.18}$$

The functions $f_n(\beta)$ are depicted in Fig. 1.5. The functions are shown in normalized form in such a way that the area under each of the curves is tak_n as unity. The normalizing factors are given in the legend of Fig. 1.5:

$$a_n = \int_0^\infty f_n(\beta) \, d\beta. \qquad (1.19)$$

Thus, the real value of the function $f_n(\beta)$ is $f_n(\beta) = a_n y_n$.

The spectral distributions of the intensity of photon flux and that of the energy in the radiation of a black body heated to the temperature of the Sun are shown in Figs. 1.6 and 1.7. The former presents the distribution in frequency, the latter in wavelengths.

As one may see in Fig. 1.5, the maximum value of the function $f_2(\beta)$, and correspondingly the distribution function of the number of photons in frequency N_ν, occurs at the value $\beta = 1.594$. For black-body radiation at the temperature of the Sun (~5785 K) this value corresponds to a frequency of 190 THz, which is thus in the infrared region. The intensity function I_ν has its maximum at $\beta = 2.817$. For solar radiation the maximum intensity also occurs in the infrared region of the spectrum at a frequency of 340 THz or a wavelength of 882 nm. The maximum of the function I_λ occurs in the green region of the spectrum at a wavelength of about 500 nm, which is rather close to the region of maximum sensitivity of the human eye.

A puzzling question may arise here: in which spectral region, the green or infrared, does the maximum energy fall? It is impossible to answer this question unambiguously because I_ν and I_λ have different dimensions. Quantities that differ
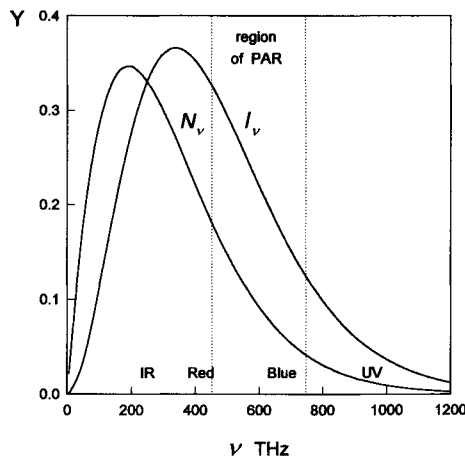
Figure 1.6   Spectral distribution in frequency of the intensity of photon flux N_ν and that of energy I_ν of black-body radiation at the temperature of the Sun (5785 K): $N_\nu = Y\,\mathrm{E/m^2 \cdot s \cdot THz \cdot sr}$; $I_\nu = Y \times 10^5$ $\mathrm{W/m^2 \cdot THz \cdot sr}$.
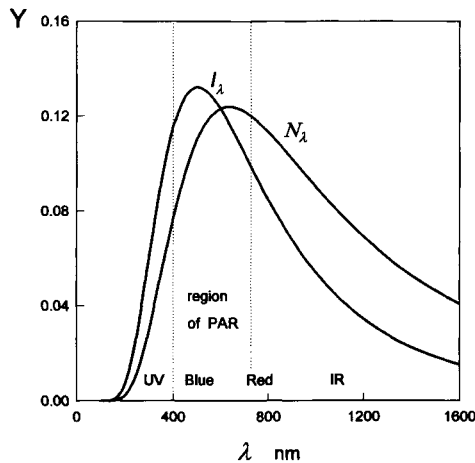
Figure 1.7 Spectral distribution in wavelength of the intensity of photon flux N_λ and that of energy I_λ of black-body radiation at the temperature of the Sun (5785 K): $N_\lambda = Y\,\mathrm{E/m^2 \cdot s \cdot nm \cdot sr}$; $I_\lambda = Y \times 2 \times 10^5\ \mathrm{W/m^2 \cdot nm \cdot sr}$.

in their dimensions cannot be compared immediately. I_ν has, in normalized form, the dimension of time (Hz^{-1} = sec), whereas the dimension of I_λ is the inverse length (nm^{-1}). The first function expresses the distribution of energy in equal intervals of frequency but nonequal intervals of wavelength, which decrease as the frequency increases. The second function, I_λ, describes the distribution of energy in equal intervals of wavelength but varying intervals of frequency. Both conventions are valid and there are no principal reasons to consider one better than the other. The choice should be based on the considerations of convenience and clarity only. With this in mind, the function I_ν, based on the uniform frequency scale, seems to have a certain advantage because it also conforms to a uniform scale of energy of quanta. Thus, equal areas under the I_ν curve correspond to equal amounts of energy. In the case of I_λ curves, such congruence does not exist. Another factor in favor of choosing the frequency scale is that the wavelength of light depends upon the refractive index of the medium through which the light propagates. Thus, the real wavelength of light in water is about one-third shorter than that in air. So yellow light with a wavelength of 580 nm (in air) changes its wavelength to about 430 nm when propagating in water. Such a value is usually associated with blue light, though it remains yellow. The point is that the frequency of light, as well as the energy of quanta, does not change when passing from one medium into another whereas the wavelength does.

As we have seen, the position of the maximum of the differential distribution function depends upon the choice of units and is different for the functions I_ν and I_λ. On the contrary, the integral characteristics are quite unambiguous: the inten-

sity of radiation within a certain finite frequency interval or the corresponding wavelength interval is the same. For example exactly one-half of the total amount of energy in the spectrum of black-body radiation falls within a low-frequency region ($0 < \beta < 3.54$), whereas the other half falls within the high-frequency region ($\beta > 3.54$). Thus, the value of parameter $\beta = 3.54$ corresponds to the median of the function I_ν. The same value of β corresponds to the median of the function I_λ as well. In case of black-body radiation emitted at the temperature of the Sun, the median falls in the region of red light at a frequency of 428 THz or at a wavelength of 700 nm. It should be noted that the position of the median of the sunlight spectrum almost exactly coincides with the shortwave boundary of the region of PAR.

DIRECTIONAL AND DIFFUSE RADIATION

Radiation emitted by an incandescent black body propagates through empty space rectilinearly and without changes in intensity or direction of rays. In a thermodynamic sense such radiation may be considered as that in equilibrium; in a geometrical sense it is directional.

The direction of radiation may be changed with the help of optical means such as mirrors or lenses, but that does not change the intensity provided the optical system is ideal. So it is possible in theory for a body placed in the focus of an optical system with a large enough aperture to be heated to a temperature near that of the source. How close could one approach this theoretical limit in practice is, nonetheless, a separate question that will not be discussed here.

The features of radiation are changed significantly, however, in passing through absorbing or scattering media. So if the light beam passes through an absorbing but nonscattering filter, the intensity of radiation diminishes in accordance with the transmission factor of the filter. In general the degree of attenuation of the light intensity may vary in different regions of a spectrum if the filter is not uniformly gray but colored, as its transmission factor will be different for rays of various wavelengths. The light beam that passed through a filter, no matter whether gray or colored, is no longer in equilibrium as its intensity is attenuated. Nevertheless, it remains directional light. Its direction may be changed with a mirror or it may be focused with a lens.

More essential qualitative changes of the properties of a light beam occur with scattering. Scattering may occur by passing the beam through a diffusive medium, say, through frosted glass, layers of clouds, or upon reflection from a scattering surface. In fact the directionality of the light beam vanishes when it is scattered, and it becomes diffuse light that propagates in all directions. In the act of scattering a directional light flux may undergo no energy loss, but all information of its initial direction is lost.

Thus light, when scattered, loses its initial quality as directional light and turns into diffuse light. In this new state, the light gains some new qualities specific to diffuse light. In contrast to directional light, for which the very first contact with any obstacle becomes the last, diffuse light may undergo a multitude of subsequent acts of scattering without changing its qualitative state as diffuse light. Therefore, it may propagate in scattering media for long distances. Thus, diffuse light penetrates comparatively freely through a thick layer of clouds and undergoes repeated acts of scattering along its way. Due to this property of diffuse light, the irradiance on the ground under an overcast sky may be rather high, even when direct sunbeams cannot struggle through the cloudy layer. On the other hand, in contrast to directional light, diffuse light cannot be focused by an optical system.

In any case, when radiation undergoes absorption or scattering, it ceases to be equilibrium radiation and becomes diluted radiation. The terms "weakened" and "attenuated" are also used as synonyms. The spectral distribution of energy in diluted radiation does not correspond with that predicted by Planck's equation. The intensity of diluted radiation is always lower than that of equilibrium radiation. If dilution of radiation is caused by absorption, the dilution factor is inversely proportional to the transmittance of the medium through which the light passes. In the case of scattering, the dilution factor equals the ratio of the solid angle at which the light propagates after scattering to the solid angle before scattering. As we have seen (Fig. 1.3), the dilution factor for scattering of directional light may attain rather large values, such as 10^5 or more.

It is useful to outline the main difference between light dilution due to absorption or due to scattering. In the former case a loss of energy occurs, while in the latter information is lost. One can see something when looking through a glass of wine (absorbing medium), but nothing can be seen through a glass of milk (scattering medium).

TEMPERATURE AND ENTROPY OF RADIATION

The radiation may be characterized by its temperature. Black-body radiation, if not altered by absorption or scattering, has the temperature of the source from which it originated. If the equilibrium black-body radiation emitted at a certain temperature is diluted by passage through an absorbing or a scattering medium, it becomes nonequilibrium radiation. The overall shape of the distribution function of diluted radiation intensity, $I_\nu(\nu)$ or $I_\lambda(\lambda)$, may be similar to that of the initial equilibrium, but it cannot coincide with the whole spectrum of the distribution function of black-body radiation at any temperature. This is shown in Fig. 1.8. It is possible to match the temperature of a black body such that the intensity of its radiation over a certain narrow frequency band will be equal to the intensity of diluted radiation over the same band. One may call this temperature as the effective temperature of the diluted radiation at the corresponding frequency.
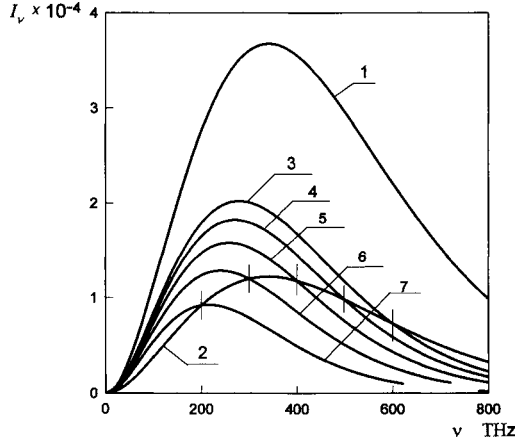
Figure 1.8 Effective temperature of nonequilibrium radiation at a given frequency may be considered as the temperature of a black body that emits radiation of the same intensity at this frequency. (1) Black-body radiation at 5875 K. (2) The same radiation diluted three times. (3–7) Black-body radiation at the temperatures 4743, 4583, 4371, 4079, and 3661 K. These curves intersect curve 2 at the frequencies 200, 300, 400, 500, and 600 THz. The effective temperatures of diluted radiation at these frequencies correspond with the values indicated.

The temperature of equilibrium radiation is the same throughout the whole range of frequencies and corresponds to the temperature of the source. In contrast, the temperature of diluted, and thus nonequilibrium, radiation cannot be characterized by a single temperature value; temperature varies over the entire spectrum. In this respect, the diluted radiation may be regarded as a series of monochrome radiation bands characterized by different temperatures.

The temperature of monochrome radiation as a function of its intensity, I_ν, may be calculated with the following equation:

$$T_\nu = \frac{h\nu}{k \ln(2h\nu^3/c^2I_\nu + 1)}. \tag{1.20}$$

This equation may be transformed to enable the calculation of the effective temperature of diluted radiation (T_ν) at given frequency, if the temperature of the initial equilibrium radiation, T_s, and the dilution factor, γ, are known:

$$T_{\nu,\gamma} = \frac{T_s\beta}{\ln[(e^\beta - 1)\gamma + 1]}. \tag{1.21}$$

The distribution of the effective temperature of radiation in the spectrum of a black body at 5800 K and at various dilution factor values is shown in Fig. 1.9. As one can seen, the effective temperature of radiation decreases as the dilution factor increases. The effect of lowering of the radiation temperature is expressed more strongly in the longwave part of the spectrum: the red rays are being
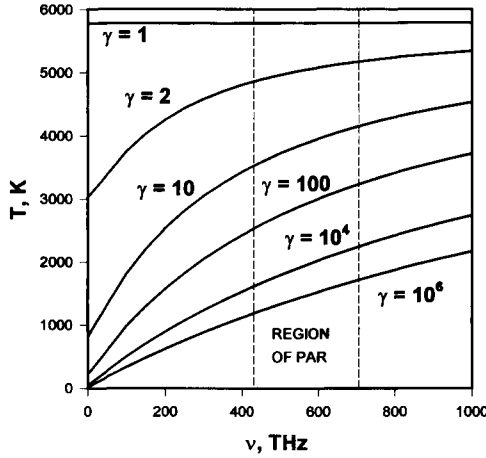
Figure 1.9 Effective temperature of radiation emitted at 5785 K and diluted by the factor γ.

"cooled" when weakened to a greater degree than the blue. The solar radiation in overcast weather is usually weakened by about $10^5 - 10^6$ times. At such values for the dilution factor, the effective temperature averaged over the region of PAR decreases to about $1000 - 2000$ K.
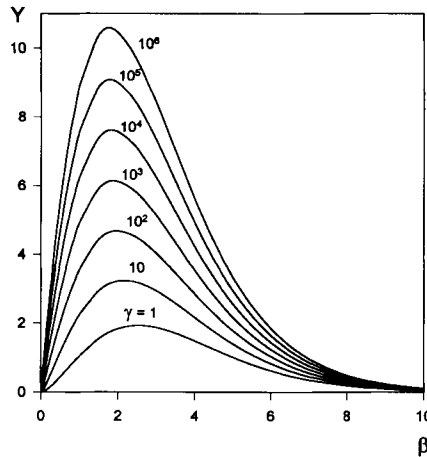
Figure 1.10 Entropy content of radiation as a function of the dimensionless frequency (β) and dilution factor (γ). The curves represent the dimensionless part of Eq. (1.23) multiplied by the dilution factor (γ). To obtain the real values of the entropy flux within a certain frequency band, the values on the y-axis must be multiplied by the factor $15h/\pi^4 kT^2$. For the case of solar radiation ($T = 5785$ K), this factor equals 2.209×10^{-4} e.u. per terahertz per kilojoule of energy (entropy units = J/K).
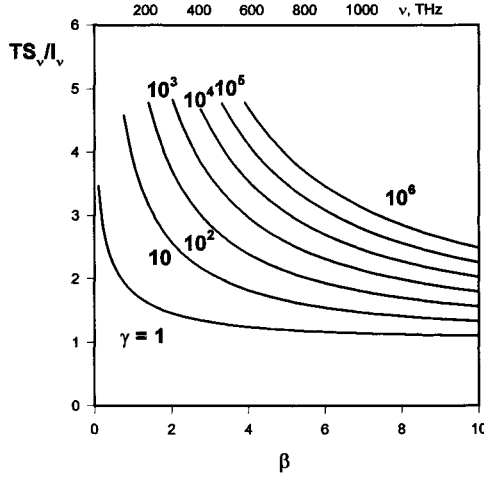
Figure 1.11 Relative entropy content of radiation. Distribution in frequencies for various values of dilution factor.

The effective temperature of radiation is the characteristic of interest when considering problems related to the thermodynamics of radiant energy conversion. Another characteristic quality of radiation that is also useful in this regard is its entropy (Landau and Lifshitz, 1958; Landsberg, 1993; Landsberg and Tonge, 1979; Ore Aadne, 1955). The entropy of equilibrium radiation is unambiguously determined by its temperature:

$$S = 4E/3T, \tag{1.22}$$

where E is the energy of radiation.

The distribution of entropy in the spectrum is not uniform. The low-frequency part of the spectrum contributes a relatively greater share to the total entropy flux than does the high-frequency one. The entropy of radiation increases as its intensity decreases. The general expression for the distribution function of entropy in frequency is as follows:

$$S_\nu = 2\frac{k^3 T^2}{c^2 h^2}\beta^2 \left[\left(\frac{z+1}{z} \right) \ln\left(\frac{z+1}{z} \right) + \frac{1}{z} \ln(z) \right], \tag{1.23}$$

where $z = (e^\beta - 1)\gamma$.

A family of curves depicting the entropy distribution for various values of a dilution factor is shown in Fig. 1.10. The maximum of the distribution function is shifted markedly into the low-frequency range. For black-body radiation at 5785 K, the maximum falls in the infrared range at a frequency of 300 THz ($\lambda = 1000$ nm). For diluted radiation the maximum is shifted more into the low-
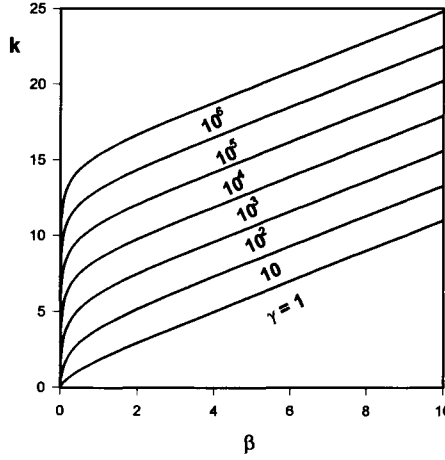
Figure 1.12   "Entropy cost" of quanta (in units of *k* per photon) as a function of their energy and the value of the dilution factor.

frequency range. So for equilibrium radiation, the low-frequency half of the spectrum contributes about 58% of the entropy, which increases to 72% when the dilution factor reaches 10^6.

The relative entropy content of radiation, defined as the ratio of entropy flux to that of energy at given frequency, increases with an increase in the dilution factor. Figure 1.11 shows a series of corresponding curves. The curves are calculated with the following formula:

$$\frac{S_\nu}{I_\nu} = \frac{1}{\beta T}[(z + 1) \ln(z + 1) - z \ln(z)]. \qquad (1.24)$$

Figure 1.12 depicts the dependence of the "entropy cost" of quanta upon their energy (frequency) and the dilution factor. The entropy per photon in the equilibrium radiation changes almost strictly in proportion to its energy. The average amount of entropy per photon in the whole spectrum equals 3.6*k*, independent of the temperature of the emitting body. Dilution of radiation results in an increase in entropy of about 0.5*k* per photon, with a 10-fold increase in the dilution factor.

SUN AND OTHER SOURCES OF RADIATION

The spectrum of solar radiation beyond the atmosphere is rather similar to that of a black body at a temperature of about 5785 K. The effective temperature in the center of the solar disk is higher, up to 6000 K, and it is lower at the edge. In
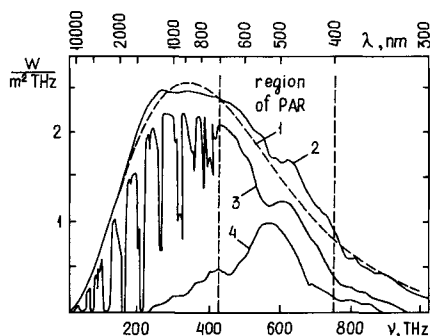
Figure 1.13 Distribution of energy: (1) black-body radiation at 5785 K; (2) solar radiation beyond the atmosphere; (3) solar radiation on a clear day at sea level; (4) radiation in overcast weather.

the ultraviolet region of the spectrum the effective temperature of solar radiation is about 4500–5000 K, whereas in the infrared region it rises to 7000 K. These details are not essential, because the spectrum of sunlight undergoes noticeable changes when light passes through Earth's atmosphere. Figure 1.13 depicts the curve of energy distribution in solar radiation beyond the atmosphere compared with the curve of equilibrium black-body radiation at 5785 K. As one may see, the deviations between the curves are small.

The Sun will always be our main source of radiant energy, whose scale will never be matched by artificial sources. Nevertheless, a large part of the available information concerning the physiology of plants and the physiological action of light has been obtained in laboratory experiments with the use of artificial sources of light. The characteristics of artificial illumination, such as the spectral distribution, intensity, effective temperature of radiation, and time course of irradiance, may differ significantly from those of natural light. Some problems may arise that are not always taken into account. One of the problems concerns the correspondence between the results obtained in daylight and those obtained under conditions of artificial lighting. As we ourselves are not indifferent to the quality of our diet, so plants probably are not quite indifferent to the quality characteristics of light. Evaluation of the efficiency of radiation only by the quantity of energy it brings, even in a specific range of a spectrum, say in the range of PAR, may be as incomplete as evaluation of the quality of our food by the caloric content only.

The regulative functions of the spectral composition of light, its intensity, and other features by no means play an essential role in the plant's life. This is shown by many experimental results. However, the theoretical notions concerning the mechanisms of observed phenomena have not yet attained the level that would make it possible to single out the effects connected with only the qualitative features of light. Therefore, the best way to avoid artifacts in experiments with plants under artificial lighting is to use light sources that have spectral features as similar

to those of the Sun as possible. Thermal light sources such as incandescent lamps are very far from perfection in this respect. Due to the low temperature of the filament (2500–3000 K), they radiate mainly in the infrared region and only 4–9% of the energy emitted falls within the PAR region. The intensity of radiation of incandescent lamps in the PAR region is 15–20 times lower than that of solar radiation.

Low-pressure gas–glow lamps have line or band spectra due to resonance emission of excited atoms of metals or inert gases. The spectra of such lamps greatly differ from that of the Sun. However, the use of luminophores can reduce the disparity. High-pressure gas–glow lamps such as high-power xenon lamps, as well as the halogen lamps with vapors of rare earth elements, emit a continuous spectrum in the PAR region with an effective temperature of close to 6000 K. Practically all of the artificial sources of light used for growing plants in laboratories, phytotrons, and greenhouses produce significant energy overloads in the infrared region.

Peculiar properties are inherent to the light emitted by quantum generators or lasers. Lasers are nonthermal sources of radiation. The word "laser" is an acronym formed from the initial letters of a short description of the principle of its functioning: light amplification by stimulated emission of radiation. The working body of the laser, which may be, for example, a ruby crystal or a mixture of gases, absorbs energy from an external source of radiation and transmits to a metastable excited state. In falling back from the excited to the base state, the working body emits the stored energy in an extremely narrow frequency range. The process of radiation is stimulated by photons that move along the axis of the laser, repeatedly reflecting from the mirrors on its edges.

Laser radiation is characterized by an extremely high degree of directness, monochromaticity, and coherence. Due to these features, the intensity of laser radiation may attain exceedingly high values. A beam from a helium–neon laser, 0.01 W in power, on a screen produces a level of irradiance approximately as high as the direct rays from the Sun, but the sunlight produces energy over a wide range of frequencies from IR to UV whereas the laser beam produces the same energy over a narrow band centered at the frequency 474 THz ($\lambda = 632$ nm). Laser radiation is characterized by extremely high values of intensity, millions of times higher than that of the sunlight, with effective temperatures in the billions of kelvins and zero entropy. Certainly one must attach no more weight to these extraordinary figures than they really have. In fact they reflect only that laser radiation is nonequilibrium to the utmost degree. If one may consider thermal radiation as a noise generated by the "voices" of a multitude of atoms that emit quite incoherently, then laser radiation is a single "note" sounding "in chorus."

It is difficult to state something definite about the effects that may be caused by the action of the laser beam on the light-accepting systems of plants. These systems are adapted, due to their long evolution history, to take up radiation from

thermal sources featuring a wide spectrum. A powerful monochromatic laser beam may, evidently, overload single components of these systems, leaving the others unloaded. In addition, various nonlinear phenomena are possible, such as radiation-induced alteration of absorption coefficients and two-photon processes, though all such effects are far beyond normal physiological conditions. The peculiarities of the action of laser radiation on plants have not been studied sufficiently to obtain adequate insights. Some interesting effects are described in the literature (Shachov, 1993), although the reliability of the data is not free from doubt.

FACTORS DETERMINING THE SCATTERING
AND ABSORPTION OF LIGHT

Light, as it passes through a medium, undergoes scattering due to interactions with molecules and more coarse particles. If scattering proceeds without the loss of energy, it is referred to as elastic (the synonyms are "pure" or "conservative scattering"). In elastic scattering the energy of the light flux remains unchanged, whereas its direction and angle of divergence do change. The entropy of the light flux increases upon scattering. The interaction of light with a medium rarely proceeds as pure scattering and may be accompanied by a partial loss of energy due to absorption. As a rule, both effects, scattering and absorption, take place simultaneously.

There are two different mechanisms of scattering: molecular or Rayleigh scattering and aerosol or Mie scattering. The first results from the interaction of the electromagnetic field of the light wave with the inhomogeneities of the medium due to fluctuations in density.

The probability of molecular scattering increases as the fourth power of the frequency of the incident light. The effect of preferential scattering of shortwave radiation by molecules of atmospheric gases makes the sky blue over our heads. Molecular scattering proceeds almost symmetrically in all directions.

The intensity of molecular scattering may be characterized by a quantity called the cross section of scattering. This value defines the probability of light scattering as it passes through a given mass of the medium. The cross section of scattering related to 1 kg of air may be expressed as $s = (1.2 \times 10^{-16})\nu^4$ m^2/kg (ν in terahertz). Values of cross section may be related not only to a unit of mass but to the whole mass of the atmosphere over a unit area of Earth's surface at sea level (10,330 kg/m^2). This quantity is given the unit "airmass one" (AM1): $s = (1.24 \times 10^{-12})\nu^4$ (dimensionless; ν in terahertz).

The atmosphere always contains suspended particles, called aerosols, whose dimensions are much larger than those of molecules. They may be particles of smoke or dust or droplets of water. The dimensions and composition of aerosols

may vary greatly. The theoretical analysis of scattering from aerosol particles is complicated, so we will make only a few generalizations. Aerosol scattering is due to the diffraction of rays by the particles. The primary parameter that determines the character of the scattering process is the ratio between the radius of the particle, r, and the wavelength of the incident light λ: $\rho = 2\pi r/\lambda$. If this parameter is small enough ($\rho < 0.1$), aerosol scattering proceeds similarly to molecular scattering, which is characterized by a very sharp dependence upon the frequency. As the dimensions of the particles increase the dependence weakens, and for particles with a radius 10–20 times larger than the maximum wavelength of the incident light the cross section of scattering becomes independent of the frequency. Atmospheric aerosols are usually polydisperse, and the cross section of scattering in such systems is proportional to an intermediate power of frequency between ν^4 and ν^0, being about $\nu^{1.3}$ on the average. In an extremely clear atmosphere the power rises to 1.5 and even to 2, but falls to approximately 0.5 when the air is dusty.

Aerosol scattering, in contrast to molecular scattering, is anisotropic. Most of the light is scattered forward in a cone with an angle of divergence of about 10–15°, although this figure may vary significantly. Aerosol scattering usually is not quite elastic. The particles suspended in the atmosphere, especially the solid ones, absorb a certain fraction of the incident light. For particles of comparatively large size ($\rho > 1$), the sum of the cross sections of scattering and absorption is equal to approximately one-half of the total area of the dust particles in a unit mass of air. The ratio between scattering and absorption is dependent on the value of the absorption coefficient of the particles.

SELECTIVE ABSORPTION BY GASEOUS CONSTITUENTS OF THE ATMOSPHERE

One may form a general impression about the character of the specific absorption of radiation by gaseous constituents of air when looking at Fig. 1.14. As shown, the whole ultraviolet part of the spectrum with frequencies higher than 1000 THz (wavelength less than 300 nm) is cut off almost completely by the absorption band of ozone. The most transparent atmosphere "window" is spread in the region between 300 and 700 nm. Here only some weak absorption bands of oxygen, ozone, and water vapor exist. Deeper into the longwave region the power of absorption bands of oxygen and water vapor increases, and in the infrared part of the spectrum at $\lambda = 1300-3300$ nm and at $\lambda > 4000$ nm the powerful bands of carbon dioxide are added to those of water. The total absorption of IR radiation by gaseous components of the atmosphere attains about 50% or more (Boer, 1977; Gates, 1965a,b, 1968, 1980, 1985, 1993; Thakaekara, 1974).

Limitation of the transparency "window" of the atmosphere by the shortwave
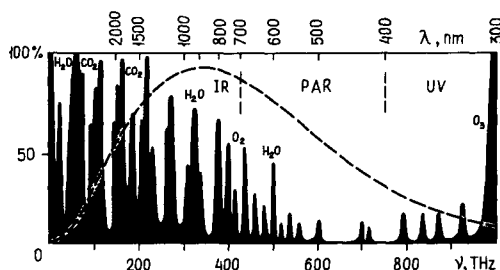
Figure 1.14 Selective absorption of solar radiation by gaseous constituents of the atmosphere: air mass AM1; moisture content = 2 cm of precipitated water; dashed line, distribution of energy in black-body radiation at 5785 K, arbitrary units.

absorption bands of ozone is of paramount importance for the whole natural history of life on Earth. In the early stages of the existence of Earth, ultraviolet radiation was possibly one of the active factors in abiogenic synthesis of organic molecules. Later it prevented living organisms in the water from moving to dry land. That became possible only when sufficient amounts of oxygen had accumulated in the atmosphere due to the photosynthetic activity of algae that lived in the water. Photolysis of atmospheric oxygen by hard ultraviolet radiation led to the formation of an ozone layer. With time, this layer shielded the ground from hard high-frequency radiation and thus created prerequisites for the evolution of terrestrial forms of life.

It should be noted that this function, of critical significance for the well-being of the biosphere, is provided by an extremely small amount of ozone, 1 molecule per 4 million molecules of other gases. The equivalent thickness of the ozone layer, if reduced to normal conditions, would only be about 2–3 mm, with a little more in the upper latitudes and a little less in the equatorial zone. Investigations show the troubling formation of large "holes" in the ozone layer of our atmosphere, especially in the polar regions (Kerr, 1994; McPeters *et al.,* 1986).

The limitation of the transparency of the atmosphere in the longwave region due to absorption bands of carbon dioxide are also of great significance for the functioning of the biosphere. These bands make the atmosphere opaque to the infrared radiation emitted by Earth, thus producing the greenhouse effect.

The content of the main gaseous constituents in the atmosphere is practically constant with the exception of water vapor, which may vary over wide limits. On a very cold clear winter day the water content in a column of atmosphere over 1 m² may amount to only 2–5 kg, whereas on a hot, humid summer day it may attain as much as 40–50 kg. The water vapor in the atmosphere, if completely condensed, would form a layer of liquid 0.2–0.5 cm thick in the former case and 4–5 cm in the latter. Variation in humidity of the atmosphere affects the absorption of light mainly in the wavelength range near 900 nm and in the far infrared.

This Page Intentionally Left Blank

Fluxes of Solar Radiation and Absorption of Light by Plants

INTRODUCTION

Earth's vegetation consists of an immeasurable quantity of light-capturing elements. These are plants or, on another hierarchical level, their individual leaves. About 2 tons of solar energy is captured every day by Earth's vegetation. This quantity is greater than 1% of the total amount of energy incident on the planet. Humans consume this amount of energy within about half a year.

The quantities of solar energy intercepted by the separate light-absorbing elements of vegetation are highly variable, depending on many different factors. These factors may be divided into at least four categories: (a) astronomical; (b) meteorological; (c) those determined by the intensity and spectral characteristics of the radiative flux; (d) those specified by the structure and properties of the light-absorbing apparatus of the plant.

Astronomical factors are well-defined and can be determined with great accuracy. For a given geographical latitude, on any day of a year, and for any hour of a day, the power of solar flux incident on a definitely oriented surface beyond the atmosphere can be calculated.

Changes in solar light that occur as it passes through the atmosphere due to scattering and absorption may also be calculated, but with a lower degree of accuracy and certainty. In this case meteorological factors, such as the transparency of the atmosphere, thickness of the cloud layer, and amounts of water vapor and dust particles in air, should all be taken into account. Meteorological factors are extremely variable and unpredictable.

The conditions of light scattering and absorption along its path through the atmosphere are essentially dependent on the spectral composition of the light flux.

Ultraviolet rays with wavelengths of less than 300 nm are almost totally absorbed by the ozone layer in the high strata of the atmosphere and do not reach the ground. Visible light, which is also effective for photosynthesis, is mainly scattered without absorption in a clean, dustless atmosphere. In the infrared region there is a series of absorption bands due to the presence of water vapor and carbon dioxide. Nevertheless, when the sky is clear, up to 50% of the total flux reaches the ground as IR radiation. Liquid water effectively absorbs infrared rays, and therefore light with wavelengths longer than 1000 nm does not reach the ground when the sky is overcast.

The characteristics of the propagation of light through scattering media are essentially distinct, depending on whether the light is direct or diffuse. Even the first act of scattering becomes "fatal" for a direct light beam as it loses its initial direction and becomes diffuse. However, diffuse light can be scattered repeatedly without a change in its qualitative state: it remains diffuse after consecutive acts of scattering. Therefore, diffuse light propagates in scattering media over longer distances than do direct beams.

The final step in the pathway of light from the Sun to plants is its capture by leaves. The conditions of this process depend on the content of light-absorbing pigments in leaves, the configuration and orientation of leaves, and the structure of the foliar system of a plant as a whole. All of these factors are greatly variable for different plant species.

The problem under consideration in this chapter is very complicated if examined fully to the minutest detail. It may be discussed, however, to various degrees of completeness within the framework of a distinct set of objectives. There are many publications about different aspects of this problem differing from each other by the approaches and by methods used. Among the works related to the matter in question, the fundamental studies of Gates (1965 a, b) and Gates *et al.* (1965) should be mentioned first. Detailed investigations were also carried out by Idso and de Witt (1970), Holmes (1981), Kleshnin (1954), Nilsen (1972), Ross (1964, 1975), Shulgin (1973), Shulgin *et al.* (1975), Thornly (1976), and Tucker and Garrat (1977). Many publications related to the problems of remote sensing of Earth's surface from satellites, atmospheric optics, and meteorology are also of interest concerning the subject matter of this section (Allen *et al.*, 1970; Boer, 1977; Chance and LeMaster, 1977; Slater, 1980; Smith and Oliver, 1974; Suits, 1972; Thomas and Thekaekara, 1976). The abundance and diversity of works concerning the topic make it worthwhile to present a brief survey of the subject that should be sufficient for further reading. The problem will be treated here in terms of the theory of radiation transfer.

In a general case, the quantity of solar energy incident upon a plant over a specific band of frequencies ($\nu_1 - \nu_2$) may be represented as follows:

$$E = \int_{\nu_1}^{\nu_2} \omega_s I(K^\circ F^\circ + K^* F^*) \, d\nu. \qquad (2.1)$$

Here ω_s is the value of a solid angle of the Sun: $\omega_s = 6.8 \times 10^{-5}$ sr. I is the inherent intensity of solar radiation beyond the atmosphere. The coefficient F considers the extinction of light while passing through the atmosphere, whereas K accounts for the orientation of a light-absorbing surface in relation to the direction of incident light flux. As the characteristics of propagation of direct and diffuse light are distinct, both components of incident radiation should be considered separately. The quantities related to direct light are indicated in Eq. (2.1) and throughout with a superscript ($^\circ$), and those related to diffuse light in a clear sky are indicated with a ($*$). In the case of overcast weather, only diffuse components of radiation exist. All quantities related to diffuse radiation from a cloudy sky will be indicated with the sign ($^=$).

Immediate use of Eq. (2.1) may be cumbersome because the intensity of radiation I and the extinction factor F depend upon the frequency or wavelength of light. The problem may be much simplified, however, by averaging the parameters within the photosynthetically active part of the spectrum (430–700 THz). In this region there are weak absorption bands (see Fig. 1.8) and, thus, such a simplification should be acceptable. Now Eq. 2.1 may be rewritten as follows:

$$\text{clear sky:} \quad E = Br(K^\circ F^\circ + K^* F^*) \tag{2.2a}$$

$$\text{cloudy sky:} \quad E = BrK^= F^= \tag{2.2b}$$

Here B is the solar constant, which equals the energy flux incident on a unit area oriented normal to the light rays beyond the atmosphere. The average value of the solar constant is assumed to be about 2 cal per cm^2 per minute or 1.39 kW/m^2. The value of B varies within $\pm 3.5\%$ in a year due to seasonal variations of the Sun-to-Earth distance; in the Northern Hemisphere B is larger in winter than in summer. The quantity r denotes the share of the photosynthetically active region (PAR) in initial solar light. The value of r is up to about 0.365 with respect to the total flux of solar light beyond the atmosphere.

ASTRONOMICAL FACTORS

Before we examine the quantities represented in Eqs. (2.2a) and (2.2b), a brief review of some basic astronomical concepts should be given.

The angular height of the Sun over the horizon is determined by the equation:

$$h_o = \arcsin(a + b \cos t), \tag{2.3}$$

where $a = \sin \phi \sin \delta$ and $b = \cos \phi \cos \delta$. ϕ is the latitude of the location, δ is the declination of the Sun, and t is the time angle of the Sun. The declination of the Sun, δ, varies within a year from -23.4° at the winter solstice (December 22) to $+23.4^\circ$ at the summer solstice (June 22). At the equinoxes (March 23 and September 22) the declination of the Sun is zero.
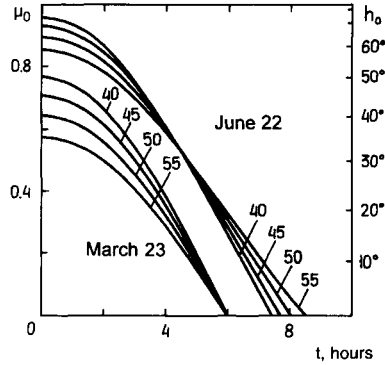
Figure 2.1 Dependence of solar elevation (h_o, μ_o = sin h_o) on the time angle (antemeridian or postmeridian) for latitudes 40–55° and for 2 days of the year.

The time angle of the Sun, t, is counted off from the meridian in hours or degrees (1 hr = 15° = 0.2618 rad). The limits of the time angle are defined by the moments of sunrise and sunset (t_s):

$$t_s = \pm\arccos(-tg\phi \cdot tg\delta). \qquad (2.4)$$

Figure 2.1 represents the dependence of solar elevation on the time angle for some latitudes and for 2 days of the year. All these astronomical parameters will be needed for further calculations.

INFLUENCE OF ORIENTATION OF THE LIGHT-ABSORBING ELEMENTS

An orientation factor for direct light ($K°$) may be derived through simple geometric consideration. It attains its largest possible value ($K° = 1$) when the light-absorbing surface is oriented normal to the incident sun rays. The leaves of some plants trace the path of the Sun, keeping an optimal position in relation to the Sun's rays during the day (Ehleringer and Forseth, 1980). Such a case is the exception rather than the rule, and the typical orientation of a leaf is random. The values of the orientation factor K for some typical cases are listed in Table 2.1.

The value 0.5 for the random orientation of a leaf is obtained as the average of a scalar product of a unit vector of a light ray and a unit vector normal to the leaf surface, with all directions of the latter vector being assumed to be equally probable:

$$\int_0^{\pi/2} \sin\theta \cdot \cos\theta \cdot d\theta = 0.5.$$

Table 2.1

Orientation Factors for Variously Oriented Leaves

| Orientation of a leaf | Clear sky | | Cloudy sky |
	Direct light, $K°$	Diffuse light, $K*$	Diffuse light, $K^=$
Normal	1	—	—
Random	0.5	—	0.5
Horizontal	$\sin h_o = \mu_o$	0.35–0.4, up to 0.5 at turbid atmosphere	0.575
Vertical (random azimuth)	$0.637 \cos h_o$	0.5–0.7	0.467

The factor 0.637 is obtained by allowing for equal probability of any orientation of an azimuth of a vertical leaf:

$$\left(\frac{2}{\pi}\right) \int_0^{\pi/2} \cos\theta \cdot d\theta = 0.637.$$

Orientation factors for diffuse light are calculated with regard for the angular distribution of brightness over the sky. As one can see from Table 2.1, the preferable orientation of a leaf for maximum energy capture is normal to the direction of the light. A leaf oriented randomly receives, on average, only half of the amount of the direct component of sunlight that falls onto a normally oriented leaf of the same area.

The values of the orientation factor for horizontally or vertically oriented leaves are dependent on the elevation of the Sun. $K°$ increases with h_o for horizontal leaves and diminishes for vertical ones. With cloudy weather the orientation coefficient depends slightly upon the leaf orientation.

Values of the orientation factor for some types of three-dimensional foliar systems are listed in Table 2.2. The coefficients refer to the unit area of a central cross section for a spherical crown and the unit area of an axial cross section for a cylindrical crown. In the case of a horizontal stratum of leaves, the factors refer to the unit area of a ground surface.

The most effective light-absorbing foliar structure is a sphere, as can be seen from Table 2.2. A spherical crown at any position of the Sun would catch the same

Table 2.2

Orientation Factors for Three-Dimensional Foliar Systems

| Light absorbing structure | Clear sky | | Cloudy sky |
	Direct light, $K°$	Diffuse light, $K*$	Diffuse light, $K^=$
Spherical crown	1	1	1
Horizontal crop layer	$\sin h_o = \mu_o$	0.35–0.4, up to 0.5 at turbid atmosphere	0.575
Vertically elongated crown	$\cos h_o$	0.8–0.9	0.733

flux of light as a normally oriented plane of area equal to that of the central cross section of the sphere. The foliar structure of any other configuration gets less energy per unit cross section. This conclusion is valid for plants that stand apart and do not shade each other. If plants are bunched together, each gets, on average, as much energy as falls upon the horizontal projection of the crown independent of its configuration.

PROPAGATION OF LIGHT IN THE ATMOSPHERE

Scattering and absorption of light, when passing through the atmosphere, may be examined with the theory of radiative transfer. This theory has been elaborated in detail and is widely used in astrophysics (Busbride, 1960; Chandrasekhar, 1960; Sobolev, 1972). It should be adequate to become acquainted with some fundamentals of the theory and to use some known results.

The basic equation of the theory of radiative transfer may be written as follows:

$$\mu \frac{dI}{d\tau} = -I + D, \tag{2.5}$$

where $\mu = \cos \theta$, the cosine of the angle between a given radius vector and the direction of radiation, τ is the optical length of the pathway of light, I is the intensity of radiation, and D is the intensity of the diffuse (scattered) component of radiation.

The physical meaning of optical length (τ) differs from that of geometric length. It is measured not with the usual units of length (meters) but by the events that may happen to light on its pathway or, more strictly, the probability of such events. There are two types of events that may happen to light: it may be scattered or it may be absorbed. The probability of any event happening to a unit length of the pathway is determined by the cross section of scattering (α) of the medium through which the light propagates. Thus, a very long geometric pathway through empty space, say 150 million km from Sun to Earth, corresponds to a negligibly small optical length. On the other hand, an optical length of several kilometers of the pathway through the atmosphere and especially through its lower strata may be quite large. The total value of the optical length of the pathway of light through the atmosphere in the zenith direction can be expressed by the following integral:

$$\tau_o = \int_\infty^0 \alpha(z) \, dz,$$

where the coordinate z is directed vertical to the zenith. The quantity τ_o is referred to as the optical thickness of the atmosphere and may be considered as the total cross section of scattering through the column of air over a unit area at sea level, which is 1 kg of air per cm^2. The term airmass one or abbreviation AM1 is used to designate this quantity.

If the Sun's rays cross the atmosphere not along the shortest path (from a ze-nith) but under a certain angle from vertical, their geometrical pathway becomes longer and the optical length correspondingly increases: $\tau = \tau_o/\mu_o$. The optical length and the airmass are doubled (AM2) when the angle between zenith and the Sun equals 60° (solar elevation = 30° over the horizon) and attain a 10-fold increase (AM10) at a solar elevation of about 5°.

The basic equation (Eq. 2.5) of the theory of radiative transfer seems simple at first. In fact, it enables one to obtain an obvious expression for an extinction factor of direct light in optically thin atmosphere when only primary scattering can be taken into account:

$$F° = \exp(-\tau_o/\mu_o). \qquad (2.6)$$

This solution is valid if the optical thickness of the atmosphere does not exceed a value of 0.5–0.7.

The optical thickness of clear atmosphere usually varies within limits of about 0.2–0.6. The lower value corresponds to a quite clear dark-blue sky and is often found in cold, dry weather. When τ_o equals 0.5–0.6, the sky looks white or milky blue. The value of τ_o for a highly dusted atmosphere may exceed 0.6. In such cases the Sun looks like a dim disk. A value for τ_o of about 0.3 is typical for the usual state of the atmosphere in good sunny weather.

It should be noted that the values of τ_o indicated in the preceding paragraph are averaged over the whole visible range of the spectrum. The real values of the optical thickness of the atmosphere in the shortwave range are greater and in the longwave range less than average, because the cross section of scattering increases with the shortening of radiation wavelength. This causes the blue color of the sky and the reddening of incident radiation, the latter effect being more evident in turbid atmosphere and at a low position of the Sun.

The dependence of F on solar elevation and the optical thickness of the atmosphere is depicted in Fig. 2.2.

Direct light, when scattered, turns into diffuse light that spreads in all directions. Equation (2.5) enables one to calculate the intensity of scattered light. For this purpose, the term D on the right side of Eq. (2.5) should be considered. If the atmosphere is clear enough, with an optical thickness no higher than 0.5–0.6, only the primary scattering should be taken into account. In such a case, the term D should be expressed as follows:

$$D = \frac{\lambda}{4} E \kappa(\gamma) \exp(-\tau_o/\mu_o), \qquad (2.7)$$

where λ is the factor of pure (conservative) scattering. If scattering is not followed by absorption, $\lambda = 1$. The function $\kappa(\gamma)$ is the indicatrix of scattering. The term indicatrix means a diagram in polar coordinates of the angular distribution of scattered light intensity. The angle γ is measured against the direction of an incident beam. In a transparent atmosphere free of coarse dust particles, the indicatrix of scattering can be considered to be roughly spherical: $\kappa(\gamma) = 1$.
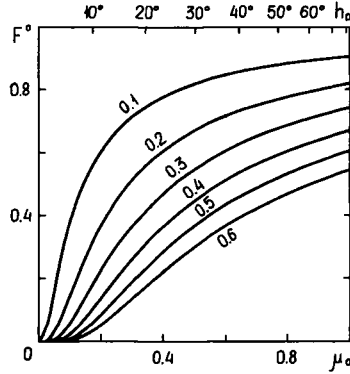
Figure 2.2 Dependence of an extinction factor for direct light incident on a horizontal surface on solar elevation and optical thickness of the atmosphere (values on the curves).

As the intensity of direct light diminishes while passing through the atmosphere due to scattering, the intensity of the diffuse component of radiation is enlarged correspondingly. By integrating Eq. (2.5) and accounting for Eq. (2.7), we obtain the following expression for the distribution of brightness of diffuse light over the sky on a clear day (Sobolev, 1972, 1975):

$$\sigma(\mu_o,\mu) = \left(\frac{1}{4}\right)\frac{\exp(-\tau_o/\mu_o) - \exp(-\tau_o/\mu)}{\mu_o - \mu} \cdot \kappa(\gamma). \qquad (2.8)$$

Here μ_o is the sine of solar height over the horizon and μ is the sine of an arbitrary direction. If the indicatrix of scattering is considered to be spherical, the indicatrix of brightness of diffuse light has the shape of a flat "cake" as shown in Fig. 2.3, curves 1–3. As the optical thickness of the atmosphere increases, the indicatrix of brightness of diffuse light becomes less flat due to an increase in the skylight flux from above. A low location of the Sun over the horizon is favorable for more
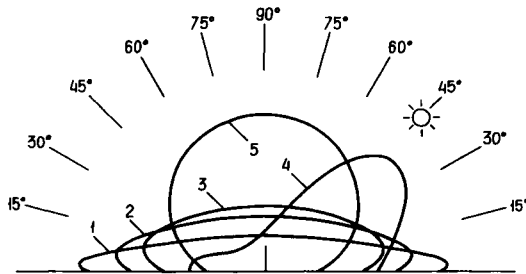
Figure 2.3 Indicatrices of brightness of diffuse light: (1–3) clear atmosphere at optical thickness $\tau_o = 0.2$, 0.4, and 0.6, respectively (spherical indicatrix of scattering of atmosphere); (4) stretched indicatrix of scattering; (5) diffuse light from a cloudy layer. Sun elevation at 45°.

uniform angular distribution of diffuse light. The effect of the sky brightening when approaching the horizon as pictured earlier may be observed more clearly from mountains or an aircraft.

A lower stratum of the atmosphere usually contains an appreciable quantity of comparatively rough aerosol particles, which scatter light very nonisotropically. The indicatrix of scattering in a turbid atmosphere is stretched forward along the incident beam. Correspondingly, the indicatrix of brightness of diffuse skylight protrudes toward the Sun. Therefore, the round Sun area of the sky becomes more bright, as shown in Fig. 2.3, curve 4.

The intensity of diffuse light over the sky is distributed in a way depending on the position of the Sun and the transparency of the atmosphere. On the other hand, the light-absorbing system has its own angular orientation. Therefore, the orientation factor K^* and the extinction factor F^* cannot be considered independently in this case. Both factors should be taken into account in combination, $K^* F^*$, which can be obtained by integrating Eq. (2.8) over the full range of μ from 0 to 1 with regard to the geometry of the light-absorbing system:

$$\text{spherical crown:} \quad K_s^* F_s^* = 2\mu_o \int_0^1 \sigma(\mu_o, \mu) \, d\mu \tag{2.9}$$

$$\text{horizontal surface:} \quad K_h^* F_h^* = 2\mu_o \int_0^1 \sigma(\mu_o, \mu)\mu \, d\mu \tag{2.10}$$

$$\text{cylindrical crown:} \quad K_v^* F_v^* = 2\mu_o \int_0^1 \sigma(\mu_o, \mu)\sqrt{1 - \mu^2} \, d\mu. \tag{2.11}$$

Figures 2.4–2.6 depict the dependence of the total flux of direct and diffuse light and the share of the latter upon the optical thickness of the atmosphere, solar
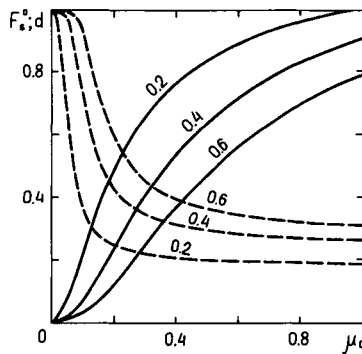
Figure 2.4 Dependence of the total (direct + diffuse) light flux on a spherical crown (solid lines) and the share of the diffuse component (dashed lines). Values on the curves are the optical thickness of the atmosphere.
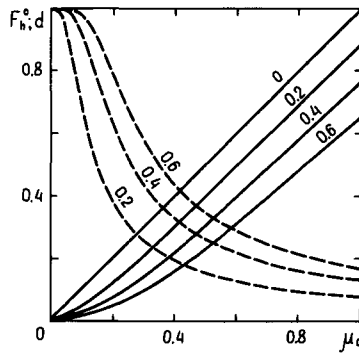
Figure 2.5   Dependence of the total (direct + diffuse) light flux or a horizontal layer of a crop (solid lines) and the share of the diffuse component (dashed lines). Values on the curves are the optical thickness of the atmosphere (values of τ_o).

elevation, and orientation of the light-absorbing system. By comparing the corresponding curves of these figures, one can see that the quantity of radiation incident on a spherical crown surpasses the values for horizontally and vertically oriented surfaces of equal cross section. The incident flux increases when the Sun rises over the horizon in cases of spherical and horizontal orientation and passes through maximum in the case of a vertical crown.

The share of energy incident in diffuse form significantly depends upon the transparency of the atmosphere and the elevation of the Sun. At a low position of the Sun the diffuse component of irradiation prevails, but its share diminishes as the Sun rises. In the case of a vertical-orientation light-harvesting system, the share of diffuse light grows again at the maximum height of the Sun.
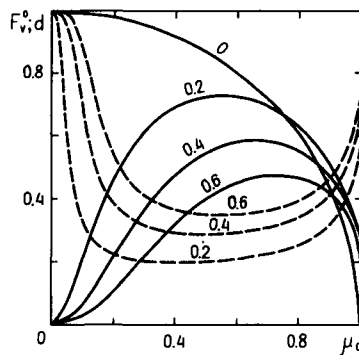
Figure 2.6   Dependence of the total (direct + diffuse) light flux on a cylindrical vertically stretched crown (solid lines) and the share of the diffuse component (dashed lines). Values on the curves are τ_o.

LIGHT SCATTERING BY A CLOUDY LAYER

When the sky is totally covered with clouds, the optical thickness of the atmosphere may be much greater than one unit. Under such conditions, light, when propagating through the atmosphere, undergoes multiple acts of scattering. To account for the effects of multiple scattering, the function D in Eq. (2.5) should be written as follows:

$$D = \lambda \int I\kappa(\gamma) \frac{d\omega}{4\pi}. \tag{2.12}$$

The basic equation of radiative transfer (Eq. 2.5), with the term D expressed by Eq. (2.12), enables one to describe the extinction of light by the cloudy layer. In this case obtaining an exact solution for Eq. (2.5) becomes a complicated problem. The point is that insertion of Eq. (2.12) into Eq. (2.5) makes the equation an integral–differential one for which no general analytical solution has been derived. In works concerning the problems of astrophysics (Busbride, 1960; Chandrasekhar, 1950; Sobolev, 1972, 1975), solutions of this equation for some special cases have been obtained. Here we will take advantage of these solutions. It was shown that in the case of optically thick medium, the solution of the equation of radiative transfer can be expressed via a function that is, in its turn, a solution of the following integral equation (sometimes referred to as the Miln equation):

$$\phi(\lambda,\mu) = 1 + \frac{\lambda}{2}\phi(\lambda,\mu)\mu \int_0^1 \frac{\phi(\lambda,\mu)}{\mu + x}dx. \tag{2.13}$$

The function $\sigma(\lambda,\mu)$, which is also known as the Hambarzumian function, is depicted in Fig. 2.7. In the case of pure scattering proceeding without absorption
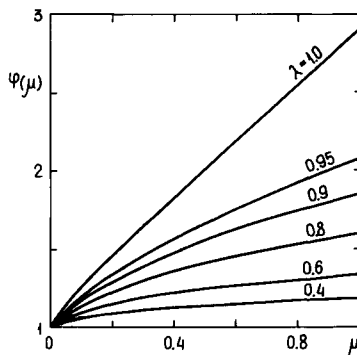
Figure 2.7 Hambarzumian function (solution of the Miln equation).

($\lambda = 1$), this function is almost linear and varies from 1 at $\mu = 0$ to 2.91 at $\mu = 1$.

The theory of planet atmospheres gives the following expression for the angular distribution of brightness of a cloudy layer of optical thickness τ_{cl}:

$$\sigma(\mu_o,\mu) = \left(\frac{1}{4}\right)\frac{\phi(1,\mu_o) \cdot \phi(1,\mu)}{\tau_{cl} + 1.42}. \tag{2.14}$$

The indicatrix of brightness expressed by Eq. (2.14) is depicted in Fig. 2.3 by curve 5. As one can see, the angular distribution of diffuse light over a cloudy sky is uniform except for low angles over the horizon, where the flux is smaller.

By integration of the function $\sigma(\mu_o,\mu)$ within the limits of μ from 0 to 1, accounting for the geometry of light-absorbing systems, the values of orientation factors may be obtained. In this way the values noted in Tables 2.1 and 2.2 for diffuse light from a cloudy sky have been calculated:

$$\text{spherical crown:}\quad K_s^= = \frac{1}{2}\int_0^1 \phi(1,\mu)\, d\mu = 1$$

$$\text{horizontal surface:}\quad K_h^= = \frac{1}{2}\int_0^1 \phi(1,\mu)\mu\, d\mu = 0.575$$

$$\text{cylindrical crown:}\quad K_v^= = \frac{1}{2}\int_0^1 \phi(1,\mu)\sqrt{1-\mu^2}\, d\mu = 0.733.$$

The factor of attenuation of light flux by the layer of clouds ($F^=$) may be expressed with the help of Eq. (2.14). The fact that the irradiance of the upper face of a cloudy layer depends on the angular height of the Sun and the optical thickness of the atmosphere above the clouds should be taken into account:

$$F^= = \frac{\phi(1,\mu_o)\mu_o}{\tau_{cl} + 1.42}\, \exp(-\tau'/\mu_o). \tag{2.15}$$

The exponent in this formula describes the extinction of radiation above the layer of clouds. The optical thickness of the upper stratum of the atmosphere, τ', is usually on the order of 0.2–0.1 or even less in the case of altitude clouds. The factor μ accounts for the declination of direct solar rays illuminating the clouds from above. The factor $(\tau_{cl} + 1.42)^{-1}$ accounts for the extinction of light by the cloudy layer. The optical thickness of clouds may vary within broad limits from 1–2 up to 10–20 and more. The values of τ_l characterize the mathematical expectancy of the number of successive acts of scattering that a photon undergoes on its path through the cloudy layer. The clouds may be of various densities, so that a unit optical thickness may refer to the thickness of a cloud from about 10 up to 100 m (Foigelson and Krasnokutskaya, 1978). A rough picture of optical characteristics of various types of clouds is given in Table 2.3.

Table 2.3

Optical Thickness of the Cloudy Layer and Attenuation of Radiation

State of cloudiness	τ_{cl}	$(\tau_{cl} + 1.42)^{-1}$	Transmission factor $(\%\%)$, $h_o = 45°$
Gray sky, very dim sun (weak shadows are visible)	0.8–1	0.4–0.45	70–75
Gray sky without sun (no shadows)	1.2–2	0.3–0.38	50–60
Overcast	2.5–4	0.18–0.25	30–45
Overcast, it rains	5–8	0.1–0.15	16–25
Heavy dark clouds	10–15	0.06–0.09	10–15
Storm clouds	20–40 and more	0.05–0.02	3–8 and less

INCIDENCE OF SOLAR ENERGY ON A PLANT

The values of the total amount of solar energy incident on a plant under various conditions and its integral radiant exposure during a light day may be determined on the basis of the regularities described earlier. Figures 2.8–2.10 depict the diurnal course of solar light flux in the photosynthetically active region (PAR) of the spectrum. The data shown refer to a midsummer day at 45° latitude. It seems interesting to first compare the curves for a hypothetical case of zero optical thickness of the atmosphere. Such a condition could only occur beyond the atmosphere. As no scattering would occur in this case, factors concerning the orientation of a leaf or the structure of a crown would be clearly manifested. A spherical crown
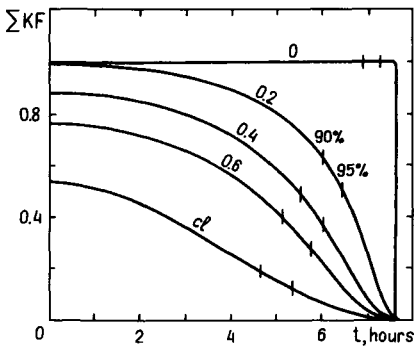
Figure 2.8 Diurnal PAR flux to a spherical crown. Latitude = 45°, June 22. Values on the curves are the optical thickness of the atmosphere; cl refers to a cloudy sky. The time ranges of obtaining 90 and 95% of a diurnal sum are shown.
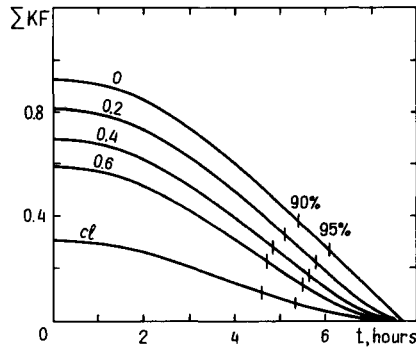
Figure 2.9 Diurnal PAR flux to a horizontal layer of a crop. Conditions and designations are the same as for the previous figure.

(or a leaf oriented normally) would receive maximum energy flux compared with any other shape of orientation of the light-absorbing system. Moreover, in this case the energy flux would be constant all day long. Energy flux incident on a horizontal surface would pass over a flat maximum at about noon and diminish in the morning and evening hours. The total amount of energy received during a day by a spherical crown would be almost twice that received by a horizontal surface. In the case of a vertical crown the situation is opposite that of a horizontal one: the energy flux is minimum at noon and comes up to a maximum value just after sunrise and before sunset. In real conditions when the light flux is being scattered as it passes through the atmosphere, the distinctions between light-absorbing systems of different configurations with respect to their ability to catch sunlight are less noticeable.
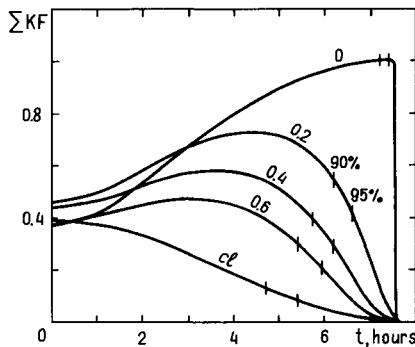
Figure 2.10 Diurnal PAR flux to a vertically stretched cylindrical crown. Conditions and designations are the same as for Fig. 2.8.

The total amount of diffuse radiation is less dependent on the optical thickness of the atmosphere, whereas its relative fraction increases with an increase in τ_o because of the corresponding decrease in the direct component. The flow of diffuse light from a clear sky varies slightly during a day, but its share of total radiant flux increases drastically at low Sun positions early in the morning and late in the evening. Horizontally oriented light-absorbing systems receive a greater fraction of diffuse light than spherical or vertical ones in the morning and evening, but the relation is reversed at a high position of the Sun.

The daily course of energy flow falling from the cloudy sky to the ground is also shown in Figs. 2.8–2.10 for a given value of optical thickness of the cloudy layer ($\tau_{cl} = 3$).

The occurrence of a minimum at midday hours and symmetric maxima in the morning and evening is peculiar to light-absorbing systems of vertical orientation. The effect is more clearly developed in summer at low latitudes. It is less marked or even disappears in spring or autumn, especially in the case of a turbid atmosphere.

It is essential to note that while the radiant flow incident on a plant varies within wide limits during a day, the main part of daily energy input occurs during the midday hours. The morning and evening hours of a light day supply only a small portion of the energy. In Figs. 2.8–2.10 the time limits at which a plant receives 90 and 95% of its total daily exposure are marked. As one can see, the periods of 1.5–3 hr after sunrise and before sunset are less energetically abundant. In these hours a plant receives only 5–10% of its total energy budget. The minute energy availability in the morning and evening hours of a day should not be a reason to conclude that these hours are insignificant for the plant in a physiological respect. In fact, the availability of periods of low-intensity irradiation may be quite essential for the physiological functions of a plant.

Apart from the morning and evening hours, the variation of irradiance during the main part of the day is not large. So within the daytime hours during which a plant receives the main portion of its energy budget, say 90–95%, the irradiance usually varies within no more than 40–50% of the mean value (for horizontal orientation). For normal and vertical orientations the variation is less. In cloudy weather the range of irradiance variation within the main part of the "working day" of a plant is of the same order but at a lower level depending upon the optical thickness of clouds.

Some generalized data for the diurnal sums of physiologically active radiation incident upon a plant under different conditions are presented in Fig. 2.11. First, the distinctions between horizontal and spherical orientations of the light-absorbing system are obvious. The spherical systems receive 40–50% more energy than horizontal systems under the same conditions. The annual cycle of energy supply is well-characterized: in low latitudes the distinctions between summer and winter are small, but they grow as one moves away from the equator. The
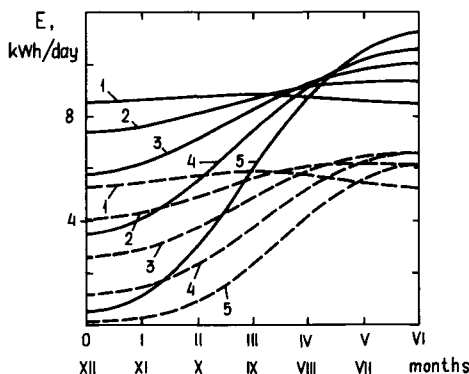
Figure 2.11   Diurnal sums of PAR in a year. Clear sky, $\tau_o = 0.3$. Solid lines: a spherical crown. Dashed lines: a horizontal layer. Latitude $= 0°, 15°, 30°, 45°$ and $60°$ (curves 1–5, respectively).

summer diurnal sums of PAR in high latitudes may exceed the corresponding values for tropical regions due to the longer duration of a day. Distinctions between south and north as well as between spring and summer are less marked for normal and vertical orientations of a light-absorbing system than for a horizontal one.

The total values of radiant fluxes including the longwave part of the spectrum may be estimated by multiplying the values of PAR by a factor of 2–2.5 in the case of a clear sky. In a cloudy sky the infrared radiation of the Sun is almost completely absorbed in the atmosphere. Under such conditions, however, the flux of low-temperature heat radiation emitted by clouds in the far infrared ($\lambda \approx$ 10,000 nm) is significantly augmented.

QUALITATIVE CHARACTERISTICS OF INCIDENT LIGHT

As was noted in Chapter 1, the light flux may be described in a qualitative way by its entropy content or, alternatively, by the effective temperature of radiation. Both quantities are immediately interconnected with each other and may be considered to be equivalent. The entropy content and the effective temperature of radiation characterize the deviation of thermodynamic parameters of light flux from those of equilibrium black-body radiation. These values are immediately dependent upon the extent of dilution of the initial light flux.

Figure 2.12 depicts the dependence of the dilution factor and the effective temperature of direct and diffuse solar radiation upon the angular height of the Sun over the horizon for various values of optical thickness of the atmosphere. All of
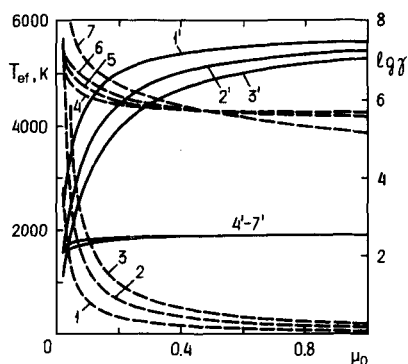
Figure 2.12 Dependence of the effective temperature of solar radiation (solid lines) and the dilution factor (dashed lines) upon solar elevation: (1–3) direct light; (4–6) diffuse light by clear sky; (7) overcast. Optical thickness of the atmosphere: 0.2 (curves 1 and 4), 0.4 (curves 2 and 5), 0.6 (curves 3 and 6).

the data relate to the PAR region of the spectrum. There is a sharp distinction between the two components of radiation flux incident on the ground, the direct and the diffuse ones. They differ from each other over about 5 orders of magnitude for their dilution factor values and by 2000–3000 for their effective temperatures. These differences are due to the abrupt change of the solid angle of an incident beam by scattering. The variation in transparency of the atmosphere exerts a comparatively slight influence in this respect. Thus, the dilution factor for direct light in a clear sky varies within the range 1.5–4 at a sufficiently high position of the Sun and grows sharply only when the Sun descends below 10°. In contrast, the dilution factor of diffuse light scattered by a clear atmosphere is about 5×10^5, almost independent of the optical thickness of the atmosphere and the solar elevation. In the case of a cloudy sky, the value of the dilution factor is on the same order.

In accordance with the variations in dilution factor, the effective temperature of radiation is significantly different for direct and diffuse components. Whereas the temperature of the direct component does not fall below 4000 K until the Sun stands high enough, the temperature of a diffuse component is much lower at 1800–2000 K. The temperature of radiation in overcast weather is also about 2000 K.

Figure 2.13 shows the diurnal course of the effective temperature of the total radiation flux on a clear day including both direct and diffuse components. The effective temperature of this "mixed" radiation is 3500–4000 K during the greater part of a day. In the case of a cloudy sky, the effective temperature of radiation varies within narrow limits around 2000 K all day.

The entropy content of the initial solar radiation in the whole spectrum equals,
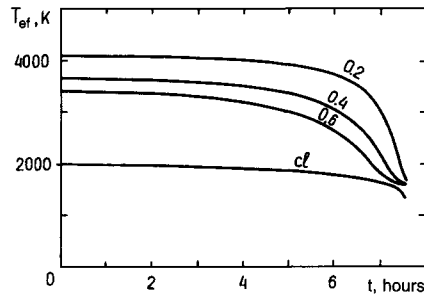
Figure 2.13 Diurnal course of the effective temperature of total radiation (direct + diffuse). June 22, latitude = 45°. Values on the curves are the optical thickness of the atmosphere; cl refers to a cloudy sky.

according to Eq. (1.16), 230 e.u. per million joules of energy (e.u. is an entropy unit, J/K). In the PAR region the value is lower, about 195 e.u. per million joules. The values of entropy of radiation (PAR) on a clear day (except the morning and evening hours) fall within limits of 250–300 e.u. per million joules and in overcast weather may amount to 650–800 e.u. per million joules.

THE INHERENT THERMAL RADIATION OF PLANTS

The region of temperatures in which various plant species survive and perform their vital functions is wide. This region extends almost from the melting point of ice up to about 50°C in diverse climatic regions of Earth and under different meteorological conditions. As with any other heated body, plants emit longwave radiation and in turn absorb thermal radiation that comes from surrounding objects: the ground, the atmosphere and clouds, nearby plants, buildings, etc. The intensity of the heat radiation of plants depends on their temperature and their absorbance features.

As plants are naturally adapted for the effective capture of radiation, they possess, due to symmetry, high radiative features as well. As the absolute temperature of a plant is approximately 20 times lower than that of the Sun, the region of maximum energy emission by the plant lies in the far infrared at frequencies correspondingly lower than those of visible light, at 15–20 THz or at a wavelength of 9000–11,000 nm. The power of thermal radiation flux, which a plant emits, is quite considerable. It amounts to about 300 W/m² at 0°C and 600 W/m² at 50°C. Say a plant with a crown radius of about 3 m emits into the upper half-space 15–35 kW of energy. The point is that the inflow of thermal radiation that comes to a plant from its surroundings is, as a rule, on the same order of magnitude because the temperature of surrounding objects usually does not significantly differ from

that of the plant. Thus, the flux of thermal radiation from the ground to a plant is essentially the same as the reverse flow from the plant to the ground (300–600 W/m^2 depending on temperature).

Radiative exchange of thermal radiation between the plant and the atmosphere may be not so symmetric, especially in clear weather. The atmosphere is almost completely opaque in the infrared region, except for a "window of transparency" at wavelengths between 8.5 and 13 μm. As the absorbance of the atmosphere is low in this window, the radiative ability of the atmosphere in this spectral region is also low. Therefore, the thermal radiation of the atmosphere is less than that of a plant or the ground at the same temperature. Thus, the downward flow of thermal radiation from the atmosphere is usually on the order of 200–400 W/m^2. A certain fraction of proper thermal radiation from vegetation escapes into space through the window of transparency. A continuous layer of clouds closes the window. In that way the downward thermal radiation of the atmosphere is increased in cloudy weather by 20–25% compared to a clear sky, and thus the balance between in- and outfluxes of thermal radiation becomes closer under such conditions.

THE CAPTURE OF LIGHT ENERGY BY LEAVES AND COMPLEX FOLIAR SYSTEMS

The leaves of plants effectively absorb solar light. The values of absorption coefficients for leaves within the visible region of the spectrum usually come to about 80%, varying for different species over the range 65–90%. Figure 2.14, constructed from data of Gates *et al.* (1965, 1971), depicts typical curves for the absorbance of leaves. The main peculiarity of the curves is the existence of a deep depression of absorbance in the red and near-infrared regions of the spectrum. One may think that this depression helps the plant to get rid of a heat overload. In
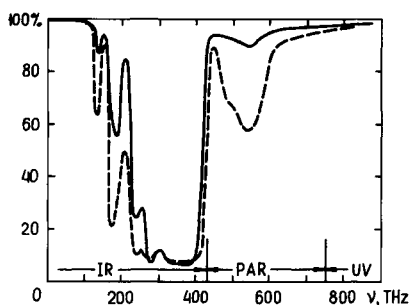

Figure 2.14 Typical curves of the spectral distribution of the absorbance of leaves: solid lines, dark green leaf; dashed lines, light green leaf.

the region of wavelengths longer than 1700 nm the leaves again become "black." The high light-absorbing ability of leaves in the far infrared provides effective removal of excess heat from a plant by emission.

To determine the energy that is actually absorbed by a leaf, the corresponding supply value should be multiplied by the absorption factor of the leaf. The problem may become more complicated, however, if a complex three-dimensional foliar system consisting of a multitude of leaves rather than an individual leaf is under consideration. The conditions of interaction of light flux by such three-dimensional light-absorbing structures should differ from those of individual leaves. A beam that passes by an individual leaf without being absorbed is lost forever, but if the beam falls onto a multileaf system and is not absorbed by the first leaf in its pathway it may be absorbed by others. It is interesting to define the interrelation between the light-absorbing properties of a single leaf and the same capabilities of a multileaf foliar structure.

This problem may be solved in different ways. The usual solution is to consider the foliar system as a series of leaves with free gaps in between them (Holmes, 1981; Idso and de Witt, 1970; Smith and Oliver, 1974; Ross, 1975; Thornly, 1976; Tucker and Garrat, 1977). An alternative approach is to consider the foliar system as a continuous light-absorbing medium characterized by a certain effective cross section of absorption. Such an approach is less specific, but makes it possible to recognize the general properties of the system more clearly. The continuous approach may be detailed if necessary by taking into account the indicatrix of scattering specific for a particular plant species. An advantage of the continual approach is that one may consider the feasibility of the immediate use of the theory of radiative transfer methods.

A simplified model of a three-dimensional foliar system can be represented by a volume in which many randomly oriented leaves are distributed homogeneously. The leaves that form such a system should be small enough compared with the size of the whole foliar system under consideration. If the total one-sided area of leaves in a unit volume equals S, then the value of effective cross section of scattering in such a system will be equal to one-half of S: $\alpha = S/2$. The factor of 1/2 accounts for the random orientation of leaves. If ϵ represents the reflection factor of a leaf, the fraction, $\alpha\epsilon\,dz$, of the incident energy should be scattered over a distance dz in the volume of foliage, and the fraction $\alpha(1-\epsilon)\,dz$ will be absorbed irreversibly.

For the sake of simplicity, only plants with optically thick foliage will be considered. This means that the characteristic size of the foliar system (L), such as the thickness of a crop layer or the radius of the crown of a tree, must satisfy the condition $L > \alpha^{-1}$. Such a condition should be met by leaf index values of about 4–6. A foliage system with such a leaf index leaves the ground almost totally in shadow, without sunlight spots on it. The sky is not visible through such foliage. A more general case of foliar systems with arbitrary optical thickness, as well as

the case of foliage with a definite prevailing orientation of the leaves, may also be examined on the basis of the theory of radiative transfer. In such cases, however, the calculations become much more complicated and the results less obvious.

The scattering and absorption of light in foliage of high optical thickness, considered to be a continual light-absorbing medium, may be described in a manner quite similar to the case of an optically thick atmosphere. For this purpose, the known solutions of the equation of radiative transfer obtained from the theory of planet atmospheres (Sobolev, 1972, 1975) can be used with only some minor modifications. The basic equation of radiative transfer (Eq. 2.5) should be written here as follows:

$$\mu \frac{dI}{dz} = -\alpha I + \alpha \epsilon \int I \frac{d\omega}{4\pi}. \tag{2.16}$$

This integral–differential equation accounts for the multiple scattering of light inside foliage. The same equation was used earlier when considering the propagation of light in clouds. The only distinction is that the scattering of light in foliage does not proceed conservatively, as in clouds, but is followed by strong absorption. Whereas the coefficient of pure scattering of clouds (λ) is near 1, the corresponding value for leaves, referred to as the reflection factor (ϵ), is about 0.15–0.3 for various plant species.

The solution of Eq. (2.16) for the case under consideration can be expressed as before via a Hambarzumian function (Eq. 2.13). The theory gives the following expression for the coefficient of the brightness of a layer of optically thick medium illuminated by a light beam:

$$\rho(\epsilon,\mu_o,\mu) = \left(\frac{\epsilon}{4}\right)\frac{\phi(\epsilon,\mu_o) \cdot \phi(\epsilon,\mu)}{\mu + \mu}. \tag{2.17}$$

Here μ_o and μ are cosines of the angles between the normal to the light-absorbing surface and the incident and scattered beams, respectively. Starting from Eq. (2.17), the fraction of radiation scattered by the foliar system into all directions, i.e., the integral coefficient of scattering or the albedo of the foliage (A), may be determined. The albedo of a flat horizontal layer of a crop illuminated with direct sunrays incident under a definite angle to the horizon can be expressed as the following integral:

$$A_{fl}^o(\mu_o) = 2 \int_0^1 \rho(\mu_o,\mu)\mu \, d\mu. \tag{2.18}$$

Integration, allowing for the function in Eq. (2.17), gives the expression for the albedo of the flat layer of a crop in explicit form:

$$A_{fl}^o(\mu_o) = 1 - \phi(\epsilon,\mu_o) \cdot \sqrt{1 - \epsilon}. \tag{2.19}$$

As one can see, the albedo of a flat layer of a crop depends on the reflectance of a leaf (ϵ) and the incidence angle of solar beams. With an increase in the incidence angle, the albedo of a horizontal layer of a crop decreases. Therefore, the fraction of reflected radiation in the morning and evening hours is larger than that at midday.

Provided the flat layer of a crop is being illuminated by diffuse light in overcast weather, the indicatrix of brightness of the cloudy sky (Eq. 2.14) must be taken into account. The angular distribution of brightness over cloudy sky as it looks from the ground depends only on the function $\phi(1,\mu)$. Thus, the albedo value of a flat layer of a crop illuminated with diffuse light in cloudy weather may be expressed by the following integral:

$$A_{\bar{\text{fl}}} = 0.869 \int_0^1 A_{\text{fl}}^\circ(\epsilon,\mu) \cdot \phi(1,\mu)\mu \; d\mu, \qquad (2.20)$$

where 0.869 is the normalizing factor.

The albedo of a spherical crown illuminated by direct rays can be found in terms of the formula (Eq. 2.19) for a flat layer. In this case the angle of incidence of the rays that fall on different segments of a spherical crown varies from 90° at the point opposite the Sun to 0° at an equatorial segment of the crown. Thus, the spherical albedo can be found by integration:

$$A_{\text{sph}}^\circ = 2 \int_0^1 A_{\text{fl}}^\circ(\epsilon,\mu)\mu \; d\mu. \qquad (2.21)$$

The proper transformations, allowing for Eq. (2.19), result in

$$A_{\text{sph}}^\circ = 1 - 2\phi_1(\epsilon)\sqrt{1 - \epsilon}, \qquad (2.22)$$

where $\phi_1(\epsilon)$ is the first momentum of the Hambarzumian function:

$$\phi_1(\epsilon) = \int_0^1 \phi(\epsilon,\mu)\mu \; d\mu. \qquad (2.23)$$

It should be noted that the albedo of a sperical crown does not depend on the character of the radiation; it is the same for either direct or diffuse light.

The dependence of the reflectance of three-dimensional foliar systems upon the reflectance of the individual leaves of which the volume foliage consists is depicted in Fig. 2.15. The curves are computed by Eqs. (2.19), (2.20), and (2.22) for various conditions of illumination and for two foliage configurations, a flat layer of a crop and a spherical crown.

The essential difference between light-absorbing systems of different shapes is illustrated by the more effective capture of light by volume structures than by simple two-dimensional systems such as individual leaves. As one can see in Fig. 2.15, the reflectance of a complex foliar system is 2–6 times lower than the reflectance of the leaves from which the system is built. In other words, **a tree is**
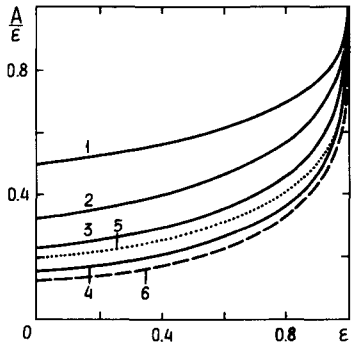
Figure 2.15 Interrelation between the reflectance (pure scattering) of a leaf (ϵ) and the albedo of a foliar system (A): (1–4) horizontal layer, sun elevation $h_o = 0°$, $11.5°$, $23.5°$, $90°$, respectively; (5) a horizontal layer, cloudy sky; (6) a spherical crown.

always much darker than its leaves. The cause of this effect is quite evident. When a beam penetrates into the depths of a mass of foliage, it falls into a trap. It is almost totally absorbed there, and only a very small fraction of the incoming light has a chance to slip out. It should be noted that in very dense foliar systems with co-lateral orientations of the leaves, the unit optical length may be less than the size of a single leaf. In such cases the incident light flux interacts mainly with the first layer of leaves and does not penetrate deep into the foliage. The value of reflectance for such foliage is usually close to that for a single leaf.

The principal results obtained earlier may be compared with some experimental data. Table 2.4 lists the measured values of the reflectance factor for leaves and the foliar system of different plant species. One can note qualitative agreement between the theoretical predictions and the experimental data. Within the range of

Table 2.4

Reflectance of Leaves and Crowns of Various Plant Species

	Reflectance (%%) ($\mu_o = 1$)					
	$\lambda = 550-590$ nm			$\lambda = 710-890$ nm		
Plant species	Leaves ϵ	Crown A	Ratio A/ϵ	Leaves ϵ	Crown A	Ratio A/ϵ
Beech, 65 years	10.8	6.3	0.58	76.0	48.7	0.64
Pine, 30 years	8.6	3.5	0.41	41.6	24.3	0.58
Pine, 160 years	10.4	5.0	0.48	55.8	24.8	0.44
Birch, 40 years	10.3	3.8	0.37	51.7	46.4	0.90
Fir, 80 years	13.2	1.7	0.13	—	—	—

Note. Data adapted from Alexeev and Belov (1960) and Arabashev and Belov (1958).

strong absorption ($\lambda = 550-590$ nm), the measured values of the reflectance factor of crowns are $2-7$ times (fir) smaller than those of leaves. According to theory, the distinctions between leaves and crowns with respect to their reflectance are less expressed in the longwave range of the spectrum ($\lambda = 710-890$ nm), where the leaves are much brighter.

Of course it would be unreasonable to expect precise quantitative agreement between the measured data and the values calculated on a theoretical basis. Deviations may be due to the initial simplifying assumptions of the theory and to natural experimental irregularities.

In the near infrared ($\lambda = 800-1300$ nm) the leaves of most plant species are very "bright" as they absorb only a small percentage of radiation ($\epsilon = 0.9-0.95$). The three-dimensional foliar systems are also very "bright" in this spectral region. The trees in infrared photographs usually look snow white.

As one can see in Fig. 2.15, the ratio of the albedo of a foliar system to the scattering factor of a single leaf, A/ϵ, tends to unity as the scattering factor increases. The organization of separate leaves in a three-dimensional foliar system significantly affects the radiative parameters of the plant in the region of PAR and in the far-infrared region, but practically it has no influence in the spectral window within $700-1700$ nm. Therefore, the heat radiation of the Sun is absorbed very faintly by separate leaves and by volume foliar systems. On the contrary, the absorbance of far-infrared rays by leaves is strong. The joining of many of leaves into a complex foliar system increases the absorbance still more to almost 100%. That makes the absorbing and, consequently, the radiative properties of a plant in the region of its proper thermal radiation (wavelengths from about 2000 nm; maximum at 10,000 nm) very close to the properties of an ideal black body. This promotes the release of surplus heat from a plant by means of emission.

The peculiarities of the light-absorbing functions of complex foliar systems may be assumed to accomplish certain roles in the life of plants. The extremely widespread occurence of foliar systems as a universal mode of organization of the light-absorbing organs of plants, due to natural evolution, favors such an assumption. It may be that the main reason that foliar systems are so widely ranged in nature is not stipulated by their higher efficiency of capturing light. In fact, the difference between the abilities of an individual leaf and a complex foliar system to absorb incident light is small, with values of about 90 and 95%, respectively. In contrast, the reflectance values of separate leaves and volume foliar systems significantly differ, by a factor of 2 (10 and 15%, respectively) in the case just considered. It seems more probable to suppose that the real reason why foliar systems are so spread widely in the plant kingdom is due to their higher reliability. The light-absorbing ability of individual leaves is more dependent upon the direction and intensity of incident radiation than that of foliar systems. In other words, the occurrence of multifoliar light-capturing structures is more significant in view of their reliability than their efficiency.

Chapter 3

Arrangement of Energy Relations in Plants

INTRODUCTION

There are many possible points of view from which a plant may be contemplated, from the aesthetic view of a painter to the pragmatic one of a forester. Even within the confined domain of a scientific approach, the ways of looking at plants may be extremely diverse. The view of plants as energy-converting engines deserves special consideration (Spanner, 1963). Such an approach is not comprehensive and only reflects a single facet of the many-sided problem in question. It is, however, of fundamental significance in obtaining an adequate picture of plant energetics.

Plants are the largest consumers of energy on Earth. Green vegetation covers more than 135 million km^2 of land on five continents and captures a large amount of solar energy every year. Plants convert a small part of this solar energy into chemical energy and annually more than 100 billion tons of biomass. In this way plants fulfill the role of providing for the perpetual functioning of the entire biosphere, including more than 6 billion human beings. The flow of solar energy pours into living matter through the leaves of plants and drives the immense multitude of biochemical processes that make matter living.

The energy flow is the actual driving force of all vital processes. Energy is a conserved entity, and thus its total amount remains constant in any process. Whenever we speak of the consumption, spending, or usage of energy, we do not mean that its quantity changes. The quantity remains the same, but the quality changes. In any spontaneous process the qualitative level of energy decreases; thus, energy degrades due to transformation into heat at the temperature of the surroundings. This change in quality enables the energy flow to perform work. The vital activity

of plants or any living organism is also driven in such a way. As H. Spencer stated, the degradation of energy and the organization of matter is the essence of life (Henderson, 1917).

The process of the degradation of energy as it flows through a living system is followed by a corresponding increase in entropy. Thus, the waste energy flow that leaves a plant carries away a greater amount of entropy than the entering flow brings in. In this way energy flow continuously washes out of a living system excess entropy generated within the organism by a multitude of irreversible processes. A highly organized and correspondingly low entropy state of the living organism is maintained. Looking from a thermodynamic point of view allows one a more contemporary conception of the energetics of life. This conception was formulated in succinct form by Schroedinger (1955) in his remarkable book "What is Life?" Schroedinger stated that all living beings feed upon negative entropy. Plants get their negative entropy and energy from sunrays, while animals get it by eating plants (as well as other animals). It should be noted here that the "negative entropy" is merely entropy with a negative sign (Brillouin, 1963). A decrease in entropy is identical to an increase in negative entropy. The point of such a substitution is connected with our routine mode of perception. Any favorable effect is usually associated with obtaining something (in this case negative entropy), not with the loss of something else (entropy).

STRUCTURE OF ENERGY PROCESSES IN PLANTS

Figure 3.1 shows in a very simple outline the general scheme of energy processes in plants. A profuse flow of energy passes through the plant. The entering energy flow is high-temperature (low-entropy) solar radiation. Almost all of the energy obtained by the plant is then removed as low-temperature heat radiation, with water vapor, and by direct heat exchange with air. In any case the energy leaves the plant at a temperature near that of its surroundings at about 300 K. Thus, the effluent energy flow is associated with much higher entropy than the influent one. Each kilojoule of radiated heat carries away with it about 4.4 entropy units (e.u. = joules per kelvin), whereas the incident radiation, depending on its effective temperature, brings in only 8–20% of this value. The continual pumping of entropy out of the plant is of fundamental significance as a prerequisite for maintaining the high organizational level of the plant organism.

The energy flow that passes through a plant initiates a flow of water through its transport systems. The flow of water brings requisite soluble substances to a plant and removes excess heat from it. A small fraction of the energy received is involved in the photosynthetic process, which provides a plant with organic materials needed to build its structures: roots, stems, branches, and leaves. A plant stores about 1% of the total amount of incident energy in these materials.

A plant uses a greater share of the energy obtained to perform its various in-
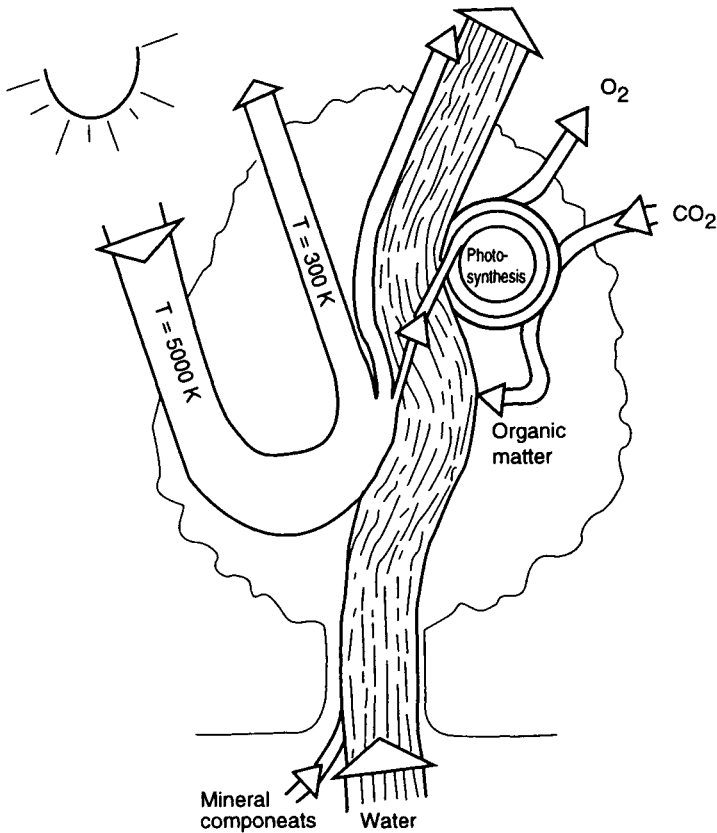
Figure 3.1 Simplified scheme of energy processes in plants.

trinsic vital functions, such as the transport of water through the xylem, with-drawal of nutrients from the soil, growth, reproduction, and defense against bio-logical rivals. All these functions are essential constituents of a plant's life. A plant has to spend the majority of its total energy resource to carry them out.

The flow of water conjugated with the energy flow that passes through a plant, is large. A plant passes 300–700 kg of water or even more through its structures for each kilogram of organic material formed. The energy needed to evaporate this mass of water exceeds the energy stored in a crop by about 100 times. It should be noted that the water flow is not only a means of cooling the plant under the Sun's hot rays but is also an effective mechanism for washing away excess entropy. The plant draws water out of the soil as a liquid and puts it into the atmosphere as vapor. The entropy content of this vapor is much higher than that of the liquid phase. The difference equals 6.6 e.u./g of water. Thus, for each kilo-

joule of heat leaving the plant with evaporated water, about 2.7 e.u. is being removed.

The main source of energy for plants is solar radiation. This source of energy is generally considered to be the only one of which plants make use. Although this is the conventional wisdom, it is not exactly true. Aside from the Sun's radiation, plants employ a supplementary source of energy, the difference in chemical potential of water between soil and air. The role of this additional energy source will be discussed in detail. Both sources of energy feature low density and high variability depending upon many factors such as the season of the year, time of day, and meteorological conditions.

Plants use energy in two types of processes: quantum and thermophysical. The processes of the first type are performed by microscopic mechanisms, which are driven by single quanta of light. Thermophysical processes are set into action by mass and energy flows and are realized by macroscopic systems. Photosynthesis is an example of a quantum process, whereas transpiration is a thermophysical one.

The basic energy relations in the plant may be depicted in more detail as shown in Fig. 3.2. Photosynthetic processes produce organic matter. Some of it is used to form various parts of the plant's structure. Another portion of synthesized matter is "eaten" by the plant itself. This process is called "respiration" and is quite similar to the process of respiration in animals. During respiration organic substances are oxidized to CO_2 and H_2O, while energy-rich compounds, such as ATP
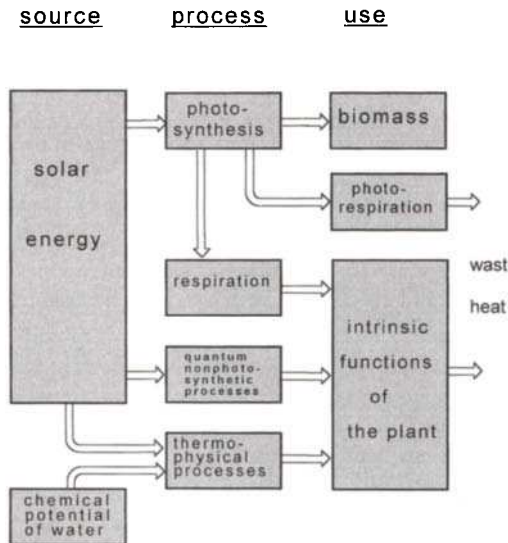

Figure 3.2   Generalized sketch of energy relationships in plants.

(adenosine triphosphate), are formed. This compound is used by living organisms as a universal energy carrier to drive various biochemical processes (Lehninger *et al.*, 1993). The only significant difference between respiration in plants and in animals is the origin of the "food" that they use. Plants create food themselves, whereas animals must search or hunt for their meals. By creating an excess of organic matter, plants store energy in chemical form and can consume it afterward when and where a need arises. By the process of respiration, up to one-half or an even larger portion of synthesized products may be consumed by the plant for its own needs.

Some plant species spend a good deal of primarily synthesized organics in another process called photorespiration (Orgen and Coollet, 1982; Osmond and Grace, 1995). The mechanism of this process is quite different from that of respiration (Leegod *et al.*, 1994). First, this process occurs only in light. Second, photorespiration, in contrast to respiration, does not produce energy-rich compounds, but instead significant amounts of ATP are consumed. The actual role of photorespiration in plant physiology still is not quite clear at this point, but it is supposed to participate in the metabolism of nitrogenous compounds. The process of photorespiration is also considered to be the consequence of the competition of CO_2 and O_2 for RuBP (ribulose bisphosphate), the key component that allows the primary act of binding carbon dioxide in photosynthesis, (Salvucci and Ogren, 1966). A few plant physiologists have searched for ways of enhancing plant productivity by inhibiting photorespiration (Zelitch, 1992). However, such an approach does not seem reasonable: our ignorance in relation to the process of photorespiration should not be taken as a reason to consider it to be useless or counterproductive. Were it really so, it would have been eliminated by evolutionary mechanisms.

In this situation a hypothesis based on purely thermodynamic factors may be advanced. One may suppose that photorespiration is necessary to maintain the entropy balance of the plant. The light is a very "pure" form of energy and it brings to the plant too great an excess of negative entropy. The plant uses photorespiration to get rid of this excess. This issue will be contemplated in more detail later.

A certain amount of solar energy absorbed by the plant is involved in quantum nonphotosynthetic processes. Its distinction from the photosynthetic one lies in the lack of a terminal synthesizing module. Therefore, it does not produce carbohydrates, as the photosynthetic process does, but only the energy-rich intermediates. In this way a plant can supply part of its energy needs in a more immediate and thrifty mode while avoiding the intermediate synthesis of such stable products as carbohydrates.

Both photosynthetic and nonphotosynthetic quantum processes in the plant start from a high-energy event in which a molecule of light-sensitive pigment absorbs a quantum of light and acquires energy in that way. Its value sums to 1.8 eV,

exceeding the mean energy of the thermal motion of a molecule at room temperature by 40–50 times. In contrast to quantum processes, all thermophysical ones are low energy. The increment of energy, which a molecule of water obtains when evaporated, exceeds its mean energy of thermal motion by no more than several times. Nevertheless, the total amount of energy involved in thermophysical processes in plants may be many times greater than that involved in quantum ones.

Thus, plants gain energy from two sources. This energy is necessary for the plant to perform the full assortment of its vital functions. These functions are rather diverse. Plants are self-sufficient organisms (at least most plant species) and they provide all that is needed to live, if external conditions are permitting. The totality of the functions plants have to carry out is shown symbolically in Fig. 3.2 within a common rectangle. A list of these functions, most likely incomplete, is as follows:

- sucking water from soil and carrying it through xylem capillaries to leaves
- extraction of mineral components from soil
- symbiotic fixation of nitrogen
- extraction of carbon dioxide from air
- synthesis of a variety of organic substances
- gathering the products of photosynthesis from an expanded surface of leaves
- transport of metabolites through phloem system
- intracellular movement of cytoplasm (cyclosis)
- maintenance of an electrochemical potential difference on cellular membranes
- propagation of electrochemical impulses
- building of plant structures on a cellular and macroscopic level
- adaptation of internal processes to changing external conditions
- regulatory processes
- movements, such as tropism

These processes are not energetically equivalent. Some of them demand a large expenditure of energy, whereas others are less "laborious" for the plant. Unfortunately, the existing information concerning the energy "costs" the plant must "pay" to perform its physiological functions cannot be considered sufficient and reliable. This is the most obscure topic of plant energetics.

Nevertheless, it seems possible to obtain some plausible estimates from general considerations. As a first step, one has to evaluate the theoretical minimum energy needed for performing a distinct process. After that, one has to make a more or less plausible assumption about the efficiency of the process under examination. The estimated value must not be too little, because a very ineffective process would have been eliminated by natural evolution. On the other hand, the value assumed must be not too large because such a process would be unstable and strongly

dependent upon external conditions. The complexity of the process under consideration must be taken into account as well. Complicated processes that run via many consecutive steps may have a lower total efficiency than more simple ones.

THE PLANT AS AN OPEN SYSTEM

The term "open" is used in thermodynamics to define systems that exchange mass and energy with their surroundings. In contrast to open systems there are "closed" ones, which exchange only energy but not mass, and "isolated" systems, which can exchange neither mass nor energy with their surroundings.

Plants are open systems, just as other living beings are. The "openness" of living organisms is a necessary prerequisite for their being alive. Only under conditions of continual exchange of mass and energy with the surroundings can organisms be maintained in a state far from equilibrium. If the exchange is stopped for any reason, in other words if the system becomes closed or isolated, it will degrade to the equilibrium state in accordance with the second law of thermodynamics. The terminal result of a such process is the transformation of a living organism into a mass of dead matter. The degradation may be comparatively quick if the normal level of metabolism in the living system is high or, on the contrary, it may proceed slowly if the metabolism is extremely slow, as for example in dormant seeds.

To avoid degradation and stay alive for a sufficiently long time, the organism must remain open and must pass energy and mass through itself. These flows are necessary to pump out entropy, which is generated in the organism by its vital processes. The storage of energy by the organism and the assimilation of substances play only a secondary role in this respect. For these needs only a minor share of the total mass and energy flows is branched out. A plant stores only about 1% of the incoming energy flow and less than 1% of the total mass flow that passes through its body in its biomass formed by photosynthesis.

It will be useful to define a quantitative measure for the openness of an organism. Unfortunately it is almost impossible to do this unequivocally and any definition adopted would be unavoidably conventional. It seems reasonable to characterize the "openness" by the ratio of the area through which a flow of energy or mass enters or leaves the organism to its volume. The value obtained may be taken as a measure of openness. Its dimension will be that of reciprocal length. Accordingly, the inverse value may be reckoned to be the "equivalent thickness" of the organism under consideration. Therefore, values obtained in this way will depend upon which flow is taken into account, whether it is the flow of water or the flow of radiant energy. Again, for the flow of water one could have at least four significantly different values of area: the total area of the roots including root hairs, the area of the roots without hairs, the total area of the leaves, or the total

cross-section area of the open stomata on the leaves. The resulting values differ by several orders of magnitude. It seems more reasonable, therefore, to take the energy flow as the basis for estimating a conventional measure of the "openness" of a plant. It may be defined as the ratio of area of the leaves to the net volume of the plant. Values estimated in such a way may have only limited meaning. In any case they may be used for the qualitative comparison of different organisms with respect to their "openness." This way one may obtain a value of about 10^3 m^{-1} as a more or less reliable figure of the openness of a foliar tree. Thus, its equivalent thickness is about 1 mm. This is, within an order of magnitude, the average distance of an arbitrary inner point of a tree from the outer medium.

The openness of a real plant is determined by the joint influence of a variety of factors. By this it is evident from the simplest geometric reasons that an increase in openness must facilitate the processes of energy and mass exchange of the plant with its surroundings. On the other hand, processes of distant transport should become more complicated due to the thinning and lengthening of their pathways. The increase in openness may also favor the formation of a more fragile and tender mechanical construction of the plant. Also, organisms with a higher degree of openness will be more vulnerable to various damaging agents, such as infections or the invasion of blights. Depending on the conditions of growth, the actual value of openness of a plant may vary within a broad range even for the same species.

It seems probable that the degree of openness of plants increased during evolution, at least in its early stages. Ancient plants had no leaves, as evidenced by paleontological data, but had thick shoots containing green photosynthesizing cells (Stewart, 1983). Over the course of time these shoots evolved by thinning and flattening, thus gradually finding forms characteristic of the leaves of present-day plants.

PLANTS AND ANIMALS: COMPARATIVE ENERGETICS

Plants in their totality play the role of prime engine of the biosphere. They capture solar radiation and convert it into the chemical energy of organic matter. All that they need to live, they produce themselves. In this respect plants are *autotrophs*. The representatives of the other biological kingdom, the animals, to which we belong, are *heterotrophs*. They can live only by consuming the organic substances synthesized by plants and breathing the oxygen that is also produced by plants. Thus, one may consider these two groups of living organisms, plants and animals, as complementary components that in conjugation provide for the functioning of the biosphere. One should bear in mind that there is significant dissymmetry between plants and animals. In a certain sense plants are more versatile. They can synthesize organic matter and consume the substances produced to obtain energy by respiration. For animals only the latter process is available. Figure 3.3 shows a generalized scheme of the interrelations between the two fundamental
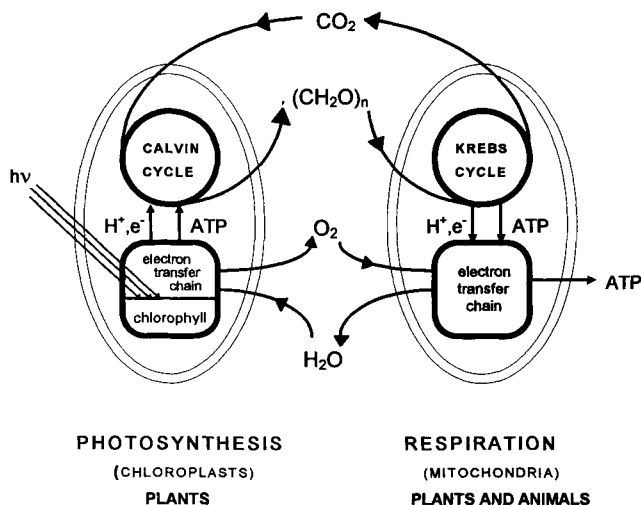
Figure 3.3 Photosynthesis and respiration, two complementary processes that provide for the functioning of a biosphere.

energy conversion processes in the biosphere, photosynthesis and respiration. The cycle shown at the left of the scheme is performed by plants, while that at the right is performed by both plants and animals.

The main topic of this book is the energetics of plants. Nevertheless, insofar as the life processes of plants and animals are bound tightly and inseparably, it may be of interest to compare the basic principles of energetics between these two groups of living organisms. The fundamental diversity of their energetics depends upon the nature of the energy that they use. Plants use energy in its "pure form": light energy is the energy of a high-frequency electromagnetic field. It is not bound up with any substance. In contrast, animals use chemical energy that becomes available only in the course of reactions between appropriate substances. These two forms of energy differ significantly. Chemical energy can be stored easily and used when necessary. In contrast, radiant energy cannot be stored and must be used instantly at the moment of its incidence.

Radiant and chemical energies are also dissimilar in a qualitative respect. The quality of energy may be defined as the amount of negative entropy that it brings in. In this respect the energy used by plants significantly surpasses that used by animals. Each kilojoule of solar radiation brings in about three units of negative entropy (joule per kelvin). The quality of energy used by animals is much lower. Each kilojoule obtained by the oxidation of glucose brings in only 0.33 unit of negative entropy, almost 10 times less than the same amount of radiant energy. This factor is of fundamental significance: to maintain approximately the same level of structural and functional organization, an animal has to consume about 10

times more energy per unit of its mass than does the plant. This ultimately determines the basic distinctions between plants and animals.

Radiant energy, which is available everywhere and is characterized with very high quality and low density, determines the relative chemical autonomy of plants, their expressed tendency to create complicated structures, and their almost total absence of locomotive activity. The chemical energy used by animals is much more concentrated, but its quality is much lower and it is not so widely available. Certain efforts are required to obtain it. These needs determine the primary features of animals: mechanical autonomy, high locomotive activity, and total chemical dependence upon autotrophs. The principal attribute of plants is the building of structures and that of animals is locomotion.

We can try to illustrate the most significant consequences that follow from the different nature of energy used by plants and animals. For this purpose it seems reasonable to compare some characteristics of a plant and an animal of approximately equal mass, say about 70 kg (Schmidt-Nielsen, 1984). A plant of 70-kg mass may be represented by a young tree, whose typical characteristics may be as follows:

- weight = 70 kg (roots, 15–20%; trunk and branches, 30–40%; foliage, up to 50%)
- height = 4–4.5 m
- diameter of the trunk = 8–10 cm
- total volume occupied = 20 m^3 (crown = 15 m^3, root system = 5 m^3)
- radius of a crown = 1.5 m
- cross section of a crown = 7 m^2
- area of leaves (one side counted) = 25 m^2
- share of leaf volume in the total volume of a crown = 0.2%
- total quantity of chlorophyll in the leaves = 5 g
- receipt of radiation (in sunny weather) = 20 MJ/hr (about 5 kW)
- total productivity = 32 g (0.7 mol) of CO_2 fixed per hour, 0.12 mol of glucose synthesized
- efficiency of utilization of radiant energy = 2%
- volume of air in contact with leaves = 100–150 m^3 or more per hour

Both subjects are shown in Fig. 3.4 for comparison. By looking at the geometric parameters of a plant and an animal of equal mass, one may see that the plant has a structure that is much looser with regard to energy flow. The plant occupies a total volume about 300 times larger than that of the animal. Their characteristic dimensions, as defined earlier via degree of openness, are about 1 mm for the plant and about 5 cm for the animal. It stands to reason that all of the values quoted here may vary within a broad range depending on specific circumstances, such as the kind and age of the tree and environmental factors. Nevertheless, the principal
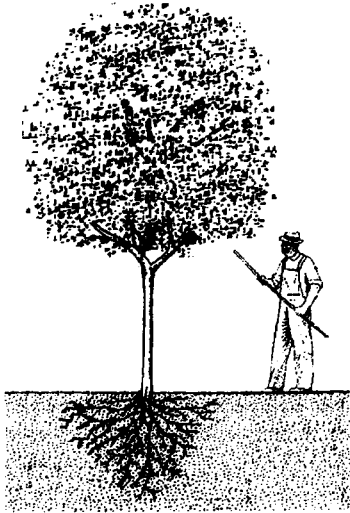
Figure 3.4 Two organisms of equal mass (70 kg) that belong to the plant and animal kingdoms.

peculiarities, which distinguish the two group of living organisms, plants and animals, remain valid. One may say briefly that the plant's life proceeds in tighter contact with the surrounding medium than the animal's. In this sense the plant is a much more "open" system.

Thus, the kind of energy used by living organisms determines the general features of their structure. Nature "designs" creatures by considering the conditions of their life (Rashevsky, 1965; Rosen, 1967). This can also be seen when comparing the energy parameters of plants and animals. Table 3.1 presents the data for such a comparison. The data of Table 3.1 show that the total energy load of a plant

Table 3.1

**Comparison of Energy Parameters of Plants and Animals
with the Same Mass of about 70 kg**

Parameter	Unit	Plant	Animal
Energy load	kJ/kg · day	500–5000	~150
Metabolism	kJ/kg · day	10–40	~150
Mass flow	kg/kg · day	0.25–1.0	0.04–0.07
Metabolism to mass flow ratio	kJ/kg	~30	~3000
Volume of air in contact	m³/hr	100–150	0.3–1.0
Characteristic dimension	mm	1–2	50–70

may be much higher than that of an animal. This may take place on a hot summer day under the direct rays of the sun. However, the specific power of metabolic processes is noticeably higher in animals than in plants. The level of metabolism markedly depends upon the dimensions of the organism. It is almost 3 times higher in a rat and about 3 times lower in an elephant than in a human being. A similar relationship between size and metabolism is also inherent in plants. Animals use their energy resources more economically and effectively, involving in metabolic processes almost all the energy they obtain. In contrast, plants use a significant share of the energy obtained in processes of a thermophysical type that are not immediately linked with metabolic processes.

Plants bring in and pass through their "bodies" immense quantities of water, more than 1000-fold more than that directly needed for photosynthesis. The water acquisition capacity of all the vegetation over Earth's surface is so great that only 10,000 years would be enough for plants to deplete the oceans if they were not continuously filled with rain. It is possible to say in a figurative sense that plants, which came out of the ocean about 400 million years ago, still pull it through their bodies. This ability could not have been maintained for such a long time as only an inheritance from their ancestors if they gained no advantages from it. In fact as the plants came out of the water, they found themselves in the field of a water chemical potential gradient. They contrived a way to use this gradient as a supplementary energy source and as an effective means for the removal of entropy.

The necessity for plants to come into tight contact with very large volumes of air is stipulated by the very low content of carbon dioxide in it (about 0.03% by volume). Thus, the plant can extract from each cubic meter of air no more than about 70–100 mg of carbon.

AUXILIARY SOURCE OF ENERGY: WATER CHEMICAL POTENTIAL DIFFERENCE

There is no question that the radiative energy captured and transformed by the quantum mechanism of photosynthesis is at the core of whole plant energetics and biochemistry. Apart from that, however, terrestrial plants use a macroscopic thermophysical mechanism of recovering an additional amount of energy from another source, the difference in chemical potentials of water in the soil and water in the air. This difference is present because air and soil usually are not at equilibrium with respect to humidity. The energy obtained from this source can play only an auxiliary role in the life of plants as it cannot actuate microscopic chemical processes. It is employed, however, for performing macroscopic processes such as the long-distance transport of water.

Though the energy recovered from the difference in chemical potentials of water fills only a secondary role, the harnessing of this source of energy turned out

to be a very significant conquest of terrestrial plants. In any case the hypothesis that this factor favored the flourishing of plant species on dry land compared with their ancestors in the water seems plausible. By assuming the diversity of a certain group of organisms as evidence for its evolutionary success one may assert that terrestrial plants have thrived much more than algae. The number of terrestrial plant species exceeds that of their multicellular water-living relatives by at least 2 orders of magnitude.

The manner in which the difference in the chemical potentials of water is used to perform work can be defined as an entropy-driven mechanism. The motive force arises because the transformation of liquid into vapor is associated with an increase in entropy. Therefore, the evaporation of liquid is a spontaneous process. It proceeds until the surrounding atmosphere is unsaturated. The transfer of liquid into the gaseous phase is followed by removal of the latent heat of evaporation.

A plant, at least a vascular plant, represents a structure that links two phases, soil and the atmosphere, via a system of conductive channels through which water can be easily transported. Water in soil is found in a liquid or a bound state, whereas in the atmosphere it is in a gaseous state. The difference between the entropy content of water in the gaseous and liquid states amounts to about 6.5 e.u./g. The heat carried away with water that leaves the plant in the form of vapor is about 2.2 kJ. Thus, due to the evaporation of water through the leaves, the waste heat and entropy are removed from the plant. The total amount of work that can be performed by the evaporation of water may vary within a broad range from 0 to 100–200 J/g or even more depending on the value of the relative humidity of the air. Such amounts of energy should be enough to raise water to a height of 1000–2000 meters.

THE ROLE OF GEOMETRIC FACTORS

Photosynthesis is surely the key process in the life activity of plants. However, plant energetics does not concern only this process. A series of contradictory conditions must be met simultaneously to allow the performance of the photosynthetic process. All components of a photosynthetic reaction, carbon dioxide and water, as well as energy in a suitable form and amount, must be delivered into a certain volume where the appropriate complex of pigments and enzymes is located. The removal of heat and the products formed in the reaction should be provided. The conditions noted can be met without difficulty for a small system, such as a single cell of algae. The transfer of reactants to such a cell and the removal of products from it are provided by diffusion. No significant problems with supplying substances arise unless the cell is small enough. On the other hand the supply of solar energy may be the limiting factor for such cells. Taking into account the solubility of carbon dioxide in water and the value of its diffusion

coefficient, we can estimate the highest possible rate of delivery of CO_2 into a cell. For a spherical cell of 1-μm radius this will be about 10^{-15} mol of CO_2 per second. To assimilate such amounts of carbon dioxide, the photosynthetic apparatus of the cell has to develop a power of about 10^{-8} W. The actual power of energy flux that can be captured by the cell under conditions of direct solar insolation is about 10^{-9} W. Thus, the rate of radiant energy supply may be the controlling factor for a very small cell.

These relations may change, however, with increasing cell dimensions. The diffusion flow into a small is approximately proportional to its radius, whereas the solar energy that may be captured by the cell is proportional to the second or an even higher power of its size. A cell of 10 μm radius will gain about as much energy as it needs to assimilate the full amount of carbon dioxide delivered by diffusion. With a further increase in dimensions the cell will find a growing disproportion between a profuse energy and poor material supply. Thus, a single cell is doomed to remain small.

Quite different relations take place for a macroscopic multicellular plant. A terrestrial plant located on the boundary between the ground and the atmosphere expands its ramified structures into both phases: its branches and leaves into the air and its roots into the soil. In this way the plant creates its own feeding zones from which it can draw requisite substances. Simultaneously the plant promotes the return of water from the soil to the atmosphere.

The solar energy incident upon a plant is approximately proportional to the second power of its radius, whereas the volume of its feeding zones is proportional to the third power of the radius. Thus, increasing a plant's dimensions should not lead to disproportion between energy and material supplies. Moreover, the conditions for mass exchange with its surroundings may be even better for a larger plant.

It should be noted, however, that the very notion of the dimension of a plant is ambiguous and can have different meanings. On the one hand these may be external dimensions such as the height of a tree or the diameter of its foliar crown. In this "global" sense the dimensions of plants may vary within extremely wide limits from millimeters up to more than 100 m. On the other hand one may have in mind a characteristic dimension defined as the ratio of the total volume occupied by the organic mass of the plant to the total area of the surface that separates this volume from its surroundings. The characteristic dimensions of plants, even of different species, vary within a narrow range from tenths of a millimeter up to about 1 cm. The global dimensions of a plant should be kept in mind when considering macroscopic processes, such as the long-distance transport of water and metabolites, or the mechanical features of a plant. Characteristic dimensions make sense in relation to processes on other scales such as the heat and moisture exchange of a plant with air and the delivery of carbon dioxide into the mesophyll of leaves.

The advantages that a large multicellular plant gains over a single cell are re-

alized due to the existence of specialized transport systems. All higher vascular plants possess such systems. These systems, the xylem and the phloem, convey water and dissolved substances in the plant over long distances much more effectively than does simple molecular diffusion. However, certain additional energy expenditures are needed to actuate these systems. These expenditures should grow with an increase in the linear dimensions of the plant due to the lengthening of transport pathways and increases in the volume of material flow. One may expect that the share of transport expenditures in the total energy balance of a plant should increase approximately proportionally to the plant's size. When the size of the plant becomes very large, the functioning of its transport systems may become the restrictive factor in its overall energy balance.

All of the regularities noted previously are derived from simple and generalized geometric and physical backgrounds. They should not be regarded as strict rules, but rather as a first approximation that only reflects trends. Under real conditions these trends may manifest themselves with significant variations depending upon the peculiarities of a specific plant species, such as its structure, conditions of growth and environmental factors.

A more thorough analysis shows that the influence of geometric factors should be more complex. One may see when comparing a young and a more aged tree of the same species that they are not quite similar in a geometric sense. The growth of a tree not only resolves into a geometrically similar enlargement of its size but is also succeeded by a gradual modification of its shape as well. As a tree grows older, an increasing fraction of its total mass is made up by the trunk and branches and the foliage fraction decreases correspondingly. Thus, the plant becomes more ponderous and less exuberant. This is simply the consequence of mechanical restrictions. As the total mass of a tree may be supposed to be approximately proportionate to the third power of its height, the cross section of its trunk should also increase in the same proportion.

Mechanical restrictions significantly influence the geometry of plants, especially for large trees with heavy foliage. Factors that affect the ability of plants to catch light are important. Among these factors are the general configuration of a plant, the regularities of branching, and the form and orientation of leaves. Computer simulations based on accounting for these factors make it possible to trace a virtual picture of the main steps in the ancient evolution of plant structures (Niklas and Kerchner, 1984).

The duality in the question of plant dimensions reflects the specific pecularities of their structure. They have such a characteristic manifestation that even the words that designate these particular structures are broadly used to denote things that bear a resemblance to them. Most common are the branched structures of various natures: we apply the word "tree" to the structure of catalogues, such as a family "tree," a genealogical "tree," and a phylogenic "tree." The principal feature of the tree's structure is not reduced to merely a ramification. The very

point is that the relation of the total area to the overall volume of the plant does not strictly follow the usual regularities inherent in simple geometric bodies. There are reasons to consider that plant structures involve certain properties of fractals.

The term "fractal" was introduced by Mandelbrot (1983). It refers to a broad class of geometric objects in which the property of self-similarity is inherent (Birdi, 1993). This property is recognized when the scale of the system is changed. Two examples of abstract fractal structures are shown in Figs. 3.5 and 3.6. The distinctive feature of such structures is that they show fractional dimensionality. The length of a fractal line may be proportional to a power of its size between 1 and 2. Thus, a fractal line possesses properties intermediate between those of one- and two-dimensional objects. Likewise, the surface area of a fractal object may be proportional not to the second but to a higher power of its dimensions. Fractal structures may occupy a large volume of space with a minimal amount of material by forming a large boundary. One may note that similar structural properties are inherent in plants.

One may illustrate the fractal character of the treelike dendrite structures of plants with Fig. 3.7, where a tree, a leaf, and the details of a leaf are depicted. Some features of resemblance between these structures are evident enough. It seems likely that considering plant structures by using the concepts of fractal geometry may be reasonable.
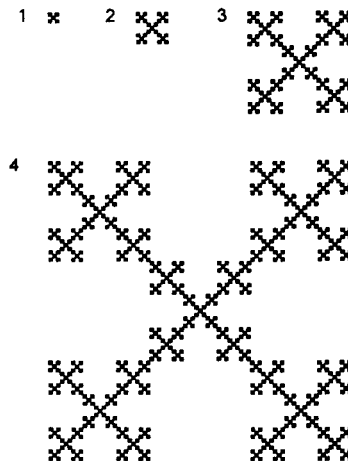

Figure 3.5 An abstract fractal structure (resembling a Ukrainian folk ornament). Each subsequent structure in the series 1–4 (which may be extended farther) repeats the overall shape of the former one, but involves more details. The density of the fractal structure decreases as the complexity increases. So, the square that circumscribes the initial element (1) is 55.5% black (nine squares, of which five are black), whereas (4) is only about 9.5% black $[(5/9)^4]$
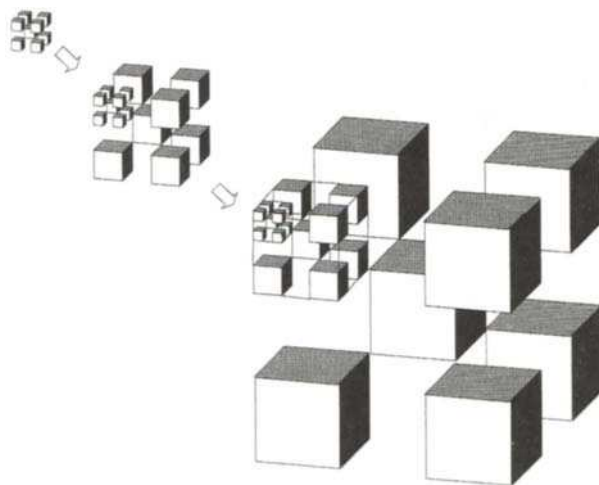
Figure 3.6 An abstract fractal structure in three dimensions; a volume analogue of the former plane model in Fig. 3.5. Each cube of higher order consists of smaller cubes (not all are shown in the picture). The volume of the smallest cube (first order) is 1/3 (9 cubes out of 27) filled, and that of the third order is less than 3% $[(1/3)^3]$ filled.
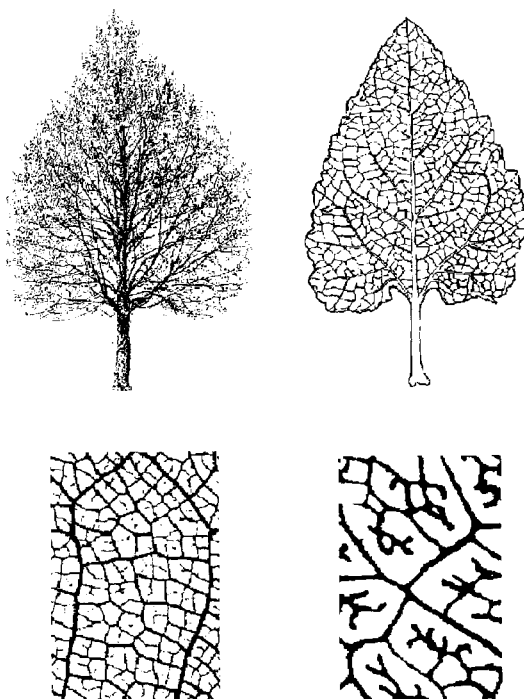

Figure 3.7 Plant structures involve some features of fractals. Subsequent structures in the series: tree, leaf, fragments of a leaf under different magnifications. They all display obvious signs of similarity.

CONVERSION OF SOLAR RADIATION: QUANTUM AND THERMOPHYSICAL METHODS

There are two fundamentally different types of processes that enable the performance of work at the cost of the consumption of solar energy: quantum and thermophysical processes. In quantum processes solar energy is immediately converted into other forms of energy such as chemical or electrical. In processes of thermophysical type, radiation first degrades into heat and only then can this heat be used to operate a heat engine. A solar battery is an example of the utilization of a quantum process in engineering that is analogous to the photosynthetic system of plants in biology. Accordingly, a solar boiler in conjunction with a steam turbine may serve as an example of a thermophysical process. Living beings, however, cannot use a temperature difference to perform work because they usually exist in conditions close to thermal equilibrium with their surroundings, whereas a large temperature difference is necessary for energy-converting systems of the thermophysical type to work efficiently.

Nevertheless, terrestrial plants employ the difference in chemical potentials of water between soil and air as a source of energy along with the quantum process of solar enegy utilization via photosynthesis. The energy from the potential difference is utilized with the help of macroscopic mechanisms. This method of generating energy may be considered a thermophysical process.

The quantum and thermophysical methods of conversion of solar energy differ in the scale of the mechanisms used. In a quantum system the mechanism must be microscopic, capable of operating under the action of a single quantum. Electrons play the role of the working body of such mechanisms. In a solar battery, an electron, after absorbing a quantum of light, moves from valence to the conduction zone of a semiconductor, thus contributing its share to the photocurrent. In a photosynthetic system, the working cycle consists of the alternating transition of an electron in a chlorophyll molecule between the ground and excited state energy levels. In contrast to quantum methods, the mechanisms of thermophysical processes are macroscopic. They use the energy flow of a working body actuated by the difference in temperature, as in the case of a boiler, or by the difference in chemical potentials of water in the case of the transpiration system.

One can explain the distinctions between the two modes of transformation of solar energy with the help of a primitive mechanical model. When waterwheels were still in use, two different types were employed, overshot and undershot wheels. In overshot wheels (Fig. 3.8A) the bowls are filled with water at the upper position and emptied at the lower one. As the filled bowls come down, each portion of water gives all of its potential energy to the axis of the rotating wheel. This energy is proportional to the mass of water in the bowl and to the difference between the upper and lower levels. All of this energy can be transformed into work
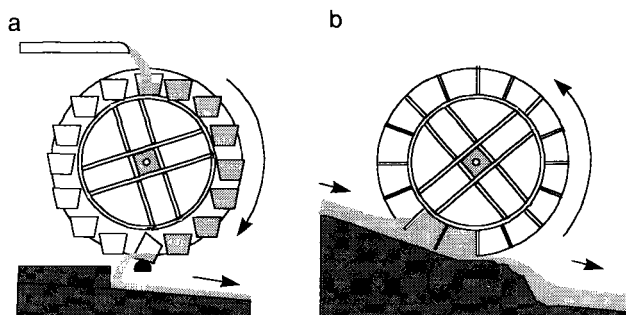
Figure 3.8   Two types of waterwheels. (A) An overshot wheel converts to work the potential energy of the water mass contained in each bowl. The level of the filling grove is the threshold: the energy of water below this level cannot be recovered. (B) An undershot wheel converts a fraction of the kinetic energy of the water stream into work.

provided that friction and other losses are small enough. A wheel of this type can work as long as the headwater is not lower than the level of the filling groove. Otherwise, the wheel will not turn at all. Raising the headwater level can quicken the filling of the bowls and, thus, the rate at which the wheel turns, but the portion of energy obtained from each bowl remains the same.

The undershot wheel (Fig. 3.8B) uses a fraction of the kinetic energy of the water stream. A wheel of this type will turn at any, even a minimum, velocity of the stream, provided that friction is absent. Yet the consumption of the kinetic energy of the stream cannot be complete because water behind the wheel does not stop but continues to flow, carrying a certain amount of energy away.

In the dynamic behavior of these two mechanical systems one may find some features resembling the behavior of the quantum (overshot wheel) and thermophysical (undershot wheel) systems for converting solar energy. Nevertheless one should not attach too much importance to this analogy, or to any other analogy in general. It is presented here exclusively to show more clearly the qualitative distinction between the quantum and thermophysical methods of solar energy conversion.

Any energy-converting system based on the quantum principle is sensitive to the spectral composition of light. To actuate the microscopic energy-converting mechanism, a certain minimum energy is needed. If a photon brings in less energy, the mechanism does not operate. Only the photons with energies above this minimum threshold level can give their energy to the conversion mechanism, as shown schematically in Fig. 3.9. In the case of photosynthesis in green plants the cutoff energy level corresponds to about 1.8 eV (frequency near 430 THz of wavelength of about 700 nm). Excess energy above the threshold level brought in by photons with higher frequencies is dissipated as heat and cannot be used beneficially.
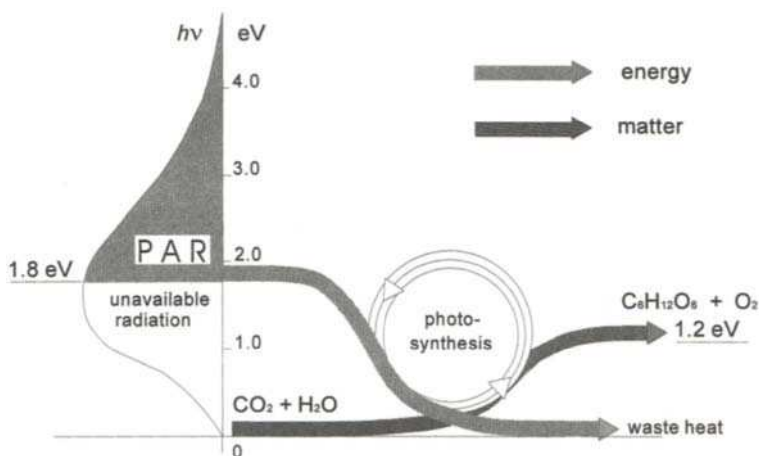
Figure 3.9   The mechanism of photosynthesis harnesses the energy of photons above the threshold level (about 1.8 eV; frequency about 430 THz). The energy of photons below this level is unavailable for photosynthesis. The energy level of the substances that are being formed as a result of photosynthesis (carbohydrates and oxygen) is about 1.2 eV higher than that of the parent compounds (carbon dioxide and water).

On the other hand, the conditions of the function of energy-converting systems of the quantum type are only slightly dependent on the intensity of incident light or the total irradiance. Each act of converting the energy of a captured photon is performed quite alike, irrespective of the power of incident flux. The total irradiance affects only how frequently a single light-converting mechanism operates. In contrast, the efficiency of thermophysical mechanisms is strongly influenced by the integral irradiance and only slightly by the spectral composition of light.

TECHNOLOGICAL PROBLEMS

The photosynthetic activity of plants is a complicated technological process. It seems reasonable to look upon the plant's photosynthetic machinery through a technologist's eyes. In doing so one can trace the intrinsic "logic" of the natural technological systems brought to a very high degree of perfection through more than hundreds of millions of years of evolution. It stands to reason that we are far from attributing nature with the ability of rational design. Nature has other means of refining the mechanisms its creatures use. Unlimited time and the lives of innumerable "experimental specimens" enable nature to create amazingly sophisticated systems excellently adapted for performing corresponding functions. Therefore, analysis of biological mechanisms from a technological point of view is quite

sound. One should bear in mind, however, some peculiarities of nature's mode of "designing." Natural evolution does not possess imagination and cannot jump through imaginary space as an engineer does when designing a new construction. Evolution solely performs continual transformations of its objects, conserving successful versions over a long time. It always uses materials at hand and makes, with each step, only insignificant deviations from the previous examples already explored. For this reason the evolutionary process has even been characterized as "tinkering" (Jacob, 1977). Thus, along with a purely technological analysis, the circumstances of the natural history of plants should be taken into account. For instance, the photosynthetic mechanism in plants is assumed to be descendent from the prokaryote blue-green algae (Margulis, 1981, 1983).

When examining the photosynthetic apparatus one may note its rational arrangement. The dimensions of the apparatus offer sufficiently favorable conditions for the local transport of reacting components by a diffusion mechanism. The primary act of capturing solar energy is then arranged by a group of pigments consisting of from 200 to 400 chlorophyll molecules. This "antenna" is associated with a single center in which the basic reactions occur. An aggregate of the antenna and the reaction center form a "photosynthetic unit." Such an arrangement offers at least two significant advantages. First of all, the absorption of light by an ordered system of pigment molecules proceeds much more effectively than by separate nonbound molecules. Due to the participation of the antenna system in collecting incident photons, the reaction center can work at a rate of about 1000 cycles per second under conditions of direct solar radiation. If the antenna system is absent, 200–400 times more reaction centers would be necessary to provide the same productivity, as each center is loaded only several times per second.

It is essential from a technological point of view that the components of the reaction center complex are incorporated into the thylakoid membrane and arranged there in a definite manner. In this way the concerted running of an intricate succession of the initial "light" stages of photosynthesis is attained. Subsequent "dark" stages are mainly run as volume reactions.

Difficult technological problems are associated with the delivery of carbon dioxide to sites where it should be involved in the photosynthetic reaction. These problems arise because of the very low content of CO_2 in air, about 330 molecules per million in all. Carbon dioxide penetrates into the mesophyll of a leaf mainly by the same pathway through which water vapor leaves: through the open stomata. The usual value of stomatal conductance varies for different plant species in the range $10^{-3}–10^{-2}$ m/s (see also Chapter 9). The concentration of carbon dioxide inside the leaf should not fall below a level of about 200 ppm. If it goes below 50 ppm, the photosynthetic mechanism of most plant species will discontinue absorbing carbon dioxide. Thus, the motive force of the diffusion of carbon dioxide through stomata should be taken to be about 100 ppm, and the values of its flow may be estimated to be about 0.01–0.1 mol/m²/hr. In addition, the counterflow of

water vapor through the stomata should be taken into account. The power of this counterflow may exceed the carbon dioxide inflow by a factor of 300–700 or more. This counterflow of water vapor from the mesophyll to some extent can hamper the inward flow of carbon dioxide. Thus, the amounts of carbon dioxide available for photosynthesis found earlier may be somewhat overrated.

The limiting value of the photosynthetic capability of a leaf can also be estimated by starting from energy considerations. Taking, for instance, the total irradiance to be 800 W/m^2 and the efficiency of photosynthesis to be 2%, one should find a value of about 0.12 $mol/m^2/hr$. This figure is commensurate with the upper value of estimations obtained earlier and exceeds the lower one by many times. The diffusion of carbon dioxide can limit the overall rate of photosynthesis under conditions of high irradiance. Many experimental data confirm this (Berry and Downton, 1982). The well-known effect of the midday depression of photosynthesis that is usually observed on hot sunny days is also connected with diffusional limitations. A plant at high temperature closes its stomata, thus protecting itself from excessive loss of water through transpiration. This also prevents the delivery of carbon dioxide to the interior of the leaves.

Natural evolution has found technological means that enable it to somewhat overcome the difficulties connected with the diffusional limitations of carbon dioxide supply. These means are mainly used by certain plants in hot and arid environments. They are known as the C_4 and CAM (Crassulacean Acid Metabolism) plants (Bassham and Buchanan, 1982; Monson and Moor, 1989). The group of C_4 plants includes corn, sorghum, amaranth, and sugarcane. CAM plants include pineapple, agave, and cacti. Plants such as wheat, barley, beans, potato, and sugar beet are examples of C_3 plants. The photosynthetic systems of C_4 and CAM plants are "improved" compared to the more simple system of C_3 plants by adjusting an additional chemical cycle at the entrance. The scheme of such a cycle is shown in Fig. 3.10. This cycle serves as a "pump" that provides more effective binding of carbon dioxide by the basic photosynthetic systems. In the C_4 and CAM plants, the initial reaction of CO_2 fixation produces four-carbon organic acids (malate, aspartate). Then carbon dioxide is released and fixed again by the normal C_3 system, forming a three-carbon compound. The difference between C_4 and CAM plants is that in the former the two carboxylation systems are separated spatially due to leaf anatomy but they operate simultaneously, whereas in the CAM plants they occur in the same cells but are separated temporally. The CAM plants absorb carbon dioxide and accumulate four-carbon acids during the night and use stored substances for photosynthesis during the day.

Therefore, rotation of the additional cycle requires additional energy, but the process is worth it under appropriate conditions. In any case these biochemical artifices enable plants to almost double their photosynthetic rate at a high radiation load.
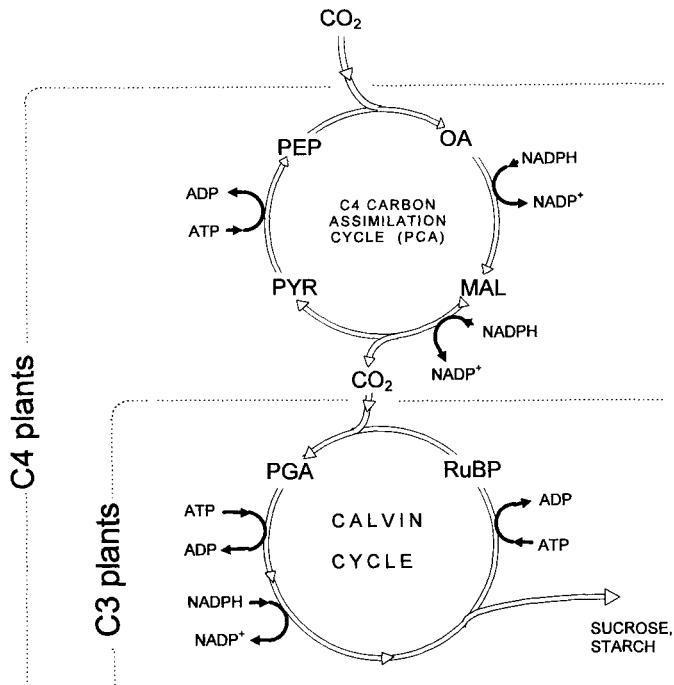
Figure 3.10 Recovery of carbon dioxide by C_3 and C_4 plants. The latter employ an auxiliary "pumping" cycle, thus providing for more efficient functioning of the photosynthetic cycle. PEP, phosphoenolpyruvate; OA, oxaloacetate; PYR, pyruvate; PGA, 3-phosphoglycerate; MAL, malate; and RuBP, ribulose 1,5-bisphosphate.

FIXATION OF NITROGEN

Nitrogen is an indispensable constituent of proteins, nucleic acids, and many other biological substances. The total content of nitrogen in plant biomass is usually 2–3% of their dry weight. Thus, an adequate supply of nitrogen is a necessary precondition for normal growth and development of a plant organism. Although molecular nitrogen is abundantly contained in Earth's atmosphere, about 8 tons per square meter of ground, higher plants are unable to assimilate it immediately. The forms of nitrogen available for plants are ammonia and nitrates. The latter are reduced in the plant to ammonia and in this form are involved in the synthesis of nitrogen-containing organic substances. In agricultural areas where sunlight or water supply does not limit crop growth, biological productivity is determined by the availability of inorganic nitrogen in the soil.

There are three main sources of the "fixed" nitrogen supply in a form available for plants. One is the lightning discharges that produce a certain amount of nitro-

gen oxides that are then transformed into nitrates. There is also the industrial catalytic binding of nitrogen with hydrogen to form ammonia; this process is performed under high pressure (200–1000 atm). In this way a large amount of nitrogenous fertilizers is produced, which meets about one-fourth of the total requirements of agricultural plants. However, the main source of fixed nitrogen for plants is biological synthesis by symbionts.

In contrast to green plants, some species of bacteria possess the capability of binding molecular nitrogen. Among the nitrogen-fixing organisms are several genera of blue-green algae and cyanobacteria. There are free-living forms among them, but those that thrive in symbiotic association with higher plants are of primary interest to us. The most well-known example is the symbiosis of the species *Rhizobium* with legumes. The *Rhizobium* forms nodules in the roots of legumes. The relationship between a host and its symbiont consists of the following. The plant secretes a certain amount of carbohydrates through its roots. The energy released by oxidation of the carbohydrates by the bacterium is used to drive the enzyme system that fixes nitrogen.

The key molecule of the nitrogen-fixation pathway is the enzyme nitrogenase. It consists of two protein components, one containing 24 iron and 2 molybdenum atoms and the other containing 4 iron atoms. The functioning of nitrogenase requires a large quantity of energy. At least 12–24 molecules of ATP are needed to convert 1 molecule of nitrogen into 2 molecules of ammonia. The actual energy consumption is much greater. The maintenance of a guest organism has a high cost in energy for the host plant. It may be as high as 15%, and possibly even 30%, of the net photosynthetic production of the plant (Beevers, 1976). The energy cost of nonsymbiotic assimilation of mineral nitrogen by the plant is much less if its content in soil is sufficient. Thus, the insertion of fixed nitrogen in the form of ammonia or nitrates into soil can relieve the life of plants, but requires vast inputs of energy for the industrial synthesis of such compounds.

Chapter 4

Problems of Integration and Hierarchy of Structures

INTRODUCTION

Problems of the integration and hierarchy of structures arise from the contrast between the microscopic dimensions of light-harvesting molecular ensembles and the macroscopic dimensions of the plant. A leaf, which the surface area is about 50 cm^2, absorbs about 5×10^{20} quanta of PAR from direct sun rays every minute. These myriad quanta are caught and their energy is utilized in individual sets of actions by innumerable of microscopic energy-converting systems distributed over the leaf's area, numbering up to 5×10^{13} units/cm^2 of a leaf's surface. Their joint activity integrated over time and space creates the consolidated energy budget of the plant. This integration is achieved due to the plant's hierarchical structure.

As many quanta fall on such a leaf, as droplets of rain fall annually onto the whole territory of 12 of the northeastern United States, from Maine to Maryland. The area of these states is about 480,000 km^2. The annual rainfall is somewhat above 1 m. Thus, the total amount of water that falls is about 5×10^{11} m^3. Taking the average volume of a droplet to be 1 mm^3, we calculate a value of 5×10^{20} droplets. Any complicated system in which processes occur on vastly different scales assumes a hierarchical structure.
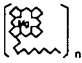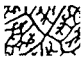
Therefore, the single drops of rain coalesce into little streams, which merge into brooks, which together form small rivers, and then larger ones, and so on. This is an example of a natural hierarchical structure. An electricity supply system may serve as an example of a technical hierarchical structure. In such systems electrical energy is transmitted in long-distance lines under hundreds of kilovolts of tension, over moderate distances the tension is under tens of kilovolts, within

urban regions it is under about 6 kV, and finally consumers receive electricity in their houses at a tension of 110–240 V. Commercial trade distribution systems offer another example of hierarchical arrangements. Complicated systems, whether natural, technical, or social, acquire a hierarchical structure as a means to reduce energy loss. Hierarchical organization enables the use of the most suitable transport mechanism on each level, providing greater efficiency for the system as a whole (Gladyshev, 1988; Nicolis, 1986).

It should be noted that any hierarchical level that is above another level cannot be considered to be the simple sum of the elements belonging to that lower level. In all cases, each step from a given level of the hierarchical staircase to the next one is followed by the development of new features not inherent in the elements of the lower level.

A plant is also a complicated, multilevel, hierarchical system, which provides a very high degree of integration, beginning from the elementary process of catching light quanta and ultimately resulting in the functioning of a macroscopic plant as an entire organism. The hierarchical structure of plants may be examined in a variety of aspects. Table 4.1 shows seven hierarchical levels of mass and energy

Table 4.1

Hierarchy of Structures and Processes of Mass and Energy Transfer in Plants

Hierar-chical level		Structure (and its charac-teristic size, m)	Transfer mechanism	Integration factor (values are tentative)
1		Antenna (2×10^{-8})	Exiton, resonant	200–400 molecules of chlorophyll per photosynthetic unit
2		Thylakoid membrane (5×10^{-7})	Electrochemical	500 photosynthetic units per thylakoid
3		Chloroplast (5×10^{-6})	Diffusion	50 thylakoids per chloroplast
4		Cell (5×10^{-5})	Diffusion, cyclosis	50 chloroplasts per cell
5		Areolae (2×10^{-4})	Diffusion	1000 cells per areola
6		Leaf (10^{-1})	Hydraulics	10^5 areolae per leaf
7		Branches, roots ($1-10$)	Hydraulics	10^4 leaves per tree

transport. The structural elements of each level differ in their characteristic size and integration factor. The overall integration factor can be calculated by multiplying the corresponding factors for each level and may attain quite a large value of about $10^{20} - 10^{21}$ or even more. These values, as well as those for individual levels, should be considered estimates only. They may vary within a wide range depending on the plant species, stage of growth, and conditions of cultivation.

Splitting the real structure of plants into seven levels is somewhat arbitrary. Some levels, such as 6 and 7, which are associated with very large integration factors may in turn be divided into sublevels differing by size but not by mechanism of transport. A multitude of plant organisms existing on a sufficiently uniform area form a plant community sometimes termed phytocoenosis (Daubenmire, 1968; Whittaker, 1975). Examples would be a meadow, a cultivated field, and a uniform parcel of wood. The next level of plant communities may be associated with specific climatic zones of a country that may be characterized by the dominant forms of plant life, such as grassland or rain forest. Such communities are termed "biomes." They may occupy vast areas of land. Finally we come to the top level of the hierarchy, to Earth's vegetation as a whole. Figure 4.1 may help to visualize the range of dimensions within which various aspects of the life of plants can be considered. The analysis of energy relationships in plant communities of various types is of extreme interest, both fundamentally and practically. These questions, however, go beyond the scope of this book. They belong mainly to the field of ecology.
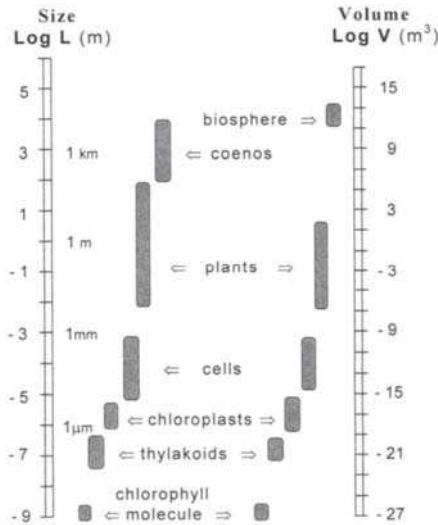

Figure 4.1   Hierarchy of scales related to plant life.

HIERARCHY OF STRUCTURES

The lowest level of the hierarchy of structures is presented by the molecular ensembles that perform the primary acts of photosynthesis. These ensembles, termed the photosynthetic units, have already been considered briefly in the preceding chapter. They are incorporated into the thylakoid membranes, the subcellular structures that in their turn represent the next hierarchical level. Each photosynthetic unit includes a spatially arranged complex of some 200–400 molecules of chlorophyll and other pigments, such as the carotenoids and phycobilins. These complexes act as "antennas" that assist in gathering incident light quanta. The integration factor of the photosynthetic unit is determined by the average number of light-capturing molecules in the antenna complex and subsequently amounts to 200–400 or sometimes more.

The next levels in the structural hierarchy are established by the thylakoids and chloroplasts. The thylakoids are thin flat membrane bags. The photosynthetic ensembles are incorporated into the thylakoid membrane (Fig. 4.2), with each unit occupying about 200 nm² of area. In their turn a number of thylakoids are grouped into lamellar structures termed grana, which form the main content of the chloroplasts. These subcellular particles are surrounded by the external membrane and contain the thylakoid membrane system within (Fig. 4.3). All thylakoid bags within a chloroplast probably are interlinked, thus forming a common internal area. The thylakoid membrane of a chloroplast contains about 1 million photosynthetic units. Chloroplasts are believed to be symbionts descended from ancient green-blue algae (Margulis, 1981). The number of chloroplasts contained in plant cells (Fig. 4.4) may vary within a wide range from 0 (colorless cells) to about 100 per cell, with the average number being about 40. The number of cells is usually about 1–2 million per square centimeter of leaf.

Thus, the sequence of the microscopic levels of structural hierarchy, from mo-
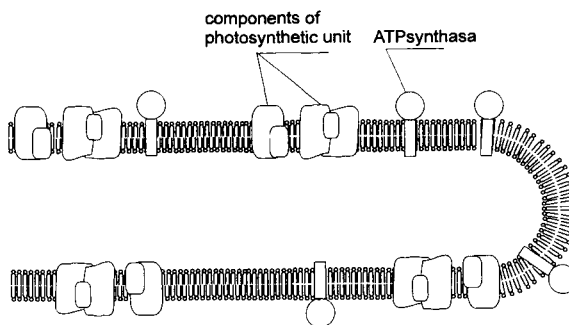
Figure 4.2   Simplified scheme of the thylakoid membrane with incorporated components of a photosynthetic unit and ATP synthase.
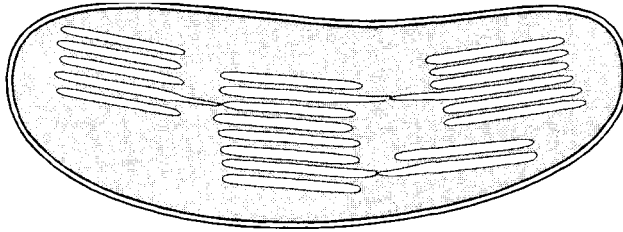
Figure 4.3 Schematic picture of a chloroplast.

lecular to cellular, provides a total integration factor of about 1 billion. The subsequent hierarchical levels relate to the macroscopic structures of the plant. They are primarily connected with the long-distance transport processer of water and metabolites. The leaf area is divided into a multitude of small domains, the areolae, in which single xylem ribs end. The areolae have dimensions of about 0.01 – 0.05 mm² and usually consist of some hundreds of cells. The number of areolae on a leaf 100 cm² in area may be as many as 1 million.

Figure 4.4 Simplified scheme of a plant cell. Only some constituents of the cell are shown: nucleus, vacuole, mitochondria, and chloroplasts.

Leaves are naturally the most significant microstructural elements of a plant. Through the leaves the plant interacts with the environment, obtains energy and carbon dioxide, and gives off water vapor and oxygen. The integration factor on this hierarchical level, in other words the number of leaves on a single plant, may vary 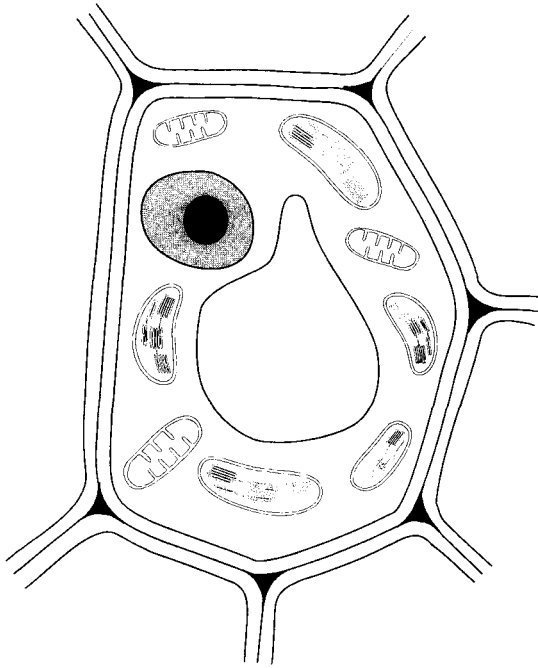from less than 10 to millions depending on the size of the plant, the stage of its growth, and the particular characteristics of any given plant species.

HIERARCHY OF PROCESSES

In analogy to the hierarchy of structures, a hierarchy of processes and corresponding mechanisms also exists. Nature usually picks out the most appropriate mechanism from those available to effect any specific process. So at the initial stage of photosynthesis a quantum of light is absorbed by an antenna complex consisting of some 200–400 pigment molecules. The quantum of light generates an excited state, or "exciton" in the antenna. The exciton may be visualized as a virtual pair of electric charges: an electron in an excited state and a positively charged hole that remains after the electron is lifted up to the higher energy level. The electron and the hole are separated with respect to energy, but they are not separated in space. Thus, the exciton behaves as an electrically neutral, fairly unstable quasi-particle that can move freely across the aggregate of closely packed chlorophyll molecules in an antenna. Once the exciton is created, it then migrates very rapidly from the site of its birth to the reaction center, which contains a specific complex of molecules that perform the primary processes of photosynthesis. It should be noted that the exciton mechanism provides for the effective transfer of energy over extremely short distances (a few nanometers). In this case an excited site in a molecular complex rather than a material particle plays the role of energy carrier. Thus, the antenna system provides for the integration of captured energy over the whole aggregate of some hundreds of chlorophyll molecules.

The next step of integration is electrochemical in nature and is realized on the thylakoid membrane. As soon as the exciton comes to the reaction center, a series of very quick primary processes converts the virtual pair of electric charges into an actual pair of separated charges of opposite signs. These charges move to opposite sides of the thylakoid membrane, thus generating a transmembrane electrochemical potential difference. The transmembrane potential is not localized but distributed over the whole area of the thylakoid membrane. The action of a multitude of reaction centers localized in the thylakoid is integrated over time and area in this way. The generation of a transmembrane potential provides a spatial and time separation between the primary and subsequent stages of the photosynthetic process. The energy stored at the thylakoid membrane as a result of the separation of charges at a reaction center can be used in other parts of the thylakoid. This makes the system more flexible.
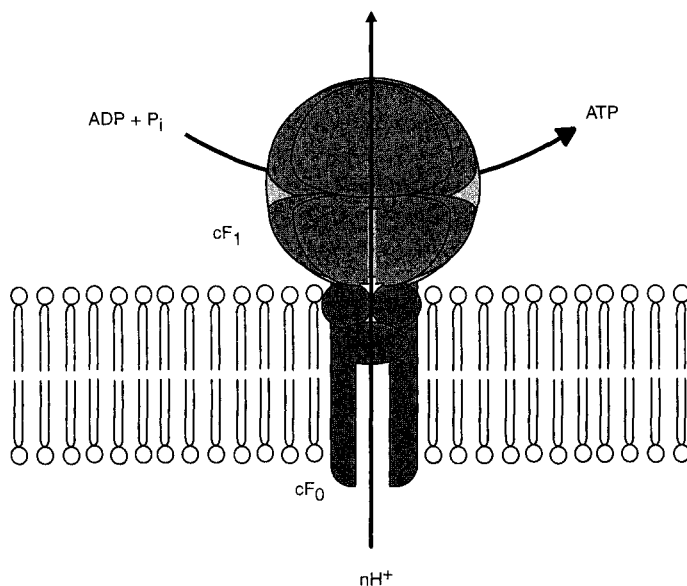
Figure 4.5 Hypothetical structure of ATP synthase.

The transmembrane electrochemical gradient serves as the driving force for ATPase, the enzyme that synthesizes ATP. The ATPase is incorporated in the thylakoid membrane and is driven by the outward flow of hydrogen ions from the inner volume of the thylakoid (Fig. 4.5). The molecules of ATP produced by a number of the ATPase complexes distributed over the membrane area then serve as energy carriers in the reaction of binding carbon dioxide. These dark reactions of photosynthesis proceed in the stroma, a matrix that fills the space between the thylakoid and the outer membrane of the chloroplast. A fraction of the ATP produced in chloroplasts permeates into the cytoplasm, where it is involved in various processes that occur in the cell.

The use of ATP as the energy carrier is based on its hydrolysis reaction, which proceeds with the participation of corresponding enzymes and is followed by the release of energy:

$$ATP + H_2O \rightarrow ADP + P_i + nH^+$$

where P_i represents inorganic phosphate.

The standard Gibbs energy of this reaction is equal to -34.5 kJ/mol at pH 7.0. Under the actual conditions in the cell the energy of hydrolysis may be higher, up to 50 kJ/mol. At the cellular level of organization many processes are dependent upon the consumption of ATP. However, this energy carrier is reactive and therefore should not be used too far from its site of generation. The transport of such a

labile substance over long distances should produce significant losses due to de-composition along the pathway. For similar reasons ATP cannot be stored and must be consumed as soon as possible after generation to reduce futile losses of energy.

At macroscopic levels energy carriers much more stable than ATP are used. These are the soluble sugars. They are quite stable and can be transported for long distances or stored for long periods without notable decomposition. On the other hand, more complicated biochemistry is needed to recover energy from such en-ergy carriers.

Thus, the change from one energy carrier to another in going from processes on one scale to those on another is quite natural. It reflects the compromise be-tween two factors, the stability of the carrier and the complexity of its processing. The long-term storage of energy is usually realized in the form of highly stable, insoluble polysaccharides such as starch.

The hierarchical organization of a plant's structure is not an accident of nature but an ordered method of joining a multitude of microscopic elements into a uni-fied system. In this way, elementary processes are integrated into the concerted vital activity of the plant. Hierarchical organization ensures minimization of losses over the entire chain of energy transformations and provides for the effective func-tioning of the system as a whole.

HIERARCHY OF TIME

One may view hierarchical relations in the plant from a somewhat different perspective to examine the photosynthetic and associated processes with respect to time. The diagram in Fig. 4.6 shows that the characteristic times of different processes in the plant vary within an exceedingly wide range, differing over about 18 orders of magnitude. It starts with the absorption of a quantum of light by a pigment molecule. Light quanta are massless particles that exist only when they move at the speed of light. At the moment the quantum is stopped, it ceases to exist but gives rise to something else, the exciton. It is almost impossible to rig-orously define the duration of this event. One may estimate it to be commensurate with the duration of several oscillations of the light wave, which is about 10^{-14} s.

The exciton may move very quickly across the aggregate of closely packed chlorophyll molecules. Its travel may last from about 50 to 200 ps (10^{-12} s) until it arrives at the reaction center (Pearlstein, 1982). After the exciton arrives at the reaction center, a sequence of reactions proceeds that leads to the separation of charges and the development of a potential difference across the thylakoid mem-brane. This sequence of reactons takes about 10^{-5}–10^{-4} s. The transmembrane potential is maintained at a constant level due to the continual arrival of new quanta. This potential serves as the energy source for a variety of reactions that
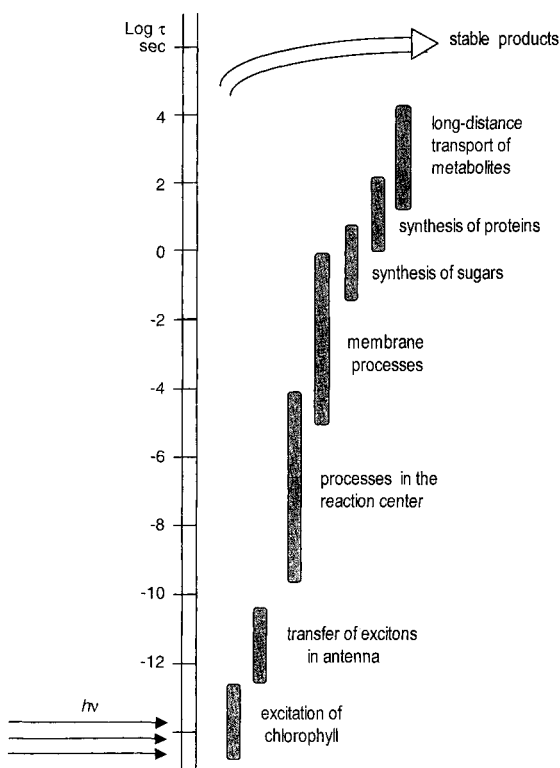
Figure 4.6   Hierarchy of characteristic times of processes in plants.

proceed with the involvement of enzymes localized in the membrane. In particular, the transmembrane electrochemical potential difference actuates ATP synthesis and the decomposition of water. The formation of reducing substances, which are used later to reduce carbon dioxide, also proceeds on the membrane. The membrane processes cover a time range from about 10^{-5} up to 1 s.

The subsequent multistage cyclic processes that perform the reduction of carbon dioxide and the synthesis of sugars use the energy released during the hydrolysis of ATP and the reducing power of corresponding substances. A characteristic rate of these cyclic processes is measured in seconds. Minutes are needed for the synthesis of more complicated substances, such as proteins.

Macroscopic plants are organized so that there are specialized organs to perform different physiological functions. The leaves capture light and synthesize metabolites, while the roots use these substances as an energy source to withdraw water and mineral components from soil and accumulate excess synthesized mat-

ter for long-term storage. These specialized organs may be separated from each other over large distances of up to tens of meters for some plant species. The transport systems of plants provide for the delivery of metabolites over such distances at a velocity of 40–120 cm/hr. Given that the transport channels may be many meters in length, the total duration of transfer of metabolites can take from one to several hours depending on the size of the plant.

HIERARCHY OF CYCLES

Nature generally likes cycles. The energy flow that occurs is perpetual, whereas the stock of available matter is limited. Nature must rotate material cycles by using that continuous flow of energy. Indeed, what has happened on Earth for billions of years is the building of changing structures from the same material powered by the energy delivered continually by photons arriving from the Sun.

The prime energy carriers, photons, and the constructive elements from which the structures are built, atoms, belong to different classes of particles that possess fundamentally different properties. Photons exist only when they move, from the moment of emission to their absorption. Photons may appear and disappear. Thus, their number is not constant. In contrast, atoms are conserved particles. They may be combined in many complicated structures, but their total number remains invariable (excluding the domain of very high energies). Thus, as matter is conserved, cycling of matter is the corollary; this is the only way to maintain life on Earth.

The functioning of biological catalysts, enzymes, may be considered the simplest type of cyclic process. The enzyme cycles within its state: it interacts with molecules of specific compounds, and when the reaction is complete it frees itself from the products formed, reverting to its initial status. All this may occur without changing position in physical space. Various enzymes cycle at different rates. Some of them can perform hundreds of thousands of cycles per second (e.g., carboanhydrase, peroxidase), while others require seconds for each cycle (e.g., protein-kinase). The enzymes that catalyze simple reactions usually cycle more quickly than those performing complicated ones.

Other types of cyclic processes are represented by various mediators and energy carriers. They loop between the sites where they are activated and the sites where they may give up excess energy. So adenosine triphosphate is produced from adenosine diphosphate (ADP) and inorganic phosphate with the participation of ATP synthase. The ATP is then used as an energy carrier in a multitude of processes that occur in cytoplasm. The energy is released while ATP undergoes hydrolysis and converts to ADP and inorganic phosphate. The reaction of ATP hydrolysis is the reverse reaction of its synthesis. It is performed with the help of the same enzyme ATP synthase, which works in the opposite direction. It is termed ATPase in this case.

   The transfer of active hydrogen in the form of highly reduced substances such as nicotinamide adenine dinucleotide phosphate (NADPH) occurs in a similar way. NADPH is formed by the addition of protons and electrons to the oxidized form NADP$^+$:

$$NADP^+ + H^+ + 2e \rightarrow NADPH$$

This process, as well as the synthesis of ATP, occurs on the thylakoid membrane. NADPH is then used in the reduction of carbon dioxide.

   The next level in the hierarchy of cycles is represented by cyclic metabolic and catabolic sequences of reactions. These cycles play a very significant role in biochemistry. As an example, a simplified scheme of the reducing pentosophosphate cycle (Metzler, 1977) also known by the names of its discoverers as the Calvin or Calvin–Benson cycle, is depicted in Fig. 4.7. In brief, the cycle functions in the following manner. A carbon dioxide molecule reacts with a molecule of ribulose 1,5-bisphosphate (RuBP), a phosphorylated five-carbon sugar. Addition of the carbon dioxide to the sugar is catalyzed by the enzyme RuBP carboxylase (Rubisco). As a result, two molecules of 3-phosphoglycerate are formed. They undergo a further series of reactions involving ATP and NADPH, the former as the energy source and the latter as a reducing agent. In each turn of the cycle one molecule of CO_2 is fixed and the initial Rubisco enzyme is regenerated. Three turns of the cycle give a three-carbon compound, glyceraldehyde 3-phosphate. Two such molecules formed within six turns of the cycle may couple to form a molecule of glucose. This, the total result of rotation of the Calvin cycle may be written in chemical terms as follows:

$$6CO_2 + 12NADPH + 18ATP \rightarrow C_6H_{12}O_6 + 12NADP + 18ADP + 18P_i + 6H_2O$$
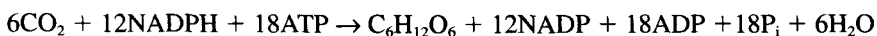
The Calvin cycle may be regarded as one of the most significant reaction systems of plant biochemistry as it is at the core of the dark stages of photosynthesis, where energy derived from absorbed quanta is used to build organic molecules.

   In the preceding chapter, Fig. 3.10 shows the scheme of an auxiliary four-carbon cycle used by C_4 plants to pump additional amounts of carbon dioxide into the main Calvin cycle. In this cycle molecules of carbon dioxide react with phosphoenolpyruvate (PEP) to form the four-carbon oxaloacetic acid (OAA), from which malic and aspartic acids are formed. Carbon dioxide is then released from these four-carbon acids and refixed by the normal Calvin cycle, whereas the remaining pyruvic acid undergoes phosphorylation and reverts to PEP.

   Along with the reduction of carbon dioxide, photosynthesis includes an oxidative process: water decomposition followed by oxygen evolution. This process requires the detachment of four electrons from two water molecules in a single act. Accumulation of the four-electron deficit at the catalytic center needed to decompose two water molecules also occurs as a cyclic process in which the corresponding complex gives away these four electrons in four subsequent steps, each

1.   **RuBP + CO₂ → 2 PGA**

BINDING OF CABON DIOXIDE

ⓟ - phosphate group PO_3^{2-}

RuBP - ribulose 1,5-bisphosphate
PGA   - 3-phosphoglycerate
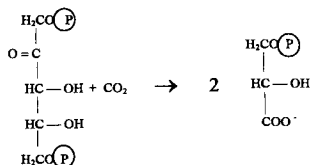
2.   **PGA → DPG**

PHOSPHORYLATION

BPG - 1,3-bisphosphoglycerate
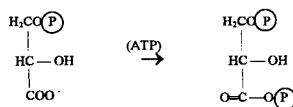
3.   **DPG → GAP**

REDUCTION

GAP - glyceraldehyde 3-phosphate
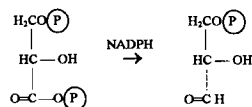
4.   **5 GAP   →   3 Ru-5-P**

CONDENSATION

Proceeds as a complicated
sequence of reactions

Ru-5-P - ribulose 5-phosphate
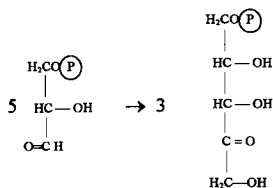
5.   **Ru-5-P → RuBP**

PHOSPHORYLATION

Regeneration of ribulose 1,5-bisphosphate
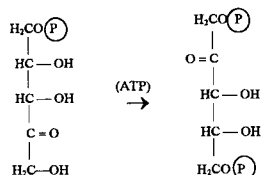
Figure 4.7   The C_3 photosynthetic carbon reduction cycle (Calvin–Benson cycle).

induced by the absorption of a photon. The cycle is complete and the complex
returns to its initial state after the withdrawal of four electrons from water
(Fig. 4.8).
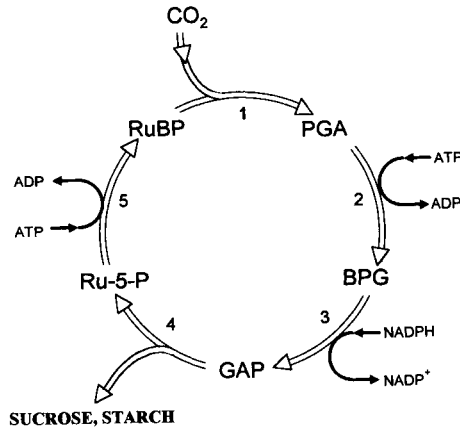
Figure 4.7—*Continued*

The scheme of the tricarboxylic acid (TCA) or Krebs cycle, which performs a function inverse in a sense to that of the Calvin cycle, is shown in Fig. 4.9. It provides for the oxidation of glucose to carbon dioxide and produces ATP and the reduced forms of the active hydrogen carriers, NADH and flavin adenine dinu-
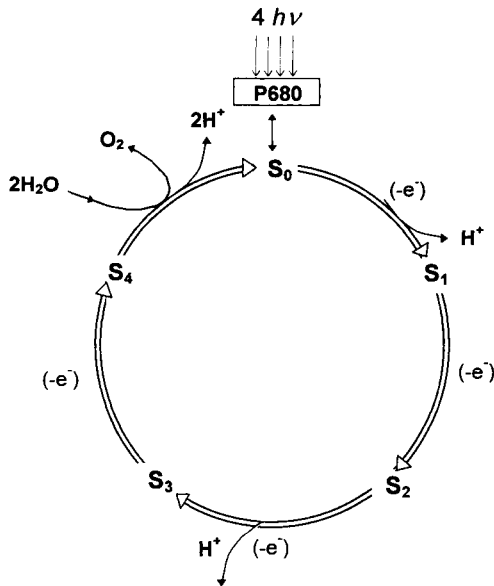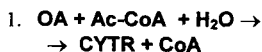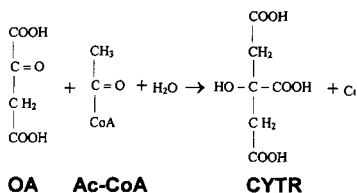

Figure 4.8 Cycle of accumulation of oxidative power needed to oxidize water to molecular oxygen.

1. **OA + Ac-CoA + H₂O →**
   → CYTR + CoA

OA - oxaloacetate
Ac-CoA - acetyl-CoA
CYTR - citrate

$$
\begin{array}{c}
\text{COOH} \\
|\\
\text{C}=\text{O} \\
|\\
\text{C H}_2 \\
|\\
\text{COOH} \\
\textbf{OA}
\end{array}
\;+\;
\begin{array}{c}
\text{CH}_3 \\
|\\
\text{C}=\text{O} \\
|\\
\text{CoA} \\
\textbf{Ac-CoA}
\end{array}
\;+\;\text{H}_2\text{O}\;\rightarrow\;
\begin{array}{c}
\text{COOH} \\
|\\
\text{CH}_2 \\
|\\
\text{HO}-\text{C}-\text{COOH} \\
|\\
\text{C H}_2 \\
|\\
\text{COOH} \\
\textbf{CYTR}
\end{array}
\;+\;C_1
$$

2. **CYTR + NAD⁺ →**
   → KGLT + CO₂ + NADH

KGLT - α-ketoglutarate

Reaction proceeds via
several stages

$$
\begin{array}{c}
\text{COOH} \\
|\\
\text{CH}_2 \\
|\\
\text{HO}-\text{C}-\text{COOH} \\
|\\
\text{C H}_2 \\
|\\
\text{COOH} \\
\textbf{CYTR}
\end{array}
\;+\;\text{NAD}^+\;\rightarrow\;
\begin{array}{c}
\text{COOH} \\
|\\
\text{CH}_2 \\
|\\
\text{CH}_2 \\
|\\
\text{C}=\text{O} \\
|\\
\text{COOH} \\
\textbf{KGLT}
\end{array}
\;+\;\text{CO}_2\;+\text{NADH}
$$

3. **KGLT + NAD⁺ + H₂O →**
   → SUC + CO₂ + NADH
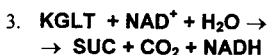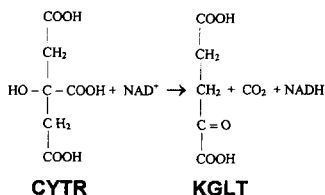
SUC - succinate

Reaction proceeds via
several stages

$$
\begin{array}{c}
\text{COOH} \\
|\\
\text{CH}_2 \\
|\\
\text{CH}_2 \\
|\\
\text{C}=\text{O} \\
|\\
\text{COOH} \\
\textbf{KGLT}
\end{array}
\;+\;\text{NAD}^+ + \text{H}_2\text{O}\;\rightarrow\;
\begin{array}{c}
\text{COOH} \\
|\\
\text{CH}_2 \\
|\\
\text{CH}_2 \\
|\\
\text{COOH} \\
\textbf{SUC}
\end{array}
\;+\;\text{CO}_2\;+\text{NADH}
$$

4. **SUC + FAD + H₂O →**
   → MAL + FADH
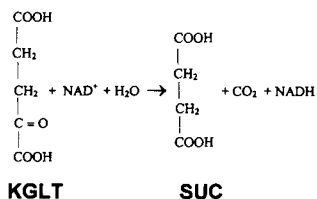
MAL - malate

Reaction proceeds via
several stages

$$
\begin{array}{c}
\text{COOH} \\
|\\
\text{CH}_2 \\
|\\
\text{CH}_2 \\
|\\
\text{COOH} \\
\textbf{SUC}
\end{array}
\;+\;\text{FAD} + \text{H}_2\text{O}\;\rightarrow\;
\begin{array}{c}
\text{COOH} \\
|\\
\text{HCOH} \\
|\\
\text{CH}_2 \\
|\\
\text{COOH} \\
\textbf{MAL}
\end{array}
\;+\;\text{FADH}_2
$$

5. **MAL + NAD⁺ → OA + NADH**

Regeneration of oxaloacetate

$$
\begin{array}{c}
\text{COOH} \\
|\\
\text{HCOH} \\
|\\
\text{CH}_2 \\
|\\
\text{COOH} \\
\textbf{MAL}
\end{array}
\;+\;\text{NAD}^+\;\rightarrow\;
\begin{array}{c}
\text{COOH} \\
|\\
\text{C}=\text{O} \\
|\\
\text{C H}_2 \\
|\\
\text{COOH} \\
\textbf{OA}
\end{array}
\;+\;\text{NADH}
$$
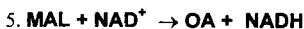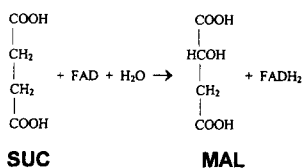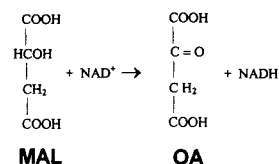
Figure 4.9   The tricarboxylic acid cycle (Krebs cycle).

cleotide (FADH₂). This cycle is the core of the respiration process. The initial compound, glucose, does not enter the cycle immediately but is oxidized in preliminary stages to form two acetyl groups (CH₃CO). Each of these groups temporarily binds to a molecule of the coenzyme CoA, forming the complex acetyl-CoA. In this form the acetyl group enters the cycle where it is added to oxaloacetic

Figure 4.9—*Continued*

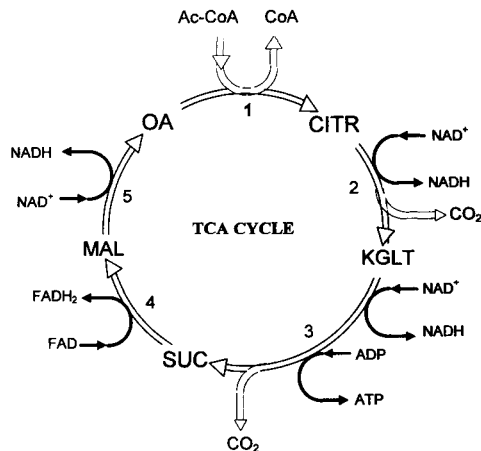acid to form citric acid. In a series of subsequent stages, the oxidation of two carbon atoms to CO_2 and the regeneration of oxaloacetic acid occur. Oxidation of carbon compounds is followed by the reduction of NAD^+ into NADH and FAD into $FADH_2$. ATP is formed simultaneously. Three molecules of NADH, one molecule of $FADH_2$, and one molecule of ATP are formed in each turn of the cycle. The cycle turns twice for each molecule of glucose oxidized.

The fundamental distinction between the Calvin and Krebs cycles is obvious. The former provides for the creation of complicated molecules from simple ones at the expense of consumed energy. The latter performs the inverse function of energy acquisition at the expense of the consumption and conversion of complicated substances into simple ones.

We have shown here only some examples of cycles on the biochemical level. In fact the total assembly of biochemical processes in any living being is represented by a multitude of various cycles. They are all interconnected and form a network of cycles. Even looking at the simplified schemes depicted here one may see that each cycle is linked with at least several other cycles, as in the loops in which the ATP/ADP and $NADPH/NADP^+$ systems circulate. In the figures referred to earlier only arclike fragments of these loops are shown.

The abundance of cyclic processes in biochemistry is not merely the corollary of the finiteness of matter and perpetuity of energy flow. The cyclic systems of reactions offer increased stability due to feedback effects. Moreover, as was shown by Eigen (1971) and Eigen and Shuster (1979), cyclic systems consisting of many links, the hypercycles, may manifest abilities of competitive selection and self-organization. These properties of hypercycles can be assumed to be an effective means of natural evolution.

Moving beyond the scope of plant energetics, one can see higher levels of hierarchy of cycles in nature. There are various cycles of physiological activity synchronized by day and night alternations. More pronounced are the annual physiological cycles. Sometimes they also have a certain relevance to plant energetics. For instance, the mineral components lost in autumn with dead leaves are reused in the spring for the formation of new foliage. The life cycles of living beings, associated with an alternation of their haploid and diploid forms, represent the next level in the hierarchy of cycles (Fig. 4.10). These cycles may be of intricate structure for certain species (Raven, 1986); Villee and Dethier, 1971).

The ecological level presents a great variety of examples of cyclic processes involving different types of organisms that interact in very intricate manners (Kershaw, 1974; Odum, 1971, 1983, 1988). The extreme complexity of such systems makes investigation of them difficult, but more significantly the complexity of natural ecological systems provides their stability.

The integral activity of the entirety of the lower hierarchical levels of the biosphere causes the turning of great biogeochemical cycles on the top of a hierarchical pyramid. These grand cycles rotate as a result of the functioning of all organisms living on Earth, mainly the plants (Fig. 4.11). Thus, all of the carbon dioxide contained in the atmosphere performs its cycle of transfer with living matter within 5–10 years. Within 4000–6000 years plants restore the full content of atmospheric oxygen. The water cycle lasts about 8 million years. Within this time
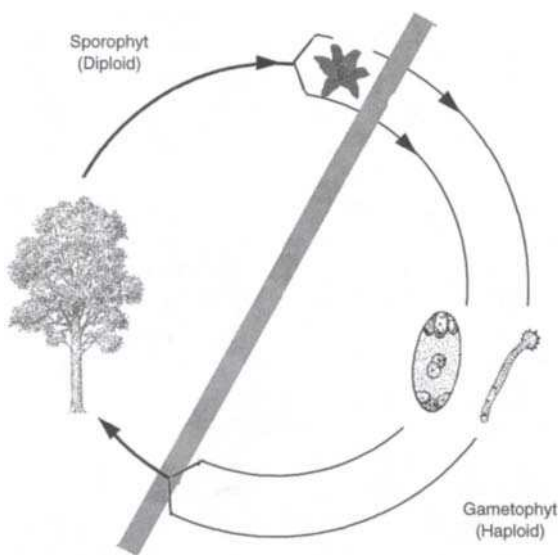

Figure 4.10 Typical life cycle of plants. Alternation of haploid and diploid forms, containing single and double sets of chromosomes, respectively.
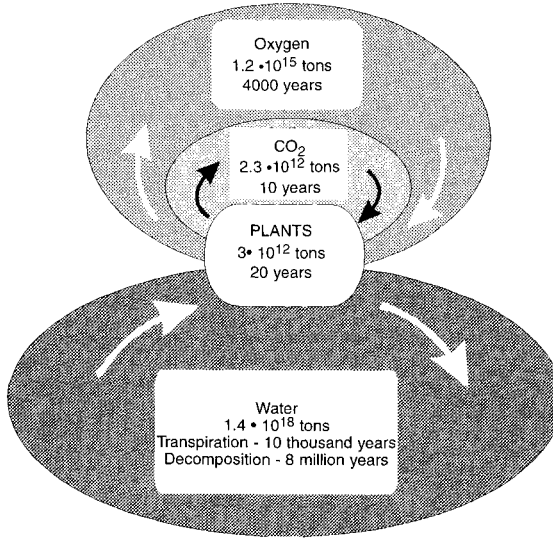
Figure 4.11 Biogeochemical cycles.

plants decompose as large an amount of water as is contained on Earth in all the oceans and seas.

HARVESTING ENERGY

A plant collects energy incident on the spread surface of its leaves. Suppose a leaf of 100 cm² in area receives up to 8 W of solar radiation from direct sun rays. A fraction of this energy, usually a few percent of the total flux, is converted into the chemical energy of metabolites. In this form it is gathered over the whole area of the leaf and removed through the thin capillaries of a phloem to the stalk. Collection of the metabolites over the leaf area requires a certain amount of energy. It seems quite reasonable to expect that the expenditure of energy for harvesting the metabolites formed will depend upon leaf size and other factors.

One may attempt to examine the process of harvesting energy in detail by using a simple model. Let us imagine a round leaf of radius R on a stalk of radius r_s, as shown in Fig. 4.12. If p is the rate of accumulation of energy in metabolites formed on a unit area of the leaf in a unit of time, then the total energy yield equals $P = \pi R^2 p$. Let G denote the energy capacity of the metabolite formed. The power of the metabolite flux crossing a concentric section of radius r of a leaf is

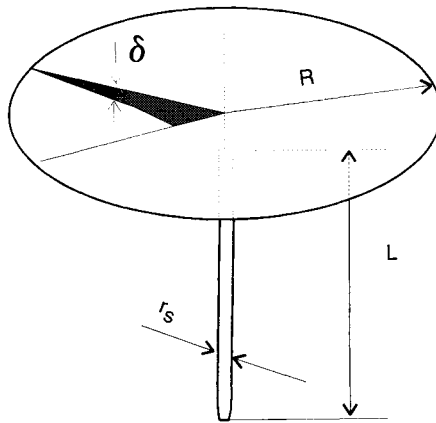$$J(r) = \pi(p/G)(R^2 - r^2). \tag{4.1}$$

Figure 4.12   Model of a leaf.

One must now make a reasonable assumption concerning the regularity of distribution of the motive force, which drives metabolite flow through the conducting pathway along the radius of a leaf. The question of the radial distribution of cross section of the transport channels in a leaf or their effective thickness is important. A straightforward assumption about the uniformity of thickness of transport channels along the leaf radius seems unsatisfactory. It would follow from such an assumption that different parts of the transport system would be loaded nonuniformly, with the central part of a leaf overloaded and its periphery underloaded. Such a construction of the transport system would be inefficient with respect to the excessive consumption of material to build it or the superfluous expenditure of energy to make it work. In biological systems neither version would be viable and both would be eliminated by natural selection. Therefore, it seems more reasonable to assume a uniform motive force tension along the transport pathway. To meet such a condition, the cross section of the phloem should grow from the periphery to the center of a leaf.

By using X as the motive force that drives metabolites through the phloem and assuming that it is constant, we can find the effective thickness of the conducting layer of a leaf as a function of its radius:

$$\delta(r) = \frac{J}{2\pi rkX} = \frac{p(R^2 - r^2)}{2rkXG}.   \tag{4.2}$$

Here k is a coefficient that features the transport capabilities of the structure through which the metabolites are conveyed.

By assuming that the tension in the stalk is equal to that in the leaf itself, its value can be found:

$$X = p\alpha/Gk,   \tag{4.3}$$

where α is the integration factor, which is the ratio of the leaf area to the cross section of phloem in the stalk: $\alpha = (R/r_s)^2$. The usual value of α is about $(1-5) \times 10^4$ for the leaves of many species.

Now the energy dissipation in the transport system can be found in the following way:

$$W = \int_0^R JX \, dr = \left(\frac{2\pi}{3}\right)\left(\frac{pX}{G}\right)R^3. \tag{4.4}$$

Thus, the efficiency of the process of harvesting energy over the leaf area equals

$$\eta = 1 - W/P = 1 - \frac{2}{3}\left(\frac{p\alpha}{G^2k}\right)R. \tag{4.5}$$

As one can see, the efficiency of collecting energy should diminish with an increase in leaf size. The maximum power that can be gathered in a stalk is

$$N_{max} = \frac{\pi}{3}\left(\frac{G^4k^2}{p\alpha^2}\right). \tag{4.6}$$

Such power can be attained at the leaf radius $R = G^2k/p\alpha$ with a low efficiency of just $\eta = 1/3$ (33%).

It should be reasonable to evaluate the biological quality of a leaf as an energy-collecting system by allowing for the ratio of the power collected to the mass (or the volume) of the system. As the radial distribution of the phloem's effective thickness is given by Eq. (4.2), its total volume can be found by integration along the radius. Accounting for Eq. (4.3), this gives

$$V = \int_0^R \delta(r)r \, dr = \frac{2}{3}\left(\frac{\pi p}{kXG}\right)R^3 = \frac{2}{3}\left(\frac{\pi R^3}{\alpha}\right). \tag{4.7}$$

Thus, the ratio of the net power collected in a stalk (N_n) to the volume of the transport system at a given value of N_n, which is the density of incident energy flux (p), can be expressed as follows:

$$\frac{N_n}{V} = \frac{9\pi}{4}\left(\frac{G^2kp}{N_n}\right)\eta^2(1 - \eta). \tag{4.8}$$

This ratio has its maximum at $\eta = 2/3$. Under such conditions the most favorable relationship between the efficiency of energy capture by a leaf and the quantity of organic matter needed to build it is maintained. To fit these conditions the leaf radius should be as half as large as in the case of maximum power, when $R = G^2k/2p\alpha$. The net power obtained under optimum conditions should also be one-half that of the maximum.

It should be noted that under other conditions the maximum value of efficiency may be different. Say under the condition of a given leaf size (R), the power to volume ratio will be

$$\frac{N_n}{V} = \frac{9}{4}\left(\frac{G^2k}{R^2}\right)\eta(1 - \eta). \tag{4.9}$$

In this case the highest value of the specific power N_n/V will be attained at an efficiency of 50%.

An assumption that the natural systems of harvesting energy are optimized for the parameter of the specific power seems quite sound. One must bear in mind, however, that biological systems usually are not rigidly optimized in relation to any single parameter. The life of a plant is under the influence of a set of continuously changing environmental factors. Therefore, its structure cannot simultaneously accommodate all of them in an optimum way. It reflects a compromise between adaptations to different effects. Even the conception of the optimum itself becomes ambiguous in relation to biological systems. The problems of optimization in biology have attracted great attention and have been discussed in detail (Rashevsky, 1965; Rosen, 1967). What may be concluded in brief is that the structure of living beings meets a certain *satisfaction principle* rather than *the principle of an optimum,* the former being more lenient than the latter. Thus, the expectation of strict agreement between the experimental data and the predictions of simple theory is not very reasonable. Nevertheless, the deviations from optimum cannot be too great. In any case, the theory set forth specifies, at least qualitatively, the basic regularities that should be observed as the result of the influence of different factors.

For instance, in considering the expression for the optimum radius of a leaf, one may expect that shaded leaves (lower values of p) should be larger than leaves in direct light. Another relation that can be expected is that of a decrease in the integration factor (α) with an increase in leaf size. In other words, the small leaves of a given species should have relatively thicker stalks than the large ones. Of course such a comparison may only be valid within the confines of the same plant species. Besides, one should take into account that the real thickness of a leaf, as well as that of its stalk, is significantly greater than the effective thickness of the transport pathways defined earlier because the cross section of the phloem composes only a fraction of the total cross section of corresponding structures.

The strong (quadratic) dependence of the optimum radius of an energy-collecting system upon the power capacity of the energy carrier (G) is of great significance. It determines the possible scale of the system.

The model of the transport system for harvesting the products of photosynthesis from the leaf area considered earlier is simplified. The transport system was assumed to be a layer of continuous conductive medium, with the thickness of the layer varying along a radius of the leaf. The real structure of the transport system of a leaf is somewhat different. It may be imagined to be a large number of think capillaries of phloem that go from the stalk of the leaf to the areolae all over the leaf surface. Thus, each capillary ends in the corresponding areola and provides for removal from the areola of the metabolites formed there. Water is delivered to the areolae in a similar way through the capillaries of the xylem. As the number of areolae in a leaf is rather large, the problem that arises is how this multitude of transport capillaries should be organized in such a way that each

could reach its corresponding areola. This problem is solved by the plants according to two main schemes. In plants known as dicotyledons (dicot plants), the capillaries enter the leaf plate as a thick midrib that then branches regularly into secondary ribs, then again into ribs of a third order, and so on until single capillaries reach the areolae. The venation of the leaves of such plants is reticulated. Plants known as monocotyledons (monocot plants) use other principles of venation, with a parallel orientation of ribs from which short single capillaries branch aside.

The leaves of different species of dicot plants show a great variety of forms, but the main pattern of their venation is always reticulated. The leaves of these plants usually have commensurate width and length. In contrast the leaves of monocot plants are stretched in length, with a ribbonlike shape being characteristic for the leaves of these plants. The conducting ribs in the leaves of monocot plants are ordered in parallel. Most grasses have such leaves. Examples of typical leaves of monocot and dicot plants are shown in Fig. 4.13, and the schemes of their venation are shown in Fig. 4.14.

The model of the transport system examined earlier evidently more closely corresponds with the geometry of the leaves of dicot plants. This model may be modified, however, quite easily with regard to the ribbonlike leaves of monocot plants. Here the total amount of energy incident on a leaf is $P = pL^2/\beta$, where β denotes the length to width ratio of the leaf: $\beta = L/b$. By repeating all of the previous derivations and accounting for corresponding modifications, we obtain the following expression for the effective thickness of the transport system:

$$\delta(x) = \frac{p}{kXG}(L - x).\qquad(4.10)$$

Accordingly, for the efficiency of the harvesting process one obtains

$$\eta = 1 - \frac{1}{2}\left(\frac{p\beta}{G^2k}\right)L.\qquad(4.11)$$

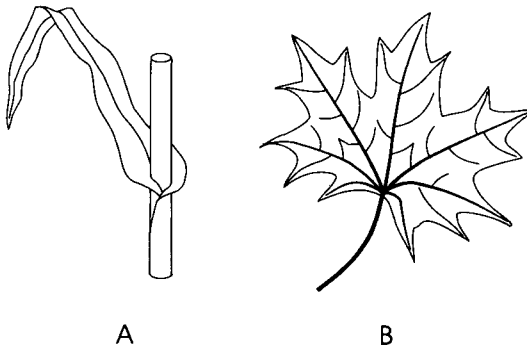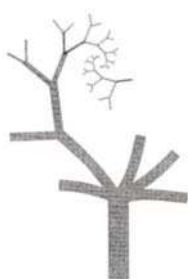A   B

Figure 4.13 Typical leaves of monocot (A) and dicot (B) plants: (A) maize; (B) maple.

times equals zero (sessile leaves) and seldom exceeds 3]. By taking γR to be the length of the stalk and $\pi R^2/\alpha$ for its cross section, we get the following corrections to the expressions found earlier. For the efficiency:

$$\eta = 1 - \left(\frac{2}{3} + \gamma\right) \frac{p\alpha}{G^2 k} R. \qquad (4.14)$$

For the radius of a leaf that provides maximum power:

$$R = \frac{G^2 k}{p\alpha} \bigg/ \left(1 + \frac{3}{2}\gamma\right). \qquad (4.15)$$

For the maximum power that can be gathered:

$$N_{\max} = \frac{\pi G^4 k^2}{3 p \alpha^2} \bigg/ \left(1 + \frac{3}{2}\gamma\right)^2. \qquad (4.16)$$

The efficiency in this case remains the same at 33%, but the power, $N_{\max}$, may be significantly lower. Thus, the length of the stalk is usually commensurate with the leaf radius or may even surpass it by 2–3 times. The radius of a leaf, which would provide maximum power, should be estimated to be several times less than in the case when only the plate of the leaf was taken into account. Correspondingly, the maximum power will be diminished by 5–25 times. Thus, the presence of stalks in the leaves of dicot plants levels out to a great extent the real differences in specific features between the leaves of both types of plants.

The leaves of most species of dicot plants contain long stalks. At the same time, the presence of a stalk decreases, as we have seen, the specific parameters of the leaf as an energy-gathering system significantly. A reasonable question arises from this contradiction: Why do leaves have stalks when this requires additional energy consumption and thus diminishes the net efficiency of their energy-harvesting function? On the one hand this means that the specific feature of the transport systems of a leaf, its power to volume ratio, is not the crucial criterion in the process of natural selection. On the other hand, the presence of a stalk as a necessary part of a leaf can hardly be explained by purely "constructive" reasons. One may think that the real cause of why the leaves of dicot plants are bound to stems or branches with long, flexible stalks is that this allows the leaves to move freely. They sway even under the lightest breath of wind, functioning as an aerodynamic device similar to helicopter blades in autorotation. Due to this effect the local velocity of movement of a swaying leaf against the adjacent layers of air may surpass the initial wind velocity by many times. This significantly promotes the processes of heat and moisture exchange between the leaf and its surrounding medium. One may suppose that this is one of the dominant factors in the evolutionary development of leaf forms.

This Page Intentionally Left Blank

Chapter 5

Thermodynamics of Energy Conversion by Plants

INTRODUCTION

   Plants perform energy-transforming processes on an extremely large scale. The conversion of energy by plants must be performed in full accordance with the general laws of thermodynamics. These laws are obligatory for energy-transforming systems of any type, whether natural or artificial.

BASICS OF THERMODYNAMICS

   Thermodynamics presents abstract and generalized approaches that enable the analysis of basic regularities of energy processes, even under conditions where the details of their intrinsic mechanisms are unknown. The methods of thermodynamics are applicable to systems that belong to diverse classes of objects, from stars to living cells (Atkins, 1994; Bazarov, 1964; Lewis and Randall, 1961; Marshall, 1978; Rumer and Ryvkin, 1980; Sivukhin, 1990; Spanner, 1964). The validity of these methods becomes limited, however, when approaching very small systems consisting of only a small number of molecules (Blumenfeld, 1983; Blumenfeld and Tikhonov, 1994; Hill, 1964).

   The basic concepts of thermodynamics are those of energy and entropy. The former concept, energy, relates to the value that quantitatively characterizes the movement of an object or its parts (kinetic energy) or the interaction of the object with its surroundings or that of the parts of the object with each other, which could cause movement (the potential energy). The latter concept, entropy, enables one to characterize the energy state of a system in a qualitative manner. Entropy mea-

sures the degree of coherence of movements and interactions in the system. The value of entropy is low in highly ordered systems and high in chaotic ones. Thus, entropy is a concept applicable to statistical systems consisting of a sufficiently large number of particles.

Thermodynamics is based on principles formulated by generalizing from experimental data: the principle of temperature or the zeroth law of thermodynamics; the principle of energy conservation or the first law of thermodynamics; the principle of entropy or the second law of thermodynamics; and the Nernst postulate or the third law of thermodynamics. The concept of temperature is based on a subjective and imprecisely defined term: the heat of a body. A thermostat will be considered to be a body whose heat capacity is large compared with that of any reference bodies with which the thermostat will be brought into contact. The internal energy of a thermodynamic system is the total energy minus the kinetic and potential energies of the system as a whole.

The first law of thermodynamics is the law of conservation of energy. It states that energy cannot be created or destroyed. Thus, an energy balance should be maintained in any system:

$$dE = dE_{in} - dE_{out}. \tag{5.1}$$

Here dE is the increment of energy in the system, and dE_{in} and dE_{out} are the energy inflows and outflows, respectively. Any transformation of one form of energy into another, say of chemical energy into heat, that may occur in the system cannot violate this balance, as the total amount of energy must remain unchanged.

Some significant notes should be made concerning different forms of energy. Mechanical energy is the energy of the directed movement of macroscopic bodies or their potential energy in any force field and is associated with zero entropy. Electrical energy, which propagates in a conductive medium along definite paths, may also be considered to be entropyless. In contrast, heat is the energy of the chaotic movement of molecules of a substance. This form of energy is associated with the highest entropy content. The value of entropy associated with a given quantity of heat (Q) is inversely proportional to the absolute temperature of the system: $S = Q/T$.

Chemical energy occupies an intermediate position in this respect. Chemical energy is mainly the potential energy of molecular structures. Accordingly, one would expect that the entropy associated with chemical energy should be zero because molecular structures are well-ordered systems. The entropy of chemical substances tends to zero at very low temperatures, but it increases as the temperature rises. The change in entropy during the course of any reactions that proceed in a system may be either positive or negative. As for the entropy of radiative energy, this question has been discussed in detail in the first chapter of this book.

Closely related to the notion of energy is the concept of *work*. Work is the transfer of entropyless energy, such as mechanical energy, into the system or out

of it. Work is performed on a system when energy is transferred to it from an external source. In the opposite case the system performs work on an external object. Gas in a cylinder compressed with a plunger and the same gas moving the plunger by expansion present examples of these two cases.

In the more general case, energy flows between the system and its surroundings or other external objects may be associated with the transfer of entropy. To make the analysis of such cases more convenient, it is useful to consider that there is free energy, which is not associated with entropy, and bound energy, which is associated with entropy. Free energy may perform work, whereas bound energy can only be transformed into heat.

We should emphasize that the term free energy, as it is used in thermodynamics, may denote different values depending on the conditions of the process under examination. If it runs in a system of constant volume (v = constant), the term Helmholz free energy should be used. In the case of an isobaric process (p = constant), the term Gibbs free energy should be used to denote the work that can be performed by the system, with the exception of the part of work consumed by expanding the volume of the system.

The second law of thermodynamics states that the occurrence of spontaneous processes is associated with an increase in entropy. In a closed system this means that its entropy tends to a maximum or, in other words, such a system evolves to its most chaotic, the equilibrium state. If the system is open, it may exchange energy and entropy with the surrounding media. The second law of thermodynamics can be presented by several statements:

- Heat can never pass from a colder to a warmer body without other changes occurring at the same time.
- It is impossible to construct a perpetual motion machine of the second kind.
- Work cannot be obtained from the energy of bodies in thermal equilibrium.
- In all thermal processes occurring in a closed system the entropy of the system increases, and the maximum possible value of the entropy of a closed system is reached in a state of thermal equilibrium.

One may write the equation of the balance of entropy for a system:

$$dS = dS_{in} - dS_{out} + dS_{gen}. \tag{5.2}$$

It should be noted that this equation for entropy balance looks different from that for the conservation of energy [Eq. (5.1)]. The existence of the dS_{gen} term in this equation, which denotes the internal generation (production) of entropy in the system, is of fundamental significance. It shows that entropy is not a conserved quantity and can be generated by the occurrence of irreversible processes.

The term *irreversible processes* needs some explanation (Prigogine, 1961, 1967). The feature that distinguishes irreversible processes from reversible ones is that the irreversibility is tied to the direction of the passage of time. Such pro-

cesses evolve in a specific direction from past to future, whereas for reversible processes past and future are indistinguishable. All irreversible processes are followed by the dissipation of energy, which is transformed into heat, the most chaotic form of energy and associated with maximum entropy. The dissipation of energy is due to effects that may be considered to be friction in the general sense of the word.

The motive force, which causes a reversible process, is proportional to the deviation of the system from its equilibrium state. In irreversible processes the motive force is proportional to the rate of the process. This may be illustrated by a simple example from mechanics. The swinging of an ideal frictionless pendulum can be described by the following equation:

$$m = \frac{d^2h}{dt^2} = -ah,$$

where m is mass, h is a coordinate, t is time, and a is a constant. The term on the left side is the force (the product of mass and acceleration), whereas the right-hand term is proportional to the deviation (h) of the pendulum from its resting position. The replacement of t by $-t$ in this equation should not alter anything because the equation contains the second derivative of time and is thus invariant with respect to the sign of the time. Thus, the oscillation of an ideal pendulum is a reversible process. If the pendulum is nonideal and moves with some friction, an additional term, proportional to the rate of movement of the pendulum, should be included in the equation:

$$m\frac{d^2h}{dt^2} = -ah - b\left(\frac{dh}{dt}\right).$$

This additional term accounts for the irreversibility that arises due to friction and manifests itself in the gradual decrease in oscillation.

Energy that dissipates in an irreversible process (the dissipation) is equal to the rate of the process multiplied by the motive force that causes it. The dissipation divided by temperature equals the rate of entropy production:

$$\frac{dS_{gen}}{dt} = \frac{1}{T}JX. \tag{5.3}$$

Here J denotes generalized flow, i.e., the rate of a certain process, and X denotes the generalized thermodynamic force that causes this process. The motive force of diffusion is the concentration gradient, and that of the transfer of heat is the temperature gradient. The motive force of a chemical reaction is the *affinity*, a thermodynamic concept that will be considered toward the end of this chapter.

Linear relationships are usually observed between the values of the motive forces and the rates of the corresponding processes:

$$J_i = L_{ii}X_i. \tag{5.4}$$

The linear relation between force and rate may be not observed in the case of very intense processes, which can significantly alter the equilibrium distribution of molecules in energy. However, such nonlinear processes are not typical for biological systems. Most of the physicochemical processes in living organisms occur under the effect of weak forces and may be considered linear. The only exception is presented by the initial stages of photosynthesis in which the extremely rapid capture of a large portion of energy occurs.

CONVERSION OF HEAT INTO WORK

Proceeding from the two basic laws of thermodynamics one can examine the transformations between various forms of energy, from heat energy into work, from radiant energy into chemical energy, and so forth. The process of transformation of any form of energy into any other one can be characterized by the value of efficiency defined as the ratio of the output flow of energy in the desired form to the input flow of the initial energy. The efficiency of the transformation of heat (Q) into work (W) may be defined as follows:

$$\eta = W/Q. \tag{5.5}$$

However, it should be noted, that, strictly speaking, the heat (at the temperature of the surroundings) cannot be transformed in any other form of energy because it presents the ultimate level of chaotic degradation associated with maximum entropy. Transformation of heat into work really means obtaining free energy from a heat flow that passes from a source maintained at a higher temperature to another held at a lower temperature. As the amount of entropy associated with the same amount of heat rises with decreasing temperature, the transfer of heat in the direction of lower temperature is an irreversible and thus spontaneous process.

The case may be examined in more detail. Let us consider the inverse temperature as a coordinate $Y = 1/T$. The functioning of a "heat engine," which transforms the energy of heat flow into work, may be represented as the movement of the working fluid of the engine along the coordinate Y in the direction of increasing value. The balance of energy in any slice of thickness dY along the pathway of the working fluid may be expressed by the first law of thermodynamics:

$$-\frac{dQ}{dY} = \frac{dW}{dY}. \tag{5.6}$$

This means that the decrement in heat flow is equal to the work performed.

The local balance of entropy involves two terms, one due to the exchange and the other due to the internal generation of entropy:

$$\frac{dS}{dY} = \frac{d}{dY}(Q \cdot Y) + \frac{dS_{gen}}{dY}. \tag{5.7}$$

The generation of entropy may be expressed as a function of the free energy produced:

$$\frac{dS_{gen}}{dY} = -Y\frac{dW}{dY}\left(\frac{1}{\rho} - 1\right). \tag{5.8}$$

Here the factor ρ shows how the free energy produced is shared between the external load and the internal resistance of the energy-transforming engine. This factor may be considered as the measure of ideality of the engine. It equals unity in the case of an ideal engine in which no dissipation of free energy occurs. The case $\rho \rightarrow 0$ corresponds to an ultimately imperfect engine in which all free energy is uselessly dissipated.

Under steady state conditions the total divergence of entropy is zero: it is neither accumulated nor discharged in any slice along the coordinate Y. Thus, by expanding Eq. (5.7) and taking into account Eqs. (5.6) and (5.8), we can write:

$$Q + \frac{Y}{\rho}\left(\frac{dQ}{dY}\right) = 0. \tag{5.9}$$

Integration of this expression within arbitrary limits of temperature leads to the following relation:

$$\frac{Q_2}{Q_1} = \left(\frac{T_2}{T_1}\right)^\rho. \tag{5.10}$$

From this relation it immediately follows that

$$\eta = 1 - \left(\frac{T_c}{T_h}\right)^\rho, \tag{5.11}$$

where T_c and T_h denote the temperatures of cold and hot reservoirs of heat, respectively.

Figure 5.1 shows the dependence of the efficiency and the relative power of the energy-transforming engine upon the value of the distribution factor ρ. In the case $\rho \rightarrow 1$ we have the ideal engine of Carnot (1887), which works with maximum efficiency but yields infinitely small power:

$$\eta = 1 - T_c/T_h. \tag{5.11a}$$

When the virtual free energy is shared equally between the engine and the load ($\rho = 0.5$), we have the case examined by Curzon and Ahlborn (1975)—the maximum power at a given temperature difference:

$$\eta = 1 - (T_c/T_h)^{1/2}. \tag{5.11b}$$

Figure 5.2 depicts the efficiency of energy conversion as a function of the ratio of temperatures of cold and hot sources according to the formulas of Carnot (1887) and Curzon and Ahlborn (1975). As one may see in the case corresponding to the
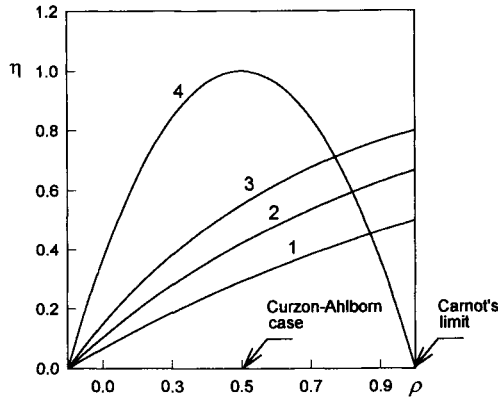
Figure 5.1 The dependence of the efficiency (curves 1–3) and the relative power of the energy-transforming engine (curve 4) upon the value of the distribution factor, p. Curves 1–3 correspond to temperatures of the hot source at 600, 900, and 1500 K and that of the cold source at 300 K.

condition of maximum power, the efficiency is markedly lower compared to Carnot's limit.

The plants cannot directly utilize heat energy to perform work because they usually live under conditions close to that of thermal equilibrium with their surroundings. The efficiency of the transformation of heat into work under such conditions should be extremely low. Nevertheless, plants use heat energy in very large amounts not to perform work directly but to compensate for heat losses due to the transpiration of water.
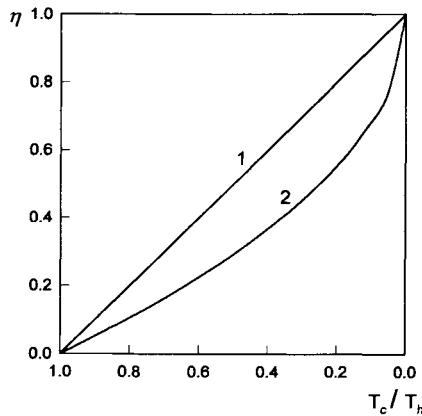

Figure 5.2 The efficiency of energy conversion as a function of the ratio of the temperatures of cold and hot sources: (1) Carnot; (2) Ahlborn and Curzon.

Despite the fact that plants do not function as heat engines, we have described the basic aspects of the transformation heat into work that follow from the laws of thermodynamics, as this information will be of use later.

THERMOPHYSICAL CONVERSION OF RADIANT ENERGY

Radiant energy can be converted into work by two considerably different means: thermophysical and quantum processes. The distinctions between them were discussed in detail in Chapter 3. The transformation of radiant energy into work is different in some aspects from the transformation of heat into work, independent of the method used. A converter of radiant energy, in contrast to a heat engine, does not directly contact the high-temperature source. Furthermore, the radiative exchange is always two-sided: if the converter obtains radiation flux from a source at a certain solid angle, it itself radiates at the same or greater angle in the reverse direction. Also, the relationships between the amount of energy and the amount of entropy in the radiative fluxes are different from those in the case of heat flows. These characteristics of radiation as a form of energy were discussed in detail in Chapter 1.

Let us consider an ideal converter of radiant energy, which does not generate entropy while it functions and which possesses the properties of a black body, i.e., it absorbs all incident radiation. Let the temperature of the converter be maintained at a constant value due to exchange with the surrounding medium which thus plays the role of a thermostat. On the other hand, the converter obtains radiation from a high-temperature source, such as the Sun. The energy balance of the converter may be written similar to Eq. (5.1) as follows:

$$W = E_s - E_c - Q, \tag{5.12}$$

where W is work performed by the converter in unit time and E_s is radiation obtained from a high-temperature source at temperature T_s within a solid angle ω_s. E_c is the energy radiated by the converter at the temperature of the thermostat, and Q is the heat that a converter gives off to its surroundings at a temperature T_c.

The values E_s and E_c are determined by the intensities of radiation at corresponding temperatures and by the values of solid angles at which the radiative exchange occurs. According to Eq. (1.6) we have:

$$E_s = \omega_s a T_s^4,$$

where $a = 2\pi^4 k^4/15c^2h^3$, and we can write a similar equation for E_c.

The heat Q can be determined from the equation of entropy balance [Eq. (5.2)] and the expression [Eq. (1.15)], which determines the relationship between entropy and energy in equilibrium radiation. The generation of entropy is taken to

be zero, because the converter is considered ideal. Now taking into account the entropy balance equation [Eq. (5.2)], one can find entropy that should be removed from the system.

$$\Delta S = \frac{4}{3}\left(\frac{E_s}{T_s} - \frac{E_c}{T_c}\right).$$ (5.13)

This entropy is carried away with the heat, the amount of which can be found easily:

$$Q = T_c \Delta S = \frac{4}{3} a\omega_s (T_c T_s^3 - T_s^4).$$ (5.14)

Now the efficiency of transformation can be found as the ratio of the work performed to the radiant energy obtained. Taking into account Eqs. (5.12) and (5.14), we have:

$$\eta = W/E_s = 1 - \frac{4}{3}(T_c/T_s) + \frac{1}{3}(T_c/T_s)^4.$$ (5.15)

Such an equation was first derived by Landsberg (1977). Figure 5.3 shows the dependence of the limiting efficiency upon the ratio of temperatures T_c/T_s compared with the line of Carnot's heat engine function and that of Curzon and Ahlborn.

Equation (5.15) was derived by conforming to equilibrium black-body radiation. If the radiation is not at equilibrium, say it is diluted due to scattering,
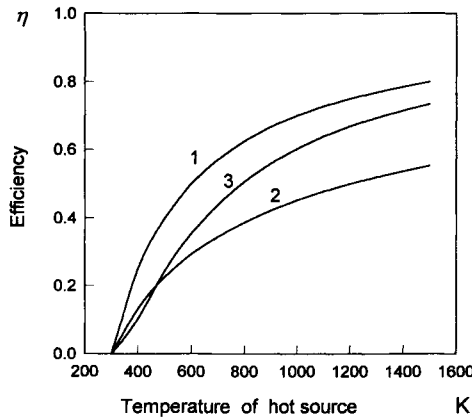

Figure 5.3 The dependence of the maximum efficiency of radiant energy conversion (3) upon the temperature of a source compared with the efficiencies of Carnot (1) and Ahlborn and Curzon (2). The temperature of the converter is 300 K.

Eq. (5.15) nevertheless can be used to obtain estimates of the efficiency, but in such cases the effective temperature of diluted radiation should be taken as the value of T_s rather than the temperature of the radiation source.

The limiting values of the efficiency of transformation of radiant energy into work according to Eq. (5.15) are always lower than those of the conversion of heat according to Carnot's equation at the same temperatures for cold and hot sources. These values remain high, however, being up to 75% for dilute radiation and more than 90% for direct sunlight. The real figures for the efficiency of the utilization of solar energy by plants are many times lower. This is caused by plants converting radiative energy by a quantum rather than a thermophysical mechanism. The peculiarities of the quantum mode transformation of radiant energy will be examined in the next section.

It is interesting to mention here that there is a theoretical possibility of obtaining work at the expense of radiating energy drawn from the surroundings into cold space (Ksenzhek, 1985, 1987). The values of the efficiency of such a process may be defined either as the ratio of available work to the energy radiated into space or to the heat withdrawn from the surroundings:

$$\eta_E = W/E_T = \frac{1}{3} - \frac{4}{3}(T_p/T_c)^3 + (T_p/T_c)^4 \qquad (5.16)$$

$$\eta_Q = W/Q = \frac{1}{4} - \frac{3}{4}(T_p/T_c)^3\frac{1 - T_p/T_c}{1 - (T_p/T_c)^3}. \qquad (5.17)$$

In these formulae, T_p denotes the temperature of space where the converter radiates. One may see that if this temperature is low enough, up to 25% of the heat energy drawn from the surroundings can be converted into work under ideal conditions. That corresponds to 33% of the energy radiated into space.

Plants do not use this theoretically available source of energy. Plants actually radiate significant quantities of energy. Say the radiative power of a tree with a crown 10 m in diameter may be as high as 20–25 kW during both day and night. The total amount of energy that leaves the plant as infrared heat radiation within 24 hr is comparable to the amount of high-temperature radiative energy that the plant receives from the Sun during daylight hours. However, the plant not only radiates but simultaneously absorbs infrared radiation proceeding from surrounding objects, the atmosphere, and the ground. Usually the flows of heat radiation in both directions are commensurate, and thus the general radiative balance of a plant in the infrared region is usually small. Only under conditions of very dry cold atmosphere the outward flux of heat radiation from a plant will significantly prevail over the inward flux from the surroundings. There are no signs, however, that the theoretically possible method of performing work using thermal radiation is used by plants.

QUANTUM MODE OF TRANSFORMATION OF RADIANT ENERGY

Thermodynamics is a science that limits the domain of the possible with no regard for the details of the mechanisms that may be used to realize this potential. The limits of the domain of the possible depend upon the conditions imposed on the energy-transforming system. The more rigid the conditions, the smaller the domain within which the process can be realized. Figure 5.3 illustrates this: the most liberal conditions for the Carnot cycle permit the highest values of efficiency. Extra constraints connected with the thermodynamic properties of black-body radiation diminish the theoretically attainable values for the efficiency of conversion. Expected limiting values of the efficiency are lower if the converter of energy is not ideal and its functioning is followed by the generation of entropy.

The quantum modes of conversion of radiant energy are associated with some peculiar conditions of fundamental significance. Quantum processes are characterized by the existence of the "red border," the threshold level of the energy of photons that can actuate the quantum mechanism of conversion. Photons with energies lower than threshold either are not absorbed or, even if they are, do not contribute energy to the work performed by the system. The second peculiarity is that all photons with energy that exceeds the threshold level contribute an equal portion of energy to the virtual work of the system. All excess energy over the threshold level is dissipated. These basic peculiarities of the quantum methods of transformation of radiant energy are illustrated by Fig. 3.9.

There are many publications related to the thermodynamics of radiant energy conversion by quantum systems (Almgren, 1978; Bolton, 1978; Byvik *et al.,* 1983; Landsberg, 1983; Landsberg and Tonge, 1979, 1982; Ross and Ta-Lee, 1977). In these publications the peculiarities of the quantum methods of conversion that have just been described are taken into account, and thus the overall results of various approaches are close to each other in spite of some secondary differences. Our presentation of the problem follows the basic aspects of the usual course of reasoning, but some details are treated in a new fashion.

The threshold energy of photons, which may be absorbed by chlorophyll molecules and cause their excitation, corresponds to the low-frequency border of the photosynthetically active region of the spectrum (PAR). The relationshp between the energy and the cutoff frequency (v_0) is as follows: $\epsilon_0 = hv_0/e_0$ eV, where $e_0 = 1.602 \times 10^{-19}$ C is the elementary charge. For the process of photosynthesis the cutoff frequency is about 430 THz and the threshold energy is correspondingly about 1.77 eV.

The PAR is limited not only on the red, low-frequency side of the spectrum but also on the blue, high-frequency side. This border corresponds to the frequency v_1 of about 750 THz (about 400-nm wavelength). Photons at higher frequencies are

absorbed by plants but are not active for photosynthesis. Thus, photosynthetically active photons are only those satisfying the condition $\nu_1 > \nu > \nu_0$. Each photon within this frequency range that is caught by the pigment brings energy in the amount $h\nu$, but only a portion of it, $h\nu_0$, can be used to perform work while the excess $h(\nu - \nu_0)$ is dissipated.

Thus, let us now consider the energy-converting device, which does not absorb radiation with frequencies lower than ν_0 and completely absorbs radiation with higher frequencies. If the spectral distribution of energy $I(\nu)$ in the incident radiation is known, the share of PAR in the total incident energy flux can be easily found:

$$\eta_1 = \int_{\nu_0}^{\nu_1} I(\nu) \; d\nu \; / \int_0^{\infty} I(\nu) \; d\nu. \tag{5.18}$$

For black-body radiation the function $I(\nu)$ is expressed by Eq. (1.8).

Figure 5.4 shows the dependence of the factor η_1 upon the temperature of the source of radiation (curve 1). This dependence shows a maximum value of about 0.4 at a temperature near 7000 K, which is higher than that of the Sun. At the temperature of the Sun (5785 K) the share of PAR is about 0.37. Thus, only a little
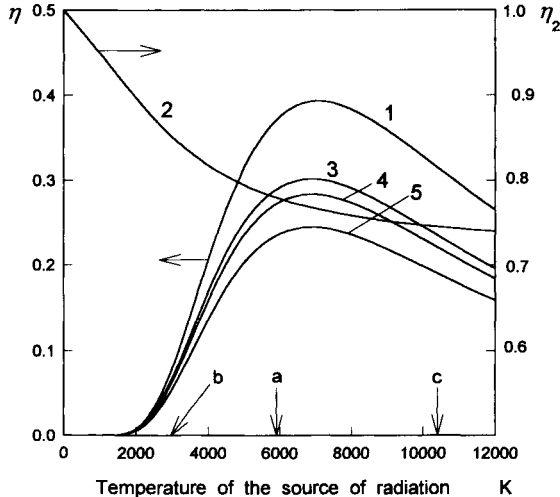

Figure 5.4 (1) The share of PAR (η_1) in the total radiation from sources of different temperature. (2) Efficiency of excitation of the working body (η_2). (3) The share of incident radiation energy transferred into energy of the excited state (η_1, η_2). (4) The share of energy of the excited state in the threshold level ($\eta_1.\eta_2.\eta_3$), direct radiation ($\gamma = 1$). (5) The same as (4), diluted radiation ($\gamma = 2 \times 10^5$). (a) The Sun; (b) incandescent lamp; (c) Sirius.

more than one-third of the unmodified solar radiation falls in the PAR. Light that has passed through the atmosphere and the diffuse radiation from an overcast sky contain a relatively greater portion of photosynthetically active rays, which may reach up to 50%. With a decrease in the temperature of the source, the share of PAR falls significantly. For example, in the radiation of an incandescent lamp ($T_s \approx 2900$ K) the share of PAR decreases to about 7%. On the other hand, in the radiation of very hot sources the relative fraction of PAR also diminishes to a certain extent.

Chlorophyll molecules almost always can be found in a state of thermal equilibrium with the surrounding medium. If a molecule of chlorophyll absorbs a photon, it is raised to an excited state. Its duration in the excited state is very short, and the difference between the ground and excited state energy levels is very large; therefore, the excited electrons have little time to lose their energy by conversion into heat. This allows one to assign to the population of excited electrons in an assembly of chlorophyll molecules a certain effective temperature that is higher than that of the surroundings. Therefore, molecular converters of radiant energy may be imagined to be heat engines, which function between these two temperature levels with the excited electrons as the working body. Captured photons bring to the system a certain amount of entropy and energy, and the process of generating an excited state of chlorophyll cannot proceed ideally as a certain share of energy is inevitably lost.

The thermodynamic efficiency of generation of the excited state can be found from the balances of energy and entropy. The balance of energy may be written as follows:

$$E_a - E_e - Q = 0, \tag{5.19}$$

where E_a is the energy absorbed by the system, E_e is the energy taken up by the working body while passing into the excited state, and Q is the heat transferred to the surrounding medium. All values from here on relate to a unit time.

If we assume the system to be ideal and thus generating no entropy, the entropy balance will consist of only two terms:

$$S_a - Q/T_c = 0. \tag{5.20}$$

The inflow of entropy by absorbed energy must be equal to its outflow through heat transferred to the surroundings. Entropy brought to the system by incident radiation is proportional to the amount of absorbed energy and depends upon the effective temperature of radiation and the extent of its dilution:

$$S_a = (E_a/T_s)r(\gamma), \tag{5.21}$$

where $r(\gamma)$ is the factor that determines the ratio of free to total energy in the incident radiation depending on the degree of dilution, γ.

Now taking into account Eqs. (5.19), (5.20), and (5.21), we can obtain the expression for the efficiency of excitation of the working body:

$$\eta_2 = E_e/E_a = 1 - (T_c/T_s)r(\gamma). \tag{5.22}$$

The factor $r(\gamma)$ can be evaluated by taking into account the spectral distribution of entropy and energy of radiation:

$$r(\gamma) = T_s\gamma\frac{\int_{\nu_0}^{\nu_1} S(T_s,\nu,\gamma)\ d\nu}{\int_{\nu_0}^{\nu_1} I(T_s,\nu)\ d\nu}. \tag{5.23}$$

For black-body radiation diluted γ times, the expression can be simplified by using Eqs. (1.8) and (1.16):

$$r(\gamma) \approx 1 + (1 + \ln\gamma)\frac{\int_{\beta_0}^{\beta_1} \beta^2\ \exp(-\beta)\ d\beta}{\int_{\beta_0}^{\beta_1} \beta^3\ \exp(-\beta)\ d\beta}. \tag{5.24}$$

Solution of Eq. (5.24) shows values of the factor $r(\gamma)$ for nondilute solar radiation to be $r(\gamma) = 1.2$ at $\gamma = 1$, and under an overcast sky $r(\gamma) = 3.6$ at $\gamma \approx 2 \times 10^5$. Factor $r(\gamma)$ equals 1.12 for the radiation of an incandescent lamp. The efficiency of excitation (η_2) in these three cases is 0.94, 0.81, and 0.88, respectively. These estimates are quite close to those that were obtained earlier from quite dissimilar theoretical assumptions and from an analysis of experimental data on fluorescence (Bell, 1980).

Although the quanta incident in the PAR bring different amounts of energy varying from 1.77 to 3 eV, the energy of electrons in their excited state that can be utilized is equal to the threshold level, $h\nu_0 \approx 1.77$ eV. The fraction of absorbed radiation that remains in a form available for further transformations can be determined as follows:

$$\eta_3 = \frac{\nu_0\int_{\nu_0}^{\nu_1} I(\nu)/\nu\ d\nu}{\int_{\nu_0}^{\nu_1} I(\nu)\ d\nu}. \tag{5.25}$$

Figure 5.4 depicts the graph of the function η_3 as curve 2. The reduction in the energy of photons to the threshold level (1.77 eV) is followed by a loss of about 20–25% of their initial energy on average, or less in the case of a low-temperature source. The value of η_3 equals 0.78 for solar radiation and about 0.86 for the light of an incandescent lamp. Curves 3 and 4 in Fig. 5.4 show what fraction of incident

energy flux can potentially be transformed into the energy of the excited state of the working body (the electrons in chlorophyll). This fraction is equal to the product of the functions η_1, η_2, and η_3.

The position of maximum efficiency, as shown in Fig. 5.4, is shifted relative to the temperature of the Sun and corresponds to about 7000 K. This means that the real threshold frequency of the photosynthetic system of green plants is higher than that referring to maximum efficiency (430 and 360 THz, respectively). This may give rise to some speculative hypotheses concerning the ancient stages of evolution of photosynthesis, including the hypothesis that the Sun was hotter 2–3 billion years ago. Those questions, while extremely intriguing, are beyond the scope of our considerations. It should be added that the maximum of the function $(\eta_1 \eta_2 \eta_3)$ is smooth, and thus the shift in the real cutoff frequency of photosynthesis against the optimal value leads to a lowering of the possible efficiency by no more than a few percent.

Figure 5.5 shows a schematic diagram of the working cycle of a molecular radiant energy converter. The incident radiation flow is absorbed by the working body of the converter at the temperature of the surrounding medium, T_c. This causes a fraction of the working body to be raised to an excited state with an effective temperature T_e. The mechanism M uses the energy of the excited state for performing work. In photosynthesis this is the chemical work performed by the mechanisms of the dark stages of the photosynthetic process.

Let the incident flow of radiant energy be E_s and the amount of absorbed energy in the PAR be $E_a = E_s \eta_1$, and the amount $E_a \eta_2$ will be transferred into excited state energy. A fraction of this energy, only $E_a \eta_2 (1 - \eta_3)$, dissipates while decreasing to the threshold level $h\nu_0$. Because the balance of entropy must be obeyed, entropy that is being generated should be removed. Various ways of removing this extra entropy are possible, for example, by radiation of excess energy
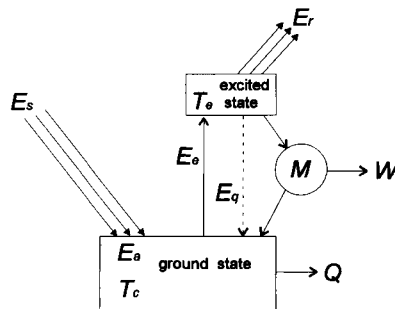

Figure 5.5   The scheme of the working cycle of quantum conversion of radiation. Description is in the text.

from higher excited levels (fluorescence) or by heat transfer to nonexcited parts of the system and then to the surroundings. Both of these ways are shown in Fig. 5.5 (E_r and E_q). Neglecting the latter process in light of its relative slowness, one may express the condition of the entropy balance as:

$$E_r = E_a \eta_2 (1 - \eta_3). \tag{5.26}$$

Continuing from this equation, one can estimate the effective temperature of the excited component of the working body. For this purpose, the values E_r and E_a should be expressed in terms of the intensity of radiation emitted by the excited component and correspondingly by the source of radiation:

$$\omega_a \eta_2 (1 - \eta_3) \frac{1}{\gamma} \int_{\nu_0}^{\infty} I(T_s, \nu) \ d\nu = \omega_r \int_{\nu_0}^{\infty} I(T_e, \nu) \ d\nu. \tag{5.27}$$

Here ω_a and ω_r are the geometric parameters that consider the values of the solid angles at which radiation arrives and is being emitted. Now, taking into account the temperature dependence of the intensity of radiation [Eq. (1.8)], one obtains after some minor approximations:

$$T_e = T_s \left[1 + \frac{kT_s}{h\nu_0} \ln \left(\frac{\omega_r \gamma}{\omega_a \eta_2 (1 - \eta_3)} \cdot \frac{T_e}{T_s} \right) \right]^{-1}. \tag{5.28}$$

Solving this transcendental equation, one may determine the temperature of the excited component of the working body for various conditions. As the calculations show, the temperature of the excited component may be as high as 1350 K under direct solar illumination. It is lower, at 1280 K, under conditions of illumination with diffuse light from an overcast sky. The radiation from a source of much lower temperature than that of the Sun, say that of an incandescent lamp, induces an effective temperature of the excited state of about 1100 K.

This raises the question of how an organic molecule, chlorophyll, can withstand such high temperatures. In spite of first impressions, there is nothing unnatural about this. The high effective temperatures relate to the excited electrons in the chlorophyll molecule and not to the molecule itself. Thus, the term "effective temperature of electrons" is used as a means to define the energy of the excited state of an electron. It should not be used in this case simply as the measure of the energy of heat motion. One should note that molecules of chlorophyll stay in darkness almost all the time, thus in a normal, nonexcited state. Even under bright solar rays the capture of a photon with sufficient energy to cause excitation is a very rare event for a given chlorophyll molecule. Such events happen only several times per second on average and last about $10^{-12} - 10^{-10}$ s. Thus, the duration of the excited state is extremely small in comparison with the duration of the "dark" state. One may try to imagine that in an absolutely dark room a single photoflash happens once every 10 years. The relationship between the duration of light and darkness will be about the same in the case of the chlorophyll molecule.

Strictly speaking, the darkness in which the chlorophyll molecule usually stays is not absolute. Low-energy red and infrared quanta hit the molecule two or even three times as frequently as the quanta of PAR, but chlorophyll does not sense or absorb these.

The total duration of the active life of a chlorophyll molecule during the vegetation period is less than one-thousandth of a second. The duration of each act of excitation is so short that the excited electron does not have enough time to give off a significant fraction of its energy to the skeleton of the chlorophyll molecule, the porphyrin ring, is endowed with a very high thermal stability.

Now we can proceed to consider the final stage of the energy transformation cycle, which is the stage of utilization of the excited state energy of the working body. As this energy has been defined in terms of temperature, we should use the general expression for the efficiency of the conversion of heat into work, Eq. (5.11). It seems expedient to use the Curzon–Ahlborn variant of the formula, which gives the value of efficiency at maximum output:

$$\eta_4 = 1 - (T/T_e)^{1/2}. \tag{5.11b}$$

The calculated values of the efficiency of conversion of radiant energy are presented in Table 5.1.

The limiting values for the efficiency of photosynthesis expected under conditions of solar illumination are about 12–14%, and are a little higher under direct sunshine than under a gloomy sky. The expected value of the efficiency in the case of illuminating a photosynthetic system with an incandescent lamp is much lower at less than 3%. This difference is connected with the low content of PAR in the radiation spectrum from a low-temperature source.

Table 5.1
Theoretical Values of Efficiency of Photosynthesis under Various Conditions

Conditions of illumination	Temperature of excited state, T_e (K)	Values of efficiency[a]				
		η_1	η_2	η_3	η_4	η_{tot}(%)
Direct solar radiation ($T_s = 5785$ K, $\gamma = 1$)	1303	0.37	0.94	0.78	0.52	14
Diluted solar radiation ($T_s = 5785$ K, $\gamma = 2 \times 10^5$)	1236	0.37	0.81	0.78	0.51	12
Incandescent lamp ($T_s = 2900$ K, $\gamma = 1$)	1097	0.07	0.88	0.86	0.48	2.6

[a] Here η_1 is the share of PAR in the incident flux, η_2 is the efficiency of excitation, η_3 is the share of energy in the PAR leveled to the threshold, η_4 is the efficiency of conversion of the excited state energy, and $\eta_{tot} = \eta_1 \eta_2 \eta_3 \eta_4$ is the total efficiency of conversion. It is the ratio of the amount of work that can be performed by the photosynthetic system to the amount of incident radiant energy.

THE EFFICIENCY OF PHOTOSYNTHESIS

One may find in the literature very diverse values for the efficiency of the energy conversion function of plants. These values range in magnitude from 10^{-1} to 10%. Usually the diversity in efficiency values is usually a consequence of the different ways of defining the values and, to a lesser degree, the physiological characteristics of the plant.

Intelligent discussion of any scientific problem requires the entities under consideration to be defined rigorously and unambiguously. The notion of the efficiency of photosynthesis does not always meet this condition. The term "efficiency" is not used in the same way by all authors. This may lead to misunderstandings and confusion that are quite superficial in most cases but sometimes can be quite serious. Occasionally the concept of the efficiency is used as a synonym for plant productivity, although these values are measured in different units and thus cannot be equivalent to each other. Efficiency is a dimensionless ratio of the output to input amounts of energy, whereas productivity has the dimension of mass (or of the energy that the mass contains) per unit area per unit time, for example, a bushel per acre (per season of vegetation).

Thus, the efficiency is the ratio of the output to input energy. The input energy flux can be defined in many ways. It may be considered the total radiation or only the photosynthetically active part. It may be the incident or the absorbed flux. Further, it may be related to a leaf, a plant, or the given area of a plantation. Finally, the amount of input energy can be related to various time periods. It could be a short time, such as seconds or hours within which no significant changes in the structure of the plant occur. There may be a 24-hr period during which day and night processes in a plant can be integrated. Last, it may be a long period commensurate with the whole life cycle of the plant or the duration of a growing season. The combination all possible variants amounts to at least 40 means of presenting the energy input.

For the output of energy there are also several possible modes of expression. The process of the conversion of radiation can be considered at different levels, for example, at the level of a chloroplast, a cell, a leaf, a whole plant, or finally a phytocoenosis. In dealing with global problems, one may consider the photosynthetic productivity of plants over large geographic regions. The amount of output energy can also be referred to in different forms. This may be the energy of the primary metabolites produced by the light stages of the photosynthetic process, such as ATP and NADPH. It may also include the energy of carbohydrates synthesized in the Calvin–Benson cycle. Next, one may take into account the total amount of energy stored in the biomass of the plant or only the energy in its economically useful parts. Thus, the output may refer to about 20 different quantities of energy.

Thus, with 40 modes in which input energy can be represented and 20 modes

for output, one can create a matrix of dimensions 40 × 20. Each of the 800 cells of such a matrix should correspond to a certain pair of output and input energy values. By dividing the output by the input, one should obtain 800 values for the efficiency of conversion of radiant energy into any other form. Of course not all of the figures obtained in this way can be considered to have practical meaning. A significant portion of the combinations are not real or present only minimal interest, and thus can be excluded from consideration. Nevertheless, the number of different modes in which the efficiency of conversion can be represented in a reasonable form is quite large. Some modes are used by investigators dealing with processes on a molecular or cellular level, while others are used by those who are interested in questions concerning plant physiology. More generalized values of the efficiency referring to a sufficiently large area of vegetation may be of more interest for ecologists. Thus, specialists in various domains of plant science considering the same plant species under equal conditions may specify the efficiency of photosynthesis in significantly different figures. The data presented in Table 5.2 serve as an illustration of how large these differences may be. This table is only a small fragment of the whole matrix of possible manners in which quantities characterizing the efficiency may be represented.

Quantities vary within wide limits depending on the mode of representation (Table 5.2). In spite of the diversity shown by the values, there is no reason to argue over which is correct. All are equally valid in this respect. Therefore, any question about the actual value of the efficiency of energy conversion, whether it is 0.5% or 24%, is meaningless unless the value under consideration is defined. On the other hand, they are all correct if properly defined.

It should be noted that the matrix of the efficiency values, such as that shown in Table 5.2, is degenerate in a mathematical sense. This means that the rows of the matrix are linearly interdependent, as are the columns. Hence, the values of the second row are one-half of the corresponding values in the third row because

Table 5.2

Efficiency of Energy Conversion Variously Defined [a]

Input	Output			
	Primary metabolites	Carbohydrates	Total production	Net production
Total flux incident on unit area	4	3	1.5	0.5
Total flux incident on a plant	8	5	3	1
Total energy absorbed	16	12	6	2
Incident flux of PAR	20	15	7.5	2.5
Absorbed PAR	24	18	9	3

[a]Tentative, mutually agreed data; in percentages.

the share of absorbed radiation is taken to be one-half of the total radiation. Similarly, the values of the fourth column are obtained by multiplying those of the third column by one-third, for that is the value used for the share of economically useful biomass.

The primary conclusion that follows is that as there are many modes of defining the efficiency of energy conversion, the selected mode in each particular case should be specified without ambiguity. The real meaning of the value considered should be clear from the context. Otherwise, any discussion concerning the values becomes pointless.

CONVERSION OF CHEMICAL ENERGY

The life of plants involves the processing of many interrelated chemical reactions. They are all accompanied by certain effects of the transfer and conversion of energy. Such processes can be examined effectively on the basis of thermodynamics. Chemical reactions as the object of thermodynamic analysis show some distinctive characteristics. During a chemical reaction the chemical bonds in reacting molecules undergo reorganization. Their spatial arrangements and their energies change. As a result, both the entropy and the energy of the whole system change. This is followed by corresponding alterations in the thermodynamic functions.

The overall change in energy of the system (dH) may be represented as the combination of two components, one of these being the change in free energy (dG) and the other that of bound energy (TdS):

$$dH = dG + TdS. \qquad (5.29)$$

According to the second law of thermodynamics the reactions may proceed spontaneously only in the direction of decreasing free energy ($dG < 0$). A zero value for free energy corresponds to the equilibrium state of the system.

The free energy of a system, in this case the Gibbs free energy, G, is also called the thermodynamic potential at constant pressure and temperature. Like any other physical value which has the meaning of potential, a thermodynamic potential unambiguously characterizes the state of a system. The work of transition of a system between two states only depends upon the difference in the potentials of these states and does not depend on the path of transition. This property of the potential values allows for the consideration of energy relations in a chemical system with no regard for the detailed mechanisms of processes that occur in it. Only the initial and ultimate states of the system must be known.

The free energy G is an *extensive* value. This means that it depends upon the amount of the substance of which the system is composed. Other examples of extensive variables are the mass or volume of a system or the number of moles of

a component. The total value of free energy of a chemical system equals the sum of the contributions of all its components:

$$G = \Sigma n_i \mu_i. \tag{5.30}$$

n_i is the number of moles of the ith component and μ_i is its chemical potential:

$$\mu_i = \left(\frac{\partial G}{\partial n_i}\right)_{T,n_j}. \tag{5.31}$$

The chemical potential, in contrast to the thermodynamic potential, is an *intensive* value. It characterizes a given component of a system irrespective of the size of the latter. This variable is similar to those such as temperature, pressure, or density. The value of the chemical potential of a component simply depends upon its concentration, provided it is low enough to consider the system as ideal (Guggenheim, 1957):

$$\mu_i = \mu_i^\circ + RT \ln n_i. \tag{5.32}$$

Biological systems usually satisfy this condition, and Eq. (5.32) can be used as a sufficiently good approximation in most cases. The value μ_i° annotated with the symbol ($^\circ$) refers to the standard state. In biochemistry the biological standard state is usually denoted by ($^{\circ\prime}$) to mean that at a temperature of 298 K (25°C) and a pressure of 101.3 kPa (1 atm) when the concentrations (the activities) of all components are unity (1 mol per liter) and the pH is 7. A reaction is described as exergonic if free energy is released and endergonic when free energy is used. It should be mentioned that in chemistry and physics the standard state corresponds to a pH of 0. $\Delta G^\circ = \Delta G^{\circ\prime}$, for reactions that do not involve water of H^+.

Linear combination of the chemical potentials of components of a reaction accounting for their stoichiometric coefficients (ν_i) is called *affinity:*

$$A = -\Sigma \nu_i \mu_i. \tag{5.33}$$

The affinity is equal to the change in free energy during a reaction (with a negative sign) and corresponds to the maximum work that a reaction can perform: $A = -\Delta G$. The affinity can be represented as a sum of two terms, where one refers to standard conditions while the other accounts for deviations in the actual state of the system from the standard one:

$$A = A^\circ - RT\Sigma \nu_i \ln c_i. \tag{5.34}$$

The standard value for affinity is directly connected with the equilibrium constant K of the reaction: $A^\circ = RT \ln K$.

Detailed tables of thermodynamic functions may be found in various sources (Fasman, 1976; Metzler, 1977). Such tables enable the calculation of energy relations in chemical systems. A fragment of a such table, containing data for the main components of the Calvin and Krebs cycles, is presented in Table 5.3. To

Table 5.3

**Free Energies of Formation and That of Oxidation of Some Compounds**

Substance	Work of formation from elements ($\Delta G°_f$, kJ/mol)	Work of oxidation with oxygen ($\Delta G°_o$, kJ/mol)	Work of oxidation with NAD$^+$, pH = 7 (ΔG_{ox}, kJ/mol)
Glucose	−917.2	−2872.2	−243.8
Oxaloacetate	−797.2	−1254.7	−79.7
Acetyl-CoA	−374.1	−889.1	−13
Citrate^{3-}	−1166.6	−2148.4	−57.3
α-Ketoglutarate	−798.0	−1885.5	−53.3
Succinate^{2-}	−690.2	−1598.9	−14.3
Malate^{2-}	−845.1	−1444.0	−49.9
Fumarate$^-$	−604.2	−1447.7	−93.6
Ribulosebisphosphate	−1597.6	−2417.1	−226.8
3-Phosphoglycerate$^-$	−1509.9	−1241.8	−106.6
Phosphoglyceraldehyde	−1285.6	−1466.0	−151.8
NADH		−219.0	0
NADPH		−219.8	0
FADH		−197.4	0
H_2O	−237,2	0	0
CO_2	−394.4	0	0

find the value of the maximum work available for a reaction, one must sum the values of the work of formation (ΔG_f) or that of oxidation (ΔG_o, ΔG_{ox}) of all reacting components, accounting for their stoichiometric coefficients in the reaction.

Consider now, from a thermodynamic point of view, the two examples of primary interest, namely, the basic Calvin and Krebs energy-converting cycles. Though both of these cycles are very complicated sets of reactions, a thermodynamic approach enables one to obtain information about their energetics without going into the details of their reactions.

CALVIN CYCLE

The overall result of the Calvin cycle may be represented as the reduction of carbon dioxide with NADPH followed by the formation of glucose as the final product:

$$6CO_2 + 12NADPH + 12H^+ \rightarrow C_6H_{12}O_6 + 12NADP^+ + 6H_2O$$
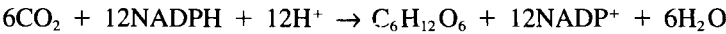
From Table 5.3 it follows that the overall change in standard free energy in the reaction is equal to +243.8 kJ/mol of glucose formed. The most convenient way to obtain this value is to use the data in the last column of Table 5.3. Under physiological conditions, the value of the free energy change, ΔG, will be higher, about

+320 kJ/mol, because of the low initial content of carbon dioxide in air, which amounts to $3 \cdot 10^{-4}$ of the atmosphere and about one-half of this value in the mesophyll of leaves. One should note that the change in ΔG in the reaction considered is positive. This means that for the components to react in the direction shown here, the reaction should be driven by an additional contribution of energy from an external source. The contribution of energy should be enough to make up for the positive increment of ΔG in the main set of reactions and force the cycle to revolve in the necessary direction at an adequate rate.

The energy required to turn the cycle is delivered by ATP. As six turns of the Calvin cycle are needed for one molecule of glucose to be synthesized, the energy cost of each turn is about 320/6 = 53.3 kJ. Each molecule of ATP can bring in 30–40 kJ of free energy. Thus, at least two molecules of ATP should be necessary to perform each revolution of the cycle under ideal conditions. Under real conditions three ATP molecules take part in each revolution of the Calvin cycle. The total excess of free energy that they bring in is 30–50 kJ. A certain portion of this energy is lost in the stage of transferring from the exoergic ATP/ADP cycle to the endoergic carbon acid cycle because energy coupling between them cannot be ideal. The energy left over drives the reactions of the cycle and finally dissipates. The Calvin cycle revolves six times to synthesize one molecule of glucose. Thus, this synthesis requires the overall consumption of 18 ATP molecules per molecule of glucose, costing 180–300 kJ of total energy.

Krebs Cycle

In the same manner, the tricarboxylic acid cycle or Krebs cycle can be examined from a thermodynamic point of view. The overall reaction that occurs in this cycle consists of the oxidation of the two-carbon acetyl residue by NAD^+ and FAD. The source component enters the cycle as a complex of acetyl with the sulfur-containing coenzyme A (CoA):

$$Ac\text{-}CoA + 3NAD^+ + FAD + 2H_2O \rightarrow 2CO_2 + 3NADH + FADH_2 + CoA$$
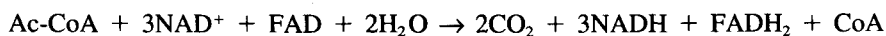
With equal validity, the reaction may be considered not as the oxidation of Ac-CoA but rather as the reduction of NAD^+ and FAD by Ac-CoA. By using the data of Table 5.3, one obtains $\Delta G = -34.6$ kJ per turn of the cycle or about -104 kJ per one molecule of glucose. In the preliminary stages of the process the molecule of glucose is transformed into three molecules of Ac-CoA; thus, three revolutions of the cycle are needed to provide its complete oxidation.

As one may see, the Krebs cycle is exergonic. Its rotation is followed by a decrease in free energy, and thus it can proceed spontaneously. The result of rotation of the cycle is the production of substances with high reducing power: three

molecules of NADH and one molecule of $FADH_2$ for each turn (nine and three molecules, respectively, per each molecule of glucose). These reduced forms play the role of carriers of active hydrogen in subsequent stages of energy transformation. It seems interesting that the energy cost of turning both cycles is similar, namely, 30–50 kJ in the case of the Calvin cycle and about 35 kJ per turn in the case of the Krebs cycle.

ADENOSINE TRIPHOSPHATE SYSTEM

The exclusively significant role of a universal energy carrier, which ATP plays in most biochemical processes, makes it necessary to consider its thermodynamics in more detail. The molecular structure of ATP (adenosine 5′-triphosphate) is as shown:
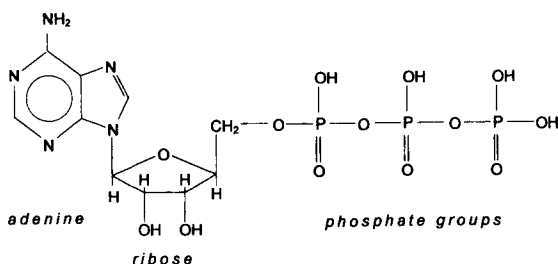
A molecule of ATP can exist in solution in various ionized forms as a result of dissociation of the hydroxyl residues of phosphate groups. ATP gives off energy when it undergoes hydrolysis followed by the departure of the terminal phosphate group. This reaction proceeds in biological systems with the participation of corresponding enzymes, the ATPases. The equation for the hydrolysis reaction may be written in the following way:

$$ATP^{4-} + H_2O \rightarrow ADP^{3-} + HPO_4^{2-} + H^+$$

The standard free energy of this reaction at 25 °C and pH = 7 is $\Delta G° = -34.5$ kJ/mol.

The actual amount of energy that can be freed by the hydrolysis of ATP depends upon the concentrations of all components of the reaction, but mainly that of H^+. The reason is that the concentrations of ATP^{4-}, ADP^{3-}, and the inorganic phosphate HPO_4^{2-} each depend upon pH, as they all take part in corresponding hydrolytic equilibria:

$$
\begin{aligned}
HATP^{3-} &\leftrightarrow ATP^{4-} + H^+ \qquad &pK = -\log K = 7.1 \\
HADP^{2-} &\leftrightarrow ADP^{3-} + H^+ \qquad &pK = 6.8 \\
H_2PO_4^- &\leftrightarrow HPO_4^{2-} + H^+ \qquad &pK = 6.8
\end{aligned}
$$
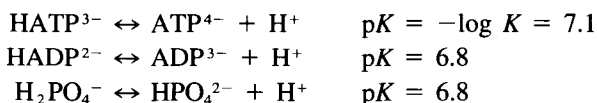
By taking into account the values for the dissociation constants, one can express the concentration of any ionic form as a function of the total content of the component. Say that for the concentration of ATP^{4-} we obtain:

$$[ATP^{4-}] = [ATP](1 + [H^+]/K_{HATP^{3-}})^{-1}, \tag{5.35}$$

where [ATP] denotes the total concentration of all forms of adenosine triphosphate. Now by using Eq. (5.34) one can derive the dependence of the maximum work available from the hydrolysis of ATP depending on the acidity of the medium:

$$A = A° - RT \ln \frac{[H^+](1 + [H^+]/K_{HATP^{3-}})}{(1 + [H^+]/K_{HATP^{3-}})(1 + [H^+]/K_{HPO_4^{3-}})} \tag{5.36}$$

The results of the calculations from this equation are presented in Fig. 5.6. As one may see the maximum energy that can be freed from hydrolysis of ATP is about 32–36 kJ mol in acidic medium, but this increases significantly at values of pH higher than 8–9. One should note, however, that Eq. (5.36) and its curve plotted in Fig. 5.6. present only an approximate picture. In more exact calculations, not only the first but all steps of hydroxyl dissociation of the components should be taken into account. In addition, ATP and ADP form complexes with the metal ions that are usually present in biological liquids. Magnesium ions have the most noticeable influence. As adenosine triphosphate binds with Mg^{2+} more strongly than does ADP, the presence of this ion diminishes the free energy of hydrolysis. The effect may attain several kilojoules per mole.
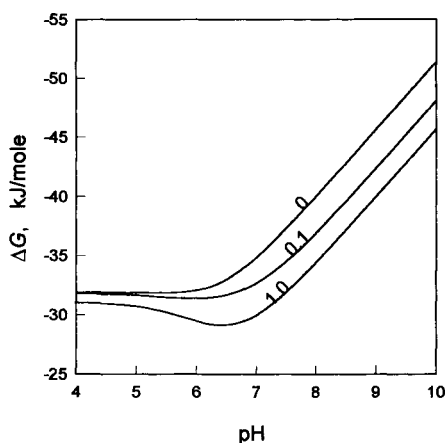
Figure 5.6 Dependence of the free energy of hydrolysis of ATP upon solution pH. Values on the curves represent the concentration of Mg^{2+} (mmol/liter).

ENERGY COUPLING OF CHEMICAL PROCESSES

The life activity of a plant can be considered as a set of a great number of various chemical reactions joined into an organized network. The individual reactions that together comprise the network are tightly linked with each other. Some are linked with common components as, for example, the series of reactions of the Calvin or Krebs cycles, in which the product of the reaction serves as the starting substrate for the next one. Other reactions are joined by energy rather than substances. For example, the energy of the flow of protons through ATP synthase causes formation of ATP from ADP and inorganic phosphate. On the other hand, under appropriate conditions the ATPase can employ the energy of the hydrolysis of ATP to pump protons out of the mitochondrion against the proton gradient. The whole set of reactions of the Calvin cycle is actuated due to the delivery of free energy from the hydrolysis of ATP.

One should note that in cases when reactions are interlinked by common components, definite stoichiometric relations between them are usually obeyed. In cases of an energy junction between reactions, the stoichiometric relations are not rigid and may vary within certain limits according to the conditions. Next we will discuss the case of an energy junction between processes.

The problem can be examined on the basis of principles of irreversible thermodynamics (Caplan and Essig, 1983; Glandsdorff and Prigogine, 1971; Hill, 1977; Katchalsky and Curran, 1965; Nicolis and Prigogine, 1977; Prigogine, 1961, 1967). We will discuss this problem according to Caplan and Essig (1983). As was shown earlier [see Eq. (5.4)], the rate of a process is usually proportional to the thermodynamic force that drives it: $J_i = L_{ii}X_i$. In a chemical reaction the affinity is the driving force (X_i). Often not one but several forces affect the system simultaneously. These may be, for example, temperature and concentration gradients or electric potential. In such cases each driving force influences not only the corresponding flow but all others too. So the temperature gradient induces, aside from the transfer of heat, diffusional flow (thermodiffusion). Also, the concentration gradient causes the diffusion of components and, simultaneously, the transfer of heat (Dufour effect). Two chemical reactions may be also coupled energetically.

The phenomenological relations between forces and the rates of the type described by Eq. (5.4) can be generalized to the case of several processes. For two processes they appear as shown:

$$J_1 = L_{11}X_1 + L_{12}X_2 \qquad (5.37)$$

$$J_2 = L_{12}X_1 + L_{22}X_2 \qquad (5.38)$$

In these equations L_{ii} is the "direct" phenomenological coefficient, such as the coefficient of diffusion or heat transfer, whereas $L_{ij}(i \neq j)$ are the cross-coefficients, such as those of thermodiffusion. Direct coefficients are always positive while cross-coefficients may be either positive or negative. They are zero if the processes

are independent and do not influence each other. The cross-coefficients are symmetric: $L_{ij} = L_{ji}$.

Now consider the thermodynamic coupling of two processes. Let the first be endergonic and thus followed by an increase in free energy, and let the second be exergonic. Therefore, only the second process should proceed spontaneously. However, if the processes are coupled, the change in free energy in the second may, under certain conditions, be sufficient to force the first process to go. The thermodynamic condition that allows such a relation between coupled processes is that the overall generation of entropy by both should be positive:

$$\Phi = J_1 X_1 + J_2 X_2 > 0. \tag{5.39}$$

Here Φ is the *dissipative function,* which equals the rate of generation of entropy multiplied by the temperature: $\Phi = T(dS/dt)$. Process (2) can be a driving force in relation to process (1) as the driven one, if it generates more entropy than the decrease in entropy due to the running of process (1).

One can further simplify the discussion of the problem by expressing the variables in a normalized form as follows: $J_i(L_{ii})^{-1/2} = j_i$ and $X_i(L_{ii})^{-1/2} = x_i$. Such normalization does not change the value of a dissipative function: $J_i X_i = j_i x_i$. Now instead of Eqs. (5.37) and (5.38) one can write:

$$j_1 = x_1 + \zeta x_2 \tag{5.40}$$

$$j_2 = \zeta x_1 + x_2, \tag{5.41}$$

where $\zeta = L_{12}(L_{11}L_{22})^{-1/2}$.

By denoting the ratio of flows as $w = j_1/j_2$ and the ratio of forces as $\psi = x_1/x_2$ and dividing Eq. (5.40) by Eq. (5.41), we can obtain an expression that shows how the ratio of reduced flows depends upon the ratio of reduced forces:

$$w = \frac{\psi + \zeta}{\zeta \psi + 1}. \tag{5.42}$$

One may see that when $\zeta = 0$, the ratio of flows is equal to the ratio of forces: $w = \psi$. This means that flows are independent of each other in this case. On the other hand when $\zeta = 1$, $w = 1$. This means that the driving process unambiguously determines the rate of the driven process. Thus, ζ may be considered to be the quantitative measure of coupling between the processes. A zero value of ζ corresponds to the absence of coupling, whereas coupling is total at $\zeta = 1$.

The dependence of the ratio of flows upon the ratio of forces for different values of the coupling factor ζ is depicted in Fig. 5.7. As one may see, the energy of reaction coupling can be efficient in the sense that the driving reaction could force the driven one to run against its natural direction, under conditions where $|\psi| < \zeta$ or in more obvious form when $X_2 > |X_1|(L_{12}/L_{11})$. If this condition is not met, the driven process may be inhibited to a certain extent, but not reversed.

As we have seen earlier [Eq. (5.39)], for the coupled processes to proceed in the desired direction, the generation of entropy by the second (the driving) process
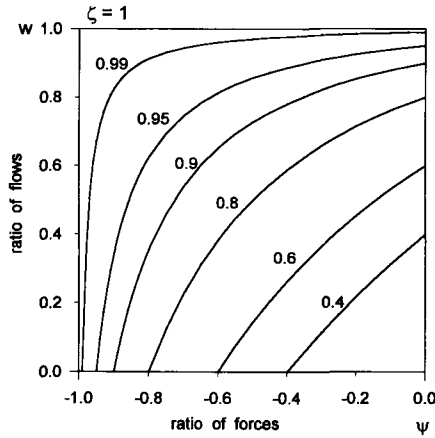
Figure 5.7   Dependence of the ratio of thermodynamic flows on the ratio of forces in coupled systems. Numbers on the curves are the values of the coupling factor, ζ.

must surpass the decrease in entropy due to the first (the driven) process: $J_2 X_2 > J_1 X_1$. The ratio of these two terms (with a negative sign) can be considered as the measure of the efficiency of coupling:

$$\eta_c = -\frac{J_1 X_1}{J_2 X_2} = -w \cdot \psi = -\frac{\psi + \zeta}{\psi\zeta + 1} \cdot \psi. \tag{5.42}$$

Figure 5.8 presents the dependence of the efficiency of coupling upon the values of the coupling factor ζ and the ratio of the forces of the driven to the driving
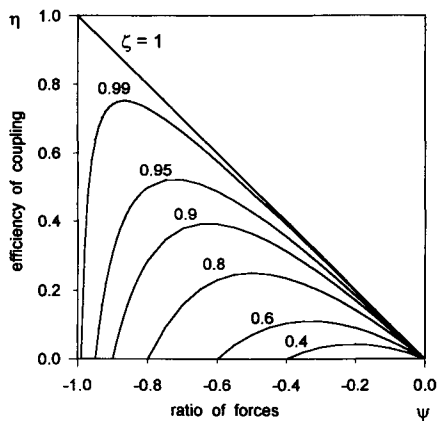
Figure 5.8   Efficiency of coupling as a function of the ratio of forces. Numbers on the curves are the values of the coupling factor, ζ.
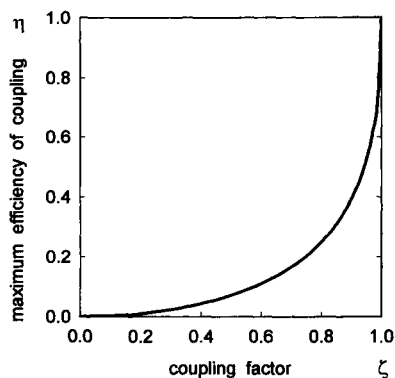
Figure 5.9 Dependence of the maximum efficiency of coupling on the value of a coupling factor.

processes, ψ. The dependence of η_c upon ψ has a higher maximum, thus the higher in the value of the coupling factor ζ. The influence of this factor on the value of maximum efficiency is very significant. As shown in Fig. 5.9, the efficiency of coupling can reach appreciable values only when ζ exceeds 0.6–0.8 and approaches unity; thus, ideal coupling is as ζ goes quite near to unity.

The primary thermodynamics rules of energy coupling, which have been presented here in brief, give grounds to think that coupled processes in biological systems are adjusted very precisely. Of course there are many other reasons for such an assumption besides thermodynamic ones, as these processes have been perfected by the long duration of natural evolution. However, a thermodynamic approach enables one to quantitatively specify the perfection of the coupling. For this purpose, the relations between forces and flows in the coupled systems should be determined experimentally. Such investigations have been carried out with various objects (Caplan and Essig, 1983; Rottenberg, 1978). For example, the most reliable data, obtained with mitochondria from rat liver, show that the coupling of oxidative processes in the Krebs cycle with the synthesis of ATP may proceed with an efficiency as high as about 50%. This corresponds to a value for the coupling factor of about 0.95. Such high values of the coupling factor and the efficiency seemingly show a fine alignment of the coupled processes. One may judge that in cases other than oxidative phosphorylation, the degree of coupling and coordination between biochemical processes is also high.
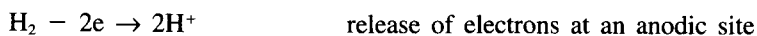
This Page Intentionally Left Blank

Chapter 6

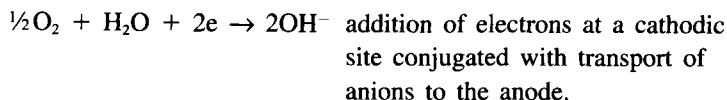# Electrochemistry and the Processes of Energy Conversion in Plants

INTRODUCTION

The life of plants is driven by the coordinated processing of a vast number of chemical reactions. Among the multitude of various chemical reactions that occur in living matter, electrochemical processes deserve special consideration. They play a very significant role in the transformations of energy in living matter and also possess some specific features that distinguish them from nonelectrochemical processes.

All chemical reactions are accompanied by a redistribution of electrical charge in the reacting molecules. In this respect, electrochemical processes significantly differ from solely chemical ones. The transfer of charge, electrons for example, can proceed in heterogeneous electrochemical processes over macroscopic distances exceeding the dimensions of the reacting molecules. In contrast, in typical chemical reactions the transfer or redistribution of charge is localized within the interacting particles. Important consequences follow from this distinction. The release of an electron from one molecule and its addition to another may be spatially separated. In electrochemical processes the overall reaction is divided into two conjugated reactions. An electron is released from a molecule in one location, whereas in another site it is added to another moleecule. According to standard chemical notation, the release of an electron corresponds to the process of oxidation, whereas the addition of an electron is considered reduction. The site of the system where the oxidative process occurs is usually called the anodic site (anode), and the site where reduction proceeds is called the cathodic site (the cathode). In the release of electrons from the anodic site or their addition at the cathode, the formation of complementary charges (ions) inevitably occurs because the electrical neutrality of the system as a whole must be maintained.

The scheme of electrochemical oxidation of hydrogen by oxygen may be written as the following pair of conjugated reactions:

$H_2 - 2e \rightarrow 2H^+$ release of electrons at an anodic site

$\frac{1}{2}O_2 + 2H^+ + 2e \rightarrow H_2O$ addition of electrons at a cathodic site
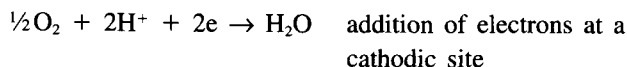
In this example, protons carry charges that are complementary to those of electrons. These ions are formed at the anode and consumed at the cathode. The ions compensating for the electron-mediated transfer of the negative charges are not necessarily positive. The transfer of negative ions in the direction opposite that of electron flow, from the cathode to an anode, gives the same result. This can be illustrated by the oxidation reaction of hydrogen in an alkaline medium.

$H_2 + 2OH^- - 2e \rightarrow 2H_2O$ release of electrons at an anodic site

$\frac{1}{2}O_2 + H_2O + 2e \rightarrow 2OH^-$ addition of electrons at a cathodic site conjugated with transport of anions to the anode.

In this example, anions formed in a cathodic reaction migrate to the anodic site, where they are consumed.

Inasmuch as the anodic and cathodic sites are separated spatially and processes at these sites are conjugated, electrochemical systems must include at least two phases with different types of conductivity. One phase can be permeable to electrons and another to ions. Electrochemical reactions proceed at interfaces, and they are heterogeneous by nature (Fig. 6.1).

Electrochemical processes depend on electrical fields. The electrochemical potential of a charged component is determined not only by its activitiy (or concentration), as in the case of uncharged substances (see Eq. 5.32), but it includes an additional term, which accounts for the interaction energy of the charge with the electric field:

$$\tilde{\mu}_i = \mu_i + z_i F \phi, \tag{6.1}$$
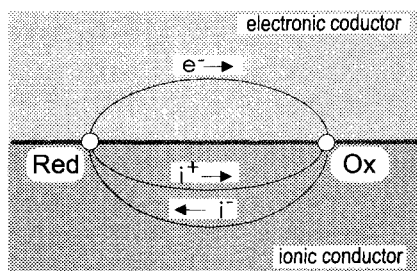
Figure 6.1   Electrochemical reactions proceed on the boundary between phases with different kinds of conductivity and are accompanied by the transfer of charge over macroscopic distances.

where $z_i F\phi$ is the electrostatic work required to bring a charge $z_i e$ from infinity in a vacuum to the inside phase, and $F = 96,500$ C is the Faraday number, the quantity of electricity associated with 1 mol of elementary charge. The electrochemical potential $\bar{\mu}_i$ is the total work required to bring particle i from a vacuum into a phase (Koryta *et al.*, 1993; Marshall, 1978). All specific features of electrochemical processes that distinguish them from the usual chemical ones are due to the dependence of the energy of charged particles on the electric field.

A very significant property of electrochemical processes is that they enable the direct transformation of chemical energy into work. In chemical reactions the total change in energy of a reacting system is transformed into heat and, thus, into the chaotic movement of molecules. If gaseous components take part in a reaction, a fraction of the energy is transformed into the work of expanding the volume. In contrast, electrochemical systems can transform the change in free energy in the reaction directly into the energy of a directed flow of electrons and therefore into electrical energy. This form of energy is not associated with entropy, and thus it may be used to perform various kinds of work.

All of the peculiarities of electrochemical processes noted earlier exist in industrial electrochemical devices and in natural systems functioning in living cells. However, another peculiarity of electrochemical processes is of distinct significance for biological systems. Electrochemical processes may serve as an effective means of summing up the effects of individual chemical acts that proceed on a molecular level into a common effect on the membrane level. If separation of charges occurs at the surface of a thylakoid membrane due to the action of a photosynthetic unit, the difference in electrical potential that arises on the membrane is not localized and spreads over the whole thylakoid surface. The energy saved in this way in the form of a transmembrane potential difference may be used to drive the mechanism localized far from the point where the potential was generated. Thus, electrochemistry enables indirect coupling of processes without the participation of common intermediate substances. The electrical field plays the role of an intermediate.

Nature employed the peculiarities of electrochemical processes in the very early stages of biochemical evolution. Life on Earth originated in an aqueous medium, which is an electrolyte solution containing significant concentrations of dissolved salts. The key event in the advent of precursors of ancient living cells may have been the formation of coacervate drops surrounded by thin films of fatty substances (Bernal, 1967; Broda, 1975; Deamer and Fleischaker, 1993; Deamer and Volkov, 1996; Kenyon, 1969; Oparin, 1969). Such films isolated two volumes of electroconductive liquid, the inner content of the drop from the surrounding medium.

We should point out another facet of the role of electrochemical processes in biochemistry. There is a certain accord between the characteristic dimensions of some biological structures and the characteristic dimensions in which electrochemical processes are developed. Electrical forces are very strong, and therefore

in any macroscopic body the strict equality of the number of positive and negative charges is always obeyed. Thus, macroscopic bodies are electrically neutral to a great extent. However, in volumes small enough to contain a low number of charged particles, the condition of electroneutrality may be less rigorously fulfilled. Thus, small volumes of matter may carry a certain electrical charge. The characteristic dimensions in which the violation of neutrality can be observed depend upon the conductivity of the medium. Higher conductivity corresponds to a smaller characteristic length on which any violation of electroneutrality decays. These dimensions may vary by about 10 nm in such liquids as cellular sap. This is approximately on the order of dimensions of the biological structures in which the primary acts of energy conversion occur. Say the hydrophilic parts of some membrane proteins stretch out from the lipid phase into the aqueous solution for several nanometers. The thickness of the aqueous interlayer between the membranes of grana in thylakoids is of the same order. This coincidence is not casual and can play a certain role in functioning biochemical mechanisms.

ELECTROCHEMISTRY IN ENGINEERING AND BIOLOGY

The generalized scheme of an electrochemical process shown in Fig. 6.1 represents a short circuit in which the complete cycle of charge transfer is implemented. Now let us depict the system as an open circuit. For this purpose, one of the conducting phases should be divided into two parts. If the divided phase is an electronic conductor, we will get the scheme shown in Fig. 6.2A. Figure 6.2B

A   B
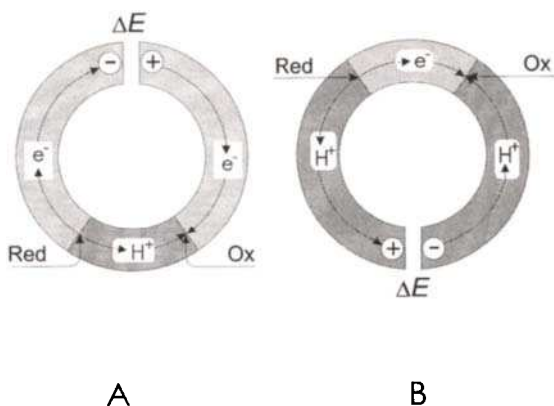
Figure 6.2   Schemes of an electrochemical systems in engineering (A) and in biology (B). In the former case the electromotive force arises across the gap in an electron conductor; in the latter it arises across a phase with ionic conductivity.

shows the case when the divided phase is an ionic conductor. Panel A represents the scheme of an electrochemical engineering device such as, for example, a battery in an electronic watch or car. In electrochemical engineering devices, metals are used as phases with electronic conductivity, and ionic conductors are usually electrolyte solutions. Both parts of the metal phase that contact the electrolyte solutions are called electrodes. One of them serves as the electron donor in the process of reduction of an oxidant. This electrode is positively charged due to the release of electrons. The opposite electrode is negatively charged due to accepting electrons from the reductant. A difference in electrical potentials arises between the two electrodes. This difference, ΔE, is called the electromotive force and can be used to perform work.

A scheme of an bioelectrochemical device is shown in Fig. 6.2B. The electron conductor is continuous, whereas the phase with ionic conductivity is split. If a part of the electrolyte phase is in contact with the site where the cathodic process occurs and where an oxidizing agent undergoes reduction, it is negatively charged while the anodic part becomes positive. Such a scheme of electrochemical process arrangement is realized in biological electrochemical systems.

Nature designed biochemical mechanisms without such electronic conductors as metal wires. At the same time, these mechanisms were tailored to operate in water, which is a conductive medium. Therefore, nature had to invent two other things: the insulator for the separation of aqueous phases and the electronic conductor to provide the transfer of electrons between the points where they are released and accepted. Phospholipid membranes, which surround cells and subcellular structures such as chloroplasts and mitochondria, play the role of insulators. The function of an electron conductor in biological systems is performed by electron transfer chains, which are incorporated in membranes and arranged as sequences of molecules that can exchange electrons with each other. Therefore, there are significant distinctions between the electrochemical systems that function in living cells and those used in our everyday life and electrochemical engineering.

THERMODYNAMICS OF ELECTROCHEMICAL SYSTEMS

The general laws of thermodynamics considered in Chapter 5 remain valid for examining electrochemical systems, which have some specific features not inherent in typical chemical systems. Their most significant advantage is the possibility of the direct conversion of free energy change during the electrochemical reaction into electrical energy. The maximum energy, which can be converted to electric work, is equal to the affinity of the reaction, A. The affinity divided by the quantity of electricity transferred during the reaction is equal to the equilibrium potential

difference of the open circuit. This value is referred to as the electromotive force:

$$E = \frac{A}{nF} = -\frac{1}{nF}\sum v_i \mu_i. \tag{6.2}$$

Here, v_i is the stoichiometric coefficient of the ith component of the reaction, and n is the number of electrons that take part in the reaction. By taking into account the expression for chemical potential (Eq. 5.32), one can define the following formula for the electromotive force as a function of the activities of the reacting species:

$$E = E° -\frac{RT}{nF}\sum v_i \ln a_i, \tag{6.3}$$

where $E° = -(1/nF)\sum v_i \mu_i°$ is the standard value of the electromotive force.

Apart from the notion of electromotive force, the concept of an *electrode potential* is also used in electrochemistry. It corresponds to the potential difference between the given electrode and an auxiliary or reference electrode, whose potential against the solution is known. According to an international agreement, the potentials of all electrodes are measured against the standard hydrogen electrode (SHE), the potential of which is taken as the conventional zero level. The potential of a standard hydrogen electrode is determined by the equilibrium $2H^+ + 2e \leftrightarrow H_2$ at standard conditions: unit activity of hydrogen ions (pH 0) and 1 atm of hydrogen partial pressure.

Equation (6.3) enables the calculation of the equilibrium electrode potential for any redox proccess. Redox reactions play a very significant role in biochemistry, particularly in energy-transforming process. The redox reaction consists of the mutual conversion of two conjugated forms of a substance, one of them oxidized (Ox) and the other reduced (Red). The conversion is followed by a transfer of electrons and protons:

$$Ox + mH^+ + ne \leftrightarrow Red$$
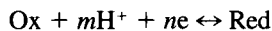
Such a system may be characterized by its *redox potential,* the thermodynamic value that describes the capability of the system to develop reducing or oxidizing properties. The value of the redox potential of a system may be measured by electrochemical means. In many cases it is adequate for this purpose to immerse an inert metal electrode in a solution containing the redox system. As the result of electron exchange with the redox components, the metal acquires a potential equal to the redox potential of the system under study. The electrode potential is the measured value, whereas the redox potential is characteristic of the reducing power of the redox couple.

The expression for the equilibrium electrode potential in the case of a redox reaction proceeding with the participation of m protons and n electrons is as follows:

$$E = E° -2.3\frac{RT}{nF}\log\frac{a_{Red}}{a_{Ox}} -2.3\frac{RT}{F}\left(\frac{m}{n}\right)(\text{pH}). \tag{6.4}$$

One can see that the redox potential shifts in the negative direction with increasing activity of the reduced form and vice versa if the activity of the oxidized form rises. Often the ratio of activities in Eq. 6.4 can be substituted with the ratio of concentrations without introducing noticeable error.

If the activities of the oxidized and reduced forms are equal ($a_{Ox} = a_{Red}$), the redox potential depends only on the value of the pH:

$$E = E° - 2.3\frac{RT}{F}\left(\frac{m}{n}\right)(\text{pH}). \qquad (6.5)$$

The equilibrium electrode potential at equal concentrations of the oxidized and the reduced forms ($c_{Ox} = c_{Red}$) is very close to this value. It is referred to as the *midpoint potential* (E_m). A difference between the value given by Eq. (6.5) and the midpoint potential may arise from an inequality of the activity coefficients of the reacting species at equal considerations, but this difference is usually very small. From the experimentally obtained value of the midpoint potential, the true value of the standard potential of the system may be calculated to a good approximation. From the experimental dependence of E_m upon pH, the ratio of the numbers of protons and electrons in the reaction can also be determined.

$$\frac{m}{n} = -\left(\frac{F}{2.3RT}\right)\frac{dE}{d\text{pH}}.$$

The redox potential of a system measures its capability to display electron donor or electron acceptor properties, or in other words its ability to function as a reducing or an oxidizing agent. A system with high positive redox potentials may act as an oxidant toward a system with less positive potentials and vice versa: a system with a more negative redox potential may act as a reductant toward a system with a more positive potential. As the values of redox potentials are specified against the standard hydrogen electrode, they characterize the reducing "power" of the redox system compared to that of molecular hydrogen at 1 atm and 25°C in acid solution (pH 0).

BIOLOGICAL REDOX SYSTEMS

Living organisms of all kinds, whether plants, animals or bacteria, contain a great number of substances capable of redox reactions. These compounds perform very significant biochemical functions. Most participate in processes of energy transformation. Biological redox systems overlap for a rather wide range of the values of redox potentials, exceeding 1.2 V. Redox systems, involved in biochemical processes, present examples of several types of substances. Among them are a variety of quinoid compounds, derivatives of isalloxazine, derivatives of nicotinic acid, metalloporphyrins and iron-sulfur proteins. We will present a short review of these compounds (Dryherst, 1977; Dryherst *et al.*, 1982; Ksenzhek and Petrova, 1986).
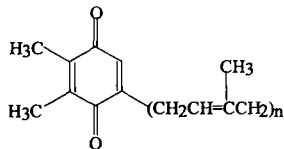
THE QUINONES

These substances are present in plants primarily as *p*-benzo- and *p*-naphtho-quinones with various side chains. The molecules of these compounds do not change their overall configuration during redox reactions. The process proceeds with the intermediate formation of a free radical (semiquinone):

| quinone | semiquinone | hydroquinone |
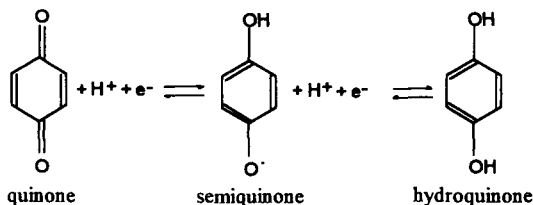
The chemical structures of two representatives of this class of compounds, the plastoq|uinones and the phylloquinones, are shown here. Living plant tissues contain these compounds in noticeable concentrations (Cramer and Crofts, 1982; Ksenzhek *et al.*, 1982; Trebst, 1978; Trumpower, 1982).
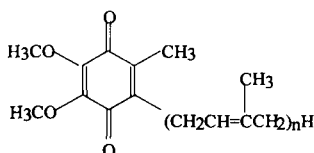
ubiquinone (n = 6 - 10)   plastoquinone (n = 3,4,9,10)

Many other quinones are also found in plants.

ISOALLOXAZINES (FLAVINS)

These compounds present a somewhat different type of quinoid structure. Their ability to undergo redox conversion is due to the ease in reorganizing their system of conjugated bonds:
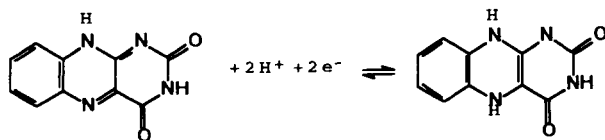
As in the case of quinones, the redox conversion of isoalloxazines may also proceed with the imtermediate formation of free radicals. The most significant

representatives of the flavins are riboflavin (vitamin B_2), flavin mononucleotide (FMN), and flavin adenine dinucleotide (FAD):
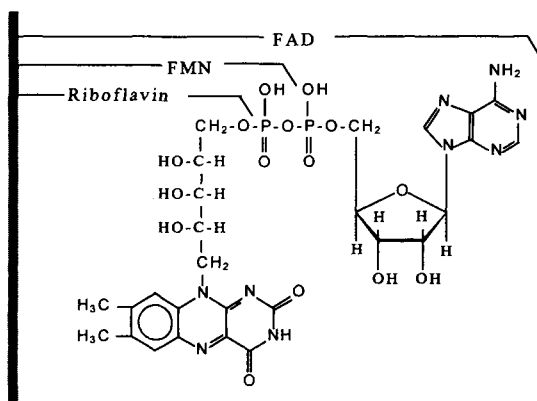
Flavins display complicated behavior as redox systems (Ksenzhek *et al.*, 1983). Their reduction proceeds with the formation of greater or lesser amounts of semiquinone in different pH regions. In this respect, noticeable distinctions between various flavins are observed. The redox behavior of flavins depends upon the composition of the solution and the presence of proteins and some metal ions. Figure 6.3 may provide an impression of the complexity of electrochemical behavior of one of the flavins, FAD, over a wide pH range.
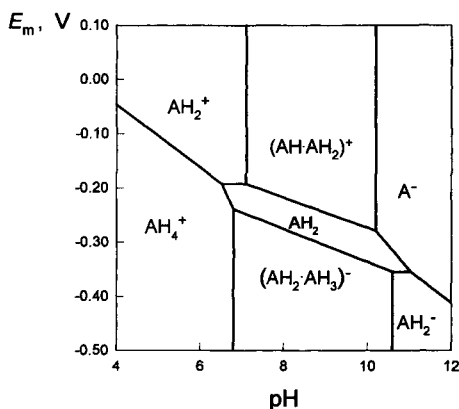
Figure 6.3 The pH–potential diagram of FAD. The lines depict the transitions between distinct forms of FAD. The areas limited by the lines show the domains of existence of corresponding forms of FAD, which differ from each other by the number of electrons and protons with which they are associated. Crossing a vertical line from right to left corresponds to the addition of a proton. Crossing an inclined line downward corresponds to the simultaneous addition of m protons and n electrons, the slope of the line being proportional to the ratio m/n. In certain areas of the pH–potential plane, FAD exists in a dimeric form.

THE DERIVATIVES OF NICOTINIC ACID

This significant group of substances capable of undergoing redox conversions is represented mainly by NAD^+ and $NADP^+$ (nicotinamide adenine dinucleotide and nicotinamide adenine dinucleotide phosphate, respectively). The structure of a molecule of NAD^+ is shown here. A molecule of $NADP^+$ differs from that of NAD^+ by the presence of an additional phosphate group linked to one of the two five-member ribose cycles.
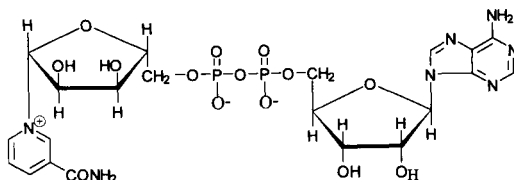
The pyridine nucleotides play the role of coenzymes of so-called pyridine-dependent dehydrogenases, enzymes that provide for the transfer of hydrogen in various reductive reactions. They function in biological systems as constituents of rather tight complexes with the protein components of the enzymes. The redox properties of pyridine nucleotides are attributed to the nicotinamide part of the molecule. The reaction is followed by a significant change in the structure of the molecule. In particular, the system of conjugated double bonds in the nicotinamide part of the molecule is broken upon reduction.
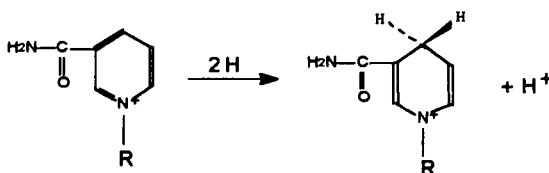
Redox conversions of the pyridine nucleotides do not proceed as freely as those of quinones. The reaction must proceed with a certain spatial arrangement of the reactants provided by the protein part of the enzyme.

METALLOPORPHYRINS

Multiple functions in biological systems are carried out by the chelate complexes of transition metals with porphyrins (Dolphin, 1979; Ksenzhek and Petrova, 1978; Volkov *et al.,* 1997a). The most significant among these are the porphyrin complexes of magnesium (chlorophylls) and iron (hemes). These porphyrin complexes serve as prosthetic groups in cytochromes participating in the process of

electron transfer. Cytochromes function as redox sustems due to the change of the valence of the iron atom in the porphyrin complex:

$$Fe^{3+} + e \leftrightarrow Fe^{2+}$$
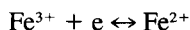
In cytochromes the heme group is linked with a protein. There is a great variety of cytochromes differing in the details of their structure and their redox properties. Redox reactions of some cytochromes proceed with the participation of a single electron, whereas the conversion of some other cytochromes is accompanied by a simultaneous transfer of protons. The values of redox potentials of cytochromes vary from -0.4 to $+0.4$ V. The cytochromes occurring in plants are mostly characterized by positive values of their redox potentials.

The molecular structure of chlorophyll *a* and the protoheme are shown:
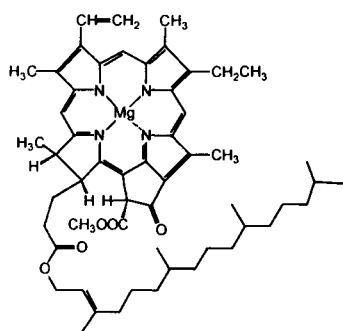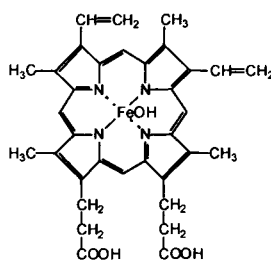
Chlorophyll   Protoheme

THE IRON–SULFUR PROTEINS

In the cells of plants, as well as those of other types of organisms, another group of compounds that displays redox properties is present. These are the iron–sulfur proteins, which contain in their active center several iron atoms (usually between one and four) linked to the protein body via sulfur bridges. Iron–sulfur proteins are also called ferredoxins:
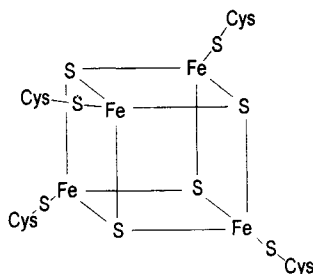
Table 6.1
Redox Potentials of Some Biologically Significant Systems

Substances and reactions		$E°$ (V) (pH 0)	$E°'$ (V) (pH 7)	Conditions
	$2H^+ + 2e^- \rightarrow H_2$	0.000	−0.414	
	$O_2 + 4H^+ + 2e^- \rightarrow 2H_2O$	1.220	0.815	
	$O_2 + 2H^+ + 2e^- \rightarrow 2H_2O_2$	0.709	0.295	
Quinones				
1,4-Benzoquinone	$Q + 2H^+ + 2e^- \rightarrow QH_2$	0699	0.285	
1,2-Benzoquinone	$Q + 2H^+ + 2e^- \rightarrow QH_2$	0.810		
1,4-Naphthoquinone	$Q + 2H^+ + 2e^- \rightarrow QH_2$	0.470		
1,2-Naphthoquinone	$Q + 2H^+ + 2e^- \rightarrow QH_2$	0.576		
Ubiquinone CoQ_{10}				
First step	$U + H^+ + e^- \rightarrow UH$	0.569		pH < 10
Second step	$UH + H^+ + e^- \rightarrow UH_2$	0.442		
Ubiquinone CoQ_6				
First step	$U + H^+ + e^- \rightarrow UH$	0.555		pH < 10
Second step	$UH + H^+ + e^- \rightarrow UH_2$	0.441		
Flavins				
FMN	$AH_2 + 2H^+ + 2e^- \rightarrow AH_4$	0.196		pH < 7
First step	$AH_2 + e^- \rightarrow AH_2^-$	−0.230		pH 7–9
Second step	$AH_2^- + e^- \rightarrow AH_2^-$	−0.297		pH 8–10
	$A^{2-} + 2H^+ + 2e^- \rightarrow AH_2^-$	0.281		pH > 10
FAD	$AH_2^+ + 2H^+ + 2e^- \rightarrow AH_4^+$	0.186		pH < 6.5
First step	$(AH \cdot AH_2)^+ + H^+ + 2e^- \rightarrow 2AH_2$	0.017		pH 7–10
Second step	$2AH_2 + H^+ + 2e^- \rightarrow (AH_2 \cdot AH_3)^-$	−0.042		pH 7–10
	$A^- + 2H^+ + 2e^- \rightarrow AH_2-$	0.285		pH 11
Cytochromes				
Cytochrome f	$(Fe^{3+}) + e^- \rightarrow (Fe^{2+})$		0.365	
Cytochrome a	$(Fe^{3+}) + e^- \rightarrow (Fe^{2+})$		0.29	
Cytochrome c	$(Fe^{3+}) + e^- \rightarrow (Fe^{2+})$		0.254	
Cytochrome b_2	$(Fe^{3+}) + e^- \rightarrow (Fe^{2+})$		0.12	
Cytochrome b_1	$(Fe^{3+}) + e^- \rightarrow (Fe^{2+})$		0.075	
Pyridine Nucleotides				
	$NAD^+ + H^+ + 2e^- \rightarrow NADH$	−0.113	−0.32	
	$NADP^+ + H^+ + 2e^- \rightarrow NADPH$		−0.324	
Ferredoxins				
From *Clostridia*	$(Fe^{3+}) + e^- \rightarrow (Fe^{2+})$		−0.413	
From spinach	$(Fe^{3+}) + e^- \rightarrow (Fe^{2+})$		−0.432	
Substrates				
Dihydroascorbic acid + $2H^+ + 2e^- \rightarrow$ ascorbic acid			0.058	
Fumarate^{2-} + $2H^+ + 2e^- \rightarrow$ succinate^{3-}			0.031	
Oxaloacetate^{2-} + $2H^+ + 2e^- \rightarrow$ malate^{2-}			−0.166	
Pyruvate$^-$ + $2H^+ + 2e^- \rightarrow$ lactate$^-$			−0.185	
Acetyl-CoA + $2H^+ + 2e^- \rightarrow \beta$-oxybutyryl-CoA			−0.238	

They play a definite role in photosynthetic electron transfer, nitrogen fixation, the reduction of nitrates and nitrites, and other processes. The ferredoxins function due to changes in the valence of their iron atoms.

Table 6.1 presents the values of the redox potentials of biological redox systems. The redox potential is a measure of the reduction ability of a system (in comparison with the reducing power of hydrogen at appropriate conditions).

The redox potential of any system depends upon the ratio of the concentrations of the reduced and oxidized forms of the substance, as well as the pH of the solution in many cases. According to Eq. (6.4), a change in the ratio $c_{Ox} : c_{Red}$ from $1 : 100$ to $100 : 1$ will shift the value of the redox potential from -116 mV in relation to the standard value to $+116$ mV, in the case of a one-electron reaction. In the case of a two-electron reaction, the shift will be one-half of these values. According to Eq. (6.4), the shift of a redox potential against the midpoint value may be of any size, provided there is correspondence in the ratio of the concentrations of reduced and oxidized forms. However, the interaction between two redox systems may be effective only under conditions where their midpoint potentials are close to each other. Should they differ significantly, electron exchange between the systems will be inhibited because the interacting forms, the donor and acceptor, respectively, will be present in very low concentrations. Besides, the conversion of a substance present in very small quantities will shift the potential of the system significantly, thus blocking any reaction progress.

In addition to the values for midpoint potentials of redox systems, the values of some substrates are also presented in Table 6.1. The redox conversions of these compounds proceed irreversibly and are followed by a significant change in the structure of their molecules.

ARRANGEMENT OF THE ELECTROCHEMICAL PROCESSES

The total effects of electrochemical processes linked with redox reactions are an indispensable part of the whole energy-transforming machinery of biological systems. They take part both in the transformation of light energy into chemical form in chloroplasts and in the processes that utilize the energy of oxidation of organic substances in mitochondria. In both cases the flow of electrons from a high energy level to a lower one takes places (Lehninger *et al.,* 1993). This flow occurs due to the consecutive transfer of electrons along a sequence of redox components with sufficiently similar values of redox potentials. This sequence is usually called the *electron transfer chain* (ETC). The mitochondrial ETC is often referred to as the *respiratory chain* because the main step of biological oxidation of organic matter and reduction of oxygen occurs here. The mitochondrial and chloroplast ETC significantly differ in their details, although they perform similar functions and contain similar components.

THE RESPIRATORY CHAIN

A simplified scheme for a probable sequence of events in the mitochondrial ETC is shown in Fig. 6.4. Electrons are delivered to the ETC from the reduced components of the Krebs cycle, such as pyruvate, isocitrate, α-ketoglutarate, succinate, and malate. The first link of the ETC consists of the enzymes known as the pyridine-dependent dehydrogenases. Their coenzymes are NAD^+ and $NADP^+$. NAD^+ is reduced by the addition of two electrons and one proton, while another H^+ is transferred to the surrounding medium. The substrate is oxidized by this release.

The next link of the chain, to which NADH releases the transferred electrons, is the flavoprotein NADH-dehydrogenase. Its prosthetic group is the flavin mononucleotide (FMN). The midpoint redox potential of FMN in its free state is -0.21 V at pH 7, but when complexed with the protein part of the enzyme it changes to a value of about -0.07 V. In addition to FMN, NADH-dehydrogenase contains another nonheme iron (FeS) centers, which also take part in electron transfer. Another component of the ETC that's very similar to NADH-dehydrogenase is another flavoprotein, succinate-dehydrogenase, which uses FAD instead of NAD^+ as its coenzyme. The midpoint potential of this enzyme is slightly more positive.
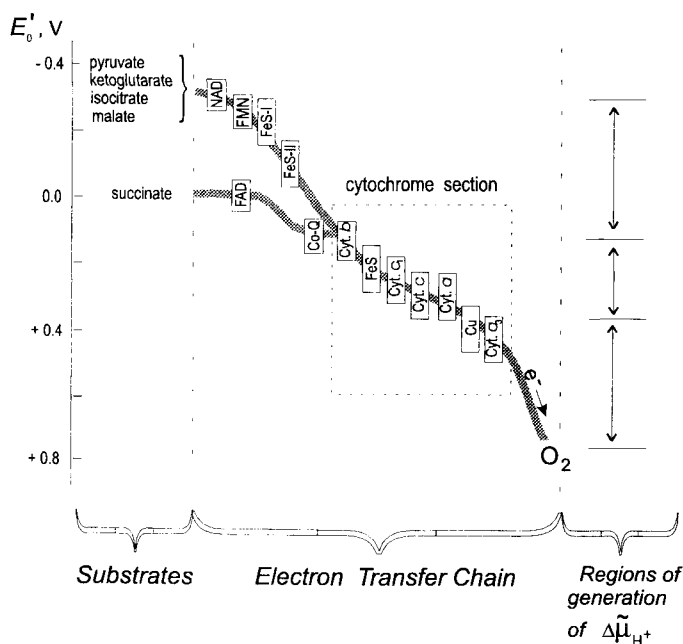

Figure 6.4   The scheme of the mitochondrial electron transfer chain.

The ubiquinones are found farther down the chain. The values of their midpoint potentials are about zero at pH 7. The subsequent path of electrons along the chain begins at the potentials of ubiquinone and continues down to the equilibrium potential of oxygen ($+0.82$ V at pH 7), starting with a set of cytochromes and ending with cytochrome-oxidase, an enzyme that contains copper and heme iron.

The electrons lower their chemical potential by $1.0-1.1$ V when descending the respiratory chain from a substrate to oxygen. This corresponds to the release of about 100 kJ of energy per mole. A fraction of this energy is saved in the form of the potential difference that arises across the mitochondrial membrane. In its turn, this potential difference is then converted into the energy stored in ATP. The conjugation of electron flow with the synthesis of ATP is termed *oxidative phosphorylation.* It is one of the two most significant processes of energy conversion in biological systems. The other is the process of photophosphorylation.

ELECTRON TRANSFER AT PHOTOSYNTHESIS

The process of photosynthesis involves the oxidation of water followed by the release of oxygen and the generation of highly reduced substances, which are then used to reduce carbon dioxide. Simultaneously, ATP is produced by the energy of electron flow down the ETC. The electron transfer chain is arranged more intricately than that in mitochondria, but the basic principle is quite similar.

A simplified scheme of electron transfer in the photosynthetic system is shown in Fig. 6.5. Higher plants use water as the prime source of electrons needed for reducing $NADP^+$ to the NADPH form. The latter in turn is required to reduce carbon dioxide. To transfer electrons from water to $NADP^+$, a redox potential difference of about 1.2 V needs to be overcome. The energy necessary to do this is imparted to an electron in two subsequent stages carried out by two distinct photosystems.

P_{680}, the component of the reaction center of photosystem II (PSII) acquires its excitation energy from the light-gathering antenna system. The electron from P^*_{680} is then taken up by the primary acceptor pheophytin (Pheo). The "holes" that remain after the detachment of electrons from P_{680} are accumulated by a special manganese-containing system, and when four are collected the oxidation of two water molecules occurs.

From the primary acceptor Pheo, the electrons move along the chain of redox components, which includes plastoquinones, cytochromes, and plastocyanine. The terminal point of this section of the ETC is the reaction center of photosystem I (P_{700}). Photosystem I provides a further rise of the energy level of electrons, but from a different energy level than photosystem II (for more details see Chapter 7). The electrons from P_{700} are then used for the production of NADPH, the strong reductant required to convert carbon dioxide into organic matter in the Calvin cycle. A fraction of the flow of high-energy electrons from PSI may branch off
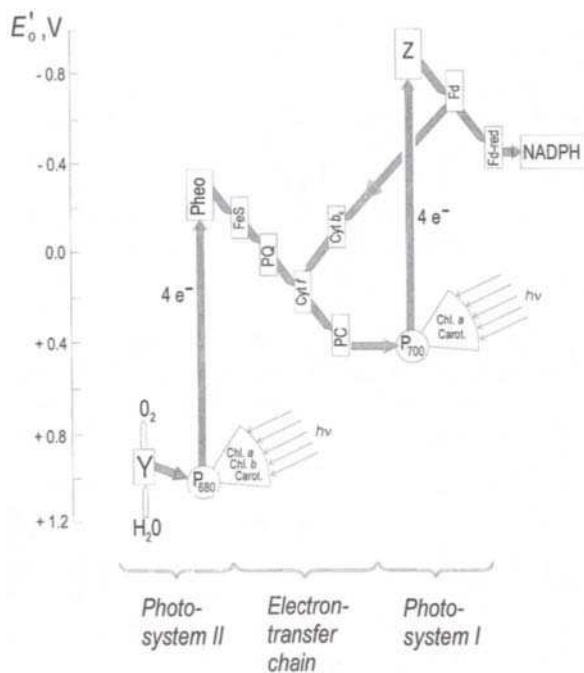
Figure 6.5 The scheme of electron transfer in a photosynthetic system.

and merge with the main stream of the electronic transfer chain, which links the primary acceptor of PSII with the reaction center of PSI.

Both PSI and PSII together perform two main functions: the generation of a substance of high reducing power and the synthesis of ATP. The latter process comes as a result of the coupling of electron flow in the electron transfer chain. The total difference in redox potentials across the ETC is about 0.8 eV in this case.

COUPLING OF ELECTRON FLOW WITH THE SYNTHESIS OF ATP

A question of great interest is how the energy of electron flow through a series of redox components of ETC is converted into the energy of ATP. The mechanism of energy coupling of electron flow and ATP synthesis remained puzzling until an electrochemical hypothesis was proposed by Mitchell (1961, 1976, 1979, 1984). This hypothesis is also known as the chemiosmotic theory (Mitchell, 1984; Nicholls, 1982). It has demonstrated its validity by explaining a great number of experimental facts although some details remain open to criticism, thus causing the appearance of other versions (Williams, 1961, 1978, 1994).

The topological aspects play a crucial role in the chemiosmotic theory. The coupling of electron flow to the synthesis of ATP is provided by the arrangement of thylakoid bags as closed containers whose internal volume is separated from the outer medium by a membrane (see Figs. 4.2 and 4.3). Because the membrane is a good insulator, a difference in electrical potentials between the inner and outer volumes of aqueous media may be created and sustained. The components of the electron transfer chain are localized across the membrane asymmetrically in quite a definite fashion. Their orientations thus define the direction of electron flow along the ETC and correspondingly the direction of the electric field that arises across the membrane as a result of the transfer of charge.

The ETC embedded in the membrane plays the role of an electronic conductor. Electrons enter the ETC and leave it as the result of anodic or cathodic electrochemical reactions at the membrane–water interface. The movement of electrons along the chain occurs as the result of subsequent transitions from one redox constituent of the chain to the next one in the sequence.

The presumed arrangement of the mitochondrial ETC, according to chemiosmotic theory, is shown Fig. 6.6A. The path of electron flow along the ETC embedded in the membrane begins at the level of NADH and terminates in the reduction of oxygen. The electrons cover this path in three subsequent loops crossing the membrane three times from the inner to the outer side and three times in the reverse direction. All of these steps are carried out with the participation of different electron carriers. All of the outward steps of electron transfer are followed by the simultaneous transfer of protons. All of the steps in the inward
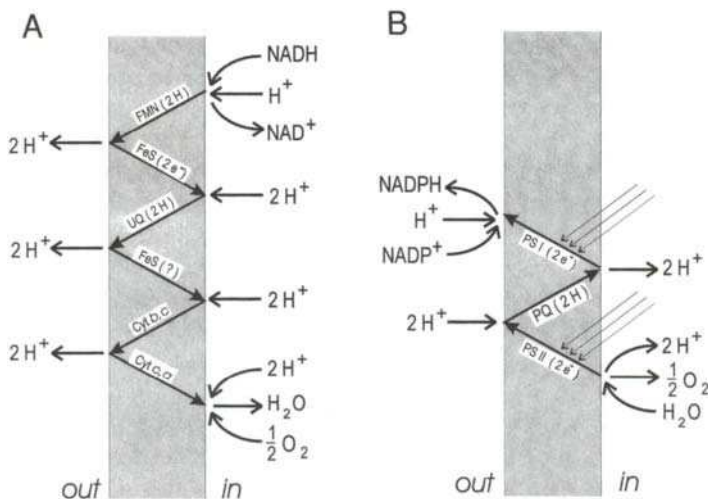

Figure 6.6 Simplified schemes of arrangement of electron transfer through the mitochondrial membrane (A) and through the thylakoid membrane (B) according to Mitchell's chemiosmotic theory.

direction are performed by the carriers that transfer only electrons. Due to the outward transfer of positively charged particles, the internal volume acquires a negative charge and the internal concentration of hydrogen ions diminishes (pH increases). As a result, an electrochemical potential gradient of protons arises across the membrane. The gradient is the form in which energy is stored across the membranes of chloroplasts and then used to produce ATP.

In this way, the large difference in the redox potentials of NADH and oxygen is divided into three parts and converted into a transmembrane gradient of proton electrochemical potential of a value of 0.25 eV. The amount of proton flux through the membrane is 3 times as large as the amount of electron flux. The passage of each electron along an ETC is followed by the transfer of three protons through the membrane. Thus, in the mitochondrial ETC a unique arrangment of the process is realized that has no direct analogue in artificial systems. Electrochemical tension is divided and current flow consequently multiplied in molecular electrical transformers. Such an arrangement makes it possible to store energy at a comparatively low voltage across the membrane. This enables the use of membranes that are thin enough, about 5–7 nm. If the transmembrane voltage were 2–3 times higher, thicker membranes would be needed to avoid rupture.

Electrochemical proton gradients comprise two components, one due to the difference in hydrogen ion concentration and the other due to the difference in electrical potential (see Eq. 6.1). The transmembrane difference in the values of proton electrochemical potential may be expressed in electric units as the proton motive force:

$$\Delta p = \frac{\Delta \tilde{\mu}_{H^+}}{F} = \Delta E - 2.3 \frac{RT}{F}(\Delta \text{pH}). \qquad (6.6)$$

The value of the proton motive force generated across the chloroplast membrane is usually about 0.25 V. The share of the electric component (ΔE) in this value is about 60% and that of the osmotic component is about 40% ($\Delta \text{pH} \sim 1.5–2$ units).

The arrangement of electron and proton transfer in chloroplasts significantly differs from that in mitochondria (Fig. 6.6B). First of all, the transmembrane movement of electrons is light-driven in this case. The functioning of both PSII and PSI is followed by the translocation of electrons from the inner side of the thylakoid membrane to the outer. In photosystem II the electrons are detached from water by the water-splitting complex. The protons released via this process remain in the inner volume of the thylakoid. The transfer of electrons along the ETC is followed by the inward translocation of protons. Thus, the overall process consists of the inward pumping through the thylakoid of four protons per two electrons used to split water and produce NADPH. In chloroplasts the direction of proton flow through the membrane is opposite that of mitochondria. The inner volume of the thylakoid becomes positively charged and more acidic than the external surroundings. The proton motive force across the thylakoid membrane reaches 0.2–0.25 V and is primarily due to the osmotic component

(ΔpH $\sim$ 3.5–4 units), whereas the electric component does not exceed 50 mV.

The fact that natural energy-transforming systems include electrochemical stages is of fundamental importance. This enables biological processes to switch between strictly localized processes, whose energy coupling requires common intermediates, to delocalized ones in which the acts of energy release and consumption can be separated in space and time. In biological electrochemical systems such as chloroplasts and mitochondria, energy is stored in the membrane structures as a transmembrane gradient of proton electrochemical potential. It is easy to notice some similar features between the biological energy conversion systems described here and electrochemical engineering systems, in which the point of energy generation is always separate from the point of its consumption. The distance may be different, from a few millimeters to many kilometers. In biological systems the transfer of energy in electrical form is limited to distances on the order of tens of nanometers.

By taking into account the dimensions of thylakoid disks (500 nm in diameter, $\sim$20-nm thickness of an aqueous layer), the buffer capacity of the internal phase of thylakoids [$\sim$0.1 mol H^+ (mol Chl)$^{-1}$ pH^{-1}], and the value of the electric capacity of the thylakoid membrane ($\sim 1 \mu F$ cm^{-2}) (Junge and Jackson, 1982), one can estimate that the absorption of two light quanta followed by the transfer of two electrons may cause a potential shift of 2 μV and a pH shift of 0.01 unit. Thus, the observed transmembrane gradient values are the result of the integration of many elementary acts executed by several thousands of photosynthetic units embedded in the membrane of a thylakoid disk. The sum of these microscopic generators jointly creates a transmembrane electric current of up to several microamperes per cm^2. Such a current density seems small compared with the values typical of engineering devices, but the total current that flows through the whole area of thylakoid membranes in a leaf is not so small. The transmembrane current within a leaf of about 50 cm^2 in area may be 0.3–0.5 or even 1 A under conditions of sufficiently intense photosynthesis.

The energy stored as the transmembrane gradient of electrochemical potential drives the processes of ATP synthesis. This function is carried out by the ATPases that are also incorporated into the membrane. Figure 6.7 shows schemes of electrochemical coupling of electron transfer and ATP synthesis. Synthesis of ATP in mitochondria is driven by the inward flow of protons through ATPase, whereas in chloroplasts the ATPase is oriented oppositely and is driven by outward proton flow.

IS THE NOTION OF REDOX POTENTIAL APPLICABLE TO SMALL SYSTEMS?

There is a question of fundamental significance that should be considered to conclude this chapter. The problem is to what extent the concept of redox potential
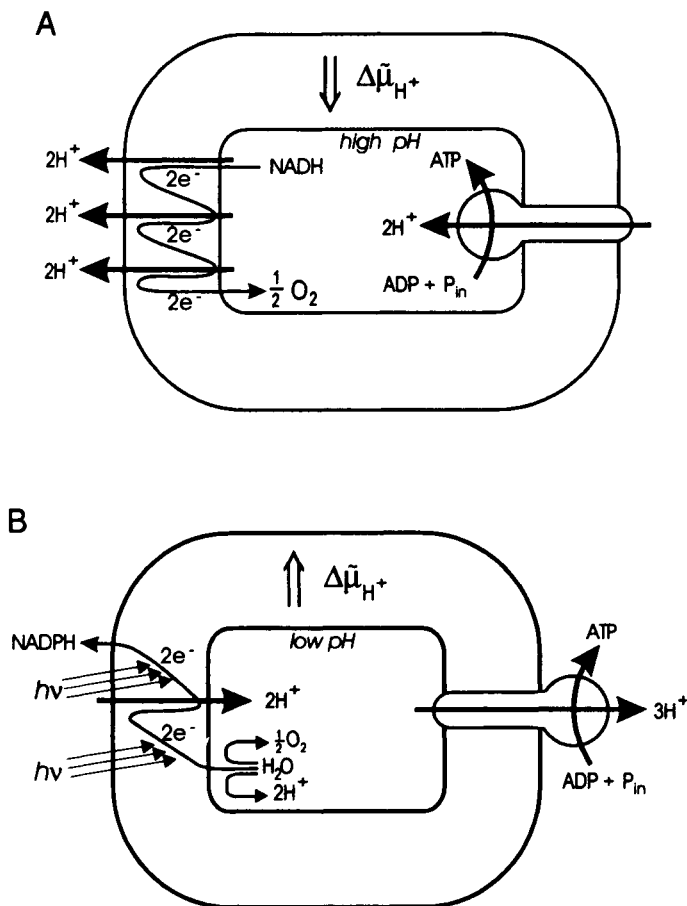
Figure 6.7   Coupling of electron transfer with ATP synthesis in mitochondria (A) and in chloroplasts (B).

may be applied to systems consisting of a small number of molecules. This concept is inherently a statistical one and is suitable for the description of large molecular ensembles. According to Eq. (6.4), the redox potential of a system depends upon the ratio between the number of molecules in an oxidized state and those in a reduced state. In large systems this ratio, i.e., the degree of oxidation, varies in a continuous manner. The situation changes, however, for a small system consisting only a few particles. An individual molecule may exist in only two discrete states, either oxidized or reduced. Therefore, the notion of degree of oxidation in its routine meaning cannot be used in relation to an individual molecule. Equation (6.4) also becomes invalid in relation to a single particle because the notion of concentration does not apply to a single molecule.

In considering biological objects, we have dealt with small, nonstatistical systems. The energy-transducing complexes embedded in the membranes of mitochondria or chloroplasts contain only a few molecules that develop redox properties and provide the translocation of electrons through the membrane. In analyzing such systems, the usual approach based on a statistical background can hardly be regarded as justified. The answer may be found in the ergodic hypothesis put forward by Ludwig Boltzmann. This hypothesis states that the time average of the state of a single molecule over a long period coincides with the average state of a sufficiently large number of molecules. As there is no possibility of determining the actual state of an individual molecule at a given moment, one should define it in terms of the probability of being in different states. This may be done by establishing the relationship between the probability of a molecule occurring in a certain state, whether oxidized or reduced, and the value of the redox potential of the macroscopic system with which the given molecule interacts. The probability of an individual molecule occurring at a given moment in a definite state is proportional to the average time of its existence in this state. This averaging must be carried out over a sufficiently long period in relation to the mean interval between the single interactions of an individual molecule with the reagents in an outer medium. The ratio of probabilities of finding the molecule in one of the possible states, either oxidized or reduced (P_{Ox}, P_{Red}), or the corresponding ratio of mean times that the molecule exists in each of them may be expressed as follows:

$$\frac{P_{Ox}}{P_{Red}} = \frac{\bar{\tau}_{Ox}}{\bar{\tau}_{Red}} = \exp\left[(E - E_m^*)\frac{nF}{RT} \right]. \tag{6.7}$$

Here E is the redox potential of the macroscopic system with which the given molecule interacts. E_m^* refers to the value of the potential when a given molecule may be found in either of two possible states with equal probability. It is easy to see that this equation and Eq. (6.3) are similar with only one distinction: in a macrosystem the redox potential is determined by the ratio of concentrations (activities) of oxidized and reduced forms, whereas in the case of a microsystem the redox potential of a component is determined by the ratio of the probabilities of the system being found in the corresponding states.

The ergodic hypothesis validates the applicability of the concept of redox potential to microscopic systems consisting of a single or several molecules. The redox potential of a small system is imposed by the redox potential of the macrosystem with which a small system is in equilibrium. The redox potential of the medium determines the ratio of probabilities of oxidized and reduced states of the small system considered. When the microsystem contacts the macrosystem with equal probability in the reduced or oxidized state, the value of the redox potential of the macrosystem in Eq. (6.7) is E_m^*. This value is characteristic of the redox properties of the microsystems under consideration. It should be emphasized that this potential does not correspond to any actual stable state of the single molecule under consideration.

If a molecule translocates from a statistical system (in solution, for example) into an isolated position (say, incorporated into a membrane complex) without a sufficient change in energy, the potential E_m^* may be accurately associated with the midpoint potential (E_m) of the appropriate macroscopic redox system. In a case where the translocation may occur with a noticeable change in energy, the potential shift may be tangible.

The relationship [Eq. (6.7)] between the redox potential and the probability that the molecule will be found in one of two conjugated redox states, i.e., to be either a donor or an acceptor of electrons, gives a key to understanding why electron transfer chains are designed from a large set of components that overlap a wide range of potential levels in small steps. Each molecule in the ETC functions in a cyclic manner by repeatedly passing from an oxidized state to a reduced one and back as a result of accepting electrons from a preceding link of the chain and passing them on to the next one. An event of electron transfer may happen only when neighboring links exist at a single time in opposite states, one being in an oxidized state and the other in a reduced one. The maximum rate of electron exchange between links may be expected under conditions where the probability of adjoining elements of the chain existing in alternate redox states does not significantly deviate from one-half. This means that the adjoining components of an ETC must have sufficiently close values of their redox potentials, E_m^*. If this condition is not satisfied, the probability of the simultaneous existence of adjoining components in the states necessary for mutual electron exchange would be low. A link in which this condition is not obeyed will limit the rate of electron flow in the chain as a whole. Thus, the design of an ETC as a series of links close to each other in potential might be expedient, making the efficient conduction of electrons through a membrane possible.

Chapter 7

Photochemistry of Photosynthesis and Mechanisms of Oxygen Evolution

INTRODUCTION

All of the energy available for life in Earth's biosphere is made available through photosynthesis. Photosynthesis is the bioelectrochemical process by which green plants, algae, and some bacteria absorb the energy of sunlight, convert it into electrochemical energy, and produce oxygen and organic compounds from carbon dioxide and water. The molecular oxygen in the atmosphere is the product of water photooxidation that occurs in the oxygen-evolving complex (OEC) of photosystem II (PSII) in photosynthesis. The most important attribute of solar energy is its ecological purity, i.e., the possibility of carrying out energy cycles without emitting harmful products into the surroundings and without additional heating of Earth. The wide-scale exploitation of solar energy requires practical solutions for the problems of the relative diffuseness of solar energy, the seasonal and daily variations in solar energy fluxes reaching Earth's surface, and the necessity to convert the energy of light quanta into an electrochemical form. Photosynthesis is our major link with the energy of the Sun.

The photosynthetic process can be divided into two main stages: a series of light-dependent photoreactions and a series of dark reactions. The first step in photosynthesis is the absorption of light by photosynthetic pigments (Fig. 7.1) such as chlorophylls, carotenoids, and phycobilins, which absorb slightly different wavelengths of light and transfer the energy to chlorophyll a pigments P_{680} and P_{700}. Accessory pigments thus broaden the spectrum of light energy that can be fixed through photosynthesis (Fig. 7.2). The photoelectrochemical processes cause the flow of an electric current, which as an intermediate converts the sunlight energy into chemical energy in the form of adenosine triphosphate (ATP) and nicotinamide adenine dinucleotide phosphate (NADPH).

155
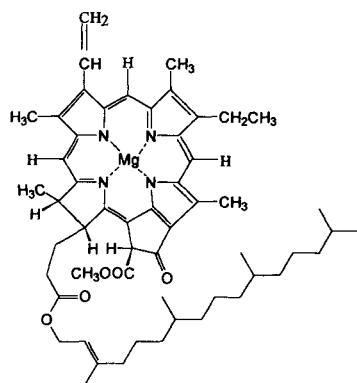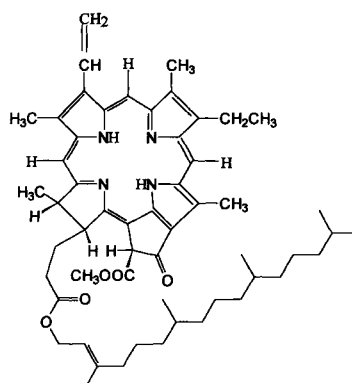
Chlorophyll a
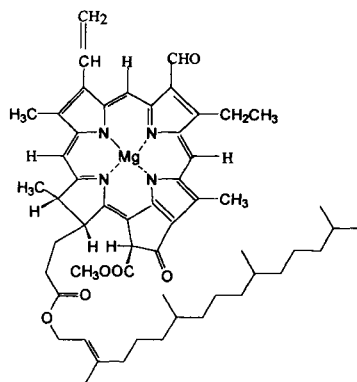
Pheophytin a

Chlorophyll b
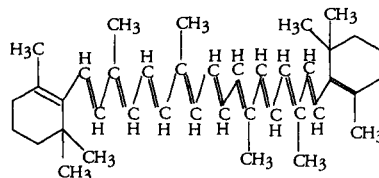
β-Carotene

Figure 7.1 Photosynthetic pigments: chlorophyll a, chlorophyll b, pheophytin a, and β-carotene.

The ability of light-excited chlorophyll molecules to become involved in reversible redox reactions underlies the primary processes of solar energy conversion into electrochemical energy that occur in chloroplasts. Some authors have proposed a molecular mechanism of water photooxidation in model systems containing chlorophyll a (Fong, 1982; Kutyurin 1965; Kutyurin *et al.*, 1975; Volkov, 1984). It is very likely that, in the earlier stages of the evolution of photosynthesis, chlorophyll was directly involved in the photooxidation of water to molecular oxygen. Such a photoelectrochemical reactor was able to operate for only a few hours (Volkov, 1984). Therefore, the structure and composition of the oxygen-evolving complex could undergo significant changes during the course of evolution of the photosynthetic apparatus to increase its stability and the functioning period.
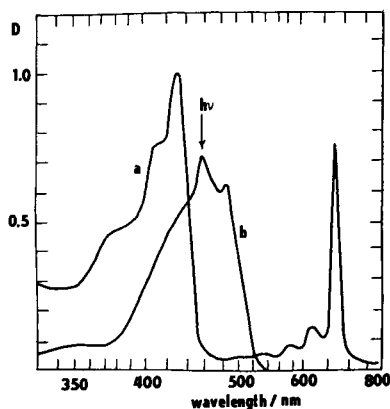
Figure 7.2   Absorption spectra of chlorophyll *a* (a) and β-carotene (b) in octane.

Carbon dioxide is reduced in the dark reaction to provide the basis for the sugar molecules. Plants reduce about 5×10^{14} kg of carbon dioxide per year during photosynthesis. The equation for photosynthesis in which water molecules serve as the electron and proton donor and carbon dioxide serves as the electron and proton acceptor is

$$6CO_2 + 6H_2O \rightarrow C_6H_{12}O_6 + 6O_2 \tag{7.1}$$
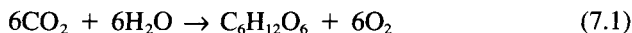
in which the following amount of Gibbs free energy is stored: $\Delta G \cong 480$ kJ (mol $O_2)^{-1}$. Chlorophyll and other plant pigments act as an antenna that traps the light of the Sun and converts it into the chemical energy of the products of photosynthesis. According to the Stark–Einstein law, one photon is required to excite one electron. To carry out one such cycle, a plant needs no fewer than eight quanta of red light at 680 nm, each with an energy of 176 kJ E^{-1}. Eight moles of photons at 680 nm contains 1408 kJ. The maximum possible efficiency of the conversion of solar energy by the eight-quantum reaction [Eq. (7.1)] is $100 \cdot 480/1408 = 34\%$ of the Sun's incident light. The theoretical maximum quantum yield is $100/8 = 12.5\%$, because eight photons are required to fix each molecule of CO_2. High efficiencies of solar energy conversion were found in maize (3.2%) and sugarcane (2.4%). The efficiency of the solar energy conversion can be defined as the ratio of the amount of energy stored to the total amount of light energy falling on the converter.

STRUCTURE AND COMPOSITION OF THE OXYGEN-EVOLVING COMPLEX *IN VIVO*

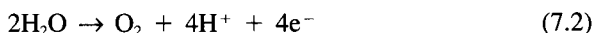The establishment of a mechanism of water photooxidation,

$$2H_2O \rightarrow O_2 + 4H^+ + 4e^- \tag{7.2}$$

Table 7.1

Polypeptides of the OEC

Molecular mass (kDa)	Functions	Bound chromophores
47	Intrinsic, antenna	Chl a
43	Intrinsic, antenna	Chl a
33	Extrinsic, regulation of Mn cluster	
34(D2)	Intrinsic, reaction center	Chl a, Pheo a, Q_A, Y_D^+
32(D1)	Intrinsic, reaction center	Chl a, Pheo a, Q_B, Y_Z^+
28	Intrinsic, electron pathway	Chl a
23	Extrinsic, regulation of Ca^{2+} effects	
22	Intrinsic	
17	Extrinsic, regulation of Cl^- effects	
9	Intrinsic	cyt b_{559}
4.5	Intrinsic	cyt b_{559}

to molecular oxygen, which takes place in photosystem II near the lumenal surface of the thylakoid membrane, is a key problem in photosynthesis. Photosystem II is an integral membrane protein complex that is present in green plants and all organisms that carry out oxygenic photosynthesis (Table 7.1).

The redox map of photosynthesis in green plants can be described in terms of the well-known Z-scheme of successive electron transfer from water to NADP proposed by Hill and Bendal (1960), with the participation of the two photosystems I and II. The main advantage of the currently accepted Z-scheme depicted in Fig. 7.3 lies in the specific mechanism of charge transfer at the stage of water photooxidation, according to the multielectron reaction mechanism involving none of the unknown intermediates of oxygen evolution. An important outcome of the photosynthetic reaction is that the light-induced electrical current causes water oxidation.

There are two independent types of photosystem in higher plants, each with its own antenna system and each carrying out quite different reactions. The first is photosystem II, whose reaction center chlorophyll a is P_{680}. The second is photosystem I, whose reaction center chlorophyll a is P_{700}. The Z-scheme should be considered not as a rigid chain of coherently linked electron carriers but rather as the kinetically most accessible path of electrons and protons in certain optimal conditions. Changes in temperature, the intensity and spectral composition of the light, electric double-layer effects, concentrations of products of photosynthesis and ionic compositions, partial pressures of carbon dioxide and oxygen, the stage of development of the chloroplast and the plant, genetic factors, and other circumstances all influence the ratio of the rates of the individual electron transport re-

Figure 7.3 Scheme of electron transfer in photosynthesis in higher plants. E_m° on the abscissa stands for the midpoint redox potential at pH 7.0. Light quanta ($h\nu$) are absorbed in two sets of antenna chlorophyll molecules. The excitation energy is transferred to the reaction center chlorophyll a molecules of photosystem II (P_{680}) and photosystem I (P_{700}), forming (P_{680})* and (P_{700})*, and the latter initiate electron transport (Volkov et al., 1995a). Reproduced by permission of Elsevier Science.

actions. These factors also lead to the locking and unlocking of the cyclic flows and the transfer of excitation energy between the parallel and serially linked photosystems, and in the negative feedback principle they correspond to homeostasis. An important factor accelerating the transfer of energy to reaction centers is the appropriate mutual orientation of the dipoles of the light-gathering molecules. The influence of the orientation factor is shown in the fact that energy is transmitted faster along ordered chains of molecules than through an ensemble with a random orientation.

The high efficiency of the supply of the energy of electronic excitation to reaction centers is ensured by the facts that the transfer of energy takes place faster than its dissipation, that the light-gathering molecules are ordered in relation to reaction centers and are oriented nonrandomly in relation to one another, and that a light-gathering antenna consists of a number of spectral forms of the pigments.

Carbon fixation uses the energy contained in ATP and NADPH to drive reactions that form organic compounds from carbon dioxide and water.

The molecular organization of a thylakoid membrane and its equivalent electrical circuit are shown in Figs. 7.4 and 7.5. The spectral characteristics of photosystem II indicate that the primary electron donor P_{680} is a dimer, or it may be a
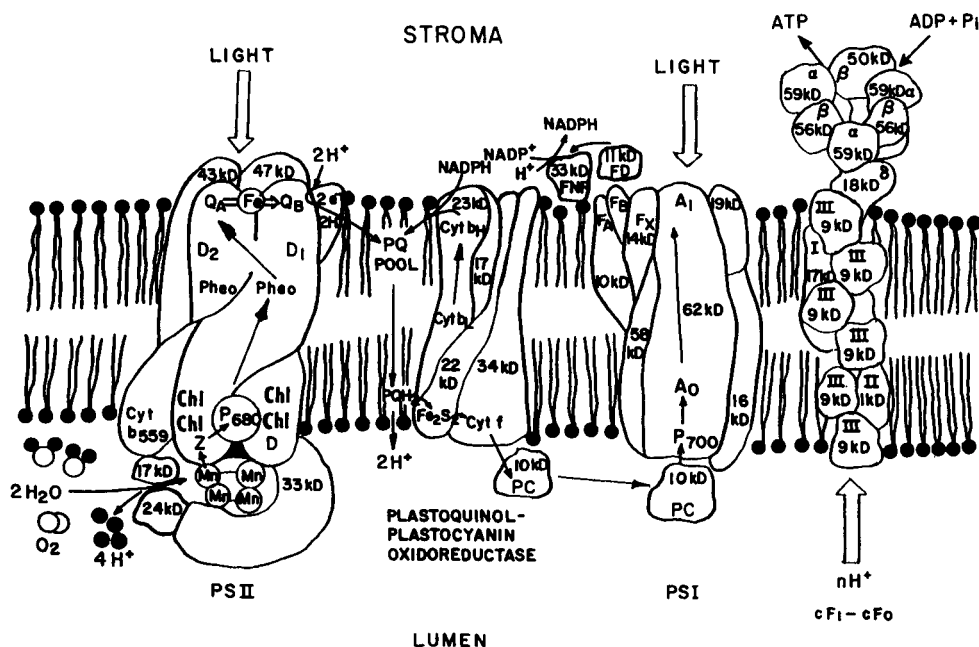

Figure 7.4   A stylized model of the electron transport chain with most of the light-harvesting pigment–protein complexes omitted (Volkov *et al.*, 1995a). Reproduced by permission of Elsevier Science.
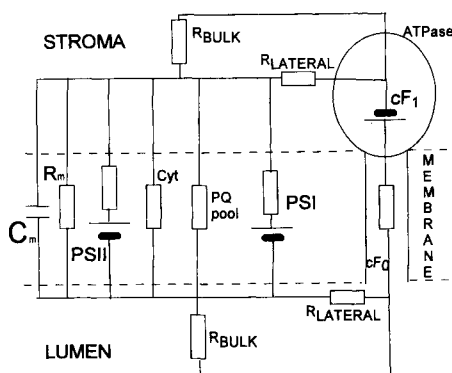
Figure 7.5 The equivalent electrical circuit of thylakoid membrane. Abbreviations: C, capacity; R, resistance; PS, photosystem; cF₁, coupling factor; PQ, plastoquinone; cyt, cytochrome (Volkov, 1989). Reproduced by permission of Elsevier Science.

monomer of chlorophyll *a* with absorption maxima near 680 and 430 nm. The photosystem II component of the plant photosynthetic apparatus oxidizes water at an oxygen-evolving complex that consists of a tetranuclear cluster of manganese ions along with the essential cofactors calcium and chloride. It was suggested that water can be oxidized by an OEC composed of several chlorophyll molecules, two molecules of pheophytin, tyrosine residues Y_Z and Y_D, plastoquinol, 2–3 calcium and several chloride ions, several plastoquinone molecules, and a manganese–protein complex containing four manganese ions. There are two redox-active tyrosine radicals in photosystem II: tyrosine 161 (Y_Z) of the D1 polypeptide, which participates in the water oxidation reaction, and tyrosine 160 (Y_D) of the D2 polypeptide, to which no function has been assigned. Although tyrosine Y_D is not directly involved in the electron transfer events that lead to water oxidation, it is in complex charge equilibrium with the water-oxidizing complex.

The Y_Z tyrosine serves as an electron transfer intermediate between P_{680} and the manganese cluster (Barry and Babcock, 1987; Debus *et al.*, 1988). Y_Z could be also involved as an intermediate in the proton transfer from a manganese cluster to the lumenal phase during water photooxidation. Gilchrist *et al.* (1995) and Hoganson *et al.* (1995) proposed a model of proton transfer from water bound to the manganese cluster through Y_Z, which can act as a photogenerated base (Fig. 7.6).

In green plants the main antenna complex spans the thylakoid membrane and contains noncovalently bound chlorophyll *a*, chlorophyll *b*, and carotenoids (Fig. 7.1). There are two populations of PSII centers, known as α- and β-centers, which have different size of the chlorophyll antenna.

Manganese-binding centers were first revealed in thylakoid membranes by EPR methods. The catalytic core of the oxygen-evolving complex is an ensemble
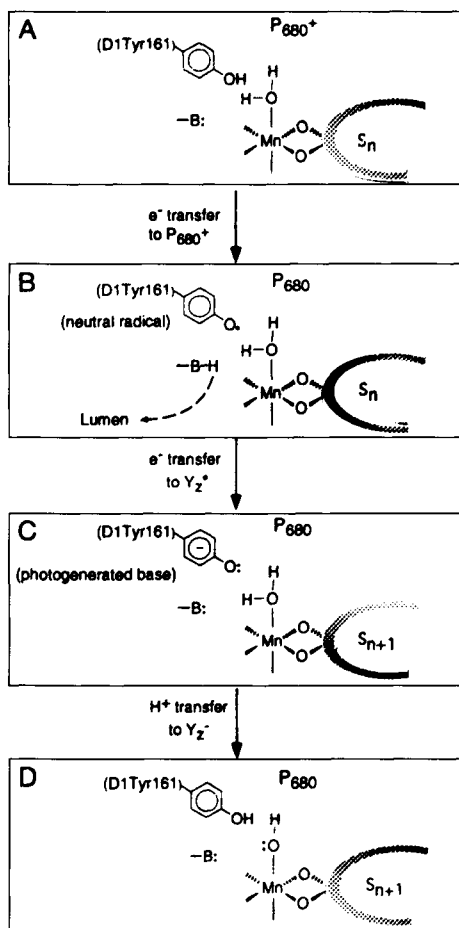
A

(D1Tyr161)

P_{680}^{+}

OH

H

H—O

—B:

O

Mn

O

S_n

e^- transfer
to P_{680}^{+}

B

(D1Tyr161)

(neutral radical)

P_{680}

O·

H

H—O

—B—H

O

Mn

O

S_n

Lumen

e^- transfer
to Y_Z^*

C

(D1Tyr161)

(photogenerated base)

P_{680}

O:

H

H—O

—B:

O

Mn

O

S_{n+1}

H^+ transfer
to Y_Z^-

D

(D1Tyr161)

P_{680}

OH

H

:O

—B:

O

Mn

O

S_{n+1}

Figure 7.6   The model (Gilchrist *et al.*, 1995) in which Y_Z, acting as a photogenerated base, abstracts protons from substrate water bound to the Mn cluster in OEC. (A) After the initial charge transfer, P_{680} is present as a cation radical, P_{680}^{+}. (B) Electron transfer to rereduce P_{680}^{+} leaves Y_Z in its neutral radical form, Y_Z^*, as the phenolic proton is transferred to a proximal base B. This proton can be quickly shuttled into the lumenal phase. (C) Y_Z^* is rereduced as an electron is transferred from the Mn cluster, advancing the S-state clock from S_n to S_{n+1}. The resulting deprotonated Y_Z is a strong base. (D) This strong base abstracts a proton from a water acidified by its ligation to a high-valence Mn ion of the cluster. A variant of this model would replace the sequential electron and proton transfers in steps B–D with a single H-atom transfer.

of four manganese atoms arranged in a cluster of undetermined structure. This manganese cluster cycles through five S-states (S_0–S_4) (Fig. 7.7) as it accumulates the four necessary oxidizing equivalents (Kok *et al.*, 1970), releasing O_2 during the S_3 to S_4 transition in one synchronous four-electron reaction or two two-

$$O_2 + 2H^+ \quad S_0$$
$$h\nu \quad \rightarrow H^+ + e^-$$
$$S_4 \quad 2H_2O \quad S_1$$
$$e^- \quad h\nu \qquad\qquad h\nu$$
$$\qquad\qquad h\nu \quad \rightarrow e^-$$
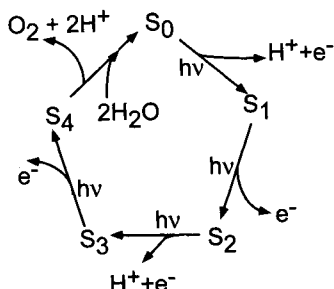$$S_3 \xleftarrow{\quad h\nu \quad} S_2$$
$$H^+ + e^-$$

Figure 7.7 S-clock of photosynthesis.

electron reactions (Volkov, 1989). Chloride and calcium are essential cofactors for oxygen evolution activity. Cl^- can be replaced with Br^- or I^- with activity retention. It has been postulated that halide is a ligand to manganese, but the evidence up to the present has not been conclusive.

In photosynthesis, one absorbed photon generates one oxidizing equivalent. Water photooxidation is a four-electron reaction, and quinone/quinol redox reactions (for example, Q_B pool) are two-electron reactions (Goldfield, 1982). Thus, the molecular "tumblers," which can accumulate redox equivalents for the multi-electron reaction, should exist in the electron transport chain of photosynthesis (Volkov, 1986 a–c, 1989). The manganese complex of PSII is a catalyst or a multielectron switch of the one-electron mechanism of P_{680}^+ reduction related to a multielectron mechanism of water photooxidation because it can donate four electrons through Y_Z to P_{680}^+ one by one in four separate redox reactions, and generate four positive equivalents in the Mn cluster for water photooxidation.

Plastoquinones Q_a and Q_b act as a transmembrane carrier of electrons and protons between the reaction centers of two photosystems in the case of noncyclic electron transfer. Besides, they may serve as a molecular "tumbler" to switch one-electron reactions over to two-electron reactions. A nonheme iron is present in close proximity to Q_a and Q_b.

Phenophytin (Pheo) is an intermediate acceptor in photosystem II. Direct formation of the $P_{680}^+ Pheo^-$ ion radical pair was revealed in the experiments on magnetic interactions between $Pheo^-$ and PQ^- reflected in the EPR spectra.

Despite considerable effort to elucidate the function of cytochrome b_{559}, its role in photosynthesis remains unclear. Cytochrome b_{559} stimulates molecular oxygen evolution in photosynthesis. It can take part in both the formation of electron pathways in the region of photosystem II and the utilization of protons.

ATP synthetase, lipids, cytochromes, plastoquinones, and polar groups of proteins are capaable of playing the role of regulators with respect to proton distribution over the thylakoid membrane (Volkov, 1987).

The oxygen-evolving complex is a highly ordered structure in which a number of polypeptides interact with one another to provide the appropriate environment

for production binding of cofactors such as manganese, chloride, and calcium, as well as for productive electron transfer within the photoact. The catalytic PSII core complex comprises at least five different hydrophobic proteins and a number of low-molecular-mass polypeptides. Table 7.1 illustrates the composition of chloroplast OEC.

This chapter discusses the physicochemical aspects of oxygen evolution during photosynthesis and does not consider the role of proteins or the mechanics and electrostatics of interactions between thylakoid membranes when photosystem II begins to function.

THERMODYNAMICS OF WATER OXIDATION

Water oxidation to molecular oxygen is a multielectron process that proceeds with a surprisingly high quantum efficiency. This process can be accomplished by a manganese cluster bound into a multicenter complex. The pathways of water oxidation to molecular oxygen are represented schematically in Fig. 7.8. Figure 7.9 shows the dependence of light energy on the wavelength of light. The water oxidation reaction can proceed upon illumination at 680 nm, a wavelength of light that excludes any process following one-electron mechanisms via hydroxyl and oxygen radicals (Fig. 7.8). For a three-electron reaction, a stronger oxidant than the cation radical P_{680}^+ is needed. A 2:2-electron pathway for the reaction is thermodynamically possible if the standard free energy of binding of the two-electron intermediate is about -40 kJ/mol. This value corresponds to the
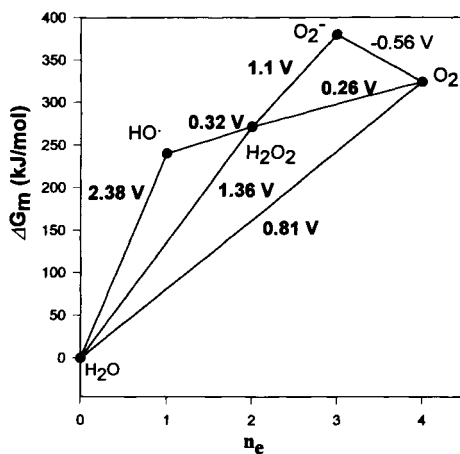
Figure 7.8 Energy schemes of possible pathways of water oxidation to molecular oxygen.
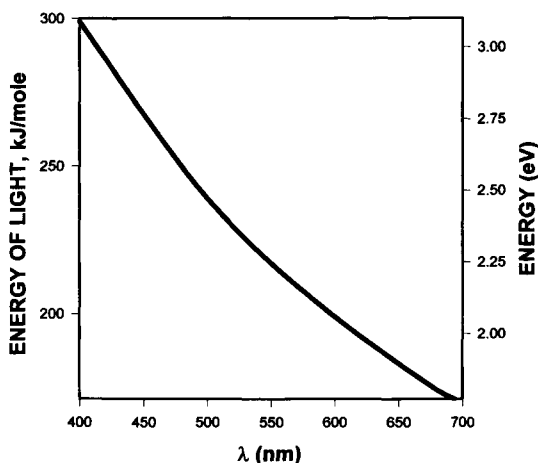
Figure 7.9   The dependence of the energy of light on its wavelength.

energy of two hydrogen bonds that form between H_2O_2 and the catalytic center. For this case, a molecular mechanism can be suggested for the reaction shown in Fig. 7.10 and will be discussed here. In fact, some authors have reported the presence of hydrogen peroxide in the functioning photosystem II. However, they performed measurements using metal electrodes immersed in incubation medium at potentials favoring the formation of hydrogen peroxide as a byproduct due to electrochemical polarization.

Even in the case where free H_2O_2 formation can be discounted on the basis of experimental setup, this finding would not eliminate the possibility of tightly bound H_2O_2 formation. Ananjev and Klimov (1988) and Klimov *et al.* (1993) discovered light-induced formation of bound hydrogen peroxide in the subchloroplast preparation of photosystem II. The results provide experimental evidence for the 2:2-electron mechanism of water photooxidation, which is suggested in Fig. 7.10. With a minimum of additional assumptions, our model corresponds to many modern views on the composition and functioning of the oxygen-evolving complex.

It should be noted that one- and three-electron mechanisms of water oxidation are thermodynamically feasible if the intermediates produced are bound in the form of cryptoradicals (Renger, 1977). Such species have never been reported to occur in natural photosynthesis. Nevertheless, the cryptoradicals are highly reactive and can readily enter into side reactions of hydroxylation, oxidation, and destruction of components of the reaction center.

Synchronous 2:2- and four-electron oxidations of water to molecular oxygen (Figs. 7.10 and 7.11) are the only two thermodynamically possible pathways.
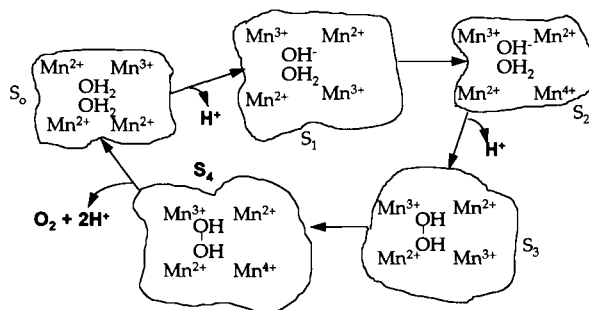
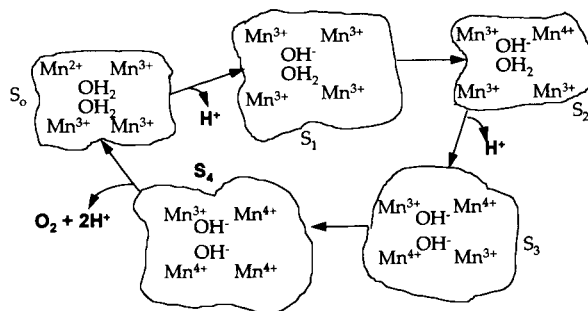**Figure 7.10** Possible 2:2-electron mechanism of water photooxidation (Volkov, 1989). Reproduced by permission of Elsevier Science.

One-electron mechanisms of water oxidation are likely to be operative in some model systems with low quantum efficiency. The intermediates formed in these systems are also highly reactive and can readily enter into side reactions of hydroxylation, oxidation, and destruction of chlorophyll and other components of the reaction center. The similar conclusion about the possibility of 2:2- or four-electron pathways of the water photooxidation reaction was drawn from a thermodynamic analysis of the conception of configurational energy instead of midpoint or standard Gibbs free energy (Krishtalik, 1986).

The configurational Gibbs free energy, ΔG_c, is the part of the free energy that does not depend on the transpositional contribution to entropy, which defines the direct dependence of ΔG on a concentration (Krishtalik and Kuznetsov, 1986). The configurational Gibbs free energy is different from the standard Gibbs free energy, ΔG^0:

$$\Delta G_c = \Delta G^0 + RT \ln \left(\prod_n X_i^0 / \prod_m X_f^0\right). \tag{7.3}$$

Figure 7.11 Possible synchronous four-electron mechanism of water photooxidation (Volkov, 1989). Reproduced by permission of Elsevier Science.

Here X_i^0 and X_f^0 are the mole fractions of n initial (i) and m final (f) reagents in their standard states. If the reaction is not accompanied by a change in the number of particles, there is no difference between the ordinary standard free energy and the configurational one. However, if it is accompanied by a change in the number of particles (e.g., in the case of decomposition of a molecule), the expression for the elementary act involves only the configurational free energy, which does not include the entropy of the particles mixing. ΔG_c is the free energy of an elementary act of the reaction, and it differs from the work of the reaction by the work of mixing reagents depending on the concentration. In the case of interfacial reactions, the quantity that corresponds to ΔG_c will be a configurational interfacial potential (Krishtalik and Kuznetsov, 1986):

$$E_c = - \Delta G_c / nF \tag{7.4}$$

The values of configurational potentials of the redox couple H_2O/O_2 are shown in Fig. 7.12. At the interfacial potential equal to E_c, the free energy of the elementary act of the interfacial reaction

$$Ox + e^- \leftrightarrow Red \tag{7.5}$$

is zero. At interfacial potentials $\Delta_\beta^\alpha \phi$ different from $\Delta_\beta^\alpha \phi_c$, the free energy of the elementary act will be $nF(\Delta_\beta^\alpha \phi - \Delta_\beta^\alpha \phi_c)$. Calculations of the configurational Gibbs energy and configurational redox and electrode potentials and the comparison of their values with standard Gibbs energies and standard redox potentials can be found in the literature (Krishtalik, 1986; Krishtalik and Kuznetsov, 1986).

Comparison of the configurational redox potential of Eq. (7.2), $\Delta_\beta^\alpha \phi_c = 1.4$ V, with the redox potential of the primary oxidant P_{680}, $E' = +1.1$ V, shows that the redox potential of an oxidant is lower than the configurational potential of the
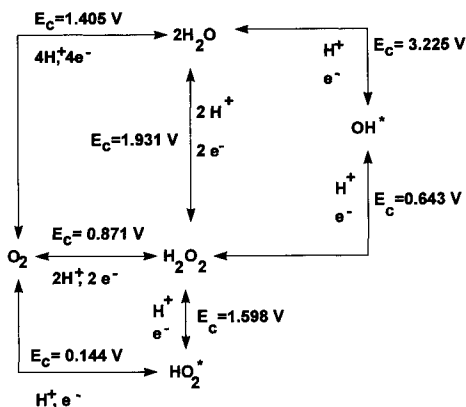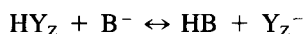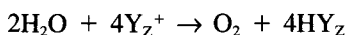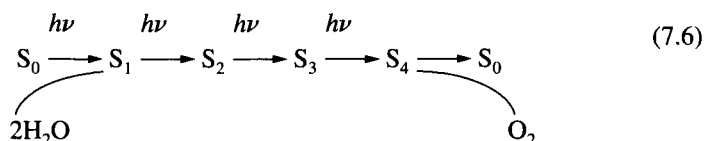

Figure 7.12 Configuration potentials of H_2O/O_2 redox reaction pathways. Values of E_c are taken from Krishtalik (1986).

water oxidation reaction. This energy deficit can be covered by protons binding to some organic groups, for example, tyrosine residues or carboxylic groups:

$$2H_2O + 4Y_Z^+ \rightarrow O_2 + 4HY_Z$$

$$HY_Z + B^- \leftrightarrow HB + Y_Z^-$$

UTILIZATION OF PROTONS
UPON OXYGEN EVOLUTION

The vectorial transport of electrons in the thylakoid membrane leads to the translocation of protons and ATP synthesis. The mechanism of oxygen evolution during photosynthesis correlates with the linear S-cycle of photosynthesis. The electron detachment in the sequence, $1:1:1:1$, is accompanied by charge formation, $0:+:+:0$, and proton release, $1:0:1:2$ (Saygin and Witt, 1985), for the following transition:

$$S_0 \xrightarrow{h\nu} S_1 \xrightarrow{h\nu} S_2 \xrightarrow{h\nu} S_3 \xrightarrow{h\nu} S_4 \rightleftharpoons S_0 \qquad (7.6)$$

$$2H_2O \qquad\qquad\qquad\qquad\qquad O_2$$

Among the S-states, only S_1 exhibits long-term dark stability. S_2 and S_3 decay to S_1 in the dark in minutes. S_0 is oxidized slowly in the dark to S_1.

Protons can be ejected from the reaction center (RC) in two ways: by regulators of proton distribution and by the Grotthus mechanism through the hydration shell of manganese or calcium ions. Exogenous manganese is known to contain, in its ligand sphere, water molecules rapidly exchanging protons with water in the bulk (Goldfeld, 1982). The presence of bivalent cations at the interface between two immiscible electrolyte solutions facilitates the strong adsorption of water molecules belonging to the second hydration shell of ions (Volkov *et al.*, 1996). Thus, a portion of coordinatively bound water enters the compact part of the electric double layer, which results in a change in its differential capacitance at the interface. In the case of multivalent ions with small radii, the electric field near a cation is large and thus disturbs the microstructure of the adjacent intrathylakoid space and causes dielectric saturation effects.

Dissociation of two water molecules during the S-cycle results first in the successive release of two protons linked within the catalytic complex, followed by the synchronized ejection of two more protons during the evolution of molecular oxygen. The estimated number of protons in a thylakoid with an inner volume of 5×10^{-22} m^{-3} at neutral pH (7.0) must be 0.03, i.e., the probability of their presence within the intrathylakoid space is far less than unity. The oxidation of

two water molecules to O_2, involving the release of four protons, formally brings the pH value to 5.0.

The problems of utilization of four protons released during the course of molecular oxygen evolution are far from being settled. These protons are basically linked with the membrane and can be used for a condensation reaction, such as the synthesis of ATP via ATP synthetase (Mitchell, 1961, 1984; Williams, 1961, 1994). The common intermediate between redox and condensation reactions is a proton gradient or, in more general terms, a transmembrane concentration gradient of any hydrophilic cation (Kornyshev and Volkov, 1984). The lateral transport of protons (Williams, 1961, 1994) for ATP synthesis is more advantageous from an electrochemical point of view in terms of energy consumption compared to chemiosmotic coupling (Mitchell, 1961, 1984) due to energy dissipation in the additional stages of proton transfer from the nonpolar membrane region into the aqueous bulk phase and back into the membrane. Williams' original idea of localized proton migration was the movement of protons around two large clusters, redox and ATP sites, in a diffusion pathway that did not allow the collapse of the ion gradient. This did not exclude limitation by a delocalized membrane system. However, the smaller the volume involved, the smaller the buffer capacity that has to be overcome (Williams, 1961). In the opinion of Dilley (1991), the protons liberated in the reaction center of photosystem II may be transported into the intramembrane domains through the amino groups in the proton channel of ATP synthetase, without leaving the thylakoid membrane. In this case, just as in Williams' scheme, ATP synthesis will occur on account of the Gibbs free energy of resolvation of the partially dehydrated protons. The Gibbs free energy of hydration of completely desolvated H^+ is 30 times greater than the energy of ATP synthesis (Kornyshev and Volkov, 1984). A total of 99% of protons generated in the reaction centers is bound to the membrane surface. Generally speaking, both pathways of proton transport, transmembrane and lateral, in membrane domains could be involved in the reaction of ATP synthesis. Both Mitchell's and Williams' mechanisms of coupling of redox chains and phosphorylation are based on the same energetic principle: the source of energy is the gradient of the electrochemical potential of protons or small hydrophilic cations.

KINETIC ASPECTS OF MULTIELECTRON REACTIONS

The probability of electron transfer between two centers in a condensed medium is determined by the probability of the electron transition from the initial to the final state and the probability of a transition of the vibratory subsystem (Kharkats and Kuznetsov, 1996). A vibratory subsystem includes both the inherent intromolecular vibration of the donor and acceptor and the vibration of the surrounding molecules if the electron interacts with them. The probability of the

transition of the vibratory subsystem reaches a maximum when the difference in the electron energies of the initial and final stages is equal to the energy of reorganization of the vibratory subsystem.

The energy of reorganization of the medium, E_s, is an important parameter in the quantum theory of charge transfer in polar medium, and in the case of homogeneous reactions that take place in one phase it can be described in the longwave approximation by the following relation:

$$E_s = \frac{1}{2\epsilon_0} \left(\frac{1}{\epsilon_{op}} - \frac{1}{\epsilon_s} \right) \int_{\infty - V_a - V_b} (\vec{D}_i - \vec{D}_f)^2 \, dV, \qquad (7.7)$$

where ϵ_{op} and ϵ_s are the optical and the static dielectric permittivities of the medium, respectively, and $\vec{D}_i$ and $\vec{D}_f$ are the induction of the electric field created in the solvent by the transfer of charge in the initial and final states, respectively. Integration in Eq. (7.7) is carried out over the entire volume of the medium except that of the reactants.

According to Marcus (1956), the energy of medium reorganization for a charge transfer between two spherical ions, with the charge uniformly distributed over their surfaces, can be computed from the formula:

$$E_s = \frac{e^2 n^2}{4\pi\epsilon_0} \left(\frac{1}{\epsilon_{op}} - \frac{1}{\epsilon_s} \right) \left(\frac{1}{2a} + \frac{1}{2b} - \frac{1}{h_{12}} \right), \qquad (7.8)$$

where n is the number of charges transferred in one act, a_i is the radius of the ith component, and h_{12} is the distance of charge transfer. It follows from Eq. (7.8) that E_s is proportional to the square of the number of charges transferred. This factor makes multielectron processes impossible in the majority of homogeneous redox reactions due to the high activation energy resulting from a sharp rise in the energy of solvent reorganization. For multielectron reactions the exchange currents of n-electron processes are small compared to those of one-electron processes, which makes the stage-by-stage reaction mechanism more advantageous. Multielectron processes can proceed only if the formation of an intermediate is energetically disadvantageous. It can, however, be seen from Eq. (7.8) that conditions can be chosen that reduce E_s, during the transfer of several charges, to the level of the reorganization energy of ordinary one-electron reactions. These conditions primarily are systems with a low dielectric constant, large reagent radii and optimized correlation of their sizes, inclusion of the substrate into the coordination sphere of the charge acceptor, and simultaneous use of several charge donors or acceptors bound into a multicenter complex. Some reports present the results of theoretical studies on the kinetics of heterogeneous multielectron reactions at the interface between two immiscible liquid media: water–oil and water–biomembrane. The interface proved to be capable of catalyzing multielectron reactions and sharply reducing the activation energy.

The energy of medium reorganization in systems with complicated charge dis-

tribution was calculated by Kharkats (1978). Reagents and products can be represented by a set of N spherical centers arbitrarily distributed in a polar medium. The charges of each of the reaction centers in the initial and final states are z^i and z^f, respectively. R_k represents coordinates of the centers and ϵ_i the dielectric constants of the reagents in the following:

$$
E_s = \frac{0.8}{4\pi\epsilon_o}\left(\frac{1}{\epsilon_{opt}} - \frac{1}{\epsilon_{st}}\right) \times \left\{ \sum_{p=1}^{N} \left[\frac{(\delta z_k)^2}{2a_p} + \sum_{\substack{k=1 \\ k\neq p}}^{N} \frac{(\delta z_p)(\delta z_k)}{2R_{pk}} \right. \right.
$$
$$
\left. \left. + \sum_{\substack{k=1 \\ k\neq p}}^{N} \sum_{\substack{l=1 \\ l\neq p}}^{N} \frac{(\delta z_p)(\delta z_k)\, a_p^3\, (\vec{R}_{pk}\vec{R}_{pl})}{R_{pk}^3\, R_{pl}^3} \left(\frac{3\epsilon_{st}^2}{(2\epsilon_{st} + \epsilon_i)^2} - \frac{1}{2} \right) \right] \right\}, \quad (7.9)
$$

where $(\delta z_k) = z_k^f - z_k^i$, $R_{pk} = R_p - R_k$, z_k^f, and z_k^i are the charge numbers of particle k in the initial and final states, respectively, a_p is the radius of particle p, R_k is the coordinate of k particle center, and ϵ_i is the dielectric constant of reactant i. Reactions with synchronous transfer of several charges present a partaicular case of Eq. (7.9). As a particular case, Eq. (7.9) gives the medium reorganization energy for several simultaneous charge transfer reactions.

The most effective coupling of ATP synthesis and the electron transport chain can be obtained if the activation energy of the coupled process is lower than that of the charge transfer in the electron transport chain. It is obvious from Eq. (7.9) that, in a general case, such a situation can be attained by the simultaneous transfer of opposite charges, so that the second and the third terms of Eq. (7.9) would be negative. An optimal geometry between the centers of charge of donors and acceptors must also be chosen.

Consider two instances of multielectron reactions: simultaneous transfer of n charges from one donor to an acceptor and simultaneous transfer of several charges (one from each of the centers) to m acceptors ($m \leq n$). In the former case E_s is proportional to n^2, while in the latter it may be significantly lower (depending on the sign of the charge being transferred and the reciprocal positions of the reagents). A multicenter process with $E_s \cong n$ is also possible. The concerted multicenter mechanism of multielectron reactions is likely to contribute to a marked reduction in E_s and, hence, in the activation energy compared with a two-center multielectron process. Electrostatic interactions between reagents may constitute an additional factor favoring the activation energy reduction of multielectron processes at the membrane–solution interface. Unlike the electron transfer process in a homogeneous dielectric medium, where the work of the mutual approach of reagents or reaction products becomes zero if one of the reagents or products is electroneutral, the energies of electrostatic interactions in the heterogeneous process in question can never be equal to zero due to interactions with image charges.

With an appropriate arrangement of the reagents, the electron transfer activation energy in such heterogeneous multielectron reactions occurring on the

surface of thylakoid membranes may be many times lower than the energy of medium reorganization (Kharkats and Volkov, 1985, 1987).

For the effective storage of electron excitation energy, the primary charge separation must satisfy the following necessary conditions:

- the transfer of an electron from donor to acceptor must occur in a time less than the lifetime of the initial excited state,
- this transfer must be sufficiently irreversible and the back processes must be sufficiently slow for the electron to move on in the transport chain,
- in this process the smallest possible share of the excitation energy must be lost.

POSSIBLE MOLECULAR MECHANISMS
OF OXYGEN EVOLUTION

Table 7.2 lists possible mechanisms of water photooxidation in reaction centers of photosystem II in green plants.

The chlorophyll dimer P_{680} incorporated into membrane becomes excited upon illumination. In dimers and other aggregated forms of chlorophyll, the quantum efficiency of triplet states is low and it is the singlet excited states that undergo photochemical transformations. The primary stages of charge separation in the reaction centers of green plants take place in $1-10$ ps, or far faster than the intramolecular waste of the energy of electronic excitation by fluorescence, transformation into heat, or conversion into a triplet state, the characteristic times of which are $1-10$ ns. In several picoseconds, an electron is first transferred to a Pheo molecule (Fig. 7.3), forming P_{680}^+ and Pheo$^-$. An electron is transferred from the oxidized primary donor P_{680}^{+*} through a chain of acceptors. Each step of transfer is accompanied by some decrease in the energy of the system and increase in the spatial separation of charges of opposite sign. Thus, at each stage the direct transfer of an electron to the following acceptor is more probable than back-reaction.

Rapid oxidation to plastoquinone Q_A then takes place, and from plastoquinone Q_A to another polypeptide-bound plastoquinone, Q_B, in the thylakoid membrane (Fig. 7.3). An oxidized form of pigment and a reduced form of acceptor are formed. The cation radical P_{680}^+ successively oxidizes four manganese ions. The transfer of four electrons results in the formation of molecular oxygen (Fig. 7.9). Formation of a cation radical of chlorophyll or oxidation of manganese ions is accompanied by dissociation of water from the reaction center and ejection of the released proton.

Anions (Cl^-, Br^-) play a functional role in electrostatic compensation of charges during redox transitions in OEC. The S-state dependence of Cl^- binding

to plant photosystem II was carefully investigated. No detectable high-affinity binding was found to particles in the S_0- and S_1-states, although binding with an affinity comparable to that which activates dioxygen evolution was found in the S_2- and S_3-states.

One-electron multistep mechanisms 1–17 of water oxidation (Table 7.2), as has been shown, are energetically unlikely. Moreover, neither intermediates nor cryptoradicals have so far been experimentally observed. Mechanisms 1–5, 7, 12–15, 18, 21, 23, 24, and 30 do not describe the sequence of H^+ ejection in the S-cycle. Two-electron mechanisms 18–20 and four-electron 21–34 are thermodynamically possible, but the molecular pathways 21, 23, and 32 were not described by the above-mentioned authors and it is not clear whether they conform to the S-cycle. Mechanisms 23, 26, 31, and 33 cannot be very effective since the energy of medium reorganization at the mononuclear center is large due to kinetic limitations [see Eq. (7.4)]. Mechanisms 20, 25, 27, and 29 conform to the aforesaid kinetic and thermodynamic features and fully comply with the S-cycle of H^+ ejection. A drawback of mechanism 26 is that it is not concrete, i.e., the nature of M_i and the oxygen-evolving enzyme is obscure.

Water oxidation can be interpreted as a four-electron process, where each S-state transition is assigned to the oxidation of one atom in a manganese cluster. It should be mentioned that Kok's original S-state hypothesis implied that a concerted four-electron process occurs upon the $S_4 \rightarrow S_0$ transition.

Moravsky and Khramov (1987), Moravsky *et al.*, (1984), and Brudvig and Crabtree (1986) have suggested structural mechanisms. In the Moravsky–Khramov model (Table 7.2, mechanism 25), the OEC contains four ions of manganese deposited at the apexes of a cube, two of which occur by μ_3-hydroxo or oxo ligands. The cubane structure represents two interpenetrating tetrahedrons, and in the corner of one of them (which is usually of a smaller size) are four oxygen atoms, resulting in a deformed cube. The S_0-state in this model contains three Mn(III), one Mn(II), and two hydroxy groups. As can be seen from pathway 25 in Table 7.2, every OH group is a μ_3-hydroxo bridge. EXAFS data show that near each manganese there is still one transition metal atom. This atom may be another atom of manganese. The distances between these atoms are similar to those in the well-known binuclear μ_2-oxo complexes, in which manganese ions are bound by two bridges from oxygen.
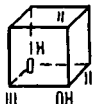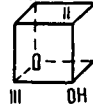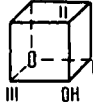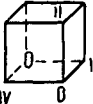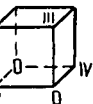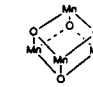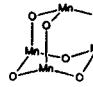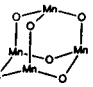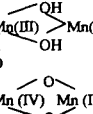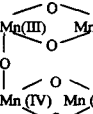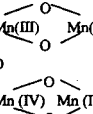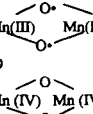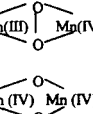
At a minimum of additional assumptions, the Moravsky–Khramov model corresponds to many modern views on the composition and functioning of the OEC, e.g., in the order of proton release at the sequential center oxidation and the presence of two pairs of manganese ions, differing in their function and the strength retaining them in the active center.

There are principal differences between pathways 25 and 27. Model 25 suggests a concrete synchronous four-electron path of water oxidation through an outer sphere mechanism of electron transfer without essential alteration in the

Table 7.2

Model	S_0 $\xrightarrow{h\nu}$ S_1	$\xrightarrow{h\nu}$ S_2	$\xrightarrow{h\nu}$ S_3	$\xrightarrow{h\nu}$ S_4
1:1:1:1 - electron	*mechanisms*			
1. Kutyurin, 1965	$2[Chl(H_2O)_xMe^{n+}]$	$[Chl^+(H_2O)_xMe^{n+}]$ $[Chl(H_2O)_xMe^{n+}]$	$2[Chl^+(H_2O)_xMe^{n+}]$	$2[Chl^+(H_2O)_{x-1}Me^{n+1}]$ [OH]	$2[Chl^+(H_2O)_{x-2}Me^{n+2}]$ $2[OH]$
2. Olson, 1970	Mn^{3+} ONOH HONO $Mn^{3+}OH_2$ Mn^{3+} $Mn^{3+}OH_2$	Mn^{3+} ONO HONO $Mn^{3+}OH$ Mn^{3+} $Mn^{3+}OH_2$	Mn^{3+} $O=N^+=O$ $Mn^{3+}OH$ Mn^{3+} $Mn^{3+}OH$	Mn^{3+} $O=N-O-H$ $Mn^{3+}OO$ Mn^{3+} Mn^{3+}	$2H_2O$ $\downarrow$ O_2
3. Mauzeral and Chivis, 1973	$Mn3+OH_2$ O O ‖ ‖ R–C–C–C–R H R	$Mn3+OH_2$ O O ‖ ‖ R–C–C–C–R H R	$Mn3+OH$ –C–C– $\overset{+}{C}$	H O $Mn3+$ –C C– C H	HO O $2H_2O$ C–C C– C H O_2
4. Earley, 1973	Mn — O O Mn Mn — O	Mn — O — OH O Mn Mn — O	Mn — O···O O Mn Mn — O	Mn — O–O O Mn Mn — O — OH	Mn HO-O-O-O Mn Mn O-OH
5. Renger, 1977	M---M^*	$(H_2O)^*$ → $(OH)^*$ +H$^-$	$(H_2O)^*+(OH)^*$→ $(H_2O_2)^{**} + H^-$	$(H_2O)^* + M^*$ → $(O_2)^{**} + 2H^+ +M$	$(O_2)^* + 2H_2O$ → $O_2 + 2(H_2O)^*$
6. Govindjee et al., 1977	Mn^{2+} Mn^{3+} OH_2 Mn^{3+} Mn^{2+} OH_2	Mn^{3+} Mn^{3+} OH_2 Mn^{3+} Mn^{2+} OH^-	Mn^{3+} Mn^{3+} OH_2 Mn^{3+} Mn^{2+} OH^-	Mn^{3+} Mn^{2+} OH Mn^{2+} Mn^{3+} OH	Mn^{3+} Mn^{2+} $2OH_2$ Mn^{2+} Mn^{3+}
7. Lawrence and Sawyer, 1978	Mn^{2+} $(OH_2)_2$ Mn^{2+} $(OH_2)_2$	Mn^{3+}-OH$^-$ OH$_2$ Mn^{2+} (OH_2)	Mn^{3+}-OH_2 O^{2-} Mn^{3+}-OH_2	Mn^{3+}-OH$^-$ O$^-$ Mn^{3+}-OH_2	Mn^{3+}-OH_2 $2H_2O$ O$_2^-$ Mn^{3+}-OH → O_2
8. Wydrzynski and Sauer, 1980	Mn^{2+} OH_2 Mn^{2+}	Mn^{3+} A$^-$ Mn^{2+} OH$^-$	$Mn^{3+}A^-$ Mn^{3+} OH$^-$	Mn^{2+}OH A$^-$ Mn^{3+} OH$^-$	Mn^{2+} Mn^{2+}
9. Fong, 1982	$H_2O[P680\ Pheo]Q$	$H_2O[P680^*Pheo^-]Q$ +[H]	$H_2O[P680^*Pheo]Q$ +[H] + 2H$^+$	[O] + [P680 Pheo]Q +[H] + 2H$^+$	$2H_2O$ O_2
10. Kusunoki, 1984	Mn^{2+} OH Mn^{2+} OH	Mn^{3+} OH H Mn^{3+} OH	Mn^{4+} OH H Mn^{3+} OH	Mn^{3+} OH H$_2$O Mn^{3+} O-H	Mn^{3+} OH ← H$_2$O Mn^{3+} O-O → O_2
11. Critchley and Sargeson, 1984	OH Cl OH Mn – Cl – Mn Cl Cl Mn-OH$_2$ Mn-OH$_2$	OH Cl OH Mn – Cl – Mn Cl Cl Mn-OH Mn-OH$_2$	O – Q – H Mn – Cl – Mn Cl Cl Mn-OH Mn-OH$_2$	O – Q Mn – Cl – Mn Cl Cl Mn-OH$_2$ Mn-OH$_2$	•O – O• Mn – Cl – Mn Cl Cl Mn-OH Mn-OH
12. Raval and Biswal, 1984	N$^+$-H H-N$^+$ O Mn^{2+} ‖ Mn^{2+} O N$^+$-H H-N$^+$	N N H-O-H Mn^{2+} Mn^{2+} H-O-H N N	N N H-O-H Mn^{3+} Mn^{2+} H-O-H N N	N N H…O-H Mn^{2+} Mn^{2+} H-O H N N	N$^+$-H H…N$^+$ O$^-$ Mn^{2+} Mn^{2+} O N$^+$-H H…N$^+$
13. Goodin et al., 1984	H_2O-Mn^{2+} D_1H H_2O-Mn^{3+} D_2H	H_2O-Mn^{2+} D_1 HO-Mn^{3+} D_2H	HO-Mn^{3+} D_1H HO-Mn^{4+} D_2H	HO-Mn^{3+} D_1 HO-Mn^{4+} D_2H	O-Mn^{3+} D_1H O-Mn^{4+} D_2H
14. Weber et al., 1985	$(H_2O)Mn^{2+}$ $(H_2O)Mn^{3+}$	$(HO)Mn^{3+}$ $(HO)Mn^{3+}$	$(HO)Mn^{3+}$ $(HO)Mn^{4+}$	Q*(OH) Q is a quinone associated with the oxidizing side of photosystem II	Q*(OH)+Q*(OH)-> HO-Q-O-O-Q-OH+ HOMn^{3+}Mn^{4+}OH-> H2OMn^{2+}Mn^{3+}OH+ 2Q+O$_2$+H$^+$
15. Kambara and Govindjee, 1985; Padhye et al., 1986	L L Mn^{3+}OH HOMn^{3+} H H H…OH HO…H Mn Mn L is a redox-active ligand	L L Mn^{4+}OH HOMn^{3+} H H OH OH Mn Mn	L$^•$ L Mn^{4+}OH HOMn^{4+} H H O…H H…OH Mn Mn	L$^•$ L Mn^{4+}OH $^-$HOMn^{4+} H H O…H OH Mn Mn	L$^+$ L Mn^{3+}-O-O-Mn^{3+} H H HO…H O…H Mn Mn
16. Renger and Weis, 1986	MH[Mn(n)OH$^-$ H$_2$OMn(m)]	M^{ox}[Mn(n)OH$^-$ H$_2$OMn(m)]	MH[Mn(n+1)OH$^-$ OH$^-$Mn(m-1)]	M^{ox}[Mn(n+1)OH$^-$ OH$^-$Mn(m+1))]	MHMn(n)…O + Mn(m)…O
1:1:2 - electron	*mechanism*			
17. Hansson and Andreasson, 1982	Mn^{3+} OH Mn^{3+}OH$^-$	Mn^{3+} OH$^-$ Mn^{3+}O^{2-}	Mn^{3+} OH$^-$ Mn^{4+}O^{2-}	Mn^{3+}-O$^-$ Mn^{3+}-O$^-$	Mn^{3+}-O$^-$ Mn^{4+}-O$^-$

Table 7.2—*Continued*

2:1:1 - electron	mechanism				
18. Dismukes *et al.*, 1982	Mn³⁺ ... Mn³⁺ 2H₂O Mn³⁺ ... Mn²⁺	Mn³⁺ ... Mn³⁺ 2H₂O Mn³⁺ ... Mn³⁺	Mn³⁺ ... Mn³⁺ OH⁻ H₂O Mn³⁺ ... Mn⁴⁺	Mn³⁺ ... Mn³⁺ OH OH Mn³⁺ ... Mn³⁺	Mn³⁺ ... Mn³⁺ O OH Mn³⁺ ... Mn³⁺
2:2 - electron	**mechanisms**				
19. Stemler, 1980	Mn^{2+} O ⌉3+ O=C-OH Mn^{2+}	Mn^{3+} O ⌉3+ C=O Mn^{2+} O	Mn^{3+} O ⌉4+ C=O Mn^{3+} O	Mn^{4+} O ⌉4+ OH Mn^{3+} O-C=O	Mn⁴⁺O ⌉4+ Mn⁴⁺O ⌉
20. Volkov, 1989	Mn²⁺ H₂O Mn³⁺ H₂O	Mn³⁺OH⁻ Mn³⁺OH₂	Mn³⁺OH⁻ Mn⁴⁺OH₂ Cl⁻	Mn³⁺OH Mn³⁺OH Cl⁻	Mn³⁺O Mn⁴⁺O Cl⁻
4 - electron	**mechanisms**				
21. Semenov *et al.*, 1975	Mn²⁺ ... Mn²⁺ H-O-H H-O-H Mn²⁺ ... Mn²⁺	?	?	Mn³⁺ ... Mn³⁺ O²⁻ O²⁻ Mn³⁺ ... Mn³⁺	Mn³⁺ ... Mn²⁺ O₂ Mn²⁺ ... Mn²⁺
22. Goldfeld *et al.*, 1980 Volkov, 1986	Mn²⁺ ... Mn²⁺ H-O-H H-O-H Mn²⁺ ... Mn²⁺	Mn³⁺ ... Mn²⁺ HO⁻ H-O-H Mn²⁺ ... Mn²⁺	Mn³⁺ ... Mn²⁺ HO⁻ Cl⁻ H-O-H Mn³⁺ ... Mn²⁺	Mn³⁺ ... Mn³⁺ HO⁻ Cl⁻ HO⁻ Mn³⁺ ... Mn³⁺	Mn³⁺ ... Mn³⁺ HO⁻ Cl⁻ HO⁻ Mn³⁺ ... Mn³⁺
23. Shilov, 1980	Mn³⁺2H₂O	?	?	?	Mn³⁺-OH₂ OH₂
24. Shilov and Dzhabiev, 1984	Mn²⁺ Mn³⁺	Mn³⁺ Mn³⁺	Mn³⁺ Mn⁴⁺	Mn⁴⁺ Mn⁴⁺	Mn³⁺ Mn⁴⁺ 2H₂O->O₂+4H⁺
25. Moravsky *et al.*, 1984					
26. Wydrzynski *et al.*, 1985	HM₀H	HM₁	HM₂⁺	M₃⁺	HOM₄²⁺OH
27. Brudvig and Crabtree, 1986					
28. Volkov, 1986	Chl₂(2H₂O)(Mn²⁺)₂	Chl₂⁺OH⁻ H₂O(Mn²⁺)₂	Chl₂⁺OH⁻ H₂OMn²⁺Mn³⁺	(Chl⁺)₂(OH⁻)₂ Mn²⁺Mn³⁺	(Chl⁺)₂(OH⁻)₂ Mn³⁺Mn³⁺
29. Volkov, 1987	Mn²⁺ ... Mn³⁺ H-O-H H-O-H Mn³⁺ ... Mn³⁺	Mn³⁺ ... Mn³⁺ HO⁻ H-O-H Mn³⁺ ... Mn³⁺	Mn³⁺ ... Mn⁴⁺ HO⁻ Cl⁻ H-O-H Mn³⁺ ... Mn³⁺	Mn³⁺ ... Mn⁴⁺ HO⁻ Cl⁻ HO⁻ Mn³⁺ ... Mn⁴⁺	Mn³⁺ ... Mn⁴⁺ HO⁻ Cl⁻ HO⁻ Mn⁴⁺ ... Mn⁴⁺
30. Likhtenstein, 1987	Mn²⁺ ... Mn³⁺ H-O-H H-O-H Mn³⁺ ... Mn³⁺	Mn³⁺ ... Mn³⁺ HO⁻ H-O-H Mn³⁺ ... Mn³⁺	HO⁻Mn⁴⁺Mn³⁺ HO⁻Mn³⁺Mn³⁺	O²⁻Mn⁴⁺Mn³⁺ HO⁻Mn³⁺Mn³⁺	O²⁻Mn⁴⁺Mn³⁺ O²⁻Mn⁴⁺Mn⁴⁺
31. Renger, 1993	Mn(II) — O — Mn(III) O	Mn(III) — O — Mn(III) O	Mn(II) — O — Mn(IV)	Mn(III)O-OMn(III) O	Mn(II)O-OMn(III) O
32. Rutherford *et al.*, 1992	Mn²⁺ Mn⁴⁺ Mn³⁺ Mn⁴⁺	Mn³⁺ Mn⁴⁺ Mn³⁺ Mn⁴⁺	Mn⁴⁺ Mn⁴⁺ Mn³⁺ Mn⁴⁺	Mn⁴⁺ His⁺ Mn⁴⁺ Mn³⁺ Mn⁴⁺	?
33. Hogansson *et al.*, 1995	(Mn)₂ⁿ⁺ H₂O Cl (Mn)₂ᵐ⁺	(Mn)₂⁽ⁿ⁺¹⁾⁺ OH Cl (Mn)₂ᵐ⁺	(Mn)₂⁽ⁿ⁺²⁾⁺ O H₂O (Mn)₂ᵐ⁺	(Mn)₂⁽ⁿ⁺²⁾⁺ O OH (Mn)₂⁽ᵐ⁺¹⁾⁺	(Mn)₂⁽ⁿ⁺²⁾⁺ O O (Mn)₂⁽ᵐ⁺²⁾⁺
34. Yachandra *et al.*, 1996	Mn(III)—OH—Mn(II) OH O Mn(IV)—O—Mn(IV)	Mn(III)—O—Mn(III) O O Mn(IV)—O—Mn(IV)	Mn(III)—O—Mn(IV) O O Mn(IV)—O—Mn(IV)	Mn(III)—O•—Mn(IV) O• O Mn(IV)—O—Mn(IV)	Mn(III)—O—Mn(IV) O O Mn(IV)—O—Mn(IV)

cubane structure. The electron transfer in model 27 occurs through an inner sphere mechanism accompanied by the structural reorganization of cubane (states S_0, S_1, and S_2) to adamantane (state S_3 and S_4). Adamantane-like structures are rather stable, and the reduction of the initial cubane complex must be a slow stage.

According to the X-ray analysis data there is structural reconstruction in the Mn cluster during the transition between S_2 and S_3, which is indirect evidence for pathway 34.

Concrete mechanisms 20, 29, and 34 do not include unknown intermediates.

ARCHITECTONICS OF THE REACTION CENTER AND ELECTRON PATHWAYS OF PHOTOSYNTHESIS

The synchronous multielectron mechanism of water photooxidation implies that the oxygen atoms belonging to two water molecules undergoing oxidation to molecular oxygen must be positioned at a sufficiently short distance from each other, as shown in Figs. 7.10 and 7.11. Otherwise, the high activation energy value will make the multielectron process impossible.

During water photooxidation in the OEC of photosystem II, electrons are transferred a relatively long distance between the electron transport chain components. According to Kulikov *et al.* (1983), the Mn–P_{680} and Mn–Pheo distances may be as great as 3.4 and 2.9 nm, respectively. Electron transfer for great distances within OEC can take place along the pathways via the systems of conjugated bonds between plastoquinones or carotenoids. There are two possible modes of such transport:

$$\overset{e}{\longleftrightarrow}$$
$$-C\!\!=\!\!C\!-\!C\!\!=\!\!C-$$
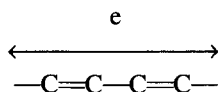
and via "bundles" or stacks of double bonds:

$$\begin{array}{c} -C\!-\!C\!\!=\!\!C- \;\uparrow \\ C\!-\!C\!\!=\!\!C- \;\Big|\,e \\ =\!C\!-\!C\!\!=\!\!C- \;\downarrow \end{array}$$
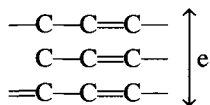
Electron transfer along electron pathways during photosynthesis is described at greater length by Debus (1992), Volkov (1989), and Yachandra *et al.* (1996).

ROLE OF MANGANESE IN PHOTOSYNTHESIS

Manganese ions play a particularly important role in the evolution of dioxygen during photosynthesis. Although there are several manganese pools in chloro-

plasts, only one is involved in water oxidation. We suggest that manganese ions associated with the chloroplast OEC perform a number of functions:

1. Mn–polypeptide complex is a redox intermediate that protects RC from redox and radical destruction.

2. Mn–cluster in OEC is a redox buffer facilitating the accumulation of four holes in the RC of photosystem II, which are needed to ensure water photo-oxidation.

3. Hydrated multivalent manganese cations bring water to the RC and maintain rapid proton exchange and transport through the hydration shell of manganese ions in the zone of water oxidation.

4. Multivalent manganese ions induce dielectric saturation effects in the polar region of the RC of photosystem II, which results in a reduction in the reorganization energy of the medium during charge transfer.

5. Ions affect the structure of the electric double layer and the membrane surface charge (Barber *et al.,* 1977), regulating the distance between thylakoid membranes by means of contraction and expansion of the diffuse part of the electric double layer. This in turn, regulates the lateral displacement of photosystems, lipids, proteins, and ATPase over the membrane surface.

This Page Intentionally Left Blank

Chapter 8

Energetics of Dark Respiration and Mechanism of Cytochrome Oxidase Functioning

INTRODUCTION

Respiration is the reduction of O_2 to H_2O during the oxidation of carbohydrate to CO_2. There are two types of respiration in photosynthetic organisms: dark respiration and a photorespiration. Dark respiration includes O_2 reduction and the oxidation of NADH and $FADH_2$ in mitochondrial membranes, glycolysis, the Krebs cycle, and the oxidative pentose phosphate pathway. Respiration is commonly subdivided into two functional components: growth respiration, supplying energy for new biomass production, and maintenance respiration, providing energy to maintain the integrity of structures already existing and their turnover. In the present chapter we will consider the thermodynamics of oxygen reduction in plant mitochondria.

Plant mitochondria have two membranes: a smooth outer membrane that surrounds an invaginated inner membrane. The respiratory chain of mitochondria is an integral part of the inner mitochondrial membrane. It is composed of four electron-transporting protein complexes (NADH dehydrogenase complex I, succinate dehydrogenase complex II, cytochrome reductase complex III, and cytochrome c oxidase complex IV), ATP synthase (complex V), and mobile electron carriers ubiquinone and cytochrome c. Plant mitochondria have additional enzymes not found in the mitochondria of animals: the cyanide-insensitive alternative oxidase, an internal rotenone-insensitive NADPH dehydrogenase, and an externally located NADPH dehydrogenase, which do not conserve energy. The alternative oxidase catalyzes the oxidation of ubiquinol to ubiquinone and the reduction of oxygen to water and is inhibited by salicylhydroxamic acid. In some photosynthetic cells, the carbohydrates formed during photosynthesis can serve as the Gibbs free energy source for respiration, which leads to ATP synthesis and

water and CO_2 production. Oxygen reduction, catalyzed by cytochrome c oxidase, accounts for a significant portion of the water eliminated from the mitochondria. About 90% of the oxygen consumed on Earth is reduced in a four-electron reaction catalyzed by cytochrome c oxidase.

Cytochrome c oxidase (EC 1.9.3.1) is the terminal electron acceptor of the mitochondrial respiratory chain. Its main function is to catalyze the four-electron reaction of dioxygen reduction to water using electrons from ferrocytochrome c (Antonini *et al.*, 1970):

$$4H^+ + O_2 + 4e^- \quad \text{respiration} \rightarrow 2H_2O$$
$$\leftarrow \text{photosynthesis} \tag{8.1}$$
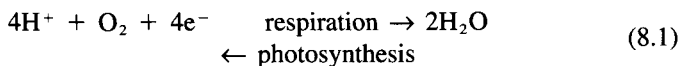
Equation (8.1) is exothermic. Liberated energy can be consumed for the transport of suprastoichiometrical protons across the mitochondrial membrane by cytochrome c oxidase or released as heat by a cyanide-insensitive alternative oxidase. The energy of oxygen reduction to water is used by the cell to synthesize ATP (Volkov and Kharkats, 1988). The enzyme is composed of several protein subunits (Fig. 8.1), two hemes A, cytochromes a and a_3, and two organocopper complexes
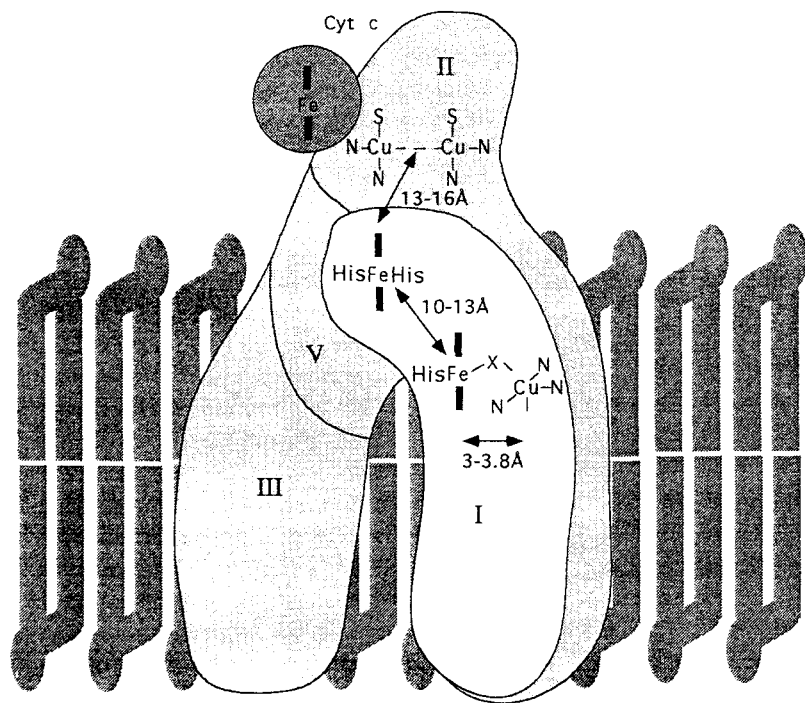
Figure 8.1   Scheme of the structural organization of cytochrome c and cytochrome c oxidase monomer in the inner mitochondrial membrane (Einarsdottir, 1995). Reproduced by permission of Elsevier Science B.V.

Cu_a and Cu_b coordinated to the protein. It has a molecular mass of about 180,000–200,000 kDa for the most active form. Cytochrome oxidases can transport up to eight H^+ across the membrane per four electrons, with four H^+ binding to the reaction complex during dioxygen reduction to water and another up to four protons transported across the membrane and used in ATP synthesis (Wikstrom, 1989). Discussed in the present chapter are possible molecular concerted $2:2:1$-electron and $2:2$-proton pump mechanisms of cytochrome c oxidase functioning.

The $1:1:1:1$-electron mechanisms of oxygen reduction by cytochrome oxidase are most frequently discussed in biochemistry. The reaction in Fig. 8.2 implies that the midpoint Gibbs free energy of the first electron transfer from cytochrome oxidase to O_2 is positive. As a result, this route either should not be followed or the reaction rate should be extremely low. Since the Gibbs free energy of O_2 binding in the catalytic site of cytochrome oxidase is -21 kJ/mol (Chance *et al.*, 1975), the cytochrome c redox potential is 0.25 V and the midpoint Gibbs free energy of the first electron donation to oxygen is $+55$ kJ/mol. The Gibbs free energy of the reaction

$$O_2 + e^- \rightarrow O_2^-, \tag{8.2}$$

in a cytochrome oxidase catalytic site is equal to $+101$ kJ/mol. Activation energy for O_2 reduction by fully reduced cytochrome oxidase amounts to 16 kJ/mol (Erecinska and Chance, 1972). Since the Gibbs free energy of the endothermic reaction [Eq. (8.2)] is 6 times the measured activation energy for O_2 reduction by cytochrome oxidase, the one-electron mechanisms $1:1:1:1$, $1:2:1$, $1:1:2$, and $1:3$ are unlikely at room temperature (Kharkats and Volkov, 1985, 1987, 1989,
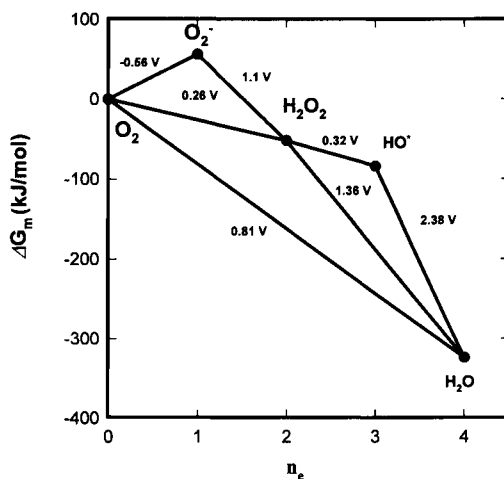
Figure 8.2 Energy diagrams for possible routes of the reaction $O_2 + 4H^+ \leftrightarrow 2H_2O$. G_m is the reaction midpoint Gibbs free energy at pH 7 (Kharkats and Volkov, 1994).

1994). They could only be feasible if the energy of the one-electron intermediate binding was negative but greater than 85 kJ/mol in magnitude. Such significant energy of covalent binding allows this intermediate to be detected experimentally. However, it has not been detected thus far.

The fact that the first electron addition to O_2 is endothermic accounts for the relative chemical inertness of oxygen in nature and permits the existence of life on Earth.

The high energy of oxy intermediate binding places a strong restriction on the energetics of the next step, including the second electron transfer and formation of a peroxide intermediate. The probability of such a pathway is too small due to kinetic and thermodynamic limits. Therefore, evolution could reserve either ecologically clean sequential $2:1:1$-mechanism, with intermediates tightly bound at the catalytic site. A possible mechanism of dioxygen reduction by cytochrome c oxidase is outlined in Fig. 8.3 and will be considered in detail after a discussion of the thermodynamic and kinetic aspects of the problem.

Synchronous multielectron reactions may proceed without the formation of intermediate radicals, which are highly reactive and can readily enter a side reaction of hydroxylation and destruction of the catalytic complex. Since multielectron reactions do not poison the environment with toxic intermediates (and so are ecologically pure), they are used by nature for biochemical energy conversion in respiration and photosynthesis (Kharkats and Volkov, 1987). In the multielectron reaction that takes place in a series of consecutive one-electron stages, the Gibbs
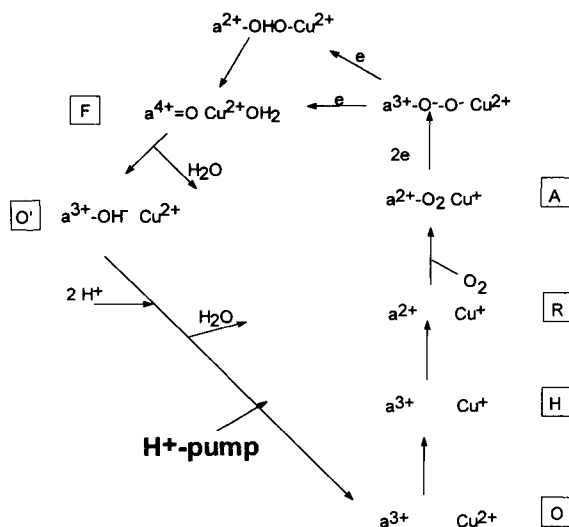
Figure 8.3 Scheme of the $2:1:1$-electron reduction mechanism at the cytochrome c oxidase active site (Kharkats and Volkov, 1994).

energy necessary per single electron transfer obviously cannot be completely uniformly distributed over the stages. The energy needs for various stages will be different, and the excess energy in the easier stages will be converted into heat. In a synchronous multielectron reaction the energy will be used very economically.

One of the important parameters in the modern quantum theory of charge transfer in polar medium is the medium reorganization energy, E_s, that determines activation energy. Medium reorganization energy for reactions involving charge transfer or redistribution in reagents with complex charge distribution [Eq. (7.9)] has been evaluated previously (Kharkats, 1978).

REACTION CENTER ARCHITECTONICS

Equation (7.9) provided conditions for the structure of a cytochrome c oxidase catalytic site necessary for dioxygen reduction to occur by the concerted n-electron mechanism. To lower medium reorganization energy and, therefore, activation energy, the following are necessary:

- The dielectric constant of the medium where oxygen reduction takes place should be low, that is, the catalytic site should be immersed in the hydrophobic phase of the membrane (protein).
- There should be n spatially separated electron donors. For the mechanism proposed, these are hemes and protein–copper complexes.
- It is desirable that electron transfer via cytochrome c oxidase be accompanied by the transport of cations (e.g., protons). If electron transfer via cytochrome oxidase is coupled with proton transport across the mitochondrial membrane, energy liberated in Eq. (8.1) will be consumed for useful work instead of being converted to heat.
- The radii of electron donors should be sufficiently large. This is achieved by using not free metal ions, but their organic complexes (hemes and cysteines) with systems of conjugated bonds and ligands capable of participating in redox reactions (Kharkats and Volkov, 1985, 1987, 1994).

THE BRIDGE ELECTRON TRANSFER MECHANISM

Electrons generated in the oligoenzyme complexes of the mitochondrial respiratory chain are transferred to the cytochrome c oxidase active site by a one-electron bridge mechanism. The reduction of the oxygen molecule to water requires the stepwise transfer of four electrons from cytochrome c to cytochromes a and a_3 as well as to two Cu-containing proteins, Cu_a and Cu_b. A quantum mechanical calculation has been made (Kharkats, 1978) for the probability of electron transfer via an intermediate virtual state as a possible model of an electron mechanism with an activated outer sphere and a bridge ion.

The stepwise transfer of electrons from cytochrome c to cytochrome a_3 via cytochrome a is kinetically favorable due to a substantial decrease in medium reorganization energy for direct electron transfer from cytochrome c to cytochrome a_3. The midpoint redox potential of Fe_c may be not smaller, but even greater than the midpoint redox potential of Fe_a. It is essential that only the minimum of the intermediate term on the reaction energy diagram be below the crosspoint of the initial and final terms.

ACTIVATION ENERGY AND MECHANISM
OF DIOXYGEN REDUCTION

Studies on the temperature dependence of the oxygen reduction rate have revealed that cytochrome oxidase exists in two conformations: "hot" (h) and "cold" (c). The respective activation energies, E_a^h and E_a^c, are equal to 16 (at 23–35° C) and 60 kJ/mol (below 20° C) (Orii *et al.*, 1977). A phase transition accompanied by changes in conformation and absorption spectrum takes place between 18 and 23° C. The temperature, T^c, depends on the composition of the surrounding lipid. The low E_a^h value means that the one-electron mechanisms $1:1:1:1, 1:2:1, 1:3$, and $1:1:2$ are unlikely at temperatures higher than T^c because the enthalpy for the transfer of the first electron from reduced cytochrome oxidase to dioxygen is 6 times the measured activation energy. If the binding energy of the one-electron intermediate $a_3-O_2^-$ is less than -85 kJ/mol, it provides thermodynamic and kinetic possibilities for a multistep one-electron mechanism of oxygen reduction. But the energy of reorganization of the medium for one-electron transfer in cytochrome oxidase in "hot" and "cold" conformations cannot be different by 4 times. From Eq. (7.8) it follows that if we change the distance h_{12} of electron transfer from $h_{12} = a_1 + a_2$ to $h_{12} > a_1 + a_2$, the energy of reorganization changes by less than 50%. E_a can be equal to 16 and 60 kJ/mol for the one-electron mechanism of oxygen reduction according to equation (7.8) only if $E_s > 770$ kJ/mol when $E_{comp} < -85$ kJ/mol. Such a high value of E_s also shows that the $1:1:1:1$-electron mechanism of oxygen reduction *in vivo* is unlikely.

For multielectron reaction $2:1:1$ according to Eq. (7.9), E_s for two-electron reactions between O_2, a_3, and Cu_b strongly depends on the geometry and distances in the catalytic site. Only the $2:1:1$-mechanism of oxygen reduction by cytochrome oxidase can be realized *in vivo* in both "hot" and "cold" conformations.

Consider the molecular mechanism of dioxygen reduction outlined in Fig. 8.3 in more detail. The oxidized catalytic site of cytochrome oxidase composed of cytochrome a_3 and Cu_b is reduced via the bridge mechanism by two electrons supplied from the electron reservoir of the respiratory chain to form a reduced complex, which then binds an oxygen molecule. The reaction center is oxidized to the initial state in a two-electron reaction with the formation of a peroxide bridge between a_3 and Cu_b. The partially reduced (to peroxide) oxygen molecule

must be bound in the reaction center since cytochrome oxidase is known to reduce dioxygen to water without the release of any intermediates from the membrane. After that, the catalytic complex in turn accepts two electrons from the electron reservoir $Fe(c) \to a_3$. In the next step, the peroxide bridge undergoes 1 : 1-electron reduction and protonation to water.

The concerted electron transfer step (10^{-15}–10^{-13} s) is followed by enzyme relaxation with a complex set of characteristic times and constants. Rate constants for such processes can range from very low (1 s^{-1}) to very high (10^9 s^{-1}). Study of the relaxation of fully reduced cytochrome oxidase upon its interaction with dioxygen allowed the following characteristic constants to be resolved: 7 $\times$ 10^7 M^{-1} s^{-1}, 6.8 $\times$ 10^4 s^{-1}, 1.7 $\times$ 10^4 s^{-1}, and 1.1 $\times$ 10^3 s^{-1} (Sucheta *et al.*, 1997). Such a complex relaxation pattern has led some authors to suggest that electron transfer to O_2 is stepwise and proceeds via the 1 : 1 : 1 : 1-mechanism. However, because no intermediate that should be formed on the first electron donation to O_2 has been detected in the native enzyme at temperatures higher than 21°C, this spectrum of characteristic times can be attributed to the relaxation of the metalloenzyme during 2 : 1 : 1-electron oxygen reduction to water. The redox potentials of cytochromes a and a_3 and Cu_a and Cu_b are about the same, which means that the energy states of all four metal centers in the reaction complex of the native enzyme are similar. This also favors concerted reactions.

Sucheta *et al.* (1997) published data, which can be considered as experimental proof of the theoretical mechanism of cytochrome *c* oxidase functioning originally proposed by Kharkats and Volkov (1994). By using time-resolved optical absorption difference spectra and singular value decomposition analysis, Sucheta *et al.* (1997) found the presence of peroxy and ferryl intermediates at room temperature during the reduction of oxygen by cytochrome *c* oxidase and measured the rate constants.

PROTON PUMP

Water molecules released during the course of oxygen reduction are removed from the hydrophobic catalytic site to the aqueous phase. Continuous removal of the product from the reaction center will shift the equilibrium of Eq. (8.1) to the right. Energy liberated in the exothermic reaction [Eq. (8.1)] is sufficient for transporting eight H$^+$ ions across the membrane. Four of them are used with O_2 to form two H_2O molecules. The rest of the H$^+$ ions can be transported across the hydrophobic zone of the membrane and used for ATP synthesis in the ATP synthetase complex, with the cytochrome oxidase H$^+$ pump serving only to transform the energy of ferrocytochrome *c* oxidation. Proton translocation can be direct if the ligands to redox centers provide the protons or indirect if the redox reactions cause conformational changes transmitted to proton-donating groups remote from the redox centers. As follows from thermodynamics (Fig. 8.2), energy for H$^+$

pump function is liberated only in the last steps of water formation upon the addition of the third and fourth electrons, independent of the reaction route (Kharkats and Volkov, 1994). The function of the proton pump after the formation of ferryl intermediate is possible only if the difference between the Gibbs energy of ferryl and peroxy intermediate binding is more negative than -35 kJ/mol.

Energy of binding of ferryl intermediate is negative and sufficiently high (Wikstrom, 1989), which makes it possible that a proton pump functions not only at the last stage of addition of the fourth electrons but also after the formation of the three-electron oxygen intermediate. The stoichiometry of proton pumping by cytochrome oxidase can be $0:2:2$ if the ferryl intermediate has -35 kJ more negative energy of binding than the peroxy intermediate.

As follows from Eq. (7.9), medium reorganization energy corresponding to simultaneous electron and proton transfer will be minimal in the case when the directions of their transfers are close. In the case of charge transfer in cytochrome oxidase, the electron donor is placed on C side and the protons come from side M. In this case the minimal activation energy will be achieved at the maximally possible system angle between the directions of electron and proton transfer.

It is to be noted that cytochrome oxidase can reduce O_2 without concomitant proton transfer. In such a case, the enzyme would work as a machine converting the energy of electron transfer to heat. It may be that evolution has preserved the e^-, H^+ form of cytochrome oxidase with minimum energy dissipation.

Chapter 9

Plants and the Atmosphere: Heat and Moisture Exchange

INTRODUCTION

The life of plants is linked inseparably with water (Kramer and Boyer, 1995). The first plants appeared approximately 2 billion years ago in the waters of an ancient sea, and their evolution in an aqueous medium continued for a very long time. An extremely important event in the history of the plant kingdom occurred 500 million years ago: the exodus of plants from water onto dry land. This step in natural history predestined an incredible bloom of plants and the appearance on Earth of a fantastic variety of plant species. The number of terrestrial plant species now known is about one-third of a million, whereas the number of species of algae is less than 10% of that value. The root cause of such evolutionary success was thermodynamic in nature. It became possible when plants were raised above the water surface to a boundary between two phases, the aqueous phase and the air. By being in contact with both phases, they were exposed to the difference in the chemical potential of water between the liquid and gaseous phases. Thus, terrestrial plants exist under thermodynamic conditions essentially different from those in the water phase. Terrestrial plants succeeded in adapting the difference in water chemical potentials between the two phases as an additional source of energy for their needs.

It should be noted that in contrast to the use of radiant energy, the difference in water chemical potentials may be used only in thermophysical processes but not in quantum ones. This question has been discussed in more detail in Chapter 3. Plants expend energy that they draw from the water chemical potential gradient for performing nonquantum processes of distant transport of water through the capillaries of their vascular system. A very important consequence of the migra-

tion of plants to dry land was that they obtained an effective channel for the disposal of entropy by the evaporation of water. One may think that this circumstance favored the appearance of a remarkable diversity of terrestrial plant species.

Although terrestrial plants migrated out of water long ago, they conserved the genetic imprint of their ancestral medium. They do not now live in water, but they draw it from the soil and pass it through their roots, stems, and leaves in immense quantities. For each kilogram of water used for photosynthesis, the plant has to uptake from the soil and eventually respirate to the atmosphere 1000 times more. The scale of water consumption by plants is so vast that during 10,000 years they pass through their bodies all of the water contained in the seas and oceans of Earth. In 8 million years plants decompose all of the water of Earth into oxygen. At the same time plants, due to their branched structures that are spread both into the ground and into air, significantly promote the exchange of water between soil and the atmosphere and thus affect the weather and even climatic conditions.

The uptake of water from soil and raising it through the long thin capillaries of the plant's vascular system to its leaves demands some work. Plants draw the energy needed to perform this work mainly from the difference in water chemical potentials. This chapter is devoted to an examination of the terminal stage of the water pathway in plants, at the stage where water leaves the plant and enters the air in the form of vapor. The problems concerning all the preceding stages of movement of water in the plant will be examined in other chapters.

A short comment on the process of evaporation is needed. The common notion that liquid evaporates due to heat is, strictly speaking, not quite correct. Liquid evaporates because this process is conjugated with an increase in entropy. The entropy of vapor is much higher than that of the liquid, and therefore the evaporation of the latter is a spontaneous process. It will proceed even without any heat until the surrounding space is saturated with vapor. If not heated, the liquid will cool when evaporation occurs due to the loss of heat with evaporation. Thus, external heating is not the direct cause of evaporation but merely compensates for the loss of heat, making the process continuous.

The conditions of energy interaction of the plant with its surroundings are extremely variable (Jones, 1992). In any concrete case they depend upon the combination of many parameters, and each may vary within wide limits. The main outer parameters are solar irradiation, the air temperature, and its humidity. The wind velocity is also a significant factor. In its turn, the plant can actively respond to the variations in external conditions by changing the permeability of its leaves to water vapor. The mutual influences of many interacting factors determine the complicated relations of heat and moisture in the plant.

A plant that lives in water has no problems with thermoregulation. Its life passes in close thermal equilibrium with a surrounding medium of constant or slowly changing temperature. In contrast, terrestrial plants exist in contact with air, whose temperature may vary over a wide range in a short time. Apart from that, the plant may be subjected to intensive heat by radiant flux. Thus, the prob-

lem of maintaining the temperature of the organism within a survivable range is quite important for the plant. As the main means of solving this vital problem, the plant uses the process of evaporation of water through the surface of leaves.

It is almost impossible to speak precisely about the temperature of the whole plant as its separate parts may have different temperatures at the same time. The roots usually are under conditions of almost constant temperature, whereas the temperature of the leaves changes during the course of a day. Therefore, the dependence of leaf temperature upon the variable environmental factors is an interesting topic.

Leaf temperature is adjusted as the result of energy balance with the environment. The thermal balance of the plant is closely connected with its water balance, and thus the heat and moisture exchange of the plant with its surrounding medium should be considered as a single process, a heat–moisture interaction. There is a large body of work devoted to the problem of thermal balance in plants. Among them the works of D. Gates (1968, 1976) are notable for being the most systematic and rigorous, providing a very detailed analysis of the thermal balance of the leaf. However, it should be noted that in most of these works this topic is considered usually in somewhat a one-sided manner. Only the influence of the surrounding medium on the plant is being taken into account whereas the reverse effects are neglected. Such an explanation is appropriate when a little plant or a separate leaf interacts with unlimited ones and, in any case, with very large volumes of air. But when the mass of vegetation is fairly large its influence on its surroundings should not be ignored. This influence may be reflected in the amount of moisture in the air and in temperature changes.

The interaction of plants with air is a process that depends upon a large number of variables, both of the plant and its surroundings, acting in various combinations at any moment. It seems reasonable to treat this complicated problem with the help of graphical methods representing heat and moisture exchange between air and the plant on a diagram for humid air.

GRAPHICAL REPRESENTATION:
THE MOTIVE FORCES

The thermodynamic state of humid air at constant pressure may be represented graphically with the help of a *t–d*, or temperature–moisture content, diagram. Such diagrams provide a clear and convenient depiction of heat–moisture interaction processes of the plant with air. A *t–d* diagram is shown in Fig. 9.1 for a temperature range that may be of interest for plant physiology.

The *t–d* diagram is based on the function that describes the dependence of the equilibrium pressure of water vapor at various temperatures:

$$p_s = \exp(s_v/R) \exp(-h_v/RT), \tag{9.1}$$

where h_v and s_v are the enthalpy and entropy of evaporation of water (h_v = 44.006 kJ/mol, s_v = 214.5 J/mol $\cdot$ K), respectively.

The partial pressure of water vapor in air (p_v) is equal to the product of the equilibrium pressure and the saturation of air or its relative humidity (ϕ): p_v = ϕp_s. The value of the moisture content of air related to 1 kg of dry air is expressed as follows:

$$d = 0.622 p_v/(p - p_v). \qquad (9.2)$$

Drawn on Fig. 9.1 are curves of constant values of relative humidity (constant ϕ lines). The system of almost straight lines at an angle to the coordinate axes shows the dependence of the specific enthalpy (h) of humid air upon its temperature and humidity. The lines are drawn according to the following relation (Voronjec and Kozic, 1980; Vukalovich *et al.*, 1969):

$$h = 1.006t + (2500 + 1.86t)d \text{ kJ/kg}, \qquad (9.3)$$

where the values of enthalpy (h) and moisture content (d) are related to 1 kg of dry air.

An arbitrary state of humid air may be depicted on Fig. 9.1 by a configurative point, the position of which can be defined unequivocally by the values of a pair of the variables, t, d, ϕ, and h in any combination. The thermodynamic state of humid air below the saturation line ($\phi = 1$) has two degrees of freedom, and the configurative point of air may lie in any position in this area. The configurative
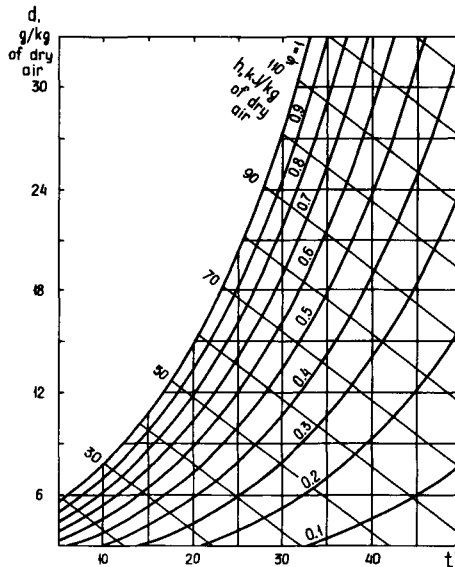
Figure 9.1 t–d (temperature–moisture content) diagram of humid air.

point corresponding to the saturated state of the system has only one degree of freedom: it may slide along the saturation line. Of course, only the states below the saturation line are attainable.

It is usually considered that the state of air in the mesophyll of a leaf is nearly saturated with water vapor. In fact this is an approximation because the water potential in the leaf is usually lower than that of free water by $1-5$ kJ/kg (or in pressure units by $1-5$ MPa). The degree of saturation should be less than 100%. The deviation may be calculated from the equation:

$$\phi = \exp(\Delta\mu/RT).$$

For the values of water potential shown here (-1 to -5 kJ/kg), the values of ϕ are 0.993 and 0.964, respectively. Thus, the configurative point of a leaf, or more strictly that of air in the mesophyll space of a leaf, lies quite close to the saturation line of the $t-d$ diagram, its position on the line being determined unambiguously by the leaf temperature. The deviation of the configurative point of the leaf from the saturation line may be more significant under water deficit conditions.

The heat–moisture interaction of a plant with air can be depicted on the $t-d$ diagram by a vector directed from the configurative point of air to that of a leaf. This vector shows the direction of thermodynamic forces that act on the system and cause its change. The vector may be expanded according to usual vector rules in two components directed along the temperature and moisture content axes of the diagram. These components are proportional to the corresponding motive forces, which are the gradients or the finite differences of both temperature and moisture content. Here the upward direction of a moisture content vector and the leftward one for that of temperature are assumed to be positive. The arrowheads of the vectors shown on the forthcoming figures show the direction of a virtual trend of a corresponding configurative point under the influence of the heat–moisture interaction.

The mutual disposition of the configurative points of air and leaf on the $t-d$ diagram may change depending upon the weather conditions, the intensity of radiation, and many other factors. The conditions of the heat–moisture interaction of a plant with air will vary accordingly.

Figure 9.2 shows how the $t-d$ diagram may be used to explain a picture of the processes of the heat–moisture interaction. Only a fragment of the diagram is shown in the figure. The point P represents the position of the configurative point of a leaf. The lines of constant t, h, d, and $\phi = 1$ drawn through the point P divide the whole area of the diagram into eight sectors. Four of them lie above the saturation line and are not of interest. Four other sectors lie below the saturation line and correspond to possible states of humid air. The configurative point of air may be found in any of these sectors, and depending on its position, the mode of the heat–moisture interaction of the plant with air will be different.

In all cases when the configurative point of air is found in sector I or II, i.e., to the left of the line of constant enthalpy (h = constant), heat is transferred from
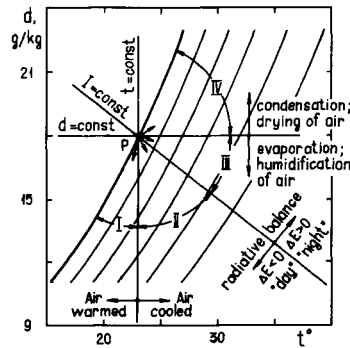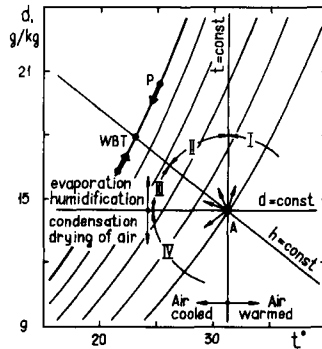
Figure 9.2 Scheme of possible modes of heat–moisture interaction of a leaf with air of various parameters. P is the configurative point of the leaf.

plant to air. In sectors III and IV to the right of the constant enthalpy line, heat transfer is directed from air to leaf. It should be noted that we have in mind here the total transfer of heat and do not divide it into components caused by gradients of temperature and moisture content.

The line of constant moisture content (d = constant) drawn through the configurative point of the leaf separates sectors I–III from sector IV. If the configurative point of air is in one of the former three sectors, then the air will be humidified due to the transpiration of water by the plant. In sector IV only the condensation of moisture from air onto the cold surface of leaves may occur.

The line of the isotherm (t = constant) separates sector I, in which warming of air occurs, from sectors II–IV where the air temperature is lowered in the course of interaction with the plant. This is all summarized in Table 9.1. The last column in Table 9.1 shows the sign of the ratio of the motive forces $\Delta t/\Delta d$.

Table 9.1

Trends of Mutual Changes of Air and Plant Parameters Under Various Conditions

Sector of the diagram	Trend of air parameters change[a]			Trend of plant temperature change	Sign of the ratio $\Delta t/\Delta d$
	t	d	h		
I	+	+	+	−	+
II	−	+	+	−	−
III	−	+	−	+	−
IV	−	−	−	+	+

[a](+) increase; (−) decrease.

It is of interest to consider the behavior of the air–leaf system in some particular cases when the configurative point of air lies on a line separating two adjacent sectors. When there is no difference in temperature between air and leaf, the temperature remains constant during heat–moisture exchange but the heat content of the air increases due to an intake of water vapor transpired from the leaf. In this particular case the transpiration of 1 g of water is connected with the transfer of 2.5 kJ of heat out of the plant. In all other cases the total release of heat accompanied by the loss of a unit mass of transpired water is not directly related to the value of the specific heat of evaporation. This point is essential and should be taken into account in the calculation of the energy balances of plants.

When the configurative points of air and plant are on the same isoenthalpic line, there is no net exchange of energy between the plant and the air. The heat content of air should be increased due to humidification, but this effect should be compensated due to an equal loss of heat because of direct heat transfer. In this case the heat–moisture interaction between the leaf and the air is quite inefficient with respect to cooling the leaf. Such conditions occur when the leaf temperature equals that of a wet-bulb thermometer.

If the air and leaf configurative points lie on the same line of constant moisture content (d = constant), i.e., on the boundary between sectors III and IV, the plant and air may exchange heat but not moisture. In this case the temperature of the plant corresponds to the dew point and the transpiration is zero. This situation can happen at night or before daybreak and is accompanied by the transfer of heat from air to plant.

Often a different mode of presentation of the heat–moisture interaction between air and plants may be more convenient. One may look at the picture from the opposite end of the vector by regarding the state of air to be fixed and that of the leaf to be variable. Such a point of view might be more natural to some extent because the parameters of the air as well as the radiation of the Sun are the factors that determine the thermal regime of the plant, but not vice versa. The scheme of possible processes in this case is shown in Fig. 9.3.

In this scheme, just as in Fig. 9.2, the configurative points of air and the plant are designated A and P, respectively, but in contrast to the previous picture, the position of A on the diagram is considered to be fixed and that of P moves along the saturation line. The scheme in Fig. 9.3 may be regarded to be the inverse of that in Fig. 9.2 with respect to the direction of the vector A–P. Accordingly, the sequence of sectors I–IV is also inverted in this picture. The scheme in Fig. 9.3 shows how the t–d diagram may be used to display the steady state of heat and moisture exchange between the air and leaf, as well as the possible variations in the state of a leaf in cases when it is not at steady state conditions.

Under conditions of normal physiological functioning of a plant, the only possible trajectory for its configurative point is along the saturation line or in close proximity to it. The equilibrium location of the configurative point of a leaf de-

Figure 9.3   Scheme of possible modes of heat–moisture interaction of a leaf with air at various conditions. *A* is the configurative point of air, *P* is the configurative point of a leaf and WBT is the wet-bulb thermometer point.

pends upon the radiative balance of the leaf and its transport facilities in relation to the flows of heat and water vapor. In the case of zero radiative balance and equal values of resistance of the pathways for both flows, the equilibrium point lies on the intersection of the saturation line with the line of constant heat content. This point corresponds to the wet-bulb temperature (WBT). In sectors I and II this process is followed by cooling of the leaf, and in sectors III and IV by its warming. It should be noted that within sector II the heat–moisture exchange causes simultaneous cooling of both the leaf and air.

To obtain a more general picture of the heat–moisture relations of a leaf with the atmosphere, beyond the above-mentioned restrictions questions concerning the resistance of the pathways of heat and moisture flows should be examined in detail.

OBSTACLES ON PATHWAYS

The *t–d* diagram enables a clear representation of the overall picture of forces acting upon the system, provided its thermodynamic state is defined; thus, the temperature and humidity of the air and the plant are known. The diagram also shows the trends of possible variations in the system due to heat–moisture interactions between plant and air.

These forces cause flows of heat and moisture, which may be depicted on the *t–d* diagram in vector form. The directions of the flow vectors should coincide with those of conjugated force vectors, whereas their lengths should relate in definite proportions. These proportions depend upon the choice of scale for the force and the flow vectors, as well as upon the transport abilities of the leaf in relation to the corresponding flows.

We can express the forces acting in a system in units of pressure. For this purpose, the difference in temperature between air and leaf should be multiplied by the value of the heat capacity of humid air and its density (ρc_p). Similarly, the scaling factor for diffusion will be the product of the specific enthalpy of water vapor and the density of air (ρh_v).

The values of c_p and h_v may be derived from Eq. 9.3:

$$c_p = 1.006 + 1.86d \text{ kJ/kg of dry air/K}$$
$$h_v = 2500 + 1.86t \text{ kJ/kg of water vapor in air.}$$

The air density value may be calculated as follows:

$$\rho = 2.167 \frac{1 + d}{(0.622 + d)} \cdot \frac{p}{(t + 273.2)} \text{ kg/m}^3, \tag{9.5}$$

where p is the total pressure in kilopascals.

Thus, forces will be expressed in units of pressure. So the equivalent pressure corresponding to the temperature difference of $1°C$ is about 1 kPa, while that of a one-gram difference in moisture content is about 2.5 kPa. The scaling in units of pressure is not quite uniform throughout the plane of the diagram because the scaling factor depends upon the temperature, humidity, and density of air. However, the deviations from uniformity are small. So the precise values of the scaling factor in the lower left and upper right corners of the diagram in Fig. 9.1 differ from the value in the center of the diagram by no more than $\pm 5\%$.

If the forces are expressed in units of pressure, the flows should be in units of power per unit area (W/m^2). Accordingly, the transfer coefficients that determine the permeability of the leaf surface to heat (U_q) and moisture (U_v) flows will be expressed in units of speed (m/s). These coefficients may be defined as permeability coefficients or conductance.

It should be noted that in the literature on plant physiology concerning the problem of transpiration, the concept of pathway resistance is also commonly used. Resistance has dimensions inverse to those of conductance. Values of conductance and resistance are easily convertible; both terms will be used herein depending on the context.

The step connected with the estimation of numerical values of permeability coefficients is more difficult. It features the kinetics of heat and moisture transfer between a leaf and air under actual conditions. This point is much more complicated because of the great diversity of factors that affect these processes. A look at the general scheme of the processes of heat and water vapor transfer in air near the leaf is useful. The diagram in Fig. 9.4 shows the pathways of these processes. One may identify on the diagram some regions that are distinguished from each other by the conditions of the transfer of mass and heat. The region of "free" air is far enough from the leaf surface. Due to the convective movement of air, transport processes effectively occur here without noticeable obstacles.
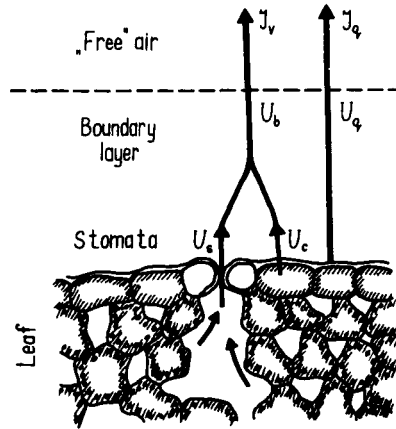
Figure 9.4   Pathways of heat and water vapor release from a leaf. The conductance of the boundary layer is U_b, that of the stomata is U_s, and that of the cuticle is U_c. J_v is the flow of enthalpy. U_q is the conductance for flow of heat J_q.

There is an adhering boundary layer close to the leaf surface. The movement of air in this region is largely hindered by viscosity. Here the predominant mechanisms of transfer are diffusion and heat conduction. These processes are subjected to identical laws. Moreover, the value of the boundary layer conductance (U_b) may be deemed the same for both processes ($U_q = U_v = U_b$). It is equal to the diffusion coefficient divided by the thickness of the boundary layer.

The thickness of the boundary layer depends upon many factors. Among the factors affecting the transport features of the boundary layer are the size and configuration of the leaf, the texture of its surface (whether it is smooth or fluffy), and the velocity of the wind. Theoretical considerations based on the principles of hydrodynamics (Bird *et al.*, 1960; Kays, 1966; Levich, 1962) give the following expression for the average thickness of a boundary layer on the surface of a plate under a laminar overflow:

$$\delta \approx \frac{3}{2}(\eta/\rho)^{1/2}(B/V)^{1/2}, \tag{9.6}$$

where η is the viscosity of air, V is the wind velocity, and B is the leaf size.

For example, for a leaf 5 cm in size and wind speeds of 1 and 10 m/s, this formula gives boundary layer thicknesses of 1.5 and 0.5 mm, respectively. By inserting the values of the basic parameters into Eq. (9.6), one can derive the following expression for the conductance of the boundary layer:

$$U_b \approx 3.5 \times 10^{-2}(V/B)^{1/2} \text{ m/s.} \tag{9.7}$$

For the conditions shown here ($B = 5$ cm, $V = 1$ and 10 m/s), the calculated values of conductance are 1.6×10^{-2} and 5×10^{-2} m/s, respectively. These values are in close agreement with the data obtained on models of leaves. Nevertheless, this formula, as well as some other equations of this type that may be seen in the literature and differ from it by the value of the numeric factor, is only valid for qualitative estimations. Representation of a leaf as a smooth plate is in most cases a rough simplification.

Deviations from measured values may be significant, especially in the case of intricately shaped leaves. The boundary layer is thicker on leaves with a rough surface structure than on those with a smooth one. The presence of fluff on the surface of leaves may favor stabilization of the boundary layer thickness and make it less dependent upon wind speed. A curved shape of a leaf surface may promote the transition of air flow from a laminar to a turbulent regime at low wind velocities. The quivering of leaves in wind flow may significantly enhance transport processes in the boundary layer.

The experimental values of boundary layer conductance for leaves of various plant species fall within the range $(0.3-10.0) \times 10^{-2}$ m/s (Gates, 1968; Holmgren *et al.,* 1965; Larcher, 1976; Slayter, 1967).

It should be noted that while heat and moisture flows overcome the same resistance when crossing the boundary layer, the situation is not quite symmetric in relation to each because of different conditions in close proximity to the surface of the leaf. The immediate transfer of heat between air and the substance of a leaf usually occurs without noticeable resistance unless the cuticular layer on the leaf surface is very thick.

In contrast to the conduction of heat, the transfer of moisture between phases must overcome significant resistance in the cuticular layer. As a result, only a small part of the total flow of moisture passes through the whole surface of a leaf (cuticular transpiration), whereas the main flow of water vapor goes through stomata that occupy only a small part of the leaf surface. The density of distribution of stomata over a leaf surface varies between different plant species and may be different even on the upper and lower sides of the same leaf. Some species have stomata on only one side of a leaf.

The conditions of transfer for the portion of water vapor flow that passes through the stomata and a cuticle are alike in the bulk of the boundary layer, but become essentially different near the leaf surface. Here spherical diffusion from the stomata takes place instead of planar diffusion along the normal to the leaf surface, as in the bulk of the boundary layer. The transition from a spherical to a linear region occurs at a distance approximately equal to the spacing between neighboring stomata. As the number of stomata usually ranges from about 5000 to 50,000 per cm^2, the average distance between them should be 20–70 μm. The thickness of the part of the boundary layer, where the diffusion of water vapor may be considered to be spherical, is about half as large.

The permeability of stomata may be estimated by analyzing diffusion through a necklike opening consisting of a pair of funnels connected with a short cylinder. Although such a model is primitive, it enables one to obtain reasonable estimates. The simplified expression for this model is as follows:

$$U_s = \pi r N D (3 + \lambda/r)^{-1}, \tag{9.8}$$

where r is the radius of the narrowest section of the stoma, λ is the length of the part of the stoma that may be regarded to be cylindrical, N is the number of stomata per unit leaf area, and D is the coefficient of diffusion. As an example, when $r = 2 \ \mu\text{m}$, $\lambda = 5 \ \mu\text{m}$, and $N = 10{,}000$ stomata/cm^2, the value of stomatal conductance is 2.2×10^{-3} m/s. Experimental data show the values of U_s to be about $(5 \div 10) \times 10^{-3}$ m/s for grasses, $(2 \div 5) \times 10^{-3}$ m/s for cereals and leaf-bearing trees, and $(0.8 \div 1.7) \times 10^{-3}$ m/s for coniferous plants. The wide variation in stomatal permeability may be connected with both stomata geometry and their number (Collatz *et al.,* 1991; Nobel, 1983).

Stomata permeability is not affected by wind speed directly, but it is dependent upon the physiological state of the plant. The closing of stomata lowers the total rate of transpiration of cereals by $5-15$ times and that of leaf-bearing plants by $35-50$ times (Lynn and Carlson, 1990).

There is another step in the stomatal pathway of water vapor. This step is caused by the evaporation of water from the surface of mesophyll cells and the diffusion of vapor to the mouths of stomata. The diffusion resistance in this step is negligible because the area of contact between the gas phase and cells in the interior of the leaf is large ($5-20$ times greater than its outer area) and the diffusion path is short.

Thus, there is a single pathway of heat flow and two parallel pathways for moisture. Along any pathway the flows overcome the resistance of the boundary layer or external resistance. Beyond that, the flows overcome resistance located immediately on the surface of the leaf, called internal resistance. External resistance is dependent upon outer conditions, such as wind speed, whereas internal resistance is not. The resistance along a single pathway is connected in series and should be added up when calculating the total resistance of the pathway. The conductance of parallel pathways should also be added up.

Table 9.2 lists some conductance values typical for certain plant species. These data are compiled from several sources (Gates, 1968; Holmgren *et al.,* 1965; Larcher, 1976; Lynn and Carlson, 1990; Slatyer, 1967; Zholkevich *et al.,* 1989).

FLOWS

Returning to the graphical representation of the processes of heat and moisture exchange between leaf and air, one could convert the system of force vectors into

Table 9.2

**Approximate Value of Resistance and Conductance
of the Diffusion Pathways of Leaves**

	Resistance (s/cm)	Conductance (m/s · 10^3)	Notes
Boundary layer	0.1–3	3–100	Higher values of resistance on large leaves at calm weather
Stomata	0.8–2	5–12	Grasses
	2–4	2.5–5	Foliar trees, cereals
	6–12	0.8–1.5	Coniferous
Cuticle	20–80	0.1–0.5	Thin leaves
	Up to 200 and more	0.05 and less	Coniferous

one of flow vectors. Such an operation can be done quite simply by rescaling the *t–d* diagram in regard to the transport abilities of the leaf. Thereby the diagram remains unchanged while the scales of axes change.

The flows of energy due to heat conduction and water vapor transfer are determined by the values of conductance U_q and U_v and the driving forces Δt and Δd:

$$J_q = U_q(\rho c_p)\Delta t \ \text{W/m}^2, \tag{9.9}$$

$$J_v = U_v(\rho h_v)\Delta d \ \text{W/m}. \tag{9.10}$$

By taking $U_q(\rho c_p)$ and $U_v(\rho h_v)$ as the scale values of t and d coordinates of the diagram, we obtain a picture of flow vectors corresponding to initial force vectors. Visually both vector systems coincide, but as a matter of fact they represent quite different diagrams. Substitution of the scales transforms the initial *t–d* diagram, which represents the thermodynamic properties of humid air, into a new diagram with coordinates representing energy flows caused by the temperature and moisture content gradients. This diagram may be considered a J_q–J_v diagram in which both flows are expressed in terms of temperature and moisture content.

One should note some peculiarities in the graphical representation of the flow vector system on the *t–d* plan compared to the corresponding force vector system. First of all, the scale values of the force vectors on a *t–d* diagram are quite definite, whereas the scale values of the flow vectors on the same diagram are determined by the individual transport features of the object under study. Another distinction of the flow diagram is the change in slope of isoenthalpic lines. On the basic *t–d* diagram the isoenthalpic lines have an almost constant slope equal to the ratio of the heat capacity of air to the specific enthalpy of water vapor ($-c_p h_v$). A system of isoenthalpic lines is depicted in Fig. 9.1. In contrast, an isoenthalpic line would

not necessarily have the same slope in the diagram depicting a flow vector system. The slopes of the isoenthalpic lines will be similar only in cases when the leaf conductance value for heat and moisture flows are equal. Such conditions may be realized when the surrounding air is quite still, the stomata are open, and crossing the boundary layer of air adhering to the surface of the leaf is the rate-determining stage of the overall process. Such a case is considered in detail in Figs. 9.2 and 9.3.

In the general case, the values of conductance of a leaf for transport of water and heat may be not equal. The line answering the condition of invariability in enthalpy content would have a slope dependent upon the ratio of the conductances $(-U_q c_p/U_v h_v)$. This ratio will be denoted as k_f. As the conductance of a leaf for heat flow is often higher than that for mass flow, the isoenthalpic line in such a case usually is more steep than in the case when the conductances for heat and mass are equal.

The diagrammatic approach can be used to obtain a more detailed depiction of the processes of heat and moisture exchange between air and leaf, taking into account that transfer resistance may be considered in two parts, an inner and an outer one. In such a case, an additional configurative point should be indicated on the diagram. This point must be located between the main configurative points of the leaf and air, and it must represent the thermodynamic parameters of air, temperature and humidity, on the surface of the leaf in the depth of the adhering air layer. To indicate the position of this intermediate configurative point on the diagram, one must divide the corresponding vectors t and d in accord with the relationships between inner and outer resistance for the flows.

MATERIAL AND ENERGY BALANCE OF A PLANT

The energy balance of leaves has been examined by many authors (Gates, 1968; Jones, 1992; Kramer, 1983; Leuning, 1989; Slatyer, 1967; Zholkevich *et al.,* 1989). Nevertheless, it is worthwhile to look at the problem again. A simplified scheme of material and energy fluxes passing through a leaf is shown in Fig. 9.5. There are two energy fluxes shown in the figure, those of radiation (E) and enthalpy (H), and two material fluxes, namely, those of air (L) and water (W). The minor components of the material and energy balances are neglected for the sake of simplicity and clarity in the general picture.

The total radiant energy influx includes high-temperature solar radiation and thermal radiation coming from the environment. The absorbed part of solar radiation is converted into heat and reradiates in the infrared region of the spectrum or aids in changing the enthalpy flow. Only a small part of solar radiation is transformed into chemical energy by photosynthesis and stored in the newly synthesized organic material.

Under steady state conditions energy and material balances are maintained.
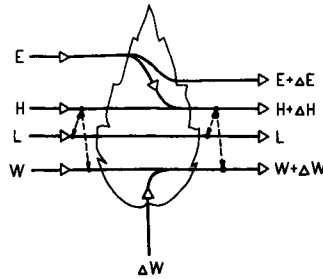
Figure 9.5 Energy and material fluxes passing through a leaf. Abbreviations: E, radiative flux; H, enthalpy flux; L, air flux; W, water flux.

This means that the total flux of energy that enters a leaf during unit time must be the same in amount as the energy flux leaving the leaf, although the qualitative parameters of the in- and outfluxes are quite different. As the total energy flux remains unchanged, only the redistribution of energy between fluxes of radiation and enthalpy may occur. Accordingly, any change in enthalpy flow should be equal in amount to that of radiative flow (taking simplifications into account) and opposite in sign.

The air flux that passes through the foliage of a plant remains unaltered in magnitude, but its qualitative parameters such as temperature and moisture content may be changed. The water flux is changed due to the transpiration of moisture from leaves. The interconnections between energy and material fluxes are shown symbolically in Fig. 9.5 by dotted arrows.

Of course the balances of both of energy and material, if treated rigorously, should include the items connected with storing a small amount of the products of photosynthesis. However, these items are usually small compared with the total flux and will be neglected here.

From the scheme of fluxes shown in Fig. 9.5, the following equations result:

$$\Delta E = -\Delta H, \tag{9.11}$$
$$\Delta H = L\delta h, \tag{9.12}$$
$$\Delta W = L\delta d. \tag{9.13}$$

In turn the change in enthalpy flow is determined by the rates of heat and moisture exchange between air and leaf:

$$\Delta H = -(J_q + J_v), \tag{9.14}$$

where the flows J_q and J_v are expressed by Eqs. (9.9) and (9.10).

The enthalpy content increment (δh) can be derived from Eq. (9.3):

$$\delta h = (1.006 + 1.86d)\delta t + (2500 + 1.86t)\delta d. \tag{9.15}$$

Within the comparatively narrow temperature range in which plants normally grow, the latter equation may be simplified without a noticeable loss of accuracy:

$$\delta h = 1.04\delta t + 2545\delta d. \tag{9.16}$$

The values of δt and δd in these equations denote the increments in the temperature and moisture content of air during its interaction with the plant. Their absolute values may be very small, especially at a high wind speed, but only their finite ratio, $\delta t/\delta d$, is significant. This ratio is determined by the direction of the resultant flow vector, and it shows the trend in the configurative point of air on the plane of the t–d diagram.

We must distinguish values of δt and δd from the values Δt and Δd. The latter symbols are finite differences in temperature and moisture content for configurative points of leaf and air, which may be read directly from the diagram. In contrast to the ratio $\delta t/\delta d$, which relates flow vectors, the ratio $\Delta t/\Delta d$ relates the resultant vector of acting forces. The relation between the two values is as follows:

$$(\delta t/\delta d) = (\Delta t/\Delta d)(U_q/U_v).$$

By excluding the variables H and L from Eqs. (9.11)–(9.13), one may derive the following relation between the radiative balance and water consumption:

$$\Delta W = (1.04k_f + 2545)^{-1}\Delta E, \tag{9.17}$$

where $k_f = (-U_q c_p/U_v h_v)$.

The expression obtained shows that the quantity of water evaporating from a leaf in unit time (ΔW) is determined by the radiative balance, i.e., by the difference between the radiative in- and outfluxes (ΔE). It is also dependent upon the ratio $\delta t/\delta d$. As mentioned earlier, when the configurative point of air moves along an isotherm ($\delta t/\delta d = 0$), the release of heat by a unit mass of transpired water is equal to the value of the specific heat of evaporation (2500 kJ/kg). The quantity of water removed from a leaf simultaneously with the release of a certain amount of heat increases as the ratio $\Delta t/\Delta d$ diminishes, and vice versa.

We have considered that the mutual location of the configurative points of air and leaf on the t–d diagram might be arbitrary. In fact, such an assumption is not exactly valid because the locations of the configurative points of air and leaf are interdependent. When the position of the configurative point of air is given, it is usually defined by the weather conditions, whereas the position of the configurative point of a leaf is determined by the energy exchange with its surroundings.

A graphical representation enables us to easily ascertain a mutual location of configurative points of air and leaf, provided the external conditions are given and the transport facilities of a leaf are known. How this can be done is shown in Figs. 9.6 and 9.7. In the former the position of the configurative point of a leaf (P) is taken as fixed. An isoenthalpic line passing through the point P gives the possible positions of the configurative point of air at zero radiative balance and equal values
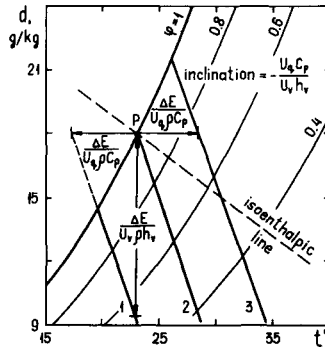
Figure 9.6 Construction of lines corresponding to the possible location of the configurative point of air at a given location of the configurative point of a leaf (P). Radiative balance: 1 means negative, $\Delta E = -100$ W/m^2; 2 means zero, $\Delta E = 0$; 3 means positive, $\Delta E = 100$ W/m^2; $U_q = 15 \times 10^{-3}$ m/s, $U_v = 4 \times 10^{-3}$ m/s.

of conductance of the pathways for heat and water vapor. In this case, the point P coincides with the position of the web-bulb thermometer point. If the conductance values are not equal, the line depicting the possible locations of the configurative point of air passes through the point P with a slope corresponding to the ratio $(-U_q c_p/U_v h_v) = k_f$. The slope is steeper when the conductance for the pathway of mass transfer is less than that of heat.

If the radiative balance of a leaf is negative $(E < 0)$, the plant absorbs more energy than it radiates and the line depicting positions of the configurative point of air would be shifted from its initial position at zero radiative balance. The line
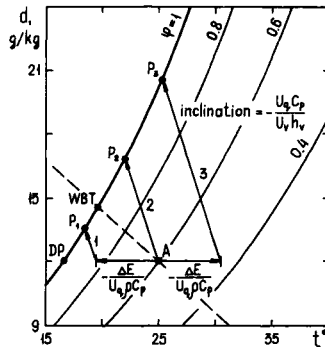
Figure 9.7 Positioning of the configurative point of a leaf (P) at a given location of the configurative point of air (A). Radiative balance: 1 means positive, $\Delta E = 100$ W/m^2; 2 means zero, $\Delta E = 0$; 3 means negative, $\Delta E = -100$ W/m^2; $U_q = 15 \times 10^{-3}$ m/s, $U_v = 4 \times 10^{-3}$ m/s.

should be shifted downward for a length equal to $\Delta E/(U_v\rho h_v)$ or leftward for a length equal to $\Delta E/(U_q\rho c_p)$. In the case of positive radiative balance, the shift should be in the opposite direction. The slope of the line depends not upon the radiative balance but only upon the ratio of conductances: $(-U_q c_p/U_v h_v)$.

Figure 9.7 shows how the position of the configurative point of a leaf may be found if the location of that of air on the t–d diagram is given. Here a straight line should be drawn through a point placed on the isotherm passing through the configurative point of air at a distance of $-\Delta E/(U_v\rho h_v)$ from the latter with a slope of k_f. The intersection of this line with the saturation line of the diagram shows the position of the configurative point of the leaf in congruence with the initial configurative point of air at a given radiative balance. The same point may be found by drawing a line of the same slope through the point on the constant d line at a distance $-\Delta E/(U_q\rho c_p)$ from the configurative point of air.

It should be noted that the position of the configurative point of air on the t–d plane of the diagram at a given radiative balance unambiguously determines the position of the configurative point of a leaf, whereas the reverse procedure is not a reciprocal process. A multitude of positions for the configurative point of air may be congruous with a single point for a leaf.

The coordinates of the configurative point of a leaf may be determined not only with the help of a t–d diagram but also analytically by the joint solution of two equations, one describing the saturation line and the second describing the inclined line constructed as shown earlier:

$$d = \frac{622}{(0.609 \times 10^{-6}) \exp(5293/T) - 1} \tag{9.18}$$

$$d = d_A + k_f(T - T_A) + \frac{\Delta E}{U_v\rho h_v}, \tag{9.19}$$

where T_A and d_A define the status of air.

Now it seems reasonable to examine the influence of basic factors upon the conditions of heat–moisture exchange of the plant with air. These conditions may vary over wide limits, which are impossible to represent completely. Nevertheless, some characteristic examples may help trace the most general regularities. To make the examples representative enough and limit their number, the following features are used:

- two levels of the humidity of air, 50% and 90%;
- temperature of air, 25° C;
- two levels of wind speed, less than 1 and 10 m/s;
- conductance of the boundary layer for vapor diffusion and heat transfer, $U_b = U_q = 15 \times 10^{-3}$ m/s for calm weather and $U_b = U_q = 50 \times 10^{-3}$ m/s for windy weather;
- conductance of stomata, $U_s = 5 \times 10^{-3}$ m/s if open and zero if closed;
- conductance of cuticle, $U_c = 0.5 \times 10^{-3}$ m/s.

The total conductance for diffusion from the leaf may be calculated by assuming that the stomatal and cuticular paths are parallel, whereas the boundary layer is in series with them:

$$U_v = \left(\frac{1}{U_b} + \frac{1}{U_s + U_c}\right)^{-1}.$$

Thus, the following set of transfer features of leaves will be used in subsequent examples:

	no wind	10 m/s wind
stomata open	$U_q = 15 \times 10^{-3}$ m/s $U_v = 4 \times 10^{-3}$ m/s $k_f = 1.53$	$U_q = 50 \times 10^{-3}$ m/s $U_v = 5 \times 10^{-3}$ m/s $k_f = 4$
stomata closed	$U_q = 15 \times 10^{-3}$ m/s $U_v = 0.5 \times 10^{-3}$ m/s $k_f = 12.2$	$U_q = 50 \times 10^{-3}$ m/s $U_v = 0.5 \times 10^{-3}$ m/s $k_f = 40$

The results are shown in a series of figures (Figs. 9.8–9.11), where the dependence of the energy flows upon the leaf's radiative balance is shown. The limits of the radiative balance depicted in the figures (± 250 W/m^2) surpass the values usually observed. This is especially true for a region of negative values, which is more characteristic under night conditions. Although the flow of heat radiation from a leaf may be as high as 450 W/m^2, during both day and night, the net radiative balance is usually much less because the heat flow incident on the leaf from surrounding objects, including the ground and the atmosphere, almost completely compensates for its inherent radiation. In daytime conditions this almost balanced heat exchange in the longwave region of the spectrum is upset due to the incident flow of high-temperature solar radiation.

One may see in the figures shown that the energy balance of a plant is attained
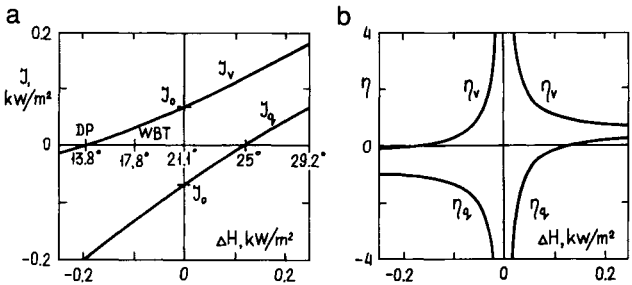
Figure 9.8 (a) Dependence of energy flows (J_v and J_q) upon radiative balance ($\Delta E = -\Delta H$). (b) Relative shares of enthalpy flow (η_v) and heat flow (η_q) in the total energy balance. Conditions: air temperature, 25° C; humidity, 50%; calm weather; $U_q = 15 \times 10^{-3}$ m/s; $U_v = 4 \times 10^{-3}$ m/s.
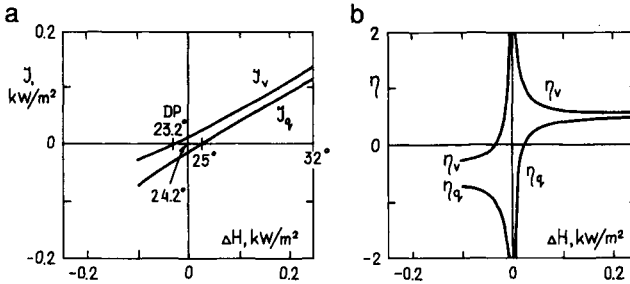
Figure 9.9 (a) Dependence of energy flows (J_v and J_q) upon radiative balance ($\Delta E = -\Delta H$). (b) Relative shares of enthalpy flow (η_v) and heat flow (η_q) in the total energy balance. Conditions: air temperature, 25°C; humidity, 90%; calm weather; $U_q = 15 \times 10^{-3}$ m/s; $U_v = 4 \times 10^{-3}$ m/s.

due to the superposition of two energy flows. The contribution of each may be negative or positive depending on conditions. The enthalpy flow J_v is positive beginning at the dew point, whereas the heat flow becomes positive from the point corresponding to the air temperature. In the region between these points the flows J_v and J_q are in opposite directions: the former draws heat out of a leaf, whereas the latter beings heat to the leaf. If the total radiative balance is high enough to raise the leaf temperature over that of air, both flows act in congruence in the same direction. Both flows also act in the same direction, but opposite that of the former case, when the leaf is cooled, due to the radiation of heat, down to a temperature below that of the dew point.

The width of the region in which the flows J_v and J_q have opposite signs depends upon the state of the air, its temperature, and its relative humidity: the drier the air the greater the distance between the dew point and air temperature:

$$t_A - t_{DP} = T_A\left(1 - \frac{1}{1 - (1.8893 \times 10^{-4})T_A \ln \phi}\right),$$
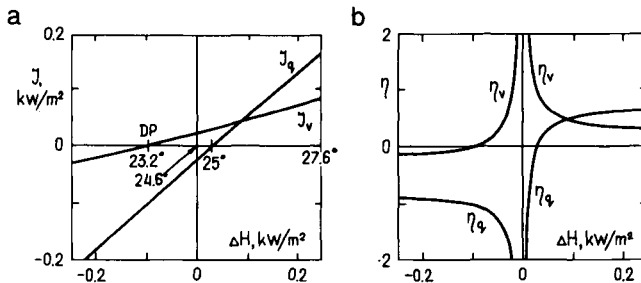
Figure 9.10 (a) Dependence of energy flows (J_v and J_q) upon radiative balance ($\Delta E = -\Delta H$). (b) Relative shares of enthalpy flow (η_v) and heat flow (η_q) in the total energy balance. Conditions: air temperature, 25°C; humidity, 90%; wind, 10 m/s; $U_q = 50 \times 10^{-3}$ m/s; $U_v = 5 \times 10^{-3}$ m/s.
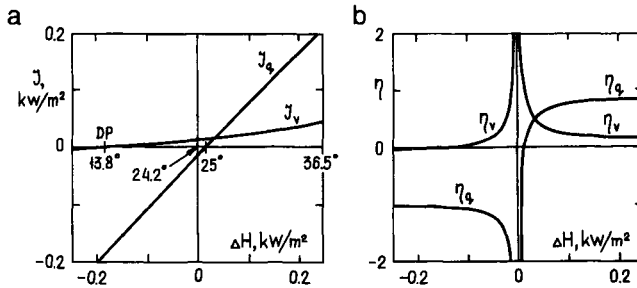
Figure 9.11 (a) Dependence of energy flows (J_v and J_q) upon radiative balance ($\Delta E = -\Delta H$). (b) Relative shares of enthalpy flow (η_v) and heat flow (η_q) in the total energy balance. Conditions: air temperature, 25° C; humidity, 50%; calm weather; stomata closed; $U_q = 15 \times 10^{-3}$ m/s; $U_v = 0.5 \times 10^{-3}$ m/s.

where $T_A = t_A + 273.2$ is the absolute temperature of air. Inside this region there is a point where both flows are equal in magnitude and thus compensate for each other. The total radiative balance at this point is evidently zero. The magnitude of either of the energy flows at zero total balance is a feature that characterizes, to a certain extent, the response of a leaf to the variation in an energy load. For reasons that are easily understood, the absolute value of the energy flow, whether J_q or J_v, at zero radiative balance should be called the "exchange flow," and we will designate it as J_0. The exchange flow is depicted in Fig. 9.8 to illustrate the meaning of this value.

By comparing Figs. 9.8–9.11, one may clearly see that the value of the exchange flow determines the relative response of a plant under varying external conditions, for example, changes in radiative balance. If the exchange flow is large compared to the external energy load of a leaf, the conditions of its functioning will only slightly deviate from those at zero load. However, in cases when the energy load considerably surpasses the exchange flow, the conditions of functioning of all the systems of a leaf linked with the transport of water will be significantly affected.

The b panels in these figures show the size of the share of each flow, J_q and J_v, in the total energy balance of a leaf. As one can see at a zero value of the balance, when both flows each have equal magnitudes, their ratio to the net energy flow approaches infinity. This means that at this point the efficiency of withdrawal of heat from a plant by water evaporation equals zero because the outflow of enthalpy with vapor is compensated by an inflow due to the conduction of heat. Beyond the zero point the heat-removing efficiency of evaporation changes in various modes, depending on the transport features of the leaf. Only in cases where the leaf temperature is equal to that of air is the efficiency of evaporation unity: each kilogram of water as it passes through the leaf carries away 2500 kJ of heat, an amount equal to its heat of evaporation.
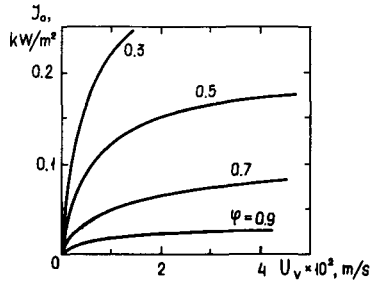
Figure 9.12 Dependence of the exchange flow upon diffusion conductance (U_v) for various values of air humidity; $U_q = 15 \times 10^{-3}$ m/s, no wind.

As for the exchange flow J_0, which determines the response of a leaf depending upon external conditions, its value may vary over a wide range from a few watts per square meter up to 200–300 W and more. Figures 9.12–9.17 show the basic regularities, such as the dependence of J_0 upon the transport features of leaves and the temperature and humidity of air. One may see that an increase in temperature and a decrease in humidity favor an increase in the exchange flow. In turn, a high exchange flow value may be considered to be a favorable factor for the plant in a limited sense. For example, if the exchange flow is high, the sunlit leaves of a plant and the shaded ones will "work" under almost the same conditions with respect to water transport and transpiration, in spite of the differences in their radiative balances. In contrast, both sunlit and shaded leaves will face significantly different loads if their exchange flow is low.

In conclusion, we will present a brief summary of the basic characteristics of the heat–moisture interaction of plants with air that can be seen in the figures. A low level of air humidity favors the broadening of the region of radiative balance, in which the flow of water varies slightly. In this region the evaporation of water,
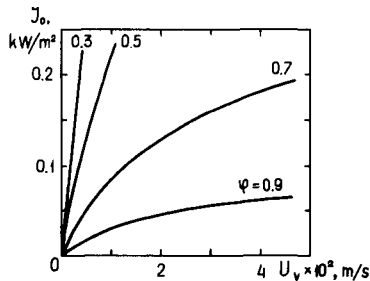
Figure 9.13 Dependence of the exchange flow upon diffusion conductance (U_v) for various values of air humidity; $U_q = 50 \times 10^{-3}$ m/s, wind 10 m/s.
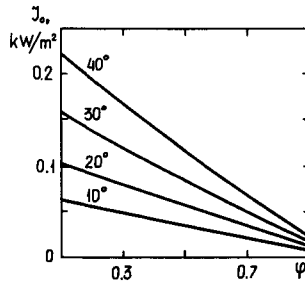
Figure 9.14 Dependence of the exchange flow upon the humidity of air for various temperatures; $U_q = 15 \times 10^{-3}$ m/s, $U_v = 4 \times 10^{-3}$ m/s, no wind.

not the direct conduction of heat, removes the wasted energy from a plant. At a high level of humidity, the share of heat conduction becomes more significant even at a low radiative balance. An increase in the wind speed broadens the region where the transfer of heat with water vapor is predominant compared to direct heat conduction. At a high wind speed the dependence of the power of water flow upon the radiative balance is less than that in calm weather. Also the shift in the temperature of a leaf with a change in radiative load diminishes. The strengthening of the wind affects heat flow J_q more strongly than the flow of enthalpy J_v. Closing of the stomata significantly diminishes the share of the enthalpy flow. This effect is expressed more sharply at high wind speeds.

WORK OF TRANSPIRATION

Transpiration is a process indissolubly bound with the vital activity of plants. It is commonly defined as the means by which a plant cools itself. Such a point of
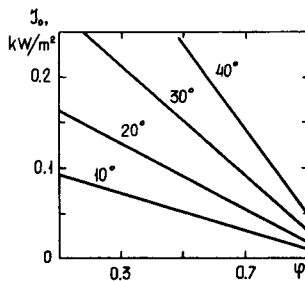
Figure 9.15 Dependence of the exchange flow upon the humidity of air for various temperatures; $U_q = 50 \times 10^{-3}$ m/s, $U_v = 5 \times 10^{-3}$ m/s, wind 10 m/s.
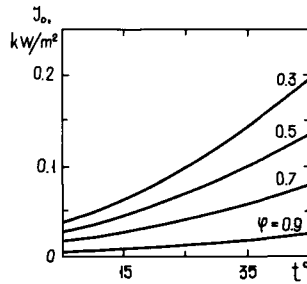
Figure 9.16   Temperature dependence of the exchange flow for various values of air humidity; $U_q =$ 15 × 10^{-3} m/s, U_v = 4 × 10^{-3} m/s, no wind.

view undoubtedly is reasonable, yet it cannot be regarded as complete. The removal of excess heat is naturally a necessary stage of the plant functioning as an energy-converting system. The withdrawal of heat is affected by two conjugated processes: direct heat exchange with the surrounding air and water evaporation. At first examination both processes seem to be fully equivalent, but such a judgment is not quite true.

There are essential distinctions between the processes of direct heat exchange and heat transfer by the evaporation of water. The former process does not involve the transfer of mass but only that of impulse, whereas the latter is coupled with the transport of molecules from the liquid phase to the gaseous one. In each elementary act of heat exchange, the average portion of energy transmitted is about 1 *kT*, whereas the transfer of one molecule of water from the liquid to the gaseous phase needs more than 17 *kT*. The status of water in liquid or gaseous phase is associated with significantly different values of entropy. Accordingly, the evaporation of liquid is an irreversible process followed by an increase in the total entropy of the system. This process proceeds spontaneously if the loss of enthalpy
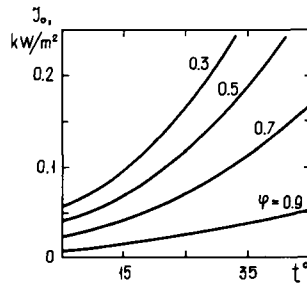
Figure 9.17   Temperature dependence of the exchange flow for various values of air humidity; $U_q =$ 50 × 10^{-3} m/s, U_v = 5 × 10^{-3} m/s, wind 10 m/s.

from evaporated water is compensated by the influx of heat from any source, and if the vapor produced is removed. Thus, the evaporation of water may perform work at the expense of heat being absorbed by the plant. In other words, this process may be regarded as the transformation into work of the difference in the water chemical potentials between the vapor and liquid phases.

It should be of interest here to elucidate two basic points connected with the problem of transpiration. The first is the amount of work that may be utilized by a plant at the expense of water transpiration. The next is how this work is performed. To find answers to these questions, one has to trace the pathway of water from soil through the plant to the atmosphere. The chemical potential of water gradually declines along this path. The crucial point on this pathway is that where the phase transition of water occurs, when liquid water is converted into vapor. This point is obviously associated with the surface of mesophyll cells that contact air in the substomatal cavity of a leaf.

Strictly speaking, water in the walls of mesophyll cells exists not in a free state but is bound with the colloidal components of the cell walls. However, this binding energy is not large, and therefore the chemical potential of the water does not significantly differ from that of free water in the liquid state. The point of principal significance is that the transition of water from a condensed state into a gaseous one is followed by a sharp increase in entropy. Due to this leap in entropy on the boundary between the phases, a mechanism that can do work may function here.

One must note that a leap in entropy between phases exists even under conditions of equilibrium, for example, in the substomatal cavity when the stomata are closed. Under such conditions the difference in water chemical potential between the phases is zero because the entropy term ($T\Delta s$) is equal to enthalpy (Δh):

$$\Delta\mu = \Delta h - T\Delta s = 0.$$

When the stomata are open, vapor can leak from the substomatal cavity, thereby perturbing the balance between the entropy and enthalpy terms, and the process of water evaporation proceeds at a rate depending upon the rate of leakage. In turn, the rate of vapor leakage into free air is determined by the difference in water chemical potential in the gaseous phase between the substomatal area and free air. This difference finally determines the rate of transpiration, but in relation to the plant it is in fact an external factor and cannot produce any work in the plant. The place where the process of transpiration can perform useful work is actually the border between a cell and the gaseous phase in the substomatal area of a leaf.

In the literature devoted to problems of plant physiology, a rather widespread concept is that the deficit of water vapor content in air is the driving force of transpiration. Such a concept should be considered, however, to be not quite true. The transfer of water vapor along a gradient of its partial pressure is in fact a passive process, which cannot act as the cause of the force that draws water through the xylem. The diffusion of water molecules from leaves only removes

the "wasted steam," whereas the withdrawing force actually originates when water transfers from a condensed into a gaseous phase.

The maximum amount of work that may be done at the expense of the transition of condensed water into the gaseous state theoretically may attain a value equal to the entropy term of the chemical potential difference ($T\Delta s$), which in turn is equal to the energy expenditure for evaporation (Δh). The real amount of work performed by the process of transpiration is much less than the theoretical limit.

One may attempt to estimate the total amount of energy potentially available for performing the work of transpiration on the basis of indirect data. It is known that plants consume a large quantity of water per unit of organic mass formed by photosynthesis. This quantity is about 500–700 kg of water/kg of dry biomass for grasses, cereals, and vegetables and somewhat less, about 300 kg/kg, for trees (Larcher, 1976). By taking into account the energy content of dry biomass, $(16-20) \times 10^3$ kJ/kg, and the value of the heat of evaporation of water (about 2500 kJ/kg), one should obtain a value of about 50 for the ratio of the amount of energy consumed by the evaporation of water to that stored in biomass. On the other hand, the efficiency of the photosynthetic conversion of absorbed radiation into the chemical energy of biomass is about 2%. Thus, one may conclude that the total amount of energy involved in photosynthesis is close to that used for water evaporation.

In the case of plants that consume water more economically, such as C_4 plants, the relation remains the same because these plants usually show correspondingly higher values of efficiency of photosynthesis. Thus, one may conclude that for its initial energy resources, plant use of the quantum process of photosynthesis and that of the thermophysical process bound with transpiration are on the same order of magnitude. Moreover, as photosynthesis proceeds with low efficiency, a large part of the energy captured is ultimately transformed into heat. This heat, being wasted energy, is quite useless for performing work. However, it may be used indirectly to compensate for heat loss during the transpiration of water.

Energetics of Permeation of Molecules and Ions across Membranes

INTRODUCTION

   Life depends on water. A number of important properties distinguish water from most other compounds and lead to the unique suitability of water as a medium for cellular activities. Water generally moves into a plant through its roots and out through its leaves. Cell membranes are semipermeable, that is, some molecules, such as water, pass through them easily, while other molecules, such as sugars and some salts, do not (Blank, 1991). The cell's cytoplasm contains large amounts of sugars and salts. Diffusion is the movement of molecules from areas of high concentration to areas of low concentration. The difference in ion concentrations causes water to diffuse into the cell. This is how water moves from the soil into the cells of plant roots. Water makes up 90–95% by weight of plant soft tissues. Water movement, associated with plants, can be into and out living cells across cell membranes, along the xylem, and from leaves to the atmosphere as water vapor.
   Ion transport across cell membranes is essential for a number of cellular functions. In cells, this process is aided by ion channels, carriers, and pumps, which lower the free energy barrier associated with the transfer of ions from the polar aqueous environment to the nonpolar interior of the membrane. However, ions can permeate lipid membranes even in the absence of special molecules to assist the transport. An understanding of the mechanism of passive ion and dipole transport at a molecular level could offer valuable insight into induced charge transport (Stein, 1967, 1986). The balance between the maintenance and dissipation of concentration gradients across cell membranes is crucial for the function of biological systems. Processes such as oxidative and photosynthetic phosphorylation require that membranes provide an effective barrier to the passive diffusion of protons. In

other cases, the rapid exchange of molecules such as water across a cell membrane is essential, which demands water channel proteins that increase the intrinsic water permeability of the membrane. The permeability coefficients of many ions and small neutral molecules have been determined experimentally and vary over a remarkably broad range. Despite the availability of these data, the mechanism of passive permeation is still not completely understood.

In the past, permeability coefficients characterizing the lipid bilayer as a barrier to permeation have been calculated from solubility–diffusion theory (Cass and Finkelstein, 1967), which is still the most generally accepted description of the water permeability of bilayers. This model treats the membrane as a thin static slab of hydrophobic matter embedded in an aqueous environment. To cross the membrane, the permeating particle must dissolve in the hydrophobic region, diffuse across, and leave by redissolving into the second aqueous phase. If the membrane thickness and the diffusion and partition coefficients of the permeating species are known, the permeability coefficient can be calculated. The partition coefficients for ions and neutral molecules are usually determined by experiment (Markin and Volkov, 1989a,b). The traditional viewpoint in the literature is that partition coefficients for ions can be derived from their Born energy, the energy required to transfer a charged particle from the high-dielectric aqueous phase to the low-dielectric membrane interior (Parsegian, 1969; Dilger *et al.,* 1979). In many cases, however, discrepancies between predicted and measured permeabilities have raised questions about this approach. For example, the observed permeability of sodium ions exceeds the calculated value by 3 orders of magnitude (Hauser *et al.,* 1973). Proton permeation rates were found to be even larger at 5–6 orders of magnitude above the values estimated from comparisons with other monovalent cations (Deamer and Nichols, 1983, 1989). Several attempts have been made to account for these discrepancies. Solvophobic and image energies have been added to the Born energy term, yielding a smaller net energy of transfer and thus increasing the predicted permeability. It has also been suggested that hydrated radii be used instead of bare ionic radii, which lead to lower translocation energies and therefore higher permeation rates (Deamer and Volkov, 1995).

An alternative to the solubility–diffusion description has been proposed, which suggests that permeation across a bilayer membrane occurs through hydrated transient defects produced by thermal fluctuations. By passing through pores, the permeating particle can avoid the Born energy barrier associated with the solubility–diffusion model. Furthermore, protons can be translocated by a Grotthus-type mechanism along water "wires" spanning the membrane in such defects. Because this process is intrinsically much faster than diffusion, the transient pore model can also explain the high permeability observed for protons. Mechanisms of ion, water, and small neutral molecule permeation across membranes will be discussed in this chapter.

The cell membrane acts as a barrier separating the cell contents from the external medium. Lipid bilayers have sufficiently low permeability such that transport

systems in the membrane can maintain suitable gradients of ions or polar solutes against a substantial leak. It has been a general assumption that the low permeability reflects the electrostatic energy for partitioning an ion or dipole in the low-dielectric hydrocarbon interior, an energy term so large that it represents a nearly insurmountable barrier (Parsegian, 1969). Although this has been a satisfying general explanation, when the expectations of electrostatic energy calculations are compared with experimental measurements of ionic flux, it becomes clear that other factors must be considered as well (Deamer and Volkov, 1995; Volkov and Deamer, 1994). For instance, the passive transfer of an ion across a lipid bilayer, although measurable, is in fact a rare event, and it is possible that transient defects can account for much if not all of the measured diffusion.

The presence of ion gradients is of vital importance to the functioning of most living cells. Ion gradients are required as an energy source, for signal transmission, and as a tool to orient proteins.

The transport across membranes can be passive or active. Passive transport operates on an existing electrochemical potential gradient of the permeant, and its work leads to the disappearance of this gradient. The passive transport requires no other input of Gibbs free energy (Shirai *et al.*, 1995, 1996).

Perhaps the most dramatic inconsistency with Born (1920) theory is seen with proton gradients. A remarkably high proton permeability was first reported by Nichols and Deamer (1978, 1980) and confirmed by other laboratories (Gutknecht, 1984; Perkins and Cafiso, 1986; Rossignol *et al.*, 1982). There is no reason to expect proton permeation to differ from that of other cations, yet calculated fluxes of protons at a concentration gradient of $10^{-6}-10^{-7}$ M (pH 6–7) are in the same range as the flux of potassium ions at a gradient of $10^{-1}-10^{-2}$ M. That is, proton and potassium fluxes at 10-fold gradients are similar even though the potassium concentration at 0.1 M is 10^5 times that of protons at pH 6.

A second unusual feature of proton translocation across membranes is that measured fluxes depend on the size of the pH gradient (or membrane potential) driving the flux, as expected, but the absolute value of the flux is essentially independent of the pH at which the measurements are made. This was first noted in liposomes by Nichols and Deamer (1978) then confirmed by Gutknecht (1984) for planar lipid bilayers over a pH range from 2 to 11. That is, at a given voltage driving proton currents, virtually the same proton conductance was measured at low, neutral, and high pH values.

It follows from these observations that protons can have a permeation mechanism quite different from that of other monovalent cations. This at first might seem to be a laboratory curiosity, but in fact proton permeation mechanisms are fundamental to our understanding of bioenergetics. For instance, electrochemical proton gradients are the energy source for ATP synthesis by cF_0cF_1 ATP synthase of thylakoid and other coupling membranes. The cF_0 subunit has a channellike structure that allows protons to be conducted to an active site at which proton translocation is coupled to the release of ATP from the cF_1 subunit (Fig. 4.5).

Parsegian (1969) first described the barrier properties of lipid bilayers in terms of the Born energy required to bring an ion from a high-dielectric aqueous phase to the low-dielectric medium of the hydrocarbon chains composing the membrane interior. This energy, in the range of 100–300 kJ/mol for inorganic monovalent cations, is an immense energy barrier and has been generally accepted as a reasonable explanation for the relative impermeability of bilayer membranes to ion flux.

The approach developed by Parsegian was elaborated by Dilger *et al.* (1979), who tested the prediction that increasing the dielectric constant of the bilayer phase would lead to significant increases in the ionic permeability of a planar lipid bilayer membrane. The membrane dielectric was increased by replacing the normal decane solvent with chlorodecane, and it was found that permeability to anions was in fact increased by 3 orders of magnitude. This result was qualitatively consistent with the expectations of Born theory, but did not represent a critical quantitative test of the hypothesis that Born energy represents the primary barrier to ion diffusion across bilayers.

Other investigators have noticed certain shortcomings of the Born theory with respect to experimental results. Among the first was Bell (1931), who noted that measured partitioning of ions between polar and nonpolar media was only in qualitative agreement with expectations from Born calculations. The initial application of the theory to lipid bilayers was attempted by Hauser *et al.* (1973), who calculated the rate at which sodium ions were expected to escape from liposomes according to Born theory. The calculated rates were then compared with measured efflux rates and found to be too slow by 3 orders of magnitude. To explain this discrepancy, it was suggested that substantial transbilayer defects were contributing to the loss of sodium ions from the vesicles, perhaps related to vesicle–vesicle fusion events.

Macdonald (1976) noted that Born energy calculations for ionic permeation predicted extreme sensitivity to the diameter of the permeating ion. Permeability was expected to vary over ranges in excess of 10^{10} when smaller and larger monovalent ions were compared. However, experimental measurements of sodium and potassium fluxes showed relatively little difference (Bangham *et al.*, 1965). Macdonald attempted to explain this by suggesting that the free energy of ion transfer from an aqueous phase to the hydrocarbon interior of a bilayer has a uniform energy minimum for all ions that is related to their hydration state. Therefore, hydrated ions would not be expected to behave according to the Born energies calculated for the bare ionic radii. This expectation was confirmed by Georgallas *et al.* (1987), who reported only small variations in the permeability of multilamellar liposomes to monovalent cations (Li^+, Na^+, K^+, and Cs^+). The permeability varied inversely with the hydrated ionic radius, suggesting that the hydrated species were permeating rather than the bare ions.

Flewelling and Hubbel (1986) noted a second discrepancy: the permeability of

bilayers to hydrophobic anions (tetraphenylboron) was considerably greater than that to cations with virtually identical size and hydrophobicity (tetraphenylphosphonium), even though Born theory would not predict any difference between monovalent anions and cations. To account for this, the authors developed a more comprehensive theory that includes not only Born energy but also dipole energy, hydrophobic energy, and image energy terms related to ions approaching and permeating an actual lipid bilayer. A major differentiating factor appears to be the dipole potential, which favors anion permeation. The expanded equation does account for the difference between anions and cations, but does not predict actual rates at which various ions permeate the bilayer.

The discrepancies described herein suggest that we must expand our consideration of ion permeation mechanisms to include other conductive processes. In this chapter, we will discuss two mechanisms of passive transmembrane transport that in a sense represent alternative hypotheses (Deamer and Volkov, 1995). The first is that ion (or dipole) permeation can be understood in terms of energy related to the partitioning of ions (or dipoles) into the nonpolar phase of the lipid bilayer and that electrostatic considerations, including electrostatic energy, are primary concerns. The second mechanism is that high-dielectric defects in the form of transient pores occur in the bilayer and allow permeating ions or dipoles to bypass the partitioning energy barriers. These two hypotheses have been tested by experimental measurements of proton, potassium, water, and small organic molecule fluxes (Paula *et al.,* 1996; Volkov *et al.,* 1997b) across lipid bilayers of varying thicknesses.

PARTITION MODEL

BORN ENERGY

We will first discuss the partition model for calculating the Gibbs free energy of ion or dipole transfer through bilayers (Fig. 10.1). In this model, an ion with radius a is transferred from the aqueous phase to the center of a bilayer with a nonpolar phase thickness d. For simplicity, we will assume that the membrane is a homogeneous liquid dielectric with a dielectric permittivity ϵ_m. To understand the energies involved in transferring an ion or dipole between two solvent phases, we must take into account the following effects: (i) electric polarization of the medium (Deamer and Volkov, 1995); (ii) production of a cavity in the medium to accommodate the ion, variously called the solvophobic, hydrophobic, or neutral effect (Volkov and Kornyshev, 1985); (iii) changes in the structure of the solvent that involve the breakdown of the initial structure and the production of a new structure close to the ion (Kornyshev and Volkov, 1984); (iv) specific interactions of the ions with solvent molecules, such as hydrogen bond forma-
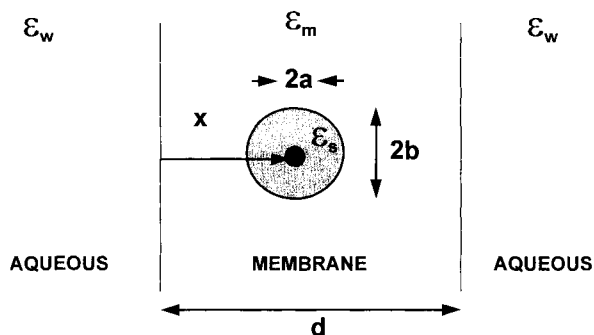
Figure 10.1 The partition model for ion permeation of a lipid bilayer, ϵ_w, ϵ_m, and ϵ_s are the dielectric constants of the aqueous phase, membrane phase, and the ion solvation shell, respectively; a is the ionic radius, x is the distance the ion penetrates into the bilayer, q is the ionic electrical charge, and d is the thickness of the hydrophobic part of the bilayer.

tion, and donor–acceptor and ion–dipole interactions (Bayliss, 1923; Markin and Volkov, 1989a,b).

This division is arbitrary to some extent because different effects may overlap (Markin and Volkov, 1987a–c). For example, the electric polarization of a solution may have a significant influence on its structure. It is possible, however, to carry out theoretical calculations of individual effects. The components mentioned earlier are sometimes grouped into "blocks," for instance, by combining solvophobic effects related to cavity formation with structural changes in the solvent surrounding the solute particle. This is justifiable because the solvophobic effect, together with the electrostatic effect, provides the major contribution to the solvation energy.

It is also necessary to take into account the differences between larger and smaller ions in the short-range interactions of the ion with each solvent. With large ions, such a contribution is primarily concerned with the work spent creating a cavity in the medium in which the ion will be placed. Entropy effects related to the disordering induced by the structure-breaking ion also fall in this category. The opposite effect may occur in the case of smaller ions, a process we will refer to as "defect annihilation." For instance, an ion may be captured in a statistically probable microcavity in the local structure of solvent, thereby releasing the energy of this defect. Other examples are the energy release due to ion–solvent hydrogen bonding via individual protons and the entropy effect of structure-making ions. Contributions of this kind are very sensitive to the nature of both the ion and the solvent.

In general, for small ions of low chemical activity (not forming solvation complexes), the electrostatic contribution dominates. With increasing ionic radius, the electrostatic contribution decreases, becoming comparable to the rising solvopho-

bic contribution. We can now discuss electrostatic considerations in more detail.

Electrostatic interactions play a central role in a variety of biophysical processes in plants. The electrostatic contribution to the Gibbs free energy of ion resolvation has often been estimated with the aid of Born's continuum model (Born, 1920) in which the ion is described as a sphere of radius a with charge q distributed uniformly over its surface, while the solvent is considered a structureless medium with a macroscopic dielectric constant ϵ. The Born model (Fig. 10.2) assumes that it is only the charge on the ion that is responsible for ion–solvent interactions. The interactions between the solvent and the ion are considered to be electrostatic in origin. The Born model considers the ion equivalent to a charged sphere and the structured solvent a structureless continuum with dielectric constant ϵ. In this model, free energy of ion transfer between two phases is considered as the sum of the work to discharge an equivalent sphere in one phase and the work to charge an equivalent sphere in another solvent. The work to charge an uncharged sphere of radius a is

$$A = \int_0^q \phi \, dq = \int_0^q \frac{q}{4\pi\epsilon_0\epsilon r} \, dq = \frac{q^2}{8\pi\epsilon_0\epsilon a}, \tag{10.1}$$

and the work of discharge can be written as

$$A = \int_q^0 \phi \, dq = \int_q^0 \frac{q}{4\pi\epsilon_0\epsilon r} \, dq = -\frac{q^2}{8\pi\epsilon_0\epsilon a}. \tag{10.2}$$
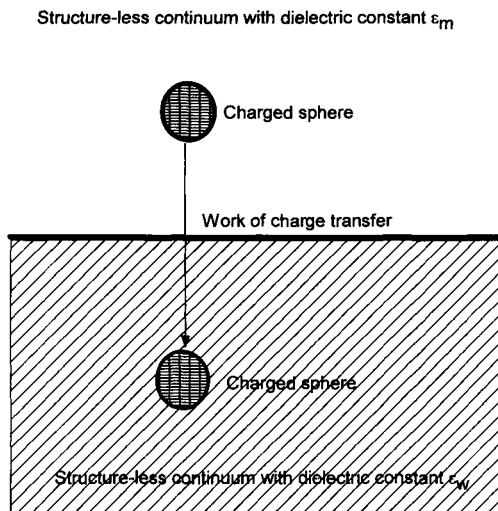
Figure 10.2 The Born model for the electrostatic contribution to ion–solvent interactions considers the ion as a charged sphere and the solvent as a structureless continuum.
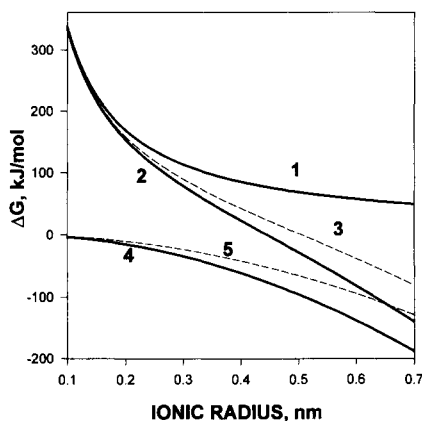
Figure 10.3 Gibbs free energy of ion transfer from water to a liquid hydrocarbon calculated according to the Born equation (1), Born equation and solvophobic effect together (2, 3), and solvophobic effect (4, 5) according to the Eq. (10.3). Conditions: $T = 25°$C; $\epsilon_w = 78.5$; $\epsilon_m = \epsilon_s = 2$; $\gamma_{w,m} = 51$ mN m^{-1} (2, 4), $\gamma_{0,m} = 35$ mN m^{-1} (3, 5).

The relationship between ionic radius a and the electrostatic (Born) component of the Gibbs energy of ion transfer from medium w into medium m is calculated from the expression

$$\Delta_m^w G(\text{Born}) = -\frac{q^2}{8\pi\epsilon_0 a} \left(\frac{1}{\epsilon_w} - \frac{1}{\epsilon_m}\right), \tag{10.3}$$

where ϵ_w and ϵ_m are the dielectric permittivities of phases w and m. The dependence of the Born component of the free energy of ion transfer between two immiscible liquid phases such as water and hexadecane on ionic radius a is shown in Fig. 10.3, curve 1. From Eq. (10.3) it follows that the Born component of the free energy of ion transfer between two immiscible liquid phases strongly depends on the dielectric permittivities of both phases (Fig. 10.4).

An obvious inherent error in this estimate is that it neglects the structural characteristics of the media being considered. The predictions of Eq. (10.3) are also in poor agreement with experimental results (Kornyshev and Volkov, 1984; Markin and Volkov, 1987a–d). Specifically, according to Eq. (10.3), for $\epsilon_w > \epsilon_m$, the lowest energy state of the ion is in medium w regardless of its radius. This is inconsistent with experimental measurements of ion distribution between two immiscible electrolyte solutions or in water–liquid membranes. The results indicate that small ions prefer the polar solvent, while large organic ions prefer the hydrophobic phase. Figure 10.5 shows that even for relatively straightforward estimates of the hydration energy of monovalent ions in water, Born theory predicts values approximately twice those of experimental results.
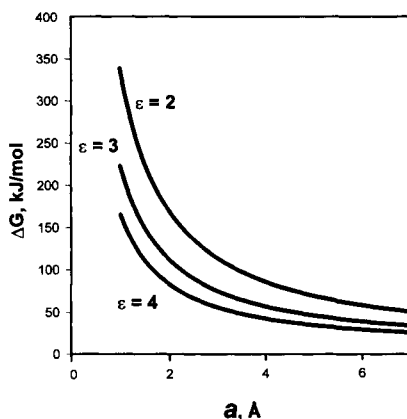
Figure 10.4 Electrostatic contribution to the Gibbs free energy of ion transport from water to a low-dielectric slab according to the Born equation.

The main weakness of the Born continuum model is that all of the information about the dielectric properties of a pure solvent is contained in the dielectric constant ϵ, which treats the solvent as a structureless screening background. However, Born formulated his model in 1920 on the basis of Lorentz macroscopic electrostatics, assuming that they could be extrapolated to localized induction and electric field effects of the ion. In calculations of fields produced by microscopic sources such as ions, it is necessary to take into account the microscopic structure of the medium. One way to do this is to apply nonlocal electrostatics, which is now widely used both in solid state theory and in the theory of liquid solutions.
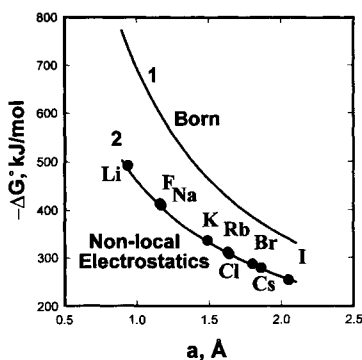
Figure 10.5 Gibbs free energy of ionic hydration as a function of ionic radius. Curve 1 was calculated from Born theory (Eq. 10.3 in text). Curve 2 was calculated from nonlocal electrostatic theory (Kornyshev and Volkov, 1984). The points are experimental data (Randles, 1956) with hydrated ionic radii taken from Gourary and Adrian (1960) ($\lambda = 0.1$ nm, $\Lambda = 0.7$ nm).

NONLOCAL ELECTROSTATICS

Nonlocal electrostatics assumes that fluctuations in solvent polarization are correlated in space because a liquid has structural features related to quantum interactions between its molecules. This means that the average polarization at each point is correlated with the electric displacement at all other points (Kornyshev, 1981). Kornyshev and Volkov (1984) used a generalization of the Born model to describe the electrostatic contribution to the free energy of resolution. In this approach, nonlocal electrostatics was used to describe the dielectric response of a solvent in terms of the static dielectric function $\epsilon(k)$. This function contains information about special features of screening at short distances associated with liquid structure. The electrostatic contribution to the free energy of ion resolution is in the form of

$$\Delta_\beta^\alpha G(\text{el}) = \frac{q^2}{4\pi^2\epsilon_0} \int_0^\infty dk \, \frac{\sin^2 ak}{a^2k^2} \left[\frac{1}{\epsilon_\beta(k)} - \frac{1}{\epsilon_\alpha(k)} \right], \qquad (10.4)$$

where $\epsilon_i(k)$ is the bulk dielectric function of the ith medium. This relation was derived from the same model as Eq. (10.3), in which ions are regarded as charged spheres to approximate a linear function. It also assumes that a foreign ion brought into the medium will not perturb the structure or screening properties of the medium.

Approximations for $\epsilon_\alpha(k)$ and $\epsilon_\beta(k)$ must be used to obtain an analytical function for $\Delta_\beta^\alpha G(\text{el})$. To this end, we can apply the results of an analysis by Dogonadze and Kornyshev (1974), according to which the expression

$$\frac{1}{\epsilon(k)} = \frac{1}{\epsilon_{\text{opt}}} - \left(\frac{1}{\epsilon_{\text{opt}}} - \frac{1}{\epsilon_*} \right) \frac{1}{1 + k^2\lambda^2} + \left(\frac{1}{\epsilon_*} - \frac{1}{\epsilon} \right) \frac{1}{1 + k^2\Lambda^2}, \qquad (10.5)$$

can serve as a reasonable approximation for $\epsilon(k)$ of polar liquids. It corresponds to provisional splitting of the medium polarization fluctuations, $\vec{P}(r)$, into three modes, $\vec{P} = \vec{P}_e + \vec{P}_i + \vec{P}_D$, associated with the excitation of electronic (e), vibrational (i), and orientational (debye, D) degrees of freedom. Because these are markedly separated in frequency, we can write

$$\langle \vec{P}(r)\vec{P}(0) \rangle \approx \langle \vec{P}_e(r)\vec{P}_e(0) \rangle + \langle \vec{P}_i(r)\vec{P}_i(0) \rangle + \langle \vec{P}_D(r)\vec{P}_D(0) \rangle \qquad (10.6)$$

Equation (10.5) corresponds to an exponential attenuation of these correlations in space with correlation radii Λ and λ for the debye and vibrational polarizations, respectively, and with a negligibly small correlation radius for the electronic polarization. Quantities ϵ_{opt} and ϵ_* are the values of the liquid's dielectric permittivities at frequencies corresponding to the transparent bands separating the electronic, vibrational, and orientational (ϵ_*) regions of the spectrum, respectively. Although the values of λ and Λ are rather uncertain, they cannot be regarded as purely adjustable parameters of the theory. By its physical meaning, λ is on the

order of the radius of a water molecule. Λ is comparable with the characteristic length of the hydrogen-bonding chain which, according to diffraction data (Palinkas *et al.*, 1977), is on the order of 0.7 nm. To test this approach for an analysis of the free energy of ion hydration in aqueous solutions, Kornyshev and Volkov (1984) used Eqs. (10.4) and (10.5) in the form

$$\Delta_{\text{water}}^{\text{vacuum}} G(\text{el}) = \frac{q^2}{8\pi\epsilon_0 a}$$

$$\times \left\{ 1 - \frac{1}{\epsilon_{\text{opt}}} + \left(\frac{1}{\epsilon_{\text{opt}}} - \frac{1}{\epsilon_*} \right) \phi\left(\frac{2a}{\lambda} \right) + \left(\frac{1}{\epsilon_*} - \frac{1}{\epsilon} \right) \phi\left(\frac{2a}{\Lambda} \right) \right\}, \quad (10.7)$$

where

$$\phi(x) = 1 - (1 - e^{-x})\frac{1}{x}. \qquad (10.8)$$

The results obtained in calculations of the electrostatic component of the Gibbs free energy of ion hydration with Eq. (10.5) are plotted in Fig. 10.5 together with data for the measured free energy of hydration of individual ions. The fit is remarkably good for both cations and anions. A minor deviation is seen for the very small Li^+ ion, which could be due to entropy effects in structure formation or to the defect annihilation effects described earlier. That is, the ion could be trapped in a statistically probable microcavity in the water structure, and this would liberate the energy of the defect microcavity. The obvious differences between theory and experiment found in the case of large ions provide evidence for the importance of hydrophobic effects in creating a cavity in the medium able to accommodate the ion.

Figure 10.5 shows the dependence of the Gibbs free energy of hydration for an ion with radius equal to 0.149 nm (for example, K^+) on correlation lengths λ and Λ. The largest value for the hydration energy is obtained in the Born limit $\lambda = 0$, that is, in a structureless solvent. The finiteness of λ and Λ reduces the contribution of any one of the three modes P_i, P_e, or P_D. In Eq. 10.5, the correlation length of the electronic mode P_e is set equal to zero. The exact values of the correlation lengths λ and Λ cannot be determined *a priori*, but they can be estimated from infrared spectral characteristics. In the infrared region, the length Λ depends on the properties of the liquid. In the case of nonassociated liquids, the correlation length for orientiational vibration is approximately equal to the intermolecular distance, while for associated liquids Λ is equal to the characteristic length of the hydrogen bond chain within an order of magnitude.

The nonelectrostatic portion of the total Gibbs energy is usually assumed to arise from the energy of solvation of a hypothetical ion that lacks electrical charge, but with all other characteristics unchanged. This can be estimated by comparison with a proper neutral analogue, such as a noble gas, and it is assumed that for particles of the same shape and size, the energies needed to form a cavity and
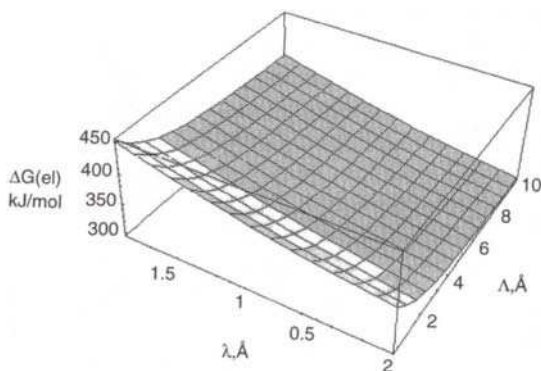
Figure 10.6 Electrostatic contribution to the Gibbs free energy of K^+ hydration ($\Delta G(el)$) as a function of correlation radii λ and Λ.

modify the solvent structure are equal, irrespective of the particle charge. This approach has an important advantage. If the ion and analogous neutral particle are assumed to be in identical standard states in the gaseous phase and solution, then a comparison of the theoretical results with experimental data no longer requires a correction for the loss of translational entropy of ions in solution.

HYDROPHOBIC EFFECT

The calculation of the hydrophobic interaction is a focus of intense interest in the context of membrane biophysics. Contemporary approaches to such problems are based on phenomenological, semiphenomenological, and microscopic statistical mechanics models. All of these use several poorly defined parameters to characterize solute interaction with the solvent. To avoid uncertainty, the solvophobic contribution to the Gibbs free energy of ion or dipole resolvation can be calculated by using the solvophobic equation (Kornyshev and Volkov, 1984). The surface energy, when expressed in terms of surface tension at the ion–solvent interface, $\gamma_{0,m}$, is equal to $4\pi a^2 \gamma_{0,m}$ (Sisskind and Kasarnowsky, 1933; Uhlig, 1937), and the difference in the surface energies in media w and m is $4\pi a^2(\gamma_{0,w} - \gamma_{0,m})$ (Volkov and Kornyshev, 1985). According to Antonov's rule (Antonov, 1907),

$$\gamma_{0,w} - \gamma_{0,m} = \gamma_{w,m} \, \text{sgn}(\gamma_w - \gamma_m), \tag{10.9}$$

where sgn $y = +1$ if $y > 0$, sgn $y = -1$ if $y < 0$, and $\gamma_{w,m}$ is the interfacial tension at the planar boundary between the media w and m. The surface tensions at the boundary between air and the solvents w and m at the same pressure and temperature are γ_w and γ_m, respectively. Here, the solvophobic equation for the solvophobic contribution to the energy of resolvation has the form

$$\Delta_\beta^\alpha G°(\text{solv}) = -4\pi a^2 \gamma_{w,m} \, \text{sgn}(\gamma_w - \gamma_m). \tag{10.10}$$

This Page Intentionally Left Blank

be reflected in the related hydrophobic effect. For example, Fig. 10.3 shows the dependence of the hydrophobic effect on the radius of transferred particles (ions, molecules) for the water–alkane and water–alkene interfaces. It is clear that the presence of double bonds should decrease diffusional transport across a membrane so long as the dielectric permittivity of the hydrocarbon (and the Born component of the resolvation energy) is unchanged. On the other hand, experimental measurements show just the opposite, that double bonds generally increase the permeability of a bilayer to ions and polar molecules. This is presumably due to the fact that although alkanes have a dielectric moment equal to zero, the double bond in alkenes induces a dielectric moment of about half a debye unit that can cause specific ion–dipole and dipole–dipole interactions among solvent molecules. This in turn produces a higher dielectric permittivity and increased partition coefficient, with the end result that unsaturated lipid bilayers are more permeable than saturated lipid bilayers.

A significant point is that the free energy of the solvophobic effect is opposite in sign to the electrostatic effect (Fig. 10.3). As a result, the sum of electrostatic and hydrophobic components of Gibbs free energy decreases with ionic size, so that $\Delta G(\text{tr}) > 0$ only for small ions. For ions with radius larger than 0.45 nm, $\Delta G(\text{tr}) < 0$. This prediction is consistent with experimental data (Kornyshev and Volkov, 1984; Markin and Volkov, 1989a,b).

IMAGE FORCES

The image forces acting on charged particles near interfaces are defined as the forces of interaction between these particles and the "image" of free and bound charges induced by them in the region next to the interface, minus the analogous quantity in one bulk phase. As a rule, positive or negative adsorption of ions arises at the oil–water interface due to the effect of image forces. This effect is caused by different dielectric bulk properties of contact phases and by the inhomogeneous transition region where the ions and their solvation shells have a different size. As a result, different planes of closest approach arise where ions and dipolar molecules can interact specifically with the interfacial region.

The electrostatic Gibbs free energy for an ion in the vicinity of a boundary between two liquids with dielectric constants ϵ_1 and ϵ_2 (Fig. 10.1) is determined by the Born ion solvation energy and by the interaction with its image charge. In research on the energy of image forces and the interactions of charges at the oil–water interface, approximate models of the interface are often employed that are based on the traditional description of the interface between two local dielectrics.

In the water–hydrocarbon system, the force of charge attraction (or repulsion) in the oil phase with its image in the aqueous phase is given by

$$f(x) = -\frac{\epsilon_w - \epsilon_{hc}}{\epsilon_w + \epsilon_{hc}} \cdot \frac{q^2}{16\pi\epsilon_0\epsilon_{hc}x^2} \tag{10.11}$$

where x is the distance from the interface (Landau and Lifshitz, 1984). If $\epsilon_w >$ ϵ_{hc}, the charge in the nonpolar phase is attracted to its image, but if $\epsilon_w < \epsilon_{hc}$, there is repulsion between the charge in a hydrocarbon phase and its image. From Eq. (10.11) it follows that charge in the hydrocarbon phase is attracted to the water–hydrocarbon interface. In the case of a thin membrane placed in a medium with high dielectric permittivity (Fig. 10.1), the sum from an infinite number of images must be calculated. The combined Born and image energies of an ion in a thin membrane can be estimated (Neumke and Lauger, 1969) as follows:

$$\Delta G(\text{el}) = \Delta G(\text{Born})$$

$$- \frac{q^2}{16\pi\epsilon_0\epsilon_w} \left\{ \frac{1}{x} + \frac{1}{d} \sum_{n=1}^{\infty} \left[\frac{\theta^{2n}}{n + x/d} + \frac{\theta^{2n-2}}{n - x/d} - \frac{\theta^{2n}}{n + a/d} - \frac{\theta^{2n-2}}{n - a/d} \right] \right\}, \quad (10.12)$$

where

$$\theta = - \frac{\epsilon_{hc} - \epsilon_w}{\epsilon_{hc} + \epsilon_w}. \quad (10.13)$$

The effect of image forces is small compared with Born electrostatic effects (Deamer and Volkov, 1995) and depends on the ion size (Fig. 10.7) and membrane thickness (Fig. 10.8).

We can calculate the Gibbs free energy of ion or dipole transfer, $\Delta G(\text{tr})$, from an aqueous phase to a hydrocarbon phase according to the following relation:

$$\Delta G(\text{tr}) = \Delta G(\text{el}) + \Delta G(\text{solv}) + \Delta G(\text{si}), \quad (10.14)$$

where $\Delta G(\text{el})$ is the electrostatic contribution, $\Delta G(\text{solv})$ is the hydrophobic effect, and $\Delta G(\text{si})$ is caused by specific interactions of the transferred particle (ion,
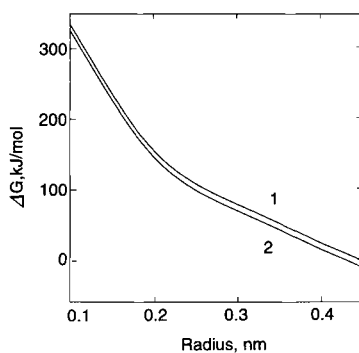
Figure 10.7 Dependence of the Gibbs free energy of ion transfer on ion size calculated according to the Born equation and solvophobic effect together (1). Curve 2 is the same as 1 corrected for image forces ($d = 6$ nm, $T = 25°$C).
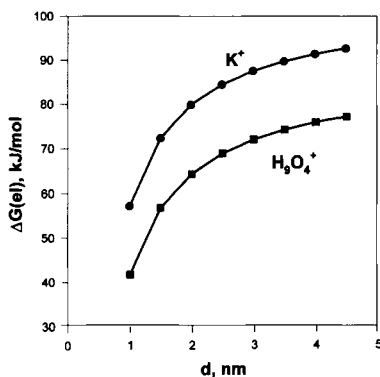
Figure 10.8 Dependence of the electrostatic Gibbs free energy of ion transfer on membrane thickness calculated according to the Born equation corrected for image forces ($T = 25°C$).

dipole) with solvent molecules, such as hydrogen bond formation or donor–acceptor and ion–dipole interactions. For simplicity we used the Born equation [Eq. (10.3)] to estimate $\Delta G(el)$ as shown in Fig. 10.3, curve 1, while the resulting calculation of $\Delta G(tr)$ is plotted in Fig. 10.3, curve 2. For small ions, the electrostatic contribution is predominant in $\Delta G(tr)$, so that the discrepancies of the solvophobic relation, which become evident with small ions, are negligible. At large ionic radius the solvophobic term predominates, so that calculations according to the solvophobic equation are consistent with experimental results (Abramson, 1981).

DIPOLE POTENTIAL

Bilayers differ from water–liquid hydrocarbon membranes by the presence of a two-dimensional layer of adsorbed water dipoles and lipid heads (Markin and Volkov, 1990). Even if lipids are neutral there is a dipolar potential within the membrane surface layer, which should be taken into account when describing specific interactions of ions with the membrane surface (Volkov 1996; Volkov *et al.*, 1997a,b). For instance, the dipole–dipole specific interactions create different concentrations of cations and anions at water–membrane interfaces. Rusanov *et al.* (1984) and Rusanov and Kuni (1982) calculated this energy as $4\pi z e \Delta P_s$, where P_s is a characteristic of the surface excess polarization, which is defined as

$$\Delta P_s = \int_a^\infty [P - P(\infty)] \, dr. \tag{10.15}$$

P is the local polarization vector, and Δ denotes a change in the quantity upon the passage of the sphere from one medium to another.

We can estimate the specific energy of the ion–dipolar layer interaction as a function of dipole potential $\Delta G(si) = -zF\phi_s$, where z is the charge of ions, F is the Faraday constant, and ϕ_s is the dipolar membrane surface potential. ϕ_s is usually estimated for bilayers to be between -100 and -200 mV (Anderson and Fuchs, 1975; Andersen *et al.*, 1978; Flewelling and Hubbel, 1986; Gawrish *et al.*, 1992; Volkov, 1996). At nitrobenzene–water and 1,2-dichloroethane–water interfaces, the dipolar potential, measured directly at the point of zero free charge, is about -20 to -50 mV (Volkov, 1996) in the absence of phospholipids and -100 to -200 mV in the presence of a phospholipid monolayer (Kakiuchi, 1996). The direct method of dipolar potential determination at the bilayer is to measure the dependence of membrane permeabilities of two oppositely charged hydrophobic ions having the same ionic radius. Such ions can be, for example, tetraphenyl-phosphonium and tetraphenylborate. They have the same electrostatic and hydrophobic effects, but opposite effects in dipole potential sign. Figure 10.9 shows the dependence of membrane permeability coefficients of cations and anions on the membrane thickness.

It is possible to calculate the ion permeability of membranes for the partition model of ion transfer by using Eqs. (10.3), (10.10), (10.12), and (10.14). The partition coefficient of an ion (K_i) is equal (Markin and Volkov, 1989a,b) to

$$K_i = \exp(-\Delta G_i^\circ(\text{tr})/RT). \qquad (10.16)$$

A permeability coefficient (P_i) is the number of ions or molecules of crossing a unit area of the membrane in unit time, when a unit concentration difference is applied across the membrane. The permeability coefficient is a directly measurable quantity and is related to the partition coefficient by the expression

$$P_i = D_i K_i/d, \qquad (10.17)$$

where D_i is the ion diffusion coefficient and d is the membrane thickness. Substitution of K_i from Eq. 10.16 into Eq. 10.17 allows P_i to be calculated directly, and the results are plotted in Fig. 10.10. From this it is clear that the partition
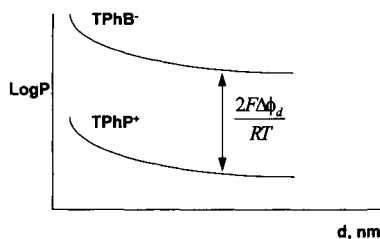
Figure 10.9 The method of membrane dipole potential determination from the measurement of the difference in membrane permeabilities of a hydrophobic cation and hydrophobic anion of the same radius.
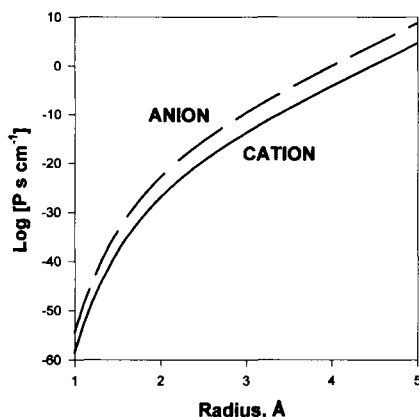
Figure 10.10 Dependence of the ionic permeability of the bilayer ($d = 3$ nm) on the radius of the permeating ion at 25° C. Conditions: $\epsilon_w = 78.5$; $\epsilon_m = \epsilon_s = 2$; $\gamma_{w,m} = 51$ mN m^{-1} (1, 2); $\gamma_{w,m} = 35$ mN m^{-1} (3, 4); ΔG(si) $= 12z$ kJ/mol, $z = +1$ for cations and -1 for anions.

coefficient and calculated permeability coefficient have extreme parameter sensitivity with respect to the ionic radius, varying over 65 orders of magnitude as the radius increases from 1 to 5 Å. Substitution of radii of bare (nonhydrated) ions (Table 10.2) such as sodium and potassium in this calculation gives values much too small for bilayer permeability when compared with experimental data, and the radius of a bare proton leads to absurd values. On the other hand, substitution of hydrated radii taken from Table 10.2 gives permeability values surprisingly close to those measured experimentally.

The transport rate of ions across bilayer membranes can be calculated from the decay times of concentration gradients or from conductance measurements. If the driving force is the concentration gradient, Δc, the permeability coefficient P can be calculated as

$$P = J/\Delta c, \tag{10.18}$$

where J is the molar ion flux per unit interfacial area. If the driving force is the transmembrane potential $\Delta\phi$, the conductance G can be calculated as

$$G = \frac{zFJ}{\Delta\phi} \tag{10.19}$$

or

$$G = \frac{cz^2F^2}{RT}P. \tag{10.20}$$

Table 10.2

Bare and Hydrated Radii of Ions[a]

Ion	Bare ion radius (nm)	Hydrated radius (nm)
H_3O^+	0.115	0.28
$H_9O_4^+$	0.395	0.395
Li^+	0.094	0.382
Na^+	0.117	0.358
Ag^+	0.126	0.341
Tl^+	0.144	0.330
NH_4^+	0.148	0.331
K^+	0.149	0.331
Rb^+	0.163	0.329
Cs^+	0.186	0.329
Be^{2+}	0.031	0.459
Mg^{2+}	0.072	0.428
Zn^{2+}	0.074	0.430
Cd^{2+}	0.097	0.426
Ca^{2+}	0.100	0.412
Pb^{2+}	0.132	0.401
Al^{3+}	0.053	0.480
OH^-	0.133	0.300
F^-	0.116	0.352
Cl^-	0.164	0.332
Br^-	0.180	0.330
I^-	0.205	0.331
NO_3^-	0.179	0.340
Me_4N^+	0.285	0.347
Et_4N^+	0.348	0.400
Pr_4N^+	0.398	0.452
Bu_4N^+	0.437	0.494

[a]Compiled from references Bockris and Reddy (1970), Conway (1981), Gourary and Adrian (1960), and Volkov and Deamer (1996).

DIPOLE RESOLVATION

It is important to analyze the energetic profile of dipole molecules at the interface between two immiscible liquids. Let us consider that a molecule has dipole moment $\vec{d}_1$ and it is located in phase m with dielectric permeability ϵ_m. Its image, $\vec{d}_2$, is located in phase w with dielectric permeability ϵ_w. The dipole $\vec{d}_1$ has angle Θ with an axis x. The interface is located at $x = 0$. The force of the interaction of a

dipole with its image is

$$f(x) = -\frac{3(\epsilon_w - \epsilon_m)\vec{d}_1{}^2}{4\pi\epsilon_0(\epsilon_w + \epsilon_m)\epsilon_m(2x)^4}(1 + \cos^2 \Theta). \tag{10.21}$$

If $\epsilon_w < \epsilon_m$, the force $f(x)$ is negative and there is attraction of the dipole to the interface. $f(x)$ is positive if $\epsilon_w > \epsilon_m$ and there is repulsion of the dipole from the interface.

The energy of the dipole interaction with its image (Arakelyan and Arakelyan, 1983; Arakelyan *et al.*, 1985) can be calculated as

$$E(x,\Theta) = \int_x^\infty f(x)\ dx, \tag{10.22}$$

and substitution of Eq. (10.21) into Eq. (10.22) gives the following equation:

$$E(x,\Theta) = -\frac{(\epsilon_w - \epsilon_m)\vec{d}_1{}^2}{8\pi\epsilon_0(\epsilon_w + \epsilon_m)\epsilon_m(2x)^3}(1 + \cos^2 \Theta). \tag{10.23}$$

There are two equilibrium dipole orientations with $\Theta = 0$ and $\Theta = \pi/2$, and a stable state will be considered when a dipole is perpendicular to the interface. It is possible to determine the thickness of a layer in which dipoles are oriented perpendicular to the interface by supposing that $E(x,0) - E(x,\pi/2)$ is equal to kT:

$$x \approx \sqrt[3]{\frac{(\epsilon_w - \epsilon_m)d_1{}^2}{64\pi\epsilon_0(\epsilon_w + \epsilon_m)\epsilon_m kT}}. \tag{10.24}$$

For the water–octane interface $x = 0.14$ nm, and this result means that only one monolayer of water is oriented at the interface by image forces.

Bell (1931) calculated the Gibbs energy of a dipole molecule transferred from a vacuum to a medium of dielectric constant ϵ_i:

$$\Delta_{vac}^i G = -\frac{d^2}{12\pi\epsilon_0 a^3}\left(\frac{\epsilon_i - 1}{2\epsilon_i + 1}\right). \tag{10.25}$$

The electrostatic ("Born") Gibbs energy of an ideal dipole transfer from phase w to solvent m can be calculated by using the thermodynamic cycle:

$$\Delta G_{dip} = -\frac{d_1{}^2}{12\pi\epsilon_0 a^3}\left(\frac{\epsilon_m - 1}{2\epsilon_m + 1} - \frac{\epsilon_w - 1}{2\epsilon_w + 1}\right)$$

$$= \frac{d_1{}^2}{4\pi\epsilon_0 a^3}\left(\frac{\epsilon_w - \epsilon_m}{(2\epsilon_w + 1)(2\epsilon_m + 1)}\right), \tag{10.26}$$

where d_1 is the dipole moment and a is the effective dipole size. Generally speaking, the dipole moment d_1 can vary from solvent to solvent. For simplicity, we will discuss the case when the dipole moment of a solute is the same in phases w and m.

The Gibbs free energy of image forces for the dipole in the membrane (Arakelyan and Arakelyan, 1983) is

$$\Delta G_{I(dip)} = -\frac{2d_1^2}{12\pi\epsilon_0\epsilon_m l^3} \sum_{i=1}^{\infty} \left(\frac{\Theta^{2i-1}}{(2i-1)^3} + \frac{\Theta^{2i-1}}{(2i-1)^3} \right). \quad (10.27)$$

The electrostatic Gibbs energy of the dipole profile can be evaluated from Eqs. (10.26) and (10.27):

$$\Delta G_{dip} = \frac{d_1^2}{4\pi\epsilon_0 a^3} \left(\frac{\epsilon_w - \epsilon_m}{(2\epsilon_w + 1)(2\epsilon_m + 1)} \right)$$

$$- \frac{(\epsilon_w - \epsilon_m)d_1^2}{6\pi\epsilon_0(\epsilon_w + \epsilon_m)\epsilon_m(2x)^3}. \quad (10.28)$$

Figure 10.11 shows the dependence of the electrostatic image energy of the water dipole on the thickness of a liquid membrane. The image energy strongly depends on the membrane thickness and decreases with increasing thickness.

The water concentration in a hydrophobic region of a membrane can be calculated from the estimated Gibbs free energy of water molecule transfer from water to the liquid hydrocarbon as

$$c_m = c_w \exp(-\Delta G(tr)/RT). \quad (10.29)$$

Figure 10.12 shows the dependence of water concentration on liquid membrane thickness.

By using Eqs. (10.10), (10.14), and (10.28), it is possible to calculate the permeability of molecules across a liquid membrane (Fig. 10.13). $\Delta G(si)$ is approximately 33 kJ/mol for the breakage of a hydrogen bond between water molecules
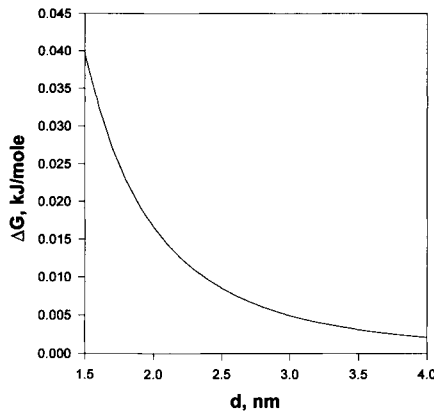
Figure 10.11 Dependence of the image energy for the water dipole on liquid membrane thickness. Parameters: $p = 1.85$ D, $l = 0.138$ nm, $\epsilon_w = 78$, $\epsilon_m = 2$.
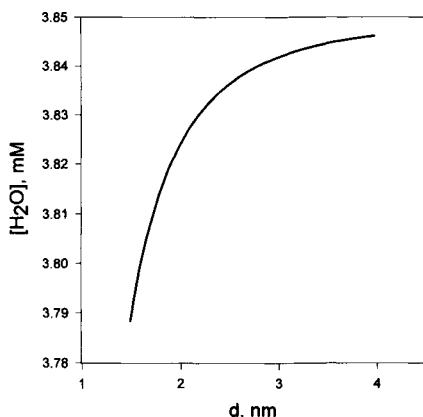
Figure 10.12 Dependence of the water concentration in a liquid membrane on membrane thickness. Parameters: $p = 1.85$ D, $l = 0.138$ nm, $\epsilon_m = 2$, $\epsilon_w = 78$, $r_{H_2O} = 0.12$ nm, $\gamma_{w,m} = 51$ mN/m, $\Delta G(\text{si})_{(\text{water})} = 33$ kJ/mol.

and 75 kJ/mol for hydrogen bonds between three water molecules and urea or a glycerol molecule (Pimentel and McClellan, 1960; Paula *et al.*, 1996).

Figure 10.13 illustrates how the water permeability coefficient is affected by the thickness of the bilayer. Although permeabilities become noticeably smaller with increasing bilayer thickness, the magnitude of this decrease is much smaller than that observed for protons. The permeability coefficient for the longest lipid (2.4×10^{-2} cm/s) is only about 5 times lower than that for the shortest (5.0×10^{-3} cm/s). Furthermore, the slope of the curve is roughly constant, which is in sharp contrast to the biphasic behavior observed for potassium ions.

Glycerol and urea display quite similar permeabilities (see Fig. 10.13), with glycerol being slightly more permeable than urea. The values were in the ranges $(1.1-6.2) \times 10^{-6}$ and $(3.4 \times 10^{-6})-(6.0 \times 10^{-7})$ cm/s for glycerol and urea, respectively. This indicates that the membrane represents a significantly higher diffusion barrier to these molecules than to water or protons. The slope of the permeability coefficient plotted against bilayer thickness resembles that of water (Fig. 10.13), with permeability values for the longest and shortest lipids differing by roughly fivefold.

Despite the interesting results arising from considerations of both electrostatic and solvophobic contributions to ionic permeation, we must be careful in uncritically applying them to ionic permeation events in bilayers and particularly to proton permeation. The main difficulty is that lipid bilayers are not ideal slabs of hydrocarbon with uniform dielectric properties, but instead are highly dynamic with considerable fluctuation around the means of thickness and intermolecular distance within the bilayer (Evans, 1992; Wiener *et al.*, 1991). Secondly, given the steepness of the slope relating ionic permeability to ionic radius (Fig. 10.10),
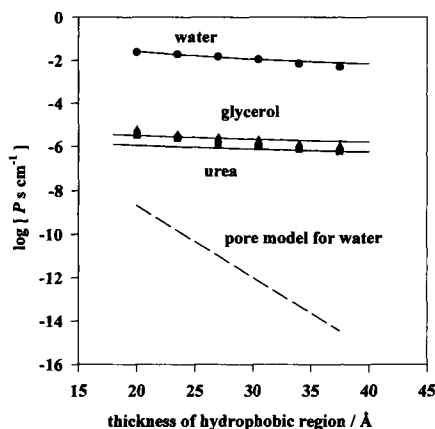
Figure 10.13 Dependence of water, urea, and glycerol permeability on membrane thickness d. Points are experimental data, and solid lines are calculated according to Eq. (10.17) for the solubility–diffusion model. Parameters: $r_{water} = 0.12$ nm, $r_{urea} = 0.28$ nm, $r_{glycerol} = 0.29$ nm, $\gamma_{\alpha,\beta} = 51$ mN m^{-1}, $p_{water} = 1.85$ D, $a_{water} = 1.38$ Å, $\Delta G(si)_{(water)} = 33$ kJ/mol, $\Delta G(si)_{(urea/glycerol)} = 3 \times 25$ kJ/mol, $D_{water} = 4.59 \times 10^{-5}$ cm^2 s^{-1}, $D_{urea} = 1.38 \times 10^{-5}$ cm^2 s^{-1}, $D_{glycerol} = 1.06 \times 10^{-5}$ cm^2 s^{-1} (Paula *et al.*, 1996). Reproduced by permission of Biophysical Society.

whereby a 0.05-nm change of radius can produce a variation of more than 10 orders of magnitude in permeability, it is a concern that estimates of hydrated ionic radii are highly dependent on the technique used to make the measurement. Last, the hydronium ion is not a hard shell of four water molecules tightly bound to a central proton. Instead, proton–water interactions are dynamic, with the proton rapidly entering and leaving clusters of water of various sizes. In the section to follow, we will examine an alternative mechanism for the permeation of ions across lipid bilayers and then compare experimental results with theoretical predictions from both models.

TRANSIENT PORE MECHANISMS OF PASSIVE TRANSPORT ACROSS LIPID BILAYERS

Although the partition model can describe the barrier properties of lipid bilayers under specified conditions, certain assumptions regarding the hydrated radius of the permeating species are required. We will now consider an alternative hypothesis, in which fluctuations in bilayer structure produce rare transient defects that allow solutes to bypass the electrostatic and solvophobic energy barriers.

For the barrier function to operate, the lipid bilayer forming the basis of the membrane must be continuous and devoid of structural defects. If the bilayer is rearranged so that the transmembrane defects appear, the membrane properties

change. If pores that are small relative to the cell radius appear, an elevated background conductance of the membrane can arise for ions from both extra- and intracellular solutions. If the pore size is comparable to that of the intracellular protein molecules, cell lysis takes place, i.e., all of the cell's contents are released into the external medium.

Two types of pore structures in the lipid bilayer are possible, which can be roughly classified as hydrophobic and hydrophilic defects. During the formation of a transient hydrophobic defect, lipid molecules are moved apart by thermal fluctuations so that the membrane hydrophobic core makes contact with and is penetrated by the aqueous bulk phase. Hydrophilic defects are formed if the lipid molecules are tilted into the transient defect so that it is lined with lipid polar head groups. In both hydrophobic and hydrophilic defects, pore formation results from dynamic properties of the lipid bilayer, and the equilibrium pore distribution is relatively constant over time. The formation of hydrophilic pores is more likely. Hydrophilic pores can arise due to thermal bilayer fluctuation or as a result of external stimuli, such as membrane extension by osmotic pressure, reactions with chemical compounds, and electrical field effects. Pore formation results in dynamic changes in the membrane properties, but thermal fluctuations in the bilayer lead to an equilibrium pore distribution in the membrane.

Markin and Kozlov (1985) analyzed the distribution of hydrophilic pore radii in a membrane at thermodynamic equilibrium from the point of view of the elasticity or flexibility of the lipid bilayer and its spontaneous curvature. The pore size distribution was calculated for three model membranes: uniform membranes with a constant spontaneous curvature, membranes with clusters of high spontaneous curvature, and membranes composed of two types of lipids, one with a high spontaneous curvature. Their calculations showed that the presence of asymmetric lipid molecules with positive spontaneous curvature should increase the number of pores in the membrane. The pore-related membrane permeability to uncharged molecules was estimated on the basis of this theory. The calculated values for water permeability were markedly lower than the experimentally estimated values, suggesting that the mechanism of water transport across the membrane is mainly due to the direct passage of water molecules across the membrane hydrophobic layer.

Although small, neutral substances like water generally move across bilayers by diffusion of individual molecules, there is still the possibility that water occasionally is involved in the formation of transient hydrated defects. A pertinent model was presented by Benjamin (1996), who used molecular dynamics and computer simulations to investigate the interface between water and a nonpolar phase. An intriguing property of the interface is that it is surprisingly rough, with "fingers" of several water molecules occasionally entering the nonpolar phase. Benjamin showed that ion permeation of the interface is linked to the presence of such water fingers. Wilson and Phorille (1996) performed molecular dynamics

simulations of the transport of Na^+ and Cl^- across a lipid bilayer located between two water lamellae. The ion located in water has no influence on the structure of the membrane. Permeation of hydrated ions into membrane is accompanied by the formation of deep, asymmetric, thinning defects in the bilayer. As the hydrated ion crosses the midplane of the membrane, the deformation switches sides. The initial defect slowly relaxes, and a defect forms in the outgoing side of the membrane (Wilson and Phorille, 1996).

Thermal fluctuations in bilayers produce transient pores lined with lipid head groups (Hamilton and Kaler, 1990a,b). The formation of pores considerably lowers the free Gibbs energy barrier to transfer of the ions across the membrane and increases the permeability of the bilayer to ions (Fig. 10.14). Ion flux was calculated from the collision frequency of the ions with the bilayer surface and the total area of pores in the bilayer that are large and deep enough to allow an ion to cross the bilayer. The total number of pores, f_p, can be expressed as the following integral:

$$f_p = \int_{s_i}^{\infty} sn(s) \, ds, \tag{10.30}$$

where $n(s) \, ds$ is the number of pores per membrane area between pore areas s and $s + ds$. The pore area distribution can be written as

$$n(s) = n_0 \exp(-k_1 s/RT) \exp(-k_2 d/RT), \tag{10.31}$$

where n_0 is the maximum number of discrete pores in the bilayer (taken to be one-half the number of lipid molecules in the bilayer), and the exponential terms are related to the probabilities of forming pores of area s and depth d, respectively (Fig. 10.14). If an ion of a given radius can permeate the bilayer, s is taken to be
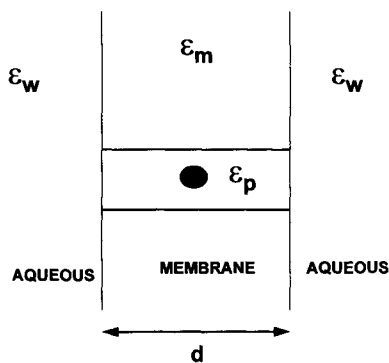
Figure 10.14   The pore model for ion permeation.

the area of that ion and d is the bilayer thickness. Given these assumptions, the ionic permeability, P_i, is

$$P_i = \frac{D_i \sigma n_0 RT}{R_{avg} A_{mem} k_1} [s_i + RT/k_1] \exp[-k_1 s_i/RT] \exp[-k_2 d/RT]. \quad (10.32)$$

Here D_i is the ion diffusion coefficient, $\exp(-k_1 s/RT)$ is the probability of forming a pore of area s, $\exp(-k_2 d/RT)$ is the probability of forming a pore of depth d, σ is the concentration enhancement at the vesicle surface due to the electric double-layer effects, R_{avg} is the vesicle radius, A_{mem} is the membrane area, R is the gas constant, and T is the absolute temperature.

PARTITIONING AND/OR TRANSIENT PORES: A CRITICAL TEST

In testing the two models described previously, an important variable under experimental control is bilayer thickness, which can be changed by choosing lipids with longer or shorter hydrocarbon chains.

Proton and potassium fluxes across liposomes composed of phospholipids with fatty acid chain lengths varying from 14 to 24 carbons were measured (Paula *et al.,* 1996). Results expressed as proton and potassium permeability coefficients are shown in Fig. 10.15 and compared with the theoretical lines calculated from Eqs. (10.31) (transient pore mechanism) and (10.14) (partitioning model). Permeability decreased logarithmically as bilayer thickness increased in the shorter chain lipids, following the slope of the line predicted by the transient pore mechanism. However, permeability tended to level off in the thicker bilayers (C_{16} and C_{18} lipids), approaching the lines predicted by the partition model (Paula *et al.,* 1996). The results suggest that the mechanism of ionic permeation may depend on bilayer thickness: thinner bilayers have many transient defects that allow the rapid permeation of small ionic species, while in thicker bilayers defects become so rare that partitioning mechanisms dominate ionic flux (Deamer and Volkov, 1995).

Earlier work has shown that the permeability of lipid bilayers to protons is 5–6 orders of magnitude greater than to other monovalent cations (Deamer and Nichols, 1989; Nichols and Deamer, 1978, 1980). This result is consistent with the partitioning model only if every proton carries at least four waters of hydration into the bilayer phase. The alternative proposed here is that transient hydrated defects occur in the bilayer. Figure 10.16 summarizes the problem at hand: an extra proton is incorporated at one end of a single file of water molecules, and a series of proton transfers takes place between adjacent water molecules until a proton is released at the other end. If water in the defects has significant hydrogen bonding, as it does in the bulk phase, hydrogen bond exchange could
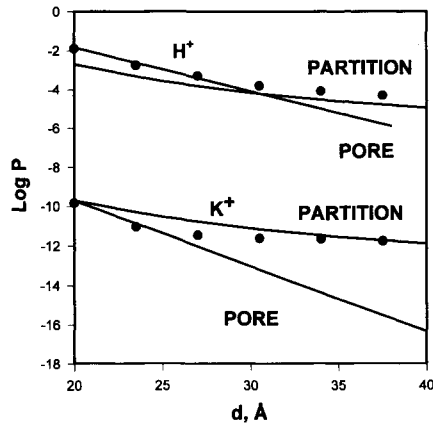
Figure 10.15 (Bottom) Dependence of K^+ permeability on d calculated from Eqs. (10.9) and (10.16). Points are experimental data. Parameters: $D_i = 2 \times 10^{-5}$ cm^2 s^{-1}, $s = 10$, $R_{avg} = 1.05 \times 10^{-6}$ cm, $A_{mem} = 26,000$ cm^{-1}, $T = 300$ K, $a = 0.149$ nm, $k_1 = 2.2 \times 10^{15}$ kJ/mol·cm^2, $k_2 = 1.9 \times 10^8$ kJ/mol·cm, $n_0 = 1.04 \times 10^{33}$ cm^5, $\phi_d = -130$ mV. (Top) Dependence of H^+ permeability on d calculated from Eqs. (10.9) and (10.16). Points are experimental data. Parameters: $D_i = 1.4 \times 10^{-4}$ cm^2 s^{-1}, $s = 10$, $R_{avg} = 1.05 \times 10^{-6}$ cm, $A_{mem} = 26,000$ cm^{-1}, $T = 300$ K, $a = 0.13$ nm, $k_1 = 2.2 \times 10^{15}$ kJ/mol·cm^2, $k_2 = 1.2 \times 10^8$ kJ/mol·cm, $n_0 = 1.04 \times 10_{33}$ cm^5, $\phi_d = -130$ mV. Ionic radii are taken from Table 10.2 (Paula *et al.*, 1996).

account for the vastly greater proton permeation rates without any assumptions regarding water of hydration. That is, protons could cross the membrane by "hopping" along hydrogen-bonded chains of water in the defect (Figs. 10.16 and 10.17). This concept was first proposed by Nagle and Morowitz (1978), who coined the term "proton wire" for hydrogen-bonded networks of amino acid side chains. Nagle and Tristram-Nagle extended this concept to more general proton transport mechanisms, including water, and developed the concept of "transient
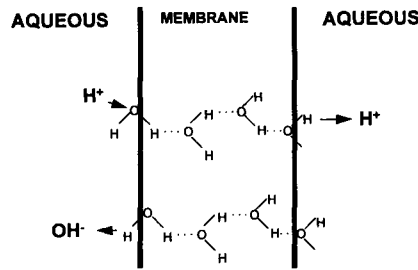
Figure 10.16   Grotthus mechanism of proton transfer through an aqueous chain.
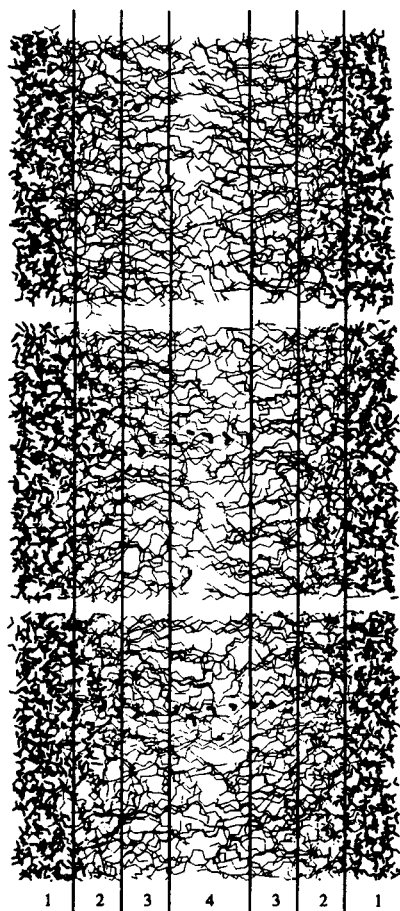
Figure 10.17 Snapshot of the water pore during formation (Marrink *et al.*, 1996). The pore molecules are drawn with bold black lines; the other water molecules are drawn in lighter lines. The four different membrane regions (small head group density, large head group density, large tail density, and small tail density, shown in sections 1–4, respectively) are also indicated. Reproduced by permission of Biophysical Society.

hydrogen bonded chains" (tHBC) to describe proton transport in clusters of water molecules associated through hydrogen bonds (Nagle and Tristram-Nagle, 1983).

Thermal fluctuations in shorter chain phospholipids produce large numbers of transient defects that cause such bilayers to be relatively permeable to ions, including protons. Because the slopes of the curves for proton and potassium flux are similar, with reasonable fits to the theoretical expectations of the pore model,

both protons and potassium ions presumably have access to the same transient defects. If protons are able to cross the bilayer by hydrogen bond exchange along water chains in the transient defects, the relatively high permeability of protons can be understood. These results are consistent with the transient pore model described earlier.

As chain length increases, the transient fluctuations become rarer, and it is possible that partitioning is the dominant factor limiting the permeation of ions such as potassium and perhaps protons, if they cross as $H_9O_4^+$. In fact, both models—partition and transient aqueous pores—contribute to the membrane permeability.

Marrink *et al.* (1996) studied proton transport across transient single-file water pores in lipid membranes by molecular dynamics simulations and found that the nature of the pore is very transient, with a mean lifetime of a few picoseconds. Figure 10.17 shows the transient pore formation process. The total excess free energy for the full water pore is 108 $\pm$ 10 kJ/mol, and this value indicates that such a complete water pore spanning the membrane is a rare phenomenon. The average free energy is 6.4 kJ/mol per pore molecule (Marrink *et al.*, 1996). The rapid translocation of protons along a chain of hydrogen-bonded water molecules, or proton wire, is thought to be an important mechanism for proton permeation through transmembrane channels or thin lipid membranes (Egberts *et al.*, 1994). Proton transfer on the wire is a semicollective process that results from the subtle interplay of rapid hydrogen bond length fluctuations along the water chain.

Two mechanisms have been proposed to account for solute permeation of lipid bilayers. Partition into the hydrophobic phase of the bilayer followed by diffusion is accepted by many for the permeation of water and other small neutral solutes, but transient pores have also been proposed to account for both water and ionic solute permeation. These two mechanisms make distinctively different predictions about the permeability coefficient as a function of bilayer thickness. Whereas the solubility–diffusion mechanism predicts only a modest variation related to bilayer thickness, the pore model predicts an exponential relationship. To test these models, Paula *et al.* (1996) measured the permeability of phospholipid bilayers to protons, potassium ions, water, urea, and glycerol. Bilayers were prepared as liposomes, and thickness was varied systematically by using unsaturated lipids with chain lengths ranging from 14 to 24 carbon atoms. The permeability coefficient of water and neutral polar solutes displayed a modest dependence on bilayer thickness, with an approximately linear 5-fold decrease as the carbon number varied from 14 to 24 atoms. In contrast, the permeability to protons and potassium ions decreased sharply by 2 orders of magnitude between 14 and 18 carbon atoms and leveled off when the chain length was extended further to 24 carbon atoms. The results for water and the neutral permeating solutes are best explained by the solubility–diffusion mechanism. The results for protons and potassium ions in shorter chain lipids are consistent with the transient pore model, but better fit the theoretical line predicted by the solubility–diffusion model at longer chain lengths.

CONCLUSIONS

Ionic permeability is extremely sensitive to ionic radius, changing by 50 orders of magnitude as ionic radius is varied from 1 to 5 Å. The Gibbs free energy of partitioning has two primary contributing factors, which were described in terms of electrostatic and solvophobic effects. The electrostatic term dominates the permeation of smaller ions, but the solvophobic effect becomes significant for larger ions to the extent that the Gibbs free energy can be negative for ions larger than 0.45 nm in diameter. A significant point is that the free energy of the solvophobic effect is opposite in sign to the electrostatic effect.

The effect of image forces is small compared with solvophobic and Born electrostatic effects and depends on ion size and membrane thickness. Even if the lipids are neutral, there is a dipole potential within the membrane surface layer, which should be taken into account when describing the specific interactions of ions with the membrane interface. For instance, the ion–dipole and dipole–dipole specific interactions create different concentrations of cations and anions at water–membrane interfaces.

Partitioning models are consistent with some features of ionic permeation, particularly if solvophobic energy is taken into account. A partition model can account for the observation that the permeability of bilayers to protons is 5–6 orders of magnitude greater than that to other monovalent cations, but only because of the extreme parameter sensitivity of the equations relating partitioning energy to permeability coefficients. An alternative hypothesis is that fluctuations in bilayer structure produce transient hydrated defects, which permit ionic solutes to bypass the electrostatic energy barrier. If water in such defects is hydrogen-bonded, permeability to protons should be relatively high because protons can rapidly move along water chains by hydrogen bond exchange mechanisms. This conductive mechanism is not available to other cations.

The two alternative hypotheses, partitioning versus transient pores, can be tested by measuring ionic permeation through bilayers of varying thickness. If the partition model is correct, a substantial barrier to ionic flux should occur as soon as a stable bilayer is produced, even with relatively short-chain lipids, and permeability will not vary significantly with bilayer thicknesses typical of biological lipids. The transient pore model predicts that ionic permeability will increase as a logarithmic function of bilayer thickness. Experimental observations for both potassium and proton permeability are consistent with the transient pore mechanism for shorter chain lipids, but trend toward the theoretical line for partitioning models for longer chain lipids. Both mechanisms may play a role for typical hydrated monovalent ions, depending on lipid chain length, but proton flux still has unexplained anomalies. The mechanism of water transport across membranes is mainly due to the direct passage of water molecules across the membrane hydrophobic layer by the solubility–diffusion mechanism.

Chapter 11

Transpiration Stream

INTRODUCTION

Photosynthesis appeared almost 3 billion years ago, and from the beginning it has occurred in microorganisms such as photosynthesizing bacteria and blue-green alga. In macroscopic green plants, photosynthetic functions have also been performed by microscopic particles such as chloroplasts. However, a macroscopic organism is not the simple sum of a large number of elements, but instead is a complicated system whose elements are self-regulated and self-organized. Functional interactions between remote parts of a large plant are possible due to the specialized vascular systems, the xylem and phloem, which provide long-distance transport of water and metabolites. Almost all terrestrial plants except primitive mossy species possess these structures.

The development of vascular systems of plants is undoubtedly the consequence of their transition to the terrestrial mode of life. The existence of long-distance transport systems in plants made it possible for large forms such as trees to arise. Plants only need to spend a minor amount of metabolic energy to drive their transport systems because they effectively utilize the energy of difference in water chemical potentials in soil and air for this purpose.

Plants conduct a huge amount of water through themselves. They consume up to 1000 mol of water per each mole of carbon dioxide assimilated. This water is extracted from the soil and released into the atmosphere. Average amounts of water consumed by some plant species are shown in Table 11.1. The actual use of water can vary within wide limits, but some general characteristics can be seen from a comparison of average values. C_3-type grassy plants expend a lot of water. Trees, referring to the same C_3 type, are about twice as economical with respect to their water needs. The C_4-type grassy plants also consume much less water in transpiration than C_3 plants with similar geometrical parameters.

Table 11.1

Water Consumption by Various Plants

Plants	mol H_2O/ mol CO_2	kg H_2O/kg dry mass
C$_3$ Plants		
Herbaceous		
Rice	1140	680
Rye	1050	630
Oats	970	580
Wheat	900	540
Barley	870	520
Alfalfa	1400	840
Bean	1170	700
Potato	1070	640
Sunflower	1000	600
Watermelon	970	580
Deciduous trees		
Oak	570	340
Birch	530	320
Beech	290	170
Conifers		
Pine	500	300
Larch	440	260
Fir	380	230
C$_4$ Plants		
Maize	620	370
Millet	500	300
Amaranth	500	300
CAM Plants		
Light	250–1000	150–600
Dark	40–250	25–150

Transpiration is responsible for cooling a plant by the removal of excess heat. If we assume that 16 kJ of energy is accumulated in 1 g of biomass and thus the efficiency of photosynthesis is 1% of absorbed photosynthetically active region (PAR), we obtain a value of absorbed energy equal to 1600 kJ. Taking into account the heat of evaporation of water, which is about 2500 kJ/kg, we determine the amount of water necessary for the removal of all absorbed energy to be about 640 g. This estimation does not contradict observed values. If we use a value for photosynthetic efficiency of about 2%, we obtain values near those that character-ize C$_4$ plants. These calculations are only approximate. The real character of the heat–moisture interaction of a plant with air is much more complicated, as is con-sidered in Chapter 9 in detail. The efficiency of water transpiration can vary within wide limits, depending on the combination of particular conditions such as tem-

perature and humidity of the air, speed of the movement, capacity of radiation flow, and physiological states of leaves. Conditions when transpiration is not accompanied by the removal of heat are also possible. There is no doubt that the main role of transpiration is the discharge of redundant heat from plants and thereby surplus entropy.

Due to the existence of vascular transport systems, plants execute the role of the binding channel between soil and atmosphere, enhancing the efficiency of moisture exchange between them. Plants make accessible for exchange with the atmosphere water in soil a few meters from the surface of the ground. Large communities of plants such as forests, meadows, and fields facilitate water exchange between soil and atmosphere to such an extent that they cause an essential influence upon the climate of different regions of the planet.

Vascular transport systems consist of two subsystems: xylem and phloem. The first conducts a continuous flow of water from soil to atmosphere. The second conducts a flow of organic substances synthesized in the leaves to other parts of the plant, including the roots. The liquid transported in xylem is a dilute solution of salts. Their total concentration is usually $5-50$ mM. The concentration of salts in the phloem sap is usually much higher, but its main components are sugars. The concentration of sugars in the phloem sap can reach $10-25\%$. The powers of the volumetric flow of liquids transported in xylem and phloem are significantly different. The volume of liquid translocated through the phloem is $20-100$ times less than that in the xylem.

HYDROSTATICS OF XYLEM

In the process of transpiration, plants lift water over a significant height, exceeding 100 m in some trees. This lifting requires significant expenses of energy. Naturally, we must answer the question of how plants can execute this function. According to thermodynamics the answer is simple for a general case. Plants use the difference in water chemical potentials in the liquid state in the soil and in the form of unsaturated vapor in air. In fact, the change in energy of 1 mol of water during the transition from the liquid state to the unsaturated vapor is equal to

$$\Delta E = -RT \ln \phi. \tag{11.1}$$

Here ϕ is the degree of the air saturation or relative humidity. Such energy is enough to lift water to a height of

$$h = -\frac{RT}{V_w \rho g} \ln \phi, \tag{11.2}$$

where V_w is the molar volume of water (1.8×10^{-5} m^3/mol), ρ is the density of water (10^3 kg/m^3). and g is the acceleration due to gravity (9.81 m/s^2). For ex-

ample, calculations using this equation show that if the degree of atmospheric saturation is $\phi = 0.9$, the energy is enough to lift water to a height of 1.4 km, and if humidity is $\phi = 0.5$ the height is 7 times greater.

Thermodynamics shows that the difference in water chemical potentials in the soil and air is enough to lift water in tall trees. However, thermodynamics does not give information about the mechanisms through which water rises. To understand how water transport mechanisms function in plants, it is necessary to consider the arrangement of the xylem and the forces acting on water and forcing it to move through the xylem from roots to leaves.

In its most simplified form, the scheme of a xylem system can be represented as shown in Fig. 11.1. There is the input device (A), a long-distance transport channel (B), and the output device (C). The input device (A) is located in the plant's root. It provides the extraction of water from soil into the long-distance transport channel (B). This channel begins in a root, lengthens in the stem, and ends in the leaves of a plant. It represents a tube formed by a sequence of long narrow cells. Xylem consists of a set of such parallel tubes. The flow of sap in xylem is set into motion by a pressure gradient quite similar to that of water flow in plumbing pipes. An output device (C) is located in the leaves. It provides for evaporation of water into the atmosphere. The pressure gradient, which is neces-
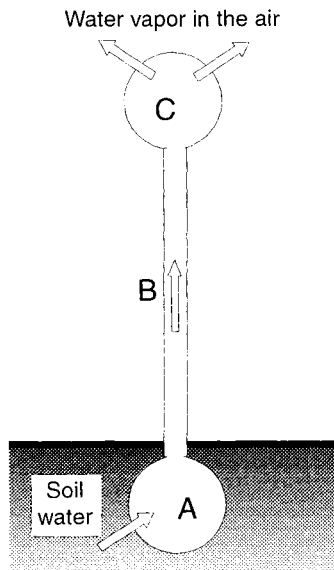
Figure 11.1 A diagram of long-distance transport in plants: (A) a lower device (a root pump); (B) transport channel; (C) an upper device (a pulling pump).

sary for the translocation of a liquid in a channel of xylem, is formed by the combined action of the input and output devices. In this sense the input device may be termed the *lower pump* and the output device the *upper pump*. The first absorbs water at the beginning of a xylem channel in the root, whereas the other pulls water through the channel and exhausts it out of the leaf. Mechanisms of function of both pumps will be discussed further.

Now let us consider the forces that act on water during its way from the soil through plants to the atmosphere. There are a few such forces, which exert a different influence on the xylem sap: the gravitational force, which acts on the mass of a substance; the hydraulic pressure, which acts on the volume of a substance; and the forces of chemical nature caused by interactions of water molecules with solutes and structural components of cells. Electrical forces usually are not taken into account in homogeneous phases due to the electroneutrality of water molecules. However, electrical fields interact with ions in the xylem sap and can cause indirect effects on water. For example, such effects exist in electro-osmosis. Electrical forces play a very important role in heterogeneous systems near cell walls and membrane surfaces. These processes are discussed in detail in Chapter 10.

The chemical potential of water can be represented as the sum of all components:

$$\mu = V_w \rho g h + V_w P + RT \ln a_w + \mu_{el}. \tag{11.3}$$

Here P is the total pressure from hydrostatic and hydrodynamic components, a_w is the activity of water, and μ_{el} is the electrical component of chemical potential caused by the action of electric fields.

It is customary in plant physiology to express the water chemical potential in units of pressure, such as pascals (Pa $= N/m^2$), kilopascals (1 kPa $= 10^3$ Pa), and megapascals (1 MPa $= 10^6$ Pa). The chemical potential of water expressed in units of pressure is termed *water potential:*

$$\Psi = (\mu - \mu^\circ)/V_w = \rho g h + P + (RT/V_w) \ln a_w + (\Delta\mu_{el}/V_w), \tag{11.4}$$

where μ° is the standard chemical potential of water.

The gravitational component of water potential has a vertical gradient equal to $\rho g h = 9.8$ kPa/m. Thus, on the top of 100-m sequoias, the gravitational component of water potential can reach about 1 MPa. A gradient of gravitational potential in a horizontally creeped plant can be close to zero regardless of its length.

The gradient of hydrostatic pressure (P_{st}) equals the gradient of gravitational potential, but it has the opposite direction:

$$\frac{dP_{st}}{dh} = -\rho g \tag{11.5}$$

In a vessel H meters tall, water has an additional energy $\rho g H V_w$ compared with water at ground level. However, the excess energy due to gravity is very small. It
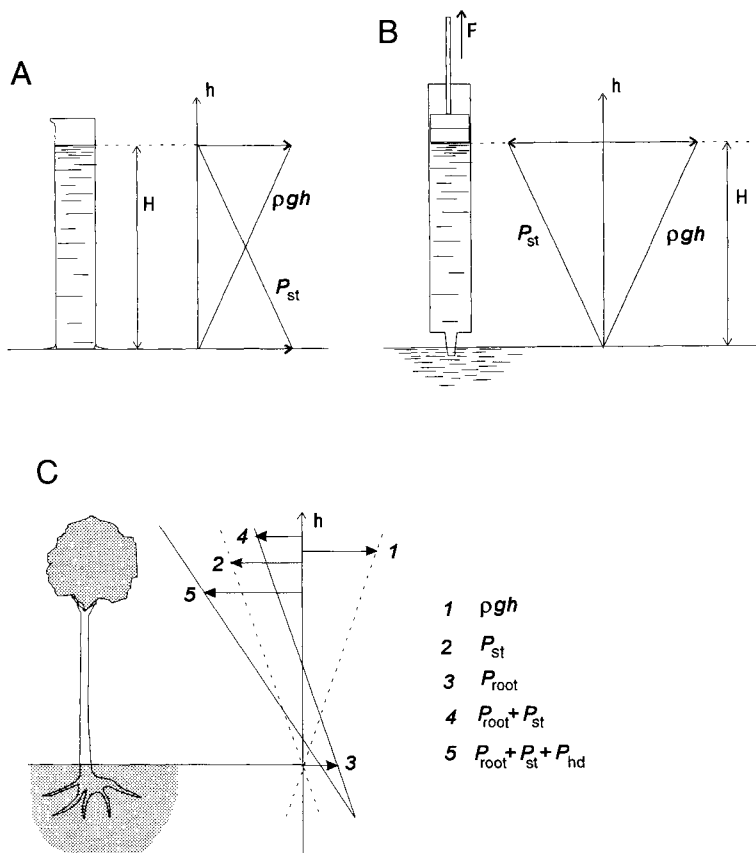
Figure 11.2 Hydrostatics of the xylem. (A) Hydrostatic equilibrium in a tall vessel filled with liquid up to level *H*. Abbreviations: ρgh, potential due to gravitation; P_{st}, hydrostatic pressure. The sum of these values is the same at any height of liquid column. (B) Hydrostatic equilibrium in a tube filled with water by pulling a plunger. Sum of the gravitational potential and the hydrostatic pressure equals zero at any height of liquid column. (C) Distribution of pressure over the height of a tree: (1) potential due to gravitation; (2) hydrostatic pressure; (3) root pressure; (4) hydrostatic pressure accounting for root pressure; (5) the same accounting for hydrodynamic pressure.

corresponds to the energy necessary to heat water by about 0.002° C in a 1-m-tall vessel.

The water in a cylindrical vessel can be lifted by a piston, as shown in Fig. 11.2B. In this case a condition of equality of gradients Eq. (11.5) will be observed, but the distribution of hydrostatic pressure along the length of the vessel will be different, as shown in Fig. 11.2B. The hydrostatic pressure of water in this case will be negative, i.e., the water will be in a "stretched" state. The chemical potentials of water in a vessel and at zero level will be equal.

An intermediate case is commonly found in xylem "vessels." Curve 4 in Fig. 11.2C shows the distribution of hydrostatic pressure in a plant under conditions when transpiration flow is absent. The water in xylem vessels in the lower part of the plant below the ground is under positive pressure, created by the root pump. In the upper part of the plant is the area in which hydrostatic pressure is negative due to the pulling action of the upper pump.

It should be noted that the hydrostatic pressure gradient does not cause the flow of liquid through xylem because the opposite gradient of gravitational potential compensates for it. The flow of liquid through the xylem vessels arises due to a hydrodynamic pressure gradient caused by the joint action of the root pump and the pulling force of the upper pump. When transpiration proceeds, the distribution of pressure along the xylem is as shown in Fig. 11.2C, curve 5. The intensity of transpiration determines the height where the positive pressure in the xylem changes to a negative value. The more intense the transpiration flow, the lower this point. Under certain conditions the region of positive pressure in xylem may stretch to the full height of the tree. In such cases the phenomenon of water exudation through leaves, guttation, can be observed. On the other hand at very intense transpiration, all of the xylem can be found to be under negative pressure.

THE CAVITATION PHENOMENON

If a tree is tall, for example, 20, 30, and even up to 100 m, the negative pressure in its upper part can reach large values of up to 1 MPa. On the other hand, it is well-known that raising water in a vessel by pulling, as shown in Fig. 11.2B, is not possible for more than about 10 m, which corresponds to a negative pressure of about 0.1 MPa. A higher column of liquid will be broken, leaving above itself a vacuum filled by saturated water vapor. If the liquid contains dissolved air, the height of such a column of liquid drawn by suction decreases. The fact that the height of a continuous column of liquid in the xylem vessels of trees can exceed 10 m gives rise to a natural question: why in this case does the rupture of the column not occur? Actually such ruptures do take place. In tall trees a gradual reduction in the quantity of functioning xylem vessels is observed because of the occurrence of air bubbles (embolisms), disturbing the continuity of water strings. The phenomenon of air bubble formation in "stretched" water is termed cavitation. It is also observed, for example, at the back edge of a screw propeller quickly rotating in water. The phenomenon of cavitation in xylem does not occur very often, so that even old trees retain large quantities of efficient vessels.

Although a column of stretched water of more than 10 m is a thermodynamically unstable system, under certain conditions it can be maintained for an indefinitely long time. A few factors promote the relative stability of long water strings in the xylem of trees. First is the cohesion of water stipulated by the presence of

hydrogen bonds between molecules, ensuring rather high resistance against rup-
ture. Moreover, the xylem sap does not contain solid particles, which could be the
nuclei of origin for embolisms. An additional stabilizing influence is provided by
the presence of a structured layer of water molecules adsorbed at the internal sur-
face of xylem vessels. Besides, there is reason to assume that the formation of
cavitation bubbles in the liquid confined in the closed space of a xylem is less
probable than under similar conditions in liquid open to air. The process of for-
mation and the initial growth of cavitation bubbles occurs quickly. With respect
to such fast processes, a xylem vessel can be considered a closed limited volume
because the displacement of an appropriate volume of sap from vessels through
thin channels into neighboring cells requires much more time. As the liquid is
practically incompressible, the formation and growth of a gas bubble under such
conditions would cause a sharp short-term increase in pressure. Such pulses of
pressure should block the growth of a bubble and promote its slamming in the
initial stages of its development. Such a mechanism can efficiently reduce the
probability of the development of embolisms. By using a microphone sensitive in
the ultrasonic region at a frequency of about 1 MHz, it is possible to register high-
frequency sonic impulses generated by the processes of nucleation and slamming
of cavitation nuclei in the trunk of a tree.

   Apparently, the whole complex of factors and mechanisms discussed is enough
to provide the expected duration of stable existence of stretched water strings in
the xylem system. However, a more difficult problem is the question of how xylem
vessels in which a rupture in the continuity of water strings has occurred can
restore their capability for work. The restoration of hydraulic conductivity of xy-
lem is sometimes observed. For example, grape xylem, after being empty for the
winter period, is filled by sap in the spring as a result of increased activity of the
root osmotic pump. However, such a simple mechanism for the restoration of
hydraulic conductivity of embolic xylem vessels is less probable for tall trees.

HYDRODYNAMICS OF XYLEM

   Xylem contains three types of cells: tracheids, fibers, and vessel elements. The
conducting elements of xylem, the tracheids, represent extended tubes with di-
ameters ranging from $10-100$ to $500\ \mu m$ for different species. The tracheid is an
elongated, tapering xylem cell having lignified, pitted, intact walls adapted for
conduction and support. Their length varies widely and can be from hundreds of
microns to greater than 1 m. The tracheids are empty structures containing no
protoplasm. The consecutive chains of tracheids connected with each other form
the vessels of xylem, continuous channels for passage of the xylem sap from roots
up to leaves. The free section for the flow of sap usually decreases in places of
connection of tracheid elements. Here the sap passes from one element to the next
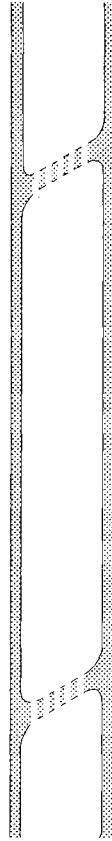
Figure 11.3 Diagram of a xylem element. The actual configurations of xylem cells of various plant species are multiform.

through thin channels. Figure 11.3 shows a single element of xylem in a very schematic way.

Flows of sap move along the tubes of xylem in a laminar regime. The dependence of the speed of flow on the hydrodynamic pressure gradient is determined according to Poiseuille's formula for the velocity of liquid flow in a cylindrical tube:

$$v_w = - \left(\frac{r^2}{8\eta} \right) \left(\frac{dP_{hd}}{dl} \right). \tag{11.6}$$

Or, accordingly, for flow:

$$J_w = - \left(\frac{\pi r^4}{8\eta} \right) \left(\frac{dP_{hd}}{dl} \right). \tag{11.7}$$

Here v_w is the average linear velocity of flow (m/s), which is equivalent to the value of flow density (m^3/m^2·s), J_w is the flow of sap (m^3/s), r is the radius of the tube, η is the viscosity of the liquid, which is equal to about 10^{-3} N·s/m^2, and P_{hd} is the hydrodynamic pressure.

The hydrodynamic pressure gradient in xylem depends upon the intensity of transpiration and usually varies within 0.05–0.3 MPa/m. It should be noted that the hydrodynamic pressure gradient is usually much higher than the hydrostatic pressure gradient caused by the gravitational potential of water and equals 9.8 $\times$ 10^{-3} MPa per meter difference in vertical levels.

The velocity of sap flow in vessels is small in coniferous trees (about 0.5 mm/s) and a little larger (0.5–1.5 mm/s) in most leaf-bearing trees, but it reaches several millimeters per second in some species of trees. The highest velocities of transpiration flow are observed in grassy plants at up to 10–20 mm/s and more. The calculation of transpiration flow velocity, using Eqs. (11.6) and (11.7), usually gives slightly underestimated values because the additional resistance of narrow channels in the connecting places of xylem elements is not taken into account.

Almost all of the water delivered through the xylem to the leaves evaporates. Only a small part of this water, about 0.1–0.3%, is used in the mechanism of photosynthesis, and just a few percent come back with phloem flow. If we assume that all heat necessary for the evaporation of water coming to the leaves is delivered at the expense of absorbed solar radiation, it will be possible to evaluate the ratio between the magnitude of a xylem cross section and an area of leaves. By multiplying the density of water flow in xylem upon the heat of evaporation ($\lambda = 2.5 \times 10^9$ J/m^3) and dividing it by the density of the flow of solar energy absorbed by a leaf (J_s), we obtain:

$$\frac{S_{\text{leaf}}}{S_{\text{xyl}}} = \frac{r^2}{8\eta} \cdot \frac{dP_{\text{hd}}}{dl} \cdot \frac{\lambda}{J_s}. \tag{11.8}$$

If we take the radius of a xylem vessel to be 20 μm, the gradient of the hydrodynamic pressure to be 0.1 MPa/m, and the density of the absorbed light flow to be 200 W/m^2, we obtain a value of about 6000 for the ratio $S_{\text{leaf}}/S_{\text{xyl}}$. Thus, one trachea string with a radius of 20 μm supplies water to about 7 mm^2 of leaf. Water arrives at this surface not directly from a trachea but through the system of thin fibers, each of which brings water to tens of cells forming separate areola. Several hundred areolae can be placed within an area of 7 mm^2.

MECHANISM OF ROOT WATER TRANSPORT

A plant acquires the water needed for carrying out its vital functions through its roots. The expanded root system of a plant provides the extraction of water from soil and pumps it into xylem vessels. The detailed structure of the root sys-

tem of a plant is rather complicated, and its functions are multiform. The extraction of moisture is only one of them. Apart from it, a root provides the extraction of mineral nutrition and delivers metabolites to microscopic symbionts that utilize molecular nitrogen. However, we will consider here only one function of root systems, the pump function ensuring the transport of water into the xylem. Energy consumption is required to perform this function.

Pumping of water into the xylem is followed by the generation of hydraulic pressure of sap in xylem vessels called root pressure. It can be directly observed and measured with a manometer placed on the cut stalk of a plant. The root pressure can reach $0.1 - 0.2$ MPa, although it is usually much less. Leaf-bearing plants can develop higher root pressures than coniferous ones. The root pressure depends upon the intensity of transpiration. It grows with decreasing transpiration and vice versa.

The structure of a root cell system is shown in Fig. 11.4. It is assumed that water generally passes through the apoplast, a continuous system of cell walls and membranes. Thus, water moves in a lateral direction along the surface of cells of a root system in the apoplast matrix. It enters the matrix at the outer side, travels some distance, and passes out into the xylem. From a topological point of view it is equivalent to the single passage of water through a membrane.

Contrary to water, ions arrive in xylem elements along the symplast through a sequence of several cells (Canny, 1965). The flow of ions crosses the cell membrane a minimum of two times: in and out of the cell. If a flow of ions passes through a sequence of cells, it can cross membranes a few times, but necessarily an even number of times. However, it is considered that ions pass from cell to cell not through membranes but through plasmodesmata, which are thin channels connecting the protoplasts of neighboring cells. To provide for a definite direction of ion flow through cells, membranes should possess asymmetric properties at places
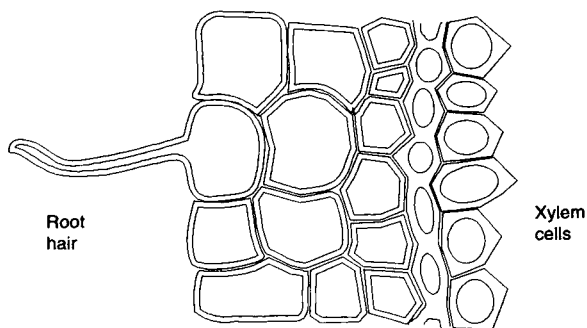
Figure 11.4 Diagram of the structure of a root cell system. Absorption of water from the soil is carried out by a multitude of very thin root hairs. Absorbed water is then translocated across the apoplast to xylem cells.

where ions enter and exit the symplast. This asymmetry means that the membrane that is in contact with the environment has a mechanism of active ion transport, whereas the membrane that is in contact with the xylem has no such mechanism.

An extremely simplified scheme of water and ion pathways in a root system and diagrams of possible distribution of ionic constituents and hydraulic pressure along the pathways are shown in Fig. 11.5.

The flow of ions from soil to xylem is an active process. It happens due to the work of ion pumps incorporated in the cell membranes and acting at the expense metabolite energy. Ion pumps selectively transport ions from the external environment, creating ion concentrations in xylem sap higher than those in the soil. This leads to a corresponding lowering of the chemical potential of water in xylem sap. The difference in water chemical potentials causes an osmotic flow of water from the soil to xylem. Osmotic flow arises when two solutions with different concentrations are separated with a semipermeable membrane through which only the solvent but not the dissolved components can pass. In such a system the solvent passes through the membrane from the side where its concentration is higher to the opposite side where the concentrations of dissolved components are lower. This flow of solvent generates an additional hydraulic pressure. This pressure
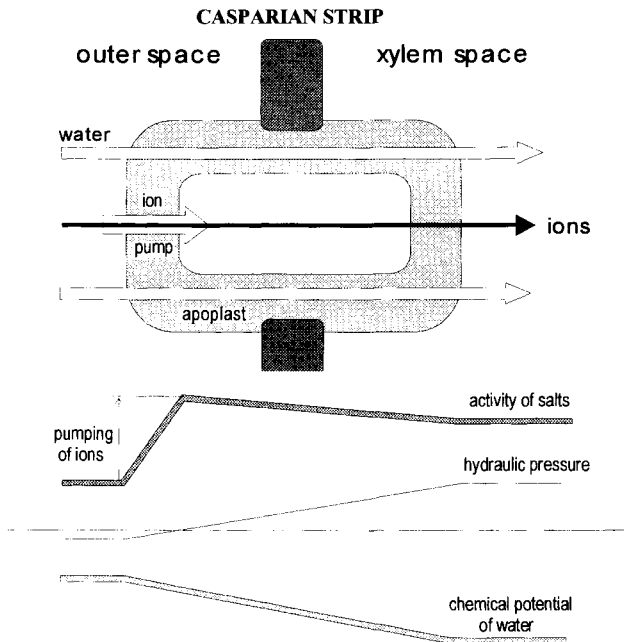
Figure 11.5   Scheme of the osmotic transport of water into xylem. Ions are actively pumped into the xylem, and water moves down its chemical potential.

reaching equilibrium equalizes the difference of water chemical potentials across the membrane. The flow of solvent generates an additional hydraulic pressure. This pressure is termed the *osmotic pressure*. A quantity of the same absolute value but opposite sign is termed the *osmotic potential.*

The osmotic potential of a water solution is related to the activity of water, a_w, as follows:

$$\Psi_{osm} = \frac{RT}{V_w} \ln a_w \tag{11.9}$$

The activity of water in dilute solutions can be taken to be equal to its mole fraction. For pure water it equals a unit. In the presence of dissolved components, the mole fraction of water decreases and the water potential is also reduced. As the sum of the mole fractions of water and the dissolved substances is equal to a unit, the water potential can be expressed via the concentration of dissolved components instead of the activity of water. Correspondingly, Eq. (11.9) can be rewritten for dilute solutions as follows:

$$\Psi_{osm} \approx -RT\nu\Sigma c_i, \tag{11.10}$$

where c is the concentration of dissolved components and ν is a correction factor that takes into account the dissociation of electrolytes in solution.

Osmosis by itself is a passive process: it proceeds along the gradient of chemical potentials. However, in the case of a plant's root system the gradient of water chemical potentials needed to transport it from soil to xylem is formed at the expense of the active process of ion pumping. Thus, the work of a root system during the transport of water should be considered an active process, claiming a portion of the plant's energy use.

It is necessary to distinguish the osmotic pressure of xylem sap from pressure created in the xylem by the root pump. The latter is equal to the difference between osmotic pressures of the xylem sap and the soil water. The content of salts in soil water depends upon the type of soil and the quantity of mineral fertilizers in it. Correspondingly, the osmotic pressure of soil can vary within wide limits: from 2–5 kPa for virgin lands to 0.2–0.3 MPa for strong, fertilized soil. It can be even higher, up to 2–3 MPa, for salted soils.

The described mechanism of water transport in xylem caused by the root pump is accepted by most researchers. However, it is also conceded that the real mechanism is more complicated. From time to time, publications with experimental results suggesting the existence of nonosmotic components of root pressure appear (Zholkevich *et al.,* 1989). For example, water flow in xylem can occur even when the osmotic pressure in the external medium is higher than that in xylem sap. This fact can hardly be interpreted within the scope of the osmotic theory of water transport.

POSSIBLE ROLE OF ELECTRO-OSMOTIC PHENOMENA IN WATER TRANSPORT IN ROOTS

Electro-osmosis is the movement of liquid along a wall of a capillary, system of capillaries, or porous plug under the influence of an externally applied electric field. In macroscopic homogeneous volumes, water is insensitive to the action of an electric field because of the electroneutrality of water molecules. The behavior of water and an electrolyte solution may be different near a solid, such as the wall of a capillary. At the boundary between the two phases the electric double layer is produced as a result of absorption of ions. It is shown schematically in Fig. 11.6. One interface of this electric capacitor is located at the surface of the solid and the other is inside the liquid. The charges at the surface of a solid are immobilized, but in liquid they can move along the surface via longitudinal electric fields. In an electric field the ions in the mobile interface of the electric double layer effect the neutral volume of liquid in the capillary and this results in the electro-osmotic
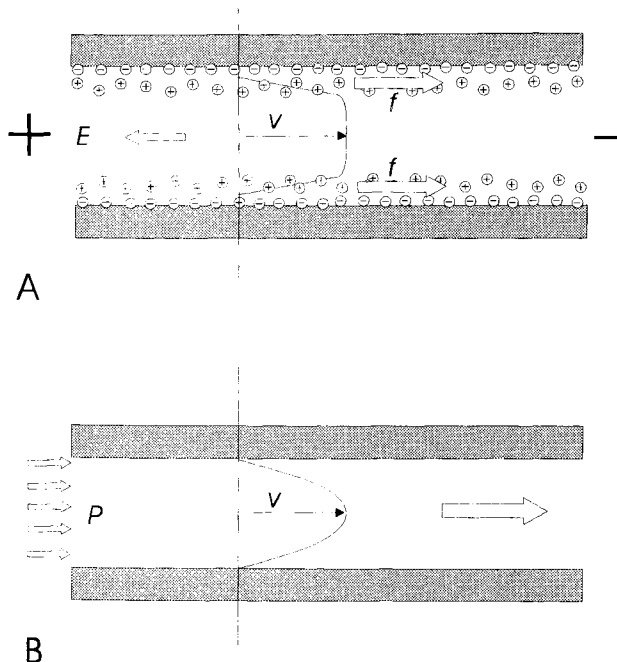
Figure 11.6 (A) Electro-osmotic flow of an electrolyte in a capillary tube. The velocity of liquid is uniform throughout the cross section of the capillary, with the exception of a charged layer near the wall. (B) Poiseuille's flow driven by the hydraulic pressure gradient. The velocity profile is parabolic. Maximum velocity in the center of capillary is twice the average velocity given by Eq. (11.6).

flow. The movement of liquid along a capillary generates a streaming potential and a streaming electrical current between the ends of capillary tubes (Fig. 7.6). Electro-osmotic flow maintains certain distinctions from Poiseuille's pressure-driven flow, as shown in Fig. 11.6. In contrast to the Poiseuille flow, the velocity of electro-osmotic flow (v_{osm}) does not depend upon the radius of the capillary. An equation for the velocity of electro-osmotic flow can be written as follows:

$$v_{osm} = \frac{\epsilon_0 \epsilon \zeta}{\eta} E, \tag{11.11}$$

where ϵ_0 is the dielectric permittivity of a vacuum (8.85×10^{-12} C/V·m), ϵ is the dielectric permittivity of the liquid (for water $\epsilon \approx 80$), η is the viscosity of the liquid phase, and ζ is the electrokinetic or zeta potential. ζ equals the potential difference between the immobilized and mobile faces of the electric double layer and varies usually from a few to some tens of millivolts. E is a longitudinal electric field gradient.

The velocity of osmotic flow under the conditions taking place in plants is usually rather moderate. For example, at a zeta potential of 20 mV and $E = 10^4$ V/m (100 mV at a 10-μm length), the velocity is about 1.4×10^{-2} cm/s. As far as the velocity of electro-osmotic flow is independent of the capillary radius, it may be supposed that the role of this mechanism may be more appreciable in very thin capillaries. In any case there are many observations that allow us to consider that electro-osmotic phenomena can play a certain role in the transport of water through the root to xylem. An electro-osmotic theory of phloem transport was suggested by Fensom and Spanner (1969). Heyl (1933) and Keller (1930) found that the electro-osmotic flow of water from soil into xylem can be responsible for root pressure. Dainty (1963) estimated the large values of the electro-osmotic pressure in roots to be about 1 MPa per 10 mV. Fensom (1958, 1980) observed a correlation between electrical potential difference and cycles of exudation. Watanabe *et al.* (1995) measured the potential distribution at the bean root surface, and Hamada *et al.* (1992) determined the occurrence of electrical current flow around plant roots. Miwa and Kushihashi (1994) published a stereoscopic electrical current density picture around the root. The distribution of electrochemical potential around the plant root surface is shown to be related to the growth of the plant. Mizuguchi *et al.* (1994) found that growth was accelerated if potential was applied to the root in a culturing bath under illumination.

THE MECHANISM OF ACTION OF THE UPPER PUMP

The root system provides for the extraction of water from soil and its delivery to xylem under some pressure. In this sense it can be considered to be the lower pump. However, the main role in the translocation of water from the root to leaves

gas

solid

θ

liquid

θ

θ
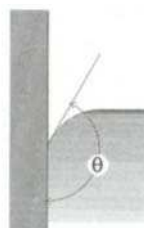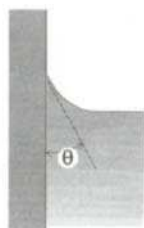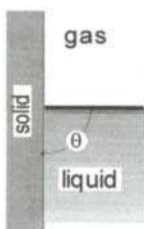
ment of gas by liquid is compensated by the expenditure of energy due to the increasing surface area of liquid.

At equilibrium conditions the phases contact at a certain angle (θ) termed the *contact angle* or the *angle of wetting*. This angle is determined by the ratio between the values of interface energy:

$$\cos \theta = \frac{\gamma_{SG} - \gamma_{SL}}{\gamma_{LG}} \tag{11.12}$$

In the case shown in Fig. 11.7B, the contact angle is acute ($\theta < 90°$) and, correspondingly, the solid phase can be defined as wetting (or hydrophilic if the liquid is water). The opposite case of a nonwetting (hydrophobic) surface is shown in Fig. 11.7C. In this case the contact angle is obtuse and the solid phase is hydrophobic. The case in Fig. 11.7A, where $\theta = 90°$, corresponds to the equality of γ_{SL} and γ_{SG}. Thus, the smaller the contact angle, the more hydrophilic the solid surface. The ultimate case is ideal wetting when the contact angle tends to zero and the meniscus is tangential to the solid surface. At the ideally hydrophilic surface, a very thin liquid film can stretch far above the contact line.

In a thin tube immersed in liquid, the meniscus takes the shape of a spherical segment with curvature radius (r') depending on the radius of the tube (r) and the angle of wetting (θ): $r' = -r/\cos \theta$. If the material of the tube is hydrophilic ($\theta \rightarrow 0$), the meniscus has the shape of a hemisphere with radius equal to that of the tube, $r' \rightarrow -r$. The minus sign indicates that the meniscus is concave. If the surface of a tube is nonwetting, the meniscus is convex. This is shown in Fig. 11.8.
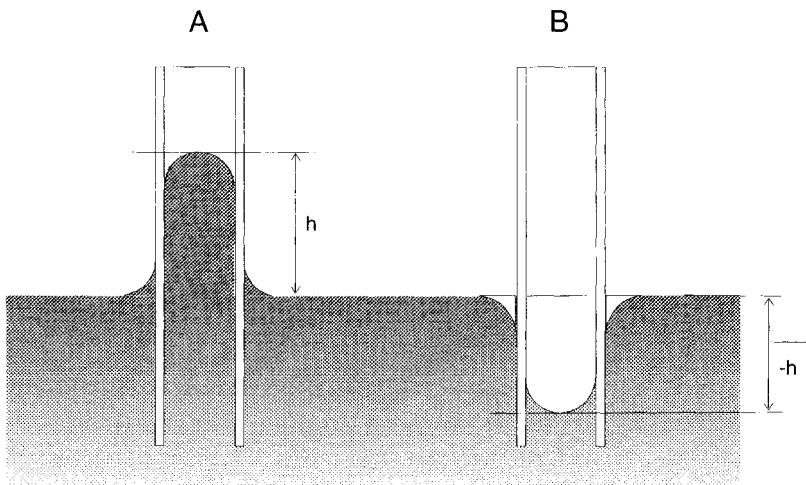
Figure 11.8   Capillary rise (A) and fall (B) of a liquid in a capillary tube: (A) hydrophilic capillary; (B) hydrophobic capillary.

Under a curved surface of liquid an additional capillary pressure arises. According to the Laplace equation, the capillary pressure is proportional to the curvature of the surface (inversely proportional to the radius of curvature) and the surface tension of the liquid:

$$P_{cap} = 2\gamma/r' = (2\gamma \cos \theta)/r. \tag{11.13}$$

Here γ is the surface tension. For pure water the surface tension is equal to 7.3×10^{-2} N/m (or J/m^2) at 20° C. The capillary pressure under a concave surface is negative whereas under a convex one it is positive. Accordingly, liquid in a tube made of a wetting material rises to a height of

$$h = \frac{P_{cap}}{\rho g} = \frac{2\gamma \cos \theta}{rg\rho}. \tag{11.14}$$

A liquid in a hydrophobic tube falls correspondingly (Fig. 11.8A,B).

The height of capillary rise can be larger if the tube is thin enough. In a hydrophilic capillary of radius 1 mm, water is lifted for 15 mm. In a tube of 1-μm radius the height of a rise is 15 m. In a tube of 1-nm radius it theoretically could reach 15 km. It is necessary to recall that water columns at heights of more than 10 m can be ruptured due to cavitation.

The upper pump, pulling water along the xylem of a plant, has to provide not only the necessary height of rising water, as determined by the height of the plant, but also a certain magnitude of water flow along the xylem. This is connected with the expenditure of energy to overcome the hydraulic resistance of vessels. As follows from a comparison of the gradients of hydrostatic and hydrodynamic pressure, this component is essential. The gradient of hydrostatic pressure is equal to 9.8 kPa/m of height. The gradient of hydrodynamic pressure varies over a wide range and, as noted earlier, can reach 100 and even 300 kPa/m of length of a plant, irrespective of how vertical or creeped the plant. For the tallest plants of about 100 m, the magnitude of negative pressure, which is created by the upper pump, can reach 10–30 MPa. The radius of a capillary that could create such a pulling force has to be between 15 and 5 nm, respectively. There are no cylindrical capillaries with such a radius in the mesophyll cells of leaves, but their role in the process of pulling water can be executed by intervals between the cellulose fibrils of a cell wall. Cellulose microfibrils are very hydrophilic. They are tightly packed in a cell wall, so that the dimensions of gaps between them are several nanometers. Correspondingly, an effective radius of curvature of a meniscus of liquid between the fibrils should have about the same value. Thus, a real system of the upper pump ensuring the transport of water along the xylem reminds one not of a system of capillary tubes but a fine-fiber wick. Nevertheless, its mechanism of action is the same.

Due to the extremely small sizes of interfibril pores, the capillary system of a cell wall can create a very large tension (negative pressure) in xylem liquid, which
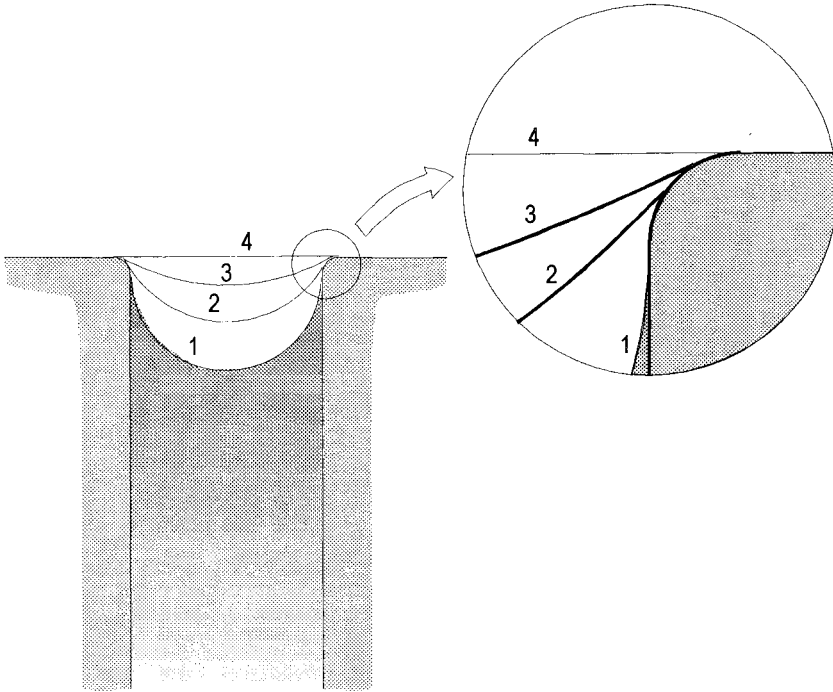
Figure 11.9 The configuration of a meniscus on the top cut of a thin capillary under the condition that negative pressure in the liquid under a meniscus does not surpass the maximum pulling power of a capillary. The less the pulling power the greater the apparent contact angle: (1) $\theta = 0°$ (true value), $P = P_{max}$; (2) $\theta = 30°$ (apparent value), $P = 0.87P_{max}$; (3) $\theta = 60°$ (apparent value), $P = 0.5P_{max}$; (4) $\theta = 90°$ (apparent value), $P = 0$.

is much higher than is required for water to rise to the tops of the highest trees. Thus, the system works with a large potential reserve. The height to which a liquid can be raised is limited by the actual height of a tree but not by the possible pulling power. The behavior of a capillary system under such conditions would show some aberrant behaviors and can be explained by using Fig. 11.9. In this case the length of the capillary tube is less than the maximum possible height of capillary rise; thus, the meniscus is situated upon the upper cut of the capillary. Because the negative pressure in the capillary is lower than that determined by Eq. (11.13), the radius of curvature of the meniscus will be greater than the radius of the tube. The meniscus will have the configuration of a spherical segment, with the radius of curvature determined by the negative pressure at the top of the capillary:

$$r' = 2\gamma/P_{top}. \tag{11.15}$$

This means that the apparent contact angle of the meniscus will be greater than the true value near zero that is characteristic of hydrophylic material. The cosine of the apparent contact angle is

$$\cos \theta' = r/r' = P_{\text{top}}/P_{\text{max}}. \tag{11.16}$$

The position of the meniscus at the upper cut of the tube remains stable until the absolute value of P_{top} is less than that of P_{max}; otherwise the meniscus can be torn off from the upper cut and moved down. Under actual conditions in plants such a tearing of the liquid column from the cell wall never occurs, but the surface curvature of a liquid in capillaries varies depending upon the intensity of transpiration. Thus, a radius of curvature of a meniscus equal to 750 nm is necessary to keep a liquid at a height of 20 m in the absence of transpiration flow. In a capillary of 10-nm radius the magnitude of the apparent contact angle will be 89°. Thus, the surface of the liquid in the capillary will be almost flat in this case. If the transpiration flow creates a hydrodynamic pressure gradient of 0.1 MPa/m under the same conditions, the appropriate value of the radius of curvature is 75 nm and the apparent contact angle in a 10-nm capillary is 82°. For 100-m eucalyptuses at the indicated hydrodynamic pressure gradient, the radius of curvature will be about 15 nm and the value of the apparent contact angle of the meniscus in a 10-nm capillary will be 48°.

In analyzing the mechanism of functioning of the upper pump based upon the phenomenon of capillary suction, it is necessary to consider the influence of surface curvature of a liquid on the motive power of transpiration. This motive power is a difference in water chemical potentials in the liquid and vapor states. Under conditions of thermodynamic equilibrium, the atmosphere is saturated by water vapor and there is no difference in the water chemical potentials between the phases. The motive power arises if the atmosphere is unsaturated. The dependence of the motive force of transpiration upon the degree of saturation of the atmosphere is determined by Eq. (11.1). The degree of saturation (the relative humidity) of the atmosphere, ϕ, is equal to the ratio of the actual pressure of water vapor to the pressure of saturated vapor at a given temperature. The pressure of saturated vapor over a flat surface of a liquid can be calculated by using Eq. (7.1). However, the pressure of saturated vapor over a concave surface of liquid is always lower than over a flat surface. It is natural because the liquid under a concave surface is under some negative pressure and, accordingly, its thermodynamic activity is lowered.

The degree of depression of the elasticity of vapor over a curved surface of liquid can be determined by the Thomson equation:

$$\frac{P_s'}{P_s} = \exp[2\gamma V_w/r'RT] = \exp[PV_w/RT]. \tag{11.17}$$

Here P_s and P_s' are the pressures of saturation over flat and curved surfaces, respectively, r' is the radius of curvature of a liquid surface, and P is the hydraulic

pressure of the liquid. Values of r' and P are negative for a concave surface. Thus, the atmosphere that is unsaturated in relation to a flat surface of water can be saturated in relation to a concave surface. The difference is quite negligible, about 0.15% at a radius of curvature of 750 nm. The saturation pressure over a surface with a radius of curvature of 75 nm corresponds to a relative humidity of the atmosphere of 98.5%. At a radius of 15 nm the value will be 93%. This value is significant. It corresponds to a reduction in the motive power of transpiration of 180 J/mol. The motive power of transpiration decreases by a value corresponding to the reduction in the chemical potential of water under a concave surface:

$$\Delta E = PV. \tag{11.18}$$

At very high relative humidity, the phenomenon of capillary condensation may occur. Since the elasticity of a saturated vapor above a very concave surface of a liquid is less than that above a flat one, the air over a concave surface may seem to be oversaturated compared to the air over a flat surface to the liquid in the thin capillaries of a cell wall. Under such conditions moisture from air will be condensed in the capillaries, and as a consequence the xylem flow can change its direction of movement from the leaves to the roots of a plant.

The availability of dissolved substances in xylem liquid can also exert an influence on the value of the motive power of capillary suction. Their presence in solution reduces the activity of water approximately in proportion to their concentration [Eqs. (11.9) and (11.10)]. As a result the elasticity of a saturated vapor is accordingly reduced compared to that over pure water. The reduction in the motive power of transpiration that occurs accurately corresponds to the osmotic component of the water potential of xylem sap.

Thus, the actual motive power of transpiration is composed of the following components:

$$E = -\frac{RT}{V_w} \ln \phi - P_{st} - P_{osm} - P_{hd}. \tag{11.19}$$

Here the first term is the initial motive power of evaporation from the flat surface of pure water. The value of this component is determined by the relative humidity of the air and can reach 14.5 MPa at 90% humidity and 95 MPa at $\phi = 50\%$. In Chapter 7 we discussed in detail the influence of various conditions on the magnitude of the motive force of transpiration that arises at the interaction of plant with humid air.

The second term in Eq. (11.19) is determined by the height of the tree and even for the tallest trees does not exceed 1 MPa. The osmotic component caused by the presence of dissolved salts is usually less than 0.2–0.3 MPa. The hydrodynamic component of pressure can reach several megapascals. All three terms P_{st}, P_{osm}, and P_{hd} reduce the acting value of the motive power, but in a dry atmosphere these effects are usually small in comparison with its initial value. However, as the relative humidity of air approaches 100%, the initial value of the motive force of
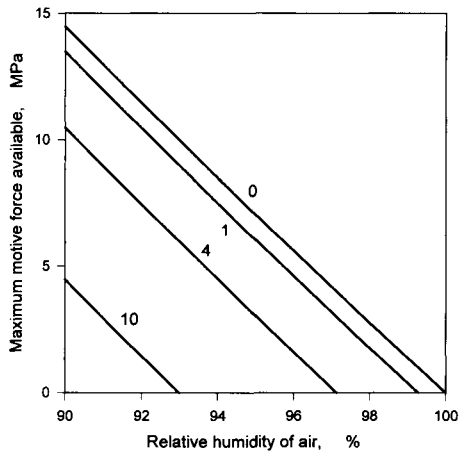
Figure 11.10   The dependence of maximum motive force of transpiration upon the relative humidity of air at high humidities. Values on the curves denote the sum of P_{st}, P_{osm}, and P_{hd}. The points of intersection with the zero line show the limiting values of humidity at which the transpiration flow should cease and capillary condensation may occur.

transpiration diminishes sharply and conditions of the function of the pulling mechanism of a plant become more difficult. Figure 11.10 shows that the motive force of the upper pump may return to zero even when the atmosphere is not fully saturated with water vapor.

IS THE UPPER PUMP
THE CAPILLARY OR MATRIX PUMP?

Along with the capillary mechanism of rising sap in xylem, the matrix mechanism can also be considered. The cell wall usually contains not only cellulose fibers but also a substantial amount of pectin-type high-molecular-weight carbohydrates. These substances have a high affinity for water, and this is displayed by their ability to swell. The process of swelling is simply the dissolving of water in a polymer matrix. The cell wall represents such a swelled film, which contacts xylem liquid on one side and air on the other in the mesophyll of a leaf. If the air is not completely saturated by the water vapor, water from the matrix can evaporate and its content in the surface layer decreases. In other words, the matrix from the external side of a cell wall dries a little. As a result, a chemical potential gradient of water in the polymer matrix of a cell wall is generated. This gradient induces the flow of water through the cell wall outward. The outflow of water from xylem vessels into the matrix creates a negative pressure there, in other words

suction, which pulls water along the xylem. The difference in water potentials on both sides of the cell wall depends upon the ratio of water activities in a matrix:

$$\Delta\Psi = \frac{RT}{V_w} \ln \frac{a_{w,in}}{a_{w,out}}, \tag{11.20}$$

where $a_{w,in}$ and $a_{w,out}$ are the activities of water at the internal and external sides of a cell wall, respectively. According to this equation, substantial suction force can be generated in the cell wall matrix even when the difference in water activities on both sides of the wall is small. For example, a 0.7% difference in water activities is enough for the creation of 1 MPa of negative pressure. A difference of 7.5% creates a negative pressure of 10 MPa.

It would be incorrect to consider the matrix and capillary mechanisms generating the pulling force as alternate mechanisms mutually excluding each other. The capillary mechanism becomes less distinguishable from the matrix mechanism at very small pore radii. If pore sizes are so small that just a few molecules of water can be placed there, the macroscopic characteristics of a system, such as contact angle and the surface curvature, lose their meaning. At the same time the relative role of effects stipulated by the interaction of water with the solid material of a cell wall is increased in a very thin capillary. These are the main interactions of the matrix mechanism. The energy characteristics of both mechanisms, capillary and matrix, are approximately equivalent.

SOME FEATURES OF THE PHLOEM TRANSPORT

The second long-distance transport system of plants is the phloem. It provides for the transport of products of photosynthesis from leaves down to the roots and distributes them in the plant. The phloem transport occurs as an active process, which requires spending a certain amount of metabolites. The products of photosynthesis are carried along phloem in the form of concentrated solutions containing 10–25% sugars, some amino acids, and ionic components. The power of liquid flows transported along xylem and phloem is significantly different. Whereas more than 300 g of water per 1 g of synthesized product is transferred along xylem, the amount of phloem sap needed to transport 1 g of product is only 4–10 g. These numbers follow directly from the concentration of sugars in the phloem. Thus, the volume of flow of liquid in the phloem is one to two orders of magnitude less than that in xylem. Water circulation is considered to occur in two parallel systems of long-distance transport: water moves from xylem to phloem in leaves and comes back to xylem in roots. As the volume of phloem flow is many times less than that of xylem flow, such circulation is essential for phloem transport but cannot render an appreciable influence upon transport in xylem.

The transport in phloem is probably caused by the osmotic mechanism. In the

leaves of plants, phloem is being loaded with sugars. The loading of phloem is an active process of the transmembrane transport of sugars from photosynthesizing cells to phloem vessels. The high concentration of sugars is accumulated in phloem sap, and therefore the osmotic pressure in it reaches $1-3$ MPa. At the same time, the unloading of sugars from phloem sap takes place in roots and other energy-consuming tissues of the plant. Sugars extracted from the sap are either spent on the actual metabolic needs of the plant or transformed into insoluble forms, such as starch, and stored. As the phloem is unloaded, the osmotic pressure of sap is reduced. An osmotic pressure gradient ensuring the flow of solution is created as a result of loading the phloem in the leaves and unloading in the places where the metabolites are consumed.

Such a model of phloem transport is now generally accepted. It was suggested by Münch 70 years ago. In general it satisfactorily explains the majority of the known facts (Zimmerman and Milburn, 1975; Kargol and Kargol, 1996; Kramer and Boyer, 1995; Kursanov, 1984; Passioura, 1988; Taiz and Zeiger, 1991). Nevertheless, from time to time other mechanisms that attempt to explain phloem transport processes are suggested.

Entropy Balance of the Plant

INTRODUCTION

In Chapter 3 we briefly discussed the thermodynamic aspects of the energy-converting functions of plants. All of the vital processes of plants, including the synthesis of complex organic substances, the building of their complicated structures, and the maintenance of a high level of organization, are due to the continuous influx of negative entropy. This influx is provided by the energy flux that passes through the plant. The entering energy flux of solar radiation has an effective temperature on the order of 2000–6000 K. The energy flux leaving the plant is almost the same in magnitude, but its effective temperature is much lower at about 300 K. Thus, the energy flux loses its high degree of negative entropy, and from this loss the plant performs all kinds of useful work necessary for its vital activity. In other words, the incoming energy flux brings little entropy to the plant, whereas the flux leaving withdraws much more entropy. Thus, the energy flux that passes through the plant continuously "pumps" entropy out of it. The entropy deficit originated in this way compensates for the entropy produced by irreversible processes that occur in a plant in various ways. Here we have to remind ourselves again of the conceptions formulated by Schroedinger (1955) and discussed in more detail by Brittin and Gamov (1961) and Broda (1975).

From the thermodynamic point of view, a plant can be considered an open system that exists in a state of continuous exchange of mass and energy with its surroundings. Under steady state conditions the inward and outward fluxes of mass and energy should be closely balanced. The difference between the in- and outflux is the fraction of matter or energy fixed by the plant: $E_{out} = E_{in} - E_{fix}$ and $M_{out} = M_{in} - M_{fix}$. The quantity of energy fixed by the plant within a definite time, E_{fix}, usually does not exceed a few percent of the total

quantity of energy that passes through the plant, E_{out} or E_{in}. The portion of mass flow that becomes part of the plant's body is at least an order of magnitude less than the equivalent portion of energy. Thus, the difference between M_{out} and M_{in} is usually quite small.

The energy balance of the plant enables one to obtain useful information concerning its temperature conditions. This balance tells us very little about the internal processes that occur in the plant. In this respect the entropy balance might be more informative. The entropy balance includes contributions from terms due to exchange with the surroundings and components due to the internal generation of entropy, S_g, in the plant. All irreversible processes that proceed in the plant generate entropy. The contribution of the internal generation of entropy to the balance may be significant. The analysis of the entropy balance may be helpful for making estimations about the general structure of the plant's energetic functions and the relative cost of certain processes of the plant.

In a general form, the expression for the entropy balance may be written as follows:

$$S_{out} = S_{in} + S_g. \tag{12.1}$$

The inward (S_{in}) and outward (S_{out}) terms of the entropy balance can be readily determined from the proper components of the energy (and material) balance. It is much more difficult to evaluate the terms related to the inner generation of entropy. Entropy is produced in the plant by various processes, both passive and active, which require work to be performed. These processes are internal to the plant and do not cause any obvious effects externally. This causes some difficulty in evaluating the energy requirements of a plant. Due to the lack of sufficiently reliable information about the energy requirements of various life functions of plants, the entropy balance may be only estimated. A balance made on the basis of probable estimations should be useful, as it may help to designate the relative "laboriousness" of different physiological functions for the plant. Qualitative deductions that may follow from such calculations are not too dependent upon the initial assumptions.

Considering all this, we will further examine the entropy balance of the plant under some arbitrary conditions. All calculations will refer to 1 million J of photosynthetically active radiation (PAR) absorbed by the plant. The longwave radiation and the fraction of PAR scattered by the plant without absorption will not be taken into account.

ENTROPY INFLUX

Let the total influx of PAR to a plant be 1 million J. A fraction of this quantity, about 10–20%, is absorbed not by light-harvesting pigments but by the

structural elements of the plant. This value roughly corresponds to the absorbance of a bleached plant leaf. All of this energy dissipates into heat, thus bringing a certain amount of entropy to the plant. This contribution can be easily determined by dividing energy by the temperature of the plant. Taking the temperature to be 27°C (300 K), we will find the value of the entropy contribution: $S_{in1} = E/T = 0.2 \times 10^6/300 = 667$ e.u. (entropy units, J/K). This value may vary within certain limits, say from 400 to 700 e.u.

Approximately 80% of PAR (0.8×10^6 J) is absorbed by such specialized pigments as chlorophylls and carotenoids. The thermalization of this energy occurs gradually as the result of a long consecutive chain of transformations starting from the generation of the pigment excited states upon the capture of quanta. The immediate contribution of entropy due to the absorption of radiation before its thermalization depends upon the intensity and spectral composition of the incident light. In Chapter 1 we discussed the question of the entropy content of radiation in detail. Here we can use an approximate formula that gives the value of the entropy of radiation. The formula is valid for the PAR:

$$S = (E/T)\,(1.12 + 0.4\,\log\gamma), \qquad (12.2)$$

where γ is the factor of radiation attenuation and T is the temperature of the source. For solar radiation, $T \sim 5785$ K.

For direct, unattenuated solar radiation $\gamma = 1$, and correspondingly $S_{in2} = 155$ e.u. (per 0.8×10^6 J of absorbed energy). For diffuse radiation from an overcast sky the attenuation factor is usually about 2×10^5 due to an increase in the solid angle at which the radiant flux arrives and to a lesser extent due to the scattering and absorption of light by the cloud layer. Assuming this value for the attenuation factor, we will calculate the entropy influx in this case to be $S_{in2} = 450$ e.u. Thus, the overall entropy influx with the radiation absorbed may vary depending upon the illumination conditions within the limits $S_{in} = S_{in1} + S_{in2} = (400 \div 700) + (155 \div 450) = 555 \div 1150$ e.u.

ENTROPY OUTFLUX

The outflux of entropy may be determined from the fact that in steady state conditions plants emit all of the energy received to their surroundings, except the share fixed by photosynthesis. Assuming a value of 5% of PAR for total photosynthesis, we will have 5×10^4 J out of 1 million as the quantity of radiation converted into the chemical energy of organic matter, and the remaining 0.95×10^6 J are lost by the plant as heat. Removal of this heat from the plant is followed by an outflow of entropy. The plant loses entropy equal to the amount of waste heat divided by the temperature of the plant. The value of S_{out} is about 3200 e.u. if the heat is removed by convection and transpiration or a little more if a significant

portion of the heat is lost as infrared radiation. Thus, the entropy outflux from a plant surpasses the influx by at least 3–5 times.

GENERATION OF ENTROPY

In a steady state the difference between the in- and outflow of entropy must be offset by the internal entropy production. The processes that produce entropy in a plant can be considered as two distinct types, passive and active. We will consider the process to be passive if it is driven by external forces, whereas processes running on the self-contained energy resources of a plant will be defined as active. In passive processes, work is performed within the plant at the cost of a decrease in the free energy of the surroundings. Generation of entropy proceeds within the plant in both cases.

We should emphasize that the division of the processes into passive and active categories is conditional to a great extent. In essence any real process is followed by a decrease in the general stock of free energy of the universe, including the system under consideration and its surroundings. The question is where we place the imaginary border between the system and its surroundings so that the source of the motive force of the process is located inside or outside the system.

The following passive processes that take place within the plant are the most significant:

- "devaluation" of the excess energy of quanta, which is over the threshold level of photosynthesis (~ 1.8 eV) in the antenna system of thylakoids;
- transport of water in the xylem due to the action of the water potential difference between the roots and the leaves;
- heat exchange between the soil and the atmosphere induced by the transfer of water.

Photosynthesis, the uptake of water by the roots, mineral nutrition, and many other vital processes in the plant are considered active.

The production of entropy by passive processes can be determined from the values of appropriate thermodynamic fluxes (J_i) and the corresponding thermodynamic forces (X_i) that cause these fluxes:

$$S = \frac{1}{T} \sum_i J_i X_i. \tag{12.3}$$

The entropy production in an active process can be estimated from the work produced (W) and the efficiency of the process (η).

$$S = \frac{W}{T} \left(\frac{1}{\eta} - 1 \right). \tag{12.4}$$

Unfortunately, there is very little reliable information about the efficiency of active processes that occur in the plant. Therefore, one has to be satisfied with plausible assumptions. Although sometimes these assumptions are hypothetical, they do not distort the general qualitative picture of the entropy balance of a plant.

DISSIPATION OF ENERGY IN THE PRIMARY STAGES OF LIGHT HARVESTING

The photosynthetic systems of chloroplasts are driven by photons, the energy of which exceeds the threshold level needed to excite the chlorophyll molecules of the reaction centers. The excitation energy of these centers is about 1.77–1.85 eV. All of the excess energy of more "energetic" photons is dissipated in the antenna while the excitation migrates to the reaction center. Thus, the energy of all photons captured by the antenna is normalized to a standard level (~ 1.8 eV). This process is followed by a partial "devaluation" of energy and the generation of corresponding quantities of entropy. As was shown earlier [Chapter 5, Eq. (5.25)], in the process of normalization about 20–25% of the absorbed energy is dissipated. Thus, the entropy produced equals $S_{g1} = (0.22 \times 0.8 \times 10^6)/300 = 587$ e.u. The real values probably vary within 530–670 e.u. (all of these data refer to solar radiation). About 6×10^6 J of energy (3.5 mol of quanta) remains available at the "standard" level (~ 1.8 eV).

PHOTOSYNTHESIS

The fraction of energy that is bound by a plant in the photosynthetic process depends upon many different factors and is therefore variable. At conditions of intense illumination it may be much less than 1%. At the most favorable conditions the efficiency of photosynthesis may reach 10% (in relation to the total PAR). In the present calculation a value of 5% for total photosynthesis is assumed; hence, 5×10^4 J of radiant energy is converted into chemical energy. This corresponds to the binding of about 0.1 mol of CO_2. The standard difference in enthalpy for the overall reaction of photosynthesis equals 466.2 kJ/mol of CO_2. The process of photosynthesis is followed by a small decrease in entropy: $\Delta S^\circ = -43.2$ e.u./mol or -4.3 e.u. per the actual quantity of carbon dioxide bound. On the other hand, the initial state of carbon dioxide in the natural photosynthetic process is not its standard state, and therefore we must take into account an additional positive component in the entropy balance:

$$\Delta S = -R \log(p/p^\circ), \tag{12.5}$$

where R is the gas constant, $p°$ is the standard pressure, and p is the partial pressure of CO_2 in air. The ratio $p/p°$ in free air is 3×10^{-4} and in the mesophyll of leaves may fall to 2×10^{-4} or less. Thus, the additional component of entropy production connected with the extraction of carbon dioxide from air can be estimated for 0.1 mol of carbon dioxide to be about 3 e.u. This value is small compared with other contributions.

The production of entropy by the irreversible processes of photosynthesis can be estimated taking into account the free energy change (ΔG) of the substances that take part in the synthesis reaction and the value of the quantum requirement n, i.e., the number of photons needed to bind 1 molecule of carbon dioxide:

$$CO_2 + H_2O + nh\nu \rightarrow 1/6C_6H_{12}O_6 \qquad (12.6)$$

The change in free energy for this reaction equals 478 kJ/mol of CO_2 and the quantum requirement usually varies from 8 to 12. Independent of the initial energy, each mole of absorbed photons brings 174 kJ, a standard portion of energy corresponding to the threshold level (1.8 eV). Eight moles of photons bring 1390 kJ; thus, for an eight-quantum requirement the efficiency of the photosynthetic process equals 34% in relation to the energy of the standard level. At a quantum requirement of 12 the efficiency equals 22%. Now we can estimate, with the help of Eq. (12.4), the entropy produced by the photosynthetic process. For an eight-quantum requirement one finds $S_{g2} = 324$ e.u., and for $n = 12$ the corresponding value is 590 e.u.

SUCTION OF WATER AND XYLEM TRANSPORT

The photosynthetic process is closely connected with the process of transpiration. The relation between the amounts of water transpired and carbon dioxide bound varies within fairly narrow limits for different plant species and over a wide range of conditions. Plants withdraw from the soil and evolve into the atmosphere approximately 500–1500 mol of water per each mole of carbon dioxide fixed. We will assume for the present calculation a mean value of 800 mol of H_2O per mole of CO_2 or 1.44 kg ($1.44 \cdot 10^{-3}m^3$) of water per 0.1 mol of CO_2. The difference in water potentials between roots and leaves may vary within extremely wide limits depending upon external conditions (Nobel, 1991). We will take, for the example under consideration, the water potential value to be 2×10^3 kJ m^{-3} = 2 MPa. To find the production of entropy by the water transport process we can use Eq. (12.3):

$$S_{g3} = (1.44 \times 10^{-3} \times 2 \times 10^6)/300 \approx 10 \text{ e.u.}$$

In Chapter 11 we mentioned that water potential consists of several components due to the action of hydrostatic, osmotic, and gravitational forces. All of

these components cause the generation of entropy except the gravitational force because the elevation of a mass is a reversible mechanical process that does not generate entropy. The gravitational component of water potential is determined directly by the height of a plant, increasing by 0.01 MPa per meter. This component may be ignored except for tall trees.

The transport of water in xylem is a passive process driven by external forces. Evidence exists that water transport depends upon metabolic processes and, thus, includes a certain active component (Zholkevich *et al.,* 1989). Unfortunately, there is little quantitative information concerning this matter. However, the root pump, one of the active mechanisms of water transport, has been studied in more detail. The work performed by the active mechanism of the root pump may be determined by using the values of root pressure. For the example under consideration it may be estimated to have a value of about 150–300 J (0.1–0.2 MPa of pressure). The efficiency of the root pump is unknown. Its value probably lies between 5 and 25%. Using these figures, we will find values from 1.5 to 20 e.u. for entropy production by the root pump. The total generation of entropy by the transport process in xylem (S_{g3}) will come to about 30–40 e.u.

GENERATION OF ENTROPY BY PHLOEM TRANSPORT

Extensive investigations have been carried out concerning the physiology of phloem transport in plants (Kursanov, 1984; Zimmerman and Milburn, 1975). The information available is very important for physiology problems. It is, however, hardly usable for calculation of the energy requirements of a plant. Therefore, we should try to estimate the value of entropy production by phloem transport in the following way. As was shown in Chapter 4, the harvest of substances produced by photosynthesis from the area of leaves requires a certain energy expenditure. It amounts to 30% of the total quantity of energy gathered if the form in which energy is transported is the prime metabolite, such as ATP. However, plants use sugars as energy-rich carriers to transfer energy over long distances. A molecule of sugar, such as glucose, when oxidized in the Krebs cycle, gives a total of up to 36 molecules of ATP, including those formed by the oxidation of NADH and $FADH_2$. Thus, sugar may be considered to be an energy carrier 36 times more "concentrated" than ATP. The use of such an energy carrier enables the plant to significantly reduce its energy expenditure for long-distance transport from 30 to 1–2%. These may be plausible estimations for energy expenditures for the transport of metabolites in leaves. The energy expenditure for the transport of metabolites in branches, stem, and roots significantly depends upon the size and macroscopic structure of a plant. Let us take this component to be 10 times greater than that of leaves. Thus, the total energy expenditure for the long-distance transport of metabolites may be estimated to be between (5×10^3) and 10^4 J. Again assum-

ing a value from 10 to 20% for the efficiency of the mechanism of phloem trans-
port, we will obtain entropy production estimates within a broad range from 50 to
300 e.u.

MINERAL NUTRITION

The work a plant has to perform to recover the basic components of mineral
nutrition out of soil theoretically is rather small. Thus, for the binding of 0.1 mol
of carbon dioxide a plant consumes about 1.5×10^{-3} mol of potassium ions.
Assuming the ratio of potassium concentrations in soil and in sap to be 1 : 100, we
find the work needed for the recovery of potassium to be 20 J. Roughly the same
amount of work is required for the recovery of phosphate and for the removal of
surplus sodium and chloride ions from the plant. The total value of work needed
to give the plant a full set of necessary ionic components (except nitrogen) comes
to 80–150 J. The work actually done by a plant is above that. By taking into
account the fact that the mechanisms that provide mineral nutrition for plants act
under difficult conditions, one may suppose their efficiency to be low, probably
no more than 1–5%. Therefore, the work actually performed by a plant should be
estimated to be 1.5–15 kJ.

The recovery of nitrogen requires much more work, especially in the case
where nitrogen is fixed symbiotically. By recalculating the experimental data
(Silsbury, 1977), one can obtain values between 7.5 and 20 kJ. Thus, the total
quantity of entropy produced by active processes of mineral nutrition (S_{g5}) may
be estimated to be within 30–120 e.u.

STRUCTURE FORMATION

The organic matter originated by photosynthetic process is incorporated into
the new structures of a plant. These structures are highly organized. Therefore,
their entropy tends to be somewhat lower. The value of the decrease in entropy
connected with the ordering of matter can be estimated in different ways. The
simplest approach may be as follows. If each of the 6×10^{22} atoms of carbon
(0.1 mol) bound by photosynthesis takes its inherent place in the newly formed
structure, we can evaluate the total decrease in entropy: $\Delta S = kN \ln N = (1.38 \times 10^{-23})(6 \times 10^{22}) \ln(6 \times 10^{22}) = 44$ e.u. Actually, it is not the indi-
vidual atoms of carbon but rather large molecules comprising hundreds of atoms
that are the distinguishable units in the structure-forming process. Therefore the
decrease in entropy due to the ordering of synthesized matter is less than this value
by at least 2–3 orders of magnitude, i.e., its amount is only some tenths or hun-
dredths of an entropy unit. These estimations are in close agreement with those

obtained by Quaster (1964) and Blumenfeld (1981) on the basis of somewhat different premises.

Thus, the absolute value of the entropy decreases as a result of the formation of an ordered structure in a plant. It is so small that it may be left out of the analysis. However, the building of a highly ordered structure is very demanding work, and a plant must pay a rather high energy cost for it. No reliable data on the energy cost of the structure-building processes in a plant are available. However, one may assume that the total efficiency of the process will be low due to its complexity. The efficiency is unlikely to exceed a few percent and probably amounts to only some tenths of a percent. By taking into account all of these considerations, one may evaluate the entropy produced by the structure formation process by dividing the supposed value of the entropy decrease by the supposed range of values for the efficiency of the process. Thus, values in the range of 2–20 e.u. for entropy production by the process of structure formation (S_{g6}) seem to be more or less probable.

ADJUSTMENT PROCESSES

A plant lives and performs its vital functions under continuously varying external conditions, such as level of irradiance, temperature and humidity of the air, and moisture content of soil. As all of the processes in a plant are more or less inertial, the plant never really works in a steady state regime. The plant changes its status, striving for complete correspondence with the external conditions, but as the conditions are also changing a true steady state remains unattainable. The continuous adjustment of life functions requires that the plant perform some work, and a corresponding amount of entropy should be produced.

Some estimates of the work needed for the continual adjustment of a complex dynamic system in which many chemical processes occur were made by several authors [see, for example, Welch (1977)]. As a first approximation, the work of adjustment may be deemed to be proportional to the product of the rate of change of the power of a process by the time constant of the system. For approximate calculations, the averaged value of the time constant for basic physiological processes in a plant may be assumed to be 10 min. The main changes in external conditions during night-to-day transitions occur within several hours. By taking into account that the energy load of a plant within this period changes from zero to maximum, we can estimate the work of adjustment to be 3×10^4 J and about 100 e.u. of entropy production.

The values that are obtained can be considered to be upper limits that are actually unattainable. The point is that a plant is not a passive system, but possesses an internal mechanism providing for the adjustment of its life functions in advance of the regular changes of external conditions. This mechanism is the circadian

rhythm, i.e., the time organization of processes into a stable dynamic cycle synchronized with natural diurnal cycles of variation of external conditions. As Glansdorff and Prigogine (1971) have shown, a dynamic system rotating around a steady state point over a stable closed trajectory produces the same amount of entropy as a steady state system. In other words, the circadian rhythm mechanism should minimize the energy requirements of the plant connected with the adjustment of the regime. This function of the circadian rhythm is effective only with respect to the processes synchronized with the diurnal cycle and does not extend to the random perturbations. To adjust the physiological regime to such perturbations, a plant must perform a certain amount of work. For example, if the total energy load of a plant changes by 20% (i.e., for 2×10^5 J) within an hour, we should obtain about the same values for the work of adjustment (3×10^4 J) and entropy production (~ 100 e.u.). Therefore, this value may vary within broad limits, say from 30 to 300 e.u.

ENTROPY BALANCE

The estimates of the individual components of the entropy balance are summarized in Table 12.1. Here values are listed for the lower and upper estimates of the main components of the entropy balance and the geometric mean values between the lower and upper estimates. Supposed values for the "uncertainty factor," defined to be the square root of the ratio of extreme estimates, are also listed. Corresponding extremes can be found in each case by multiplying or dividing the mean value by the uncertainty factor.

Table 12.1

Entropy Balance of a Plant

	Items of the balance	Estimates Lower	Upper	Mean	Uncertainty Factor
S_{in}	Influx with solar radiation	555	1150	800	1.4
S_{out}	Outflux	3200	3600	3395	1.1
S_{g1}	Dissipation in antenna	530	670	595	1.1
S_{g2}	Photosynthesis	320	590	435	1.4
S_{g3}	Xylem transport	30	40	35	1.2
S_{g4}	Phloem transport	50	300	122	2.5
S_{g5}	Mineral nutrition	30	120	60	2
S_{g6}	Structure building	2	20	6	3.2
S_{g7}	Adjustment	30	300	95	3.5
S_g	Total entropy generation	992	2040	1348	
	Entropy deficit	1653	410	1247	

As one can see, the individual components of the balance are estimated with essentially different accuracy. Some, S_{in} and S_{out} as well as S_{g1}, S_{g2}, and S_{g3}, can be calculated precisely. The values of the uncertainty factors for these contributions merely represent the possible range of their variation due to external conditions. The other components, especially those connected with active processes, may now be only tentatively evaluated. There are no reliable data, which is necessary for exact calculations of these components of the entropy balance. In this sense the "uncertainty factor" actually reflects the deficit in our present knowledge of this question. Even so, the estimates shown in Table 12.1 may form the basis for some important speculations and conclusions despite their approximate character.

WHAT FOLLOWS FROM THE BALANCE OF ENTROPY?

Attention should be paid to the large deficit in the entropy balance. The outflux of entropy greatly exceeds the sum of entropy influx and its generation. Mean estimates of the entropy deficit reach about 60% of the total amount of entropy acquired from outside of and generated within a plant. The deficit exceeds 100% of the total income at lower estimates and remains significant even at upper estimates. The presence of such a dramatic deficit in the entropy balance in fact means that some source of entropy has not been taken into account in our calculations. Some minor components were ignored because of their small size. The question concerns the destiny of 40–75% of the energy absorbed by specialized pigments of a plant. The ways in which this energy is ultimately thermalized in the plant remain vague. The assumption that this energy "simply" dissipates, being transformed into heat without the performance of any work, may be oversimplified and does not elucidate the problem. Such an assumption takes the problem from a physical ground onto a biological one, raising a new question: If the highly specialized light-absorbing systems of a plant are idle to such a great extent and even load the plant with surplus heat from which it has to free itself, why have these systems not been reduced by natural evolution?

The entropy balance can be squared under conditions of keeping equality between the influx of entropy and its generation and the outflux. In such a case, estimates of entropy production should be taken as significantly greater than those used earlier. The question about the sources of energy needed for performing the necessary work becomes more acute. If this energy is supplied by respiration, the plant would consume, for this purpose, about 75% of the products accumulated by photosynthesis even if the lower estimates of entropy generation by active processes (about 120 e.u.) are taken into account. The net photosynthesis would amount to only 1.25% in relation to PAR and not 5% as was assumed earlier. The energy requirements of a plant for the performance of its active processes on the mean level (~280 e.u.) and more so on the top level (~740 e.u.) are not provided

because the total exhaustion of photosynthetic products by respiration can provide no more than 170 e.u.

The way out of these contradictions may be as follows. One must suppose that a plant utilizes, for its inherent energy needs, not only the energy accumulated by the photosynthetic process but essentially a larger share of the energy absorbed. A substantial part of useful work may be performed by the plant not through the cycle of carbon dioxide fixation and subsequent oxidation of the products but in a roundabout way, which is not directly linked with the cycle of CO_2 assimilation. This may be the cyclic loop of electron transfer in photosystem I, which produces ATP but is not immediately bound to the synthesizing block. Thus, energy can be stored here without the participation of carbon dioxide.

There are a lot of experimental data showing that such nonphotosynthetic ways of capturing solar energy really do play a significant role in plant energetics. This is born out by the disagreement between the results of direct calorimetric measurements and those of gas exchange. All of these data are not quite consistent, and there is now no agreed-upon theory about the probable estimates of the share of solar energy utilized by a plant in a nonphotosynthetic way. Hypotheses about the nature and mechanisms of nonphotosynthetic processes are diverse, and this question evidently is beyond the limits of the thermodynamic approach considered here. One may judge that plants may use a significant amount of energy in non-photosynthetic processes.

Another way to find an acceptable explanation for the entropy deficit may be connected with the process of photorespiration. It seems possible that this process, whose actual purpose is not quite yet clear, exists as a means to compensate for the entropy deficit that arises continuously because of the extreme "purity" of energy that the plant feeds upon. One must bear in mind that solar radiation as a form of energy is characterized by a very low entropy content. This question was discussed in some detail in Chapters 3 and 4. This may be a plausible explanation for the role that photorespiration plays in a plant's life.

Chapter 13

Electrical Signals and Long-Distance Communication in Plants

INTRODUCTION

The problem of action and resting potentials in plants has a rich and dramatic history, which has been discussed by Bose (1924, 1926, 1927a,b, 1964), Du Bois-Reymond (1848), Pickard (1973), and Sinukhin (1972). Plants have a specific property: excitability (Volta, 1816). This is the ability of cells, tissues, and organs to change their internal conditions and external reactions under the influence of various environmental factors, referred to as irritants. The high sensitivity of protoplasm and all cell organelles to any natural and chemical effects is the basis for excitability.

According to Goldsworthy (1983), electrochemical signals that look like nerve impulses exist in plants at all levels of evolution. Gunar and Sinukhin (1963) proposed the idea that the excitation waves or action potentials in higher plants could be information carriers in intercellular and intracellular communication in the presence of environmental changes. The irritability of plants developed during their evolution and improved as adaptation to changes in their environment and the increasingly complicated organization of plants. It has acquired complex forms among the modern higher plants (Abe, 1981; Abe et al., 1980). A plant consists of interconnected cells, tissues, and organs. The integral organism of a plant can be maintained and developed in a continuously varying environment only if all cells, tissues, and organs function in concordance. Plants are continuously balancing with the external world. The coordination of internal processes and their balance with the environment are connected with the excitability of plant cells.

A large amount of experimental material testifies that the main laws of excitability, such as the inducement of nonexcitability after excitation and the summa-

tion of subthreshold irritations, were developed in the vegetative and animal kingdoms in protoplasmatic structures before the morphological differentiation of nervous tissues (Bentrup, 1979; Bertholon, 1783; Davis and Shuster, 1981a,b). These protoplasmatic excitable structures consolidated into the organs of a nervous system and adjusted the interactions of the organism with the environment.

The response reactions of plant tissues and organs can be local or can be transmitted from cell to cell over long distances via the plasmodesmata. Excitation functions as a carrier of information about changes in environmental conditions (Dixon, 1924; Siomons, 1981). Action potentials are signals caused by the depolarization of cellular membrane potentials. Bose (1914) tried to examine the coordinating theme of response reactions of so-called sensitive plants, such as *Mimosa pudica*. He noted that the response reactions of these plants to external effects were not as slow as they seemed at first sight. Bose registered the quickly transmitted reactions by electrophysiological equipment without causing rough damage to the plants.

External mechanical, physical, or chemical irritants act not only at the place of occurrence, but the excitation can also be transferred along the whole plant. The speed of transfer depends on many factors, such as the intensity of the irritation, temperature, chemical treatment, or mechanical wounding, and is also influenced by previous excitations. The excitation reaction proceeds in both directions from the top of a stem to roots and vice versa, but not always at identical rates. The transfer of excitation has a complicated character, accompanied by an internal change in cells and tissues. Bose (1914) has also established the availability of a reflex arch in such plants as *Mimosa pudica*. By being excited, sensor cells generate impulses, which reach motor cells. The character of their distribution depends upon the physiological condition of the plant. The signal from a sunbeam is transmitted to the tissues of a stem at an extremely high speed, and the stem begins to curve toward the source of light. The reflex arch appears. The illuminated top of a stem, being excited, causes an impulse, which is distributed among tissues. When the impulse reaches motor cells, the stem bends. Electrophysiological phenomena are primary, and then deep cytophysiological reactions occur. Of particular concern is the redistribution of biologically active substances. The discovery of hormones in plants was the result of analysis of these phenomena.

Conductive bundles of vegetative organisms not only facilitate the movement of substances but also actuate the transfer of bioelectrical impulses (Gradmann and Mummert, 1980). This phenomenon underlies the coordination of the vital activities of vegetative organisms (Sinukhin and Gorchakov, 1968). The bioelectrical impulses arise under the influence of various chemical compounds (herbicides, salts, water, plant growth stimulants) and physical factors such as mechanical wounding, electromagnetic or gravitational fields, and temperature effects (Fig. 13.1, Table 13.1).
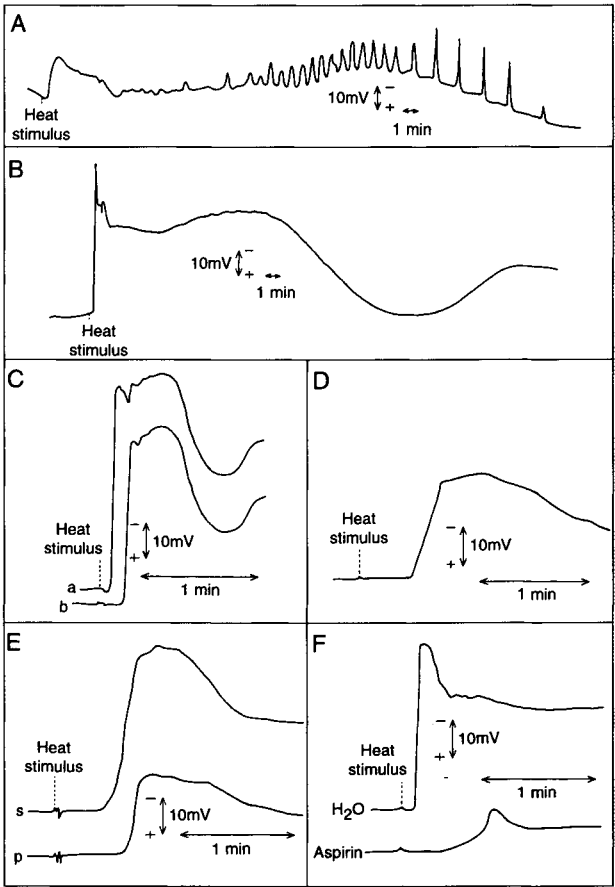
Figure 13.1 (A) Intact tomato plant with heat (from a flame) applied to the tip of the terminal leaflet for 5 s. Recording on the petiole using a wick electrode with a Ag/AgCl reference electrode located in the compost. (B) Excised tomato shoot with heat (from a metal block heated in a boiling water bath) applied to the tip of the terminal leaflet. Recording on the petiole using a thread electrode with a calomel reference electrode connected by a salt bridge to the bath solution (C–E) Intact tomato plants with heat (from a metal block heated in a boiling water bath) applied to the tip of the terminal leaflet. (C) Recording on the petiole using two thread electrodes located approximately 28 mm apart and a Ag/AgCl reference electrode located in the compost. Electrical response was seen first at the electrode nearer to the site of stimulus and then at the electrode farther from the stimulus site. (D) Recording on the stem with a Ag/AgCl reference electrode located in the compost. (E) Recording on the stem and on the petiole using a thread electrode with a Ag/AgCl reference electrode located in the compost. (F) Excised tomato shoots, one with its cut end in distilled water (pH 5.5) and the other with its cut end in 2 m*M* aspirin (pH 5.5). Heat (from a metal block heated in a boiling water bath) was applied to the tip of the terminal leaflet. Recording on the petiole using a thread electrode with a calomel reference electrode connected by a salt bridge to the bath solution (Wildon *et al.,* 1989). Reproduced by permission of Annals of Botany Company.

Table 13.1

**Comparative Characterization of the Action Potentials Spreading
in the Acropetal Direction in Various Plants upon Heat Stimulation[a]**

Plants	Site of stimulation	Latent period (sec)	Mean amplitude of action potentials (mV)	Speed of propagation of action potentials (cm/min)
Sunflower, *Helianthus annus* L.	Leaf	3.2 ± 0.3	24.4 ± 2.4	161.0 ± 7.4
Buckwheat, *Fagopyrum sagittatum*	Leaf	6.2 ± 0.4	19.5 ± 3.0	69.4 ± 7.1
Gilib Bean, *Phaseolus multiflorus*	Leaf	4.7 ± 0.2	27.0 ± 2.6	38.4 ± 4.1
Wild Pumpkin, *Cucurbita pepo* L.	Leaf	4.2 ± 0.2	25.3 ± 1.9	62.5 ± 6.0
Bean, *Phaseolus multiflorus*	Root system	21.4 ± 3.2	22.0 ± 3.4	31.2 ± 0.0
Wild Pumpkin, *Cucurbita pepo* L.	Root system	4.7 ± 0.8	8.5 ± 1.3	45.4 ± 8.7

[a] From Sinukhin and Gorchakov (1966a).

The generation and propagation of action potentials and electrical impulses between the tissues in higher plants can be measured by reversible, nonpolarizable electrodes. Impulses take an active part in the expedient character of the response reactions of plants as a reply to external effects. These impulses transfer a signal about the changes in conditions in a conducting bundle of the plant from the root system to the point of growth and vice versa. Action potentials are now found in many plants, such as beans, bindweed, *Solanaceae,* tomato, cucumber, potato, and buckwheat. The generation of action potentials is used for the transfer of information and the response reaction occurs: the leaf is folded up and lowered under the influence of an external effect.

A number of plants can eat insects. These plants are called insectivorous. Examples include the *Drosera, Dionaeva* (Williams and Pickard, 1972a,b), Venus flytrap, pitcher plants, sundew, and bladderworts. Insectivorous plants are most often found in moist and nutrient-poor habitats. The insects, which the plants trap, provide mineral nutrients. The amazing speeds of electrical impulses are illustrated by the capture of insects by these plants and by tropism. Action potentials in the plants that do not process motor activity are similar in their characteristics to the action potentials of "sensitive" plants of the *Mimosa pudica* and insectivore type, such as *Drosera rotundifolia* and *Dionaea muscipula,* and the cells of algae *Nitella* and *Chara* (Fromm and Eschrich, 1988, 1989a,b; Fromm and Spanswick,

1993; Sinukhin and Gorchakov, 1966a,b; Williams and Pickard, 1980; Zimmer-man and Beckers, 1978).

The most rapid methods of long-distance communication between plant tissues and organs are bioelectrochemical and electrophysiological signals (Volkov and Haack, 1995a,b). The effectiveness of such long-distance communication is clear as plants can rapidly respond to external stimuli (e.g., changes in temperature, osmotic environment, or illumination level, wounding, cutting, mechanical stimu-lation, water availability) and changes can be detected in distant parts of the plant soon after the injury. Wounding stress is accompanied by the rapid long-distance propagation of electrochemical signals, known as action potentials, which switch on the membrane enzymatic systems that initiate biochemical reactions, accelerate ethylene synthesis, increase the concentration of proteinase inhibitor, and decrease or increase the formation of polysomes and protein synthesis. Action potentials have been induced in higher plants by cold or heat shock (Bose, 1926, 1927a; Davies *et al.*, 1991; Jones and Wilson, 1982; Volkov and Haack, 1995a,b; Wildon *et al.*, 1989, 1992), wounding (Frachisse and Desbiez, 1989; Malone and Stan-kovic, 1991; Van Sambeek and Pickard, 1976; Van Sambeek *et al.*, 1976; Volkov and Haack, 1995a,b), chemical treatment (Bose, 1926, 1927a, 1964; Davies, 1987a,b; Fromm, 1991; Gunar and Sinukhin, 1963; Jones and Wilson, 1982; Kursanov, 1984; Pickard, 1973, 1984b; Sinukhin and Britikov, 1967; Volkov and Haack, 1995a,b; Wildon *et al.*, 1989, 1992), and a change in the orientation of gravitational or magnetic fields.

Physiological mechanisms for rapid long-distance communication between plant tissues and organs, particularly in response to external stimuli, are poorly understood (Greppin *et al.*, 1991). The translocation of phytohormones or other endogenous organic and inorganic compounds has been traditionally viewed as the primary means of signaling between stimulated and specific remote tissues in the plant where physiological responses are observed. A significant limitation of communication systems involving the transport of chemical compounds is the relatively slow response kinetics. Many systemic physiological responses within higher plants are known to occur within seconds of treatment with specific stimuli (Sibaoka, 1962, 1969, 1980).

The velocities of the propagation of electrical signals that have values from 0.05 to 20 cm/s (Bose, 1914, 1925, 1926, 1927a,b; Burdon-Sanderson, 1873, 1882, 1888; Burdon-Sanderson and Page, 1876; Davies, 1987a,b; Davies *et al.*, 1991; Edwards and Pickard, 1987; Eschrich *et al.*, 1988; Opritov and Pyatygin, 1989; Opritov *et al.*, 1992; Pickard, 1973, 1984a; Pyatygin and Opritov, 1990, 1992; Pyatygin *et al.*, 1989, 1992; Raven, 1987; Volkov and Haack, 1985a,b; Wildon *et al.*, 1989, 1992) are sufficiently high to facilitate rapid long-distance communication and to account for the rapid response phenomena observed in plants. Both the speed of propagation and the amplitude (5–70 mV) of action

potentials depend on the type of external stimulus (Kursanov, 1984; Pickard, 1973; Sinukhin and Britikov, 1967; Volkov and Haack, 1995a,b,).

Fromm and Bauer (1994) found that action potentials in maize sieve tubes change phloem translocation. By using macro- and microautoradiography in mature leaves of maize, Fromm and Bauer (1994) studied the inhibition of phloem translocation caused by electric and cold shock. They stimulated the leaf tip with ice water and found that the velocity of signal transmission was 3–5 cm/s, whereas the microelectrode recorded a basipetally propagating action potential with a depolarizing amplitude of 80 mV in the sieve tubes (Fig. 13.2). During electrical stimulation, an action potential with a speed of 5 cm/s was measured in the sieve tube system.

The action potential propagates rapidly throughout the plant (Volkov and Haack, 1995a). Phloem consists of two types of conducting cells, the characteristic type known as sieve tube elements and another type called companion cells. Sieve tube elements are elongated cells that have end walls perforated by many pores, through which dissolved chemical compounds can pass. Companion cells are found next to the sieve tube elements and are believed to control the conduc-
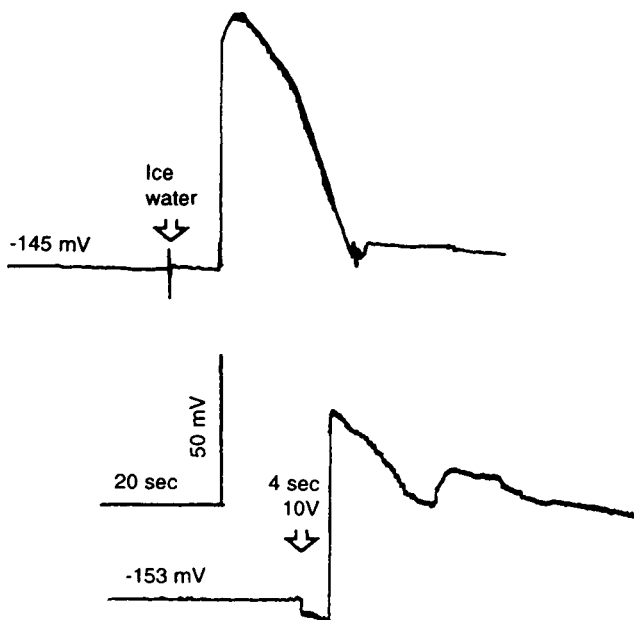
Figure 13.2   Measurements of intracellular potentials in sieve tubes of maize via severed aphid stylets. Stimulation by ice water (top) and electric shock (bottom) evoked action potentials that were propagated at a velocity of 3–5 cm s^{-1} in a basipetal direction (Fromm and Bauer, 1994). Reproduced by permission of Oxford University Press.

tion process in the sieve tubes. A potential pathway for transmission of this electrical signal might be the phloem sieve tube system because it represents a continuum of plasma membranes (Kursanov, 1984). Phloem is an electrical conductor of bioelectrochemical impulses over long distances (Gunar and Sinukhin, 1963; Sinukhin and Britikov, 1967).

Many systemic physiological responses within higher plants are known to occur within seconds of treatment with specific stimuli: gravitropic responses (Volkmann and Sievers, 1979), thigmotropic responses in *Mimosa pudica* L. and *Dionaea muscipula* Ellis (Burdon-Sanderson, 1873; Pickard, 1973), growth responses to salinity (Matsuda and Riazi, 1981), and stomatal closure following the treatment of *Salix* roots with abscisic acid (Fromm, 1991). At the cellular level in plants, electrical potentials exist across membranes and, thus, between cellular compartments, as well as within specific compartments. K^+, H^+, Na^+, Ca^{2+}, and Cl^- ions represent electrolytic species involved in the establishment and modulation of electrical potentials. Electrical potentials have been measured at the tissue and whole plant levels.

Because electrical potential differences are expressed spatially within biological tissue and are modulated over time, many investigators have postulated the involvement of electrical potentials in inter- and intracellular communication (Bose, 1925, 1926, 1964; Burdon-Sanderson, 1873, 1882, 1888; Burdon-Sanderson and Page, 1876; Davies, 1987a,b; Du Bois-Reymond, 1848; Pickard, 1973; Roberts, 1992) and, thus, in the regulation of such physiological plant processes as phloem unloading (Fromm, 1991). Action and resting potentials represent the primary candidates for signaling between cells because they can be rapidly induced and transmitted within plant tissue. Specificity of communication can be achieved through modulation of the amplitude, duration, direction of polarity change, and rate of propagation of the electrical potential signal.

The ability of a given stimulus to elicit electrical signals in plants and perhaps even the extent of receptor tissue response to the electrical signal are influenced by the physiological conditions of the plant and plant species (Pickard, 1973; Schroeder and Hendric, 1989). Zavadzki *et al.* (1991) showed that many electrophysiological parameters are highly variable within higher plants, including the excitability state, excitability threshold, velocity of impulse movement, and length of the refractory period.

Action potentials and resting potentials were measured (Volkov and Haack, 1995a,b) in potato plants (*Solanum tuberosum* L.) under different physiological conditions. External stimuli (e.g., changing temperature, wounding or exposing plant leaves or soil to certain chemical compounds) cause an action potential to be generated and change the resting potential from the original steady state level. The amplitude, polarity, and the speed of action potential propagation depend on the type of external stimulus or stress. The kinetics and amplitude of the resting potential also change depending on the nature of the external stimulus.

Mizuguchi *et al.* (1994) found that the application of DC voltage to a cultured solution accelerates plant growth rate by 30%. The authors considered such an accelerating effect to be related to the stimulation of the ion pumps for growth metabolism. The effect of voltage acceleration was observed only under illumination.

ELECTROCHEMICAL CIRCUITS, CHAINS, AND ELECTRODES

A correctly constructed electrochemical circuit, on the ends of which it is possible to measure an electrical potential difference, must always have metals or conductors with identical chemical composition (Fig. 13.3). It is usually achieved by the simple connection of two metals, Me(1) and Me(2), by copper wires. The inclusion of a third metal conductor between these two metals according to Volta's law does not change the difference in potentials at the circuit output. The difference in potentials of an electrochemical circuit at equilibrium is caused by the change in Gibbs free energy during the appropriate electrochemical reaction:

$$E = -\Delta G/nF, \qquad (13.1)$$

where $F = 96,500$ C is the Faraday constant and n is the number of electrons. The difference in electrical potentials of an electrochemical circuit at equilibrium (E) is the electromotive force (EMF). The value of nFE characterizes the maxi-
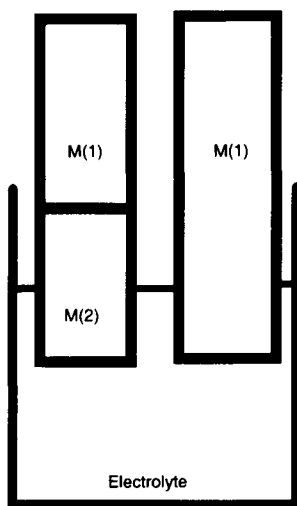
Figure 13.3   The electrochemical cell

mum electrical work that can be received through an electrochemical circuit. Equation (13.1) is the basis for calculation of the Gibbs free energy for different electrochemical reactions. The electrode potential at a given temperature and pressure is determined by the magnitude of the standard electrode potential and the activities of the substances taking part in the electrode reaction. The standard potential is a constant that is specific for each electrode, whereas the activities of the reacting species may be different, depending on the concentration of the reaction medium (Felle and Bertl, 1986).

The classification of electrodes is based upon the chemical nature of the substances participating in the electrochemical process. Electrodes of the first type are systems in which the reduced forms are metals forming the electrodes and oxidized forms are ions of the same metal. Electrodes of the second type are systems in which the metal is covered by a layer of low-solubility salts (or oxide), and the solution contains anions of these salts (for oxide ions OH^-). The Nernst equation for electrodes of the second type can be written as

$$E = E^\circ - \frac{RT}{nF} \ln a_{A^{n-}},\qquad(13.2)$$

where E° is the standard potential of the second kind of electrode. As follows from Eq. (13.2), electrodes of the second kind are anions reversible. The potential of an electrode of the second kind depends on the anionic activity of the sparingly soluble compound of the electrode material. The values of the potentials of electrodes of the second kind are readily reproducible and stable. These electrodes are often employed as standard half-cell or reference electrodes with respect to which the potentials of other electrodes are measured. Of greatest interest in practice are silver–silver chloride, calomel, mercury–mercurous sulfate, mercury–mercuric oxide, and antimony electrodes.

Let us consider two examples of electrodes of the second type that are important for plant electrophysiology:

1. The silver chloride electrode $Cl^-/AgCl$, Ag with the electrode reaction:

$$AgCl + e^- \leftrightarrow Ag^+ + Cl^-.\qquad(13.3)$$
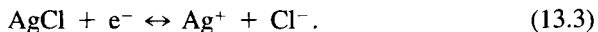
2. The calomel electrode Cl^-/Hg_2Cl_2, Hg with the electrode reaction:

$$Hg_2Cl_2 + 2e^- \leftrightarrow 2Hg + 2Cl^-.\qquad(13.4)$$
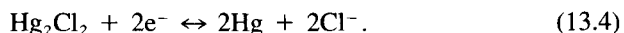
Both such reversible electrodes of the second type have electrode potentials equal to

$$E = E^\circ - \frac{RT}{F}a_{Cl^-}.\qquad(13.5)$$

Silver-silver chloride electrodes are reversible or nonpolarizing (Markin and Volkov, 1990). Ag/AgCl electrodes consist of a piece of silver wire covered with
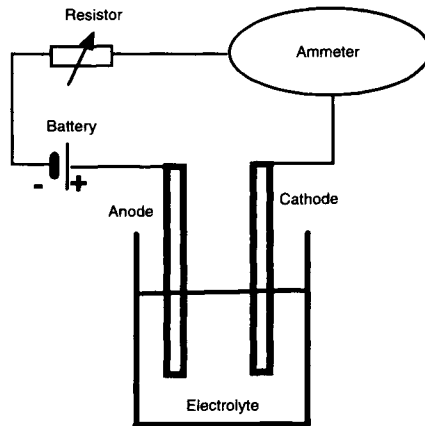
Figure 13.4   The setup for chloridizing a silver electrode.

a layer of silver chloride and immersed in an electrolyte solution containing chloride ions.

Figure 13.4 shows a simple method for the preparation of Ag/AgCl electrodes. The anode should be a clean, high-purity silver wire and the cathode should be a platinum plate. Electrolytes could be, for example, 0.05 M KCl, HCl, or NaCl. Electrical current in the cell is limited to 1 mA/cm^2 of the anode surface. Because Ag/AgCl electrodes are photosensitive, it is better to produce them in the dark. Ag/AgCl electrodes are initially unstable. Stabilization can be accomplished by placing two electrodes in a 0.05 M KCl solution for 24 hr and connecting a short circuit between them. Ag/AgCl electrodes should be stored in the dark and protected from light while in use.

A saturated calomel electrode consists of a mercury electrode in contact with a solution saturated with respect to both mercurous chloride and potassium chloride. The calomel electrode has a constant and reproducible potential.

Ag/AgCl and saturated calomel electrodes are sensitive to temperature (Fig. 13.5) and should be maintained at constant temperature.

Lucas and Kochian (1984) described an approach utilizing microelectrode techniques for the study of electrochemical phenomena in plants.

MEASUREMENT OF ACTION AND RESTING POTENTIALS IN PLANTS

An example of the experimental setup for the measurement of action and resting potentials is shown in Fig. 13.6. All electrochemical measurements can be conducted at constant temperature inside a Faraday cage mounted on a vibration-
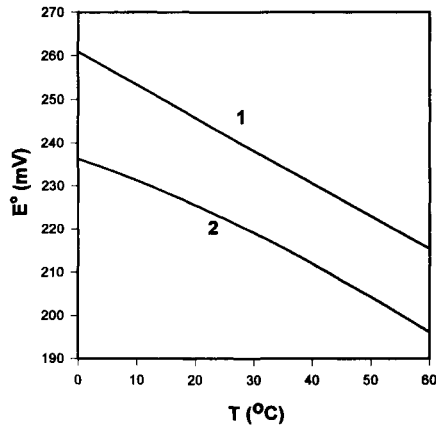
Figure 13.5 Temperature dependence of the standard potential of the saturated calomel electrode (1) and the Ag/AgCl electrode (2).

stabilized table in a laboratory (Fig. 13.6). Reversible electrodes, such as Ag/AgCl or calomel, can be connected to a programmable electrometer with high input impedance (greater than 200 TΩ). A microcomputer with a multiple input–output plugin data acquisition board (for example, Keithley MetraByte DAS-8pga or DAS-1601) can be interfaced with the electrometer and used to record digital data. When multiple electrode pairs (measuring and reference) are monitored simultaneously on a plant, each electrode pair should be connected to a separate electrometer and interfaced with the computer.
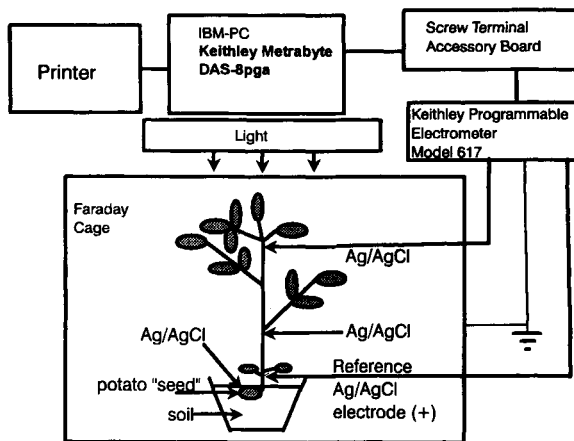
Figure 13.6 The arrangement of Ag/AgCl electrodes in the stem and potato seed.

   Action potentials, induced by mechanical wounding, have been measured by Volkov and Haack (1995a,b) in the stem tissue of potato plants using a few Ag/AgCl electrodes and an amplifier recording system. To measure electrical signal transmission through the phloem tissue, changes in the potential differences over time can be determined as follows. A few Ag/AgCl electrodes should be inserted in the plant at different positions at least 2 hr before electrical measurements to ensure that a steady state level of resting potential is reached. Insertion of the electrodes in the plants induces an action potential across the stem. After approximately 1–2 hr the resting potential stabilized and spikes in the potential–time dependence disappeared. In measurements of voltage between different electrodes in the plant, Volkov and Haack (1995a,b) did not change positions of the inserted electrodes but switched the electric contact between the electrometer and different electrodes. Because insertion of the electrodes elicited a wound response, each plant to be measured was allowed to stabilize for a minimum of 2 hr before treatment. Following insertion of the electrodes, the plants were allowed to rest until a stable potential difference was obtained between the measuring and reference electrodes. For characterization of the electrical signals, including the amplitude, duration, and velocity of propagation, one pair of electrodes was spaced 2 cm apart at an apical position on the stem axis but subtending the leaf to be treated, while a second set of electrodes was positioned at an equidistant spacing on a more basal region of the stem. The apical set of electrodes could also be inserted into the petiole of the leaf under investigation.

ACTION AND RESTING POTENTIALS IN POTATO PLANTS (*SOLANUM TUBEROSUM* L.)

   The cells of many biological organs generate an electrical potential that may result in the flow of electric current. Electrical impulses may arise spontaneously or they may result from stimulation; once initiated, they can propagate to adjacent excitable cells. The change in transmembrane potential creates a wave of depolarization, or action potential, that affects the adjoining, resting membrane. Thus, when the phloem is stimulated at any point, the action potential is propagated over the entire length of the cell membrane and along the phloem with a constant voltage. Once initiated, the action potential has a stereotyped form and an essentially fixed amplitude—an "all or none" response to a stimulus. The propagation of each impulse is followed by the absolute refractory period during which the fiber cannot transmit a second impulse. Excitability returns when the membrane repolarizes.

   Two hours after the insertion of reversible Ag/AgCl electrodes in the stem of a potato plant the difference in electrical potentials between electrodes separated by a distance of 5–10 cm is equal to 30 ± 5 mV (Fig. 13.7a). Insertion of electrodes
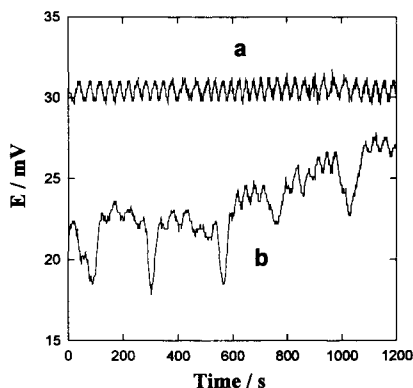
Figure 13.7 Potential difference between two Ag/AgCl electrodes in the stem of a potato plant 2 hr after the insertion of electrodes in the stem before any treatment of the plant (a) and immediately after the insertion of electrodes (b). Frequency of scanning is 1 Hz. Distance between Ag/AgCl electrodes is 5 cm (From Volkov and Haack, 1995b).

in stem, leaf, or tuber (Fig. 13.7b), pinching of a young terminal leaf (Fig. 13.8a), and application of a thermal shock to the terminal leaflet by using a flame (Fig. 13.8b) all result in the propagation of an action potential along the stem, probably via the phloem. The amplitude, duration, and velocity of the propagation of action potentials depend on the external stimulus. Production of the action potential ceases 2 hr after mechanical wounding of plants by inserting electrodes in the stem because a steady state has been established. The potential difference in the potato stem remains stable for many hours if experimental conditions such as temperature, humidity, or illumination are not changed. In the absence of illumination at night the resting potential dropped to a level of 15–20 mV, but returned to the level of 30 mV in the morning. If artificial illumination was used during the night, the steady state potential difference did not drop.

Action potentials are the most extensively studied forms of potential electrical signals in plants (Hejnowicz *et al.,* 1991; Hope and Walker, 1975; Huang *et al.,* 1992). They are characterized as being of short duration, relatively constant amplitude, and propagated at high velocities within plants (Davies *et al.,* 1991). Resting potentials are of longer duration, higher magnitude, slower velocity, and more variable in response to stimuli than action potentials (Davies *et al.,* 1991). Thus, resting potentials are thought to involve larger changes in ion flux and recompartmentation and to have a greater potential for influencing physiological processes in receptor tissues. Roblin (1985) concluded that resting potentials are ubiquitous in herbaceous plants.

Measured velocities for the transmission of action potentials that have been reported include 20 (Burdon-Sanderson, 1873, 1882, 1888; Burdon-Sanderson
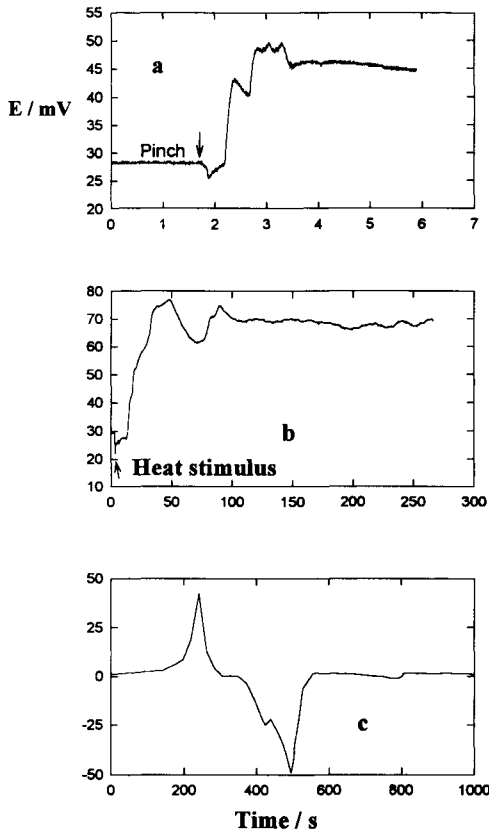
Figure 13.8   Resting and action potentials of a potato plant after (a) pinching along the midrib in the center of the young terminal leaflet by forceps; (b) thermal shock of the terminal leaflet by a flame; (c) single spraying of 0.3 ml of a 1 mM aqueous solution of pentachlorophenol. The soil around the plant was treated with water every day. Distance between Ag/AgCl electrodes is 5 cm (a), 5 cm (b), and 9 cm (c) (Volkov and Haack, 1995a). Reproduced by permission of Elsevier Sequoia S.A.

and Page, 1876) and 0.5 cm/s in *Drosera* (Williams and Spanswick, 1972), 1.8 cm/s following cold stimulation in *Cucurbita pepo* (Pickard, 1973), 0.05–0.08 cm/s in etiolated pea plants that were wounded (Davies, 1987a,b), up to 10 cm/s via sieve tubes in *Cucurbita pepo* (Eschrich *et al.*, 1988,1994), and 0.1–0.6 cm/s in response to wounding (Van Sambeek and Pickard, 1976; Franchisse and Desbiez, 1989; Wildon *et al.*, 1989).

Malone and Stankovic (1991) concluded that hydraulic signals, pressure waves, can also elicit changes in the apoplasmic electrical potential similar to resting potentials within shoot tissue due to altered ion flux rates from the symplast. It was hypothesized that ion fluxes associated with stomatal opening or closing may dominate the electrical activity in leaves (Edwards *et al.*, 1988; Malone and Stan-

kovic, 1991). The surface potentials measured by Malone and Stankovic (1991) in response to heat wounding were erratic and highly variable from plant to plant.

The speed of the propagation of action potentials in potato plants also depends on the external stimulus. The action potential speed induced by pinching the terminal leaflet of a potato plant is equal to 7 ± 2 cm/s (Volkov and Haack, 1995a). The speed of propagation of the action potential induced in the terminal leaflet by thermal shock is equal to 0.7 ± 0.2 cm/s (Volkov and Haack, 1995b).

The effect of chemical treatment of potato leaves by pentachlorophenol, which is known to be a protonophore or uncoupler (Yaguzhinsky *et al.,* 1975), was studied by Volkov and Haack (1995a,b). After a single spray of 0.3 ml of 1 mM aqueous solution of pentachlorophenol on potato leaves, the potential difference between two silver chloride electrodes, inserted in the stem and separated by a distance of 9 cm, decreases monotonously during 1 hr from 30 to 0 ± 3 mV and has a steady state zero value for at least a couple of days. The potato plant treated with pentachlorophenol generates an action potential with an amplitude of 40 ± 10 mV at the zero resting potential every 2 ± 0.5 hr over a period of 2 days and nights (Fig. 13.8c). The speed of propagation of the action potential induced by pentachlorophenol in the potato plant is very slow, approximately 0.05 cm/s.

Plants require all of the essential ingredients of photosynthesis to construct the necessary compounds and structures. Water is especially important, because cell enlargement is the result of internal water pressure (turgor) extending the walls. Water generally moves into a plant through its roots. The water inside a plant creates pressure against the cell walls called turgor. Most plants require large quantities of water to grow and reproduce. Turgor causes expansion of the cell wall and stimulates cell growth. It also keeps cells rigid and so enables the plant to remain upright. Loss of water, and consequently turgor, from plant cells causes the entire plant to wilt.

If the soil is sufficiently wet, the further addition of water to the soil or spraying of water on the leaves does not result in the generation of action potentials or any essential change in the resting potential (Fig. 13.9a). If the soil had not been watered for a few days, the water stress of the plant was deserved. After the addition of water to the soil surrounding the plant or the spraying of 0.3 ml of water on the leaves, action potentials with amplitude 7 ± 2 mV were generated over a period of 20–30 min (Fig. 13.9b). The speed of propagation of electrical signals is sufficiently high to facilitate rapid long-distance communication and account for the rapid response phenomena ovserved in plants.

INSECT-INDUCED BIOELECTROCHEMICAL SIGNALS IN POTATO PLANTS

Volkov and Haack (1995a) were the first afforded a unique opportunity not only to investigate the role of electrical signals induced by insects in the long-
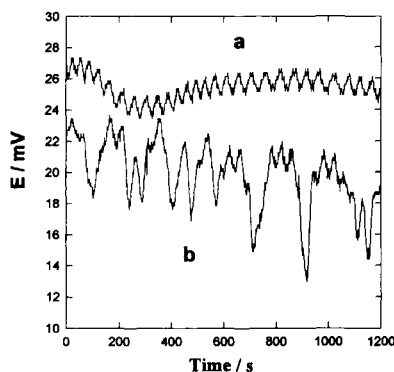
Figure 13.9   Potential difference between two Ag/AgCl electrodes in the stem of a potato plant mea-
sured after (a) spraying of leaves with 0.3 ml of distilled water (the soil was treated with water every
day) and (b) adding 50 ml of distilled water to dry soil (the soil in the plant pot was not treated with
water for 2 days). Frequency of scanning is 1 Hz. Distance between Ag/AgCl electrodes is 5 cm (From
Volkov and Haack, 1995b)

distance communication of plants but also to confirm the mechanism by which
electrical signals can directly influence both biophysical and biochemical pro-
cesses in remote tissues.

   Action and resting potentials were measured in potato plants (*Solanum tuber-
osum* L.) in the presence of leaf-feeding larvae of the Colorado potato beetle [*Lep-
tinotarsa decemlineata* (Say); Coleoptera: Chrysomelidae]. When the larvae were
allowed to consume the upper leaves of the potato plants, after 6–10 hr action
potentials with amplitudes of 40 ± 10 mV were recorded every 2 ± 0.5 hr during
a 2-day test period. The speed at which insect-induced action potentials moved
downward through the stem was about 0.05 cm/s. The resting potential decreased
from 30 mV to a steady state level of 0 ± 5 mV. This drop in resting potential
appeared similar to the effect that known protonophores such as pentachlorophe-
nol (PCP) have on the potato plant. When the upper leaves of potato plants were
sprayed with 0.3 ml of a 1 m*M* aqueous solution of pentachlorophenol, the effect
was nearly identical to that induced by the Colorado potato beetle.

   Figure 13.10 shows that positive spikes and negative humps appear during
measurement of the electrical potential difference between two reversible silver
chloride electrodes. High-resolution analysis of more short time intervals shows
that these spikes are action potentials (Figs. 13.11 and 13.12). The action potential
induced by the Colorado potato beetle in potato plants propagates slowly, and
hence the speed of propagation can be measured with two Ag/AgCl electrodes.
The action potential propagates from plant leaves with Colorado potato beetles
down the stem (Fig. 13.11 a–c) to the potato tuber (Figs. 13.11d and 13.12). The
action potential induced by the Colorado potato beetle on the young terminal leaf
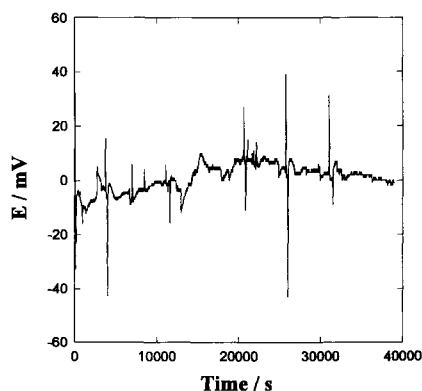
Figure 13.10 Potential difference between two Ag/AgCl electrodes in the stem of a potato plant in the presence of five Colorado beetles on the leaves of the plant. Frequency of scanning is 0.07 Hz. Distance between Ag/AgCl electrodes is 10 cm.
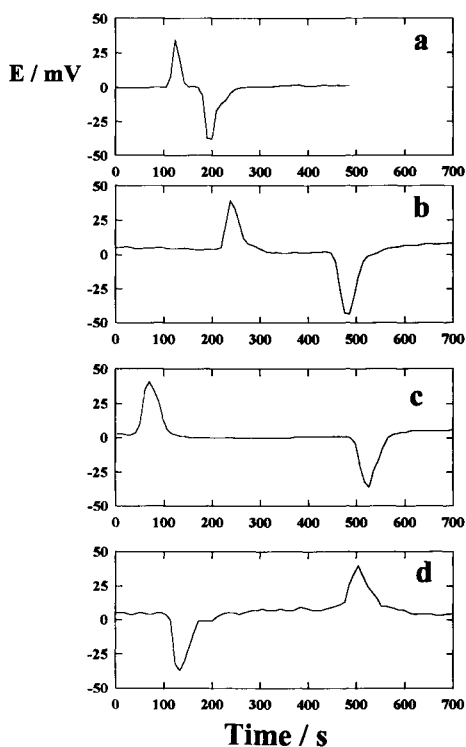
Figure 13.11 Action potential in the stem of a potato plant in the presence of Colorado beetles on young terminal leaves of the plant. Distance between electrodes is (a) 3.5 cm, (b) 12 cm, (c) 22 cm, and (d) 20 cm. The reference Ag/AgCl electrode was inserted in the stem between cotyledons. The working Ag/AgCl electrode was inserted in the stem (a–c) or in the potato seed (d) (Volkov and Haack, 1995a). Reproduced by permission of Elsevier Sequoia S.A.
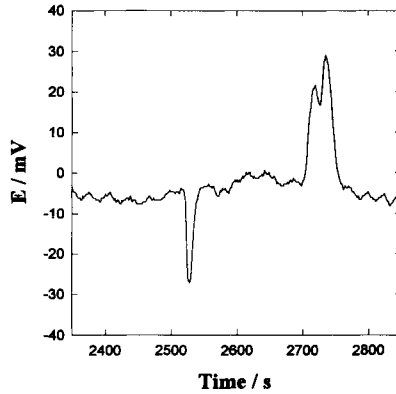
Figure 13.12   Potential difference between two Ag/AgCl electrodes in the presence of five Colorado beetles on leaves of the plant. The reference Ag/AgCl electrode (+) was inserted in the stem of the potato plant and the second Ag/AgCl electrode was immersed in the potato seed, as shown in Fig. 13.6. Frequency of scanning is 0.07 Hz. Distance between Ag/AgCl electrodes is 10 cm.

reaches a working electrode in the plant stem, which changes its potential relative to the reference electrode. Hence, it is possible to measure the peak potential of the working electrode compared to the reference electrode. The action potential slowly propagates along the stem and after some time reaches the reference electrode, which gives a mirror image of the potential peak with opposite sign from that of the first peak (Figs. 13.10–13.12) because during this process the potential of the reference electrode changes relative to that of the working electrode.
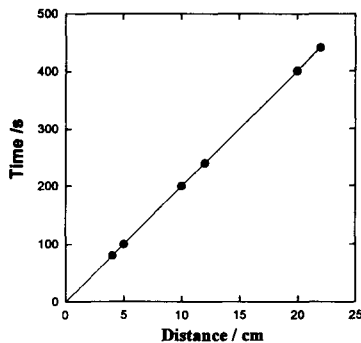
Figure 13.13   The time dependence between positive and negative action potential peaks induced by Colorado potato beetles on the distance between electrodes. A few electrodes were immersed in the potato seed and different parts of the plant stem 2 hr before measurement of the potential difference (Volkov and Haack, 1995a). Reproduced by permission of Elsevier Sequoia S.A.

The speed of propagation of the action potential does not depend on the location of the working electrode in the stem of the plant (Figs. 13.11 a–c) or in the tuber (Figs. 13.11d and 13.12) or on the distance between the working and reference electrodes (Fig. 13.12). The speed of propagation of the action potential induced by the Colorado potato beetle can be determined from the slope of the dependence of the time interval between peaks on the distance between electrodes (Fig. 13.13) and is about 0.05 cm/s.

A similar effect of slow action potential generation was observed after a terminal leaflet was sprayed with a protonophore such as pentachlorophenol. In contrast, when an upper leaf was wounded mechanically by pinching, single action potentials with amplitudes of 3–4 mV were generated with a propagation velocity in the stem of 7 cm/s. Therefore, response of the potato plant to insect feeding appears to have more similarities with that induced by a protonophore than that induced by simple mechanical wounding. This suggests the presence of a protonophore-like substance in the saliva and/or feces of the Colorado potato beetle.

The automatic measurements of the electrical potential difference can be used effectively in plant electrophysiology for the study of molecular mechanisms of ion transport, the influence of external stimuli on plants, and the bioelectrochemical aspects of the interaction between insects and plants.

This Page Intentionally Left Blank

Chapter 14

Artificial Photosynthesis in Organized Assemblies of Photosynthetic Pigments

INTRODUCTION

Photosynthesis is the process by which chlorophyll-containing organisms capture solar energy and convert it to electrochemical energy. All energy available for life in Earth's biosphere is made available through photosynthesis.

Light energy is harvested for the biosphere by photosynthetic pigment systems in which the electronic structure of excited-state chlorophyll donates an electron to a primary acceptor, pheophytin, the first component in an electron transport chain. The electron carries with it the energy of the original photon of light that was absorbed, and in the process of electron transport energy is captured in two ways. The first involves coupling of a proton pump mechanism to the sequential redox reactions in one part of the electron transport chain, so that a proton gradient is established across the membrane. The electrochemical energy of the proton gradient is then used to drive ATP synthesis by ATP synthase (Mitchell, 1961; Williams, 1961). The second means of energy capture occurs when an acceptor molecule such as NADP is reduced to NADPH, which in turn is used to reduce carbon dioxide in the Calvin cycle. It follows that systems modeling photosynthesis should have the capability of carrying out relatively simple versions of these fundamental reactions (Volkov *et al.*, 1995a,b).

An understanding of the photosynthetic mechanisms is essential for the successful design of artificial solar energy utilization systems (Bard and Fox, 1995; Lewis, 1995; Zamaraev and Parmon, 1983). The quantum yield of any photochemical reaction first depends on the efficiency of charge separation (Durr *et al.*, 1996; Kotov and Kuzmin, 1990a,b, 1991, 1992, 1996; Volkov, 1984, 1986a–c). It follows that heterogeneous systems (Fig. 14.1) will be most effective in this re-

gard, where the oxidants and reductants are either in different phases or sterically separated (Volkov, 1985, 1986a–c). Furthermore, different solubilities of the substrates and reaction products in the two phases of heterogeneous systems can also shift the reaction equilibrium (Kharkats *et al.*, 1977). The redox potential scale is thereby altered, making it possible to carry out reactions that cannot be performed in a homogeneous phase. If phototransfer of electrons or protons occurs in homogeneous solution, the resulting products usually rapidly recombine and the light energy is converted to thermal energy. The closest to natural photosynthesis are molecular photocatalytic systems at liquid interfaces such as oil–water, micelles, microemulsions, vesicles, bilayers, monolayers, thin films, polymers, and colloids (Fig. 14.1). Comprehensive reviews of artificial photosynthesis in lipid membrane systems have been published by Tien (1974, 1980, 1986, 1989), Krysinski and Tien (1986), and Ottova-Leitmannova and Tien (1993).

In the case of artificial photosynthesis in organized molecular assemblies, the reaction of interest is water photooxidation. The design of systems for this reaction is often based on mimicking the function and structure of natural photosynthesis (Volkov *et al.*, 1995a). Photocatalytic splitting of water is usually a se-
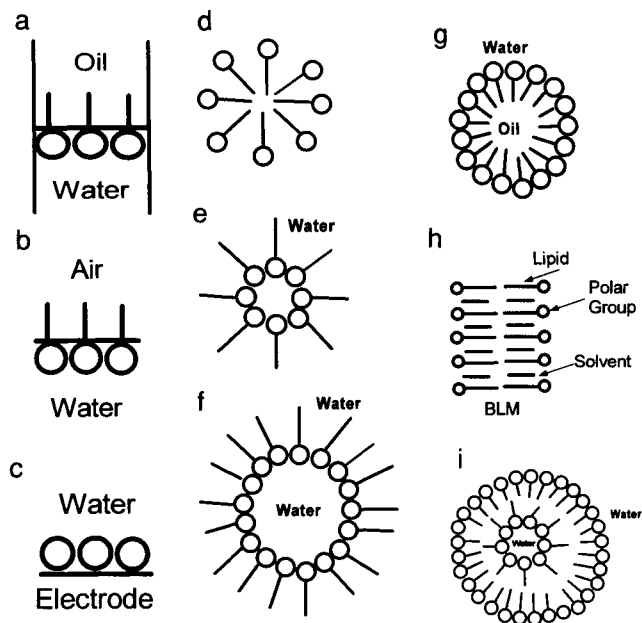
Figure 14.1 Structures or organized molecular assemblies at interfaces: (a) amphiphilic compounds at the oil–water interface; (b) monolayers at the air–water interface; (c) monolayers or thin films at the semiconductor–water interface; (d) micelle; (e) inverted micelle; (f) oil–water microemulsion; (g) water–oil microemulsion; (h) bilayer lipid membrane; (i) vesicle.

quence of three steps. The first is charge separation under the action of solar radiation in the presence of a photocatalyst. Photocatalysts are substances that can induce, by the absorption of light, quantum chemical reactions between the components of a reaction and then regenerate themselves after interaction with the substrates. A strong oxidant and reductant are formed, followed by subsequent catalytic reactions of oxygen evolution that may not necessarily require light. The major problem in this approach is suppressing the recombination of the strong oxidant and reductant, a simple bimolecular process that is very rapid. One way to overcome this problem might be to use heterogeneous photocatalytic systems such as oil–water interfaces or lipid vesicles.

The interface of two immiscible liquids is a widely used example of a heterogeneous system for energy conversion. For instance, fundamental processes of photosynthesis (Volkov *et al.*, 1986, 1991, 1992a,b, 1994), biocatalysis (Volkov and Deamer, 1997; Volkov and Kharkats, 1988), membrane fusion (Volkov *et al.*, 1997a), ion pumping, and electron transport (Casta and Porter, 1977; Brown *et al.*, 1993; Volkov *et al.*, 1982, 1983a–c) have all been investigated in interfacial systems. Extraction of the reaction products and adsorption of the reaction components can establish catalytic properties at interfaces, now recognized as interfacial catalysis (Kharkats and Volkov, 1985, 1987; Volkov and Kharkats, 1985, 1986, 1987). The interface between two immiscible liquids with immobilized photosynthetic pigments can serve as a convenient model for investigating photoprocesses that are accompanied by the spatial separation of charges (Brody and Owens, 1976). The present chapter focuses on electrochemical mechanisms of photocatalytic systems at liquid interfaces.

ARTIFICIAL PHOTOSYNTHESIS AT LIQUID INTERFACES

Although many photochemical reactions of artificial photosynthesis have been studied in homogeneous systems, they are characterized by low quantum yield and low efficiency. Interfacial chemistry, being a highly creative discipline, generates innovative new ideas constantly. Over time, these ideas are incorporated into the corpus of the science, and often subsequently into the technology that drives chemical and biotechnological enterprises. Sometimes, however, a new idea has such innovative force that it sweeps through the discipline like a fast-moving brush fire through dry chaparral. This is the case with artificial photosynthesis at liquid interfaces, a term that describes a very effective type of solar energy conversion that came from nature during chemical evolution on Earth (Deamer and Volkov, 1996; Gugeshashvili *et al.*, 1992; Volkov, 1989; Volkov and Kharkats, 1985).

From thermodynamic and kinetic principles, the interface between two immis-

cible liquids can have catalytic properties for interfacial charge transfer reactions. For example, at the oil–water interface the following redox reaction can occur:
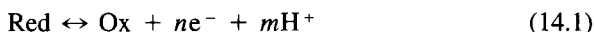
$$\text{Red} \leftrightarrow \text{Ox} + n e^- + m\text{H}^+ \tag{14.1}$$

The electrons that are the products of Eq. (14.1) can be accepted at the interface by another substance if it is dissolved in one of the two phases.

The standard Gibbs energies of Eq. (14.1) for each phase, α and β, are

$$\Delta G_\alpha^\circ = {}_\alpha\mu_{\text{Red}}^\circ - {}_\alpha\mu_{\text{Ox}}^\circ - n\mu_e^\circ - m_\alpha\mu_{\text{H}^+}^\circ \tag{14.2}$$

$$\Delta G_\beta^\circ = {}_\beta\mu_{\text{Red}}^\circ - {}_\beta\mu_{\text{Ox}}^\circ - n\mu_e^\circ - m_\beta\mu_{\text{H}^+}^\circ \tag{14.3}$$

Subtraction of Eq. (14.2) from Eq. (14.3) gives the change in the standard Gibbs energy at the interface, if the electron acceptor is located in only one phase or localized at the phase boundary:

$$\Delta G_\beta^\circ - \Delta G_\alpha^\circ = ({}_\beta\mu_{\text{Red}}^\circ - {}_\alpha\mu_{\text{Red}}^\circ) - ({}_\beta\mu_{\text{Ox}}^\circ - {}_\alpha\mu_{\text{Ox}}^\circ)$$
$$- m({}_\beta\mu_{\text{H}^+}^\circ - {}_\alpha\mu_{\text{H}^+}^\circ) \tag{14.4}$$

or

$$\Delta G^\circ = RT \ln \frac{P_{\text{Red}}}{P_{\text{Ox}}(P_{\text{H}^+})^m} \tag{14.5}$$

where P_i is the partition coefficient of the ith ion:

$$RT \ln P_i = {}_\beta\mu_i^\circ - {}_\alpha\mu_i^\circ \tag{14.6}$$

In the case of an n-electron reaction, the standard redox potential, ΔE°, at the interface is determined by

$$\Delta E^\circ = -\frac{RT}{nF} \ln \frac{P_{\text{Red}}}{P_{\text{Ox}}(P_{\text{H}^+})^m} \tag{14.7}$$

A thermodynamic analysis of redox and mixed potentials at the liquid–liquid interface was published by Markin and Volkov (1987d, 1989b, 1990).

It is possible to shift the redox potential scale in a desired direction by selecting appropriate solvents, thereby permitting reactions to occur that are highly unfavorable in a homogeneous phase. If the resolution energies of substrates and products are very different, the interface between two immiscible liquids may act as a catalyst. The kinetic mechanism underlying the catalytic properties of the liquid–liquid interface was discussed by Kharkats and Volkov (1985, 1987).

PHOTOSYNTHETIC REACTION CENTERS AT THE OIL–WATER INTERFACE

A method for investigating fast photoelectrical phenomena in the presence of photosynthetic reaction centers or pigments at oil–water interfaces suggested by
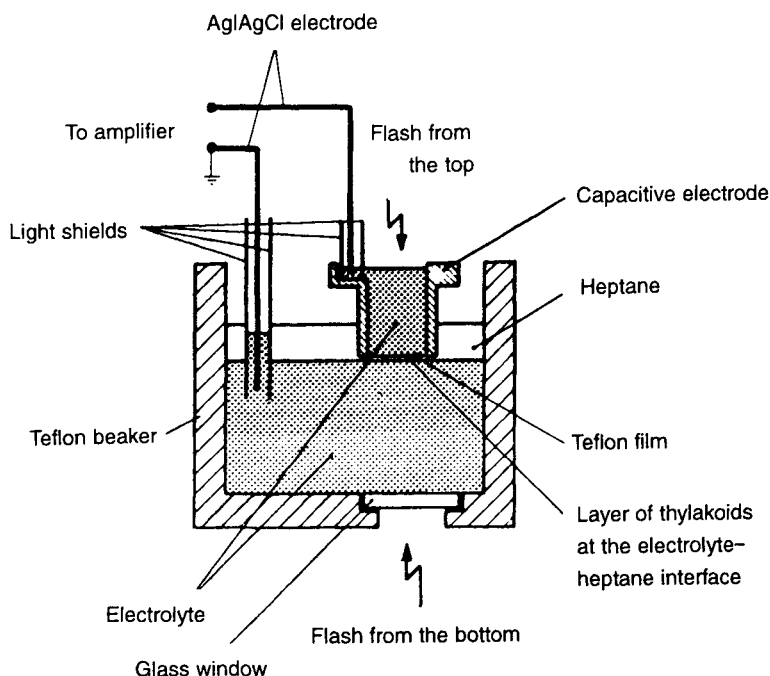
Figure 14.2 Schematic drawing of the capacitative electrode (Trissl and Graber, 1980). Reproduced by permission of Elsevier Science.

Trissl (1980) and Trissl and Graber (1980), who described the construction and electrical properties of a novel capacitative electrode with a wide frequency range (Fig. 14.2). The electrode can measure flash-induced photopotentials in monolayers at the oil–water interface with a sensitivity of 0.05–0.10 mV. The method is based on capacitive coupling of two aqueous compartments separated by a thin Teflon film, and the electrode is placed with its planar bottom about 0.01 mm above the interface. The aqueous subphase and the inner electrolyte are connected with Ag/AgCl electrodes to voltage amplifiers. A schematic representation of the experimental setup is shown in Fig. 14.2. The main advantage of this method is that it can measure rapid electrical signals with nanosecond resolution during photochemical processes at the oil–water interface. Its main disadvantage is that it can only be used in the absence of ions, microemulsions, or a diffuse double layer in the nonaqueous phase. Generally speaking, Trissl's method does not measure interfacial potentials between two phases, but instead monitors rapid light-induced electrochemical effects at the interphase boundary. The physical basis for such effects can vary between systems and must be analyzed carefully before drawing conclusions.

Trissl and Graber (1980) measured the photopotential at the heptane–water

interface in the presence of photosynthetic reaction centers induced by single laser flashes. The photopotential shows characteristics similar to the photosynthetic primary charge separation. Figure 14.3 shows the photopotential at the oil–water interface in the presence of adsorbed chloroplasts or individual photosynthetic pigments. 3-(3',4'-Dichlorophenyl)-1,1-dimethylurea (DCMU), the inhibitor of pho-
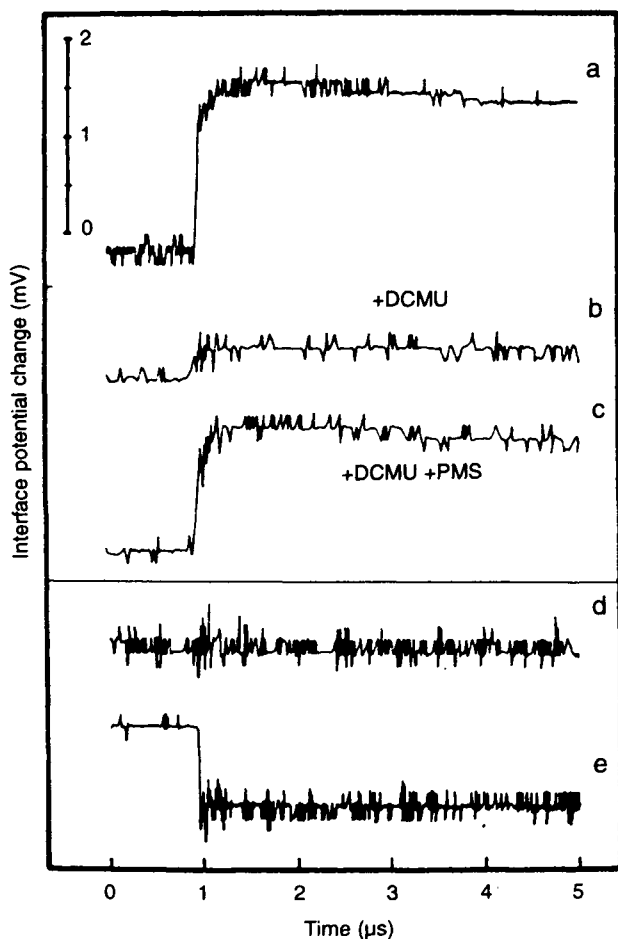
Figure 14.3 Interfacial potential changes induced by single flashes from chloroplasts spread at the heptane–water interface. Signals a–c were recorded 200 ms after a preillumination of 2 s duration with red light ($\lambda = 684$ nm) of intensity 4.5×10^{15} quanta cm^{-2} s^{-1}. (a) Thylakoid membrane layer, aqueous subphase, 10^{-2} M NaCl, pH 5.5. (b) Thylakoid membrane layer, aqueous subphase, 10^{-2} M NaCl, 10^{-5} M DCMU, pH 5.5. (c) Thylakoid membrane layer, aqueous subphase, 10^{-2} M NaCl, 10^{-5} M DCMU, 10^{-4} M PMS, 10^{-2} M ascorbate, pH 5.5. (d) Lutein layer, aqueous subphase, 10^{-2} M NaCl, pH 5.5. (e) Chlorophyll a layer, aqueous subphase, 10^{-2} M NaCl, pH 5.5 electrode (Trissl and Graber, 1980). Reproduced by permission of Elsevier Science.
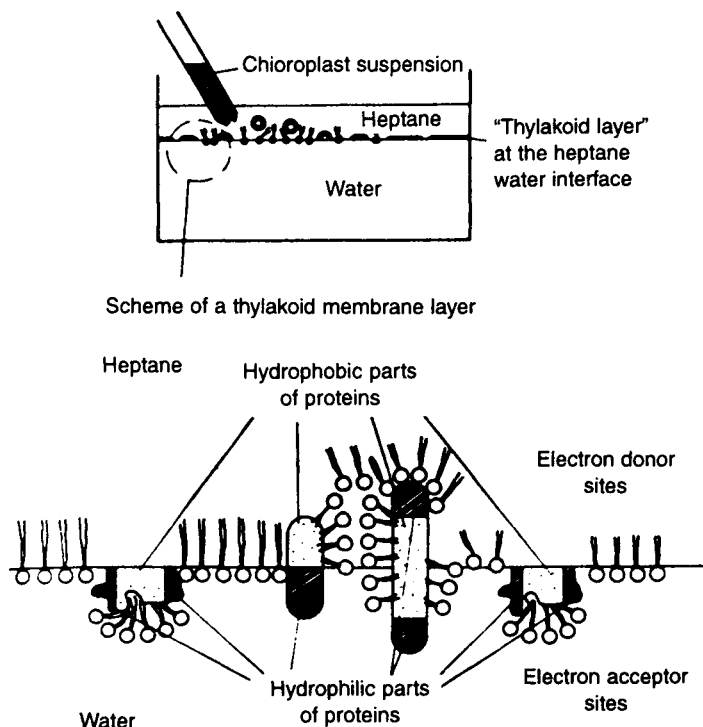
Figure 14.4 Schematic drawing of the spread of chloroplasts at the heptane–water interface and hypothetical structure of the resulting interfacial layer electrode (Trissl and Graber, 1980). Reproduced by permission of Elsevier Science.

tosynthetic electron transport in chloroplasts, decreases the photoeffect (Fig. 14.3). Figures 14.3d and 14.3e show control experiments with monolayers of pure photosynthetic pigments lutein and chlorophyll *a* in the absence of electron donors and acceptors. Figure 14.4 shows the possible structure of the interfacial layer in the presence of chloroplasts at the oil–water interface. Trissl and Graber (1980) concluded that the photopotential in the presence of an adsorbed thylakoid membrane layer at the oil–water interface shows properties similar to those known for the primary photosynthetic process in chloroplasts.

P_{745}: HYDRATED OLIGOMER OF CHLOROPHYLL *A* AT THE OIL–WATER INTERFACE

The photoelectrochemical properties of chlorophyll *a* in monolayers, multilayers, and thin films at oil–water, gas–water, and solid–water interfaces have been

studied extensively to obtain a thorough understanding of their role in the primary events of plant photosynthesis, i.e., light harvesting, energy transfer, and charge separation in the photosynthetic unit. The state of chlorophyll molecules in the photosynthetic apparatus, believed to be in various aggregated forms, is still under active investigation.

Several forms of chlorophyll are involved in the primary events of photosynthesis. Absorbance peaks at longer wavelengths than those characteristic of chlorophyll in solution have been observed *in vivo* and attributed to varying degrees of chlorophyll aggregation (Anderson and Calvin, 1964). Chlorophyll *a* dissolved in anhydrous liquid hydrocarbons (hexane, octane, decane) gives the characteristic absorption spectrum shown in Fig. 14.5 (curve 2). This spectrum does not change if the solution is allowed to contact water for a short time (5 min). However, when chlorophyll *a* is dissolved in water-saturated hydrocarbons, an additional band appears in the absorption spectrum with a maximum between 740 and 745 nm, which reflects the hydrated oligomer of chlorophyll *a* (Fig. 14.5, curve 1). The electronic adsorption spectrum of anhydrous chlorophyll *a* solution shows two bands at 428 and 660 nm, similar to the absorption spectra of chlorophyll *a* in nonpolar solvents. The hydrated oligomer of chlorophyll *a* is characterized by shifts in its absorption spectrum to lower energy wavelengths with maxima at 448 and 745 nm (Helenius *et al.*, 1993, 1994). It is worth noting that the intensity ratio of the blue-to-red adsorption bands is 1.3 for the dry sample and 0.6 after hydration. The differences in the absorption spectra of dry and wet solutions, coupled with marked decreases in the energy of the lowest electronic transition of
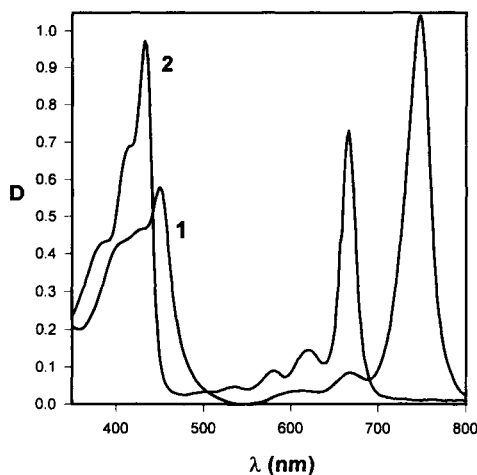
Figure 14.5   Electronic absorption spectra of dry (2) and hydrated (1) chlorophyll *a* in *n*-hexane (Volkov *et al.*, 1993). Reproduced by permission of Elsevier Science.

the hydrated oligomer of chlorophyll a ($\Delta\nu = 1700$ cm^{-1}), show that in water-saturated hydrocarbons chlorophyll a exists as organized aggregates. Such self-organized molecular assemblies of hydrated chlorophyll a molecules are characterized by lower energy electronic transitions with an absorption band between 740 and 745 nm and a fluorescence band at 755 nm. The lifetime of the emission is 0.1–0.2 ns.

Chlorophyll a dissolved in anhydrous hydrocarbon solvents at relatively high concentrations (1–10 mM) also undergoes aggregation to form oligomers. For instance, in hexane at higher concentration ranges, chlorophyll a is present as tetramers and dimers, provided that its concentration is sufficiently high. In the range of chlorophyll a concentrations examined in water-saturated hexane ($<10^{-5} M$), it is present mostly as a mixture of its hydrated oligomers and monomers, as can be inferred from the fluorescence and circular dichroism spectra.

Circular dichroism (CD) spectra of chlorophyll a in water-saturated hexane (Fig. 14.6) have negative bands at 765 nm in the region of the Q_y transition. This suggests that the oligomer consists of at least four or six chlorophyll molecules. The aggregate exhibits a relatively strong optical rotation with a Kuhn anisotropy factor of 0.05 at 748 nm, which is 500 times that of monomeric chlorophyll (Kandelaki *et al.*, 1987, 1988).

Hydrated oligomers of chlorophyll a in n-octane have a narrow, intense dark ESR signal (Fig. 14.7) with a linewidth of 4.7 G (Volkov *et al.*, 1993) and a g value of 2.0025 ± 0.0003. Hydrated oligomers of chlorophyll a in the form of solid colloidal particles have been investigated as well, and it was found that
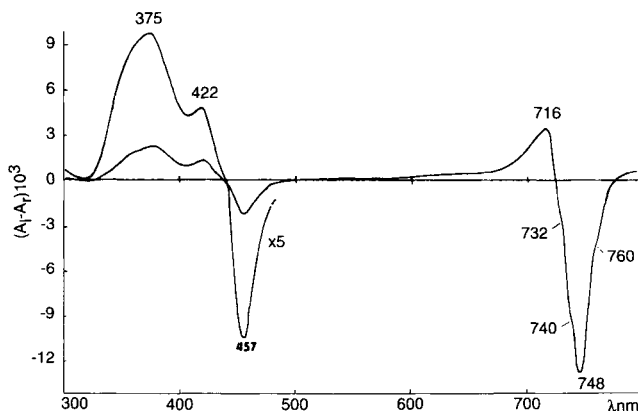
Figure 14.6 Circular dichroism spectrum of chlorophyll a in water-saturated octane. Chlorophyll a concentration in octane is 10^{-5} M, and optical density $A_{742} = 0.27$ (Kandelaki *et al.*, 1987). Reproduced by permission of Elsevier Science.
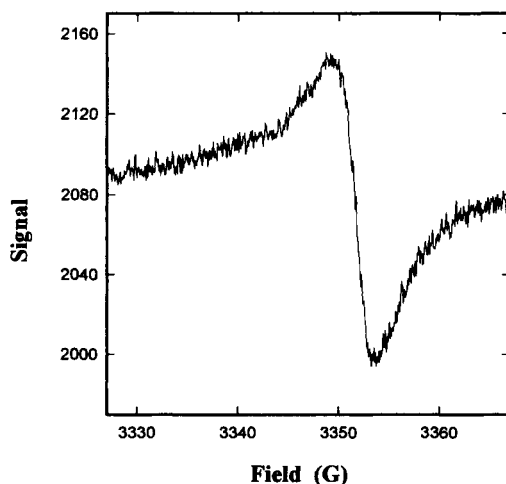
Figure 14.7   X-band ESR spectrum of wet chlorophyll *a* radicals at 298 K. Conditions: microwave power, 20.7 mW; gain, 10^6; time constant, 200 ms. The spectrum is an average of 25 scans (Volkov *et al.*, 1993). Reproduced by permission of Elsevier Science.

colloidal particles of dry and hydrated chlorophyll *a* have different EPR signals. The linewidth for dry chlorophyll *a* was 12 G, while the linewidth for colloidal particles of hydrated chlorophyll *a* was 1.6 (Sherman and Fujimory, 1968), 2–3 (Brody *et al.*, 1960), 6 (Anderson and Calvin, 1963), or 1–14 G (Garcia-Morin *et al.*, 1969) due to different aggregation states of hydrated chlorophyll in solid films or colloidal suspensions. The number of chlorophyll molecules (N) in the cluster of hydrated oligomers of chlorophyll *a* can be found by the following equation (Norris *et al.*, 1971):

$$N = (\Delta H_m / \Delta H_n)^2, \tag{14.8}$$

where ΔH_m is the linewidth of chlorophyll *a* monomer and ΔH_n is the linewidth when the unpaired spin is delocalized over N molecules. It follows from Eq. (14.8), that a hydrated oligomer of chlorophyll *a* in hexane solution consists of six molecules of chlorophyll *a*. CD spectra and surface tension measurements show the same number of molecules in a cluster of hydrated chlorophyll (Markin *et al.*, 1992; Markin and Volkov, 1996; Volkov *et al.*, 1994.

Chlorophyll molecules in monolayers, multilayers, and thin films also form aggregates due to the strong attraction between the pigment molecules in the densely packed monolayer. Results of NMR and IR spectroscopic studies revealed the formation of coordination linkage between the carbonyl group of the chlorophyll molecule and the magnesium atom of another molecule. In densely packed structures such as monolayers or films, thermal vibrations lead to the attenuation

of luminescence due to the overlap of porphyrin ring electron clouds during molecular collisions.

Hydration of chlorophyll oligomers inhibits the expected coordination interaction between carbonyl oxygen and magnesium in chlorine rings:

$$C=O\cdots Mg$$
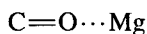
Instead, water molecules are coordinated by the central magnesium atom of chlorophyll:

$$=C=O\cdots H-O-H\cdots O=C=$$
$$\vdots$$
$$Mg$$
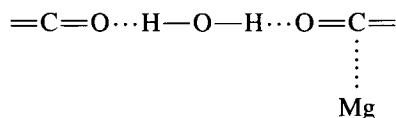
with an adsorption maximum at 720 nm or

$$=C=O\cdots H-O-H$$
$$\vdots$$
$$Mg$$
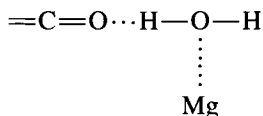
with an adsorption maximum at 740–745 nm.

ARTIFICIAL PHOTORESPIRATION: OXYGEN PHOTOREDUCTION BY MONOLAYERS OF HYDRATED CHLOROPHYLL *A* OLIGOMER

Optically transparent electrodes, modified with monolayers of photosynthetic pigments using the Langmuir–Blodgett technique, are suitable for the investigation of chemical models of photosynthesis (Gugeshashvili *et al.*, 1995; Leblanc *et al.*, 1991; Munger *et al.*, 1992a,b; Volkov *et al.*, 1992a,b, 1993, 1994, 1995a,b; Zelent *et al.*, 1993). The phenomenon of photorespiration by a hydrated chlorophyll *a* monolayer deposited on an optically transparent electrode was studied by Volkov *et al.* (1993). A SnO_2 optically transparent electrode (OTE) doped with antimony is a quasi-metallic conductor. The SnO_2 electrode is transparent in the visible region of the optical spectrum. The SnO_2 OTE is often used as a working electrode in photoelectrochemistry due to its large potential window and its optical transparency in the visible region. By using such an electrode, the electronic absorption spectrum of a wet chlorophyll *a* monolayer on SnO_2 OTE was measured (Fig. 14.8). The oligomer possesses a Soret band at 425 nm and low-energy bands at 664 and 742 nm, while the glass side of the OTE gives absorption maxima at 434, 676, and 744 nm. Under the deposition of one monolayer at the OTE, both forms of chlorophyll *a* (dry and wet) are present.
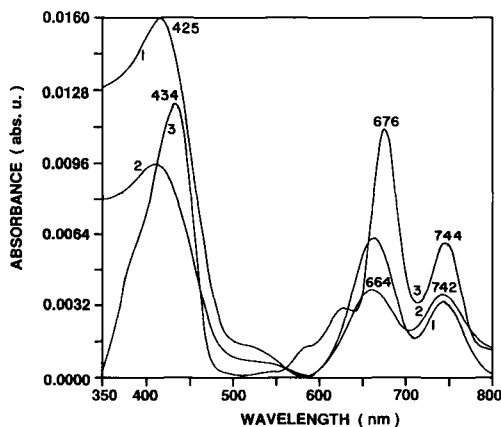
Figure 14.8 Electronic absorption spectra of a wet chlorophyll *a* monolayer on SnO₂ OTE before contact with the electrolyte solution (1), after photoelectrochemical experiments (2), and on the glass side of OTE (3) (Volkov *et al.*, 1993). Reproduced by permission of Elsevier Science.

During illumination of the hydrated oligomers of the chlorophyll *a* monolayer at the SnO_2 OTE in the presence of an artificial electron donor, hydroquinone (QH_2), anodic photocurrents can be measured at voltages between $+200$ and $+50$ mV (Fig. 14.9, curves 1–4). The action spectra under these conditions coincide with the absorption spectrum of a dry chlorophyll *a* monolayer. At more negative polarization of the electrode in the presence of oxygen, cathodic photocurrents are observed. The action spectra of these cathodic photocurrents correspond to the absorption spectra of hydrated oligomers of chlorophyll *a*. Under polarization in the range -50 to -150 mV, both cathodic and anodic photocurrents caused by hydrated and dry chlorophyll *a* appear in the action spectra (Fig. 14.9, curves 5–9). Two types of particles exist in the chlorophyll *a* monolayer: molecules of dry chlorophyll *a* and clusters of hydrated oligomers of chlorophyll *a*. Dry chlorophyll *a* is capable of the phototransfer of electrons from QH_2 to SnO_2 OTE, whereas the hydrated oligomers of chlorophyll *a* can transfer electrons from the SnO_2 electrode to molecules of oxygen in an aqueous solution of the electrolyte. These processes of phototransfer of electrons in opposite directions are caused by the difference in redox potential of dry and wet chlorophyll *a* and by the capability of clusters of wet chlorophyll *a* to undergo synchronous multielectron reactions (Volkov, 1984). If oxygen is carefully removed from the aqueous solution, the cathodic photocurrent disappears (Volkov *et al.*, 1992a,b).

When QH_2 is absent from the aqueous solution initially saturated with O_2 before illumination, only a cathodic photocurrent appears (Fig. 14.10). This results from oxygen reduction by the hydrated oligomers of the chlorophyll *a* monolayer. The cathodic photocurrent is proportional to the O_2 concentration and strongly
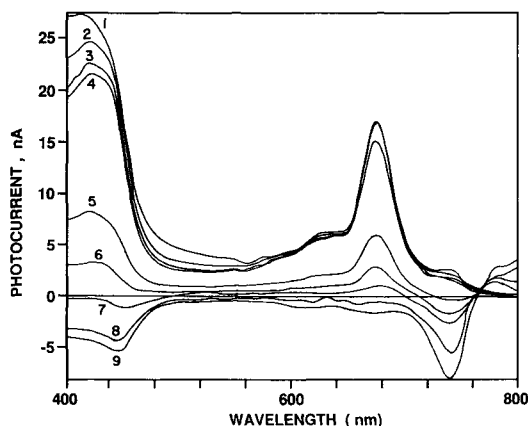
Figure 14.9   Action spectra of a hydrated chlorophyll *a* monolayer on SnO_2 OTE in the presence of hydroquinone. Medium: 0.1 *M* KCl, 0.05 *M* QH_2, 0.025 *M* NaH_2PO_4, pH 6.9. Electrode potentials against a saturated calomel electrode: (1) +200 mV, (2) +150 mV, (3) +100 mV, (4) +50 mV, (5) −50 mV, (6) −100 mV, (7) −150 mV, (8) −200 mV, (9) −250 mV. The aqueous solution was deaerated by argon (Volkov *et al.*, 1993). Reproduced by permission of Elsevier Science.

depends on the electrode potential and wavelength of the incident light. The action spectrum of the cathodic photocurrent coincides with the absorption spectrum of a hydrated oligomer of chlorophyll. The number of electrons transferred through the electrode interface is thousands of times higher than the number of chlorophyll
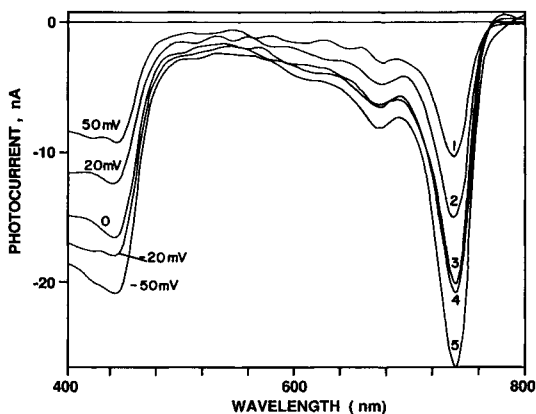
Figure 14.10   Action spectra of a wet chlorophyll *a* monolayer on SnO_2 OTE in the absence of QH_2 in aerobic conditions. Medium: 0.1 *M* KCl, 0.025 *M* NaH_2PO_4, pH 6.9. The aqueous solution was saturated by air (Volkov *et al.*, 1993). Reproduced by permission of Elsevier Science.
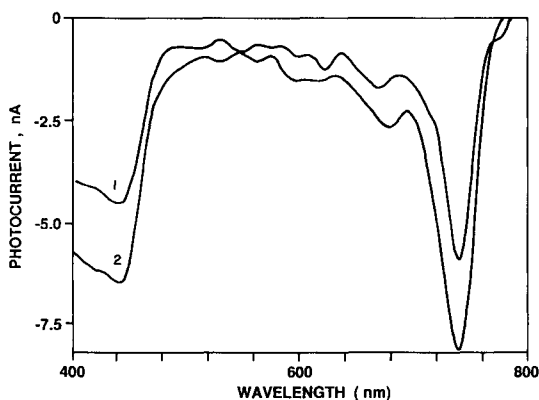
Figure 14.11   Action spectra of a wet chlorophyll *a* monolayer on SnO_2 OTE. Medium: 0.1 *M* KCl, 0.025 *M* NaH_2PO_4, pH 6.9. Electrode potential against saturated calomel electrode was +50 mV. The aqueous solution was initially saturated with argon (1) or air (2) (Volkov *et al.*, 1993). Reproduced by permission of Elsevier Science.

molecules in the monolayer. The absorption spectra of wet chlorophyll before and after the photoreaction coincide. The monolayer of hydrated oligomers of chlorophyll *a* is the photocatalyst of oxygen reduction. The cathodic photocurrent depends on the concentration of oxygen in the aqueous solution (Fig. (4.11).

Quantum efficiency, Θ_λ, for photocurrent generation at wavelength λ was calculated by the following equation:

$$\Theta_\lambda = I_\lambda/qn(1 - 10^{-A_\lambda}), \tag{14.9}$$

where I_λ is the photocurrent density at wavelength λ, q is the elementary charge, n is the number of incident photons, and A_λ is the absorbance of the chlorophyll *a* monolayer in contact with the aqueous solution. By using this relation, the maximum quantum yield of oxygen photoreduction at pH 6.9 and an electrode potential of −50 mV was found to be 0.45 ± 0.05%. If three or five monolayers are deposited on the SnO_2 OTE instead of one, the cathodic photocurrent increases but the quantum yield of oxygen reduction decreases slightly (Volkov *et al.*, 1993).

P_{745}: WATER PHOTOOXIDATION

The ability of light-excited chlorophyll molecules to be involved in reversible redox reactions underlies the primary process by which chloroplasts convert solar energy into electrochemical energy. A few years ago, hydrated oligomers of chlorophyll immobilized on the interface between two immiscible liquids (Boguslavsky *et al.*, 1977; Kandelaki and Volkov, 1991, 1993; Kandelaki *et al.*, 1983a,b,

1984; Volkov, 1984, 1985, 1986a–c, 1988; Volkov *et al.,* 1986), on a bilayer lipid membrane (Toyoshima *et al.,* 1977), on an electrode (Fong, 1982; Fong *et al.,* 1977; Fruge *et al.,* 1979, Galloway *et al.,* 1978; Miyasaka *et al.,* 1981; Showell and Fong, 1982), in liquid crystals (Aizawa *et al.,* 1979), in lipid gel (Agostiano *et al.,* 1992), in Aerosil (Kachan and Negievich, 1978), or present in nonaqueous solvents containing traces of water (Kutyrin, 1965, 1970; Kutyurin *et al.,* 1968, 1973, 1975) were found to catalyze oxygen evolution during the photooxidation of water. The quantum efficiency in the model oil–water system in terms of oxygen production amounted to 10–20% in the absence of transition metal ions. Oxygen production was measured both polarographically (Boguslavsky *et al.,* 1976a,b, 1977) and by mass spectral analysis (Boguslavsky *et al.,* 1978). Investigations with the Clark oxygen electrode and mass spectrometry conclusively proved the presence of oxygen resulting from the following reaction:

$$2H_2O \leftrightarrow O_2 + 4H^+ + 4e^- \qquad (14.10)$$
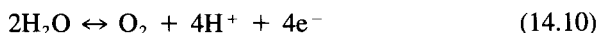
If chlorophyll *a* was replaced by chlorophyll *b,* no oxygen evolution occurred, presumably due to different supramolecular structures of chlorophyll *a* and *b* aggregates.

Several authors have proposed a molecular mechanism for water photooxidation in model systems containing chlorophyll (Kutyurin, 1970; Pinchuk, 1993; Riveros, 1991; Volkov, 1984). It is likely that chlorophyll was directly involved in the photooxidation of water to molecular oxygen early in the evolution of light-harvesting pathways. However, because hydrated chlorophyll aggregates can operate for only a few hours, the structure and composition of the oxygen-evolving complex must have undergone significant evolutionary changes to increase its stability (Volkov, 1984).

When reactions attended by charge separation occur in homogeneous solution, the resulting products usually recombine rapidly, so that the light energy is converted to thermal energy. Separation of reactants in two different phases can delay recombination of the products of electron phototransfer. The interface between two immiscible liquids with immobilized photosynthetic pigments can serve as a simple model convenient for studying the photoprocesses accompanied by the spatial separation of charges, as in biological membranes. Upon illumination of the octane–water interface in the presence of P_{745}, proton acceptors in octane, and electron acceptors [nicotinamide adenine dinucleotide (NAD^+), nicotinamide adenine dinucleotide phosphate ($NADP^+$), or $K_3Fe(CN)_6$], oxygen evolution from water takes place at the oil–water interface. Oxygen production is proportional to the area of the interface and does not depend on the volume of the oil or water phase.

Illumination also induces an interfacial photopotential if chlorophyll *a* and $K_3Fe(CN)_6$ are added to the previously equilibrated octane–water system containing 2,4-dinitrophenol (Fig. 14.12). The magnitude of this potential depends on the
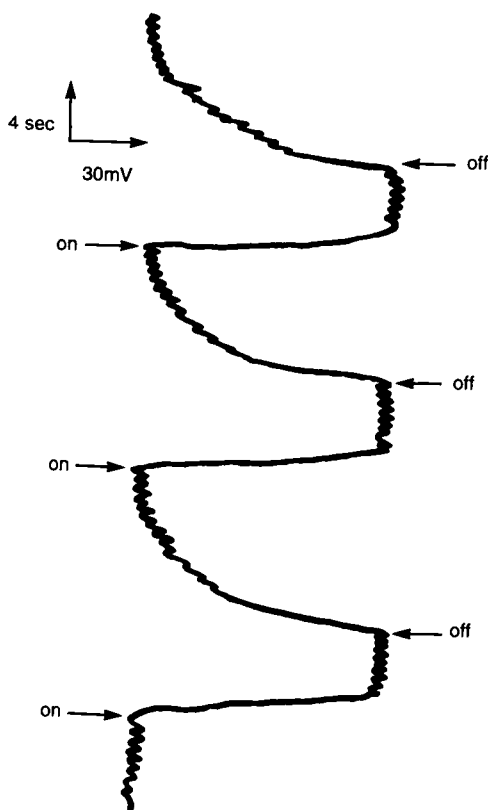
Figure 14.12   Photopotential at the octane–water interface. Composition: 10 mM $K_3Fe(CN)_6$, 1 mM 2,4-dinitrophenol, 10^{-5} M chlorophyll a, 10 mM Tris-HCl, pH 7.7 (Kandelaki *et al.*, 1987). Reproduced by permission of Elsevier Science.

wavelength and intensity of the incident light, as well as the concentrations of all reagents. Photopotentials do not occur if octane and water are not mutually saturated and equilibrated (Fig. 14.13). The absence of a photopotential in the dry octane–water system and the dependence of its amplitude in water-saturated octane on the chlorophyll incubation time prove that photopotential generation requires a certain structural organization of the interfacial layer. A high surface concentration of the adsorbed chlorophyll favors its aggregation, whereas contact between the porphyrin ring and the aqueous phase ensures the high dielectric permeability of the surroundings necessary for the formation of chlorophyll cation radicals. Because it can hardly be assumed that the hydration of monomer chlorophyll in the octane phase is essential for pigment organization at the interface,
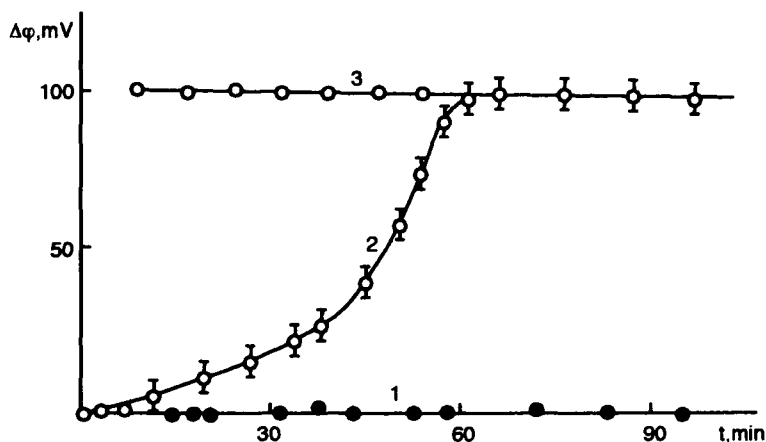
Figure 14.13 Dependence of photopotential measured in the electrochemical chain on the time of illumination with different contact times of the aqueous phase with dry n-octane. Medium: 1 mM dinitrophenol, 10 mM $K_3Fe(CN)_6$, 10 mM Tris-HCl, pH 7.7. Chlorophyll a in 10^{-5} M concentration was added after 0–1 min, 2–10 min, and 3–24 hr (Kandelaki *et al.*, 1987). Reproduced by permission of Elsevier Science.

where the porphyrin ring is in aqueous medium, the observed dependence of the photopotential on the presence of water in octane is more likely to be explicable in terms of the effect of water on the aggregation of chlorophyll in octane and the subsequent adsorption of aggregates at the interface. Similar effects were observed in other experiments in which chlorophyll was used to catalyze redox reactions. Photopotential was measured as a difference between Volta potentials in the dark and under illumination. The electrochemical chain for measuring Volta potentials is shown here:

Au	Air	Octane, chlorophyll, proton acceptor	Water, electron acceptor	Water, KCl-saturated	Hg_2Cl_2, Hg
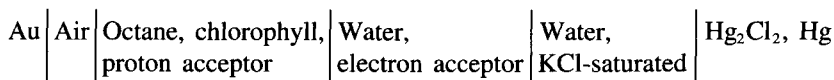
All of the methods of measuring Volta potentials between immiscible phases use compensation (Markin and Volkov, 1990). This means that a potential difference is applied between the water and octane that is equal in magnitude to the Volta potential but of opposite sign (Bewig, 1964; Boguslavsky and Volkov, 1975; Guyat, 1924; Kenrick, 1886; Knotz and Dubovik, 1985; Randles, 1956). Changes in Volta potentials and Galvani potentials can be measured by the dynamic capacitor method, radioactive probe method, jet electrode method, and by using concentration chains. The dynamic capacitor method was proposed by Kelvin (1898) and later developed by Zisman (1932).

A schematic diagram of the setup for measuring Volta potentials by the dy-
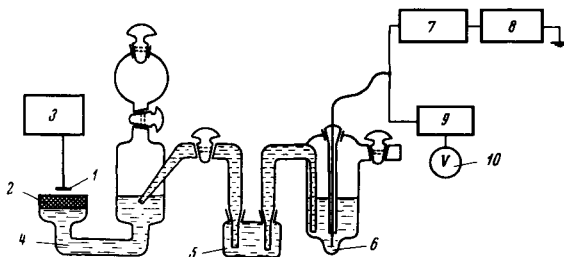
Figure 14.14   Schematic diagram of the setup for measuring Volta potentials or photopotentials at the interface between two immiscible liquids. Notation: (1) vibrating gold electrode; (2) layer of oil; (3) generator; (4) aqueous solution; (5) salt bridge; (6) calomel electrode; (7) amplifier; (8) oscillograph; (9) compensating device. The compensating potential was measured by a voltmeter (10).

namic capacitor method is shown in Figure 14.14. A generator of mechanical vibrations drives a gold electrode to vibrate at a distance 0.2–1.0 mm from the surface of the liquid phase in question. To eliminate the effect of the diffusion potential, the aqueous solution is connected to a reversible reference electrode via a salt bridge filled with saturated KCl solution. The displacement current, which occurs due to the vibration of the gold electrode, is compensated by applying to the vibrating electrode a potential equal in magnitude to the measured Volta potential but of opposite sign.

The photopotential results from the following reaction taking place at the interface:

$$2H_2O + 4A + 4PCP^- \rightarrow O_2 + 4PCPH + 4A^- \qquad (14.11)$$
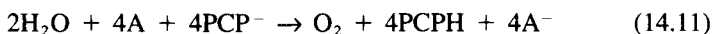
The reaction is accompanied by the capture of protons released by proton acceptors. Dinitrophenol (DNP) or pentachlorophenol (PCP^-) is present in the adsorbed state at the interface between two immiscible liquids, such as octane and water. Such compounds dissociate to produce a net negative charge on the octane phase relative to water. The magnitude of the measured potential was -0.2 V following the addition of DNP to the octane–water system. When the photoreaction [Eq. (14.11)] was initiated, the potential abruptly shifted in the positive direction by 0.1 V. The stoichiometry of Eq. (14.11) was verified polarographically (Boguslavsky and Volkov, 1987).

Figure 14.15 shows an absorption spectrum for chlorophyll in water-saturated octane and an action spectrum of the water photooxidation reaction. The action spectrum in Fig. 14.15 suggests that hydrated chlorophyll oligomers, P_{745}, and dry chlorophyll monomers are involved in the reaction. Monomeric forms of chlorophyll *a* may serve as sensitizers or antennae in this system. These results support the molecular mechanism of water photooxidation in model systems involving the oxidized form of hydrated chlorophyll oligomers (Volkov, 1984).
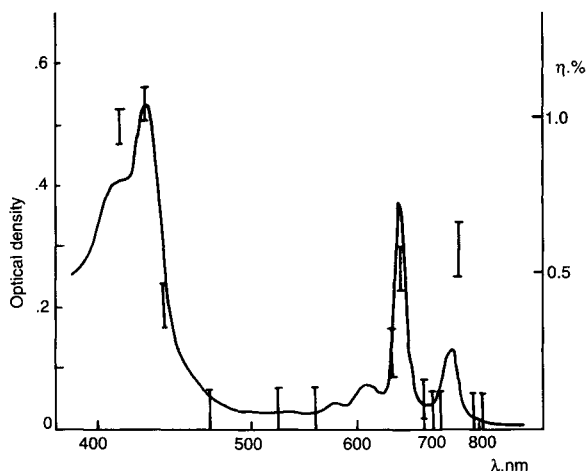
Figure 14.15 Action spectrum (I) of water photooxidation in the presence of chlorophyll. Medium: 1 mM pentachlorophenol, 10 mM Tris-HCl (pH 7.7), 10^{-5} M chlorophyll a, 1 mM NAD$^+$, octane–water. For comparison, the absorption spectrum of chlorophyll solution in octane equilibrated with water is presented (solid line).

The hydrated chlorophyll oligomer, $Chl_6(H_2O)_n$ ($n > 2$), adsorbed on the surface and closely packed so that the electron clouds of porphyrin rings may overlap enters an excited state upon illumination, which leads to pigment oxidation and acceptor reduction. In the reaction center, water is coordinated to the magnesium atom of one chlorophyll molecule and linked by hydrogen bonds to the carbonyl group of a second chlorophyll molecule and a pentachlorophenol anion, which is also adsorbed at the interface and forms part of the catalytic reaction center. The PCP$^-$ anion is required for water binding at the reaction center and protection of chlorophyll against pheophytinization during the reaction. The redox potential of a hydrated chlorophyll oligomer is about 0.92 V (Showell and Fong, 1982), so that only one possible pathway is available for water oxidation—a direct four-electron oxidation that produces molecular oxygen. It should be mentioned that one- and two-electron reactions are formally possible if their intermediates are absorbed at the interface and their binding energies are high enough. However, the radicals formed in the course of multistage processes would inevitably oxidize and destroy the catalytic complex. The quantum yield of fluorescence of the aggregate shows that it is 10^3 less than the quantum yield of monomer fluorescence. This indicates that the molecular ensemble responsible for the reaction of water oxidation to molecular oxygen, in addition to hydrated oligomer, involves other catalytic sites (e.g., chlorophyll dimers, trimers, and monomers).

In the reaction described, P_{745} acts as both a photosensitizing agent and a catalyst. Photosensitizers are substances that induce reactions by energy transfer to

the reactants rather than by forming chemical intermediates with them. It is possible to uncouple these functions by adding a dye (β-carotene) that can also sensitize the photooxidation of water (Volkov *et al.*, 1985). Carotene not only protects chlorophyll against photodynamic destruction but also is capable of absorbing light and imparting the excitation energy to chlorophyll *a*. The van der Waals interaction known to exist between the tetrapyrole ring of chlorophyll and β-carotene apparently stabilizes a weak complex. The complex can then participate in water photooxidation at wavelengths where β-carotene rather than chlorophyll absorbs light.

Figure 14.16 illustrates the relationships between oxygen evolved, length of the illumination period, and different sequences of reagent addition to the octane–water system. Addition of a proton acceptor (PCP), an electron acceptor (NAD^+), and chlorophyll results in the light-induced evolution of oxygen. No oxygen was evolved during illumination at 462 nm (Fig. 14.16a), but the addition of β-carotene caused oxygen evolution at this wavelength. The process stops completely in the dark and returns to its initial rate upon reillumination. In the presence of β-carotene, the quantum yield at the incident light wavelength 462 nm is approximately 0.5% (calculated on the basis of incident light quanta). Figure 14.16 shows that oxygen evolution in the complete system is independent of the order of chlorophyll and β-carotene addition. However, no oxygen evolution was found in the absence of chlorophyll (Fig. 14.16b).

Carotenoids do not appear to be directly involved in water photooxidation during photosynthesis, but perform several other functions. Due to their optical properties, they absorb shortwave blue light and excite chlorophyll by resonance
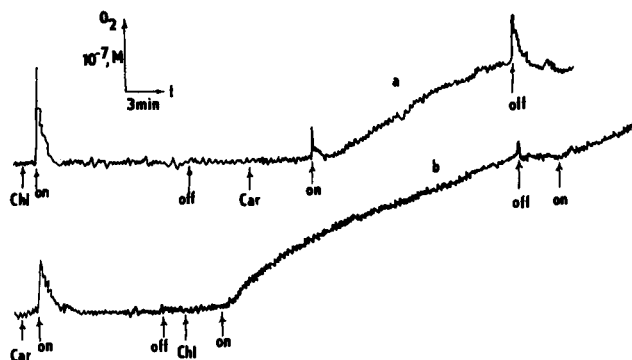
Figure 14.16 Dependence of the amount of oxygen evolved on the incubation time and sequence of reagent addition. Composition: water–octane, 1 m*M* NAD^+, 20 m*M* Tris-HCl (pH 7.4), 1 m*M* pentachlorophenol. Chlorophyll and β-carotene were added to the octane fraction in concentrations of 4 and 10 μM, respectively. The interface was illuminated with monochromatic light at a wavelength of 462 nm (Volkov *et al.*, 1995b). Reproduced by permission of Elsevier Science.
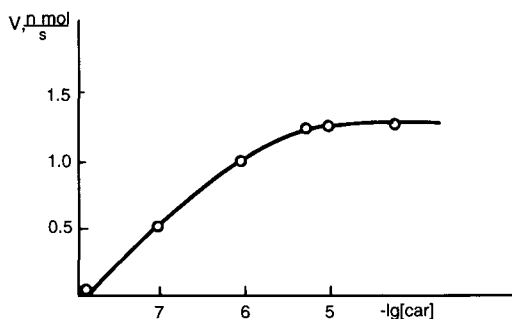
Figure 14.17 Dependence of the oxygen release rate on β-carotene concentration. Medium: octane, water, 10 mM pentachlorophenol, 20 mM Tris-HCl (pH 7.4), and β-carotene in the concentrations indicated on the figure. The octane–water interface was illuminated with monochromatic light at 462-nm wavelength (Volkov *et al.*, 1995b). Reproduced by permission of Elsevier Science.

energy transfer, thus increasing the efficiency of light energy utilization. As anti-oxidants, carotenoids protect chlorophyll from oxidation by singlet oxygen produced during photosynthesis. Carotene can also participate in electron transfer through its system of conjugated bonds.

Additional experiments were carried out to establish the duration of oxygen evolution. The results show that the oxygen evolved without β-carotene was proportional to the illumination time during the first 2 hr and that the absorption spectrum of the octane phase was coincident with the initial spectrum. The rates of oxygen evolution began to decrease after 3 hr and ceased entirely between the fourth and fifth hours of illumination. At that time, chlorophyll in the octane phase was discolored as a result of pheophytinization and photobleaching, even though the pH of the aqueous phase remained neutral (buffered by 20 mM Tris-HCl at pH 7.4). Addition of β-carotene (10^{-5} M) did not significantly increase either the duration of molecular oxygen evolution or the stability of chlorophyll *a*. Figure 14.17 shows the dependence of the molecular oxygen evolution rate on the β-carotene concentration in octane. The oxygen release rate grows with increasing β-carotene concentration and reaches its maximum value when the carotene concentration equals 10^{-5} M.

ARTIFICIAL PHOTOSYNTHESIS IN MONOLAYERS AND LANGMUIR–BLODGETT FILMS

Photoelectrochemistry is a very well-established technique that has been widely used to investigate charge separation phenomena following the absorption of light on a modified electrode. A great deal of work has been performed on inorganic

complexes and organic molecules, particularly the chlorophyll molecule, which plays a fundamental role in the overall conversion of solar energy in the biosphere.

Chlorophyll *a* in photosystem II of green leaf chloroplasts serves as a primary electron donor, P_{680}. On the other hand, pheophytin *a* is well-recognized as a primary electron acceptor of P_{680}. This indicates that these two photosynthetic pigments are directly involved in the conversion of light energy to chemical energy in the primary process of charge separation. Pheophytin *a* is a derivative of the chlorophyll *a* molecule in which magnesium has been replaced by two hydrogens in the center of the porphyrin ring. The spectroscopic and electrochemical properties of pheophytin *a* are different from those of chlorophyll *a*. Pheophytin *a* absorbs more weakly in the red region and more strongly at 505 and 535 nm than chlorophyll *a*. The midpoint redox potential of pheophytin *a*, which is -0.84 V (against the saturated calomel electrode), is less negative than that of chlorophyll *a* (Seely, 1977). Moreover, in the reaction center pheophytin *a* is in monomer form.

Chemical models of photosynthetic processes are used for the investigation of two types of reactions. In photosynthesis, the standard Gibbs free energy of the reaction is positive, and solar energy is utilized to perform work. In photocatalytic processes, the Gibbs free energy is negative, and solar energy is used to overcome the activation barrier. Optically transparent electrodes, modified with monolayers of photosynthetic pigments using Langmuir–Blodgett techniques, are well-suited for the investigation of both types of chemical models of photosynthetic processes.

The optically transparent SnO_2 electrode doped with antimony is a quasi-metallic conductor. The tin oxide electrode is transparent in the visible region of the optical spectrum (Fig. 14.18) and has a high reflectivity for infrared radia-
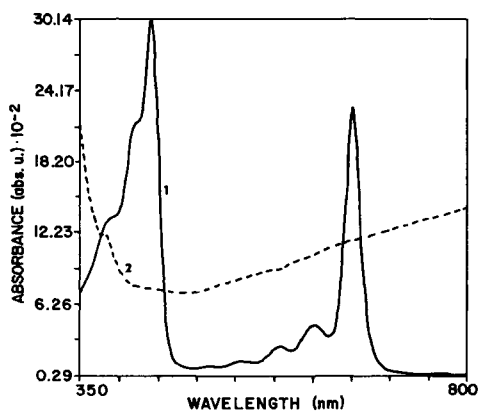
Figure 14.18   Absorption spectra of chlorophyll *a* in (1) benzene solution and (2) SnO_2 OTE (Volkov *et al.*, 1995b). Reproduced by permission of Elsevier Science.

Table 14.1

Location of Adsorption Bands with the Ratio of the Intensities for Chlorophyll *a* and Pheophytin *a* in *n*-Hexane and in Monolayer Langmuir–Blodgett Films[a]

Pigment and conditions	λ_{max}(Soret) (nm)	λ_{max}(Q$_y$) (nm)	$\dfrac{\epsilon_{max}(\text{Soret})}{\epsilon_{max}(Q_y)}$
Dry chlorophyll *a*, $3 \times 10^{-7}\,M$ in *n*-hexane	428	660	1.34
Dry chlorophyll *a* in Langmuir–Blodgett films	440	680	1.33
Pheophytin *a*, $3 \times 10^{-7}\,M$ in *n*-hexane	409	670	1.89
Pheophytin *a* in Langmuir–Blodgett films	412 (422)	674	2.24

[a] Data are taken from Volkov *et al.* (1994) and Zelent *et al.* (1993).

tion. This type of electrode is often used as a working electrode in photoelectro-chemistry due to its sufficiently large potential window and its optical transparency in the visible region. For chlorophyll *a* in benzene, two absorption maxima are observed at 428 and 660 nm (Fig. 14.18, Table 14.1). Upon deposition of a chlorophyll *a* monolayer on the substrates, the absorption maxima are shifted (Fig. 14.19). For the spectrum recorded with the monolayer of chlorophyll *a* deposited on the glass side of the electrode, the blue maximum is at 428 nm. In the red region, the maximum at 660 nm moves to 676 nm. When the monolayer of chlorophyll *a* is on the tin oxide side, the absorption spectrum is also different
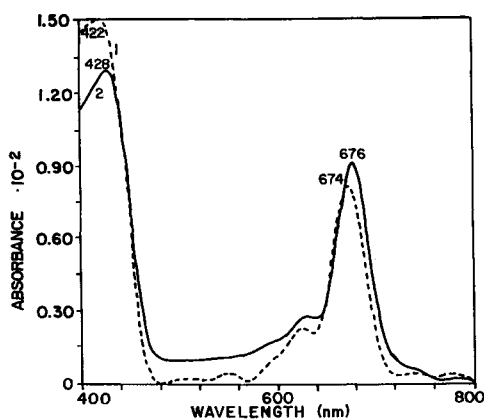
Figure 14.19 Absorption spectra of chlorophyll *a* monolayers on SnO$_2$ OTE (1) and on the glass side of the substrate (2) (Volkov *et al.*, 1995b). Reproduced by permission of Elsevier Science.
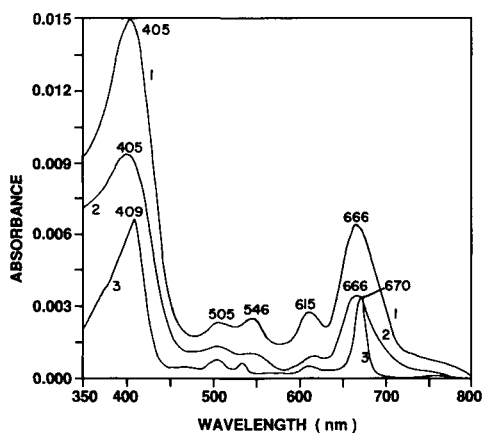
Figure 14.20 Adsorption spectra of pheophytin *a* on SnO₂ OTE before the photoelectrochemical measurements (1), after immersion in electrolyte solution (2), and in *n*-octane (3).

from the absorption spectrum of chlorophyll *a* in solution. The maximum in the blue region is shifted from 428 to 422 nm; the maximum in the red region moves to 674 nm.

Pheophytin *a* has primary absorption maxima in benzene at 414 and 670 nm. Under deposition of a pheophytin *a* monolayer on the SnO₂ OTE, absorption maxima are shifted to higher energy (Fig. 14.20, curve 1). The absorption spectrum of the pheophytin *a* monolayer is quite different when compared with the absorption of pheophytin *a* in benzene. The blue maximum is shifted from 414 to 405 nm, and the red maximum is moved to 666 nm.

Upon immersion of the modified electrode (SnO₂ OTE covered by a chlorophyll *a* or pheophytin *a* monolayer) in an aqueous solution at pH 6.9, the positions of the maxima in both regions are not affected. However, the intensity of the peaks decreases by a factor of 30–40% for chlorophyll *a* and pheophytin *a*.

It has been shown that pheophytinization takes place when the aqueous solution is acidified. The absorption spectrum of the chlorophyll *a* monolayer at the SnO₂ OTE subsequent to incubation with an aqueous solution at pH 3.1 is shown in Fig. 14.21. The spectrum shows the formation of a pheophytin *a* monolayer from the chlorophyll *a* monolayer at the SnO₂ OTE. The absorbance of the substrate varies with pH as shown in Fig. 14.22, where the difference between absorption spectra at pH 3.1 and 6.9 is represented. After acidification, a decrease in light absorption by chlorophyll *a* is observed, along with an increase in the absorption maximum of pheophytin *a* at 506 nm.

Illumination of chlorophyll *a* or pheophytin *a* monolayers at SnO₂ OTE in aqueous solution, in the absence of artificial electron donors, gave rise to a small anodic photocurrent at potentials higher than +20 mV (less than 2 nA/cm²) or a small cathodic photocurrent in the acidic pH range under negative polarization up
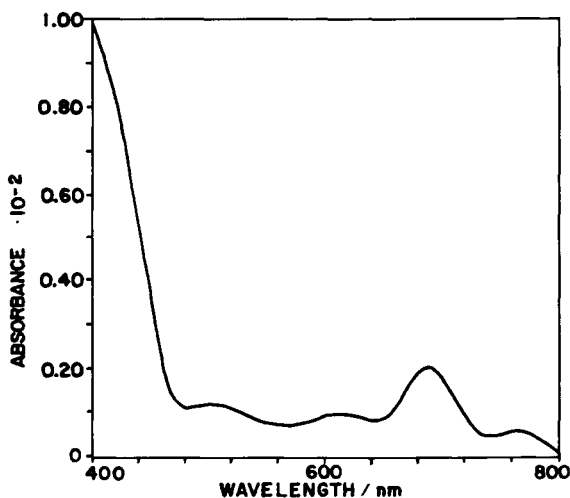
Figure 14.21 Absorption spectra of the chlorophyll a monolayer on SnO_2 OTE after immersion in the electrolyte solution. Medium: 0.1 M Na_2SO_4, 0.05 M QH_2, 0.025 M NaH_2PO_4, pH 3.1 (Volkov *et al.*, 1995b). Reproduced by permission of Elsevier Science.

to -100 mV (less than 4 nA/cm^2). If hydroquinone (QH_2) is added to the aqueous solution, the anodic photocurrent increases by a factor of $10–100$. Cathodic photocurrent can be explained by the reduction in impurities of dioxygen on the order of 10^{-12} mol s^{-1}.
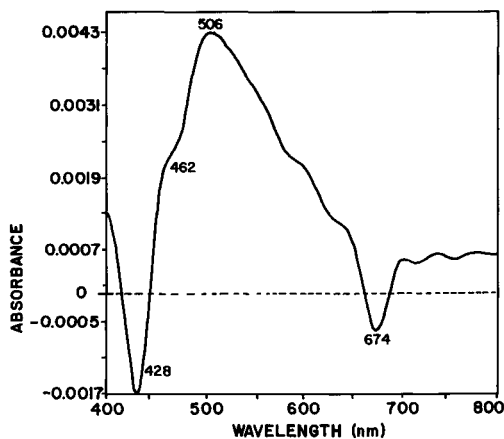
Figure 14.22 Difference in absorption spectra of chlorophyll a monolayers at SnO_2 OTE at pH 6.9 and 3.1. Composition of solution: 0.1 M Na_2SO_4, 0.05 M QH_2, 0.025 M NaH_2PO_4 (Volkov *et al.*, 1995b). Reproduced by permission of Elsevier Science.
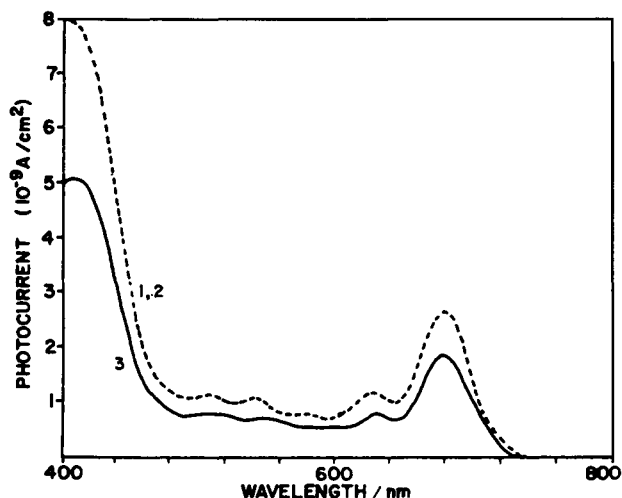
Figure 14.23   Action spectra of the chlorophyll *a* monolayer at SnO_2 OTE. Medium: 0.1 *M* Na_2SO_4, 0.05 *M* QH_2, 0.025 *M* NaH_2PO_4, pH 6.9, electrode potential = 15 mV. Time of exposition: 0–1, 1–2, and 3–4 hr (Volkov *et al.*, 1995b). Reproduced by permission of Elsevier Science.

Figures 14.23–14.26 illustrate the dependence of photocurrent on the wave-length of light in the presence of QH_2. The action spectra correlated with absorption spectra of photosynthetic pigments at the SnO_2 OTE. The photoeffect is a function of time of illumination (Fig. 14.23), electrode potential (Fig. 14.24), solution pH (Figs. 14.23 and 14.25), and hydroquinone concentration (Fig. 14.28).

During the first hour of illumination, when the electrode potential is positive, the photocurrent was shown to be independent of the time of illumination or incubation in the dark. However, after a period of 4 hr, the anodic photocurrent decreased by 30% (Fig. 14.23). This effect is related to the oxidation of QH_2 under both illumination and dark incubation with anodic polarization. After 4 hr, by using a fresh electrolyte solution it is possible to reproduce an initial action spectrum (Fig. 14.23, curve 1). At a potential of +15 mV, the dark current during 4 hr corresponds to the oxidation of 20–40% of QH_2 molecules at SnO_2 OTE. With acidification of the electrolyte solution from a pH of 6.9 to 3.5, the photo-current increases, as observed in Fig. 14.24. Both the value and the sign of the photocurrent depend on electrode potential. Under even stronger acidification conditions than pH 3.5, the values of the anodic and cathodic photocurrents decrease (Fig. 14.25). The voltammetric characteristics of the SnO_2 OTE depend on the composition of the electrolyte solution. It is possible to measure the photoeffect in the potential window in the presence of various inorganic salts in aqueous solution (Figs. 14.25 and 14.26). If NADH is used as an electron donor rather than QH_2, the photocurrent generated is notably smaller than that in the presence of
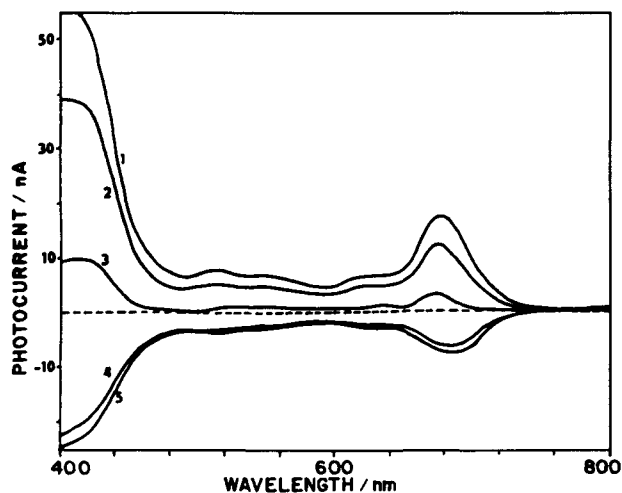
Figure 14.24 Action spectra of the chlorophyll *a* monolayer at SnO_2 OTE. Medium: 0.1 M Na_2SO_4, 0.05 M QH_2, 0.025 M NaH_2PO_4, pH 3.5. Electrode potentials: (1) +190, +200 mV; (2) +160 mV; (3) +100 mV; (4) −50, −100 mV; (5) −150 mV (Volkov *et al.*, 1995b). Reproduced by permission of Elsevier Science.

QH_2, in spite of the fact that the redox potential of NADH is more negative. Apparently, this phenomenon is connected with the kinetic barrier of formation of a one-electron intermediate during the oxidation of NADH or the catalytic oxidation of NADH on the Pt electrode.
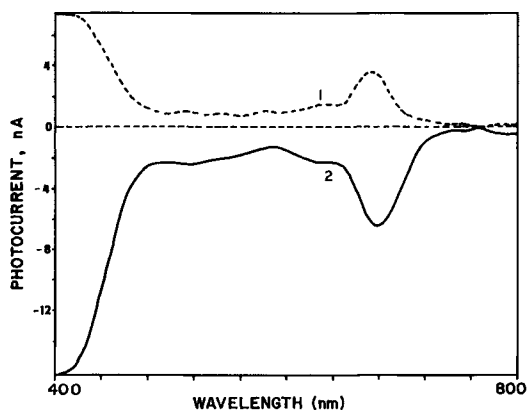
Figure 14.25 Action spectra of the chlorophyll *a* monolayer at SnO_2 OTE. Medium: 0.1 M Na_2SO_4, 0.05 M QH_2, 0.025 M NaH_2PO_4, pH 3.0. Electrode potentials: (1) +14 mV; (2) −50 mV (Volkov *et al.*, 1995b). Reproduced by permission of Elsevier Science.
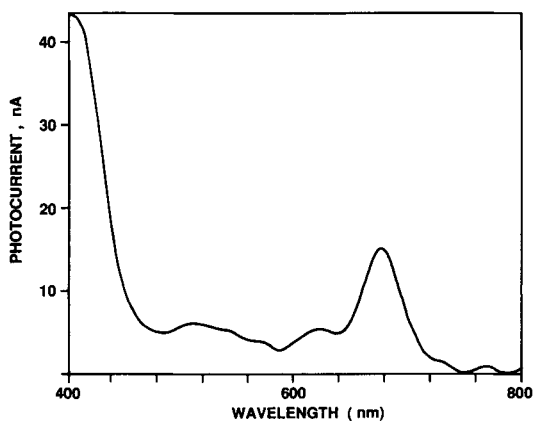
Figure 14.26   Action spectrum of the chlorophyll *a* monolayer at SnO_2 OTE. Medium: 0.1 *M* KCl, 0.05 *M* QH_2, 0.025 *M* KH_2PO_4, pH 3.6, electrode potential $= 100$ mV (Volkov *et al.*, 1995b). Reproduced by permission of Elsevier Science.

Quantum yields for a pheophytin *a* (chlorophyll *a*) monolayer in the presence of QH_2 at pH 6.9 were found to equal 0.7% (0.4%) for the red and 0.6% (0.3%) for the blue maxima.

The ability of light-excited chlorophyll and pheophytin molecules to be in-
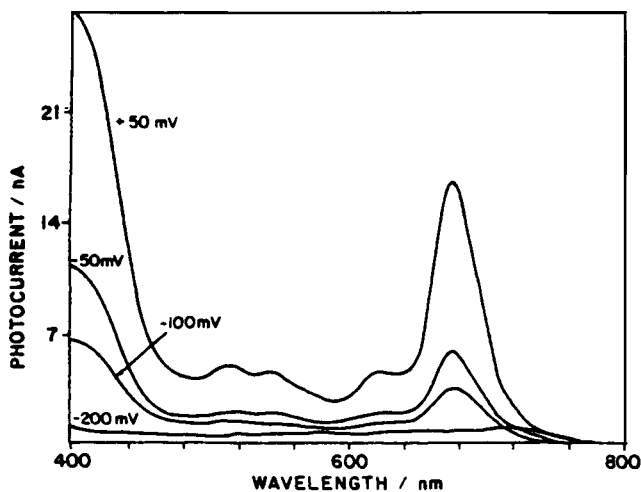
Figure 14.27   Action spectra of the pheophytin *a* monolayer at SnO_2 OTE. Medium: 0.1 *M* KCl, 0.05 *M* QH_2, 0.025 *M* NaH_2PO_4, pH 6.9 (Volkov *et al.*, 1995b). Reproduced by permission of Elsevier Science.
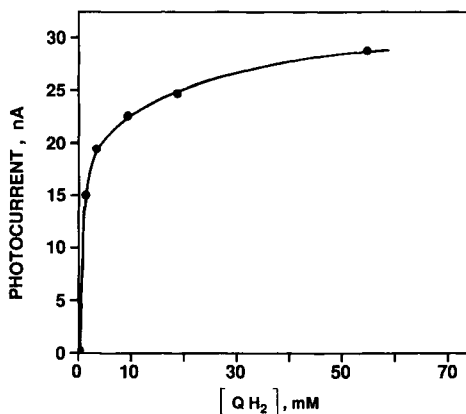
Figure 14.28 Dependence of the photocurrent at SnO_2 OTE in the presence of the pheophytin *a* monolayer on the concentration of hydroquinone at illumination of 400-nm wavelength. Medium: 0.1 *M* KCl, 0.05 *M* hydroquinone, 0.025 *M* KH_2PO_4, pH 6.9, electrode potential $= +50$ mV vs saturated calomel electrode.

volved in reversible redox reactions underlies the primary process of solar energy conversion into electrochemical energy occurring in chloroplasts. The most important process in the bioenergetics of natural photosynthesis is the utilization of solar energy for the transport of electrons from H_2O to $NADP^+$. In the experiments described earlier involving the photocatalytic oxidation of QH_2 by chlorophyll and pheophytin monolayers, the standard Gibbs free energy of the electrochemical reaction is negative; solar energy is used to overcome the activation barrier. In the absence of QH_2, it is possible to use water molecules as electron donors and $NADP^+$ as an electron acceptor. In this case, solar energy can be used to perform work because the standard Gibbs free energy of the reaction of water photooxidation and $NADP^+$ reduction is positive. This process of artificial photosynthesis is the chemical model of natural photosynthesis.

The midpoint redox potential of the chlorophyll cation radical at pH 7 is 0.52 V vs SCE (standard calomel electrode). Because the midpoint redox potential for the reaction $2H_2O = O_2 + 4H^+ + 4e^-$ is 0.57 V vs SCE, the oxidation of water by Chl$\overset{.}{:}^+$ cannot be an effective process. If pheophytin is used as a photocatalyst, its redox potential is equal to $+0.86$ V vs SCE, and the reaction resulting in water oxidation is thermodynamically feasible. If the chlorophyll *a* monolayer at the SnO_2 OTE after a 20-min incubation in aqueous solution at pH 3.5 is placed in a solution of $NADP^+$ at pH 7, the anodic photocurrent arises at a potential of $+400$ mV. This photocurrent may correspond to the reactions of water photooxidation at SnO_2 OTE covered by the pheophytin monolayer and $NADP^+$ reduction on the Pt electrode. The quantum yield of this photocurrent is very low, approxi-
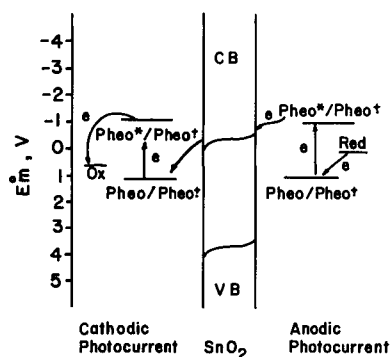
Figure 14.29 A working scheme of anodic and cathodic photocurrent generation by the pheophytin *a* monolayer on SnO_2 OTE. E_m is the midpoint redox potential, which corresponds to the standard redox potential at pH 7.0 against a saturated calomel electrode; CB and VB are the conduction and valence bands of SnO_2, respectively.

mately 0.02%. The mechanism of anodic and cathodic photocurrent generation at the SnO_2 OTE can be illustrated as shown in Fig. 14.29.

Pheophytin *a* in *n*-hexane possesses two well-defined electronic transitions, which in the absorption spectrum are manifested by two bands in the blue region at λ_{max} = 409 nm and in the red region at λ_{max} = 670 nm (Fig. 14.30, curve 2). The comparison of the absorption spectra of pheophytin *a* in *n*-hexane and in benzene indicates that the long-wavelength band essentially is not affected by solvent polarity. However, the short-wavelength band, in going from benzene to
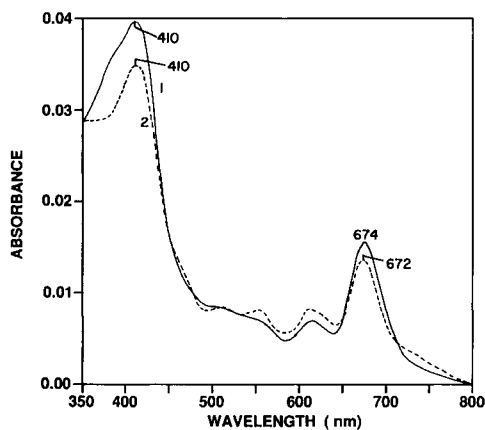
Figure 14.30   Absorption spectra of pheophytin *a* in *n*-hexane (10^{-5} *M*) (1) and in a monolayer on a quartz slide (2) (Volkov *et al.*, 1995b). Reproduced by permission of Elsevier Science.

n-hexane, is shifted slightly to higher energy ($\Delta\nu = 300 \text{ cm}^{-1}$) due to the decrease in the static dielectric constant of the solvent from 2.3 to 1.9, respectively. In absorption spectra of pheophytin a there is a visible change in going from dilute n-hexane solution to a Langmuir-Blodgett monolayer on quartz slides. This is shown in Fig. 14.30 (curve 1). Two broad absorption bands of pheophytin a in Langmuir–Blodgett films in the blue and red regions possess maxima at 412 and 674 nm, respectively (Volkov *et al.*, 1994). A more dramatic change is observed in the fluorescence spectra of pheophytin a in the same samples (see Fig. 14.31). A typical emission spectrum of pheophytin a in dilute n-hexane solution possesses a maximum at $\lambda_{em} = 674$ nm and a low-intensity band at $\lambda_{em} = 723$ nm. However, the emission spectrum of pheophytin a in a Langmuir–Blodgett film is shifted to lower energy with a maximum at $\lambda_{em} = 695$ nm and a large shoulder at $\lambda_{em} = 750$ nm. Note that the fluorescence excitation spectra of pheophytin a (see Fig. 14.32) measured at the maxima of the emission spectrum at 674 and at 695 nm correspond well with the absorption spectra of pheophytin a in n-hexane and the Langmuir–Blodgett film (see Fig. 14.30), respectively. The observed changes in the absorption and fluorescence spectra indicate that pheophytin a in a Langmuir–Blodgett film exists in an aggregated form. This is also supported by the fluorescence lifetime values presented in Table 14.2.

Monoexponential decay has been measured for a 674-nm emission band of pheophytin a in dilute n-hexane solution with $\tau_1 = 5.79 \pm 0.02$ ns. Such a lifetime value indicates monomer emission for pheophytin a. Similar lifetime values
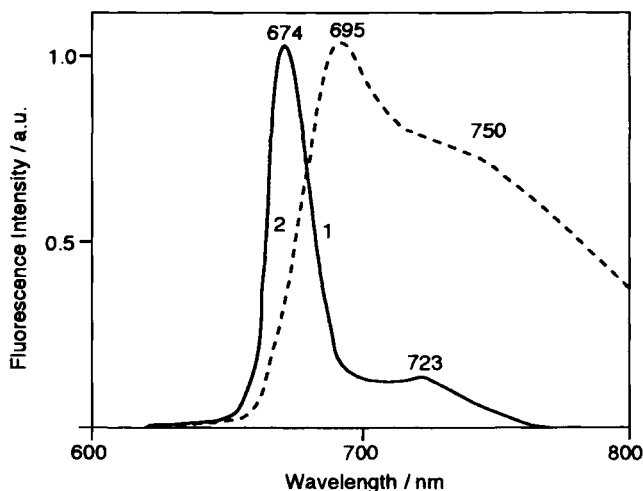
Figure 14.31 Corrected fluorescence spectra of pheophytin a in n-hexane ($c = 3 \times 10^{-7} M$, $l = 1.0$ cm) (1) and in a monolayer on the quartz slide (2); $\lambda_{exc} = 410$ nm (Volkov *et al.*, 1995b). Reproduced by permission of Elsevier Science.
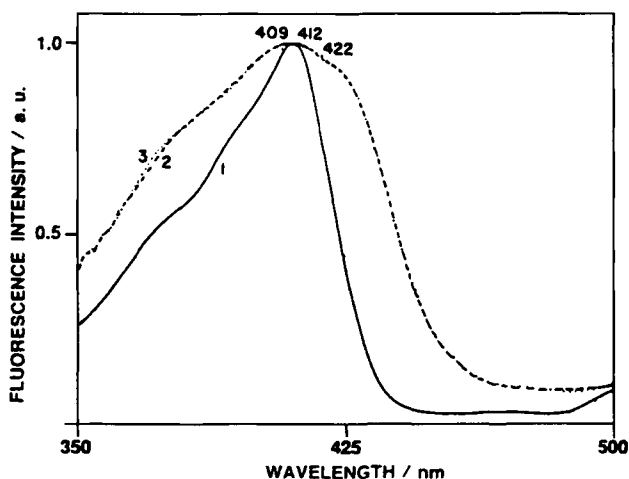
Figure 14.32   Fluorescence excitation spectra of pheophytin *a* in *n*-hexane (*c* = 3 × 10⁻⁷ *M*, *l* = 1.0 cm) at λ_{em} = 674 nm (1) and in a monolayer on the quartz slide at λ_{em} = 695 nm (2) and λ_{em} = 750 nm (3) (Volkov *et al.*, 1995b). Reproduced by permission of Elsevier Science.

have also been reported for the monomer emission of chlorophyll *a* in solution (Connoly *et al.*, 1982). However, the decay of the emission of pheophytin *a* in a Langmuir–Blodgett film possesses biexponential character. The lifetime values

Table 14.2

**Fluorescence Lifetimes of Pheophytin *a* in *n*-Hexane,
Thin Films, and Langmuir–Blodgett Films[a]**

Conditions	Excitation λ_{max} (±1 nm)	Emission λ_{max} (±1 nm)	τ_1 (ns)	τ_2 (ns)
n-Hexane (3 × 10⁻⁷ *M*)	409	674	5.79 ± 0.02 (100%)	–
Thin film on quartz slide adsorbed from dry	410	680	5.61 ± 0.02 (100%)	–
benzene		726	5.82 ± 0.10 (87%)	1.32 ± 0.35 (13%)
Thin film on quartz slide adsorbed from wet	410	675	5.16 ± 0.14 (74%)	2.40 ± 0.32 (26%)
benzene		722	5.16 ± 0.28 (56%)	2.45 ± 0.27 (44%)
Langmuir–Blodgett film, one monolayer on	412 (422)	695	3.03 ± 0.27 (17%)	0.46 ± 0.06 (83%)
quartz slide		750	3.10 ± 0.51 (12%)	0.72 ± 0.06 (88%)

[a]Volkov *et al.* (1995b).

measured at 695 nm are $\tau_1 = 3.03 \pm 0.27$ ns (17%) and $\tau_2 = 0.46 \pm 0.06$ ns (83%). These two lifetime components can be assigned to dimeric and oligomeric forms of pheophytin a, respectively. Only small changes in the contribution of τ_1 and τ_2 lifetime components are observed when measurements are carried out at 750 nm (see Table 14.2). This is consistent with the fact that the fluorescence excitation spectra of pheophytin a in a Langmuir–Blodgett film measured at $\lambda_{em} = 695$ nm and at $\lambda_{em} = 750$ nm are the same (see Fig. 14.32).

It is known from monolayer studies of pheophytin a at the air–water interface, by absorption spectroscopy and other methods, that at pressures above a critical value of 15 mN m^{-1} pheophytin a aggregates in an arrangement with coplanar stacking of the porphyrin rings. Moreover, such a monolayer is also stable for pressures below the critical value. We can expect a similar type of arrangement of pheophytin a molecules in Langmuir–Blodgett films, because the deposition of the pheophytin a monolayer on the hydrophilic surface of a quartz slide was performed at 16 mN m^{-1} (Volkov *et al.*, 1994). Going back to the lifetime measurements, the data obtained support the conclusion on the aggregate state of pheophytin a in Langmuir–Blodgett films. The effect of aggregation of pheophytin a molecules can only be explained by the π–π interaction of the porphyrin rings in the coplanar arrangement (Volkov *et al.*, 1994).

The state of pheophytin a molecules on a quartz slide depends on the procedure of pigment deposition. The spectroscopic and photophysical properties of pheophytin a in a thin film on a quartz slide are different from those of pheophytin a in Langmuir–Blodgett films. Figure 14.33 shows the absorption spectra
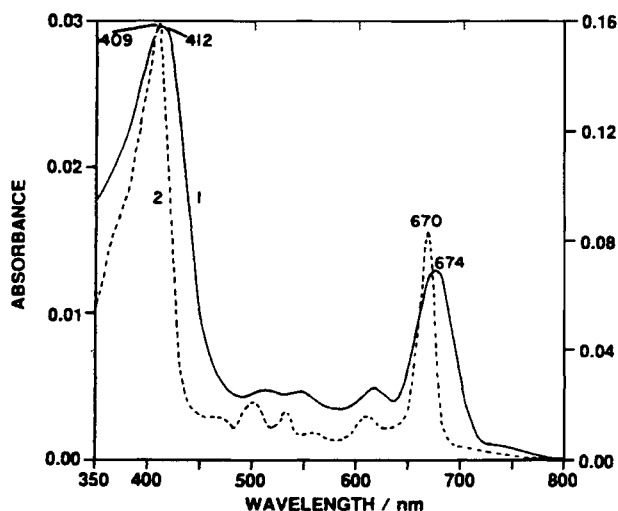
Figure 14.33   Absorption spectra of pheophytin a in thin films on quartz slides adsorbed from dry (1) and wet benzene (2) (Volkov *et al.*, 1995b). Reproduced by permission of Elsevier Science.
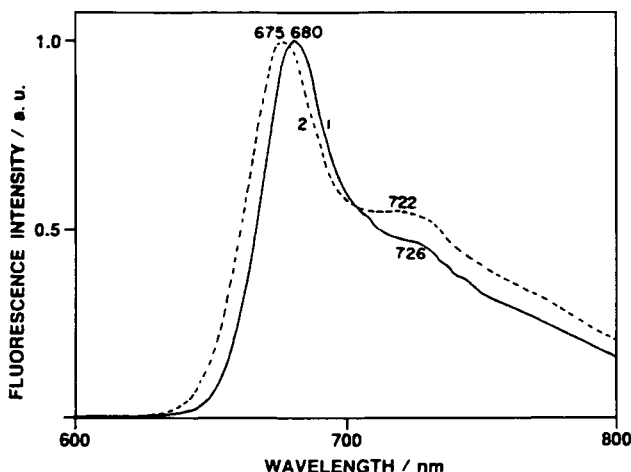
Figure 14.34 Corrected fluorescence spectra of pheophytin *a* in thin films on quartz slides adsorbed from dry (1) and wet benzene (2); λ_{exc} = 410 nm (Volkov *et al.*, 1995b). Reproduced by permission of Elsevier Science.

of pheophytin *a* in thin films on quartz slides deposited by adsorption from dry and wet benzene. These spectra are shifted slightly to lower energy compared with the spectrum of pheophytin *a* in *n*-hexane. In the blue region, the absorption bands for both samples appear at λ_{max} = 410 nm. One can see that the Soret band of dry pheophytin *a* is larger than the Soret band of wet pheophytin *a*. In the red region, the absorption bands for dry and wet pheophytin *a* appear at λ_{max} = 674 and 672 nm, respectively. Fluorescence spectra of pheophytin *a* in thin films (Fig. 14.34) are shifted to lower energy by less than in Langmuir–Blodgett films as compared to the fluorescence spectrum of the same pigment in *n*-hexane (see Fig. 14.31). For wet pheophytin *a*, the fluorescence spectrum possesses maximum emission at 675 nm and a lower intensity broad band at 722 nm. For dry pheophytin *a* these two emission bands appear at 680 and 726 nm, respectively. The absorption and emission spectra presented indicate that the state of pheophytin *a* in thin films is less ordered than that in Langmuir–Blodgett films.

Fluorescence excitation spectra of pheophytin *a* in thin films measured at emission maxima (see Figs. 14.35 and 14.36) correspond well with the Soret absorption bands of the pigment. However, the fluorescence excitation spectra measured at λ_{em} = 750 nm in both cases are broader. This shows that emission at lower energy comes from more aggregated forms of pheophytin *a*.

Fluorescence decay kinetics measured for pheophytin *a* in thin film adsorbed from wet benzene yields two lifetime values (see Table 14.2). For the 675-nm emission band, τ_1 = 5.16 ± 0.14 ns (74%) and τ_2 = 2.40 ± 0.32 ns (26%). These lifetime values also remain the same for the decay of the lower energy emission
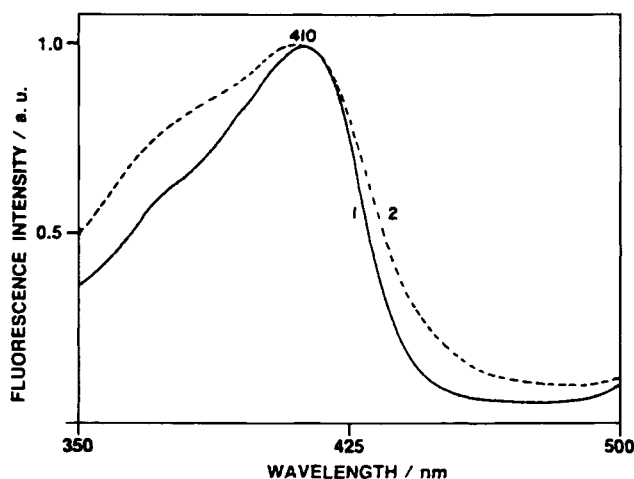
Figure 14.35 Fluorescence excitation spectra of pheophytin *a* in a thin film on a quartz slide adsorbed from dry benzene at λ_{em} = 680 nm (1) and λ_{em} = 750 nm (2) (Volkov *et al.*, 1995b). Reproduced by permission of Elsevier Science.

band at 722 nm. However, in this case, the contribution of the long-lived component decreases to 56% while the contribution of the short-lived component increases to 44%. These two lifetime components in the time-resolved fluorescence
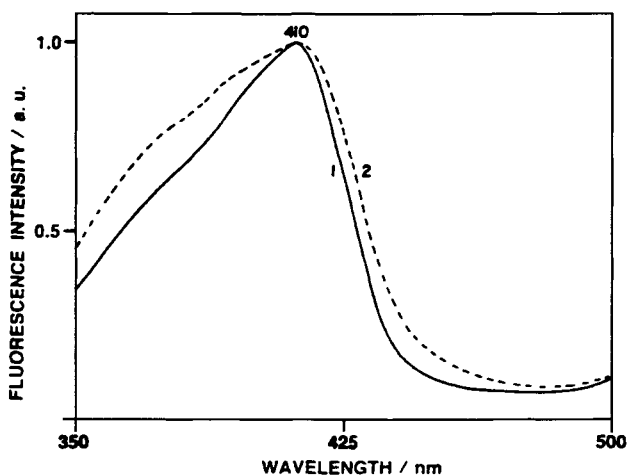
Figure 14.36 Fluorescence excitation spectra of pheophytin *a* in a thin film on a quartz slide adsorbed from wet benzene at λ_{em} = 675 nm (1) and λ_{em} = 750 nm (2) (Volkov *et al.*, 1995b). Reproduced by permission of Elsevier Science.

decay curves describe the state of pheophytin *a* in thin films as single molecules and dimers. These lifetime results also indicate that the adsorption of pheophytin *a* on a quartz slide from wet benzene gives rise to the formation of a very unified film. Different results were obtained when the adsorption of pheophytin *a* on a quartz slide was carried out with dry benzene. The monoexponential decay of the emission at 680 nm yields $\tau_1 = 5.61 \pm 0.02$ ns (see Table 14.2). This lifetime value can be assigned to monomeric states of pheophytin *a*. However, the decay of the 726-nm emission band possesses biexponential character with the lifetime values $\tau_1 = 5.82 \pm 0.10$ ns (87%) and $\tau_2 = 1.32 \pm 0.35$ ns (13%). The results of lifetime measurements show that pheophytin *a* in such thin films exists not only in monomeric but also in oligomeric form.

Chlorophyll *a* and pheophytin *a* in monolayers are capable of effectively transforming light energy into electrical energy. The quantum yields of the process in the presence of hydroquinone have been found to equal $0.7 \pm 0.1\%$ for pheophytin *a* and $0.4 \pm 0.1\%$ for chlorophyll *a* in monolayers. The photoeffect depends on the electrode potential, concentrations of the redox components, and pH of the aqueous solution.

From absorption and fluorescence studies it follows that pheophytin *a* in Langmuir–Blodgett films exists in aggregated forms. Two lifetime components in the biexponential decay of the emission at 695 nm, which are $\tau_1 = 3.03 + 0.27$ ns (17%) and $\tau_2 = 0.48 + 0.06$ ns (83%), have been assigned to dimeric and oligomeric forms of pheophytin *a* in Langmuir–Blodgett films, respectively. This is in agreement with the conclusion that the effect of the aggregation of pheophytin *a* molecules is due to the π–π interactions of the porphyrin rings in the coplanar arrangement. The state of pheophytin *a* in thin films adsorbed from benzene solutions is less ordered than that in Langmuir–Blodgett films.

The pheophytin *a* in monolayers deposited on a SnO_2 optically transparent electrode by means of the Langmuir–Blodgett technique is characterized by stability higher than that of chlorophyll *a* and can be used in nanotechnology for the production of molecular electronic devices and biosensors.

The interface between two immiscible liquids has unusual properties that follow from thermodynamic and kinetic principles controlling reactions in biphasic environments. Photochemical reactions in particular have remarkable characteristics when carried out at interfaces. Biological reaction pathways such as oxygen evolution, photorespiration, and synthesis of organic molecules can be investigated in systems involving liquid–liquid interfaces. Early photochemical processes that may have permitted light harvesting by primitive cells can also be studied at the liquid–liquid interfaces of emulsified alkanes and polycyclic aromatic hydrocarbons (Deamer and Volkov, 1996). An important general insight is that multielectron reaction centers in biological membranes can be understood as self-organized catalytic interfaces. In the future, such molecular ensembles will likely be central features of systems that capture solar energy by artificial photosynthesis.

Chapter 15

Humans and Plants

An artificial satellite that revolves around Earth is equipped with solar battery panels, which transform solar energy into electricity and sustain the potential difference in the power system needed to actuate all electronic devices inside. Earth also has its panels of "solar batteries." They gird the globe with a green belt stretching from the southern to the northern polar circle. These solar batteries feed energy to Earth's biosphere. This is not electric energy as in the case of the system made by humans, but the chemical energy of organic matter and oxygen. The chemical potential difference between them is the motive force for most processes in the biosphere. This potential difference is small. If expressed in electric units, it equals about 1.2 V. However, the amount of matter involved in the process is huge. The total production of organic matter by plants reaches 200 billion metric tons annually. About three-fourths of this mass is produced by terrestrial plants and one-fourth by microscopic algae in oceans. The amount of oxygen produced simultaneously is about the same. Up to 1% of the total yield of organic matter is produced by cultivated plants. This matter, the product of humankind's agricultural activity, is of paramount significance to us.

Agriculture is an essential part of human culture. Moreover, it is a domain that determines the existence of a developed society. In fact it is quite easy to imagine a society without computers, aircraft, cars, or electricity. Without it people could live for centuries and create pretty complicated forms of culture and public organizations. However, during the times when agriculture did not exist, there were just primitive tribes of hunters and collectors. Thus, historical experience tells us that agriculture plays a specific and exceptional role in the development of society, incomparable in its consequences to any branch of manufacturing. One may even state that manufacturing could have arisen only when people had satisfied their

food requirement due to agricultural activity and, thus, created the possibility of doing something else besides supplying themselves with food. The historic role of agriculture is quite prominent. We presume that its role in the future will not decrease, but on the contrary will grow with continual growth in Earth's human population.

Taking agriculture's outstanding role into account, we have reason to consider it not simply as one among other branches of manufacture but as a sphere of human biological activity. This activity consists of obtaining food and raw materials from specifically controlled and stimulated biological communities. In essence, agriculture is nothing but the realization of symbiosis between humans as a biological species and selected species of plants and animals (Whittaker, 1975).

This point of view may appear unacceptable and may cause negative reactions. Indeed, we have become used to considering humans as being of higher rank, on the top of evolution, the only thinking beings on Earth. Therefore, the assumption that the "King of Nature" may be joined in symbiotic relations with any primitive organisms, say with plants or even worse with cows, may seem almost blasphemous. Two specifics should be noted about this. First, the term "symbiosis" should not be understood in too simple of a sense. At the level being considered, the term *symbiosis* defines a conjugated system of humans and other components of the biosphere providing a division of labor and pooling of efforts. Second, in the course of self-consciousness humankind more than once faced a situation when feelings of exclusivity were subjected to serious challenges. Such was the case when Copernicus showed that Earth was not the center of the universe but only an ordinary planet.

Humans as a biological species exist in symbiotic relations with some portion of the whole of plants and animals, which we call "agricultural" or "domesticated." Our welfare as a biological species directly depends upon the extent to which we provide for the welfare of our symbionts: the agricultural plants and animals.

Right now humankind is surely the most prosperous species among all animals living on Earth. The size of the human population is nearly 6 billion individuals, with a total mass of about 300 million tons. Its natural habitat spreads over the whole Earth. Humans consume the greater part of Earth's food resources.

Among the plants that grow on Earth, the most prosperous species are those cultivated by people. The total number of plant species on Earth is estimated to be about 300,000. Their total productivity is estimated to be 150 billion tons annually. Thus, the mean yield of a single species should equal 0.5 million tons based on the assumption that all species are equally productive. However, such an assumption is unrealistic. Some of the 300,000 plant species are more prosperous, whereas others are less successful. One may use the productivity of a species as a tentative criterion for its evolutionary success. By arranging the plant species in descending order of productivity, one can determine a certain distribution. The law of such distributions is not known, but plausible assumptions may be made

on the basis of general considerations. Various mathematical expressions are used for describing biological diversity (Gray, 1988; Greig-Smith, 1983; Maguarran, 1988). There are reasons to think that for the case under consideration the distribution proposed by Mandelbrot (1983) may be suitable. This distribution is described by the following expression:

$$p(r) = M(N + r)^{-s} \qquad (15.1)$$

Here $p(r)$ is the productivity of a species whose rank in the descending arrangement is r. M, N, and s are certain constants. The first determines the general scale of values, and the second shows the number of species whose productivity appreciably surpasses the average level. The value of the constant s is connected with the extent of diversity of the species in the distribution. Unfortunately, there are no reliable data concerning the actual distribution of the productivity of different plant species. Nevertheless, possible estimates of the constants cannot go beyond certain reasonable limits. The constant M is determined by the total productivity value of all plants that exist. The constant N probably lies in the range 1000–10,000. If it were less we would have noticed the evident predominance of a few species. In the opposite case the distribution would be too uniform.

Figure 15.1A shows several examples of the distribution curves for various values of parameters M, N, and s. One can see that the expected productivity of the most abundant species may be estimated to be 10–200 million tons, whereas
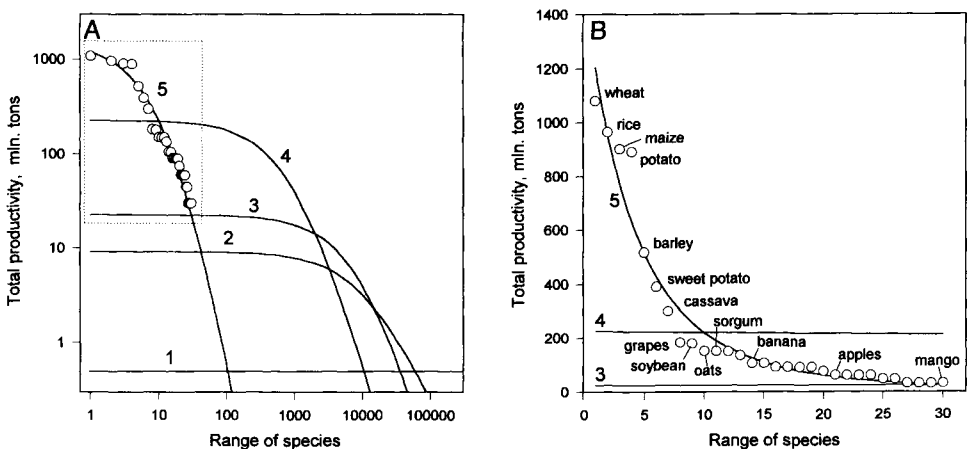
Figure 15.1 (A) Supposed distribution of total productivity of plant species. Curve 1: the uniform distribution of 150 billion tons of biomass over 300,000 species (unrealistic supposition). Curves 2–4 are plotted according to Eq. (15.1) with the following values of parameters: $M = 9.14$, 22.6, 225.6, $N = 10^4$, 10^4, 10^3, and $s = 1.5$, 2.5, 2.5, respectively. Curve 5 refers to cultured plants, plotted on the basis of data for the 30 most abundant crops. Parameters of best fits: $M = 1534$, $N = 16$, $s = 4$. (B) Distribution of total productivity of the most abundant cultured crops. Curves 3–5 are the same as in (A). The region selected in a dotted rectangle is in linear coordinates.

the productivity of species on the tail of the distribution (not shown in the figure) may be as little as 50,000 tons or even only 10 tons. In spite of a certain arbitrariness of the initial estimates, there is no reason to think that the real distribution of the productivity of wild species may significantly deviate from the limits depicted in the figure (curves 2–4).

It is interesting to compare the wild and cultivated plants with respect to their productivity. Curves 5 in Fig. 15.1A,B enable us to do that. The curves are plotted on the basis of productivity data for 30 of the most abundant crops from wheat to mango. More than 1.5 billion tons of grain (wheat, rice, and maize) are produced on Earth annually. Each type of crop accounts for 300–400 million tons of pure product or 2–3 times that for total organic mass, taking into account leaves, stems, and roots. Thus, the humble grasses, the predecessors of contemporary cereals, by being domesticated became the most prosperous plants, surpassing the most prosperous wild species by many times in productivity.

Thus, on the one hand the most prosperous species on Earth is people, and on the other hand it is agricultural plants and animals. Striving for welfare, humankind also has to provide for the thriving of its "symbionts." The evolutionary success of both humankind and its plant symbionts is linked with the rise of a strong mutual dependence between the partners. Many domesticated plants cannot survive in nature without human assistance. On the other hand, the survival and prosperity of the human population of the world absolutely depends upon the performance of the main domesticates. The fact that humankind kills its symbiont, the domestic animals, and uses their meat as food is not a reason to reject their relation as symbiotic. The symbiosis between humans and agricultural plants and animals is realized at the species level, not at the level of single beings.

In a broad sense the term "symbiosis" refers to different forms of interaction between species. There are strong reasons to believe that symbiosis played a very large role in the evolution of living beings. Even the appearance of advanced organisms, the eukaryotes, probably happened as a result of multistage symbiosis (Margulis, 1983). According to this assumption, plants were "designed" as a symbiotic system of a prokaryotic amoeboid cell as host, primitive blue-green algae as the ancestors of chloroplasts, and aerobic bacteria as those of mitochondria. Animals are supposed to have originated in a similar manner, with the only distinction being that blue-green algae were not involved in their formation. These assumptions are illustrated in Fig. 15.2 [from Margulis (1983)].

Here we must specify the term "symbiosis" as applied to the problem under consideration. Relationships between humankind and its main agricultural symbionts are, as we have seen, mutually beneficial for both participants and favor their thriving. Moreover, these relationships are essentially necessary at least for one party, the humans. Such a form of symbiosis is known as obligate mutualism. A classic example of mutualism in nature is represented by lichens, which are the result of symbiosis between algae and fungi. In the lichen, the alga component performs photosynthesis and provides itself as well as the fungus component with
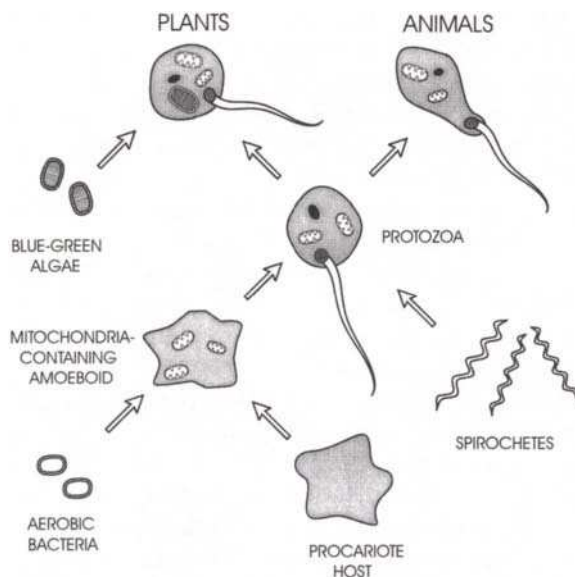
Figure 15.2 Symbiosis theory of the origin of eukaryotic cells, animals, and plants, as a result of the union of prokaryotic predecessors.

food, whereas the fungus protects the alga from external threats and supplies it with water and mineral salts. Due to such joining of efforts of the components, the lichens are highly adaptable organisms. They manifest their vitality under severe conditions of Arctic regions and on lifeless rocks at heights where no plants are found. Therefore, symbiosis in the case of lichens and symbiosis realized in the agricultural activity of humankind are qualitatively different phenomena. It would be an oversimplification to try to find too straightforward a similarity, as in a comparison between human society and the colonies of social insects such as ants or bees.

Any form of symbiosis presumes the existence of a single biological system consisting of two interacting subsystems. In the case under consideration, one of the subsystems is represented by humankind and the other by the totality of agricultural plants and animals. The symbiotic system is not a simple sum of two subsystems, but includes the processes of their interactions manifested in mutual flows of matter and energy. The nature and structure of these flows will be interpreted in detail later. Here we will only estimate their scales. Let us designate, for the sake of convenience and brevity, the human subsystem by the letter H and the agricultural subsystem by the letter A. Having in mind agricultural production in the United States only, we may estimate the material flow in the direction A → H as 400 million tons annually, 200 million being cereals. The reverse flow in the direction H → A may be estimated as 200 million tons annually. This flow in-

volves such components as fertilizers, machinery, fuel, and materials. Is this flow large or small? One may think that there are reasons to consider it large as it amounts to about 3 kg per capita daily.

Let us now compare the power of mutual energy flows between the subsystems. The population of the United States obtains from its partner in symbiosis about 10^{15} kcal or 10^{12} kW·h annually in the form of chemical energy stored in farm products. This is a unique form of energy that cannot be replaced by any other form, whether electrical, mechanical, or nuclear. This energy is necessary to maintain the life and activity of 260 million inhabitants, each consuming from 2500–5000 kcal daily depending on their physical load. Thus, the total power of energy flow in the direction A → H is very great. It is commensurable with the power of all the atomic stations in U.S. territory.

The reverse energy flow in the direction H → A may be estimated as follows. The annual consumption of electrical energy by agriculture in the United States is 1.3×10^{11} kW·h. Consumption of other forms of energy such as heat and mechanical are presumably 10–15 times higher. The total energy flow from subsystem H to A is on the same order of magnitude as that in the direction A → H.

The scale of interrelations between the subsystems H and A in the symbiotic system of agriculture may also be illustrated by another criterion: the cost that subsystem H pays to subsystem A for all that it obtains from the latter. These are the payments for foodstuff, which cannot be obtained from any other source but subsystem A. This cost cannot be expressed in dollars or yen or in tons of gold or silver. Such things are of value only for people, but not for their symbionts. Subsystem A is in need of a "currency" of quite a different sort, one that is of real value for it. Such a "currency" is human labor either in its immediate or material form. Thus, humankind must spend a lot of time satisfying the requirements of its symbionts.

More than one-half of the world's population is directly engaged in agriculture. In developing countries most people are occupied with rather primitive agriculture. The inhabitants of industrialized countries are concerned with agriculture to a lesser degree, but it would be erroneous to implicitly trust the statistical data on the subject. The smaller the value provided by statistics, the greater the correction that should be introduced to obtain an impression of the actual number of people involved in agriculture either directly or indirectly. Statistical data usually deal with the number of farmers, but it is not only farmers that drive the agricultural industry. The more advanced the country, the greater the number of people that are indirectly involved in the agricultural industry. These are the people that produce fertilizers and pesticides, farm machinery, fuel, and electricity. They also work at amelioration, transport, agricultural building, education and research, and food processing. If all of these are summed, the values that characterize the fraction of the population involved in the agricultural industry in any way will be much greater than the formal statistical data. These values will be no less than 30–

40% even for the most advanced countries with the most developed agriculture. That is the immensity of the price humankind pays to its symbiotic partners.

At the dawn of history, some 5000–7000 years ago, almost 100% of human labor, time, and creative capacity were occupied by agriculture. Now this figure is smaller but is not significantly lower. Despite the remarkable industrial progress of the past century, the total share of the world's population whose lives are connected with agriculture exceeds 50% at this time.

Thus, our symbiont, subsystem A, must be considered a serious partner in our coexistence on Earth. Therefore, we must know all about our partners, or at least the most important facts. It is necessary for humankind to perform its functions within the symbiotic alliance H ↔ A in the best way possible.

We should emphasize here another fundamental distinction of agriculture from any other kind of industrial activity, say mining or the production of steel or cars. In all these cases except for agriculture, the term "exploitation" may always be used. One may speak of exploiting an oil field, an auto factory, or a railway. The term may be also in order when discussing some forms of social relations. It does not seem pertinent, however, in relation to the symbiotic system under consideration. The point is that the term exploitation supposes a certain asymmetry in relations between the parts of the system. These relations are always one-sided. One of the allies leads the other to do something to obtain some profit for itself without equivalent compensation for the partner. However, interactions between subsystems H and A in the symbiotic system of agriculture should not be interpreted as one-sided. Therefore, it would not be correct to think that humankind exploits its biological partners. That falls out of the nature of things. One-half of human population expends its time and labor to meet the needs of its symbionts and does its best to offer them optimal conditions for production. Humankind literally feeds them. Cultivated plants in developed countries now obtain from people about one-half the necessary amount of nitrogen, about one-third of their potassium, and almost the full amount of necessary phosphorus. Thus, symbiotic relations in the H ↔ A system consist of a mutually profitable, although rather specific division of labor.

What is the basis for this division? To determine an answer for this question, the abilities and needs of both subsystems should be taken into account. Assuming that we know enough about ourselves in this respect, we must look upon the real abilities of our biological partners. Our partners can transform the energy of solar rays into the chemical energy of proteins, carbohydrates, and fats, the substances we need for food. We still cannot perform this function in spite of all our scientific advances. Thus, the conversion of solar energy into the chemical energy of organic substances is the most significant and, for us, indispensable function performed by our symbiotic partners. This function is fulfilled by domesticated plants. Domesticated animals only provide "conditioning" of the substances originated by the plants. They chew coarse vegetable food, transforming it into

meat or milk for us. This is by no means an essential function, but it is in any case a secondary one in relation to that performed by plants. Thus, plants cultivated by people provide the grounds of our prosperity.

Unlike animals, plants almost seem to be creatures from a different world. They are constructed from the same materials, but the basic principles of their design are quite different from those of animals. Meanwhile, we are related to plants, although much more remotely than to animals. The genealogical paths of humans and plants diverged some $1-2$ billion years ago. Up to that point, the evolutionary "design" of biochemical processes had been essentially complete. Therefore, the biochemistry of plants and animals is compatible, and we can feed on substances produced by plants. As for physiological mechanisms, nature needed some hundreds million more years to develop them. Several fundamentally differing variants of living beings have been created. We belong to one category, whereas plants belong to quite another one. Though humankind has dealt with plants throughout its history, and though it examines their life and function both in day-to-day practice and with the help of the most modern scientific methods, nevertheless it knows far less about plants than about its closer relatives, the animals.

Let us now return to our examination of the plant component of the symbiotic system H $\leftrightarrow$ A. Its inherent and most significant function for us is photosynthesis, because this is the process that supplies us with substances to eat. However, that aspect is seen from humankind's point of view, from the outlook of the consumers of plant products. If one looks at the problem from the plant's point of view, the situation would seem somewhat different. Photosynthesis is, of course, a fundamental process that provides indispensable life necessities for the plant, but it can hardly be considered the main objective of the plant's life. This process is surely not the goal but only the means by which the plant supplies itself with material to build its body and energy to perform its various life functions. As humankind in its symbiotic relation with the plants is after all concerned with obtaining a greater yield, its efforts should be directed toward making easier some of the life functions of its symbionts. In this way humans can facilitate the redistribution of the energy balance of the plant in favor of the accumulation of excess energy in additional biomass.

The total human contribution into the energy balance of agricultural plants is quite minor, not exceeding 1%, compared with energy that plants obtain from the Sun. At the same time this contribution is large if compared with the energy that plants accumulate in the organic matter that they produce. In any case, the purposeful and directed energy contribution makes it possible for humankind to be of service to its symbiotic partners. Important services of diverse kinds are rendered to plants on both biological and technological levels.

The most effective and most impressive results of human activity on the biological level are those concerned with the process of evolution of cultured plants. It would not be an exaggeration to suppose that the rate of evolution of agricultural

plants has increased by at least 1000 or even 10,000 times since the mechanism of natural selection has been substituted by advanced methods of selection and genetics. No wild species changes its genetic aspects as fast as species that "collaborate" with humankind.

Humankind's contribution to plant functioning on the technical level mainly consists of soil cultivation, water delivery, and nutrient supply. These operations facilitate plant activities such as forming their structures, defending against biological competitors, and extracting nutrients from the soil.

Humankind spends a great deal of labor, including primitive handwork, mechanized work in developed societies, and intellectual work, to fulfill its functions and obligations to the symbiotic system H $\leftrightarrow$ A. What assumptions should be made about an optimum strategy that humankind should adopt toward its symbionts? On the whole, human efforts are directed toward a continual increase in the total productivity of the H $\leftrightarrow$ A system along with a gradual decrease in the relative expenditure of human labor. The current strategy includes the further mechanization of agricultural processes, use of increasing amounts of fertilizers, and selection for high-yield crops. This strategy is in essence an extension of the same principles used by humankind at the beginning of its agricultural activity thousands of years ago. This strategy will satisfy the needs of humankind for yet some time. One should note, however, that each subsequent step in this direction provides diminishing returns and demands greater cost. Eventually the increasing demands on food supply for the increasing population of Earth will cause a deepening of the interdependence between humankind and its plant domesticates. This will manifest itself in the gradual transition from current agricultural practice, which can be characterized as a strategy of "engines," to a string of "structures."

A strategy of engines represents a direct extension of the traditional mode of progress in agriculture. The major steps along this path are as follows: hoe and sickle, wooden plow, iron plow, tractors, and finally combines and other farm machinery. These are all qualitative stages on the road of agricultural development. Nevertheless, it is an extensive mode of development. It demands the use of vast areas of land. It is connected with the huge expenditure of energy, water, and human labor. It retains a seasonal character and strong dependence upon climatic and weather conditions. One may project that in the future the tendency to use biotechnological systems with some "structures" partly or completely isolated from the environment will increase. These structures will resemble the current hothouse to a certain degree. Technological process within such structures will be not so rigidly bound to seasonal conditions, and thus they can be organized more rationally as continuous operations. In such structures, closed water cycles can be implemented, thus making agriculture much more independent from water supplies, which are becoming increasingly scarce. The efficiency of utilization of fertilizers may also increase.

A gradual transition to the strategy of structures will demand a certain tight-

ening of all symbiotic human–plant interrelations. Humans should free their sym-
bionts from performing their most unproductive biological functions. In a sense,
plants should be transformed into "parasites" of the engineering system to allow
them to focus their potential on performing two basic processes: reproduction and
the production of organic material by photosynthesis. Humans require only these
products of plant processes.

Industrial systems in which tight interactions between engineering and bio-
logical components are in place for the sake of maximum productivity are now
widely used. Examples are modern farms for the industrial breeding of pork and
poultry. An animal in such places is a true "parasite" of the engineering system,
performing only the functions of gaining weight and reproducing.

Therefore, the strategy of structures will be put into practice gradually, over a
rather long time. It will require prodigious investments. Many problems concern-
ing both engineering and biology will arise and should be solved. However, the
need for food will force humankind to take this path sooner or later. In fact we are
already advancing in this direction step by step.

The transition to growing plants in biotechnological structures will make agri-
culture more similar to other branches of industry, but some fundamental distinc-
tions will remain. It seems reasonable to emphasize the specific features of agri-
culture that distinguish it from mechanical industries. Any type of industry deals
with passive, dead materials, whereas the objects of farm production are living
things that can actively respond to any external input. A passive material may be
affected by any means consistent with the objective of this influence. A living
system demands much more delicate handling: a rough approach is impermissible.
Any attempt to force a living thing to do something that it is not able to do will
fail. Living systems may be adapted and acclimated, but they cannot be compelled.
Humankind in its turn must also acclimate and adapt to the living systems with
which it interacts. This is, of course, a difficult, complicated, and delicate task.

A qualitative difference between agriculture and industry may be visualized by
comparing the course of their development as a function of engineering progress.
This is shown symbolically in Fig. 15.3. Progress in industry is impossible if the
level of engineering is too low. Some initial threshold level of technical ability
must be achieved before initiating the development of industry. However, once
started, this process will proceed with self-acceleration, because engineering is
the prerequisite and at the same time the product of the development of industry.
Through engineering a positive feedback loop that determines the self-accelerating
character of the process as a whole is formed.

Agricultural activity, in contrast to industry, is possible even at a minimal level
of skill. It is, however, rather primitive, unproductive, and unreliable in this case.
Progress in engineering holds particular promise for progress in agriculture by
increasing its productivity and efficiency. But engineering itself cannot cause the
self-accelerating development of agriculture because the products of agriculture
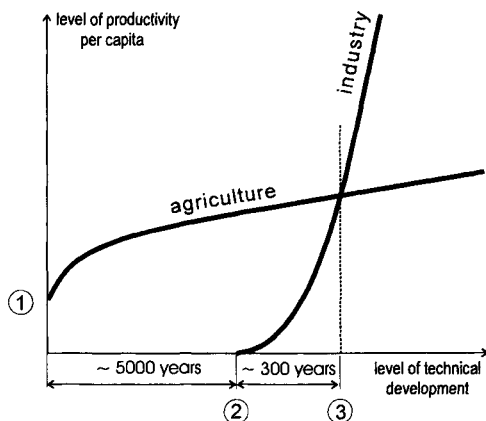
Figure 15.3 Agriculture and industry develop according to fundamentally different laws. The industry develops with self-acceleration due to positive feedback, whereas in the case of agriculture the feedback is negative.

do not engage in a feedback loop. Hence, even the progressive introduction of new techniques in agriculture leads only to the gradual increase in production, much less than in industry. This peculiarity of agriculture results from the fact that agriculture is in a certain sense more complicated than any other kind of industry, even the most sophisticated ones. It is more complicated because it deals with the intricacies of living matter, in contrast to other kinds of industry, which deal with dead matter only.

Humankind laid the foundation for further prosperity when it succeeded in establishing symbiotic relations with some plant and animal species. On the long and not always straightforward path of its presence on Earth, humankind has imagined its own role in nature in different ways. In the early stages humans fetishized nature, and then they intended to conquer it. These were, however, nothing but signs of human immaturity. Only now we are coming close to understanding our indispensable connection with other forms of life on Earth. As the only thinking creature, humankind must recognize its responsibility to maintain Earth in a state suitable for life.

This Page Intentionally Left Blank

Appendix

SYMBOLS

CHAPTER 1

BB, black-body radiation
c, light velocity ($2.998 \cdot 10^8$ m/s)
D, volume density of photons
D_ν, volume density of photons at frequency ν (E/m^3)
E, Einstein = one mole of photons = $6.02 \cdot 10^{23}$ photons
E, irradiance (W/m^2)
I, intensity of radiation (W/m^2 sr)
h, Planck constant ($6.626 \cdot 10^{-34}$ J $\cdot$ s)
I_λ, intensity of radiation at wavelength λ (W/m^2 sr nm)
I_ν, intensity of radiation at frequency ν (W/m^2 sr Thz)
k, Boltzmann constant ($1.38 \cdot 10^{-23}$ J/K)
N, intensity of photon flux (mol/m^2 sr s or E/m^2 sr s)
N_λ, intensity of photon flux at wavelength λ (mol/m^2 sr s nm)
N_ν, intensity of photon flux at frequency ν (mol/m^2 sr s Thz)
PAR, photosynthetically active radiation
r, radius of an aerosol particle
s, cross section of scattering
S, intensity of radiation of entropy (J/K)/m^2 sr s)
S_ν, intensity of radiation of entropy at frequency ν (J/K)/m^2 sr s Thz)
T, absolute temperature (K)
t, time (s)
$T_{\nu,\gamma}$, effective temperature of diluted radiation at frequency ν (K)
T_s, temperature of a source of radiation (K)
U, volume density of radiation (J/m^3)
U_ν, volume density of radiation at frequency ν (J/m^3 Thz)
α, an incidence angle
β, ratio of energy of quanta to average energy of heat motion (hν/kT)
γ, dilution factor

λ, wavelength (nm = 10^{-9} m)
ϕ, azimuth angle
λ, wavelength
ν, frequency (THz = 10^{12} Hz)
ρ, factor determining relation between the size of aerosol particle and the wavelength of light
σ, area (m^2)
ω, solid angle (steradian (sr))

CHAPTER 2

A, albedo of a foliar system
B, solar constant equal to 1.39 kW/m^2
D, intensity of diffuse light
d, share of diffuse component in daylight
E, irradiation (W/m^2)
F, attenuation (extinction) factor
I, intensity of radiation
K, an orientation factor
L, characteristic size of foliar system
r, share of PAR in the incident radiation
S, a foliar index
Superscripts ∘, ∗, and = denote the quantities related accordingly to direct light, diffuse light from clear sky, and diffuse light from cloudy sky, respectively
Subscripts s, h, and v denote the quantities related to spherical, horizontal, and vertical foliar systems, respectively
t, a time angle of the Sun
α, cross section of scattering in atmosphere
δ, declination of the Sun
ϵ, coefficient of pure scattering of leaves
ϕ, latitude of a place
$\phi(\lambda, \mu)$, Hambarzumian function
$\kappa(\gamma)$, indicatrix of scattering in atmosphere
λ, coefficient of pure scattering in atmosphere
μ, a cosine of an angle between vertical line and the direction of a light beam
$\mu_\circ$, a sine of the angle of solar elevation
ν, frequency of radiation
θ, angle between vertical line and the direction of the light beam
$\rho(\epsilon, \mu, \mu_\circ)$, coefficient of brightness of a foliar layer
$\sigma(\mu, \mu_\circ)$, coefficient of brightness of diffuse light
τ, optical thickness

τ_o, optical thickness of atmosphere at AM1
ω, a solid angle of light flux (ster)

CHAPTER 3

ATP, adenosine triphosphate
RuBP, ribulose bisphosphate

CHAPTER 4

G, energy capacity of metabolites (J/mol)
J, flow of metabolites through transport system of a leaf (mol/s)
k, permeability of the phloem (mol^2/m^2 s N)
L, length of a leaf (m)
N, a net rate of harvesting energy in a leaf (W)
p, a potential rate of accumulation of energy in metabolites per unit area per unit time (W/m^2)
P, potential rate of accumulation of energy by a leaf (W)
R, radius of a leaf (m)
r_s, an equivalent radius of transport channels in a stalk (m)
V, effective volume of phloem system in a leaf (m^3)
W, rate of dissipation of energy in transport system of a leaf (W)
X, motive force of phloem transport (N/mol)
α, ratio of the leaf area to effective cross section of a phloem in a stalk
β, length to a width ratio of a ribbon-like leaf
δ, effective thickness of the transport system (m)
γ, length of the stalk to the leaf radius ratio
η, efficiency of harvesting energy

CHAPTER 5

A, affinity (J/mole)
E, energy (J/mole)
G, Gibbs free energy
H, enthalpy
J, generalized thermodynamic flux
j, normalized thermodynamic flow
L, phenomenological coefficient defining the relation between force and flux
Q, heat (J/mole)

r(γ), auxiliary function
S, entropy (J/mole · K)
T, temperature (K)
T_s, temperature of a source of radiation
T_c, temperature of a cold source
T_h, temperature of a hot source
W, work (J)
X, generalized thermodynamic force
x, normalized thermodynamic force
$Y = T^{-1}$, auxiliary coordinate
Φ, dissipative function
γ, a dilution factor
η, efficiency of energy conversion
μ, chemical potential
ρ, factor defining the relation between the values of external load and the internal resistance of the energy transforming engine
ω, a solid angle (steradian (sr))
ζ, coupling factor

CHAPTER 6

A, affinity
a_i, activity of i-th component
E, redox potential
$E^{\circ\prime}$, midpoint potential at pH = 7
E°, standard redox potential (pH = 0)
F, Faraday number (96500 C)
m, number of protons
n, number of electrons
ϕ, electrical potential
μ_i, chemical potential of i-th component
ν_i, stoichiometric number of i-th component

CHAPTER 7

a, radius
ATP, adenosine triphosphate
$\vec{D}$, induction of the electric field
E_c, configurational potential

E_s, reorganization energy
F, Faraday constant
ΔG_c, configurational Gibbs free energy
h, distance of charge transfer
n, number of charges
NADH, nicotinamide adenine dinucleotide
OEC, oxygen evolving complex
Pheo, pheophytin
PSI, photosystem I
PSII, photosystem II
Q, plastoquinone
R, coordinate
X^0, mole fraction
Y_D, tyrosine 160
Y_Z, tyrosine 161
$\Delta_\beta^\alpha \phi$, interfacial potential between phases α and β
ϵ_0, dielectric permittivity of a vacuum
ϵ_{op}, optical dielectric permittivity
ϵ_{st}, static dielectric permittivity

CHAPTER 8

ATP, adenosine triphosphate
E_a, energy of activation
E_s, reorganization energy
NADH, nicotinamide adenine dinucleotide

CHAPTER 9

B, leaf size (m)
c_p, heat capacity of air
D, diffusion coefficient (m^2/s)
d, moisture content of air (g/kg of dry air)
E, radiation flux (W/m^2)
ΔE, radiative balance (W/m^2)
H, enthalpy flux (W/m^2)
ΔH, total enthalpy balance (W/m^2)
h, enthalpy of air (kJ/kg)
h_v, enthalpy of water vapor (kJ/kg of water)

h_w, enthalpy of evaporation (44.006 kJ/mol)

J_0, exchange flow (W/m^2)

J_q, flow of heat (W/m^2)

J_v, flow of enthalpy (W/m^2)

k_f, an inclination factor of isoenthalpic line ($U_q \cdot c_p / U_v \cdot h_v$)

L, total flow of air

N, number of stomata per unit area (cm^{-2})

p, atmospheric pressure (Pa)

p_s, saturation pressure of water vapor (Pa)

p_v, partial pressure of water vapor (Pa)

R, gas constant (8.314 J/mol)

s, entropy of evaporation (214.5 (J/K)/mol)

T, absolute temperature (K)

t, temperature ($^\circ$C)

U_b, conductance of the boundary layer (m/s)

U_c, conductance of a cuticle (m/s)

U_q, conductance of the pathway for heat flow (m/s)

U_s, conductance of stomata (m/s)

U_v, conductance of the pathway for diffusion (m/s)

V, wind velocity (m/s)

W, total flow of water vapor

ΔW, amount of evaporating water (kg/m^{2}s)

δ, thickness of a boundary layer (m)

η, viscosity of air (Pa $\cdot$ s)

ϕ, relative humidity of air

ρ, density of air (kg/m^3)

CHAPTER 10

A_{mem}, membrane area

D, diffusion coefficient

d, thickness of hydrophobic part of a membrane

f_p, total number of pores

$\Delta_\beta^\alpha G(el)$, electrostatic component of the Gibbs free energy of ion transfer

$\Delta_\beta^\alpha G(svph)$, solvophobic component of the Gibbs free energy of ion transfer

$\Delta_\beta^\alpha G(tr)$, the Gibbs free energy of transfer

hc, hydrocarbon

n(s), number of pores per membrane area between pore area s and s + ds

$\underset{\sim}{n}_o$, pore formation frequency factor

$\tilde{P}$, medium polarization fluctuation

P_i, permeability coefficient
R, gas constant
R_{avg}, the vesicle radius
T, absolute temperature
w, aqueous phase, water
α or β, phase α or β
ϵ, macroscopic dielectric constant
$\epsilon(k)$, static dielectric function
ϵ_{opt}, optical dielectric permittivity
γ, interfacial tension
Λ and λ, correlation radii for Debye and vibrational polarization

CHAPTER 11

a_w, activity of water
a_{win}, activity of water at internal side of a cell wall
a_{wout}, activity of water at external side of a cell wall
c, concentration
E, energy
g, gravitational constant
J_s, density of flow of solar radiation
J_w, flow of water
P, pressure
P_{cap}, capillary pressure
P_{hd}, hydrodynamic pressure
P_{st}, hydrostatic pressure
P_{top}, pressure at the top of a capillary
V_w, molar volume of water ($1.8 \cdot 10^{-5}$ m^3/mole)
ν_{osm}, velocity of electro-osmotic flow
ν_w, average linear velocity of a liquid flow
ζ, electrokinetic or zeta potential
ϵ_0, dielectric permittivity of a vacuum
γ, interfacial tension
η, viscosity
ϕ, degree of air saturation or relative humidity
λ, heat of evaporation
μ^0, standard chemical potential
v, correction factor
Θ, contact angle or angle of wetting
Θ', apparent contact angle

ρ, density of water (10^3 kg/m^3)
Ψ, water potential
Ψ_{osm}, osmotic potential

CHAPTER 12

E, energy
J, flux
NADH, nicotinamide adenine dinucleotide
p, partial pressure
p^0, standard pressure
S, entropy
X, force
η, efficiency

CHAPTER 13

a, activity
E, electrode potential
E^0, standard electrode potential
F, Faraday constant
ΔG, Gibbs free energy
R, gas constant
T, absolute temperature

CHAPTER 14

A_λ, absorbance at the wavelength λ
DNP, 2,4-dinitrophenol
ΔG^0, standard Gibbs free energy
ΔH_m, linewidth of chlorophyll a monomer
ΔH_n, linewidth when the unpaired spin is delocalized over N molecules
I_λ, photocurrent at wavelength λ
m, number of protons
N, number of chlorophyll a molecules
n, number of electrons
OTE, optically transparent electrode
PCP, pentachlorophenol
P_i, partition coefficient

q, elementary charge
QH_2, hydroquinone
Θ_λ, quantum efficiency
μ^0, standard chemical potential

CHAPTER 15

A, agriculture subsystem
H, human subsystem
p(r), productivity of a species

This Page Intentionally Left Blank

References

Abe, T. (1981). Chloride ion efflux during an action potential in the main pulvinus of *Mimosa pudica. Bot. Mag. (Tokyo)* **94,** 379–383.

Abe, S., J. Takeda, and M. Senda (1980). Resting membrane potential and action potential of *Nitella expansa* protoplasts. *Plant Cell Physiol.* **21,** 537–546.

Abramson, A. A. (1981). "Surface Active Compounds. Properties and Applications." Khimiya Publ. House, Leningrad.

Agostiano, A., M. Dellamonica, and A. Mallardi (1992). Chlorophyll *a* dimer photoreactions in lecithin organogels. *J. Photochem. B* **13,** 241–251.

Aizawa, H., M. Hirano, and S. Suzuki (1979). Photoelectrochemical oxygen evolution from water by a manganese clorophyll-liquid crystal electrode. *Electrochim. Acta* **24,** 89–94.

Alekseev, V. A., and S. V. Belov (1960). Spectral reflectance of trees and other objects of western Ukraine. *Trud. Lab. Aerometeorol.* **10,** 105–122.

Allen, W. A., T. V. Gayle, and A. J. Richardson (1970). Plant-canopy irradiance specified by Duntley equations. *J. Opt. Soc. Am.* **60,** 372–376.

Almgren, M. (1978). Thermodynamic and kinetic limitations on the conversion of solar energy into storable chemical free-energy. *Photochem. Photobiol.* **27,** 603–609.

Ananjev, G. M., and V. V. Klimov (1988). Light induced formation of bound hydrogen peroxide in subchloroplast preparation of photosystem II. *Dokl. Acad. Nauk SSSR* **298,** 1007–1011.

Andersen, O. S., and M. Fuchs (1975). Potential energy barriers to ion transport within lipid bilayers. Studies with tetraphenylborate. *Biophys. J.* **15,** 795–830.

Andersen, O. S., S. Felberg, H. Nakadomari, S. Levy, and S. McLaughlin (1978). Electrostatic interactions among hydrophobic ions in lipid bilayer membranes. *Biophys. J.* **21,** 35–70.

Anderson, A. F. H., and M. Calvin (1963). Electron spin resonance of crystalline chlorophyll *a* and crude mixtures of chlorophyll *a* with normally associated pigments. *Nature* **199,** 241–243.

Anderson, A. F. H., and M. Calvin (1964). The aggregation of chlorophylls. *Arch. Biochem. Biophys.* **107,** 251–259.

Antonini, E. M., C. Brunory, C. Greenwood, and B. G. Malmstrom (1970). Catalytic mechanism of cytochrome oxidase. *Nature* **228,** 936–937.

Antonov, G. (1907). Sur la tension superficielle a la limite de deux couches. *J. Chim. Phys.* **5**, 372–385.

Arakelyan, V. B., and S. B. Arakelyan (1983). Energetic profile of a dipole molecule in the thin membrane. *Biol. Zh. Armen.* **36**, 775–779.

Arakelyan, V. B., S. B. Arakelyan, T. M. Avakyan, and V. M. Aslanyan (1985). Electrostatic effect on transport of water across bilayer lipid membrane. *Biophysics* **30**, 186–187.

Arcibashev, E. S., and S. V. Belov (1958). The reflectance of tree species. *Trud. Lab. Aerometeorol.* **10**, 105–122 (in Russian).

Atkins, P. W. (1994). "Physical Chemistry," 5th ed. W. H. Freeman, New York.

Bangham, A. D., M. M. Standish, and J. C. Watkins (1965). Diffusion of monovalent ions across the lamellas of swollen phospholipids. *J. Mol. Biol.* **13**, 238–252.

Barber, J., J. Mills, and A. Love (1977). Electrical diffuse layers and their influence on photosynthetic processes. *FEBS Lett.* **74**, 174–181.

Bard, A. J., and M. A. Fox (1995). Artificial photosynthesis—solar splitting of water to hydrogen and oxygen. *Acc. Chem. Res.* **28**, 141–145.

Barry, B. A., and G. T. Babcock (1987). Tyrosine radicals are involved in the photosynthetic oxygen-evolving system. *Proc. Natl. Acad. Sci. USA* **84**, 7099–7103.

Bassham, J., and D. Buchanan (1982). Carbon dioxide fixation pathways in plants and bacteria. *In* "Photosynthesis" (Govinjee, ed.), Vol. 2, pp. 143–189. Academic Press, New York.

Bayliss, W. M. (1923). "Interfacial Forces and Phenomena in Physiology." Methuen & Co. Ltd., London.

Bazarov, I. P. (1964). "Thermodynamics." Pergamon Press, Oxford.

Beevers, L. (1976). "Nitrogen Metabolism in Plants." Elsevier, New York.

Bell, R. P. (1931). The electrical energy of dipole molecules in solution and solubilities of ammonia, hydrogen chloride, and hydrogen sulfite in various solvents. *J. Chem. Soc.* **32**, 1371–1381.

Bell, L. N. (1980). "Energetics of Photosynthesizing Plant Cell." Nauka Publ. House, Moscow.

Bell, C. G., and D. A. Rose (1981). Light measurement and the terminology of flow. *Plant Cell Environ.* **4**, 89–96.

Benjamin, I. (1996). Molecular dynamics of charge transfer at the liquid/liquid interface. *In* "Liquid-Liquid Interfaces. Theory and Methods" (A. G. Volkov and D. W. Deamer, eds.), pp. 179–211. CRC Press, Boca Raton, FL.

Bentrup, F. W. (1979). Reception and transduction of electrical and mechanical stimuli. *In* "Encyclopedia of Plant Physiology N.S." (W. Haupt and M. E. Feinleib, eds.), Vol. 7, pp. 42–70. Springer-Verlag, Berlin.

Bernal, J. D. (1967). "The Origin of Life." World Publ. Co., Cleveland.

Berry, J., and W. J. Downton (1982). Dependence of photosynthesis upon environmental factors." *In* "Photosynthesis" (Govinjee, ed.), Vol. 2, pp. 263–343. Academic Press, New York.

Bertholon, M. (1783). "De l'electricite des vegetaux: ouvrage dans lequel on traite de l'electricite de l'atmosphere sur les plantes, de ses effets sur leconomie des vegetaux, de leurs vertus medico." P. F. Didotjeune, Paris.

Bewig, K. W. (1964). Ionization method of measuring contact potential differences. *Rev. Sci. Instrum.* **35**, 1160–1162.

Bird, R. B., W. E. Stewart, and E. M. Lightfoot (1960). "Transport Phenomena." Wiley and Sons, New York.

Birdi, K. S. (1993). "Fractals in Chemistry, Geochemistry and Biophysics. An Introduction." Plenum Press, New York.

Blank, M. (1991). Membrane transport: insights from surface science. *In* "Interfacial Phenomena in Biological Systems" (M. Bender, ed.). M. Dekker, Inc., New York.

Blumenfeld, L. A. (1981). "Problems of Biological Physics." Springer-Verlag, New York.

Blumenfeld, L. A. (1983). "Physics of Bioenergetic Processes." Springer-Verlag, New York.

Blumenfeld, L. A., and A. N. Tikhonov (1994). "Biophysical Thermodynamics of Intracellular Processes. Molecular Machines of Living Cell." Springer-Verlag, New York.

Bockris, J. O., and A. K. N. Reddy (1970). "Modern Electrochemistry," Vol. 1. Plenum Publishing Corporation, New York.

Boer, K. W. (1977). The solar spectrum of typical clear weather days. *Solar Energy* **19**, 525–538.

Boguslavsky, L. I., and A. G. Volkov (1975). Photoinduced proton transfer across decane/water interface in the presence of chlorophyll. *Dokl. Akad. Nauk SSSR* **224**, 1201–1204.

Boguslavsky, L. I., A. G. Volkov, M. D. Kandelaki, and E. A. Nizhnikovsky (1976a). Photooxidation of water and proton transport through the interface between two immiscible liquids in the presence of chlorophyll. *Dokl. Akad. Nauk SSSR* **227**, 727–730.

Boguslavsky, L. I., A. G. Volkov, and M. D. Kandelaki (1976b). Transfer of electrons and protons at the decane/water interface in the presence of chlorophyll. *FEBS Lett.* **65**, 155–158.

Boguslavsky, L. I., A. G. Volkov, M. D. Kandelaki, E. A. Nizhnikovsky, and M. A. Bibikova (1977). Photooxidation of water in the presence of chlorophyll and the iron complex of coproporphyrin-III adsorbed at the octane/water interface. *Biofizika* **22**, 223–227.

Boguslavsky, L. I., Zhuravlev, M. D. Kandelaki, and K. Shengeliya (1978). Study of water photooxidation at the octane/water interface in the presence of chlorophyll by a mass-spectrometric method. *Dokl. Akad. Nauk SSSR* **240**, 1453–1456.

Boguslavsky, L. I., and A. G. Volkov (1987). Redox and photochemical reactions at the interface between immiscible. *In* "The Interface Structure and Electrochemical Processes at the Boundary Between Two Immiscible Liquids" (V. E. Kazarinov, ed.), pp. 143–178. Springer-Verlag, Berlin.

Bolton, J. R. (1978). Solar fuels. The production of energy-rich compounds by the photochemical conversion and storage of solar energy. *Science* **202**, 705–711.

Born, M. (1920). Volumen und Hydrationswarme der Ionen. *Z. Phys.* **1**, 45–48.

Bose, J. C. (1907). "Comparative Electrophysiology." Longman, Green and Co., London.

Bose, J. C. (1914). An automatic method for the investigation of velocity of transmission of excitation in Mimosa. *Philos. Trans. B* **204**, 63–97.

Bose, J. C. (1924). "Physiology of Photosynthesis." Longmans, Green and Co., New York.

Bose, J. C. (1925). Transmission of stimuli in plants. *Nature* **115**, 457.

Bose, J. C. (1926). "The Nervous Mechanism of Plants." Longmans, Green and Co., New York.

Bose, J. C. (1927a). "Plant Autographs and their Revelations." The Macmillan Company, New York.

Bose, J. C. (1927b). Transmission of excitation in plants. *Nature* **119**, 48–48.

Bose, J. C. (1964). "Selected Works." Nauka Publ. House, Moscow (in Russian).

Brillouin, L. (1963). "Science and Information Theory." Academic Press, New York.

Brittin, W., and G. Gamov (1961). Negative entropy and photosynthesis. *Proc. Natl. Acad. Sci. USA* **47**, 724–727.

Broda, E. (1975). "The Evolution of Bioenergetic Processes." Pergamon Press, New York.

Brody, S. S., G. Newel, and T. Castner (1960). Paramagnetic resonance of chlorophyll crystals and solutions. *J. Phys. Chem.* **64**, 554–557.

Brody, S. S., and N. F. Owens (1976). Photosynthetic electron carriers at a heptane/water interface. *Z. Naturforsch.* **31**, 567–571.

Brown, A. R., L. J. Yellowlees, and H. H. Girault (1993). Photoinduced electron-transfer across the interface between two immiscible electrolyte solutions. *J. Chem. Soc., Faraday Trans.* **89**, 207–212.

Brudvig, G. W., and R. H. Crabtree (1986). Mechanism for photosynthetic O_2 evolution. *Proc. Natl. Acad. Sci. USA* **83**, 4586–4588.

Burdon-Sanderson, J. (1873). Note on the electrical phenomena which accompany stimulation of the leaf of *Dionaea muscipula*. *Proc. R. Soc. London* **21**, 495–496.

Burdon-Sanderson, J., and F. J. M. Page (1876). On the mechanical effects and on the electrical disturbance consequence on excitation of the leaf of *Dionaeva* muscipula. *Proc. R. Soc. London* **25**, 411–434.

Burdon-Sanderson, J. (1882). On the electromotive properties of *Dionaeva* in the excited and unexcited states. *Philos. Trans.* **173**, 1–53.

Burdon-Sanderson, J. (1888). On the electromotive properties of the leaf of *Dionaeva* in the excited and unexcited states. *Philos. Trans. B* **179**, 417–449.

Busbride, I. W. (1960). "The Mathematics of Radiative Transfer." Harvard University Press, Cambridge, MA.

Byvik, Ch. E., A. M. Buoncristiani, and B. T. Smith (1983). Limits to solar power conversion efficiency with application to quantum and thermal systems. *J. Energy* **7**, 581–588.

Canny, M. J. (1995). Apoplastic water and solute movement: new rules for an old space. *Annu. Rev. Plant Physiol. Plant Mol. Biol.* **46**, 215–236.

Caplan, S. R., and A. Essig (1983). "Bioenergetics and Linear Nonequilibrium Thermodynamics: The Steady State." Harvard University Press, Cambridge, MA.

Carnot, N. L. S. (1887). "Reflexions sur la puissance motrice du feu et sur les machines propres a developper cette puissance." Librarie Philosophique, J. Vrin, Paris.

Cass, A., and A. Finkelstein (1967). Water permeability of thin lipid membranes. *J. Gen. Physiol.* **50**, 1765–1784.

Casta, S., and G. Porter (1974). Model systems for photosynthesis. Photosensitization by chlorophyll *a* monolayers at a lipid/water interface. *Proc. R. Soc. London* **A341**, 167–176.

Chance, B., C. Saronio, and I. S. Leigh (1975). Functional intermediates in the reaction of membrane-bound cytochrome oxidase with oxygen. *J. Biol. Chem.* **250**, 9226–9237.

Chance, J. E., and E. W. LeMaster (1977). Suits reflectance models for wheat and cotton: theoretical and experimental tests. *Appl. Optics* **16**, 407–412.

Chandrasekhar, S. (1960). "Radiative Transfer." Dover Publications, New York.

Collatz, G. J., J. T. Ball, C. Grivet, and J. A. Berry (1991). Physiological and environmental

regulation of stomatal conductance. Photosynthesis and transpiration: a model that includes a laminar boundary layer. *Agr. Forest Meteorol.* **54**, 107–136.

Connoly, J. S., A. F. Janzen, and E. B. Samuel (1982). Fluorescence lifetimes of chlorophyll *a*: Solvent, concentration and oxygen dependence. *Photochem. Photobiol.* **36**, 559–563.

Conway, B. E. (1981). "Ionic Hydration in Chemistry and Biophysics." Elsevier, New York.

Cramer, W., and A. Crofts (1982). Electron and proton transfer. *In* "Photosynthesis," (Govindjee, ed.), Vol. I, Energy Conversion by Plants and Bacteria, pp. 387–468. Academic Press, New York.

Critchley, C., and A. M. Sargeson (1984). A manganese chloride cluster as the functional centre of the O_2 evolving enzyme in photosynthetic systems. *FEBS Lett.* **177**, 2–5.

Curzon, F. L., and B. Ahlborn (1975). Efficiency of a carnot engine at maximum power output. *Am. J. Phys.* **43**, 22–23.

Dainty, J. (1963). Water relations of plant cells. *Adv. Bot. Res.* **1**, 279–326.

Daubenmire, R. (1968). "Plant Communities." Harper & Row, New York.

Davies, E., and A. Shuster (1981a). Intercellular communication in plants: Evidence for a rapidly generated, bidirectionally transmitted wound signal. *Proc. Natl. Acad. Sci. USA* **78**, 2422–2426.

Davies, E., and A. Shuster (1981b). Wounding, action potentials and polysome formation. *Plant Physiol.* **67**, 96.

Davies, E. (1987a). Action potentials as multifunctional signals in plants: a unifying hypothesis to explain apparently disparate wound responses. *Plant Cell Environ.* **10**, 623–631.

Davies, E. (1987b). Wound responds in plants. *In* "The Biochemistry of Plants" (D. D. Davies, ed.), Vol. 12, pp. 243–264. Academic Press, New York.

Davies, E., T. Zawadzki, and D. Witters (1991). Electrical activity and signal transmission in plants: How do plants know? *In* "Plant Signalling, Plasma Membrane and Change of State" (C. Penel and H. Greppin, eds.), pp. 119–137. Universite de Geneve.

Deamer, D. W., and J. W. Nichols (1983). Proton-hydroxide permeability of liposomes. *Proc. Natl. Acad. Sci. USA* **80**, 165–168.

Deamer, D. W., and J. W. Nichols (1989). Proton flux mechanisms in model and biological membranes. *J. Membr. Biol.* **107**, 91–103.

Deamer, D. W., and G. R. Fleischaker (1993). "Origins of Life. The Central Concepts." Jones and Bartlett Publishers, Boston.

Deamer, D. W., and A. G. Volkov (1995). Proton permeation of lipid bilayers. *In* "Permeability and Stability of Lipid Bilayers" (E. A. Disalvo and S. A. Simon, eds.), pp. 161–178. CRC Press, Boca Raton, FL.

Deamer, D. W., and A. G. Volkov (1996). Oil/water interfaces and the origin of life. *In* "Liquid-Liquid Interfaces. Theory and Methods" (A. G. Volkov and D. W. Deamer, eds.), pp. 375–400. CRC Press, Boca Raton, FL.

Debus, R. J., G. T. Babcock, B. A. Barry, and L. McIntosh (1988). Site-directed mutagenesis identifies a tyrosine radical involved in the photosynthetic oxygen-evolving system. *Proc. Natl. Acad. Sci. USA* **85**, 427–430.

Debus, R. J. (1992). The manganese and calcium ions of photosynthetic oxygen evolution. *Biochim. Biophys. Acta* **1102**, 269–352.

Dilger, J. P., S. McLaughlin, T. J. McIntosh, and S. A. Simon (1979). Dielectric constant

of phospholipid-bilayers and the permeability of membranes to ions. *Science* **206,** 1196–1198.

Dilley, R. A. (1991). Energy coupling in chloroplasts: A calcium-gated switch controls proton fluxes between localised and delocalised proton gradient. *Curr. Top. Bioenerg.* **16,** 265–318.

Dismukes, G. C., K. Ferris, and P. Watnic (1982). EPR spectroscopic evidence for a tetra-nuclear manganese cluster as the site for photosynthetic oxygen evolution. *Photobio-chem. Photobiophys.* **3,** 243–256.

Dixon, H. H. (1924). Transmission of stimuli in plants. *Nature* **114,** 626.

Dogonadze, R. R., and A. A. Kornyshev (1974). Polar-solvent structure in theory of ion solvation. *J. Chem. Soc., Faraday Trans. 2* **70,** 1121–1132.

Dole, S. H. (1970). "Habitable Planets for Men." American Elsevier Publ. Co., Inc., New York.

Dolphin, D., ed. (1979). "The Porphyrins." Academic Press, New York.

Dryherst, G. (1977). "Electrochemistry of Biological Molecules." Academic Press, New York.

Dryherst, G., K. Kadish, F. Scheller, and R. Renneberg (1982). "Biological Electrochem-istry." Academic Press, New York.

Du Bois-Reymond, E. (1848). "Untersuchungen über Thierishe Elektrizität," Vol. 1. G. Reiner, Berlin.

Durr, H., E. David, M. Seiler, and I. Willner (1996). Model systems for artificial photosyn-thesis—supramolecular relays assemblies. *J. Inf. Record.* **22,** 417–419.

Earley, J. E. (1973). Oxygen evolution: a molecular model for the photosynthetic process, based on an inorganic example. *Inorg. Nicl. Chem. Lett.* **9,** 487–490.

Edwards, K. L., and G. G. Pickard (1987). Detection and transduction of physical stimuli in plants. *In* "The Cell Surface in Signal Transduction" (E. Wagner, H. Greppin, and B. Millet, eds.), pp. 41–66. Springer-Verlag, Berlin.

Edwards, M. C., G. N. Smith, and D. J. F. Bowling (1988). Guard cells extrude protons prior to stomatal opening. *J. Exp. Bot.* **39,** 1541–1547.

Egberts, E., S. J. Marrink, and H. J. Berendsen (1994). Molecular dynamics simulation of a phospholipid membrane. *Eur. Biophys. J.* **22,** 423–436.

Ehleringer, J., and I. Forseth (1980). Solar tracking by plants. *Science* **210,** 1094–1098.

Eigen, M. (1971). Self-organization of matter and the evolution of biological macromole-cules. *Naturwissenshaften* **58** (October), 10.

Eigen, M., and P. Shuster (1979). "The Hypercycle. A Principle of Natural Self-Organization." Springer-Verlag, Berlin.

Einarsdottir, O. (1995). Fast reactions of cytochrome oxidase. *Biochim. Biophys. Acta* **1229,** 129–147.

Erecinska, M., and B. Chance (1972). Studies on the electron transport chain at subzero temperatures: electron transport at site III. *Arch. Biochem. Biophys.* **151,** 304–315.

Eschrich, W., J. Fromm, and R. F. Evert (1988). Transmission of electrical signals in sieve tubes of zucchini plants. *Bot. Acta* **101,** 327–331.

Eschrich, W., and J. Fromm (1994). Evidence for two pathways of phloem loading. *Physiol. Plant.* **90,** 699–707.

Evans, E. (1992). Composite membranes and structured interfaces: From simple to complex design in biology. *In* "Biomembrane Structure and Function: The State of

the Art" (B. P. Gaber and K. R. K. Easwaran, eds.), pp. 81–101. Adenine Press, New York.

Fasman, G. D., ed. (1976). "Handbook of Biochemistry and Molecular Biology," 3rd ed., Vol. I. CRC Press, Boca Raton, FL.

Felle, H., and A. Bertl (1986). The fabrication of H^+-sensitive liquid membrane micro-electrodes for use in plant cells. *J. Exp. Bot.* **37,** 1416–1428.

Fensom, D. S. (1958). The bioelectric potentials of plants and their functional significance. II. The patterns of bioelectric potential and exudation rate in excised sunflower roots and stems. *Can. J. Bot.* **36,** 367–383.

Fensom, D. S., and D. C. Spanner (1969). Electro-osmotic and biopotential measurement on phloem strands of Nymhoides. *Planta* **88,** 321–331.

Fensom, D. S. (1980). Problems arising from Munch-type pressure flow mechanism of sugar transport in phloem. *Can. J. Bot.* **59,** 425–432.

Flewelling, R. F., and W. L. Hubbel (1986). The membrane dipole potential in total membrane potential model. Applications to hydrophobic ion interactions with membranes. *Biophys. J.* **49,** 541–552.

Foigelson, E. M., and L. D. Krasnokutskaya (1978). "Solar Radiation Fluxes and Clouds." Hydrometeoizdat, Leningrad.

Fong, F. K. (1982). *In* "Light Reaction Path of Photosynthesis," (F. K. Fong, ed.), pp. 277–321. Springer-Verlag, Heidelberg.

Fong, F. K., I. S. Poles, L. Galloway, and D. R. Fruge (1977). Far red photogalvanic splitting of water by chlorophyll a dihydrate. A new model of plant photosynthesis. *J. Am. Chem. Soc.* **99,** 5902–5805.

Frachisse, J. M., and M. O. Desbiez (1989). Investigation of the wave of electric depolarization induced by wounding in *Bidens pilosus* L. *Biochem. Physiol. Pflanz.* **185,** 357–368.

Fromm, J., and W. Eschrich (1988). Transport processes in stimulated and non-stimulated leaves of *Mimosa pudica.* I. The movement of ^{14}C-labelled photoassimilates. *Trees* **2,** 7–17.

Fromm, J., and W. Eschrich (1989a). Correlation of ionic movements with phloem unloading and loading in barley leaves. *Plant Physiol. Biochem.* **27,** 577–585.

Fromm, J., and W. Eschrich (1989b). Electric signals released from roots of willow (*Salix viminalis* L.) change transpiration and photosynthesis. *J. Plant Physiol.* **141,** 673–680.

Fromm, J. (1991). Control of phloem unloading by action potentials in Mimosa. *Physiol. Plant.* **83,** 529–533.

Fromm, J., and R. Spanswick (1993). Characteristics of action potentials in willow (*Salix viminalis* L.). *J. Exp. Bot.* **44,** 1119–1125.

Fromm, J., and T. Bauer (1994). Action potentials in maize sieve tubes change phloem translocation. *J. Exp.* **45,** 463–469.

Fruge, D. R., G. D. Fong, and F. K. Fong (1979). Photosynthesis of polyatomic organic molecules from carbon dioxide and water by photocatalytic action of visible light illuminated platinized chlorophyll *a* dihydrate polycrystals. *J. Am. Chem. Soc.* **101,** 3694–3697.

Galloway, L., I. Roettger, D. R. Fruge, and F. K. Fong (1978). Photochemical conversion in the chlorophyll *a* water light reaction: Causative factors underlying the two-quanta/electron requirement in plant photosynthesis. *J. Am. Chem. Soc.* **100,** 4635–4638.

Garcia-Morin, M., R. A. Uphaus, J. R. Norris, and J. J. Katz (1969). Interpretation of chlorophyll electron spin resonance spectra. *J. Phys. Chem.* **73**, 1066–1070.

Gates, D. M. (1965a). Energy, plants and ecology. *Ecology* **46**, 1–13.

Gates, D. M. (1965b). Radiant energy, its receipt and disposal. *Meteorol. Monogr.* **6**, 1–26.

Gates, D. M., H. J. Keegan, J. C. Schleter, and V. R. Weinder (1965). Spectral properties of plants. *Appl. Optics* **4**, 11–20.

Gates, D. M. (1968). Transpiration and leaf temperature. *Annu. Rev. Plant Physiol.* **19**, 211–238.

Gates, D. M., and E. Papian (1971). "Atlas of Energy Budgets of Plant Leaves." Academic Press, London.

Gates, D. M. (1976). Energy Exchange and Transpiration. *In* "Water and Plant Life, Modern Approaches" (O. L. Lange, L. Kappen, and E. D. Schulze, eds.). Springer-Verlag, Berlin.

Gates, D. M. (1980). "Biophysical Ecology." Springer-Verlag, New York.

Gates, D. M. (1985). "Energy and Ecology." Sinauer Associates, Sunderland, MA.

Gates, D. M. (1993). "Climate Change and Its Biological Consequences." Sinauer Associates, Sunderland, MA.

Gawrish, K., D. Ruston, J. Zimmerberg, V. A. Parsegian, R. P. Rand, and N. Fuller (1992). Membrane dipole potentials, hydration forces, and the ordering of water at membrane surfaces. *Biophys. J.* **61**, 1213–1223.

Georgallas, A., J. D. MacArthur, X. P. Ma, C. V. Nguyen, and G. R. Palmer (1987). The diffusion of small ions through phospholipid bilayers. *J. Chem. Phys.* **86**, 7218–7226.

Gilchrist, M. L., J. A. Ball, D. W. Randall, and R. D. Britt (1995). Proximity of the manganese cluster of photosystem II to the redox-active tyrosine Y-Z. *Proc. Natl. Acad. Sci. USA* **92**, 9545–9549.

Gladyshev, G. P. (1988). "Thermodynamics and Kinetics of Natural Hierarchical Processes." Nauka Publ. House, Moscow.

Glansdorff, P., and I. Prigogine (1971). "Thermodynamic Theory of Structure, Stability and Fluctuations." John Wiley & Sons, New York.

Goldfeld, M. G., L. A. Blumenfeld, L. G. Dmitrovsky, and V. D. Mikoyan (1980). Plastoquinone function in photosystem 2. *Mol. Biol.* **14**, 804–813.

Goldfeld, M. G. (1982). Paramagnetic centres of the electron transport chain of photosynthesis of higher plants. *Biofizika* **27**, 954–965.

Goldsworthy, A. (1983). The evolution of plant action potentials. *J. Theor. Biol.* **103**, 645–648.

Goodin, D. B., V. K. Yachandra, R. D. Britt, K. Sauer, and M. P. Klein (1984). The state of manganese in photosynthetic apparatus. 3. Light-induced changes in X-ray absorption (K-edge) energies of manganese in photosynthetic membranes. *Biochim. Biophys. Acta* **767**, 209–216.

Gourary, B. S., and F. S. Adrian (1960). Wave functions for electron-excess color centers in alkali halide crystals. *Solid State Physics* **10**, 127–247.

Govindjee, T. Wydrzynski, and S. B. Marks (1977). *In* "Bioenergetics of Membranes" (L. Packer, G. Papageorgiou, and A. Trebst, eds.), pp. 305–316. Elsevier, Amsterdam.

Gradmann, D., and H. Mummert (1980). Plant action potentials. *In* "Plant Membrane Transport: Current Conceptual Issues" (R. M. Spanswick, W. J. Lucaas, and J. Dainty, eds.), pp. 333–347. Elsevier, Amsterdam.

Gray, J. S. (1988). Species Abundance Patterns. *In* "Organization of Communities, Past and Present." Blackwell, Oxford.

Greig-Smith, P. (1983). "Quantitative Plant Ecology." Blackwell, Oxford.

Greppin, H., M. Bonzon, P. Crespi, M. Crevecoeur, R. degli Agosti, C. Penel, and P. Tacchini (1991). Communication in plants. *In* "Plant Signalling, Plasma Membrane and Change of State" (C. Penel and H. Greppin, eds.), pp. 139–177. Universite de Geneve.

Gugeshashvili, M. I., A. G. Volkov, A. Tessier, P. F. Blanchet, D. Cote, G. Munger, and R. M. Leblanc (1992). Light energy conversion with chlorophyll *a* monolayers. *Biol. Membr.* **9,** 862–873.

Gugeshashvili, M. I., A. G. Volkov, B. Zelent, Ju. Galant, G. Munger, and R. M. Leblanc (1995). Self-organized molecular amphiphilic assemblies of wet chlorophyll *a* in monolayers and thin films. *Membr. Cell Biol.* **9,** 1–12.

Guggenheim, E. A. (1957). "Thermodynamics," 3rd ed. North-Holland, Amsterdam.

Gunar, I. I., and A. M. Sinyukhin (1963). Functional significance of action currents affecting the gas exchange of higher plants. *Sov. Plant Physiol.* **10,** 219–226.

Gutknecht, J. (1984). Proton/hydroxide conductance through lipid bilayer membranes. *J. Membr. Biol.* **82,** 105–112.

Hamada, S., S. Ezaki, K. Hayashi, K. Toko, and K. Yamafuji (1992). Electric current precedes emergence of a lateral root in higher plants. *Plant Physiol.* **100,** 614–619.

Hamilton, R. T., and E. W. Kaler (1990a). Alkali metal ion transport through thin bilayers. *J. Phys. Chem.* **94,** 2560–2566.

Hamilton, R. T., and E. W. Kaler (1990b). Facilitated ion transport through thin bilayers. *J. Membr. Sci.* **54,** 259–269.

Hansson, D., and L. E. Andreasson (1982). EPR-detectable magnetically interacting manganese ions in the photosynthetic oxygen-evolving system after continuous illumination. *Biochim. Biophys. Acta* **679,** 261–268.

Hauser, H., D. Oldani, and M. C. Phillips (1973). Mechanism of ion escape from phosphatidylcholine and phosphatidylserine single bilayer vesicles. *Biochemistry* **12,** 4507–4517.

Hejnowicz, Z., E. Krause, K. Glebicki, and A. Sievers (1991). Propagated fluctuations of the electrical potential in the apoplast of *Lepidium sativum* L. roots. *Planta* **186,** 127–134.

Helenius, V. M., P. H. Hynninen, and J. E. I. Korppi-Tommola (1993). Chlorophyll *a* aggregates in hydrocarbon solution, a picosecond spectroscopy and molecular modeling study. *Photochem. Photobiol.* **58,** 867–873.

Helenius, V. M., J. O. Sikki, P. H. Hynninen, and J. E. I. Korppitommola (1994). Femtosecond study of relaxation of hydrated chlorophyll *a* aggregate in hydrocarbon solution. *Chem. Phys. Lett.* **226,** 137–143.

Henderson, L. (1917). "The Order of Nature." Harvard Univ. Press, Cambridge, MA.

Heyl, J. G. (1933). Der Einfluss von Aussenfaktoren auf das Bluten der Pflanzen. *Planta* **20,** 294–353.

Hill, R., and P. Bendal (1960). Function of the two cytochrome components in chloroplasts: A working hypothesis. *Nature* **186,** 136–137.

Hill, T. L. (1964). "Thermodynamics of Small Systems." Benjamin, New York.

Hill, T. L. (1977). "Free Energy Transduction in Biology." Academic Press, New York.

Hoganson, C. W., N. Lydakis-Simantiris, X. S. Tang, C. Tommos, K. Warncke, G. Bab-

cock, B. A. Diner, J. McCracken, and S. Styring (1995). A hydrogen-atom abstraction model for the function of YZ in photosynthetic oxygen evolution. *Photosynth. Res.* **46,** 177–184.

Holmes, M. G. (1981). Spectral distribution of radiation within plant canopies. *In* "Plants and Day-Light Spectrum" (H. Smith, ed.), pp. 147–158. Academic Press, London.

Holmgren, P., P. G. Jarvis, and M. Jarvis (1965). Resistances to carbon dioxide and water vapour transfer in leaves of different plant species. *Physiol. Plant.* **18,** 557–573.

Hope, A. B., and N. A. Walker (1975). Action potentials in charophyte cells. *In* "The Physiology of Giant Algae Cells," pp. 111–119. Cambridge University Press, Cambridge, UK.

Huang, J. W., J. E. Shaff, D. L. Grunes, and L. V. Kochian (1992). Aluminum effects on calcium fluxes at the root apex of aluminum-tolerant and aluminum-sensitive wheat cultivars. *Plant Physiol.* **98,** 230–237.

Idso, S. B., and C. T. de Witt (1970). Light relations in plant canopies. *Appl. Optics* **9,** 177–184.

Jacob, F. (1977). Evolution and tinkering. *Science* **196,** 1161–1167.

Jones, C., and J. M. Wilson (1982). The effects of temperature on action potentials in the chill sensitive seismonastic plant *Biophytum sensitivum. J. Exp. Bot.* **33,** 313–320.

Jones, H. G. (1992). "Plants and Microclimate," 2nd ed. Cambridge University Press, Cambridge, UK.

Junge, W., and J. B. Jackson (1982). Formation of electrochemical potential difference on photosynthetic membranes. *In* "Photosynthesis, Energy Conversion by Plants and Bacteria" (Govindjee, ed.), Vol. 1, pp. 589–646. Academic Press, New York.

Kachan, A. A., and L. A. Negievich (1978). Oxidation of water by methyl red sensitized by chlorophyll *a* absorbed on aerosyl. *Dokl. Akad. Nauk SSSR* **241,** 1204–1206.

Kakiuchi, T. (1996). Phospholipid monolayers and phospholipases. *In* "Liquid-Liquid Interfaces. Theory and Methods" (A. G. Volkov and D. W. Deamer, eds.), pp. 317–331. CRC Press, Boca Raton, FL.

Kambara, T., and Govindjee (1985). Molecular mechanism of water oxidation in photosynthesis based on the functioning of manganese in two different environments. *Proc. Natl. Acad. Sci. USA* **82,** 6119–6123.

Kandelaki, M. D., A. G. Volkov, A. L. Levin, and L. I. Boguslavsky (1983a). Photooxidation of water by chlorophyll adsorbed on an octane water interface. *Dokl. Akad. Nauk SSSR* **271,** 462–465.

Kandelaki, M. D., A. G. Volkov, A. L. Levin, and L. I. Boguslavsky (1983b). Oxygen evolution in the presence of chlorophyll adsorbed at the octane/water interface. *Bioelectrochem. Bioenerg.* **11,** 167–172.

Kandelaki, M. D., A. G. Volkov, A. L. Levin, and L. I. Boguslavsky (1984). Oxygen evolution in the presence of chlorophyll adsorbed at the octane/water interface. "Bioconversion of Solar Energy" (I. V. Berezin, ed.), pp. 18–21. Akad. Nauk SSSR, Pushchino.

Kandelaki, M. D., A. G. Volkov, V. V. Shubin, and L. I. Boguslavsky (1987). Chlorophyll-water interaction during oxygen photoevolution at the octane/water interface. *Biochim. Biophys. Acta* **893,** 170–176.

Kandelaki, M. D., A. G. Volkov, V. V. Shubin, A. L. Levin, and L. I. Boguslavsky (1988). Interaction of chlorophyll with water during oxygen photoevolution reaction at the octane/water interface. *Electrokhimiya* **24,** 288–294.

Kandelaki, M. D., and A. G. Volkov (1991). The influence of dielectric permittivity of the nonaqueous phase on the photooxidation of water at the interface of two immiscible liquids in the presence of a hydrated oligomer of chlorophyll. *Can. J. Chem.* **69,** 151–156.

Kandelaki, M. D., and A. G. Volkov (1993). Influence of permittivity of the nonaqueous phase on water photooxidation at interfaces between immiscible liquids in the presence of a hydrated chlorophyll oligomers. *Russ. J. Electrochem.* **29,** 1158–1164.

Kargol, A., and M. Kargol (1996). The plant root as an osmo-diffusive converter of free energy. *Gen. Physiol. Biophys.* **15,** 17–26.

Katchalsky, A., and P. F. Curran (1965). "Nonequilibrium Thermodynamics in Biophysics." Harvard University Press, Cambridge, MA.

Kays, W. M. (1966). "Convective Heat and Mass Transport." McGraw-Hill, New York.

Keller, R. (1930). Der elektrische Factor des Wassertransporte in Luhte der Vitalfarbung. *Ergeb. Physiol.* **30,** 294–407.

Kelvin, W. (1898). Contact electricity of metals. *Plilos. Mag.* **46,** 82–120.

Kenrick, F. B. (1886). Die potentialspringe zwischen Gasen und Flüssigkeiten. *Z. Phys. Chem.* **19,** 625–656.

Kenyon, D. H. (1969). "Biochemical Predestination." McGraw-Hill, New York.

Kerr, R. A. (1994). Environment—Antarctic ozone hole fails to recover. *Science* **266,** 217–219.

Kershaw, K. A. (1974). "Quantitative and Dynamic Plant Ecology." American Elsevier Publ. Co., New York.

Kharkats, Yu. I., A. G. Volkov, and L. I. Boguslavsky (1977). Transfer of ions and electrons across the interface between two immiscible liquids in functioning enzyme membrane systems. *J. Theor. Biol.* **65,** 379–391.

Kharkats, Yu. I. (1978). The calculation of the solvent energy reorganization of reactions with complex distribution of charges in reactants. *Sov. Electrochem.* **14,** 1721–1724.

Kharkats, Yu. I., and A. G. Volkov (1985). Interfacial catalysis: Multielectron reactions at liquid/liquid interface. *J. Electroanal. Chem.* **184,** 435–439.

Kharkats, Yu. I., and A. G. Volkov (1987). Membrane catalysis: Synchronous multielectron reactions at the liquid-liquid interface. Bioenergetical mechanism. *Biochim. Biophys. Acta* **891,** 56–67.

Kharkats, Yu. I., and A. G. Volkov (1989). Cytochrome oxidase: The molecular mechanism of functioning. *Bioelectrochem. Bioenerg.* **22,** 91–103.

Kharkats, Yu. I., and A. G. Volkov (1994). 2:1:1 molecular mechanism of cytochrome oxidase functioning. *In* "Charge and Field Effects in Biosystems-4" (M. J. Allen, S. F. Cleary, and A. E. Sowers, eds.), pp. 70–77. World Scientific, Singapore.

Kharkats, Yu. I., and A. M. Kuznetsov (1996). Quantum theory of charge transfer. *In* "Liquid-Liquid Interfaces. Theory and Methods" (A. G. Volkov and D. W. Deamer, eds.), pp. 139–154. CRC Press, Boca Raton, FL.

Kleshnin, A. F. (1954). "Plant and Light." Nauka Publ. House, Moscow.

Klimov, V. V., G. Ananyev, O. Zastryzhnaya, T. Wydrzhinski, and G. Renger (1993). Photoproduction of hydrogen peroxide in Photosystem II particles: A comparison of four signals. *Photosynth. Res.* **38,** 409–416.

Knots, L. L., and G. G. Dubovik (1985). A method of exciting self-oscillations in a cell for measuring contact potential difference by the capacitor method. *Sov. Electrochem.* **1,** 701–705.

Kok, B., B. Forbush, and M. McGloin (1970). Cooperation of charges in photosynthetic O_2 evolution. 1. A linear four step mechanism. *Photochem. Photobiol.* **11**, 457–475.

Kornyshev, A. A. (1981). Nonlocal screening of ions in a structurized polar liquid. New aspects of solvent description in electrolyte theory. *Electrochim. Acta* **26**, 1–20.

Kornyshev, A. A., and A. G. Volkov (1984). On the evaluation of standard Gibbs energies of ion transfer between two solvents. *J. Electroanal. Chem.* **180**, 363–381.

Koryta, J., J. Dvorak, and L. Kavan (1993). "Principles of Electrochemistry." Wiley, New York.

Kotov, N. A., and M. G. Kuzmin (1990a). The photocurrent kinetics across the polarizable interface of immiscible electrolyte solutions in the protoporphyrine-quinone system. *Sov. Electrochem.* **26**, 1484–1488.

Kotov, N. A., and M. G. Kuzmin (1990b). A photoelectrochemical effect at the interface of immiscible electrolyte solutions. *J. Electroanal. Chem.* **285**, 223–240.

Kotov, N. A., and M. G. Kuzmin (1991). Analysis of photocurrent kinetics in photoelectro-chemical effect at polarizable interface between electrolyte solutions by mathematical modelling method. *Sov. Electrochem.* **27**, 76–81.

Kotov, N. A., and M. G. Kuzmin (1992). Nature of the processes of charge-carrier genera-tion at ITIES by the photoexitation of porphyrins. *J. Electroanal. Chem.* **338**, 99–124.

Kotov, N. A., and M. G. Kuzmin (1996). Photoelectrochemical effect at interface between two immiscible electrolyte solutions. *In* "Liquid-Liquid Interfaces. Theory and Meth-ods" (A. G. Volkov and D. W. Deamer, eds.), pp. 213–253. CRC Press, Boca Raton, FL.

Kramer, P. J. (1983). "Water Relations of Plants." Academic Press, New York.

Kramer, P. J., and J. S. Boyer (1995). "Water Relations of Plants and Soil." Academic Press, New York.

Krishtalik, L. I. (1986). Energetics of multielectron reactions. Photosynthetic oxygen evo-lution. *Biochim. Biophys. Acta* **849**, 162–171.

Krishtalik, L. I., and A. M. Kuznetsov (1986). Energetics of the elementary reaction act and the "configurational" electrode potential. *Sov. Electrochem.* **22**, 218–221.

Krysinski, P., and H. Ti Tien (1986). Voltammetric studies of electron-conducting modified bilayer lipid membranes. *Bioelectrochem. Bioenerg.* **16**, 185–191.

Ksenzhek, O. S., and S. Petrova (1978). Redox properties of ferriprotoporphyrin IX in aqueous solutions. *Bioelectrochem. Bioenerg.* **5**, 661–670.

Ksenzhek, O. S., S. Petrova, and M. Kolodyazhny (1982). Redox properties of ubiquinones in aqueous solutions. *Bioelectrochem. Bioenerg.* **9**, 167–174.

Ksenzhek, O., S. Petrova, and I. Pinielle (1983). Thermodynamic parameters of flavins in aqueous solutions. *Bioelectrochem. Bioenerg.* **11**, 105–127.

Ksenzhek, O. S. (1985). Thermodynamic limits of efficiency of conversion of radiant en-ergy. *Dokl. Akad. Nauk Ukr. SSR, Ser. A* **9**, 56–59.

Ksenzhek, O. S., and S. Petrova (1986). "Electrochemical Properties of Reversible Bio-logical Redox Systems." Nauka Publ. House, Moscow.

Ksenzhek, O. S. (1987). Thermodynamics of radiant energy conversion. *In* "Thermody-namics of Irreversible Processes" (A. I. Lopushanskaja, ed.), p. 292. Nauka Publ. House, Moscow.

Kulikov, A. V., V. R. Bogatyrenko, G. I. Likhtenstein, S. I. Allakhverdiev, V. V. Klimov, V. A. Shuvalov, and A. A. Krasnovsky (1983). Magnetic interaction of manganese with the anion-radical of pheophytin and the cation radical of chlorophyll at the reaction centers of photosystem II. *Biophysics* **28**, 381–388.

Kursanov, A. L. (1984). Phloem as a conductor of bioelectric pulses. *In* "Assimilate Transport in Plants." Chapter V, pp. 422–429. Elsevier, New York.

Kusunoki, M. (1984). *In* "Advances in Photosynthesis Research" (C. Sybesma, ed.), Vol. 1, pp. 275–278. Martinius Nijhoff/Dr. W. Junk Publ., Den Haag.

Kutyurin, V. M. (1965). About the mechanism of water oxidation and oxygen evolution in the course of photosynthesis. *Uspek. Sovr. Biol.* **59**, 205–225.

Kutyurin, V. M., I. Yu. Artamkina, and I. N. Anisimova (1968). On the interaction between oxidized form of chlorophyll and water. *Dokl. Akad. Nauk SSSR* **180**, 1002–1004.

Kutyurin, V. M. (1970). Mechanism of water decomposition during photo-synthesis. *Izv. Acad. Nauk. SSSR (Ser. Biol.)* **4**, 569–580.

Kutyurin, V. M., I. Yu. Artamkina, A. D. Korsun, I. N. Anisimova, and I. V. Matveeva (1973). On the interaction between oxidized form of chlorophyll and water. *Dokl. Akad. Nauk SSSR* **212**, 243–245.

Kutyurin, V. M., I. Yu. Artamkina, N. P. Melnikov, and I. N. Anisimova (1975). Mechanism of water oxidation by oxidized chlorophylls. *Theor. Exp. Chem.* **11**, 831–834.

Landau, L. D., and E. M. Lifshitz (1958). "Statistical Physics." Pergamon, New York.

Landau, L. D., and E. M. Lifshitz (1984). "Electrodynamics of Continuous Media," 2nd ed. Pergamon, New York.

Landsberg, P. T. (1977). A note on the thermodynamics of energy conversion in plants. *Photochem. Photobiol.* **26**, 313–314.

Landsberg, P. T., and G. Tonge (1979). Thermodynamics of conversion of diluted radiation. *J. Phys. A* **12**, 551–562.

Landsberg, P. T., and Tonge G. (1982). Kinetic photochemical and photovoltaic energy conversion models. *Photochem. Photobiol.* **35**, 769–781.

Landsberg, P. T. (1983). Some maximal thermodynamic efficiencies for the conversion of blackbody radiation. *J. Appl. Phys.* **54**, 2841–2843.

Landsberg, G. S. (1993). Advances in light scattering. *Uspek. Fiz. Nauk* **163**, 33–50.

Larcher, W. (1976). "Okologie der Pflanzen." Verlag Eugen Ulmer, Stuttgart, Germany.

Lawrence, C. D., and D. T. Sawyer (1978). The chemistry of biological manganese. *Coord. Chem. Rev.* **27**, 173–193.

Leblanc, R. M., P. F. Blanchet, D. Cote, M. I. Gugeshashvili, G. Munger, and A. G. Volkov (1991). Light energy conversion with pheophytin *a* and chlorophyll *a* monolayers at the optical transparent electrode. *Proc. Soc. Photo-Opt. Instrum. Eng.* **1436**, 92–102.

Leegood, R. C., P. J. Lea, M. D. Adcock, and R. E. Hausier (1994). The regulation and control of photorespiration. *J. Exp. Bot.* **46**, 1397–1414.

Lehninger, A. L., D. L. Nelson, and M. M. Cox (1993). "Principles of Biochemistry." 2nd ed. Worth Publishers Inc., New York.

Leuning, R. (1989). Leaf Energy Balances: Developments and Applications. *Philos. Trans. R. Soc. London B* **324**, 191–206.

Levich, V. G. (1962). "Physicochemical Hydrodynamics." Prentice-Hall, Englewood Cliffs, NJ.

Lewis, G. N., and M. Randall (1961). "Thermodynamics." McGraw-Hill, New York.

Lewis, N. S. (1995). Artificial Photosynthesis. *Am. Sci.* **83**, 534–541.

Likhtenstein, G. I. (1987). Clusters in biological materials. *J. All-Union Mendeleev Chem. Soc.* **32**, 61–69.

Lucas, W. J., and L. V. Kochian (1984). Ion transport processes in corn roots: An approach utilizing microelectrode techniques. *In* "Advanced Agricultural Instrumenta-

tion" (W. Gensler and M. Nijhoff, eds.). Proceedings of NATO Advanced Studies Inst., Pisa, Italy.

Lynn, B. H., and T. N. Carlson (1990). A stomatal resistance model illustrating plant vs. external control of transpiration. *Agr. Forest Meteorol.* **52,** 5–43.

Macdonald, R. C. (1976). Energetics of permeation of thin lipid membranes by ions. *Biochim. Biophys. Acta* **448,** 193–198.

Maguarran, A. E. (1988). "Ecological Diversity and Its Measurement." Croom Helm, London.

Malone, M., and B. Stankovic (1991). Surface potentials and hydraulic signals in wheat leaves following localized wounding by heat. *Plant, Cell and Environ.* **14,** 431–436.

Mandelbrot, B. (1983). "The Fractal Geometry of Nature." Freeman & Co., San Francisco.

Marcus, R. A. (1956). On the theory of oxidation-reduction reactions. *J. Chem. Phys.* **24,** 966–978.

Margulis, L. (1981). "Symbiosis in Cell Evolution. Life and Its Environment on the Early Earth." Freeman & Co., San Francisco.

Margulis, L. (1983). "Symbiosis in Cell Evolution. Life and Its Environment on the Early Earth." Freeman & Co., San Francisco.

Markin, V. S., and M. M. Kozlov (1985). Pore statistics in bilayer lipid membranes. *Biol. Membr.* **2,** 205–223.

Markin, V. S., and A. G. Volkov (1987a). The standard Gibbs energy of ion resolvation and nonlinear dielectric effects. *J. Electroanal. Chem.* **235,** 23–40.

Markin, V. S., and A. G. Volkov (1987b). The standard free energy of ion resolvation and nonlinear dielectric effects. *Electrokhimiya* **23,** 1105–1112.

Markin, V. S., and A. G. Volkov (1987c). Theoretical description of Gibbs energy of ion transfer. *Russ. Chem. Rev.* **56,** 1953–1972.

Markin, V. S., and A. G. Volkov (1987d). Interfacial potentials at the interface between two immiscible electrolyte solutions. *Electrokhimiya* **23,** 1405–1413.

Markin, V. S., and A. G. Volkov (1989a). The Gibbs free energy of ion transfer between two immiscible liquids (review). *Electrochim. Acta* **34,** 93–107.

Markin, V. S., and A. G. Volkov (1989b). Interfacial potentials at the interface between two immiscible electrolyte solutions. Some problems in definitions and interpretation. *J. Colloid Interface Sci.* **131,** 382–392.

Markin, V. S., and A. G. Volkov (1990). Potentials at the interface between two immiscible electrolyte solutions. *Adv. Colloid Interface Sci.* **31,** 111–152.

Markin, V. S., M. I. Gugeshashvili, A. G. Volkov, G. Munger, and R. M. Leblanc (1992). The standard Gibbs free energy of adsorption equilibrium and isotherms of adsorption of amphiphilic molecules and clusters at the oil/water and gas/water interfaces. Adsorption of dry and hydrated chlorophyll. *J. Colloid Interface Sci.* **154,** 264–275.

Markin, V. S., and A. G. Volkov (1996). Absorption isotherms and the structure of oil/water interface. *In* "Liquid–Liquid Interfaces: Theory and Methods" (A. G. Volkov and D. W. Deamer, eds.), pp. 63–75. CRC-Press, Boca Raton, FL.

Marrink, S. J., F. Jahnig, and H. J. C. Berendsen (1996). Proton transport across transient single-file water pores in a lipid membrane studied by molecular dynamics simulations. *Biophys. J.* **71,** 632–647.

Marshall, A. G. (1978). "Biophysical Chemistry." John Wiley & Sons, New York.

Marshall, T. J., and J. W. Holmes (1988). "Soil Physics," 2nd ed. Cambridge University Press, New York.

Matsuda, K., and Riazi, A. (1981). Stress induced osmotic adjustment in growing regions of barley leaves. *Plant Physiol.* **68,** 571–576.

Mauzerall, D., and A. Chivis (1973). A novel cyclical approach to the oxygen producing mechanism of photosynthesis. *J. Theor. Biol.* **42,** 387–395.

McPeters, R. D., P. A. Newman, and J. C. Alpert (1986). Nimbus 7 satelite measurements of springtime Antarctic ozone decrease. *Nature* **322,** 808–811.

Metzler, D. E. (1977). "Biochemistry. The Chemical Reactions of Living Cells." Academic Press Inc., New York.

Mitchell, P. (1961). Coupling of phosphorylation to electron and hydrogen transfer by a chemiosmotic type of mechanism. *Nature* **191,** 144–148.

Mitchell, P. (1976). Vectorial chemistry and the molecular mechanics of chemiosmotic coupling: Power transmission by proticity. *Biochem. Soc. Trans.* **4,** 399–430.

Mitchell, P. (1979). Compartmentation and communication in living systems. Ligand conduction: A general catalytic principle in chemical, osmotic and chemiosmotic reaction systems. *Eur. J. Biochem.* **95,** 1–2.

Mitchell, P. (1984). Chemiosmosis: A term of abuse. *Trends Biochem. Sci.* **9,** 205–205.

Miyasaka, T., A. Frushima, and K. Honda (1981). Photochemical behavior of chlorophyll *a*–lipid films on a platinum electrode in an aqueous electrolyte. *Bull. Chem. Soc. Jpn.* **54,** 957–961.

Mizuguchi, Y., Y. Watanabe, H. Matsuzaki, Y. Ikezawa, and T. Takamura (1994). Growth acceleration of bean sprouts by the application of electrochemical voltage in a culturing bath. *Denki Kagaku* **62,** 1083–1085.

Monson, R., and B. Moor (1989). On the significance of C_3–C_4 intermediate to the evolution of C_4 photosynthesis. *Plant, Cell Environ.* **12,** 689–699.

Moravsky, A. P., A. V. Khramov, and A. E. Shilov (1984). 4th International Symposium on Homogeneous Catalysis, Abstracts, Book 4, September 24–28, Leningrad, pp. 219–220.

Moravsky, A. P., and A. V. Khramov (1987). A theoretical model for the manganese cluster of photosystem II oxygen evolving center. *In* "Chemical Physics of Enzyme Catalysis," Program and Abstracts, p. 54. Tallinn, September 21–24, 1987.

Munger, G., R. M. Leblanc, B. Zelent, A. G. Volkov, M. I. Gugeshashvili, J. Gallant, H. A. Tajmirriahi, and J. Aghion (1992a). Characterization of monolayers and Langmuir-Blodgett films of dry and wet chlorophyll *a*. *Thin Solid Films* **210,** 739–942.

Munger, G., R. M. Leblanc, B. Zelent, J. Gallant, H. A. Tajmirriahi, J. Aghion, M. I. Gugeshashvili, and A. G. Volkov (1992b). The hydrated chlorophyll *a* oligomer in monolayers and Langmuir-Blodgett films. *Biol. Membr.* **9,** 874–880.

Myers, N. (1984). "The Primary Source: Tropical Forests and Our Future." W. W. Norton & Co., Inc., New York.

Nagle, J. F., and H. J. Morowitz (1978). Molecular mechanisms for proton transport in membrane. *Proc. Natl. Acad. Sci. USA* **75,** 298–302.

Nagle, J. F., and S. Tristram-Nagle (1983). Hydrogen bonded chain mechanisms for proton conduction and proton pumping. *J. Membr. Biol.* **74,** 1–14.

Nagle, J. F. (1987). Theory of passive proton conductance in lipid bilayer. *J. Bioenerg. Biomembr.* **19,** 413–426.

Neumke, B., and P. Lauger (1969). Nonlinear electrical effects in lipid bilayer membranes. II. Integration of the generalized Nernst-Plank equations. *Biophys. J.* **9**, 1160–1170.

Nicholls, D. (1982). "Bioenergetics. An Introduction to the Chemiosmotic Theory." Academic Press, New York.

Nichols, J. W., and D. W. Deamer (1978). Proton and hydroxide permeability coefficient measured for unilamellar liposomes. *In* "Frontiers of Biological Energetics" (P. L. Dutton, J. S. Leigh, and A. Scarpa, eds.), Vol. 2, pp. 1273–1283. Academic Press, New York.

Nichols, J. W., and D. W. Deamer (1980). Net proton–hydroxyl permeability of large unimolecular liposomes measured by an acid–base titration technique. *Proc. Natl. Acad. Sci. USA* **77**, 2038–2042.

Nicolis, G., and I. Prigogine (1977). "Self-Organization in Nonequilibrium Systems." John Wiley & Sons, New York.

Nicolis, J. S. (1986). "Dynamics of Hierarchical Systems. An Evolutionary Approach." Springer-Verlag, Heidelberg.

Niklas, K., and V. Kerchner (1984). Mechanical and photosynthetic constraints on the evolution of plant shape. *Paleobiology* **10**, 79–101.

Nilsen, T. (1972). Radiative relations in plant canopies. *In* "Theoretical Principles of Photosynthetic Productivity" (A. A. Nichiporovich, ed.), pp. 420–424 (in Russian). Nauka Publ. House, Moscow.

Nobel, P. S. (1983). "Biophysical Plant Physiology and Ecology." W. H. Freeman, San Francisco.

Nobel, P. S. (1991). "Physicochemical and Environmental Plant Physiology." Academic Press, San Diego.

Norris, J. R., R. A. Uphaus, H. L. Crespi, and J. J. Katz (1971). Electron spin resonance of chlorophyll and the origin of signal 1 in photosynthesis. *Proc. Natl. Acad. Sci. USA* **68**, 625–628.

Noyes, R. W. (1982). "The Sun. Our Star." Harvard University Press, Cambridge, MA.

Odum, E. P. (1971). "Fundamentals of Ecology." Wiley-Interscience, New York.

Odum, E. P. (1983). "Basic Ecology." Saunders College Publ., Philadelphia.

Odum, E. P. (1988). "Ecology and Our Endangered Life-Support System." Sinauer Associates, Sunderland, MA.

Olson, J. M. (1970). The evolution of photosynthesis. *Science* **168**, 438–446.

Oparin, A. (1969). "Biogenesis and Early Development of Life." Academic Press, New York.

Opritov, V. A., and S. S. Pyatygin (1989). Analysis of coupling of the electrogenic ion pump operation in the excitable membrane with the action potential generation in higher plants. *Izv. Akad. Nauk SSSR Ser. Biol.* **5**, 739–744.

Opritov, V. A., V. A. Khudyakov, and S. S. Pyatygin (1992). Role played by plasmalemma lipid matrix fluidity in modulation of H^+-ATPase activity in higher plant cells subjected to different forms of moderate cold influence. *Sov. Plant Physiol.* **39**, 340–344.

Ore Aadne (1955). Entropy of radiation. *Phys. Rev.* **98**, 887–888.

Orgen, W. L., and R. Coollet (1982). Photorespiration. *In* "Photosynthesis" (Govinjee, ed.), Vol. 2, pp. 191–230. Academic Press, New York.

Orii, Y. M., M. Manabe, and M. Yoneda. (1977). Molecular architecture of cytochrome oxi-

dase and its transition on treatment with alkali or sodium dodecyl sulfate. *J. Biochem.* **81,** 505–517.

Osmond, C. B., and S. C. Grace (1995). Perspectives on photoinhibition and photorespiration in the field: Quintessential inefficiencies of the light and dark reactions of photosynthesis? *J. Exp. Bot.* **46,** 1351–1362.

Ottova-Leitmannova, A., and H. Ti Tien (1993). Bilayer lipid membranes: An experimental system for biomolecular electronic devices development. *Prog. Surf. Sci.* **41,** 337–445.

Padhye, S., T. Kambara, D. N. Hendrickson, and Govindjee (1986). Manganese-histidine cluster as the functional center of the water oxidation complex in photosynthesis. *Photosynth. Res.* **9,** 103–112.

Palinkas, G., E. Kalman, and P. Kovacs (1977). Liquid water. II. Experimental atom pair correlation functions of liquid D_2O. *Mol. Phys.* **34,** 525–537.

Parsegian, A. (1969). Energy of ion crossing a low dielectric membrane: Solutions to four relevant electrostatic problems. *Nature* **221,** 844–846.

Passioura, J. B. (1988). Water transport in and to roots. *Annu. Rev. Plant Physiol. Plant Mol. Biol.* **39,** 245–265.

Paula, S., A. G. Volkov, A. N. Van Hoek, T. H. Haines, and D. W. Deamer (1996). Permeation of protons, potassium ions, and small polar molecules through phospholipid bilayers as a function of membrane thickness. *Biophys. J.* **70,** 339–348.

Pearlstein, R. H. (1982). Chlorophyll singlet excitons. *In* "Photosynthesis" (Govinjee, ed.), Vol. 1. Academic Press, New York.

Perkins, W. R., and D. Cafiso (1986). An electrical and structural characterization of H^+/OH^- currents in phospholipid vesicles. *Biochemistry* **25,** 2270–2276.

Pickard, B. G. (1973). Action potentials in higher plants. *Bot. Rev.* **38,** 172–201.

Pickard, B. G. (1984a). Voltage transients elicited by sudden step-up of auxin. *Plant, Cell Environ.* **7,** 171–178.

Pickard, B. G. (1984b). Voltage transients elicited by brief chilling. *Plant, Cell Environ.* **7,** 679–681.

Pimentel, G. C., and A. L. McClellan (1960). "The Hydrogen Bond." Freeman, San Francisco.

Pinchuk, V. M. (1993). Quantum chemical modeling of the photodecomposition of the water dimer in chlorophyll complexes of magnesium and manganese. *J. Struct. Chem.* **34,** 203–207.

Planck, M. (1923). "Vorlesungen uber die Theorie der Warmestralung." 5 Aufl., Leipzig.

Prigogine, I. (1961). "Thermodynamics of Irreversible Processes." Wiley, New York.

Prigogine, I. (1967). "Introduction to Thermodynamics of Irreversible Processes." John Wiley & Sons, New York.

Pyatygin, S. S., V. A. Opritov, V. A. Khudyakov, and A. V. Gnezdolov (1989). Temperature dependence of the resting potentials in cells of the cold-sensitive pumkin plant. *Sov. Plant Physiol.* **36,** 96–102.

Pyatygin, S. S., and V. A. Opritov (1990). Effect of temperature on action potentials generating in higher plant excitable cells. *Biophysics* **35,** 444–449.

Pyatygin, S. S., and V. A. Opritov (1992). Role of membrane potential changes of higher plant cells for formation of adaptation syndrome at cooling. *Dokl. Akad. Nauk SSSR* **326,** 202–205.

Pyatygin, S. S., V. A. Opritov, and V. A. Khudyakov (1992). Subthreshold changes in excitable membranes of *Cucurbita pepo* L. stem cells during cooling-induced action-potential generation. *Planta* **186,** 161–165.

Quaster, H. (1964). "The Emergence of Biological Organisation." Yale University Press, New Haven, CT.

Randles, J. E. B. (1956). The real hydration energies of ions. *Trans. Faraday Soc.* **52,** 1573–1581.

Rashevsky, N. (1965). Models and mathematical principles in biology. *In* "Theoretical and Mathematical Biology" (T. Waterman and H. Morowitz, eds.). Blaisdell Publishing Co., New York.

Raval, M. K., and U. C. Biswal (1984). Oxidation of water in photosynthesis. *Bioelectrochem. Bioenerg.* **12,** 57–61.

Raven, P. H., R. F. Evert, and S. E. Eichhorn (1986). "Biology of Plants." Worth Publ., New York.

Raven, J. A. (1987). Electrochemistry of plant and signal transduction. *In* "The Cell Surface in Signal Transduction" (E. Wagner, H. Greppin, and B. Millet, eds.), pp. 205–235. Springer-Verlag, Berlin.

Renger, G. (1977). A model for the molecular mechanism of photosynthetic oxygen evolution. *FEBS Lett.* **81,** 223–228.

Renger, G., and W. Weiss (1982). The detection of intrinsic 320 nm absorption changes reflecting the turnover of the water splitting enzyme system Y which leads to oxygen formation in trypsinized chloroplast. *FEBS Lett.* **137,** 217–221.

Renger, G. (1993). Water cleavage by solar radiation—An inspiring challenge of photosynthesis research. *Photosynth. Res.* **38,** 229–247.

Riveros, O. J. (1991). Dynamics of electron transfer in the oxidation of water by chlorophyll *a* dimer. *Biophys. Chem.* **40,** 109–115.

Roberts, K. (1992). Potential awareness of plants. *Nature* **360,** 14–15.

Roblin, G. (1985). Analysis of the variation potential induced by wounding in plants. *Plant Cell Physiol.* **26,** 455–467.

Rosen, R. (1967). "Optimaity Principles in Biology." Butterworths, London.

Rosenberg, T., and W. Wilbrandt (1957). Uphill transport induced by counterflow. *J. Gen. Physiol.* **41,** 289–296.

Ross, Yu. K. (1964). Towards the mathematical theory of photosynthesis in plant canopies. *Dokl. Akad. Nauk SSSR* **157,** 1239–1244.

Ross, Yu. K. (1975). "Radiative Relations and Architectonics of Plant Canopies" (in Russian). Hydrometeoizdat, Leningrad.

Ross, R. T., and Hsiao Ta-Lee (1977). Limits on the yield of photochemical solar energy conversion. *J. Appl. Phys.* **48,** 4783–4785.

Rossignol, M., P. Thomas, and C. Grignon (1982). Proton permeability of lyposomes from natural phospholipid mixture. *Biochim. Biophys. Acta* **684,** 195–199.

Rottenberg, H. (1978). An irreversible thermodynamic approach to energy coupling in mitochondria and chloroplasts. *In* "Progress in Surface and Membrane Science" (J. F. Danielli, ed.), Vol. 12, pp. 245–325. Academic Press, New York.

Rumer, Iu. B., and M. Sh. Ryvkin (1980). "Thermodynamics, Statistical Physics and Kinetics." Mir, Moscow.

Rusanov, A. I., and F. M. Kuni (1982). Theory of nucleation on charged nuclei. 1. General thermodynamic relationships. *Kolloid. Zh.* **44,** 934–941.

Rusanov, A. I., S. S. Dukhin, and A. E. Yaroshchuk (1984). Problem of the surface layer in liquid mixtures and the electric double layer. *Kolloid. Zh.* **46,** 490–494.

Rutherford, A. W., J. L. Zimmermann, and A. Boussac (1992). Oxygen evolution. *In* "The Photosystems: Structure, Function and Molecular Biology" (J. Barber, ed.), pp. 179–229. Elsevier, Amsterdam.

Salvucci, M. E., and W. L. Ogren (1996). The mechanism of Rubisco activase: Insight from studies of the properties and structure of the enzyme. *Photosynth. Res.* **47,** 1–11.

Saygin, O., and H. T. Witt (1985). Evidence for the electrochromic identification of the change of charges in the four oxidation steps of the photoinduced water cleavage in photosynthesis. *FEBS Lett.* **187,** 224–226.

Schmidt-Nielsen, K. (1984). "Scaling. Why Is Animal Size So Important?" Cambridge Univ. Press, London.

Schroeder, J. I., and R. Hendric (1989). Involvement of ion channels and active transport in osmoregulation and signalling of higher plant cells. *Trends Biochem. Sci.* **14,** 187–192.

Schroedinger, E. (1955). "What Is Life? The Physical Aspects of the Living Cell." Cambridge University Press, Cambridge, UK.

Seely, G. R. (1977). Chlorophyll in model systems: Clues to the role of chlorophyll in photosynthesis. *In* "Primary Processes of Photosynthesis" (J. Barber, ed.), pp. 1–53. Elsevier, Amsterdam.

Semenov, N. N., A. E. Shilov, and G. I. Likhtenstein (1975). Multielectron oxidation-reduction processes in the chemistry and biology. *Dokl. Acad. Nauk SSSR* **221,** 1374–1377.

Shachov, A. A. (1993). "Photoenergetics of Plants and Yield." Nauka Publ. House, Moscow.

Sherman, G., and E. Fujimory (1968). Interactions between chlorophyll and water in the solid state: electron spin resonance. *Nature* **219,** 375–377.

Shilov, A. E. (1980). Activation of small molecules by metal complexes. *Kinet. Katal.* **21,** 26–35.

Shilov, A. E., and T. S. Dzabiev (1984). "Solar Energy Bioconversion" (I. V. Berezin, ed.), pp. 22–34. ONTI AN SSSR, Pushchino.

Shirai, O., S. Kihara, Y. Yoshida, and M. Matsui (1995). Ion transfer through a liquid membrane or a bilayer lipid membrane in the presence of sufficient electrolytes. *J. Electroanal. Chem.* **389,** 61–70.

Shirai, O., Y. Yoshida, M. Matsui, K. Maeda, and S. Kihara (1996). Voltammetric study on the transport of ions of various hydrophobicity types through bilayer lipid membranes composed of various lipids. *Bull. Chem. Soc. Jpn.* **69,** 3151–3162.

Showell, M. S., and F. K. Fong (1982). Elementary reconstitution of the water splitting light reaction in photosynthesis. 3. Photooxidative properties of chlorophyll dihydrate on metal as catalyst for water photolysis. *J. Am. Chem. Soc.* **104,** 2773–2781.

Shulgin, I. A. (1973). "Plant and Sun" (in Russian). Hydrometeoizdat, Leningrad.

Shulgin, I. A., S. V. Klimov, and A. A. Nichiporovich (1975). Adaptation of plant architectonics to solar radiation. *Sov. Plant Physiol.* **22,** 40–48.

Sibaoka, T. (1962). Excitable cells in *Mimosa. Science* **137**, 226–228.

Sibaoka, T. (1969). Physiology of rapid movements in higher plants. *Annu. Rev. Plant Physiol.* **20**, 165–184.

Sibaoka, T. (1980). Action potentials and rapid plant movements. *In* "Plant Growth Substances" (F. Skoog, ed.), pp. 462–469. Springer-Verlag, Berlin.

Silsbury, J. (1977). Energy requirement for symbiotic nitrogen fixation. *Nature* **267**, 149–150.

Sinukhin, A. M., and V. V. Gorchakov (1966a). Action potentials of higher plants not possessing motor activity. *Biophysics* **11**, 966–975.

Sinukhin, A. M., and V. V. Gorchakov (1966b). Characteristics of the action potentials of the conducting systems of pumkin stems evoked by various stimulu. *Sov. Plant Physiol.* **13**, 727–733.

Sinukhin, A. M., and I. V. Rutkovskii (1966). An electrophysiological method of recording the vitality of woody plants. *Sov. Plant Physiol.* **13**, 310–316.

Sinukhin, A. M., and E. A. Britikov (1967). Action potentials in the reproductive system of plant. *Nature* **215**, 1278–1280.

Sinukhin, A. M., and V. V. Gorchakov (1968). Role of the vascular bundles of the stem in long-distance transmission of stimulation by means of bioelectric impulses. *Sov. Plant Physiol.* **15**, 400–407.

Sinukhin, A. M. (1972). Plant signalling. *Priroda* **11**, 40–47.

Siomons, P. J. (1981). The role of electricity in plant movements. *New Physiologist* **87**, 11–37.

Sisskind, B., and J. Kasarnowsky (1933). Studying of gases solubilities. 2. The solubility of argon. *Zh. Fiz. Khim.* **4**, 683–690.

Sivukhin, D. V. (1990). "General Physics. Thermodynamics and Molecular Physics," Vol. 2. Nauka, Moscow.

Slater, P. N. (1980). "Remote Sensing: Optics and Optical Systems." Addison-Wesley, London-Amsterdam.

Slatyer, R. O. (1967). "Plant-Water Relationships." Academic Press, London.

Smith, J. A., and R. E. Oliver (1974). Effects of changing canopy directional reflectance on feature selection. *Appl. Optics* **13**, 1599–1604.

Sobolev, V. V. (1972). "Light Scattering in the Atmospheres of Planets." Nauka Publ. House, Moscow.

Sobolev, V. V. (1975). "Course of Theoretical Astrophysics," Nauka Publ. House, Moscow.

Spanner, D. C. (1963). The green leaf as a heat engine. *Nature* **198**, 934–937.

Spanner, D. C. (1964). "Introduction to Thermodynamics." Academic Press, New York.

Stein, W. D. (1967). "The Movement of Molecules across Cell Membranes." Academic Press, New York.

Stein, W. D. (1986). "Transport and Diffusion across Cell Membranes," Academic Press, New York.

Stemler, A. (1980). Inhibition of photosystem II by formate. Possible evidence for a direct role of bicarbonate in photosynthetic oxygen evolution. *Biochim. Biophys. Acta* **593**, 103–112.

Stewart, W. (1983). "Paleobotany and the Evolution of Plants." Cambridge University Press, New York.

Sucheta, A., K. E. Georgiadis, and O. Einarsdottir (1997). Mechanism of cytochrome *c* oxidase-catalysed reduction of dioxygen to water: Evidence for peroxy and ferryl intermediates at room temperature. *Biochemistry* **36**, 554–565.

Suits, G. H. (1972). The calculation of the directional reflectance of a vegetative canopy. *Remote Sensing Environ.* **2**, 117–125.

Taiz, L., and E. Zeiger (1991). "Plant Physiology." The Benjamin/Cummings Publ. Company, Inc., Redwood City, CA.

Thekaekara, M. P. (1974). Extraterrestrial solar spectrum 3000–6100 Å at 1-Å intervals. *In* "The Energy Crisis and Energy from the Sun: Papers Presented at the Symposium on Solar Energy Utilization." Institute of Environmental Sciences, Mount Prospect, IL.

Thomas, A. P., and M. P. Thekaekara (1976). Experimental and theoretical studies on solar energy for energy conversion. *In* "Sharing the Sun: Solar Technology in the Seventies" (K. W. Boer, ed.), Vol. 1, pp. 338–355. Winnipeg, American Section of the International Solar Energy Society, Cape Canaveral, FL.

Thornly, J. H. M. (1976). "Mathematical Models in Plant Physiology." Academic Press, London.

Tien, H. Ti. (1974). "Bilayer Lipid Membranes (BLM). Theory and Practice." M. Dekker, Inc., New York.

Tien, H. Ti. (1980). Energy conversion via pigmented bilayer lipid membranes. *Sep. Sci. Technol.* **15**, 1035–1058.

Tien, H. Ti. (1986). Redox reactions in lipid bilayers and membrane bioenergetics. *Bioelectrochem. Bioenerg.* **15**, 19–38.

Tien, H. Ti. (1989). Membrane photobiophysics and photochemistry. *Prog. Surf. Sci.* **30**, 1–199.

Toyoshima, Y., M. Marino, H. Motoki, and M. Sukigara (1977). Photo-oxidation of water in phospholipid bilayer membranes containing chlorophyll *a. Nature* **265**, 187–189.

Trebst, A. (1978). Plastoquinones in photosynthesis. *Philos. Trans. R. Soc. London* **284**, 591–599.

Trissl, H. W. (1980). Novel capacitive electrode with a wide frequency range for measurements of flash-induced changes of interface potential at the oil/water interface. Mechanical construction and electrical characteristics of the electrode. *Biochim. Biophys. Acta* **595**, 82–95.

Trissl, H. W., and P. Graber (1980). Properties of chloroplasts spread at the heptane/water interface. Measurements of the photosynthetic charge separation in the nanosecond range. *Bioelectrochem. Bioenerg.* **7**, 167–186.

Trumpower, B. (ed.) (1982). "Functions of Quinones in Energy-Conserving Systems," Vol. 1. Academic Press, New York.

Tucker, C. J., and M. W. Garrat (1977). Leaf optical system modeled as a stochastic process. *Appl. Optics* **16**, 635–642.

Uhlig, H. H. (1937). The solubilities of gases and surface tension. *J. Phys. Chem.* **41**, 1215–1225.

Van Sambeek, J. W., and B. G. Pickard (1976). Mediation of rapid electrical, metabolic, transpirational, and photosynthetic changes by factors released from wounds. I. Variation potential and putative action potentials in intact plants. *Can. J. Bot.* **54**, 2642–2650.

Van Sambeek, J. W., B. G. Pickard, and C. E. Ulbright (1976). Mediation of rapid electrical, metabolic, transpirational, and photosynthetic changes by factors released from wounds. II. Mediation of the variation potential by Ricca's factor. *Can. J. Bot.* **54**, 2651–2661.

Villee, C. A., and V. G. Dethier (1971). "Biological Principles and Processes." W. B. Saunders Co., Philadelphia.

Volkmann, D., and A. Sievers (1979). Graviperception in multicellular organs. *In* "Encyclopedia of Plant Physiology, Vol. 7: Physiology of Movements" (W. Haupt and M. E. Feinleib, eds.), pp. 573–600. Springer, New York.

Volkov, A. G., M. I. Gugeshashvili, A. F. Mironov, and L. I. Boguslavsky (1982). Reduction of hydrophobic porphyrin at the octane/water interface controlled by the specific adsorption of halogen anions. *Bioelectrochem. Bioenerg.* **9**, 551–558.

Volkov, A. G., M. A. Bibikova, A. F. Mironov, and L. I. Boguslavsky (1983a). Adsorption and catalytic properties of an iron complex of coproporfyrin III at the octane/water interface. *Elektrokhimiya* **19**, 1398–1401.

Volkov, A. G., M. A. Bibikova, A. F. Mironov, and L. I. Boguslavsky (1983b). Adsorption and catalytic properties of iron coproporphyrin II complex at the octane/water interface. *Bioelectrochem. Bioenerg.* **10**, 477–483.

Volkov, A. G., M. I. Gugeshashvili, A. F. Mironov, and L. I. Boguslavsky (1983c). Oxidation of NADH and reduction of vitamin K_3 at the octane/water interface with ethioporphyrin complexes as catalysts. *Bioelectrochem. Bioenerg.* **10**, 485–491.

Volkov, A. G. (1984). A possible mechanism of the photooxidation of water sensitized by chlorophyll adsorbed at the interface. *J. Electroanal. Chem.* **173**, 15–24.

Volkov, A. G. (1985). Possible mechanism of the photooxidation of water sensitized by chlorophyll adsorbed on an interface. *Sov. Electrochem.* **21**, 91–98.

Volkov, A. G., and Yu. I. Kharkats (1985). Catalytic properties of the interface between two immiscible liquids during redox reaction. *Kinet. Katal.* **26**, 1322–1326.

Volkov, A. G., and A. A. Kornyshev (1985). Dependence of the Gibbs free energy of resolvation during ion transfer from one solvent to another on the ion size. *Electrokhimiya* **21**, 814–817.

Volkov, A. G., V. D. Kolev, A. L. Levin, and L. I. Boguslavsky (1985). Oxygen photoevolution at the octane/water interface in the presence of β-carotene and chlorophyll *a*. *Photobiochem. Photobiophys.* **10**, 105–111.

Volkov, A. G. (1986a). The electrochemical mechanism of functioning of photosystem II in higher plants. *J. Electroanal. Chem.* **205**, 245–257.

Volkov, A. G. (1986b). The molecular mechanism of functioning of photosystem II in higher plants. *Photobiochem. Photobiophys.* **11**, 1–7.

Volkov, A. G. (1986c). Molecular mechanism of the photooxidation of water during photosynthesis: Cluster catalysis of synchronous multielectron reactions. *Mol. Biol.* **20**, 728–736.

Volkov, A. G., and Yu. I. Kharkats (1986). Synchronous multielectron reactions at the liquid/liquid interface. *Chem. Phys.* **5**, 964–971.

Volkov, A. G., V. D. Kolev, A. L. Levin, and L. I. Boguslavsky (1986). Oxygen photoevolution at the octane/water interface in the presence of β-carotene and chlorophyll *a*. *Electrokhimiya* **22**, 1303–1307.

Volkov, A. G. (1987). Thylakoid membrane: electrochemical mechanisms of photosynthesis. The mechanism of oxygen evolution in the reaction center of photosystem II of green plants. *Biol. Membr.* 4, 984–993.

Volkov, A. G., and Yu. I. Kharkats (1987). Membrane catalysis: Synchronous multielectron reactions at the interface between two liquid phases. Bioenergetic mechanisms. *In* "Chemical Physics of Enzyme Catalysis" (A. Aaviksaar, ed.), pp. 87–90. Publ. House Estonian Academy of Sciences, Tallinn.

Volkov, A. G. (1988). The molecular mechanism of oxygen evolution (Review). *Uspek. Sovr. Biol. (Prog. Modern Biol.)* 105, 467–487.

Volkov, A. G., and Yu. I. Kharkats (1988). Cytochrome oxidase: Mechanism of functioning. *Biol. Membr.* 5, 920–931.

Volkov, A. G. (1989). Oxygen evolution in the course of photosynthesis. *Bioelectrochem. Bioenerg.* 21, 3–24.

Volkov, A. G., M. I. Gugeshashvili, M. D. Kandelaki, V. S. Markin, B. Zelent, G. Munger, and R. M. Leblanc (1991). Artificial photosynthesis at octane/water interface in the presence of hydrated chlorophyll *a* oligomer thin film. *Proc. Soc. Photo-opt. Instrum. Eng.* 1436, 68–79.

Volkov, A. G., M. I. Gugeshashvili, G. Munger, and R. M. LeBlanc (1992a). Light-dependent oxygen uptake by hydrated oligomer of chlorophyll. *Biol. Membr.* 9, 576–580.

Volkov, A. G., M. I. Gugeshashvili, G. Munger, R. M. Leblanc, B. Zelent, Ju. Galant, H.-A. Tajmir-Riahi, and J. Aghion (1992b). The hydrated chlorophyll *a* oligomer in monolayers and Langmuir-Blodgett films. *Biol. Membr.* 9, 874–880.

Volkov, A. G., M. I. Gugeshashvili, G. Munger, and R. M. Leblanc (1993). The light-dependent oxygen reduction by monolayers of hydrated chlorophyll *a* oligomer. *Bioelectrochem. Bioenerg.* 29, 305–314.

Volkov, A. G., and D. W. Deamer (1994). Mechanisms of the passive ion permeation of lipid bilayers: Partition or transient aqueous pores. *In* "Charge and Field Effects in Biosystems-4" (M. J. Allen, S. F. Cleary, and A. E. Sowers, eds.), pp. 145–155. World Scientific, Singapore.

Volkov, A. G., V. S. Markin, R. M. Leblanc, M. I. Gugeshashvili, B. Zelent, and G. Munger (1994). Monolayers of pheophytin *a* at the oil/water, gas/water and SnO_2/water interfaces: Adsorption and photoelectrochemistry. The general isotherm of adsorption of amphiphilic molecules. *J. Sol. Chem.* 23, 223–248.

Volkov, A. G., and R. A. Haack (1995a). Insect induces bioelectrochemical signals in potato plants. *Bioelectrochem. Bioenerg.* 35, 55–60.

Volkov, A. G., and R. A. Haack (1995b). Bioelectrochemical signals in potato plants. *Russ. J. Plant Physiol.* 42, 17–23.

Volkov, A. G., M. I. Gugeshashvili, and D. W. Deamer (1995a). Energy conversion at liquid-liquid interfaces: Artificial photosynthetic systems. *Electrochim. Acta* 40, 2849–2868.

Volkov, A. G., M. I. Gugeshashvili, B. Zelent, D. Cote, G. Munger, A. Tessier, P. F. Blanchet, and R. M. Leblanc (1995b). Light energy conversion with chlorophyll *a* and pheophytin *a* monolayers at the optically transparent SnO_2 electrode: Artificial photosynthesis. *Bioelectrochem. Bioenerg.* 38, 333–342.

Volkov, A. G. (1996). Potentials of thermodynamic and free zero charge at the interface between two immiscible electrolytes. *Langmuir* **12**, 3315–3319.

Volkov, A. G., and D. W. Deamer (eds.) (1996). "Liquid-Liquid Interfaces: Theory and Methods." CRC Press, Boca Raton, FL.

Volkov, A. G., D. W. Deamer, D. I. Tanelian, and V. S. Markin (1996). Electrical double layers at the oil/water interface. *Prog. Surf. Sci.* **53**, 1–136.

Volkov, A. G., and D. W. Deamer (1997). Redox chemistry at liquid/liquid interfaces. *Prog. Colloid Polym. Sci.* **103**, 21–27.

Volkov, A. G., D. W. Deamer, D. I. Tanelian, and V. S. Markin (1997a). "Liquid Interfaces in Chemistry and Biology." J. Wiley, New York.

Volkov, A. G., S. Paula, and D. W. Deamer (1997b). Two mechanisms of permeation of small neutral molecules and hydrated ions across phospholipid bilayers. *Bioelectrochem. Bioenerg.* **42**, 153–160.

Volta, A. (1816). "Collezione dell' opere del cavaliere Conte Alessandro Volta," Vol. 1, pp. II, 257. Nella stamperia di G. Piatti, Firence.

Voronjec, D., and D. Kozic (1980). "Humid Air." Smeits, Belgrade.

Vukalovich, M. P., S. L. Rivkin, and A. A. Alexandrov (1969). "Tables of Thermophysical Properties of Water and Water Vapour." Izdatelstvo Standartov, Moscow.

Watanabe, Y., S. Takeuchi, M. Ashisada, Y. Ikezawa, and T. Takamura (1995). Potential distribution and ionic concentration at the bean root surface of the growing tip and lateral root emerging points. *Plant Cell Physiol.* **36**, 691–698.

Weber, A. N., L. Spencer, D. T. Sawyer, and R. L. Heath (1985). Photosynthetic water oxidation. A new chemical model. *FEBS Lett.* **189**, 258–262.

Welch, G. R. (1977). On the free energy "cost of transition" in intermediary metabolic processes and the evolution of cellular infrastructure. *J. Theor. Biol.* **68**, 267–291.

Whittaker, R. H. (1975). "Communities and Ecosystems." Macmillan Publ. Co., New York.

Wiener, M. C., G. I. King, and S. White (1991). Structure of a fluid dioleoylphosphatidylcholine bilayer determined by joint refinement of X-ray neutron diffraction data. 1. Scaling of neutron data and the distribution of double bonds and water. *Biophys. J.* **60**, 568–576.

Wikstrom, M. (1989). Identification of the electron transfers in cytochrome oxidase that are coupled to proton-pumping. *Nature* **338**, 776–778.

Wildon, D. C., H. M. Doherty, G. Eagles, D. J. Bowles, and J. F. Thaine (1989). Systemic responses arising from localized heat stimuli in tomato plants. *Ann. Bot.* **64**, 691–695.

Wildon, D. C., J. F. Thain, P. E. H. Minchin, I. R. Gubb, A. J. Reilly, Y. D. Skipper, H. M. Doherty, P. J. O'Donnell, and D. J. Bowles (1992). Electric signalling and systemic proteinase inhibitor induction in the wounded plant. *Nature* **360**, 62–65.

Williams, R. J. P. (1961). Possible functions of chains of catalysis. *J. Theor. Biol.* **1**, 1–17.

Williams, S. E., and B. G. Pickard (1972a). Properties of and action potentials in *Drosera* tentacles. *Planta (Berlin)* **103**, 222–240.

Williams, S. E., and B. G. Pickard (1972b). Receptor potentials and action potentials in *Drosera* tentacles. *Planta (Berlin)* **103**, 193–221.

Williams, S. E., and R. M. Spanswick (1972). Intracellular recording of the action potentials which mediate the thigmonastic movements of *Drosera*. *Plant Physiol. (Lancaster)* **49** (Suppl.), 64.

Williams, R. J. P. (1978). The multifarious coupling of energy transduction. *Biochim. Biophys. Acta* **505**, 1–44.

Williams, S. E., and B. G. Pickard (1980). The role of action potentials in the control of capture movements of *Drosera* and *Dionaea*. *In* "Plant Growth Substances" (F. Skoog, ed.), pp. 470–480. Springer-Verlag, Berlin.

Williams, R. J. P. (1994). Energy coupling: An introduction. *Biochim. Biophys. Acta* **1187**, 125–128.

Wilson, M. A., and A. Phorille (1996). Mechanism of unassisted ion transport across membrane bilayers. *J. Am. Chem. Soc.* **118**, 6580–6587.

Wydrzynski, T., and K. Sauer (1980). Periodic changes in the oxidation state of manganese in photosynthetic oxygen evolution upon illumination with flashes. *Biochim. Biophys. Acta* **589**, 56–70.

Wydrzynski, T., B. J., Higgins, and P. A. Jursinic (1985). Uncoupling of detectable O_2 evolution from the apparent S-state transitions in photosystem II by lauroylcholine chloride: Possible implications in the photosynthetic water-splitting mechanism. *Biochim. Biophys. Acta* **809**, 125–136.

Yachandra, V. K., K. Sauer, and M. P. Klein (1996). Manganese cluster in photosynthesis: Where plants oxidize water to dioxygen. *Chem. Rev.* **96**, 2927–2950.

Yaguzhinsky, L. S., L. I. Boguslavsky, A. G. Volkov, and A. B. Rakhmaninova (1975). Synthesis of ATP coupled with action of membrane protonic pumps at the octane-water interface. *Nature* **259**, 494–496.

Zamaraev, K. I., and V. N. Parmon (1983). Molecular photocatalytic systems for solar energy conversion: Catalysts for the evolution of hydrogen and oxygen from water. *Uspek. Khim.* **52**, 1433–1467.

Zavadzki, T., E. Davis, H. Dziubinska, and K. Trebacz (1991). Characteristics of action potentials in *Helianthus annus*. *Physiol. Planetar.* **83**, 601–604.

Zelent, B., Ju. Gallant, A. G. Volkov, M. I. Gugeshashvili, G. Munger, H.-A. Tajmir-Riahi, and R. M. LeBlanc (1993). Hydrated chlorophyll alpha oligomers in solutions, monolayers, and thin films. *J. Mol. Struct.* **297**, 1–11.

Zelitch, I. (1992). Control of plant productivity by regulation of photorespiration. *BioScience* **42**, 519–516.

Zholkevich, V. N., N. A. Gusev, A. V. Kaplya, G. I. Pakhomova, N. V. Pilschikova, F. D. Samuilov, P. S. Slavnyj, and I. G. Shmat'ko (1989). "Water Exchange of Plants." Nauka Publ. House, Moscow.

Zimmerman, M. N., and J. A. Milburn (1975). Transport in Plants. 1. Phloem Transport. *In* "Encyclopedia of Plant Physiology," New Series, Vol. 1. Springer-Verlag, New York.

Zimmerman, V., and F. Beckers (1978). Generation of action potentials in *Chara cirallina* by turgor pressure changes. *Planta* **138**, 173–180.

Zirin, H. (1988). "Astrophysics of the Sun." Cambridge University Press, New York.

Zisman, W. A. (1932). A new method of measuring contact potential differences in metals. *Rev. Sci. Instr.* **3**, 367–370.

This Page Intentionally Left Blank

Index

This Page Intentionally Left Blank